First Row Transition Metal Perfluoro-Alkyls and -Carbenes: Synthesis, Metathesis and More

Alexander Daniels

A thesis submitted in conformity with the requirements
for the degree of Philosophy Doctorate-Science

Chemistry
University of Ottawa

First Row Transition Metal Perfluoro-Alkyls and -Carbenes: Synthesis, Metathesis and More

Alexander Daniels

Philosophy Doctorate - Science

Chemistry
University of Ottawa

2019

Abstract

Organofluorine compounds are highly sought-after products owing to the unique physical and chemical properties imparted by fluorine. However, the use of hazardous HF, reactive F_2 and environmentally persistent long chain fluorosurfactants, all staples of the industrial processes used to prepare refrigerants, pharma-/agrochemicals and fluoropolymers, make the preparation of organofluorine compounds difficult. Therefore, new routes to some *or* all of these value-added products are desirable. Efficient transition metal-mediated or -catalyzed processes within the arena of fluoro-organic chemistry, however, are significantly less well developed than similar processes for both non-fluorinated and even halogenated compounds. For example, analogs of Group 4 metallocene catalysts for controlled polyolefin formation, or Ru and Group 6 catalysts for alkene metathesis are not generally useful with fluoroalkene substrates. Recent progress has focused on first row metal fluoroalkyl ($M\text{-}R^F$) and fluorocarbene ($M{=}CFR^F$) complexes that tend to have weaker M-C bonds than their second and third row counterparts. The synthesis, electronic structure and chemistry of such complexes is summarized in Chapter 1 along with an assessment of their potential for catalyzed C-C bond formation with fluoroalkenes via insertion or cycloaddition reactions. In Chapter 2 the synthesis and reactivity of new d^8 [Co]-CF_3 carbonyl complexes and their corresponding electrophilic $\{[Co]{=}CF_2\}^+$ complexes is described. In Chapter 3 we introduce the first examples of d^{10} metal fluorocarbenes, $P_3Ni{=}CF_2$ [P = $P(O^iPr)_3$; P_3 = dppe, $P(O^iPr)_3$] along with their facile cycloaddition reactions with tetrafluoroethylene and some reactivity of the resulting stable perfluoronickelacyclobutanes (dppe = 1,2-bis(diphenylphos-

phino)ethane). In Chapter 4 exploration of the more reactive Ni fluorocarbenes, Ni=CF(CF_3)-[$P(OR)_3$]$_3$, (R = Me, ^{i}Pr) leads, in reactions with fluoroalkenes, to formation of both metalla-cycles and metathesis products via separate pathways, in the first example of metathesis of fluoro-alkenes with a perfluoro-carbene. Detailed analysis of the latter by Texas A&M collaborators Guan and Hall using density functional theory showed that the nature of the reaction products depends on the geometry of the four-coordinate C-C bond forming transition state. In Chapter 5 this novel fluoroalkene metathesis process is probed further by extending the substrate scope to additional fluoroalkenes and several non-fluorinated variants. In Chapter 6 a series of new Mn-CF_3 carbonyl complexes are prepared with a view to enabling fluoroalkene insertion reactions. Although this goal has not yet been achieved, fluoride abstraction using Lewis acids afforded the first examples of [Mn]=CF_2 complexes. Finally, in Chapter 7 the findings of this thesis are placed in the context of the current state of the art and logical next steps for further understanding and catalytic process development are proposed.

Acknowledgments

When I think about my time during my PhD I am filled with a pride that I can be welcomed into the ranks of so many of those that I respect and admire: Newton, Galileo, Da Vinci, Einstein, Kekule and a near infinite number of philosophers who came before me who dreamt of what could be and what magic they might discover by the simple act of asking, 'why?'. The road to my PhD was paved with the support of good friends, family and mentors who deserve to be mentioned here. My mother and father, Rosemary and Steven are, quite honestly, my heroes. Both coming from modest backgrounds in England and travelled to Canada to new adventures they both strived towards doing the right thing even if it meant the hardest of multiple paths. They taught me the importance of knowledge, family, love, truth and adventure. As the son of both an engineer and a PhD in literature I was gifted with both a love of science but also a whimsical desire to pursue the unknown. They always encouraged going to University and reaching for the lofty goal of becoming a scientist even as an adult student whose high school grades would suggest this was a rather poor idea. If it wasn't for their loving guidance, support and sympathetic ears when times became tough, I would never have made it through. My friend, who is probably better described as a brother from another mother, Dan Courtney, and all of the Courtney's, Sue, Steve, Tizzy, and Dan are all family to me and have all supported me in their own way as I threw myself into my studies. Dan, someone who is one of the most driven and intelligent scientists I have met never stopped pushing me to go back to school even when I had given up on myself and through his example gave me a blueprint on what I needed to do to succeed. I treasure his friendship even when time and space separate us. Friends that I've made during my PhD were always a source of comic relief, new ideas and shoulders to cry on. Dr. Dan Harrison was not only one of the first people I encountered during my entry into graduate studies. Similarly, to many that have met Dan, I was immediately intimidated by his gruff exterior and his extraordinary brilliance and work ethic. It was these qualities that made me strive to be a better scientist. However, as time passed, I was no longer intimidated but instead had a truly kind friend and mentor who always seemed to look out for me and my interests. Without Dan, I would not have a thesis to defend. His ideas and the formation of the compounds with which I worked most intimately with carved a path that I could follow throughout my studies. For that I am truly thankful. Graham Lee, the red menace, was a brilliant scientist and one of the most well-read people I came across. Graham was typically quiet however as we

worked in silence you would always hear his clever quips resonating from his office that would give everyone wholehearted belly laughs that would always alleviate the stresses of failed experiments. Matt Leclerc, one of my favorite people in the lab, had an absolutely outrageous sense of humor and a heart of gold. We would spend most days attempting to humiliate, degrade and insult one another to within an inch of each other's lives while simultaneously talking shop, movies, gossip and life's little foibles and I wouldn't have wanted it any other way. Kelvin Tso, my organic chemistry friend, I met during my first-year chemistry TA position as we worked together where he informed me that I was explaining TLC's incorrectly and promptly assumed I must have been an inorganic chemist. Throughout the years our friendship grew where we discussed inorganic vs organic chemistry, our favorite TV shows, video games and geeked out about everything while opening up about our most vulnerable moments. No matter how deflated, busy or stressed I was Kelvin always was able to pull me out from the darkness. I hope to always have my personal organic chemist in my corner. I should also take a moment to thank the Baker lab old and new for their constant assistance, moral guidance and friendship. Alex Sicard, a wealth of knowledge about anything phosphine, NHC, organometallic or pretty much whatever he finds interesting. Nicholas Andrella, the resident vegan, a wonderfully optimistic scientist who was always a real treat to talk with. Karine 'Ghost' Ghostine, the resident pessimist, is one of my favorite people to gossip and complain with, a true kindred spirit and a wonderful person. My personal lab slaves otherwise known as undergraduates, Jason De Gama, Raquel Edjoc and most recently Alex Watson were amazing students, quick learners and I wish them the best in their future careers. The Baker lab has seen many previous master's and PhDs who helped along the way: Katie, Sarah, Jenny, and Brandon to name a few who were always there to help. I would also like to thank the staff, technicians and administration at the University, especially, Ilia Korbkov, Bulat Gabidullin, Josee Rouleau, Annette Campeau, NMR Geniuses – Glen Facey and Peter Pallister and an army of others dedicated to their students. Of course, I would also like to thank Prof. Tom 'the beard' Baker. Baker is a supervisor to which there is no equal. Baker is one of the most optimistic men I have ever met, always encouraging thought experiments and new ideas and who even after a lifetime of science has never grown tired of the thrill of discovery. Baker has been an invaluable source of optimism, genesis of ideas, intelligence and friendship and I am honored to have been given the opportunity to work with him. Finally, to my beautiful wife Natalie, you have been, and I'm sure will continue to be a guiding light in my life. You have been there through my worst and enjoyed every moment of

joy at my best. During periods of imposter syndrome, depression and hardships you, as a strong and compassionate woman, helped me persevere and learn from my mistakes. To have found a scientist, friend and fellow adventurer such as you, who grounds me while simultaneously lifting me up is something I consider to be one of my greatest discoveries.

"Anybody who has been seriously engaged in scientific
work of any kind realizes that over the entrance to the
gates of the temple of science are written the words:
Ye must have faith." – Max Planck

Table of Contents

Table of Contents

Acknowledgments iv

Table of Contents vii

List of Figures x

Chapter 1 . Introduction and Background 1

1 C–F bonds 1

1.1 Industrial Synthesis and Relevance 1

1.2 The Problem with C–F 3

1.3 Modern Methods Towards C–R^F Manipulation 4

1.3.1 Organic Reagents 4

1.3.2 Organometallic M–F/ M–R^F Complexes 4

1.3.3 M-R^F in R^F transfer, Insertion and Cross-Coupling Reactions 8

1.4 Carbenes 10

1.4.1 M=CR_2 carbenes (R = alkyl, aryl, H) 10

1.4.2 NHCs (‘pure’ Fischer carbenes) 14

1.4.3 Metal Carbenes and Olefin Metathesis 16

1.4.4 M=CR^F_2 vs. M=CR_2 (R^F = F, CF_3, R = alkyl, aryl, H) 17

1.4.5 Fluoroalkenes: Fluoropolymers, Refrigerants and More 20

1.4.6 Fluoroalkene Metathesis 22

1.5 Summary and Thesis Outline 25

2 Tetracarbonyl(trifluoromethyl)cobalt(I) [$Co(CO)_4(CF_3)$] as a Precursor to New Cobalt Trifluoromethyl and Difluorocarbene Complexes 41

2.1 Context 41

2.1.1 Published Contribution. 42

2.2 Introduction 43

2.2.1 Results and Discussion 45

2.2.2 Conclusion 52

2.2.3 Supplemental 59

3 Chapter 3: d^{10} Nickel Difluorocarbenes and their Cycloaddition Reactions with Tetrafluoroethylene 73

3.1 Context 73

3.1.1 Published Contribution 73

3.2 **Introduction** 74

3.2.1 Results and Discussion 76

3.2.2 Conclusion 80

3.2.3 Experimental Section 80

4 Nickel Fluorocarbene Metathesis with Fluoroalkenes 103

4.1 Context 103

4.1.1 Published Contribution 103

4.2 **Introduction** 104

4.2.1 Results and Discussion 106

4.2.2 Conclusion 111

4.2.3 Experimental Section 111

^{1}H NMR, ^{19}F NMR and ^{31}P NMR Spectra 120

5 Metathesis and Metallacycle Reactivity of $P_3Ni{=}CF(CF_3)$ with Alkenes [P = $P(O^{i}Pr)_3$] 169

5.1 Context 169

5.2 Introduction 171

5.3 Results 174

5.4 Conclusion 181

5.5 Experimental Section 182

5.6 Supplemental 188
6 Synthesis and Reactivity of Mn–CF_3 Complexes 216
6.1 Context 216
6.1.1 Published Contribution 217
6.2 Introduction 217
6.2.1 Results 220
6.2.2 Discussion/Conclusion 226
6.2.3 Materials and Methods 227
6.2.4 IR Spectra 232
6.2.5 NMR Spectra 234
6.2.6 Cyclic Voltammetry 244
6.2.7 EI-MS Data 247
7 Summary and Outlook 259
7.1 Overview 259
7.2 Chapter 2 259
7.3 Chapter 3 260
7.4 Chapter 4 260
7.5 Chapter 5 262
7.6 Chapter 6 263
7.7 Outlook 264

List of Figures

Figure 1.1: Selection of important fluorine containing HFOs [GWP = Global Warming Potential] 2

Figure 1.2: Selected examples of F^- and CF_3^- transfer reagents 4

Figure 1.3: Metal perfluoroacyl decarbonylation route to M-CF_3 complexes 5

Figure 1.4: General trend of bonding between early to late metals and CF_3 ligands 7

Figure 1.5: Outer sphere fluoride 'rebound' reaction for the formation of R-CF_3 bonds. 9

Figure 1.6: First proven existence of dibromo-carbene utilized in the cyclopropanation of an alkene also showing the diradical behavior of a *triplet* carbene. 10

Figure 1.7: Chugaev's Salt (first synthesis of a metal carbene complex) Pt=C! 11

Figure 1.8: Trends in metal group, oxidation state, ligand environment and carbene R groups in regards to electronic state and reactivity of M=CRR.' 14

Figure 1.9: Chauvin's mechanism showing both the metallacyclobutane intermediate and the production of both degenerate and productive metathesis products. 17

Figure 1.10: Overview of currently known metal perfluoro-carbenes 19

Figure 1.11: Most common alkene monomers in the fluoropolymer industry 21

Figure 1.12: Example of Grubbs 2nd gen catalyst becoming deactivated upon reacting with fluoro-olefins due to the formation of singlet-stabilizing carbene fragment. 22

Figure 1.13: Mechanistic differences between traditional [2+2] cycloaddition (Chauvin mechanism) and the singlet diradical mechanism which forms a stable metallacyclobutane. 24

Figure 1.14: Synthesis and reactivity of nucleophilic d^8 [Co]=CFR^F complexes and corresponding metallacyclobutanes. 25

Figure 2.0.1: ORTEP structures of **2**, **3**, **4**, and **5** with 50% ellipsoids. Hydrogen atoms are omitted. Toluene solvent molecules appearing in the unit cells of **3** and **5** are not shown..... 47

Figure 2.0.2: ORTEP representation of the molecular structure of **7** with 50% thermal probability ellipsoids. Hydrogen atoms, the rotationally disordered OTf^- anion and benzene solvent molecule are omitted and the carbon frame-work of the P3 ligand is shown as a wire cage structure for clarity. Selected bond distances [[Å]: Co(1)-C(35) = 1.787(3), Co(1)-C(36) = 1.757(3), O(1)-C(36) = 1.128(3), F(1)-C(35) = 1.340(3), F(2)-C(35) = 1.322(3)..... 52

Figure 2.0.3: FT-IR spectra (Nicolet Nexus 6700 instrument, neat/solid samples) for tri-carbonyl/trifluoromethyl complexes $Co(PPh_3)(CO)_3(CF_3)$,$Co[P(O\text{-}o\text{-}Tol)_3](CO)_3(CF_3)$ (**2**) and $Co(SIPr)(CO)_3(CF_3)$ (**5**) (metal carbonyl region). 62

Figure 2.0.4: FT-IR spectra (Nicolet Nexus 6700 instrument, neat/solid samples) for di- and mono-carbonyl/trifluoromethyl complexes $Co(DPPE)(CO)_2(CF_3)$ (**3**) and $Co(P_3)(CO)_3(CF_3)$ (**4**) (metal carbonyl region). 63

Figure 2.0.5: FT-IR spectra (Nicolet Nexus 6700 instrument, neat/solid samples) for di- and mono-carbonyl/difluorocarbene complexes $[Co(DPPE)(CO)_2(=CF_2)](OTf)$ (**6**) and$[Co(P_3)(CO)(=CF_2)](OTf)$ (**7**) (metal carbonyl region). 64

Figure 2.0.6: FT-IR spectra (Nicolet Nexus 6700 instrument, neat/solid samples) for all new compounds and $Co(PPh_3)(CO)_3(CF_3)$. 65

Figure 2.0.7: Variable-temperature (–40 to 20°C) ^{19}F NMR (282 MHz, $CDCl_3$) spectra of **3**. The inset illustrates the proposed exchange process. 66

Figure 2.0.8: Variable-temperature (–10 to 10 °C) ^{19}F NMR (282 MHz, $CDCl_3$) spectra of **3**.... 67

Figure 3.1: ORTEP representation of the X-ray crystal structure of **1** with 50% probability thermal ellipsoids. Hydrogen atoms are omitted and the carbon framework of the DPPE ligand is depicted as a wire cage structure for clarity. One orientation is shown for the disordered (over two positions) oxygen atoms, O2' and O3'. Selected bond distances [Å]: Ni1–C27 = 1.771(4), Ni1–P1 = 2.183(1), Ni1–P2 = 2.2100(9), Ni1–P3 = 2.148(1), C27–F1 = 1.340(5), C27–F2 = 1.327(5). 77

Figure 3.2: ORTEP representation of the X-ray crystal structure of 3 with 50% probability thermal ellipsoids. Hydrogen atoms are omitted and the carbon framework of the DPPE ligand is depicted as a wire cage structure for clarity. Selected bond distances [Å]: Ni1–P1 = 2.1861(6), Ni1–P2 = 2.1701(5), C27–F1 = 1.383(3), C27–F2 = 1.377(3), C28–F3 = 1.368(3), C28–F4 = 1.356(3), C29–F5 = 1.388(3), C29–F6 = 1.367(3). Additional distances and angles are displayed in the inset. 79

Figure 3.3: ^{19}F NMR (282 MHz, CH_2Cl_2 with C_6D_6 capillary) spectrum of **5** [Ni(DPPE)(OTf)(cis- and trans-CF=CFCF$_3$)]. The product peaks are expanded in the insets. Note that the top of the BTB peak is off-scale. 87

Figure 3.4: $^{31}P\{^1H\}$ NMR (121 MHz, CH_2Cl_2 with C_6D_6 capillary) spectrum of **5** [Ni(DPPE)(OTf)(cis- and trans-CF=CFCF$_3$)]. The product peaks are expanded in the insets. Minor contaminants are not labeled. 88

Figure 3.5: ^{19}F NMR (282 MHz, CH_2Cl_2 with C_6D_6 capillary) spectrum of **6** [Ni(DPPE)(η^2-CF_2=CFCF$_3$)]. The product peaks are expanded in the insets. Minor contaminants are not labeled. Note that the top of the BTB peak is off-scale. 89

Figure 3.6: $^{31}P\{^1H\}$ NMR (121 MHz, CH_2Cl_2 with C_6D_6 capillary) spectrum of **6** [Ni(DPPE)(η^2-CF_2=CFCF$_3$)]. The product peaks are expanded in the insets. Minor contaminants are not labeled. 90

Figure 3.7: Reaction of **1** with excess TFE: Ni(=CF_2)(DPPE)(P(OMe)$_3$) [1], Ni(=CF_2)(P(OMe)$_3$)$_3$ [2] and Ni(κ^2-$CF_2CF_2CF_2$-)(DPPE)] [3] vs. time. $[1]_o$ = 0.080 M in toluene-d_8; P_{TFE} = 1.7 atm; T = 30.0^{o}C. 92

Figure 3.8: Ln[1] vs. time. The linear least-squares best fit (y = 1.49*10–4*x – 2.70; R2 = 0.9972, S = 0.06359) is displayed as a dotted line, corresponding to k = 1.5*10–4 s–1 (0.54 h–1) for the decay of Ni(=CF_2)(DPPE)(P(OMe)$_3$) **1**. 92

Figure 3.9: Ln{[1]o – [3]} vs. time. The linear least-squares best fit (y = 9.40*10–5*x – 2.83; R2 = 0.9805, S = 0.1069) is displayed as a dotted line, corresponding to k = 9.4*10–5 s–1 (0.34 h–1) for the growth of Ni(κ^2-$CF_2CF_2CF_2$-)(DPPE)] (**3**). 93

Figure 3.10: Reaction of Ni(=CF_2)($P(OMe)_3$)$_3$ (**2**) with excess TFE: [2] and Ni(κ^2-$CF_2CF_2CF_2$-)[$P(OMe)_3$]$_2$ [4] vs. time. [2]^o = 0.080 M in toluene-d^8; PTFE = 1.7 atm; T = 30.0^{o}C..... 93

Figure 3.11: Ln[2] vs. time. The linear least-squares best fit (y = 1.48*10–4*x – 2.99; R2 = 0.9918, S = 0.07389) is displayed as a dotted line, corresponding to k = 1.5*10–4 s–1 (0.54 h–1) for the decay of Ni(=CF_2)($P(OMe)_3$)$_3$ (**2**). 94

Figure 3.12: Ln{[2]o – [4]} vs. time. The linear least-squares best fit (y = 1.42*10–4*x – 2.98; R2 = 0.9881, S = 0.08526) is displayed as a dotted line, corresponding to k = 1.4*10–4 s–1 (0.50 h–1) for the growth of Ni(κ^2-$CF_2CF_2CF_2$-)[$P(OMe)_3$]$_2$ (**4**)..... 95

Figure 3.13: Reaction of Ni(=CF_2)($P(OMe)_3$)$_3$ (2) with excess TFE and 20 equiv of $P(OMe)_3$: [2] and [4] vs. time. [2]o = 0.080 M; [$P(OMe)_3$]$_o$ = 1.6 M in toluene-d_8; PTFE = 1.7 atm; T = 30.0^{o}C..... 96

Figure 3.14: Ln[2] vs. time [with 20 equiv of $P(OMe)_3$]. The linear least-squares best fit (y = 1.32*10–5*x – 2.56; R2 = 0.9974, S = 0.03634) is displayed as a dotted line, corresponding to k = 1.3*10–5 s–1 (0.047 h–1) for the decay of Ni(=CF_2)($P(OMe)_3$)$_3$ (**2**)..... 96

Figure 3.15: Ln{[2]o – [4]} vs. time [with 20 equiv of $P(OMe)_3$]. The linear least-squares best fit (y = 4.44*10–6*x – 2.66; R2 = 0.9347, S = 0.06352) is displayed as a dotted line, corresponding to k = 4.4*10–6 s–1 (0.016 h–1) for the growth of Ni(κ^2-$CF_2CF_2CF_2$-)[$P(OMe)_3$]$_2$ (**4**)..... 97

Figure 4.1: Reaction coordinate for reaction of **1** with TFE..... 109

Figure 4.2: Fluorine labeling scheme for complex 2a,c and Ni(κ^2-P_3)[-$CF(CF_3)CF_2CF_2$-] (**7**).. 120

Figure 4.3: ^{19}F NMR (282 Hz, C_6D_6) spectrum of TFE from PTFE pyrolysis..... 121

Figure 4.4: ^{1}H NMR (300 Hz, C_6D_6) spectrum for Ni[$P(O\text{-}i\text{-}Pr)_3$]$_3$(=$CFCF_3$) (**1**, sublimed) at RT. 122

Figure 4.5: ^{19}F NMR (282 Hz, C_6D_6) spectrum for Ni(=$CFCF_3$)[$P(O\text{-}i\text{-}Pr)_3$]$_3$ (**1**, sublimed) at RT. The inset shows an expansion of the target CF_3 peak. Note that the $CFCF_3$ peak (24.6 ppm) is

barely visible in this view. Also, F-F coupling is observed at RT but F-P co coupling is not. See below for the low-temperature spectrum. 122

Figure 4.6: Partial ^{19}F NMR (282 Hz, toluene-d8) spectrum for $Ni[P(O\text{-}i\text{-}Pr)_3]_3(=CFCF_3)$ (1) at –45°C, showing the expanded $CFCF_3$ and $CFCF_3$ signals with F-P coupling. 123

Figure 4.7: $^{31}P\{^1H\}$ NMR (121 MHz, C_6D_6) spectrum for $Ni(=CFCF_3)[P(O\text{-}i\text{-}Pr)]_3$ (1, sublimed) at RT. The inset shows an expansion of the target and minor contaminant {i.e., < 2% $Ni[P(O\text{-}i\text{-}Pr)_3]_4$} peaks. 124

Figure 4.8: $^{31}P\{^1H\}$ NMR (121 MHz, toluene-d_8) spectrum for $Ni(=CFCF_3)[P(O\text{-}i\text{-}Pr)]_3$ (**1**) at –45 °C, showing P-F coupling. 125

Figure 4.9: ^1H NMR (300 MHz, CD_2Cl_2) of $Ni(=CFCF_3)(P_3)[P_3 = MeC(CH_2PPh_2)_3]$ (**7**). The limited solubility of 7 accounts for the low signal/contaminant ratio. 126

Figure 4.10: ^{19}F NMR (282 MHz, CD_2Cl_2) spectrum of $Ni(=CFCF_3)(P_3)$ $[P_3 = MeC(CH_2PPh_2)_3]$ (**7**). 127

Figure 4.11: $^{31}P\{^1H\}$ NMR (121 MHz, CD_2Cl_2) spectrum of $Ni(=CFCF_3)(P_3)$ $[P_3 = MeC(CH_2PPh_2)_3]$ (**7**). 128

Figure 4.12: ^{19}F NMR (282 MHz, THF with C_6D_6 capillary) spectrum for the reaction of $Ni(=CFCF_3)(P_3)$ (**7**) with TFE. $[P_3 = MeC(CH_2PPh_2)_3]$ 129

Figure 4.13: ^{31}P NMR (121 MHz, THF with C_6D_6 capillary) spectrum for the reaction of $Ni(=CFCF_3)(P_3)$ (**7**) with TFE. $[P_3 = MeC(CH_2PPh_2)_3]$. 130

Figure 4.14: ^1H NMR (300 MHz, C_6D_6) spectrum for the reaction of $Ni(=CFCF_3)[P(O\text{-}i\text{-}Pr)_3]_3$ (**1**) with TFE. 130

Figure 4.15: ^{19}F NMR (282 MHz, C_6D_6) spectrum (upfield) for the reaction of $Ni(=CFCF_3)[P(O\text{-}i\text{-}Pr)_3]_3$ (**1**) with TFE. The insets show expanded spectral regions and the labeling scheme. ... 131

Figure 4.16: ^{19}F NMR (282 MHz, C_6D_6) spectrum (downfield) for the reaction of $Ni(=CFCF_3)[P(O\text{-}i\text{-}Pr)_3]_3$ (**1**) with TFE. The inset shows expanded $Ni=CF_2$ region. 132

Figure 4.17: $^{31}P\{^{1}H\}$ NMR (121 MHz, C_6D_6) spectrum for the reaction of Ni(=CFCF$_3$)[P(O-i-Pr)$_3$]$_3$ (**1**) with TFE. 132

Figure 4.18: ^{19}F NMR (282 MHz, C_6D_6) spectrum (downfield) for the reaction of Ni(=CFCF$_3$)[P(O-i-Pr)$_3$]$_3$ (**1**) with TFE. Spectrum includes the calculation of the metallacycle/metathesis ratio. 133

Figure 4.19: Two-dimensional ^{19}F COSY experiment in C_6D_6 to help in the assignment of the hydrofluoroalkene metathesis peaks and the CF_2 peaks of the metallacycle product. 134

Figure 4.20: Low temperature ^{19}F NMR (282 MHz, C_6D_6) spectra of metallacycle product formed from Ni(=CFCF$_3$)[P(O-i-Pr)$_3$]$_3$ **1** and VDF showing inequivalent CF_2 resonances overlapped with that due to excess VDF. 135

Figure 4.21: ^{19}F NMR (282 MHz, C_6D_6) spectrum (upfield) for the reaction of Ni(=CFCF$_3$)[P(O-i-Pr)$_3$]$_3$ (**1**) with VDF. 136

Figure 4.22: ^{19}F NMR (282 MHz, C_6D_6) spectrum (downfield) for the reaction of Ni(=CFCF$_3$)[P(O-i-Pr)$_3$]$_3$ (**1**) with VDF. Spectrum includes the calculation of the metallacycle/metathesis ratio. 137

Figure 4.23: $^{31}P\{^{1}H\}$ NMR (121 MHz, C_6D_6) spectrum for the reaction of Ni(=CFCF$_3$)[P(O-i-Pr)$_3$]$_3$ (**1**) with VDF. 137

Figure 4.24: $^{31}P\{^{1}H\}$ NMR (121 MHz, C_6D_6) low temperature (-40^{o}C) spectrum for the reaction of Ni(=CFCF$_3$)[P(O-i-Pr)$_3$]$_3$ (**1**) with VDF. 138

Figure 4.25: ^{1}H NMR (300 MHz, C_6D_6) spectrum for the reaction of Ni(=CFCF$_3$)[P(O-i-Pr)$_3$]$_3$ (**1**) with VDF. 138

Figure 4.26: Two dimensional (^{1}H - ^{19}F) HMBC spectrum for the reaction of Ni(=CFCF$_3$)[P(O-i-Pr)$_3$]$_3$ (**1**) with VDF 139

Figure 4.27: ^{19}F NMR (282 MHz, C_6D_6) spectrum of Ni(=CFCF$_3$)[P(OMe)$_3$]$_3$ (**6**). 140

Figure 4.28: $^{31}P\{^{1}H\}$ NMR (121 MHz, C_6D_6) spectrum of Ni(=CFCF$_3$)[P(OMe)$_3$]$_3$ (**4**). 141

Figure 4.29: ^{1}H NMR (300 MHz, C_6D_6) spectrum of$Ni(=CFCF_3)[P(OMe)_3]_3$ (**6**)). 142

Figure 4.30: ^{19}F NMR (282 MHz, C_6D_6) spectrum for the reaction of $Ni(=CFCF_3)[P(OMe)_3]_3$ (**6**)with TFE. 143

Figure 4.31: ^{1}H NMR (300 MHz, C_6D_6) spectrum for the reaction of $Ni(=CFCF_3)[P(OMe)_3]_3$ (**6**) with TFE. 144

Figure 4.32: ^{19}F NMR (282 MHz, C_6D_6) spectrum for the reaction of $Ni(=CFCF_3)[P(OMe)_3]_3$ (**6**) with TFE showing the integrations of the $Ni=CF_2$ peak and the $Ni(-CFCF_3-CF_2-CF_2-)$ used to calculate the metallacycle/metathesis ratio. 145

Figure 4.33: Proposed reaction mechanism for the reaction of **1** with T'FE 146

Figure 4.34: Stacked ^{19}F NMR (282 MHz, C_6D_6) spectra for the reaction of **1** with $CFH=CF_2$ showing the reaction before the solvent was removed and after showcasing the formation of several volatile fluorinated products. 147

Figure 4.35: ^{19}F NMR (282 MHz, C_6D_6) spectrum for the reaction of **1** with $CHF=CF_2$ focusing on the peaks associated with volatile fluorinated compounds. 148

Figure 4.36: ^{1}H NMR (300 MHz, C_6D_6) spectrum for the reaction of **1** with $CHF=CF_2$ focusing on the olefinic region of the spectrum where the compounds cis/trans-$CHF=CFCF_3$ are observed. 149

Figure 4.37: Two-dimensional ^{19}F COSY experiment of the reaction mixture of **1** with $CFH=CF_2$ after the volatiles were removed in C_6D_6 to help in the assignment of the major products from the non-metathesis pathways. 150

Figure 4.38: ^{19}F NMR (282 MHz, C_6D_6) spectrum for the reaction of **1** with $CHF=CF_2$ after the solvent was removed focusing on the peaks associated with E/Z-**4** 151

Figure 4.39: ^{19}F NMR (282 MHz, C_6D_6) spectrum for the reaction of 1 with $CHF=CF_2$ after the solvent has been removed focusing on the peaks associated with cis isomer of **5**. 152

Figure 4.40: ^{19}F NMR (282 MHz, C_6D_6) upfield spectrum for the reaction of 1 with $CHF=CF_2$ focusing on Ni-F peaks. Nickel vinyl compounds A and B are the major products of this reaction

while compound C and D are predicted to be formed through a 2,1 fluoride shift of the β-CHF metallacycle pathway (Fig. 4.33) however could not be fully characterized. 153

Figure 4.41: $^{31}P\{^{1}H\}$ NMR (121 MHz, C_6D_6) of the reaction of **1** with HTFE after the volatiles had been removed 154

Figure 4.42: ^{1}H NMR (300 MHz, C_6D_6) spectrum for the reaction of 1 with $CHF=CF_2$ after the removal of volatiles..... 155

Figure 4.43: ^{19}F NMR Overlapped with $^{19}F\{^{1}H\}$ NMR (282 MHz, C_6D_6) showing the proton coupling of E-**4** 156

Figure 4.44: ^{19}F NMR Overlapped with $^{19}F\{^{1}H\}$ NMR (282 MHz, C_6D_6) showing the proton coupling of Z-**4** 157

Figure 4.45: ^{19}F NMR Overlapped with $^{19}F\{^{1}H\}$ NMR (282 MHz, C_6D_6) showing the proton coupling of Z-**5** 158

Figure 4.46: ^{19}F NMR Overlapped with $^{19}F\{^{1}H\}$ NMR (282 MHz, C_6D_6) showing the proton coupling of the E/Z- 1,2,3,3,3-pentafluoro-1-propene..... 158

Figure 4.47: ^{19}F NMR (282 MHz, C_6D_6) full spectrum for the reaction of **1** with $CHF=CF_2$ including F-labelling of all major products. Structural isomers of compound **3** were not capable of being fully characterized. 159

Figure 4.48: ^{19}F NMR (282 MHz, C_6D_6) full spectrum for the reaction of **1** with $CHF=CF_2$. Included is the calculation used to determine the ratio of metathesis versus metallacycle formation..... 160

Figure 4.49: ORTEP molecular structure of **7** with 50% probability thermal ellipsoids. Hydrogen atoms are not shown, and the phenyl groups are depicted as wire cage structures for clarity. .. 161

Figure 4.50: Qualitative kinetic experiment between complex **1** (labelled in NMR with an asterisk) and excess TFE showing the progression of the reaction over an hour at room temperature. Spectra shows the product ratio remaining relatively unchanged throughout the course of the reaction. Reaction is complete within an hour. 162

Figure 4.51: Qualitative Kinetics experiment between complex **1** (labelled in NMR with an asterisk) and excess TFE in the presence of 20 equiv. of $P(O^iPr)_3$. Experiment shows the product ratio remaining relatively unchanged throughout the course of the reaction. Unlike the same experiment without excess phosphite the reaction only begins to form products after 10 min. and the starting material (**1**) is still present after an hour of reaction time at room temperature. 163

Figure 4.52: Proposed mechanism in the formation of (**5**) via β-Fluoride abstraction of metallacyclobutane B forming Ni-F allyl complex followed by 1,3 F-shift leading to the observed product. 164

Figure 5.1: Transition states for formation of metallacycle vs. metathesis products from $P_3Ni=CF(CF_3)$ and fluoroalkenes. 172

Figure 5.2: Constituent effect on the electronic state of a transition metal carbene 173

Figure 5.3: Reaction coordinate of **1** with ethylene showing the parallel reaction pathways for metallacycle formation (green) and metathesis (blue) 178

Figure 5.4: ^{19}F Cosy of reaction of **1** with $CF_2=CF(OCF_3)$ producing complex **3**, **4**, **5**, and **6** .. 187

Figure 5.5: ^{19}F NMR of reaction between **1** with $CF_2=CF(OCF_3)$. Close-up view of resonances associated with **3**-cis/tran, and nickel carbenes **5** and **6**. 188

Figure 5.6: ^{19}F NMR of reaction between 1 with $CF_2=CF(OCF_3)$. Close-up view of resonances associated with complex **4b** 189

Figure 5.7: ^{19}F NMR of reaction between 1 with $CF_2=CF(OCF_3)$. Close-up view of resonances associated with complex **4a**. 190

Figure 5.8: ^{31}P NMR of complex **1** reacted with $CF_2=CF(OCF_3)$. 191

Figure 5.9: ^{19}F NMR of complex **7**. 192

Figure 5.10: ^{31}P NMR of complex **7**. 193

Figure 5.11: Stacked $^{19}F/^{19}F[^1H]$ NMR of complex **8**. 194

Figure 5.12: HMQC of Complex **8**. 195

Figure 5.13: ^{1}H NMR of complex **8**. 196

Figure 5.14: ^{31}P NMR of complex **8**. 197

Figure 5.15: Stacked ^{19}F/^{19}F[^{1}H] NMR of complex **9.** 198

Figure 5.16: ^{31}P NMR of complex **9**. 199

Figure 5.17: HMQC of complex **9** used to discern identity of metallacycle protons. 200

Figure 5.18: ^{19}F NMR of complex **12**, **13**. 201

Figure 5.19: ^{31}P NMR of complex **12**, **13**. 202

Figure 5.20: ^{1}H NMR of complex **12**, **13**..... 203

Figure 5.21: ^{19}F NMR of complex **2** reacting with 4-methoxy styrene showing how product distribution is dependent on sterics of ancillary ligands. 204

Figure 5.22: ^{19}F COSY showing correlation of α and β C - F of complex **14**. 205

Figure 5.23: ^{19}F COSY showing β-C-F and CF_2 groups' viscinal to spyro-carbon of complex **14**. 206

Figure 5.24: Time-resolved ^{19}F NMR of the reaction of 1 with perfluoro-cylobutene showing the formation of a new carbene (possible formation of ring opened carbene intermediate). 207

Figure 5.25: ^{19}F NMR of complex **14** with fluorine assignments..... 208

Figure 5.26: ^{31}P NMR of complex **14**. 209

Figure 5.27: Stacked ^{19}F/^{19}F[^{1}H] spectra of complex **15** cis/trans. 210

Figure 5.28: ^{31}P NMR of complex **15** cis/trans..... 211

Figure 5.29: Stacked ^{19}F/^{19}F[^{1}H] spectra of complex **16**. 212

Figure 5.30: ^{31}P NMR of complex **16** with phosphine assignments. 213

Figure 6.1: ORTEP structures of **3** and **6** with 50% ellipsoids. 222

Figure 6.2: ORTEP structure of $Mn(Phen)_2(OTf)_2$, **9** (Mn-N1 = 2.2262, Mn-N2 = 2.2397 Å) with 50% ellipsoids. 226

Figure 6.3: FT-IR spectra (Nicolet Nexus 670 instrument, neat/solid samples) for $MnCF_3(CO)_2(Phen)$ (**1**) 232

Figure 6.4: FT-IR spectra (Nicolet Nexus 670 instrument, neat/solid samples) for $MnCF_3(CO)_3(Bipy)$ (**2**). 233

Figure 6.5: FT-IR spectra (Nicolet Nexus 670 instrument, neat/solid samples) for $MnCF_3(CO)_5$. 233

Figure 6.6: FT-IR spectra (Nicolet Nexus 670 instrument, neat/solid samples) for $MnCF_3(CO)_2(NNS)$ (**4**) 234

Figure 6.7: ^{19}F NMR (282 Mhz, CD_3CN) spectrum of $MnCF_3(Bipy)(CO)_3$ **3**. 234

Figure 6.8: ^{1}H NMR (300 Mhz, CD_3CN) of $MnCF_3(Bipy)(CO)_3$ (**3**). 235

Figure 6.9: ^{19}F NMR (282 Mhz, $CDCl_3$) of $MnCF_3(CO)_2(Tpy)$ **4**. 235

Figure 6.10: ^{1}H NMR (300 Mhz, $CDCl_3$) of $MnCF_3(CO)_2(Tpy)$ **4**. 236

Figure 6.11: ^{19}F NMR (282 MHz, CD_3CN) spectrum of $MnCF_3(CO)_2Tpy$ (**6**). Spectrum shows a minor Mn-CF_3 peak which is proposed to be the trans-Mn-CF_3 product. 236

Figure 6.12: ^{1}H NMR (300 MHz, CD_3CN) spectrum of $MnCF_3(CO)_2Tpy$ **6**. 237

Figure 6.13: ^{19}F NMR (282 Mhz, CD_3CN) of complex $MnCF_3(CO)_2(NNS)$ (**7**). 238

Figure 6.14: ^{1}H NMR (300 MHz, CD_3CN) spectrum of $MnCF_3(CO)_2(NNS)$ (**7**). 239

Figure 6.15: ^{19}F NMR (282 Mhz, C_6D_6) downfield spectrum of $[Mn(=CF_2)(CO)_3(Phen)][OTf]$ (**8**). 240

Figure 6.16: ^{19}F NMR (282 Mhz, C_6D_6) upfield spectrum of [Mn(=CF_2)$(CO)_3$(Phen)][OTf] (**8**). 241

Figure 6.17: ^{1}H NMR (300 MHz, $CDCl_3$) spectrum of [Mn(=CF_2)$(CO)_3$(Phen)][OTf] (**8**)..... 241

Figure 6.18: ^{19}F NMR (282 MHz, C_6D_6) downfield spectrum of (NNS)$(CO)_2$Mn=CF_2 complex. 242

Figure 6.19: ^{19}F NMR (282 MHz, C_6D_6) downfield spectrum of (Bpy)$(CO)_3$Mn=CF_2 complex. Minor peak at 156.3 is proposed to be an isomeric Mn=CF_2 complex..... 243

Figure 6.20: Blank Cyclic Voltammogram (0.1M THF solution of [$(Bu)_4N$][BF_4])..... 244

Figure 6.21: Cyclic Voltammogram of $MnCF_3$(Bipy)$(CO)_3$ (**3**) in THF (100mV/s sweep rate) 244

Figure 6.22: Cyclic Voltammogram of -0.5V - +1.5V region of $MnCF_3(CO)_2$(Tpy) (**4**) in THF (100mV/s sweep rate) showing quasi-reversible reduction at -2.1 V vs. ferrocene 245

Figure 6.23: Cyclic voltammogram of -1.5 - 2.5 V region for $MnCF_3(CO)_2$(Tpy) (**4**) in THF (100mV/s sweep rate) showing non-reversible oxidation at 0.66V vs ferrocene 245

Figure 6.24: Cyclic voltammogram of -0.5V - -1.5V region for $MnCF_3(CO)_2$(Tpy) (**4**) in THF (100 mV/s sweep rate) showing possible irreversible oxidation and quasi-reversible reduction246

Figure 6.25: Cyclic voltammogram of $MnCF_3(CO)_2$(NNS) (**7**) in THF (100 mV/s sweep rate) showing possible irreversible oxidation and quasi-reversible reduction 246

Figure 6.26: Cyclic voltammogram of $MnCF_3(CO)_2$(NNS) (**7**) in THF (100 mV/s sweep rate) showing possible irreversible oxidation and quasi-reversible reduction 247

Figure 6.27: Hypothetical fragmentation of complex **3** and **4** after electron impact (EI) mass spectrometry (shown in Figures 6.28-6.32) 247

Figure 6.28: Exact mass search for N_2(F)Mn=CF_2 (N_2 = Bipy) of mass 280.00375 Da 248

Figure 6.29: EI-MS spectrum of fragmentation of complex **3** showing N_2(F)Mn=CF_2 fragment. 249

Figure 6.30: EI-MS for complex **4** showing $N_2Mn\text{-}CF_3$ and $N_2Mn\text{-}F$ fragments (304.0 and 254 Da respectively) 250

Figure 6.31: Exact mass for $N_2Mn\text{-}CF_3$ (N_2 = Phen) exact mass of 303.99905 Da 251

Figure 6.32: Exact mass of $N_2Mn\text{-}F$ (N_2 = Phen) exact mass of 254.00625 Da..... 251

Chapter 1 . Introduction and Background

"The fury of the chemical world is the element fluorine. It exists peacefully in the company of calcium in fluorspar and also in a few other compounds; but when isolated, as it recently has been, it is a rabid gas that nothing can resist." – unattributed author? *Scientific American **1888** when fluorine was first isolated.*

"Fluorine leaves nobody indifferent; it inflames emotions be they affections or aversions. As a substituent, it is rarely boring, always good for a surprise, but often completely unpredictable." - M. Schlosser, *Angew. Chem. Int. Ed.* **1998**, *37*, 1496-1513.

1 C–F bonds

1.1 Industrial Synthesis and Relevance

Since their discovery by Alexander Borodin in 1862,[1] organofluorine compounds and their properties have been exploited by many industries such as agrochemicals, pharmaceuticals and refrigerants, as well as being useful as blowing agents, surfactants and advanced materials. In fact, global demand for fluorine-containing compounds continues to rise (ca. 4% per year) and in 2016 was worth a combined $20 billion dollars.[2] The synthesis of many organofluorine compounds generally follows a simple nucleophilic displacement of another halogen using a fluorinated salt (Scheme 1.1). Industrially, this general method remains relatively unchanged besides the addition of catalysts such as antimony trifluoride and Co-F complexes known as the Swarts and Fowler/Flutec processes respectively.[3,4]

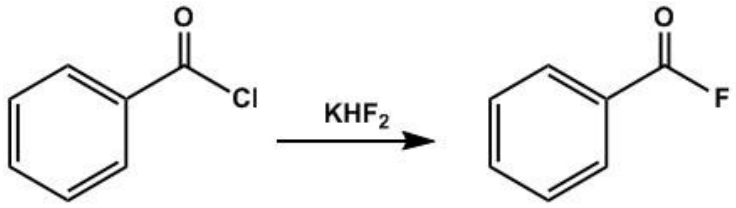

Scheme 1.1

However, these processes are only used for unselective fluorinations of halogenated alkyls/alkenes and perfluorination of saturated hydrocarbons, respectively. Additionally, the conditions for these processes are harsh, precluding functional group tolerance. As a result,

products of these reactions tend to be early-stage synthons in the synthesis of value-added fluorinated compounds. As a functional group, fluorine often brings unusual and surprising characteristics to the various molecular scaffolds in which it is incorporated. In agrochemicals and pharmaceuticals, fluorine, as the most electronegative element, drastically affects the polarity of the parent molecule and with a van der Waals radius similar to hydrogen (1.47 vs. 1.20 Å) does not usually alter the metabolic pathways that the mimicked non-fluorinated molecules undergo.[5] This alters the bio-availability, lipophilicity and metabolism of biologically active molecules, thereby increasing their efficacy.[6,7] The drive to incorporate fluorine into these products is evidenced by the large number of pharma- and agrochemicals which contain fluorine or fluorinated substituents (20-30% as of 2016).[5,8,9]

The above examples rely heavily on first incorporating –F, $–CF_3$ or $–OCF_3$ moieties into early-stage alkyl or aryl organic fragments which can then be utilized for the synthesis of these pharmaceuticals, herbicides and pesticides. Meanwhile, fluoro-olefins are mainly synthesized for use as blowing agents and refrigerants or as monomers in the fluoropolymer industry.[10] Fluorine's increased molecular repulsion (large van der Waals radius) between adjacent molecules tends to give fluorocarbons high volatility which is essential for refrigeration and inert blowing agents (cf. HFO-R1234-yf and -ze; Figure 1.1)[11]. Refrigerant synthesis originally utilized chlorofluorocarbons (CFCs) following simple Swarts methods for their synthesis. However,

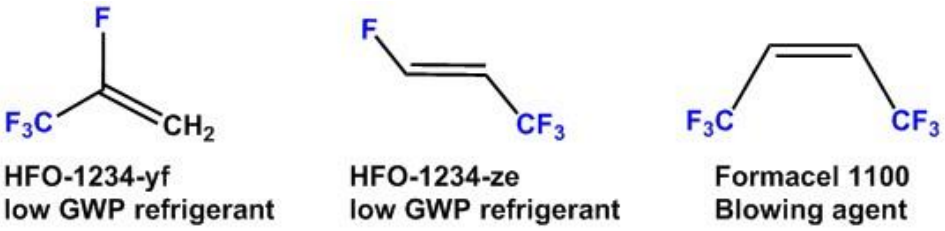

Figure 1.1: Selection of important fluorine containing HFOs [GWP = **G**lobal **W**arming **P**otential]

as of 1987 the Montreal Protocol came into effect, banning the use of CFCs entirely due to their environmental impact for both ozone depletion and high global warming potential (GWP) and newer refrigerants were developed that required more complicated synthetic routes (*vide infra*).[12] Fluorine, due to its high charge density, lone pairs and inductive electron-withdrawing effect,

renders its materials chemically and oxidatively inert (cf. highly fluorinated polymers such as Teflon®, Viton®, and Krytox®). Unfortunately, polymerization of fluorinated monomers is almost exclusively carried out through free radical polymerization in water using fluorosurfactants,[13] offering little control of the morphology and tacticity of these polymers while also creating toxic and environmentally long-lived waste products.[14] These surfactants are now under review by the US EPA and European parliament[15] due to the presence of long-chain fluorinated molecules such as perfluorooctanoic acid (PFOA) in the blood of large portions of the populations of both humans and animals.[16] The above limitations have led to increasing demand for shorter fluorinated chains and for alternative late-stage fluorination approaches through higher efficiency metal-mediated and -catalyzed reactions as discussed below.

1.2 The Problem with C–F

Carbon-fluorine bonds do not exist in nature, other than low concentrations of F-substituted enzymes and proteins from plant/animal metabolisms (*vide infra*), despite having the most thermodynamically stable bond to carbon of any element, with bond dissociation energies from 130 to ~ 545 kJ/mol depending on the number of fluorines present on carbon.[17,18] This stability is due to the significant overlap of the non-bonding electrons of fluorine with the π-orbitals of carbon. This effect, coupled with the high electronegativity of fluorine that is stabilized via the least electronegative hybridization of carbon (low s-character), leads to a thermodynamic stabilization when fluorine resides on sp^3 carbons, an effect that is compounded when additional fluorines are present.[19] Despite these factors, the smallest building block for organic synthesis is not a C-F containing organic (although several natural products can have very low concentrations of fluorinated adducts present[20]) but hydrofluoric acid (HF), which comes mainly from processing the mineral fluorite (CaF_2) into anhydrous HF.[21] Handling of this highly corrosive and toxic substance makes its processes less appealing and therefore efforts towards more benign and effective fluoride and fluoroalkyl (R^F) transfer reagents are desirable.

Several methods for late-stage fluorination and perfluoroalkylation have been developed. These include nucleophilic F^- and CF_3^- transfer reagents[22] as well as use of these reagents in conjunction with transition metals to allow for electrophilic transfer, milder reaction conditions and greater selectivity.[23] However, these methods are often encumbered by the expense of the

reagents and stoichiometric reaction conditions. Owing to the massive thermodynamic and kinetic stability[24] of C–F and C–R^F, manipulation of these bonds is a considerable burden.

1.3 Modern Methods Towards C–R^F Manipulation

1.3.1 Organic Reagents

In an attempt to serve the growing number of industries reliant on fluoro-organic compounds, where late-stage C–R^F functionalization represents a profitable endeavor, a significant number of mild and functional group tolerant reagents have been developed (Figure 1.2).[25] These include electrophilic, nucleophilic and radical additions of a trifluoromethyl group such as trifluoromethyl halides, trifluoromethyl silane, trifluoroacetic acid (TFAA) and its derivatives, trifluoromethane, trifluoromethanesulfonyl chloride and its derivatives all of which have been shown to work in aqueous media.[26] Additionally there are various electrophilic fluorination reagents such as Selectfluor (*vide supra*), N-fluorobenzenesulfonamide (NFSI)[27] and several others.[26] These utilize the inductive electron-withdrawing effect to polarize the N–F bond to encourage nucleophilic attack on fluorine, thus providing a mild oxidizing reagent. These perfluoroalkylation /fluorination reagents suffer from either being highly deactivated due to the polarized bond that is typically formed, making them relatively unreactive, or conversely being highly oxidizing such as XeF_2 leading to low functional group tolerance.[28] For these reasons many of these fluoride sources need to be utilized with various transition metals in metal mediated/catalyzed processes (Chapter 1.3.3).

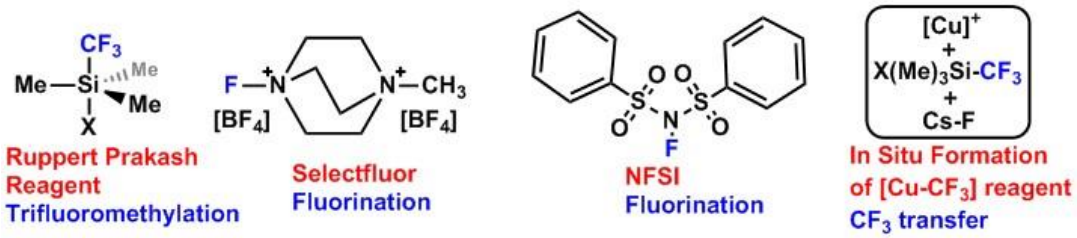

Figure 1.2: Selected examples of F^- and CF_3^- transfer reagents

1.3.2 Organometallic M–F/ M–R^F Complexes

Since the 1950's organometallic complexes containing M–C_{RF} (R^F = F, CF_3, CF_2CF_3) bonds have been studied. This spanned the initial formation of M–CF_3 via thermal decarbonylation of

$(CO)_5Mn\text{-}C(O)CF_3$ by Ethyl[29], McClellan[30], and Stone groups[31] nearly simultaneously while similar syntheses of the cobalt analogues $(CO)_4CoC(O)CF_3$ were pursued by Hieber and Beck (Figure 3).[32]

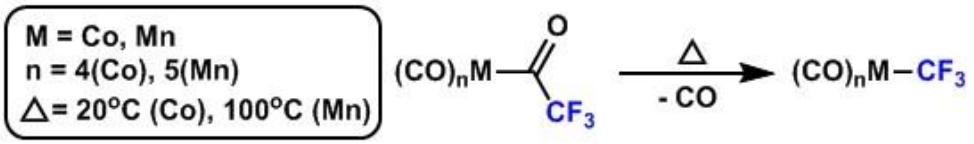

Figure 1.3: Metal perfluoroacyl decarbonylation route to M-CF_3 complexes

This decarbonylation requires an open coordination site for the formed CF_3 group and therefore mainly occurs with metal carbonyls that have thermally labile CO ligands. An early, non-carbonyl example by Chee and Robertson using $PtCl(COCF_3)(PMePh_2)_2$ required much more forcing conditions, with temperatures exceeding 200 ^oC.[33] Another route to M–CF_3 complexes involves oxidative addition of ICF_3, taking advantage of the orbital mismatch between iodine and the high charge density CF_3 group. This transformation is more likely to occur with electron-rich metal centers.[34] Additionally, examples of organometallic fluorine compounds reported by Wilkinson and Parshall in the 1960s utilized both perfluorinated alkenes and dienes.[35] After this initial surge of publications, however, research involving M-R^F complexes slowed and, in regards to some metals like manganese, nearly halted completely for over a decade. This may have been due to the pronounced stability and unreactive nature of these complexes when compared to non-fluorinated metal-alkyl analogues which benefited from reactivity of the M–C bond, activation of α/β-C–H bonds and a wide variety of useful catalytic transformations such as cross-coupling and polymerization that did not appear to occur with M–C_{RF} examples. The first fluoro-alkyl manganese carbonyl complex, $Mn(CF_3)(CO)_5$, for example, exhibits little to no substitution chemistry of the CO ligands with ANY donor ligand besides isoelectronic nitrosyl ($N{\equiv}O^+$),[36] whereas analogous [Mn]-R, -H, and even -Br complexes all show rich ligand substitution chemistry.[37]

Fluorine and fluorinated ligands show pronounced bonding effects due to the coexistence of a significant inductive electron withdrawing effect coupled with π-donation of electron density back to its neighbors.[38] This often leads to unpredictable chemistry, especially when fluorine-containing substituents are associated with the d-orbitals of transition metals. The pronounced difference in reactivity between fluorinated and non-fluorinated alkyl ligands is reflected in their

bond dissociation energies (BDEs); cf. the M-C bond difference in Mn–CF_3 vs. Mn–CH_3 in $MnR(CO)_5$ is 20 kJ/mol,[39] as well as M-C bond distances {Mo-C_3F_7 = 2.288(9) vs. Mo-C_2H_5 = 2.397(19) Å and Pt-C_2F_5 = 2.002(8) vs. Pt-CH_3 = 2.081(6) Å}.[40] The rationale for both the high BDE and M-C bond shortening was originally attributed to back-bonding from metal d-orbitals to low lying C–F σ*-orbitals. This belief was propagated when pronounced C–F bond elongation and low energy IR absorption shifts of ν_{C-F} were observed upon metal complexation.[41] However, Fenske-Hall calculations suggested that the CF_3 group is as poor a π-acceptor as CH_3. An electrostatic interaction between the metal and CF_3 due to the carbon having significant positive charge would account for the high BDE and shorter bonds as well as the subsequent stabilization of the d-orbitals in M–R^F complexes.[42] This idea was complicated further when recent studies on M–C_{CF3} bond distances showed deviation from this behavior and noted *elongation* of these bonds in *early* as opposed to late metals. This suggests that all interactions (σ-bonding, π-bonding, σ*, π*, and electrostatic) should be taken into account when analyzing M-R^F bonds. For early metals (Ti) electrostatic interactions appear to be dominant for the unusual elongated bond due to repulsion of the electropositive metal and highly electropositive CF_3 carbon. Conversely, the Ti–C_{CH3} bond is *shortened* due to a significantly more negative carbon (-0.96 for CH_3 vs. +0.79 for CF_3).[43] Bonds to intermediate (Mn, Fe) and late metals such as Ni, Cu and Pd, however, have multiple interactions that lead to dramatically shortened M-C bonds for CF_3 when compared to CH_3. These bonds are considered more covalent in nature (L→M σ-bond with M →L π-backbonding) although π-backbonding is still thought to be a minor contributor to the overall bonding interaction with a maximum bond contribution of < 8% in the case of several Pd examples.[44] Middle to late metal M–R^F bonds are shortened due to the presence of strong F→C π-donation into p-orbitals on carbon. This leads to a destabilization of the carbanion lone pair and resonance with low-lying C–F σ* orbitals as shown in natural bond order (NBO) analyses.[44,45] These antibonding orbitals are significantly smaller and have more 2s character than the 2p orbitals that the lone pair of the CH_3 congeners utilize for bonding (Scheme 1.2). Secondly, unlike typical CR_3 ligands, CR^F_3 ligands can participate in retro-dative bonding

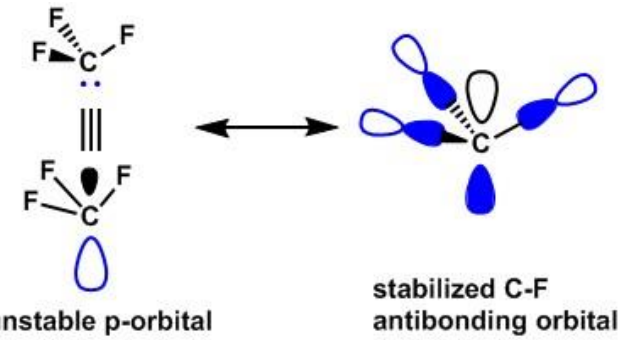

Scheme 1.2

with the parent metal and this interaction increases from left to right across the same period. Finally, there is a significant increase in the overall C lone pair to metal donation when compared with CR_3 ligands, with ionic bonding to early metals becoming more covalent for late metals (Figure 1.4).

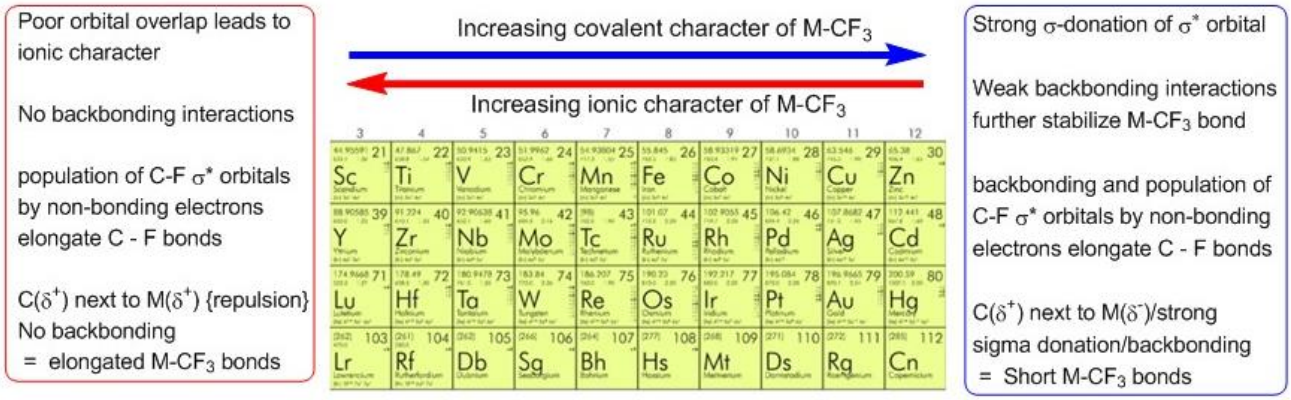

Figure 1.4: General trend of bonding between early to late metals and CF_3 ligands

These interactions not only affect the reactivity of M–CF_3 bonds but also the overall reactivity of the complex itself. Having such an electropositive ligand, with a shorter, high s-character M-C_{RF} bond significantly stabilizes the metal's remaining d-orbitals, thereby reducing the overall reactivity of the metal complex.[46] In fact, replacement of CH_3 with a CF_3 ligand in square planar $RhX(PPh_3)_3$ (X = CH_3 or CF_3) results in a 9-15 kcal mol^{-1} stabilization of the metal d-orbitals.[44] The strong sigma-donor properties of CF_3, while being a diminishingly poor π-acceptor, increases the electron density/negative charge on the metal, while stabilized d-orbitals lead to a counter-intuitive increase in the electrophilic nature of the metal.[44] Being a strong Lewis base also makes CF_3 a good trans-directing ligand although the degree of trans-influence is less than alkyl-ligands. The trans-influence decreases with α-fluorination of the alkyl ligand (CFR_2 > CF_2R > CF_3). It should also be noted that in square planar Pd(II) complexes there was a strong

cis-influence that was associated with steric effects due to the fluoro-alkyl ligand being held more closely to the metal, pushing the cis-alkyl ligand away without affecting bond angles.[44,47]

Metal fluoride complexes {[M]F_n; n = 1 – 5}, on the other hand, are synthetically useful in reactions involving fluoride transfer and subsequent reduction of fluorocarbons, as hydrogen bond acceptors and as mediators in C-F bonding processes. Formation of the M–F bond is traditionally accomplished through oxidative addition of activated C-F bonds, although typically as intermediates or by-products of catalytic cycles or metal-mediated processes respectively.[48] Another route involves salt metathesis of M-X complexes with nucleophilic fluoride sources (i.e., KF•2H_2O, Ag-F, Cs-F and others)[49] or oxidative fluorination using XeF_2.[50] These methods have been utilized in the formation of metal fluoride complexes from groups 3-11[51] which experience the same orbital stabilizing effects as organometallic M-R^F complexes. Metal fluorides are beyond the scope of this thesis, however, and so will not be discussed in detail.

1.3.3 M-R^F in R^F Transfer, Insertion and Cross-Coupling Reactions

Although relatively unreactive, transition metal perfluoroalkyl complexes have been employed successfully in the formation of sp, sp^2 and sp^3 C-C_{RF} bonds. For example, $Cu^{(I)}$–CF_3 intermediates were invoked in the stoichiometric trifluoromethylation of aryl iodides by McLoughlin and Thrower in a patent in 1965[52] and later in the open literature in 1969 (Scheme 1.3).[53]

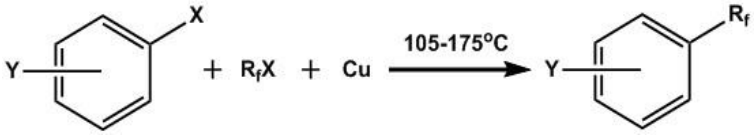

Scheme 1.3

Since then, many prominent researchers have contributed and expanded this game-changing reaction.[54] In 2008 a report by Vicic presented the first *well defined,* crystallographically characterized NHC-supported $Cu^{(I)}$–CF_3 trifluoromethylating reagent[55] and later work by Amii in 2009 showcased the first copper-catalyzed aryl trifluoromethylation utilizing trifluoromethyl trimethylsilane (TMS-CF_3) otherwise known as Ruppert's or Ruppert-Prakash reagent.[56] Another report by Grushin described the first example of a stoichiometric, selective coupling reaction via reductive elimination from a Pd(II) center (Scheme 1.4).[57]

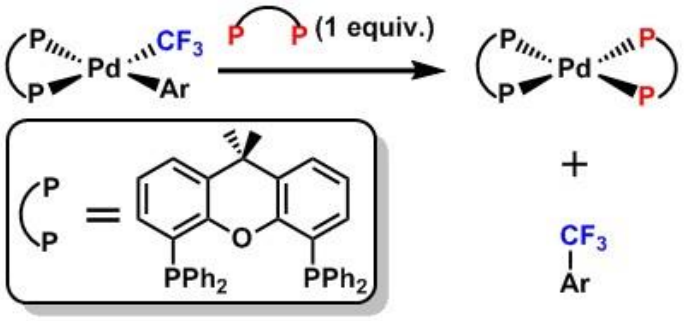

Scheme 1.4

Intriguingly, there are extensive examples of both Pd(II) and Pd(IV) trifluoromethyl complexes coplanar to aryl and alkyl ligands and none of these complexes undergo reductively elimination to produce the coupled products.[58] The reductive elimination reaction achieved by Grushin was aided by the large bite angle of the Xantphos ligand as attempts with other P and N donor ligands were unsuccessful.[59] Work by Sanford showed that a $Pd^{(IV)}$–CF_3 complex readily undergoes reductive elimination of aryl–CF_3 under similar reaction conditions to Grushin's (80 ^oC, 3 h) while being able to utilize a variety of ancillary ligands, due to the greater oxidizing power of $Pd^{(IV)}$.[60] Several examples exist in the literature for the metal-mediated formation of C^{sp3}–CF_3 compounds although the involved metals acted purely as electron-transfer reagents to produce reactive CF_3 radicals.[61] More recently, cross-coupling processes have been discovered for the formation of C^{sp3}-C_{RF} bonds. Due to the stability of M-C_{RF} bonds the reductive elimination step is often rate-limiting and as such requires forcing conditions such as the use of $Ni^{(III)}$ [where a $Ni^{(IV)}$ via disproportionation pathway was invoked][62] or $Cu^{(III)}$ [with a competing 1 electron reduction of the benzylic substrate].[63] A final example shows the *catalytic* formation of R–CF_3 bonds using a $Au^{(III)}$ complex. This research postulates a unique fluoride 'rebound' mechanism whereby fluoride abstraction from a CF_3 ligand is followed by migration of the M-R to the M=CF_2 carbon. Nucleophilic addition of the abstracted fluoride then leads to displacement of the desired CF_3–R (5).[64]

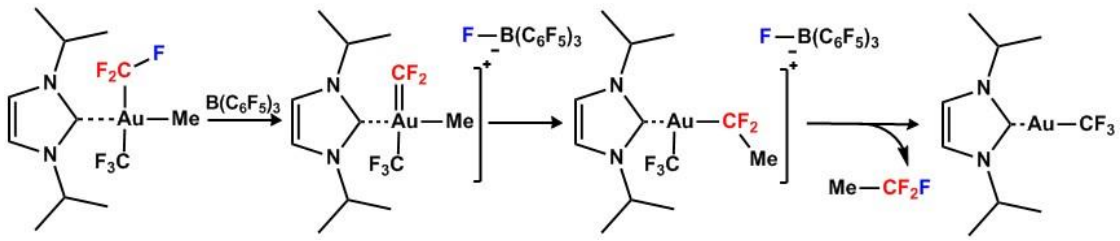

Figure 1.5: Outer sphere fluoride 'rebound' reaction for the formation of R-CF_3 bonds.

A similar formal 1,1-insertion of a $M=CF_2$ into a metal *fluoroalkyl* was reported by Baker and co-workers, joining just two previous examples[65] of insertions into typically inert $M\text{-}C_{RF}$ bonds.[66] Due to the inherent strength of $M\text{-}C_{RF}$ bonds, conversion of these moieties into more reactive $M=CF_2$ carbenes via fluoride abstraction may provide more reactive ligands with which to work. However, besides the examples given, no such research has yet to implement this strategy in earnest or incorporate it into a catalytic cycle.

1.4 Carbenes

1.4.1 $M=CR_2$ Carbenes (R = alkyl, aryl, H)

Carbenes contain a neutral, divalent carbon atom with six electrons in its valence shell and have been major curiosities and research subjects in chemistry for the last 160 years.[67] The first work by Geuther and Hermann was a postulation of a "carbonic" intermediate in an alkaline hydrolysis utilizing a dichlorocarbene.[67] Their idea regarding the existence of a carbene was truly recognized after work by Staudinger and Kupfer on methylene derivatives and diazomethane was undertaken,[68] then much later work by Doering finally proved the existence of a dibromo-carbene via its addition to an alkene (Figure 1.6).[69]

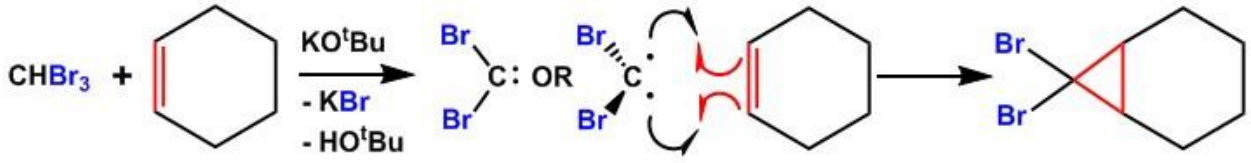

Figure 1.6: First proven existence of dibromo-carbene utilized in the cyclopropanation of an alkene also showing the diradical behavior of a *triplet* carbene.

The above figure also showcases the two different electronic structures of a carbene, either singlet (carbon with sp^2 hybridization with both electrons in a single orbital with s-character) or triplet (carbon with sp^3 hybridization with two orbitals with unpaired electrons). These electronic states are dependent on both the inductive and mesomeric effects of the carbene substituents.[70] Triplet carbenes generally behave like diradicals. Their reactivity consists of dimerization[71], C–H insertion/abstraction[72], cyclopropanation of alkenes[73], as well as formation of other radicals via abstraction reactions.[73] They do not tend to abstract halogens,[74] however, and can be protected/stabilized utilizing larger substituents (Br, CF_3) or through delocalization of

radicals onto aryl substituents.[75] Singlet states are stabilized with inductive electron-withdrawing α-groups which give the carbon greater s-character.[71, 76] Singlet carbenes show a variety of different reactivity dependent on the mesomeric effects the α-groups contribute, and can behave as nucleophiles or electrophiles[77] the specifics of which are beyond the scope of this thesis.

Metal carbenes, [M]=CRR', have had a long history, starting in 1915 when Chugaev reacted hydrazine and methylisocyanide with a Pt(II) complex, forming a hydrazide-bridged Pt metallacyclic carbene complex (Figure 1.7).[78] Although this was the first synthesis of a metal carbene complex it wasn't until 1973 that a definitive structure was determined.[79] The first

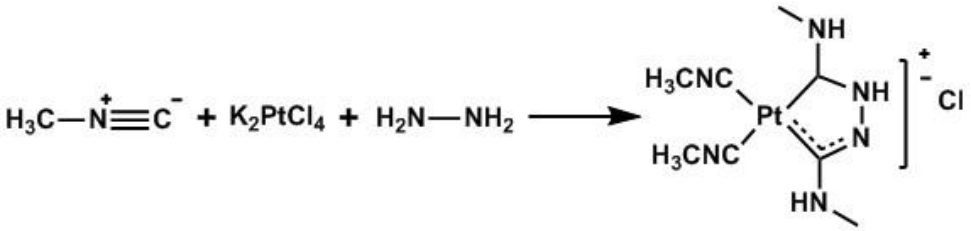

Figure 1.7: Chugaev's Salt (first synthesis of a metal carbene complex)

recognized metal carbene, on the other hand, was discovered by Fischer and Öfele in the 1960s[80] from nucleophilic addition of a phenyl group to a tungsten-coordinated carbonyl, yielding (methoxyphenyl)methylene tungsten(0) pentacarbonyl. This was followed by similar syntheses of chromium(0), iron(0) and manganese(0) carbene complexes bearing various α-substituents.[81] Schrock in 1974 isolated the first high oxidation state metal alkylidene complex - tris (2,2-dimethylpropyl)methyl-(2,2-dimethylpropyl) tantalum(V) (Scheme 1.5).[82]

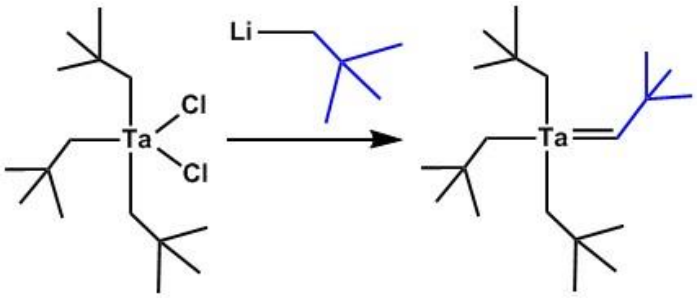

Scheme 1.5

To a first approximation, metal carbenes can be derived from singlet or triplet carbene fragments. The so-called Fischer carbenes typically contain a singlet carbene fragment stabilized by heteroatoms that can π-donate their lone pair into the empty p-orbital of the carbene carbon (Scheme 1.6).[83] As such, metal→carbene back-donation is diminished, depending on the degree of π-donation of the heteroatom constituents. The metal-carbene bond thus behaves like a traditional dative bond with σ-donation of the carbene lone pair into an empty metal orbital and a π-bond that is polarized towards the metal.[84] More electron-rich, low oxidation state metal fragments stabilize these types of metal carbenes[84,85] that tend to be electrophilic and prone to nucleophilic attack on the carbene carbon.[86] Conversely, so-called Schrock carbenes contain triplet carbene fragments[84,87] and do not require stabilizing heteroatoms. The M=C bonds are more covalent with the π-bond being equally shared between the metal and the carbene (Scheme 1.6). Schrock carbenes normally contain early, high oxidation state metals (d^0) and tend to be nucleophilic at the carbene carbon.[84,88]

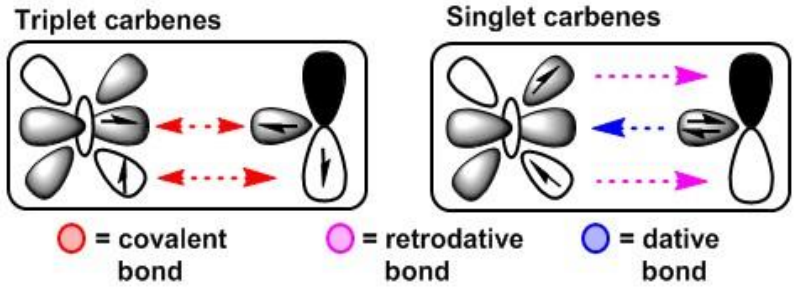

Scheme 1.6

However, the reality of transition metal carbenes is they exist in a continuum between true Fischer carbenes (electrophilic, highly polarized, hetero-atom stabilized, donor-acceptor complexes) and true Schrock carbenes (nucleophilic-carbene, electron sharing, covalent [M]=CRR' complexes) that take into account both the carbene and metal fragment individually and as a whole. The reactivity of carbenes does depend on the covalency of the [M]=CRR' bond and this can be modified depending on the nature of both the carbene and metal fragments. For example, generally speaking Schrock carbenes contain constituents that stabilize triplet states such as CH_2 which has a ground triplet state and CPhH which has a ground singlet state with a highly accessible triplet state (difference of only 7.3 $kcalmol^{-1}$)[89]. The metal fragment of covalent carbenes also tend to have geometries, oxidation states, electronegativities (based on position on the periodic table) and ligands that decrease crystal field stabilization energies (CFSE), making singly occupied d-orbitals more accessible. Dative/retrodative carbenes, on the

other hand, tend to have π-donor groups which not only stabilize the highly electrophilic carbene carbon from nucleophilic attack (non-hetero-atom stabilized carbenes are prone to decomposition with water and much more difficult to isolate)[87] but also stabilize singlet ground states [cf. C(OMe)Me; singlet ground state with high-energy triplet state, 42.1 kcalmol^{-1}].[89] The metal fragments also tend to be low-valent, late-transition metals coordinated by strong-field π-accepting ligands that increase CFSE, thereby encouraging molecular orbitals (MOs) with spin-paired electrons. This can be seen when comparing Grubbs Ru(II) carbenes with stereotypical Schrock carbenes [W/Mo(VI)]. The W/Mo(IV) d^2 fragments each contain two singly occupied MO's in addition to triplet-stabilized alkylidenes yielding a π-orbital that contains near equal metal(d_π) and carbene (C_{2p}) character (≈ 50% metal character). In contrast, Ru(II), a low spin d^6 complex, has a M=C bond that has significantly polarized π-bonds (>70% metal character) although the 14e$^-$ metathesis intermediate (4-coordinate; pseudo-tetrahedral; high-spin) has significant covalent character (≈ 55% metal character) as shown by Occhipinti and Jensen (Scheme 1.7). [90]

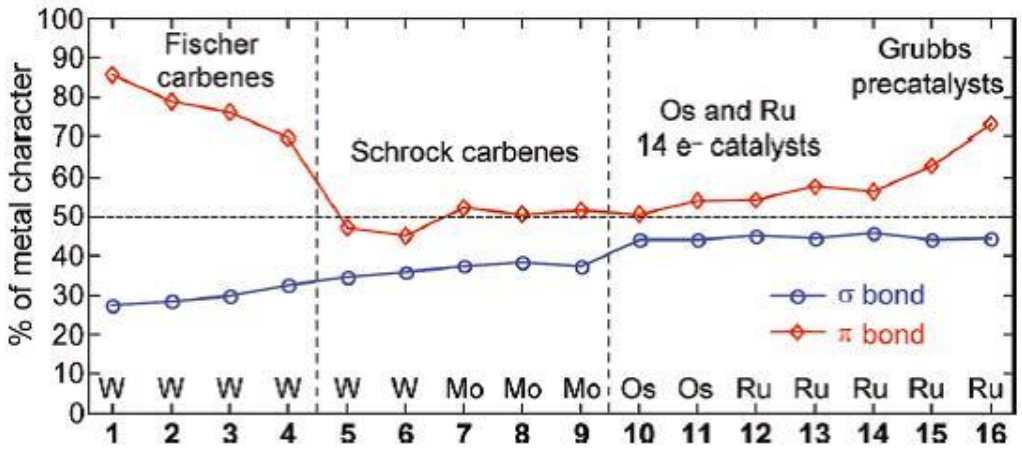

Scheme 1.7

Additionally, properties of the metal and carbene fragment can be modified to change the reactivity of the transition metal carbene as a whole. For example, Fischer carbenes, whose reactivity is mostly associated with alkene cyclopropanations are capable of metathesis reactions when the carbene is no longer stabilized with π-donor groups as shown by Casey using $(CO)_5W{=}CPh_2$.[91] When utilized with electron-rich olefins, this complex gave both cyclopropanation and metathesis products.[92] However, changing one aspect of the transition metal carbene does not necessarily alter the nature of the molecule as a whole. Grubbs has

published on this very subject, where he modified $Cl_2Ru{=}CH_2(PCy_3)_2$ by incorporating a stabilizing C-R-group such as -OEt, -SEt and -N(carbazole) to make, “Fischer type carbenes”. These were shown to catalyze metathesis reactions with strained ring-systems but were determined to be significantly de-activated, albeit with significantly enhanced thermal stability.[93] These examples show the correlation between transition metal carbenes that have covalent character and those that possess a more traditional dative/retrodative style bond in regards to their reactivity (Figure 1.8). Similar effects can be seen with double heteroatom–stabilized carbenes such as the recently employed N-heterocyclic carbenes (NHCs).

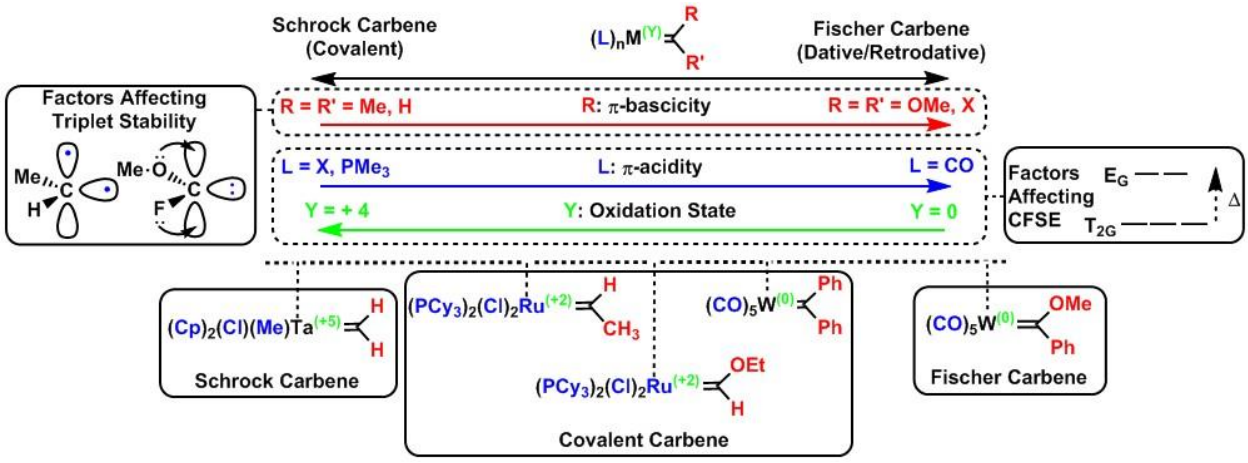

Figure 1.8: Trends in metal group, oxidation state, ligand environment and carbene R groups in regards to electronic state and reactivity of M=CRR.'

1.4.2 NHCs (‘pure’ Fischer carbenes)

As previously mentioned, although alkylidene fragments are formally considered as dianionic, carbenes are neutral species that feature a two-coordinate carbon atom possessing two non-bonding electrons.[94] N-heterocyclic carbenes (NHCs) are perfect examples of stable, singlet-state (Fischer) carbenes. They have found utility in both organic and inorganic chemistry and as ligands for early-, late- and post-transition metals.[95] As very strong σ-donors and relatively weak π-acceptors, NHCs are often compared to phosphines, especially as ligands.[94a] In general, NHCs are better electron donors than phosphines, and tend to form stronger metal-ligand bonds.[95b,d] Since the first report of a stable and isolable NHC by Arduengo *et al*. in 1991,[96] a staggering number of examples featuring varying steric and electronic parameters have been synthesized and characterized.[95]

Electronic stabilization plays a considerable role in these molecules as less sterically demanding NHCs, like IMe_4, were shown to be stable with only limited steric hindrance being provided by the methyl substituents on the nitrogen and carbon atoms.[97] Much like Schrock vs. Fischer carbenes, the electronic stabilization of NHCs stems from both σ and π factors.[98] The σ stabilization is due to inductive effects from the electronegative nitrogen atoms on the carbene carbon bearing the non-bonding lone pair. This effect controls the nucleophilic character of the carbene making it less likely to react via undesired pathways. The stability from π interactions, similar to π-donor R-groups on carbene fragments, arises from donation of the nitrogen lone pairs into the empty out-of-plane p-orbital on the carbene carbon. These combined σ- and π-effects increase the singlet-triplet gap of the carbene, favouring the less reactive singlet state .[99] The energy difference between the highest occupied molecular orbital (HOMO) and lowest unoccupied orbital (LUMO) can be manipulated, however, through conjugation (employing a saturated vs unsaturated C2 backbone) or modification of the N-R substituents.[100] This is especially evident on moving from imidazolium-based NHCs to cyclic (alkyl)-(amino) carbenes (CAACs) in which replacement of one N-donor destabilizes the singlet state (similar to replacing an -OMe group with -Me in M=CRR'). These were shown to outperform traditional NHCs as both σ-donors and π-acceptors due to the inclusion of an electron-releasing quaternary carbon and a more accessible LUMO.[101] This effect is further enhanced with Bertrand's new bicyclic (alkyl)(amino) carbene (BICAAC; Scheme 1.8). By forcing the geometry of BICAACs to mimic traditional diamino containing NHCs, the HOMO-LUMO gap is further reduced, increasing both the donor and acceptor properties of these carbenes. These examples show that even within the realm of 'pure' Fischer carbenes, a spectrum of chemical bonding is observed that affects their overall reactivity as has been extensively reviewed[102] elsewhere and is beyond the scope of this thesis.

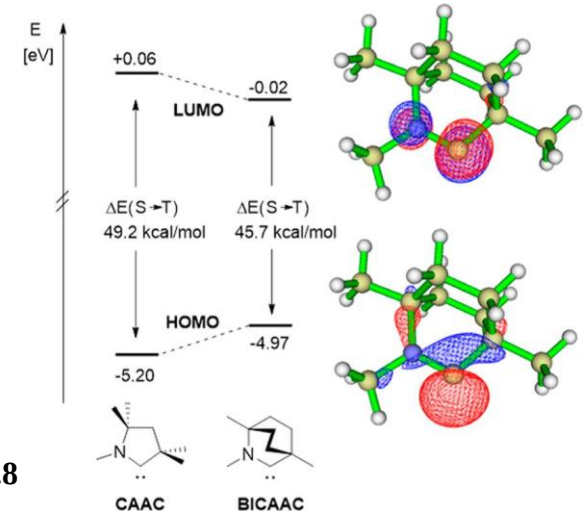

Scheme 1.8

1.4.3 Metal Carbenes and Olefin Metathesis

Metathesis, directly translated from Greek, means transposition, and what metal carbenes are best known for is their ability to construct new C-C bonds through exchanging the metal carbene with one carbon of an olefin. This transformation has a rich history that began in 1931 when propene was transformed into ethylene and 2-butene at 725 ^{o}C. A catalyzed metathesis reaction was later discovered when chemists from Dupont, Standard Oil and Phillips Petroleum determined that heating propene at 150-500 ^{o}C with an alumina-supported $Mo(CO)_6$ catalyst gave both ethylene and 2-butenes.[103] The mechanism for this unusual reaction remained a mystery until the 1970's when Yves Chauvin and his student, Jean-Louis Herrison, published a manuscript detailing their proposed mechanism.[104] The mechanism involves olefin coordination to an open site on the metal carbene followed by metallacyclobutane formation via a 2+2 cycloaddition. Subsequent retro-cycloaddition then affords a new carbene- olefin pair (Figure 1.9 top). The newly formed metal carbene can then perform this transformation again, either forming the same starting alkene + carbene pair (degenerate metathesis) OR the symmetrical olefin (Figure 1.9 bottom). Each step in an effective metathesis mechanism needs to be reversible to guarantee the propagation of this reaction. Unfortunately for Chauvin, there was hesitation in accepting his proposal and it wasn't until the 1980's when Schrock performed the metathesis reaction using non-heteroatom stabilized metal carbenes, that universal acceptance of the Chauvin Mechanism was established. This mechanism showed the importance of the metal carbene complex and the metallacycle intermediate as it allows transfer of the original metal carbene to the carbene fragment of the starting material olefin. Early studies by Grubbs, in fact, confirmed the presence of metallacycle intermediates by showing that Tebbe's complex $\{Cp_2Ti(\mu\text{-}CH_2)(\mu\text{-}Cl)AlMe_2)\}$ reacts to form stable, well defined metallacyclobutanes that can be pressed to slowly catalyze olefin metathesis.[105] The metallacycle intermediate can also be utilized in other transformations including sigma-bond metathesis, olefin-insertion, alkyne-polymerization and alkyne-metathesis as shown in other reviews.[106] The olefin metathesis reaction earned the early pioneers in this field, Yves Chauvin, Robert H. Grubbs and Richard R. Schrock the Nobel Prize in 2005. Capable of much more than olefin cross-metathesis (Figure 1.9), such as production of cyclic structures through ring closing metathesis (RCM) and of polymers through ring-opening metathesis polymerization (ROMP), this transformation now represents an essential tool in the organic chemist's toolbox.

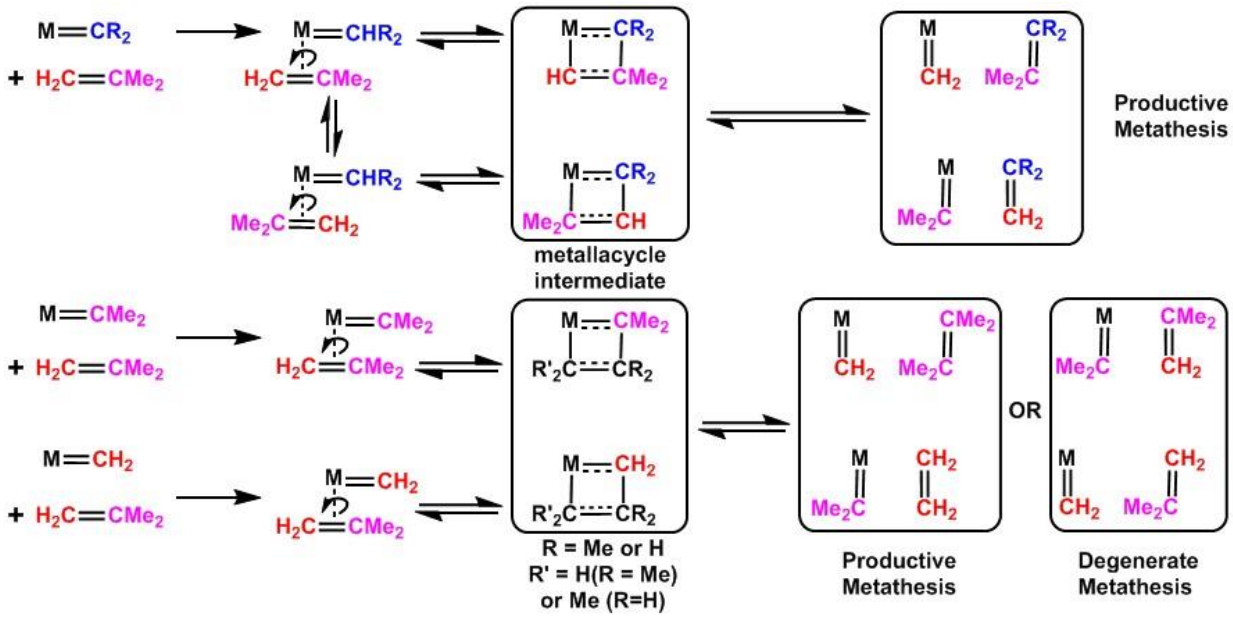

Figure 1.9: Chauvin's mechanism showing both the metallacyclobutane intermediate and the production of both degenerate and productive metathesis products.

1.4.4 M=CR^F_2 vs. M=CR_2 (R^F = F, CF_3, R = alkyl, aryl, H)

Given the significant academic and industrial interest in transition metals complexes containing both hetero-atom stabilized (Fischer) and unstabilized (Grubbs/Schrock) carbenes there are surprisingly few that contain fluorine/perfluoro-alkyl α-substituents. Syntheses of perfluorinated carbenes comes from only a handful of methodologies, including: intramolecular α-fluoride elimination from a Lewis acidic metal[34,75](Scheme 1.9A), intermolecular α-fluoride abstraction utilizing a Lewis-acid (Scheme 1.9B), reduction utilizing powerful reductants containing Lewis-acidic counter cations,[107] (Scheme 1.9C) simultaneous transfer and F^--abstraction using $Hg(CR^F)_2$ and $Cd(CR^F)_2$ reagents,[108] (Scheme 1.9D) and Lewis acid-catalyzed direct difluorocarbene addition utilizing the Ruppert-Prakash reagent (Scheme 1.9E).[109]

The lack of examples of isolated metal perfluorocarbenes is due to several factors. Firstly, given that most metal perfluorocarbenes traditionally begin their life as metal perfluoroalkyl ligands the lack of general routes to M–R^F complexes limits the number of derived metal carbenes. Secondly, perfluorinated carbenes are often brutally electrophilic and decompose even with trace water to produce HF and a coordinated carbonyl in place of the CF_2. In fact, there are so few M=CR^F_2 complexes that they can be included in the figure below with only a handful of

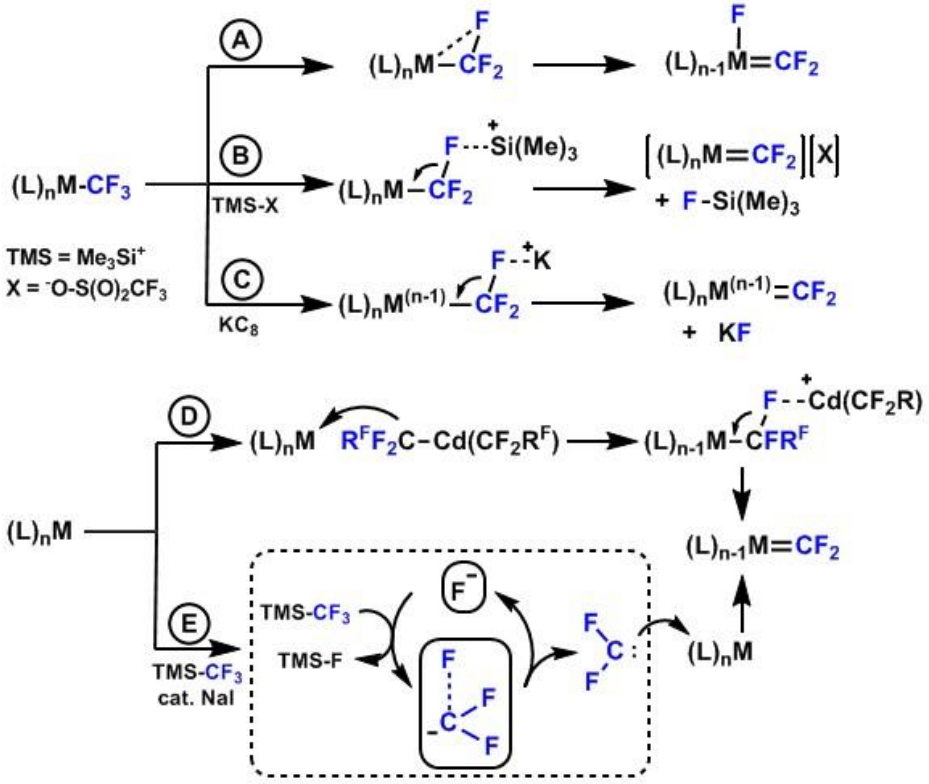

Scheme 1.9

researchers responsible for their synthesis. The vast majority of these examples are 2nd and 3rd row metals including: Rh[43a,110], Ir[111], Os[112], Mo[113], and Ru.[112,114,115] One of the ruthenium examples was isolated by the Grubbs group after attempted catalytic metathesis of tetrafluoroethylene (TFE) as discussed further in section 1.4.6. The only other example of first row metal perfluoro-carbenes other than the significant contributions by the Baker lab is a piano-stool iron(II) example by Shriver.[116] Over the last decade the Baker group has prepared and characterized metal perfluorocarbenes of manganese,[117] iron,[118]cobalt[66, 119,120,121,122] and nickel.[107,123]

The majority of these exhibit electrophilic character mainly due to the singlet stabilization and resistance to π-backbonding that fluorine substituents have on the carbene fragment.

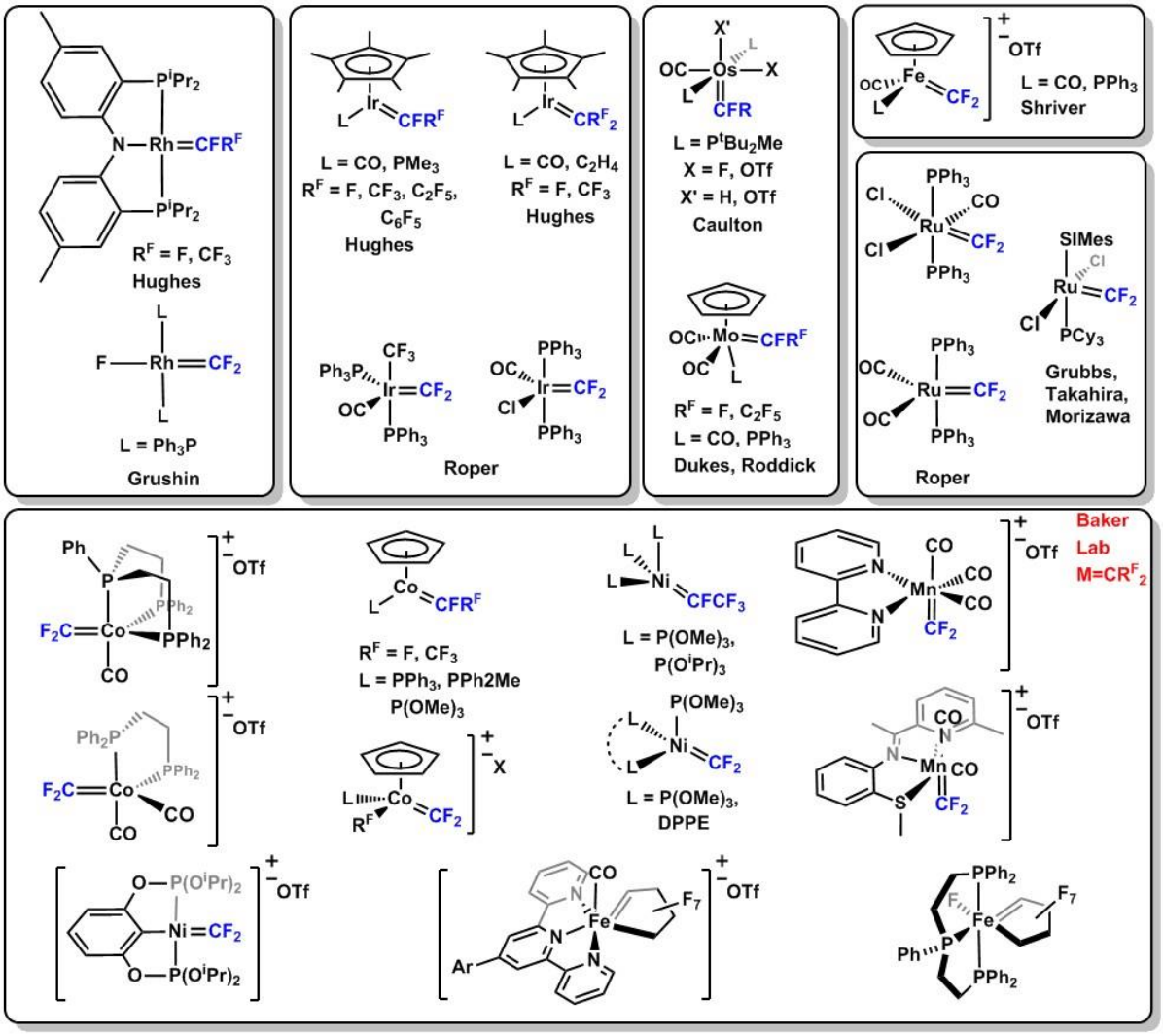

Figure 1.10: Overview of currently known metal perfluoro-carbenes

Additionally, late metals with low-oxidation states additionally increase the CFSE, making access to singly occupied MOs difficult. As fluorine is moved further away from the carbene carbon there is a drop in the electrophilic nature of the carbene with a complementary increase in its ability to accept electron-density in the form of π-back-bonding from the metal (Scheme 1.10). In this regard reactivity of metal carbenes may be dictated by both the dampening of electron density by induction and the degree of back-bonding which is determined by the nature of the metal fragment. This can be observed with late metal perfluorocarbenes where moving from Ru(II) to Ru(0) changed the reactivity from electrophilic to nucleophilic[114a] as well as our

own example involving Ni(0)[123] which shows markedly different reactivity than typical heteroatom-stabilized Fischer carbenes as discussed at length in chapters 4 and 5.

1.4.5 Fluoroalkenes: Fluoropolymers, Refrigerants and More

The importance of fluoroalkenes in industry will be briefly discussed here as they are essential in several key applications. Firstly, however, the physical and electronic properties of fluorine in unsaturated organics should be illuminated. Again, fluorine's strong electronegativity and interactions of its lone pairs with adjacent orbitals lead to unpredictable chemistry. In unsaturated systems fluorine has a marked destabilizing effect. Fluroalkenes are destabilized by the inductive effect of fluorine as well as the repulsive π-interaction of fluorine lone-pairs with the alkene π-system.[124] Additionally, there is a thermodynamic driving force for fluorine to be attached to sp^3 carbons that increases as fluorine is added to the alkene. For example the π-bond BDE in TFE is ca. 29 kcal mol^{-1} weaker than that of ethylene[125] although this reasoning alone may not paint a clear picture, as that of vinylidene fluoride (VDF; CF_2=CH_2) is 12.5 $kcalmol^{-1}$ *stronger* than ethylene, presumably due to increased electrostatic forces.[111] Another interesting feature in partially fluorinated alkenes is the cis-effect, where the cis-conformation is thermodynamically more stable (4-8 kJ mol^{-1}) in 1,2-difluoroethylene, an effect seen in the preferential gauche rotomer in 1,2-difluoro*ethane* as well. The most reasonable explanation for this is that the destabilizing interaction between fluorine lone pairs and the alkene π-system is exacerbated in the trans-isomer versus the cis.[124,126]

Fluoroalkenes play prominent roles in both the refrigeration[127] and polymer industries. Since the implementation of the Montreal protocol in 1987[127] that banned the use of ozone-depleting substances such as chlorofluorocarbons (CFCs)[128] which was a mainstay of the refrigeration industry, significant efforts were put towards the development of hydrochloro-fluorocarbons (HCFCs) followed by hydrofluorocarbons (HFCs) which were determined to have little to no impact on the ozone layer. However, with increasing concerns over production of greenhouse gases, the industry has recently transitioned to hydrofluoroalkenes (HFAs) which are both ozone-friendly and have both significantly reduced global warming potential (GWP) than saturated HFCs.[129] Unfortunately, selective fluorination and hydrodefluorination processes involving alkenes is challenging, and most successful examples require strict control over substrates and conditions. This lack of control is exemplified when looking at the cost of TFE

($0.44/g), VDF (0.50/g), vinyl fluoride (VF; CH_2=CHF $2.00/g) and trifluoroethylene (T^rFE; $11.00/g), where the cost of partially fluorinated products increases dramatically. For this reason, cost-effective and selective methods for the synthesis of new fluoro-alkenes are an area of active and continued research.

Fluoro-olefins are also heavily utilized by the fluoro-polymer industry. Fluorine not only significantly stabilizes the adjacent carbon backbone of a polymer making it resistant to cleavage and thermal decomposition (thermal stability), but its high electronegativity and lone pairs also make highly fluorinated polymers chemically resistant, especially to oxidation. Other properties that are common for fluoropolymers are low-friction coefficients and resistance to UV and aging.[14,124,130] These properties make them ideal materials for harsh environments such as, but not limited to, non-stick frying pans, gaskets, seals, membranes, and insulators.[131] The major monomers for the formation of fluoropolymers (including their common names) are shown in Figure 1.11.

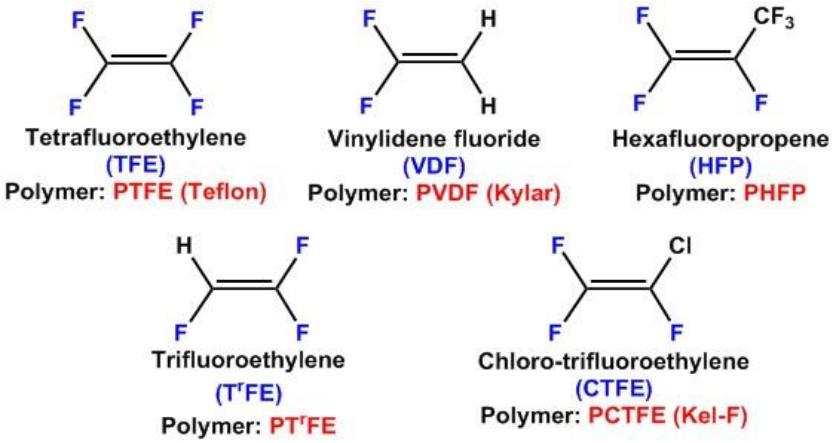

Figure 1.11: Most common alkene monomers in the fluoropolymer industry

Unlike non-fluorinated polymers there are no metal-mediated/catalyzed methods for the formation of fluoropolymers which are almost exclusively synthesized through radical polymerization (typically carried out with fluorosurfactants in aqueous emulsions; Chapter 1.1). As such, control over the tacticity and morphology of fluoropolymers has not been aided by such breakthroughs as the Ziegler-Natta catalyst and metallocene systems that have revolutionized hydrocarbon polymer synthesis and instead are limited to kinetic control.[14]

1.4.6 Fluoroalkene Metathesis

The fluoro-variant of the catalyzed alkene metathesis reaction has yet to be realized and is difficult for several key reasons. The electrophilic nature of the substrate would presumably require the use of a highly nucleophilic (Schrock-type) carbene whereas after a single turnover utilizing, for example, the Grubbs-II catalyst would then produce a more electrophilic (Fischer-type) carbene (Figure 1.12).

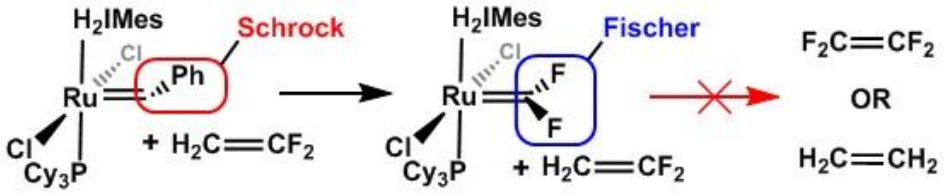

Figure 1.12: Example of Grubbs 2nd gen catalyst becoming deactivated upon reacting with fluoro-olefins due to the formation of singlet-stabilizing carbene fragment.

In fact, the above example is based on research by Grubbs where he showed that only a single turnover occurred with VDF regardless of the temperature being utilized. However, when the product of this reaction, the Ru=CF_2 complex was later isolated and utilized for the ROMP of 1,4-cyclooctadiene (COD) a much more electron-rich substrate, it successfully catalyzed this reaction. A key detail however was the requirement of HCl to help dissociate a normally labile phosphine, further showcasing the orbital stabilization effect of fluorinated ligands.[115] To state that by moving from a M=CHPh to a M=CF_2 carbene is the same as moving from a Schrock to a Fischer carbene is of course a generalization as a review by Roper states.[132] The major effects of this transformation are: formation of a carbene with α-substituents that reduce π-backbonding, stabilization of singlet carbene that deactivates the carbene towards nucleophilic reactions and stabilization of the d-orbitals rendering the complex sluggish towards dissociative mechanisms (Chapter 1.4.4). The idea that metathesis of fluorinated substrates leads to the flipping of carbene reactivity, was exploited recently for catalytic cross-metathesis of fluoro-olefins utilizing the Grubbs catalyst. Takahira and Morizawa utilized two substrates, highly fluorinated alkenes *and* electron-rich alkenes that would be more likely to react with a Fischer carbene (Scheme 1.11), allowing them to realize more than one turnover.[133] Reactions of the difluorocarbene with

the vinyl ethers were still sluggish, however, and only a low turnover number (TON) of 14 was obtained with only moderate conversions (< 45%).

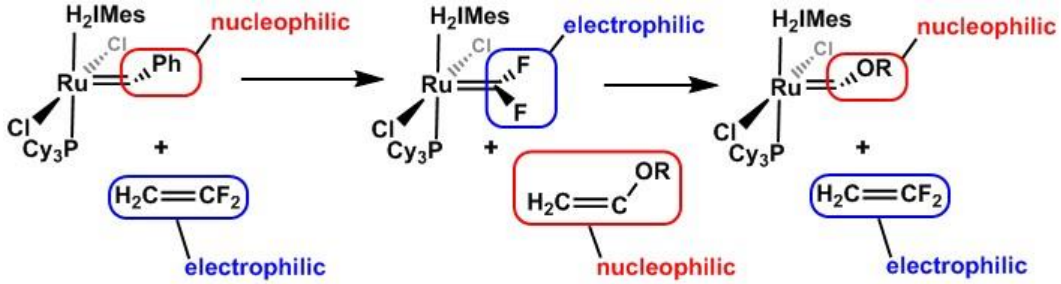

Scheme 1.11

This reduction in reactivity is due, in part, to the carbene stability and the singlet-triplet energy gap. For example, a 2011 study by O'Ferrall on carbene stabilization enthalpies (CSEs; determined using the singlet-triplet energy gap) of various CRR' carbenes showed a dramatic effect when moving from a perfluorinated carbene ($Ru=CF_2$) to a partially fluorinated carbene (Ru=CFH) the overall stability decreases by ca. 42 $kcalmol^{-1}$.[134] This can be seen in recent work by Schrock and Hoveyda who reported Z-selective catalytic cross-metathesis of fluorinated substrates using Group 6 catalysts. Their process avoids formation of the perfluorinated carbene altogether by utilizing 1,2-difluoroethylene and 1,2-bis(trifluoromethyl)ethylene.[135] The more reactive [Mo]=CFR ($R \neq F$, CFR_2) carbene can perform these difficult transformations, whereas the highly stabilized $Mo=CF_2$ carbene cannot. The first step towards true catalytic metathesis of fluoroalkenes, then, likely requires a nucleophilic transition metal perfluorocarbene complex and the absence of a terminal CF_2-containing fluoralkene to ensure the catalyst does not become de-activated after carbene exchange. The Baker lab took first steps towards this by focusing on first-row metal fluorocarbenes.

Developing a first-row alkene metathesis catalyst is not as simple as replacing the Ru in Grubbs catalyst by iron. Research by Dixon et al. suggests that the first step in ethylene metathesis using $M=CH_2(Cl)_2(PH_3)(NHC)$ catalysts , ligand dissociation, has significantly lower activation barriers for first row metal $M=CF_2$'s than those for both ruthenium and osmium (20 – 26 kcal mol^{-1} respectively).[136] Although they also studied the metal fluorocarbenes [M]=CFH with both TFE and 1,2-difluoroethylene, formation of a tetravalent Fe metallacycle is unlikely and additional trends were thus not identified. Returning to the need for a nucleophilic metal

fluorocarbene, early gas phase chemistry by Beauchamp suggested that d^9 Ni^+ may be capable of mediating fluoro-metathesis. They noted, however, that this process would be highly dependent on the overall energy of metal fluorocarbene + fluoroalkene pairs on either side of the required equilibrium.[137] Indeed when the Baker group reported the first nucleophilic first-row metal fluorocarbenes, $CpCo{=}CFR^F(PR'_3)$ (R^F = F, CF_3; R' = Ph; R'_3 = $MePh_2$).[119] their reaction with TFE gave cobaltacyclobutanes[121] that were more than 30 kcal more stable than $[M]{=}CF_2$ + TFE.[138] It was also shown that this occurred through a diradical mechanism where the carbene carbon reacted directly with the alkene, unlike the pre-coordination of the alkene substrate followed by concerted [2+2] addition for both the Grubbs and Schrock catalysts (Figure 1.13).

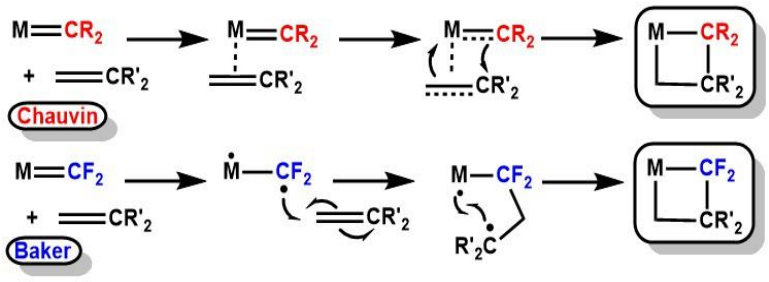

Figure 1.13: Mechanistic differences between traditional [2+2] cycloaddition (Chauvin mechanism) and the singlet diradical mechanism which forms a stable

While the stability of the resulting metallocyclobutanes precluded any retrocycloaddition needed for metathesis, abstraction of fluoride utilizing a Lewis-acid gave cobalt perfluoroalkenyl complexes and catalytic Bronsted acid led to perfluorometallacyclopropanes (Figure 1.14). Both sets of products were attributed to activation of the Cβ-F bond, in contrast to the Cα-F bond activation observed in typical metal perfluoroalkyls. Given the stabilizing effect that perfluoroalkyl groups have on d-orbitals, formation of such stable metallacycles is yet another hurdle that must be overcome to develop successful first-row metal-catalyzed fluoroalkene metathesis.

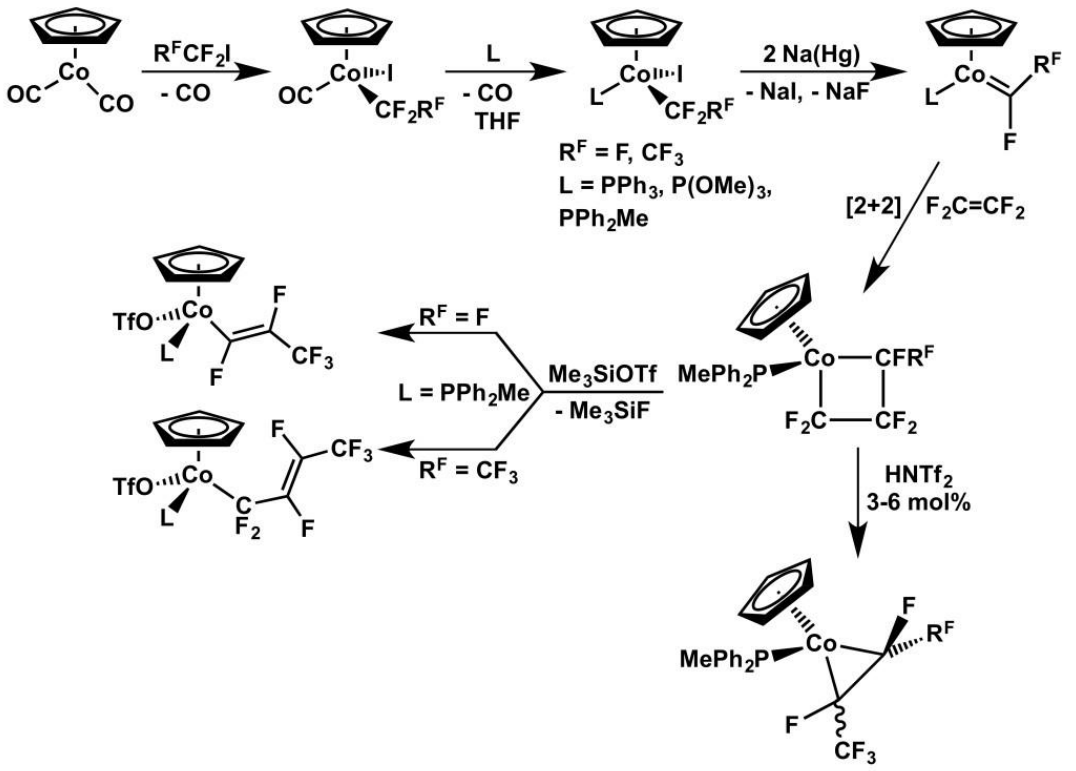

Figure 1.14: Synthesis and reactivity of nucleophilic d^8 [Co]=CFR^F complexes and corresponding metallacyclobutanes.

1.5 Summary and Thesis Outline

The benefits that fluorine imparts to molecular scaffolds especially in the arenas of materials, such as fluoropolymers, coatings, and heavy-duty valves and gaskets, as well as in the pharmaceutical and agrochemical industries towards the bioactivity of compounds, have been discussed here in detail. The inherent difficulty of incorporating fluorine into organic molecules has also been described with specific emphasis on how fluoride and fluoro-alkyl ligands impart new electronic and physical properties. These properties hinder our ability to mimic non-fluorinated organic transformations such as metal-catalyzed polymerization, alkylation and metathesis. A detailed look at transition metal carbenes and their fluorinated congeners showed the dramatic and often counterintuitive differences fluorine can have on both carbene and metal reactivity as demonstrated in several prominent publications on metathesis of fluorinated substrates utilizing transition metal carbenes. Chapter 2 of this thesis focuses on the design of a

coordinatively labile [Co]–CF_3 complex that provides an easily modified scaffold on which to build new [Co]=CF_2 metal carbenes. The C-based Lewis acidity of the latter was nicely demonstrated by its conversion of a different [Co]-CF_3 complex to new [Co]=CF_2 and [Co]-CF_3 complexes. Chapter 3 details the synthesis and characterization of the first isolable nickel(0) fluorocarbenes and features comparisons between nucleophilic cobalt(I) perfluorocarbenes with a specific focus on the dramatic increase in the rate of metallacyclobutane formation. Chapter 4 expands on chapter 3, introducing the more reactive [Ni]=CF(CF_3) carbenes. The latter are shown to react with fluoro-alkenes to produce both metathesis and metallacycle products through disparate reaction pathways as elucidated by detailed computational analysis with Texas A&M university collaborators. Chapter 5 features a comprehensive look at how various substrates, when combined with our new Ni=CF(CF_3) metal carbene, dramatically affect both metallacycle and metathesis reaction pathways. In addition, computational and experimental data is utilized to determine certain trends regarding regio- and chemoselectivity. Next, Chapter 6 covers the synthesis of new Mn–CF_3/Mn=CF_2 complexes and their potential use as fluoro-cross-coupling/polymerization catalysts. Finally, Chapter 7 places the learnings derived from this thesis work in context of the current state of the art and points to potentially fruitful avenues for future research.

References

[1] Banks, R. E.; Tatlow, J. C. *J. Fluorine Chem*. **1986**, *33*, 71-108.

[2] Feedonia World Fluorochemicals-Industry Study with Forecast for 2016 & 2021.www.feedoniagroup.com (2012).

[3] (a) Swarts, F. *Bull. Soc. Chim. Belg*. **1926**, 35, 412. (b) Swarts, F. *Bull. Soc. Chim. Belg*. **1926**, 12, 679. (c) Swarts, F. *Bull. Soc. Chim. Belg*. **1927**, *13*, 175.

[4] Burford III, W. B.; Fowler, R. D.; Hamilton Jr., H. C.; Anderson, C. E.; Weber, C. E.; Sweet, R. G. *Ind. Eng. Chem.* **1947,** *39*, 319-329.

[5] Fujiwara, T.; O'Hagan, David. *J. Fluorine Chem*. **2014**, *167*, 16-29.

[6] Böhm, H.-J.; Banner, D.; Bendels, S.; Kansy, M.; Kuhn, B.; Müller, K.; Obst-Sander, U.; Stahl, M. *ChemBioChem* **2004**, *5*, 637–643.

[7] Hagmann, W. K. *J. Med. Chem.* **2008**, *51*, 4359–4369.

[8] O'Hagan, D. *J. Fluorine Chem.* **2010**, *131*, 1071–1081.

[9] Wang, J.; Sánchez-Roselló, M.; Aceña, J. L.; del Pozo, C.; Sorochinsky, A. E.; Fustero, S.; Soloshonok, V. A.; Liu, H. *Chem. Rev.* **2014**, *114*, 2432–2506.

[10] (a) Kim, C. U.; Lee, J. M.; Ihm, S. K. *J. Fluorine Chem.***1999**, *96*, 11. (b) Kim, C. U.; Lee, J. M.; Ihm, S. K. *J. Appl. Polym. Sci*.**1999**, *73*, 777-793.

[11] Emani, M. S.; Roy, R.; Mandal, B. K. *Indian. J. Sci. Res*. **2017**, *14*, 175-181.

[12] Benhadid-Dib, S.; Benzaoui, A. *Energy Procedia*, **2012**, *18*, 807-816.

[13] Ameduri, B., Boutevin, B. *Well-Architectured Fluoropolymers: Synthesis, Properties and Applications*; Elsevier: Oxford, 2004.

[14] (a) Kim, C. U.; Lee, J. M.; Ihm, S. K. *J. Fluorine Chem.***1999**, *96*, 11. (b) Kim, C. U.; Lee, J. M.; Ihm, S. K. *J. Appl. Polym. Sci*.**1999**, *73*, 777-793.

[15] (a) U.S. Environmental Protection Agency. PFOA Stewardship Program, *http://www2.epa.gov/assessing-and-managing-chemicals-under-tsca/20102015-pfoa-stewardship-program*, Accessed 15/02/2019 (b) 39 Directive 2006/122/EC Of The European Parliament and Of The Council, *Official Journal of the European Union*, **2006**, L372/32–L372/34.

[16] S. K. Ritter, *Chem. Eng. News*, **2010**, *88*, 12–17.

[17] sp^3 carbons bearing more than one F; CF_2-F have higher BDEs than singly bound C-F BDEs

[18] Lemal, D. M. *J. Org. Chem.* **2004**, *69*, 1–11.

[19] Hughes, R. P. *Adv. Organomet. Chem.* **1990**, *31*, 183.

[20] D. O'Hagan, D. B. Harper. J. Fluorine Chem., **1999**, *100*, 127.)

[21] (a) Aigueperse, J.; Mollard, P.; Devilliers, D.; Chemla, M.; Faron, R.; Romano, R.; Cuer, J. P. In *Ullmann's Encyclopedia of Industrial Chemistry*; John Wiley & Sons, Inc., 2000.

(b) Harsanyi, A.; Sandford, G. *Green Chem.* **2015**, *17*, 2081–2086.

[22] (a) Stavber, S. *Molecules*. **2011**, 16, 6432-6464 (b) Liu, X.; Xu, C.; Wang, M.; Liu, Q. *Chem. Rev*. **2015**, *115*, 683-730.

[23] (a) Yang, X.; Tsui, G. C. *Org. Lett*. **2018**, *20*, 1179-1182. (b) Barata-Vallejo, S.; Postigo, Al. *Coord. Chem. Rev*. **2013**, *257*, 3051-3069. (c) Mormino, M. G.; Fier, P. S.; Hartwig, J. F. *Org. Lett*. **2014**, *16*, 1744-1747.

[24] (a) Lemal, D. M. *J. Org. Chem.* **2004**, *69*, 1–11. (b) O'Hagan, D. *Chem. Soc. Rev.* **2008**, *37*, 308–319.

[25] Selected Reviews: (a) Meyer, F. *Chem. Commun*., **2016**, *52*, 3077–3094 (b) Clarke, S. L.; McGlacken, G. P. *Chem. – Eur. J.*, **2017**, *23*, 1219–1230 (c) Kohlhepp, S. V.; Gulder, T. *Chem. Soc. Rev*., **2016**, *45*, 6270–6288 (e) Tomashenko, O. A.; Grushin, V. V. *Chem. Rev*., **2011**, *111*, 4475–4521.

[26] Song, H.; Han, Q.; Zhao, C.-L.; Zhang, C.-P. *Green Chem*. **2018**, *20*, 1662-1731.

[27] Differding, E.; Ofner, H. *Synlett* **1991**, *1991*, 187–189.

[28] Chernick, C. L.; Claassen, H. H.; Fields, P. R.; Hyman, H. H.; Malm, J. G.; Manning, W.

M.; Matheson, M. S.; Quarterman, L. A.; Schreiner, F.; Selig, H. H.; Sheft, I.; Siegel, S.; Sloth, E. N.; Stein, L.; Studier, M. H.; Weeks, J. L.; Zirin, M. H. *Science* **1962**, *138*, 136–138.

[29] Coffield, T. H.; Kozikowski, J.; Closson, R.D. Abstr. I.C.C.C. Conference, vol. Special Publication No. 13, The Chemical Society, London, 1959, p. 126.

[30] Kaesz, H. D.; King, R. B.; Stone, F. G. A. Z. *Naturforsch.* **1960**, *15*, 763–764.

[31] McClellan, W. R. *J. Am. Chem. Soc*. **1961**, *83*, 1598–1600.

[32] Hieber, W.; Beck, W.; Lindner, E. *Z. Naturforsch. B*, **1961**, *16b*, 229–231.

[33] Bennett, M. A.; Chee, H.; Robertson, G. B. *Inorg. Chem*. **1979**, *18*, 1061.

[34] (a) King, R. B.; Treichel, P. M.; Stone, F. G. A. *Proc. Chem. Soc*. **1961**, 69–70. (b) Manuel, T. A.; Stafford, S. L.; Stone, F. G. A. *J. Am. Chem. Soc*. **1961**, *83*, 249–250.

[35] (a) Hoehn, H. H.; Pratt, L.; Watterson, K. F.; Wilkinson, G. *J. Chem. Soc*. **1961**, 2738–2745. (b) Parshall, G. W.; Wilkinson, G. *J. Chem. Soc*. **1962**, 1132.

[36] Shin, S. K.; Beauchamp, J. L. *J. Am. Chem. Soc*. **1990**, *112*, 2057-2066.

[37] (a) Lumsden, S. E. A.; Durgaprasad, G.; Muthiah, K. A. T.; Rose, M. J. *Dalton Trans*. **2014**, 43, 10725–10738. (b) Welch, K. D.; Dougherty, W. G.; Kassel, W. S.; Dubois, D. L.; Bullock, R. M. *Organometallics*, **2010**, 29, 4532–4540. (c) Van Putten, R.; Uslamin, E. A.; Garbe, M.; Liu, C.; Gonzalez-de-Castro, A.; Lutz, M.; Junge, K.; Hensen, E. J. M.; Beller, M.; Lefort, L.; Pidko, E. A. *Angew. Chem. Int. Ed*. **2017**, 56, 7531–7534.

[38] Taw, F. L.; Clark, A. E.; Mueller, A. H.; Janicke, M. T.; Cantat, T.; Scott, B. L.; Hay, P. J.; Hughes, R. P.; Kiplinger, J. L. *Organometallics*. **2012**, *31*, 1484 – 1499.

[39] Connor, J. A.; Zafarani-Moattar, M. T.; Bickerton, J.; El Saied, N. I.; Suradi, S.; Carson, R.; Al Takhin, G.; Skinner, H. A. *Organometallics*. **1982**, *1*,1166.

[40] (a) Churchill M. R.; Fennessey, J. P. *Inorg. Chem*. **1967**, *6*, 1213. (b) Bennett M. J.; Mason, R. *Proc. Chem. Soc*., *London*, 273 (1963). (c) Bennett, M. J. Ph.D. Thesis, University of Sheffield, England, 1965. (d) Bennett, M. A.; Chee, H.-K.; Robertson, G. B. *Inorg. Chem*. **1979**, *18*, 1061.

[41] (a) King, R. B.; Bisnette, M. B. *J. Organomet. Chem*. **1964**, *2*, 15. (b) Cotton F. A.; McCleverty, J. A. *J. Organomet. Chem*. **1965**, *4*, 490. (c) Cotton F. A.; Wing, R. M. *J. Organomet. Chem*. **1967**, *9*, 511 (d) Clark H. C.; Tsai, J. H. *J. Organomet. Chem*. **1967**, *7*, 515.

[42] Hall M. B.; Fenske, R. F. *Inorg. Chem*. **1972**, *11*, 768.

[43] (a) Goodman, J.; Grushin, V. V.; Larichev, R. B.; Macgregor, S.A.; Marshall, W. J.; Roe, D. C. *J. Am. Chem. Soc*. **2009**, *131*, 4236. (b) Goodman, J.; Grushin, V. V.; Larichev, R. B.; Macgregor, S. A.; Marshall, W. J.; Roe, D. C. *J. Am. Chem. Soc*. **2010**, *132*, 12013.

[44] Algarra, A. G.; Grushin, V. V.; Macgregor, S. A. *Organometallics*. **2012**, *31*, 1467-1476.

[45] (a) Yang, D.-S.; Bancroft, G. M.; Puddephatt, R. J.; Tse, J. S. *Inorg. Chem*. **1990**, *29*, 2496. (b) Evans, S.; Green, J. C.; Green, M. L. H.; Orchard, A. F.; Turner, D. W. *Discuss. Faraday Soc*. **1969**, *47*, 112.

[46] Morrison, J. A. *Adv. Organomet. Chem*. **1993**, *35*, 211.

[47] Hughes, R. P.; Meyer, M. A.; Tawa, M. D.; Ward, A. J.; Williamson, A.; Rheingold, A. L.; Zakharov, L. N. *Inorg. Chem*. **2004**, *43*, 747-756.

[48] Selected oxidative addition examples: (a) Zhu, F.; Wang, Z.-X. *J. Org. Chem*. **2014**, *79*, 4285-4292. (b) Kuehnel, M. F.; Lentz, D.; Braun, T. *Angew. Chem. Int. Ed*. **2013**, *52*, 3328-3348.

[49] Selected salt metathesis of M-X with fluoride salts: (a) Veltheer, J. E.; Burger, P.; Bergman, R. G. *J. Am. Chem. Soc*. **1995**, *117*(50), 12478–12488. (b) Osterberg, C. E.; King, M. A.; Arif, A. M.; Richmond, T. G. *Angew. Chem. Int. Ed. Engl*. **1990**, *29*(8), 888–890. (c) Poulton, J. T.; Sigalas, M. P.; Folting, K.; Streib, W. E.; Eisenstein, O.; Caulton, K. G. *Inorg. Chem*. **1994**, *33*(7), 1476–1485.

[50] Mankad, N. P.; Toste, F. D. *J. Am. Chem. Soc*. **2010**, *132*(37), 12859–12861.

[51] Selected examples of M-F complexes in order from group 3-11: (a) Bottomley, F.; Paez, D. E.; White, P. S. J. *Organomet. Chem*. **1985**, *291*(1), 35–41. (b) Murphy, E. F.; Yu, P.; Dietrich, S.; Roesky, H. W.; Parisini, E.; Noltemeyer, M. *J. Chem. Soc. Dalton Trans*. **1996**, *No. 9*, 1983–1987. (c) Antiñolo, A.; Lappert, M. F.; Singh, A.; Winterborn, D. J. W.; Engelhardt, L. M.; Raston, C. L.; White, A. H.; Carty, A. J.; Taylor, N. J. *J. Chem. Soc. Dalton Trans*. **1987**, *No. 6*, 1463–1472. (d) Gowik, P.; Klapötke, T.; Thewalt, U. *J. Organomet. Chem.* **1990**, *385*(3), 345–350. (e) Roesky, H. W.; Sotoodeh, M.; Xu, Y. M.; Schrumpf, F.; Noltemeyer, M. *Z.Anorg. Allg. Chem*. **1990**, *580*(1), 131–138. (f) Roesky, H. W.; Schrumpf, F.; Noltemeyer, M. *J. Chem. Soc. Dalton Trans*. **1990**, *No. 2*, 713–714. (g) Thomas, B. J.; Mitchell, J. F.; Theopold, K. H.; Leafy, J. A. *J. Organomet. Chem*. **1988**, *348*(3), 333–342. (h) Ellis, R.; Henderson, R. A.; Hills, A.; Hughes, D. L. *J. Organomet. Chem*. **1987**, *333*(1), C6–C10. (i) Green, M. L. H.; Hughes, A. K.; Lincoln, P.; Martin-Polo, J. J.; Mountford, P.; Sella, A.; Wong, L.-L.; Bandy, J. A.; Banks, T. W.; Prout, K.; Watkin, D. J. *J. Chem. Soc., Dalton Trans*. **1992**, *No. 13*, 2063–2069. (j) Abel, E. W.; Towle, I. D. H.; Cameron, T. S.; Cordes, R. E. *J. Chem. Soc., Dalton Trans*. **1979**, *No. 12*, 1943–1949.

[52] McLoughlin, V. C. R.; Thrower, J. U.S. Patent 3,408,411, **1968**.

[53] McLoughlin, V. C. R.; Thrower, J. *Tetrahedron*, **1969**, *25*, 5921.

[54] Selected Reviews: (a) Burton, D. J.; Lu, L. *Top. Curr. Chem*. **1997**, *193*, 45. (b) McClinton, M. A.; McClinton, D. A. *Tetrahedron*, **1992**, *32*, 6555. (c) Burton, D. J.; Yang, Z. Y. *Tetrahedron*, **1992**, *48*, 189.

[55] (a) Dubinina, G. G.; Furutachi, H.; Vicic, D. A. *J. Am. Chem. Soc*. **2008**, *130*, 8600. (b) Dubinina, G. G.; Ogikubo, J.; Vicic, D. A. *Organometallics*. **2008**, *27*, 6233.

[56] Oishi, M.; Kondo, H.; Amii, H. *Chem. Commun*. **2009**, 1909.

[57] Grushin, V. V.; Marshall, W. J. *J. Am. Chem. Soc*. **2006**, *128*, 12644.

[58] Selected examples of $L_2(R)Pd - CF_3$: (a) Umemoto, T. *Chem. Rev*. **1996**, *96*, 1757. (b) Ruppert, I.; Schlich, K.; Volbach, W. *Tetrahedron Lett*. **1984**, *25*, 2195. (c) Folleas, B.; Marek, I.; Normant, J.-F.; Saint-Jalmes, L. *Tetrahedron*. **2000**, *56*, 275. (d) Grushin, V. V.; Marshall, W. J. *J. Am. Chem. Soc*. **2006**, *128*, 4632. (e) Culkin, D. A.; Hartwig, J. F. *Organometallics*. **2004**, *23*, 3398.

[59] Bakhmutov, V. I.; Bozoglian, F.; Gómez, K.; González, G.; Grushin, V. V. Macgregor, S.A.; Martin, E.; Miloserdov, F. M.; Novikov, M. A.; Panetier, J. A.; and Romashov, L. V. *Organometallics*. **2012**, *31*, 1315-1328.

[60] Ball, N. D.; Kampf, J. W.; Sanford, M. S. *J. Am. Chem. Soc*. **2010**, *132*, 2878 – 2879.

[61] Xu, J.; Liu, X.; Fu, Y. *Tetrahedron Lett*. **2014**, *55*, 585-594.

[62] Bour, J. R.; Camasso, N. M.; Meucci, E. A.; Kampf, J. W.; Canty, A. J.; Sanford, M. S. *J. Am. Chem. Soc*. **2016**, *138*, 16105-16111.

[63] Paeth, M.; Tyndall, S. B.; Chen, L-Y.; Hong, J-C.; Carson, W. P.; Liu, X.; Sun, X.; Liu, J.; Yang, K.; Hale, E. M.; Tierney, D. L.; Liu, B.; Cao, Z.; Cheng, M-J.; Goddard III, W. A.; Liu, W. *J. Am. Chem. Soc*. **2019**, *141*, 3153-3159.

[64] Levin, M. D.; Chen, T. Q.; Neubig, M. E.; Hong, C. M.; Theulier, C. A.; Kobylianskii, I. J.; Janabi, M.; O'Neil, J. P.; Toste, F. D. *Science*. **2017**, *356*, 1272-1276.

[65] Wilford, J. B.; Stone. F. G. A. *Inorg. Chem*. **1965**, *4*, 93-97

[66] Leclerc, M. C.; Bayne, J. M.; Lee, G. M.; Gorelsky, S. I.; Vasiliu, M.; Korobkov, I.; Harrison, D. J.; Dixon, D. A.; Baker, R. T. *J. Am. Chem. Soc*. **2015**, *137*, 16064-16073.

[67] Geuther, A.; Hermann, M. *Liebigs Ann. Chem*. **1855**, *95*, 211.

[68] (a) Staudinger, H.; Kupfer, O. *Berichte der Deutschen Chemischen Gesellschaft*. **1911**, *44*, 2194. (b) Staudinger, H.; Kupfer, O. *Berichte der Deutschen Chemischen Gesellschaft*. **1912**, *45*, 501.

[69] Doering, W. E.; Hoffmann, A. K. *J. Am. Chem. Soc*. **1954**, *76*, 6162.

[70] (a) Harrison, J. F. *J. Am. Chem. Soc*. **1971**, *93*, 4112 (b) Harrison, J. F.; Liedtke, C. R.; Liebman, J. F. *J. Am. Chem. Soc*. **1979**, *101*, 7162 (c) Pauling, L. *J. Chem. Soc., Chem. Commun*. **1980**, 688.

[71] (a) Zimmerman, H. E.; Paskovich, D. H. *J. Am. Chem. Soc*. **1964**, *86*, 2149. (b) Tomioka, H.; Okada, H.; Watanabe, T.; Hirai, K. *Angew. Chem., Int. Ed. Engl*. **1994**, *33*, 973 (c) Sander, W.; Kirschfeld, A.; Kappert, W.; Muthusamy, S.; Kiselewsky, M. *J. Am.Chem. Soc*. **1996**, *118*, 6508.

[72] (a) Hirai, K.; Komatsu, K.; Tomioka, H. *Chem. Lett*. **1994**, *23*, 503. (b) Griffin, G. W.; Horn, K. A. *J. Am. Chem. Soc*. **1987**, *109*, 4919 (c) Platz, M. S. (Ed.), Kinetics and Spectroscopy of Carbenes and Biradicals, Plenum, New York, 1990 (d) Itoh, T.; Nakata, Y.; Hirai, K.; Tomioka, H. *J. Am. Chem. Soc*. **2006**, *128*, 957.

[73] Hideo, T.; Kumiko, O.; Yasuji, I.; Moss, R. A.; Ramesh, M. C. *Tetrahedron Lett*. **1984**, *25*, 5415.

[74] Roth, H. D. *Acc. Chem. Res*. **1977**, *10*, 85.

[75] Tomioka, H.; Watanabe, T.; Hattori, M.; Nomura, N.; Hirai, K. *J. Am. Chem. Soc*. **2002**, *124*, 474.

[76] Irikura, K. K.; Goddard III, W. A.; Beauchamp, J. L. *J. Am. Chem. Soc*. **1992**, *114*, 48.

[77] (a) Moss, R. A.; Perez, L. A.; Wlostowska, J.; Guo, W.; Krogh-Jespersen, K. *J. Org.Chem*. **1982**, *47*, 4177 (b) Moss, R. A.; Kmiecik-Lawrynowicz, G.; Krogh-Jespersen, K. *J. Org. Chem*. **1986**, *51*, 2168 (c) Moss, R. A.; Shen, S.; Hadel, L. M.; Kmiecik-Lawrynowicz, G.; Wlostowska, J.; Krogh-Jespersen, K. *J. Am. Chem. Soc*. **1987**, *109*, 4341 (d) Mieusset, J. –L.; Brinker, U. H. *J. Org. Chem*. **2008**, *73*, 1553.

[78] (a) Chugaev, L.; Skanavy-Grigorizeva, M. *J. Russ. Chem. Soc*. **1915**, *47*, 776. (b) Chugaev, L.; Skanavy-Grigorizeva, M.; Posniak, A. *Z. Anorg. Allg. Chem*. **1925**, *148*, 37.

[79] Butler, W. M.; Enemark, J. H.; Parks, J.; Balch, A. L. *Inorg. Chem*. **1973**, *12*, 451.

[80] (a) Fischer, E. O.; Öfele, K. *Angew. Chem*. **1961**, *73*, 581 (b) Fischer, E. O.; Öfele, K. *Angew. Chem*. **1962**, *74*, 76 (c) Fischer, E. O.; Fichtel, K.; Öfele, K. *Chem. Ber*. **1962**, *85*, 249.

[81] Cardin, D. J.; Cetinkaya, B.; Lappert, M. F.; *Chem. Rev*. **1972**, *72*, 545.

[82] Schrock, R. R. *J. Am. Chem. Soc*. **1974**, *96*, 6796.

[83] Bourissou, D.; Guerret, O.; Gabbaï, F. P.; Bertrand, G. *Chem. Rev*. **2000**, *100*, 39.

[84] Taylor, T. E.; Hall, M. B. *J. Am. Chem. Soc*. **1984**, *106*, 1576.

[85] Cardin, D. J.; Cetinkaya, B.; Lappert, M. F. *Chem. Rev*. **1972**, *72*, 545.

[86] (a) Schoeller, W. W.; Eisner, D.; Grigoleit, S.; Rozhenko, A. B.; Alijah, A. *J. Am. Chem. Soc*. **2000**, *122*, 10115 (b) Canac, Y.; Soleilhavoup, M.; Conejero, S.; Bertrand, G. *J. Organomet. Chem*. **2004**, *689*, 3857.

[87] S.F. Vyboishchikov, G. Frenking, *Chem. Eur. J.* **1998**, *4*, 1428.

[88] Lappert, M. F. *J. Organomet. Chem*. **1988**, *358*, 185, and references therein.

[89] Gronert, S.; Keefe, J. R.; O'Ferrall, R. A. M. *J. Am. Chem. Soc*. **2011**, *133*, 3381-3389.

[90] Occhipinti, G.; Jensen, V. R. *Organometallics*, **2011**, *30*, 3522-3529.

[91] Casey, C. P.; Burkhardt, T. J. *J. Am. Chem. Soc*. **1974**, *96*, 7808-7809.

[92] Santamaria, J.; Aguilar, E. *Org. Chem. Front*. **2016**, *3*, 1561.

[93] Louie, J.; Grubbs, R. H. *Organometallics*, **2002**, *21*, 2153-2164.

[94] (a) Hopkinson, M. N.; Richter, C.; Schedler, M.; Glorius, F. *Nature* **2014**, *510*, 485–496.

(b) Diez-Gonzalez, S., ed. In *N-Heterocyclic Carbenes - From Laboratory Curiosities to Efficient Synthetic Tools, 2nd Edition*; Royal Society of Chemistry, 2016.

[95] (a) Glorius, F., ed. In *N-Heterocyclic Carbenes in Transition Metal Catalysis*; Springer International Publishing, 2007. (b) Velazquez, H. D.; Verpoort, F. *Chem. Soc. Rev.* **2012**, *41*, 7032–7060. (c) Cazin, C. S. J., ed. In *N-Heterocyclic Carbenes in Transition Metal Catalysis and Organocatalysis*; Springer International Publishing, 2010.(d) Nelson, D. J.; Nolan, S. P., eds. In *N-Heterocyclic Carbenes: Effective Tools for Organometallic Synthesis*; John Wiley & Sons, Inc., 2014.

[96] Arduengo III, A. J.; Harlow, R. L.; Kline, M. *J. Am. Chem. Soc.* **1991**, *113*, 361–363.

[97] Arduengo III, A. J.; Dias, H. V. R.; Harlow, R. L.; Kline, M. *J. Am. Chem. Soc.* **1992**, *114*, 5530–5534.

[98] Wanzlick, H. W. *Angew. Chem. Int. Ed.* **1962**, *1*, 75–80.

[99] (a) Dixon, D. A.; Arduengo III, A. J. *J. Phys. Chem.* **1991**, *95*, 4180–4182. (b) Irikura, K. K.; Goddard, W. A.; Beauchamp, J. L. *J. Am. Chem. Soc.* **1992**, *114*, 48–51.

[100] Huynh, H. V. *Chem. Rev*. **2018**, *118*, 9457-9492.

[101] (a) Lavallo, V.; Canac, Y.; Donnadieu, B.; Schoeller, W. W.; Bertrand, G. *Angew. Chem., Int. Ed*. **2006**, *45*, 3488. (b) Droege, T.; Glorius, F. *Angew. Chem., Int. Ed.* **2010**, *49*, 6940. (c) Hopkinson, M. N.; Richter, C.; Schedler, M.; Glorius, F. *Nature*. **2014**, *510*, 485. (d) Vatsadze, S. Z.; Loginova, Y. D.; dos Passos Gomes, G.; Alabugin, I. V. *Chem. - Eur. J.* **2017**, *23*, 3225.

[102] (a) Flanigan, D. M.; Romanov-Michailidis, F.; White, N. A.; Rovis, T. *Chem. Rev*. **2015**, *115*, 9307-9387. (b) Danopoulos, A. A.; Simler, T.; Braunstein, P. *Chem. Rev*. **2019**, *119*, 3730-3961. (c) Kühl, O. *Chem. Soc. Rev*. **2007**, *36*, 592-607.

[103] (a) Banks, R. L.; Bailey, G. C. *Int. Eng. Prod. Dev*. **1964**, *3*, 170 (b) Eleuterio, H. S. *J. Mol. Catal*. **1991**, *65*, 55. (c) Eleuterio, H. S. German Pat. 1,072,811, 1960. (d) Truett, W. L.; Johnson, D. R.; Robinson I. M.; Montague, B. P. *J. Am. Chem. Soc*. **1960**, *82*, 2337 (e) Rouhi, M. R. *Chem. Eng. News*, **2002**, 29 (December 23).

[104] Chauvin, Y. and Herisson, J. –L. *Makromol. Chem.* **1971**, *141*, 161.

[105] (a) Tebbe, F. N.; Parshall, G. W.; Reddy, G. S. *J. Am. Chem. Soc.* **1978**, *100*, 3611. (b) Howard, T. R.; Lee, J. B.; Grubbs, R. H. *J. Am. Chem. Soc*. **1980**, *102*, 6876. (c) Anslyn, E. V.; Grubbs, R. H. *J. Am. Chem. Soc*. **1987**, *109*, 4880. (d) Hawkins, J. M.; Grubbs, R. H. *J. Am. Chem. Soc*. **1988**, *110*, 2821.

[106] Astruc, D. *New J. Chem*. **2005**, *29*, 42-56.

[107] Harrison, D. J.; Daniels, A. L.; Korobkov, I.; Baker, R. T. *Organometallics* **2015**, *34*, 5683–5686.

[108] (a) S. D. Ittel, *Inorg. Synth*. **1990**, *28*, 98-104. (b) Lange, H.; Naumann, D. *J. Fluorine Chem*. **1984**, *26*, 1-18.

[109] (a) Wang, F.; Luo, T.; Hu, J.; Wang, Y.; Krishnan, H. S.; Jog, P. V.; Ganesh, S. K.; Prakash, G. K. S. and Olah, G. A. *Angew. Chem., Int. Ed*. **2011**, *50*, 7153–7157. (b) Liu, X.; Wang, M.; Liu, Q. *Chem. Rev*. **2015**, *115*, 683-730.

[110] Pell, C. J.; Zhu, Y.; Huacuja, R.; Herbert, D. E.; Hughes, R. P.; Ozerov, O. V. *Chem. Sci.* **2017*, 8***, 3178-3186.

[111] (a) Brothers, P. J.; Burrell, A. K.; Clark, G. R.; Rickard, C. E. F.; Roper, W. R. *J. Organomet. Chem.* **1990**, *394*, 615–642. (b) Bourgeois, C. J.; Hughes, R. P.; Yuan, J.; DiPasquale, A. G.; Rheingold, A. L. *Organometallics* **2006**, *25*, 2908–2910. (c) Hughes, R. P.; Laritchev, R. B.; Yuan, J.; Golen, J. A.; Rucker, A. N.; Rheingold, A. L. *J. Am. Chem. Soc.* **2005**, *127*, 15020–15021. (d) Yuan, J.; Hughes, R. P.; Golen, J. A.; Rheingold, A. L. *Organometallics* **2010**, *29*, 1942–1947.

[112] Huang, D.; Koren, P. R.; Folting, K.; Davidson, E. R.; Caulton, K. G. *J. Am. Chem. Soc.* **2000**, *122*, 8916–8931.

[113] (a) Reger, D. L.; Dukes, M. D. *J. Organomet. Chem.* **1978**, *153*, 67–72. (b) Koola, J. D.; Roddick, D. M. *Organometallics* **1991**, *10*, 591–597.

[114] (a) Clark, G. R.; Hoskins, S. V.; Roper, W. R. *J. Organomet. Chem.* **1982**, *234*, C9–C12.

(b) Clark, G. R.; Hoskins, S. V.; Jones, T. C.; Roper, W. R. *J. Chem. Soc. Chem. Commun.*

1983, *13*, 719–721.

[115] Trnka, T. M.; Day, M. W.; Grubbs, R. H. *Angew. Chem. Int. Ed.* **2001**, *40*, 3441–3444.

[116] (a) Richmond, T. G.; Crespi, A. M.; Shriver, D. F. *Organometallics* **1984**, *3*, 314–319. (b) Crespi, A. M.; Sabat, M.; Shriver, D. F. *Inorg. Chem.* **1988**, *27*, 812–816. (c) Crespi, A. M.; Shriver, D. F. *Organometallics* **1985**, *4*, 1830–1835.

[117] Daniels, A. D.; Da Gama, J. G.; Edjoc, R.; Gabidullin, B. M.; Baker, R. T. *Inorganics*. **2019**, *7*, 3.

[118] Ghostine, K. Reactivity of low-valent Iron and Cobalt Complexes with Fluoroalkenes. M.Sc. Dissertation, University of Ottawa, Ottawa, ON, 2018.

[119] Harrison, D. J.; Gorelsky, S. I.; Lee, G. M.; Korobkov, I.; Baker, R. T. *Organometallics*

2012, *32*, 12–15.

[120] Lee, G. M.; Harrison, D. J.; Korobkov, I.; Baker, R. T. *Chem. Commun.* **2013**, *50*, 1128–

1130.

[121] Harrison, D. J.; Lee, G. M.; Leclerc, M. C.; Korobkov, I.; Baker, R. T. *J. Am. Chem. Soc.*

2013, *135*, 18296–18299.

[122] Harrison, D. J.; Daniels, A. L.; Korobkov, I.; Baker, R. T. *Organometallics* **2015**, *34*,

4598–4604.

[123] Daniels, A. L.; Harrison, D. J.; Guan, J.; Gabidullin, B. M.; Hall, M. B.; Baker, R. T. *Angew. Chem. Int. Ed*. **2018**, *57*, 5772-5776.

[124] Chambers, R. D. In *Fluorine in Organic Chemistry*; CRC Press, 2004.

[125] Wang, S. Y.; Borden, W. T. *J. Am. Chem. Soc*. **1989**, *111*, 7282.

[126] O'Hagan, D.; Rzepa, H. S. *Chem. Comm*. **1997**, 645-652.

[127] Calm, J. M. *Int. J. Refrig.* **2008**, *31*, 1123–1133

[128] Kim, K.-H.; Shon, Z.-H.; Nguyen, H. T.; Jeon, E.-C. *Atmos. Environ.* **2011**, *45*, 1369–1382.

[129] McLinden, M. O.; Brown, J. S.; Brignoli, R.; Kazakov, A. F.; Domanski, P. A. *Nat. Commun.* **2017**, *8*, 14476.

[130] Boday, D. J. The State of Fluoropolymers. In *Advances in Fluorine-Containing Polymers*; Smith, D. W. Jr., Iacono, S. T., Boday, D. J., Kettwich, S. C., Eds.; American Chemical Society: Washington, 2012; pp 1-5.

[131] Banks, R. E.; Smart, B. E.; Tatlow, J. C., eds. In *Organofluorine Chemistry - Principles and Commercial Applications*; Springer International Publishing, 1994.

[132] Brothers, P. J.; Roper, W. R. *Chem. Rev*. **1988**, *88*, 1293-1326.

[133] Takahira, Y.; Morizawa, Y. *J. Am. Chem. Soc*. **2015**, *137*, 7031-7034.

[134] Gronert, S.; Keefe, J. R.; O'Ferrall, R. A. M. *J. Am. Chem. Soc*. **2011**, *133*, 3381-3389.

[135] Koh, M. J.; Nguyen, T. T.; Lam, J. K.; Torker, S.; Hyvl, J.; Schrock, R. R.; Hoveyda, A. H. *Nature* **2017**, *542*, 80.

[136] Vasiliu, M.; Arduengo III, A. J.; Dixon, D. A. *J. Phys. Chem. C*. **2014**, *118*, 13563-13577.

[137] Halle, L. F.; Armentrout, P. B.; Beauchamp, J. L. *Organometallics*. **1983**, *2*, 1829-1833.

[138] (a) Steinborn, D. *Fundamentals of organometallic catalysis*; Wiley-VCH: Weinheim, 2012. (b) Metal-Catalysis in Industrial Organic Processes; Chiusoli, G. P.; Maitlis, P. M., Eds.; RSC Publishing: Cambridge, 2006.

2 Tetracarbonyl(trifluoromethyl)cobalt(I) [$Co(CO)_4(CF_3)$] as a Precursor to New Cobalt Trifluoromethyl and Difluorocarbene Complexes

"A journey of a thousand miles begins with a single step."

– Lao Tzu

2.1 Context

As previously noted, with the successes of the Baker lab toward the first step of the Chauvin mechanism utilizing cobalt difluorocarbenes with TFE, specifically the [2+2] cycloaddition producing perfluorinated metallacyclobutanes, and with the inherent difficulty in the synthesis of [M]=CR^F_2 complexes, we pursued the synthesis of an easily modified M–CF_3 starting material. As mentioned in section 1.4.4, most difluorocarbenes are synthesized through intra- or intermolecular abstraction of fluorine by a Lewis acidic metal fragment or external Lewis acid respectively. This chapter aims to discern a methodology for the easy synthesis of [Co]=CF_2 carbenes and to showcase the effect of formal charge on reactivity of fluorocarbenes.

Transition metal fluoro-alkyls and perfluoro-carbenes are difficult to synthesize due to the lack of readily available –R^F sources outside of trifluoromethyl halides. In this Chapter we introduce a modification of the known synthesis of Na[$Co(CO)_4$] that was originally utilized in the formation of $Co(CF_3)(CO)_4$ which we then show to be an effective route to new difluoro-carbenes. This allowed us to synthesize and fully characterize 5 new Co–CF_3 complexes including a novel NHC-containing complex. Abstraction of a fluoride utilizing a Lewis acid then gave us ready access to two new cationic Co(I) difluorocarbenes which allowed us to more carefully discern the reactivity and behavior of these types of complexes.

These cationic cobalt carbenes did not exhibit the same nucleophilic character that previous neutral d^8 [Co]=CF_2 complexes had in that they reacted readily with water and did not undergo the same [2+2] cycloaddition reaction with TFE. These complexes did, however, exhibit unique Lewis-acidic properties in that a cobalt difluorocarbene was capable of fluoride abstraction from a [Co]–CF_3, further confirming the necessity for electron-donating ancillary ligands to stabilize heteroatom-containing carbenes.

2.1.1 Published Contribution

Harrison, D. J.; Daniels, A. L.; Korobkov, I.; Baker, R. T. *Organometallics* **2015**, *34*, 4598-4604.

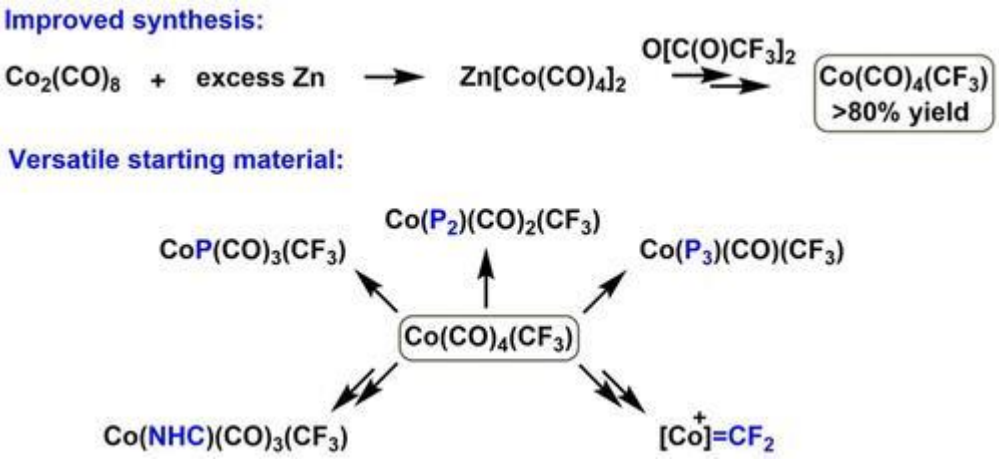

Here we present an improved synthesis of the known trifluoromethyl cobalt compound $Co(CF_3)(CO)_4$ (**1**), which gives significantly higher yields than previously reported methods. Treatment of **1** with P-donor ligands of varying denticity under thermal conditions afforded $Co(CF_3)(CO)_3[P(O\text{-}o\text{-}tolyl)_3]$ (**2**), $Co(CF_3)(CO)_2(DPPE)$ (**3**) and $Co(CF_3)(CO)(P_3)$ (**4**) in high isolated yields [DPPE = $Ph_2PCH_2CH_2PPh_2$; P_3 = $PhP(CH_2CH_2PPh_2)_2$]. The new cobalt N-heterocyclic carbene complex, $Co(CF_3)(CO)_3(SIPr)$ (**5**) [SIPr = 1,3-bis(2,6-diisopropylphenyl)imidazolidin-2-ylidene)], was obtained by phosphine substitution from $Co(CF_3)(CO)_3(PPh_3)$, a known compound efficiently prepared from **1**. Additionally, we report the synthesis of two rare cobalt difluorocarbene complexes ([Co]=CF_2) produced by fluoride

abstraction from **3** or **4**. These results are relevant to our efforts to assess the reactivity of first-row metal perfluoroalkyl and fluorocarbene complexes.

Author Contributions: The original concept for the paper (IE: synthesis of easily substituted $Co(CF_3)(CO)_4$) and writing of the manuscript was done by DJH with contributions and editing by ALD and RTB. ALD and DJH were responsible for the synthesis and characterization of all complexes listed within the manuscript. IK performed X-ray crystallography.

2.2 Introduction

Transition metal alkyl compounds ([M]–R) are tremendously important intermediates in catalysis[1] but the remarkable stability of perfluorinated analogues ([M]–R^F; R^F = perfluoroalkyl) has severely limited the scope of transition metal-mediated/-catalyzed processes[2] for the important field of fluoro-organic synthesis.[3,4,5] Notable exceptions include [Cu]–R^F reagents for stoichiometric perfluoroalkyl transfer to organic substrates[6] and increasing numbers of transition metal (e.g., Cu, Ni, Pd)[7] catalyzed C–R^F (where R^F is usually CF_3) bond-forming processes,[8] with relevance to high-value pharmaceuticals and agrochemicals.[3,4] Similarly, metal alkylidenes ([M]=CRR$^{'}$; R, R$^{'}$ = H, alkyl, aryl) are involved in a variety of catalytic transformations, most prominently alkene metathesis,[9] while fluorocarbenes (here, [M]=CFR^F, R^F = F or perfluoroalkyl) are quite rare and, until very recently, had not been implicated in catalysis. Importantly, Takahira and Morizawa reported (2015) catalytic cross metathesis between fluoroalkenes and *electron-rich* alkenes (CH_2=CHOR), with the participation of [Ru]=CF_2 intermediates, albeit with modest activities/yields.[10]

Recently, we reported the first formal [2+2] cycloaddition reactions of tetrafluoroethylene (TFE) to difluoro- and fluoro(trifluoromethyl)carbenes of cobalt ([Co]=CFR^F, R^F = F or CF_3) to afford metallacyclobutane products (Scheme 2.1).[11,12] These reactions constitute the first step in a perfluoroalkene/metal perfluorocarbene metathesis sequence[13] and could also be mechanistically relevant to metal-catalyzed fluoroalkene polymerization.[11,14,15,16] However, the metallacyclobutanes [i.e., bis(perfluoroalkyl) complexes] are considerably more stable than the metal-fluorocarbenes/free alkene, likely precluding catalysis for this system. Thus, significant

challenges confront fluoro-organometallic catalysis and we are undertaking fundamental studies on metal perfluoroalkyl and fluorocarbene complexes of first-row transition metals to assess their viability as catalytic intermediates in perfluoroalkene metathesis, polymerization and other reactions.

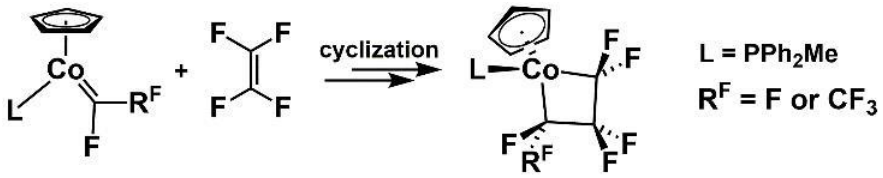

Scheme 2.1

Tetracarbonyl(trifluoromethyl)cobalt(I) $[Co(CF_3)(CO)_4]$ (**1**), first reported in the 1960s,[17] is a potentially useful precursor to cobalt trifluoromethyl and difluorocarbene complexes (i.e., [Co]–CF_3 and [Co]=CF_2) and was the subject of a recent computational investigation.[18] However, reactivity studies concerning this compound have been extremely limited over the past >50 years, presumably because of its cumbersome and low-yielding (<10% or unreported)[17,19] syntheses. To our knowledge, the substitution of carbonyl groups with PF_3 to yield $Co(CF_3)(CO)_{4-n}(PF_3)_n$ are the only reported reactions of **1**.[17c,20] The first preparations of **1** used sodium-mercury amalgam in large excess to reduce $Co_2(CO)_8$ to $Na[Co(CO)_4]$[17a,c] but it was later discovered that the amalgam was ineffective unless water was present.[21] Thus, anhydrous NaOH (in excess) can be used as the reductant to form $Na[Co(CO)_4]$[17d,21] but the process gives peroxide and/or water side-products (*via* OH radicals; Scheme 2.2A), which must be removed before using the sodium tetracarbonylcobaltate. The reaction of $Na[Co(CO)_4]$ with trifluoroacetic anhydride {$O[C(O)CF_3]_2$} followed by decarbonylation of the cobalt acyl intermediate[20,22] at 55°C gives **1** (Scheme 2.2B). Here, we report a more convenient, higher-yielding method for making **1**, which uses zinc metal as the reductant. Several carbonyl-substitution reactions to give phosphine, phosphite and N-heterocyclic carbene (NHC) cobalt(I) trifluoromethyl complexes from **1** are described and selected examples were converted to rare cobalt(I) (d^8) difluorocarbene complexes ($\{[Co^I]=CF_2\}^+$).[11,12]

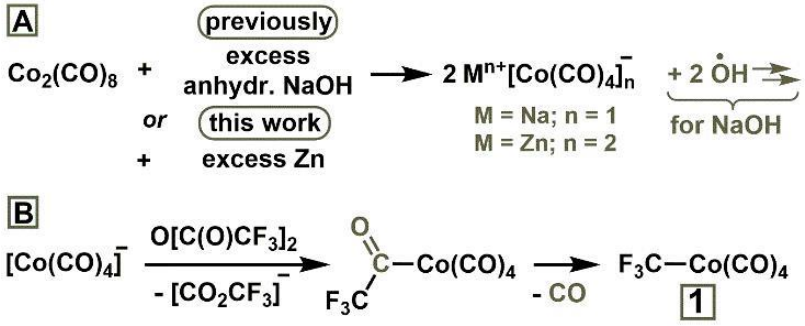

Scheme 2.2

2.2.1 Results and Discussion

Synthesis of 1. Our synthetic route to **1** uses zinc metal to reduce $Co_2(CO)_8$ (Scheme 2A) under mild conditions (RT, <2 atm).[23] As in the original procedure, the cobaltate reacts with electrophilic trifluoroacetic anhydride to form a cobalt acyl complex.[24] We did not isolate the [Co]–$C(O)CF_3$ intermediate but, rather, converted it to **1** at 55°C (Scheme 2B).[17a] The THF solvent and **1** (b.p. ~ 90°C)[17b,18] were transferred, under vacuum at room temperature, away from the non-volatile by-products, to give **1** (~0.5 M in THF; purity ≥ 98% by ^{19}F NMR spectroscopy) in ~80% yield based on $O[C(O)CF_3]_2$ (24 mmol scale).[25] Note that a sub-stoichiometric quantity of anhydride (0.8 equiv) was used to avoid contamination of the product with this volatile compound. Substantially better yields of **1** were obtained when zinc metal was employed as the reductant, compared to analogous reactions with NaOH,[21] under otherwise similar conditions (86% vs. 73%, 4.4 mmol scale, 1 equiv of anhydride). Although our results indicate a distinct advantage to using zinc metal, the low or unreported yields for **1** in the literature are likely accounted for by inefficient separation of **1** from the solvent[24] or failure to remove the by-products from the NaOH reduction (Scheme 2A) which results in decomposition of **1** during subsequent synthesis. With our approach, **1** is obtained in high purity as a THF solution, which was conveniently used in the following reactions.

Substitution reactions of 1; new [Co^I]–CF_3 complexes. With multi-gram quantities of **1** available, we began exploring its ligand substitution chemistry. The reaction of **1** with PPh_3 gives the known compound $Co(CF_3)(CO)_3(PPh_3)$, by carbonyl substitution,[17a,20,26] in >85% isolated yield (quantitative by ^{19}F and $^{31}P\{^1H\}$ NMR) (20 h, 22°C). Less Lewis-basic tri(o-tolyl)phosphite [P(O-*o*-Tol)$_3$] also displaces a CO group to furnish a new phosphite complex (**2**) (18 h, 50°C). The substitution of two or three carbonyl groups can be achieved with bi- and

tridentate phosphines, respectively, to produce **3** (18 h, reflux) and **4** (72 h, reflux) (Scheme 2.3; isolated yields are given in the scheme).

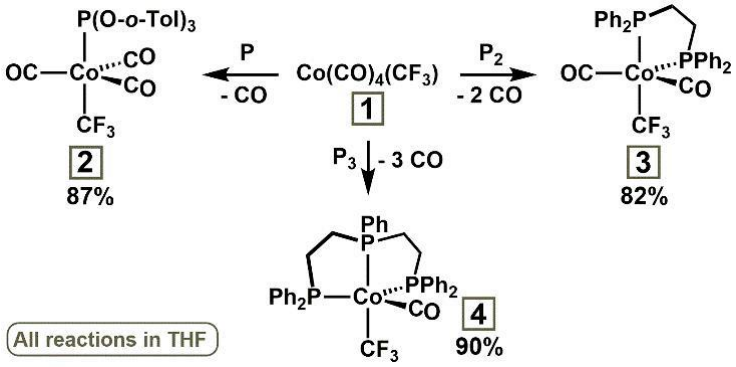

Scheme 2.3

The bulky diaryl N-heterocyclic carbene (NHC) compound, SIPr [bis(2,6-diisopropylphenyl)-4,5-dihydroimidazol-2-ylidene], reacts with **1** to afford a number of products, including the target $Co(CF_3)(CO)_3(SIPr)$ (**5**) (<30% NMR yield). However, **5** was obtained in 63% isolated yield by substitution of the phosphine ligand from $Co(CF_3)(CO)_3(PPh_3)$ with SIPr (120 h, reflux; Scheme 2.4), following a procedure similar to the one used by Llewellyn and Malcolm for making a related alkyl/NHC complex, $Co(CH_3)(CO)_3(IMes)$ [IMes = 1,3-bis(2,4,6-trimethylphenyl)imidazol-2-ylidene].[27] Compound **5** features three types of carbon-donor ligands bound to cobalt (i.e., CO, NHC, CF_3) and appears to be the first cobalt trifluoromethyl/NHC complex. Vicic and coworkers reported $Cu(CF_3)(NHC)$ (NHC = diisopropyl-4,5-dihydroimidazol-2-ylidene) compound.[6d]

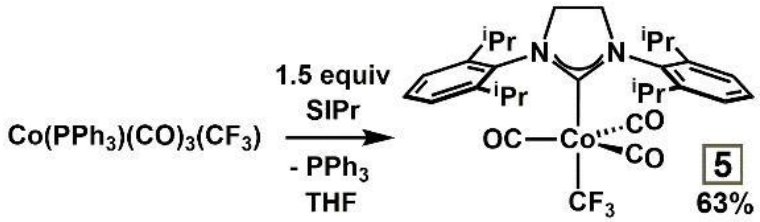

Scheme 2.4

Solid state structures of $[Co^I]$–CF_3 complexes. The molecular structures of **2**, **3**, **4**, and **5**, determined by single-crystal X-ray diffraction, are shown in Figure 2.1 and selected bond lengths are listed in Table 1 for the new compounds, $Co(CF_3)(CO)_3(PPh_3)$ [26] and **1** (computed[18]). The

variation in the Co–CF_3 bond length is generally small and within standard deviation for compounds **2**, **3** and **5**, although these bonds are marginally longer than the same bond in

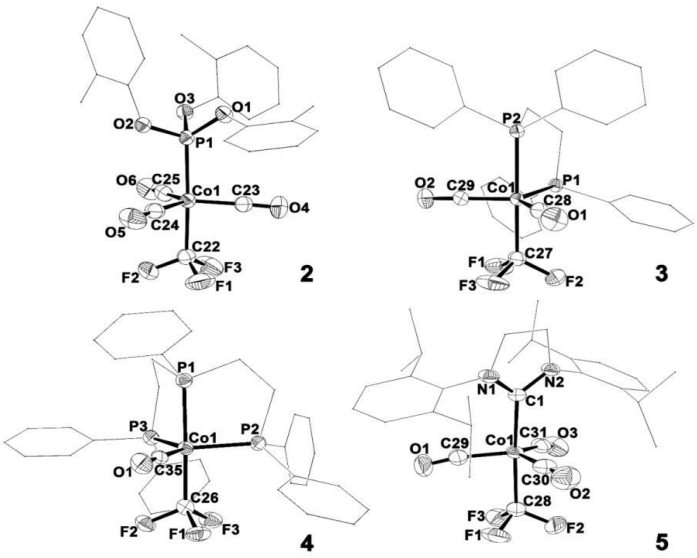

Figure 2.0.1: ORTEP structures of **2**, **3**, **4**, and **5** with 50% ellipsoids. Hydrogen atoms are omitted. Toluene solvent molecules appearing in the unit cells of **3** and **5** are not shown.

$Co(CF_3)(CO)_3(PPh_3)$ (Table 1). The Co–CF_3 bond in **4**, with the tridentate phosphine co-ligand, is shorter compared to the other complexes in Table 1, possibly reflecting a greater degree of π back-donation from the relatively electron-rich metal center to the C–F σ* orbitals.[2a] Also, the average C–F distance is slightly greater in **4** than the other compounds, although computational work has shown that this feature might be unrelated to the short metal-perfluoroalkyl bond.[2a] Compound **4** also features a relatively short Co–CO bond, likely due to π back-bonding effects. As expected, the metal-carbonyl bonds of **2**, with the π-accepting P(O-*o*-Tol)$_3$ co-ligand, are longer compared to $Co(CF_3)(CO)_3(PPh_3)$, which bears the stronger σ-donating PPh_3 ligand. However, Co–CO bonds of latter compound are shorter than those in **5**, despite the greater σ-donor ability of the NHC ligand. The longer Co–CO bonds in the NHC complex are likely caused by steric pressure between the carbonyl groups and the bulky NHC ligand. Indeed, the CO ligands are bent out of the equatorial plane, with the effect most pronounced for the two carbonyl ligands nearest to the isopropyl groups of the NHC.[28]

NMR data for [Co^{I}]–CF$_3$ complexes. The solution-phase NMR data is consistent with the solid-state structures for Co(PPh$_3$)(CO)$_3$(CF$_3$) and **2**, **4** and **5**. Complex **3**, however, gives a single ^{19}F NMR coupling constant [$^3J_{FP}$(avg) = 31 Hz] to the two non-equivalent (by ^{31}P NMR) phosphorous atoms of the DPPE ligand at RT, consistent with rapid axial/equatorial exchange of the P-atoms on the NMR timescale. Indeed, at –40°C, the ^{19}F NMR signal for **3** is a doublet-of-doublets [$^3J_{FP}$(*cis*) = 22 Hz, $^3J_{FP}$(*trans*) = 39 Hz] and variable temperature experiments established $\Delta G^{\ddagger}$ = 13.0 ± 0.3 kcal mol^{-1} for the exchange process (see Supporting Information). On the other hand, Co(PPh$_3$)(CO)$_3$(CF$_3$) and **4** showed no sign of fluxionality from –40°C to 40°C.

Complex	**Co–CF$_3$**	**C–F**	**Co–CO**	**C–O**
Co(PPh$_3$)(CO)$_3$(CF$_3$)[17a,20,26]	1.953(6)	1.358(7)	1.751(5)	1.172(7)
		1.344(8)	1.742(5)	1.175(7)
		1.352(8)	1.763(6)	1.177(8)
Co[P(O-*o*-tol)$_3$](CO)$_3$(CF$_3$) (**2**)	1.963(2)	1.355(3)	1.7919(18)	1.132(2)
		1.347(2)	1.795(2)	1.131(2)
		1.335(2)	1.796(2)	1.130(2)
Co(DPPE)(CO)$_2$(CF$_3$) (**3**)	1.9601(14)	1.345(5)[a]	1.7663(15)	1.143(2)
		1.347(6)[a]	1.7673(14)	1.1379(18)
		1.371(5)[a]		
Co(P$_3$)(CO)(CF$_3$) (**4**)	1.938(4)	1.382(4)	1.744(4)	1.138(4)
		1.383(4)		
		1.363(4)		

$Co(CF_3)(CO)_3(SIPr)$ (**5**)	1.964(2)	1.368(3) 1.359(3) 1.365(2)	1.777(2) 1.802(2) 1.799(2)	1.137(3) 1.135(2) 1.147(3)
$Co(CO)_4(CF_3)$ (**1**) (*computed*)	1.989	NA	1.828[b] 1.831	NA NA

Table 1: Selected bond distances (Å). All CO ligands are in the equatorial plane of the trigonal bipyramidal complexes, except where noted. The metric data for compound **1** are from DFT (B3LYP) computations.[18]

[a] Rotationally disordered CF_3 group; bond lengths for one of two orientations are given

[b] CO ligand in axial position (*trans* to CF_3)

IR data. Selected FT-IR data are listed in Table 2. As expected, the CO stretches move to lower energies with increasing σ electron donor ability of the ancillary ligands/electron density at the metal. The trend holds for the tricarbonyl complexes $Co(CF_3)(CO)_3(PPh_3)$, **2** and **5**: the electron-rich NHC complex (**5**) has the lowest ν(CO) and **2**, with the π-accepting $P(O\text{-}o\text{-}Tol)_3$ ligand, has the highest ν(CO). Likewise, the cationic difluorocarbenes (**6** and **7**, see below), have the highest frequency carbonyl stretches of all the complexes in Table 2, presumably due to the positive charge and π-accepting CF_2 ligand.

Complex	**CO stretching frequencies (cm^{-1})[a,b,c]**
$Co(PPh_3)(CO)_3(CF_3)$[17a,20,26]	**1993(s)**, 2004(s), 2071(w)
$Co[P(O\text{-}o\text{-}tol)_3](CO)_3(CF_3)$, **2**	**2002(s)**, 2017(m), 2085(w)
$Co(DPPE)(CO)_2(CF_3)$, **3**	1915(sh), **1941(s)**, 2000(s)
$Co(P_3)(CO)(CF_3)$, **4**	**1901(s)**
$Co(SIPr)(CO)_3(CF_3)$, **5**	**1975 (s)**, 1990(sh), 2061(w)

$[Co(DPPE)(CO)_2(=CF_2)](OTf)$, **6**	2012 (s), **2033 (s)**, 2078 (s)
$[Co(P_3)(CO)(=CF_2)](OTf)$, **7**	**2019(s)**

Table 2: FT-IR peaks for the metal carbonyl region.

[a] w = weak, m = medium, s = strong, sh = shoulder

[b] The highest-intensity peaks are bolded

[c] All data collected for the current study on a Nexus 6700 spectrometer (see Experimental section for additional details)

Fluoride-abstraction from $[Co^I]–CF_3$; new $[Co^I]=CF_2$ complexes. Having established **1** as a versatile precursor to new cobalt(I) trifluoromethyl complexes, we turned our attention to reactions of the trifluoromethyl group. Compounds **3** and **4** were cleanly converted to their respective difluorocarbenes, **6** and **7**, by fluoride-abstraction with Me_3SiOTf ($Tf = SO_2CF_3$) (Scheme 2.5A).[29] Attempts to generate the difluorocarbene complexes, using the same approach, from $Co(CF_3)(CO)_3(PPh_3)$, **2** and **5** were unsuccessful, likely indicating that two or more phosphine (strong σ donor) co-ligands are required to stabilize the cationic difluorocarbene complexes. The ^{19}F NMR spectrum of **6** does not change from –40°C to 40°C, pointing to a static structure in solution. In contrast, the parent trifluoromethyl complex, $Co(CF_3)(CO)_2(DPPE)$ (**3**), undergoes axial/equatorial phosphine exchange at RT on the NMR timescale (see above).

Interestingly, fluorocarbene complex **6** cleanly abstracts a fluoride from the trifluoromethyl complex **4** to produce **7** and **3** (Scheme 2.5B; quantitative ^{19}F NMR yield). Thus, we have demonstrated unusual fluoride-abstraction from a metal trifluoromethyl complex using an electron-deficient metal fluorocarbene, to give new $[M]–CF_3$ and $[M]=CF_2$ species. This finding supports the idea that electron-releasing co-ligands stabilize the $[Co]=CF_2$ motif.

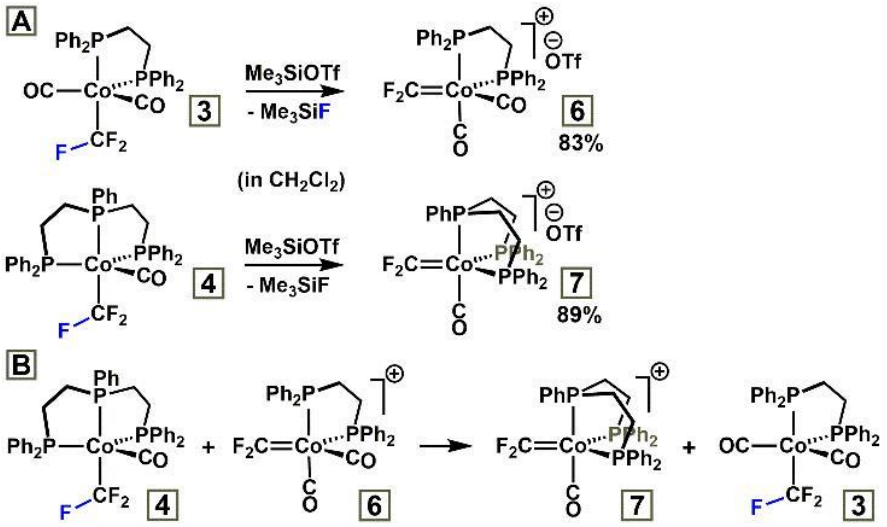

Scheme 2.5

Terminal first row metal fluorocarbenes (here, [M]=CFR^F; R^F = F or perfluoroalkyl) are very rare[2c,30] and, prior to our work, isolable [Co]=CFR^F complexes were unknown. The new compounds contain formally Co^I d^8 centers[31] and, in that regard, are similar to the cobalt fluorocarbenes we reported previously, which react with tetrafluoroethylene (CF_2=CF_2) to furnish cycloaddition products (see above).[11] Although the new complexes contain formally d^8 metals, they are also cationic and possess carbonyl co-ligands. We have noted the need for electron-rich metal fluorocarbenes for reactions with electron-deficient/electrophilic perfluoroalkenes.[11] Perhaps unsurprisingly, **6** and **7** failed to react with CF_2=CF_2 under thermal or photolytic conditions,[32] unlike the more electron-rich/charge-neutral CoCp(L)(=CFR^F) complexes (see above). Note that CpCo(PPh_2Me)(=CF_2) reacts with TFE in an associative fashion,[11] so ligand dissociation is not necessarily required for metallacycle formation.

Solid state structure of 7. The molecular structure of the P_3 difluorocarbene complex (**7**) (Figure 2) reveals Co=CF_2 and Co–CO bond lengths of 1.787(3) Å and 1.757(3) Å, respectively. For comparison, the cobalt-carbene contacts in CpCo(L)(=CF_2) are appreciably shorter [1.7395(14) for L = PPh_3; 1.743(2) for L = PPh_2Me]. We propose that the longer Co=CF_2 bonds in **7** indicate less effective M→CF_2 π overlap due to the cationic and relatively electron-poor nature of the cobalt center. Further, the apparent lack of electron density in the metal-carbene π bond is consistent with the fact that **7** does not form a cycloaddition product with tetrafluoroethylene.[32] The carbon atom of the CF_2 group is in the equatorial plane and the CO ligand occupies an axial sites *trans* to a phosphine donor. In complexes Co(CF_3)($CO)_3$(PPh_3)

and **2-5**, the carbonyl groups are invariably in the equatorial plane and not directly *trans* to other ligands (Figure 2.2).

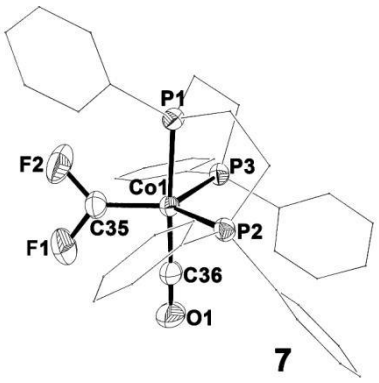

Figure 2.0.2: ORTEP representation of the molecular structure of **7** with 50% thermal probability ellipsoids. Hydrogen atoms, the rotationally disordered OTf^- anion and benzene solvent molecule are omitted and the carbon frame-work of the P3 ligand is shown as a wire cage structure for clarity. Selected bond distances [[Å]: Co(1)-C(35) = 1.787(3), Co(1)-C(36) = 1.757(3), O(1)-C(36) = 1.128(3), F(1)-C(35) = 1.340(3), F(2)-C(35) = 1.322(3).

2.2.2 Conclusion

In summary, we have described an improved route to $Co(CF_3)(CO)_4$ (**1**), which provides relatively convenient access to the rich thermal substitution chemistry of this long-known but little-studied compound. Mono-, di-, tridentate phosphine and NHC complexes were prepared in good to excellent yields. Metal fluoroalkyl compounds are potentially valuable for stoichiometric or catalytic fluoroalkyl group transfer but, as discussed above, the unusual stability of metal-perfluoroalkyl bonds poses an obstacle to such applications. The cobalt trifluoromethyl compounds described here and new derivatives should be useful for assessing factors that stabilize/destabilize metal-perfluoroalkyl bonding, which could lead to new catalytic processes involving fluorinated substrates/products. The structural data presented above shows that the $Co–CF_3$ bond lengths are quite insensitive to the other ligands on the metal but more detailed reactivity studies will be required to establish whether the manipulation of co-ligands can facilitate metal-perfluoroalkyl bond activation. It should also be possible to study the effect of

metal oxidation state on Co–CF_3 bonding; for example, oxidation of the Co^{I} compounds to substitutionally labile Co^{II} is likely to give relatively reactive metal perfluoroalkyl complexes. Finally, we demonstrated that the metal-bound CF_3 groups could be converted to difluorocarbene ligands (CF_2) by fluoride-abstraction, depending on the electronic environment at the metal, with relatively electron-releasing ligands favoring the formation of carbene complexes. First-row metal fluorocarbenes are uncommon and we are investigating potential applications for these compounds.

2.2.2.1 Experimental Section

General. Experiments were conducted under nitrogen, using Schlenk techniques or an MBraun glove box. All solvents were deoxygenated by purging with nitrogen. Toluene, hexanes, diethyl ether (DEE) and tetrahydrofuran (THF) were dried on columns of activated alumina using a J. C. Meyer (formerly Glass Contours) solvent purification system. Dichloromethane (DCM) and $CDCl_3$ were dried by refluxing solution over calcium hydride (CaH_2) followed by distillation. C_6D_6 was dried over activated alumina (heated at 300°C > 8 h under vacuum) (~15 wt. %), All solvents were stored over activated (heated at 250°C for >6 h under vacuum) 4 Å molecular sieves. Glassware was oven-dried at 150°C for > 2 h. The following chemicals were obtained commercially: $Co_2(CO)_8$ (Strem, stabilized with 1-5% hexane), trifluoroacetic anhydride (Aldrich, >99%), PPh_3 (Strem, 99%), tri(o-tolyl)phosphite (Alfa Aesar, ~97%), 1,2-bis(diphenylphosphino)ethane (Strem, 99%), bis(2-diphenylphosphinoethyl)phenylphosphine (Strem, 97%), zinc dust (Alfa Aesar, 100 mesh, 99.9%), trimethylsilyl triflate (Aldrich, 98%), C_6D_6/$CDCl_3$ (Cambridge Isotope Labs, d-99.5%). SIPr was made following a literature procedure.[33] ^{1}H, ^{19}F and $^{31}P\{^{1}H\}$ NMR spectra were recorded on 300 MHz Bruker Avance or AvanceII instruments at RT (21-23°C). ^{1}H NMR spectra were referenced to the residual proton peaks (C_6D_6: 7.16 ppm; $CDCl_3$: 7.26 ppm). ^{19}F NMR spectra were referenced to internal 1,3-bis(trifluoromethyl)benzene (BTB) (Aldrich, 99%), set to –63.5 ppm. ^{19}F NMR yields were calculated from product integration relative to a known quantity of BTB using 9 s delay times. $^{31}P\{^{1}H\}$NMR data were referenced to external H_3PO_4, set to 0.0 ppm. IR data were obtained on a Nicolet Nexus 6700 FT-IR spectrometer using neat/solid samples for compounds $Co(PPh_3)(CO)_3(CF_3)$ and **2-7**. For **1**, the IR spectrum was collected with a Nicolet NEXUS 670 FT-IR instrument and the sample was prepared by allowing a THF solution of **1** to evaporate on

a NaCl plate under a stream of nitrogen. Elemental analyses were performed at the University of Montreal (Montreal, Quebec, Canada).

Preparative synthesis of $Co(CF_3)(CO)_4$ (1) using $Zn[Co(CO)_4]_2$. $Co_2(CO)_8$ (5.00 g, 14.6 mmol) and activated[34] zinc powder (2.00 g, 30.6 mmol, 2 equiv) were combined as solids and cooled to –80°C (acetone/dry ice). THF (35 mL), also cooled to –80°C, was added with stirring. The flask was removed from the dry ice bath and sealed with a pressure release valve calibrated to vent at ~2 atm to account for CO loss [$Co_2(CO)_8$ gradually evolves CO in THF]. Vigorous stirring was continued for 18 h; the color of the solution changed from dark red to green-yellow. The mixture was purged with nitrogen for 2 min to remove CO and then filtered to remove unreacted zinc. The origin flask/zinc were washed with THF (1 mL x 3) and these washings were collected with the rest of the filtrate. The $Zn[Co(CO)_4]_2$/THF solution was cooled to –80°C and $O[C(O)CF_3]_2$ (3.2 mL, 23 mmol; 0.8 equiv relative to Co to avoid unreacted anhydride in the product) was added dropwise over 10 min to the stirred/cooled solution. Once the addition was complete, the vessel was removed from the cooling bath and allowed to come to RT, over ~0.5 h, with stirring (color changed to orange-yellow upon warming to RT). The flask was then fitted with a nitrogen-flushed condenser and heated to 55°C for 1 h to induce decarbonylation of the $Co(CO)_4[C(O)CF_3]$ intermediate (caution: carbon monoxide is released; color became darker orange-brown). The mixture was degassed with three freeze-pump-thaw cycles. The volatile components (i.e., **1** and THF) were transferred under static vacuum (<10 mTorr) to a liquid nitrogen-cooled flask, keeping the origin flask at or below RT, leaving behind dark brown-orange residue. THF (~3 mL) was added to the residue and, after three freeze-pump-thaw cycles, the remaining THF/**1** were transferred under vacuum to the receiving flask (as above). The resulting yellow-orange **1**/THF solution {40 mL, 0.47 M, 19 mmol (4.3 g) of **1**; 83% based on $O[C(O)CF_3]_2$, purity ≥ 98%}, or similar solutions, were used in all further reactions involving **1**. IR (neat on NaCl, Nexus 670 instrument) 701 (m), 796 (w), 1032 (m), 1074 (m), 1152 (w), 1207 (w), 1259 (w), 1680 (w, br), 1851 (s), 2051 (s), 2082 (sh), 2121 (m), 2810-3010 (w) cm^{-1}. ^{19}F NMR (282 MHz, THF with C_6D_6 capillary) 8.3 (s, $C\underline{F}_3$).

Synthesis of 1 using $Na[Co(CO)_4]$ (for comparison to $Zn[Co(CO)_4]_2$). $Na[Co(CO)_4]$ was made using a slightly modified literature procedure[21] as follows: $Co_2(CO)_8$ (1.50 g, 4.41 mmol) and anhydrous NaOH (702 mg, 17.5 mmol) were combined as solids and cooled to –80°C in an acetone/dry ice bath. THF (10 mL), also cooled to –80°C, was added by canula with stirring.

After 15 min, the vessel was removed from the acetone/dry ice bath and stirred at RT for 1.5 h. The mixture was filtered; the purple solid was washed with THF (~1 mL x 3) and these washings were collected with the rest of the faintly yellow filtrate. The solvent/volatiles were removed under vacuum, yielding white solid. Note: if the volatile components (including water and/or peroxide by-products) are not removed before the reaction with $O[C(O)CF_3]_2$, the preparation of **1** fails outright. The solid was dissolved in THF (~12 mL) and the solution was cooled to –80°C before adding $O[C(O)CF_3]_2$ (1.2 mL, 1.8 g, 8.6 mmol, ~1 equiv relative to Co) was added dropwise over 10 min to the cooled/stirred solution. The vessel was allowed to come to RT, fitted with a nitrogen-flushed condenser, and heated at 55°C for 1 h (caution: carbon monoxide is released). After degassing with three freeze-pump-thaw cycles, the volatile components were transferred under static vacuum (<10 mTorr) to a liquid nitrogen-cooled vessel, which gave yellow solution. Yield: 13 mL (**1**: 0.48 M in THF), 6.2 mmol, 70% based on $Co(CO)_4(CF_3)$. Note that the sample was contaminated with a large number of minor, unknown species in the –50 to –150 ppm region (12% of total ^{19}F NMR integration).

Synthesis of 1 using $Zn[Co(CO)_4]_2$ (for comparison to $Na[Co(CO)_4]$). The procedure was identical to the one described above, except activated Zn powder (574 mg, 8.78 mmol) was substituted for NaOH and the reduction was allowed to proceed at RT for 17 h. Also, after filtering to remove excess Zn, and washing the solid with THF (~1 mL x 3), the solvent was not removed from the filtrate/washings; the resulting solution was used directly for the reaction with $O[C(O)CF_3]_2$, as detailed above. Yield: 12 mL (**1**: 0.63 M in THF), 7.6 mmol, 86% based on $Co(CO)_4(CF_3)$. Note that the sample contained unreacted anhydride (0.1 equiv relative to **1**) but was otherwise pure.

Modified synthesis of $Co(CF_3)(CO)_3(PPh_3)$[17a,20,26] PPh_3 (250 mg, 0.953 mmol) was combined with **1** (3.2 mL, 0.33 M, 1.05 mmol) and the solution was stirred at RT for ~20 h under nitrogen (vented to an oil bubbler to allow CO to escape). A portion of the yellow solution was removed for NMR analysis. ^{19}F NMR data showed a very small peak for **1** and the PPh_3 was completely consumed, as determined by $^{31}P\{^1H\}$ NMR. ^{19}F NMR (282 MHz, THF with C_6D_6 capillary) δ 8.2 (minor s, residual **1**), 8.4 [d, $^3J_{FP}$ = 40 Hz, $C\underline{F}_3$]. Removal of the volatiles, including **1**, under vacuum afforded $Co(C\underline{F}_3)(CO)_3(PPh_3)$ (>98% purity by ^{19}F and ^{31}P NMR) in >85% yield on 0.3-1.5 mmol scale (off-white solid). This experiment also corroborated the concentration of the **1**/THF solution, determined by product integration relative to the internal standard, BTB. IR

(neat, Nexus 6700 instrument) 541(w), 570(m), 650(w), 691(s), 708(m), 749(m), 807(m), 849(w), 923(w), 992(s), 1000(s), 1027(s), 1042(m), 1096(m), 1188(w), 1263(w), 1310(w), 1434(m), 1483(w), 1827 (w), 1905(w), 1935(m), 1993(s), 2004(s), 2071(w), 2830-3150(w) cm^{-1}. ^{1}H NMR (300 MHz, C_6D_6) δ 6.78-7.02 (ov m, 9H, Ar–H), 7.35 (m, 6H, Ar–H). ^{19}F NMR (282 MHz, C_6D_6) δ 9.3 (d, $^{3}J_{FP}$ = 40 Hz, CF_3). $^{31}P\{^{1}H\}$ NMR (121 Hz, C_6D_6) δ 50.7 ppm (q, $^{3}J_{PF}$ = 40 Hz).

Synthesis of $Co(CF_3)(CO)_2[P(O\text{-}o\text{-}tol)_3]$ (2). $P(O\text{-}o\text{-}Tol)_3$ (285 mg, 0.810 mmol), dissolved in THF (0.5 mL), was added to a stirred THF solution of **1** (0.33 M, 2.7 mL, 0.89 mmol). The mixture was stirred at 50°C for 18 h under nitrogen (vented to an oil bubbler to allow CO to escape), giving faintly yellow solution. The solvent/volatiles were removed under vacuum to yield colorless oily residue. DEE (1.5 mL) was added to the residue and removed under vacuum (x2), giving off-white powder. Yield: 440 mg, 0.78 mmol, 87% based on **1**. IR (neat, Nexus 6700 instrument) 542 (w), 568 (m), 605 (m), 705 (m), 716 (m), 750 (s), 754 (s), 796 (m), 802 (m), 919 (s), 926 (sh), 937 (m), 987 (w), 1030 (s), 1057 (m), 1105 (m), 1162 (m), 1182 (w), 1221 (w), 1228 (sh), 1259 (w), 1382 (w), 1436 (w), 1463 (w), 1490 (m), 1584 (w), 1939(w), 1975(sh), 2002(s), 2017(m), 2085(w), 2830-3110 (w) cm^{-1}. ^{1}H NMR (300 MHz, C_6D_6) δ 1.97 (s, 9H, CH_3), 6.70-6.91 (ov m, 9H Ar–H), 7.18-7.28 (m, 3H Ar–H). ^{19}F NMR (282 MHz, C_6D_6) δ 7.6 ppm (d, $^{3}J_{FP}$ = 64 Hz, CF_3). $^{31}P\{^{1}H\}$ NMR (121 MHz, C_6D_6) δ 147.1 ppm (q, $^{3}J_{PF}$ = 64 Hz). Anal. Calc. for $C_{25}H_{21}CoF_3O_6P$: C, 53.20, H, 3.72. Found: C, 52.97, H, 3.83. Crystals suitable for X-ray analysis were grown from hexanes at –35°C.

Synthesis of $Co(CF_3)(CO)_2$(DPPE) (3). A THF solution of **1** (0.33 M, 5.7 mL, 1.9 mmol) was added to DPPE (765 mg, 1.92 mmol). The mixture was heated to reflux under nitrogen (vented to an oil bubbler to allow CO to escape), with a reflux condenser, for 18 h, yielding homogeneous yellow solution. The vessel was allowed to cool to RT and approximately half of the solvent was removed under vacuum; hexanes (~12 mL) were added, causing yellow solid to form. The suspension was cooled in the GB freezer at –35°C overnight before recovering the yellow solid by filtration, washing with hexanes (~3.0 mL x 4) and drying under reduced pressure. Yield: 910 mg, 1.56 mmol, 82%. IR (neat, Nexus 6700 instrument) 529(w), 542(w), 553(m), 566(m), 617(w), 649(m), 674(s), 691(s), 701(s), 747(m), 806(m), 878(m), 930(m), 975(sh), 983(s), 1002(m), 1038(s), 1101(m), 1179(w), 1312(w), 1410(w), 1435(m), 1481(w), 1915(sh), 1941(s), 2000(s), 2072(w), 2760-3130 cm^{-1}. ^{1}H NMR (300 MHz, C_6D_6) δ 1.91 (m,

4H, C<u>H</u>$_2$C<u>H</u>$_2$), 6.89-7.14 (ov br m, 12H, Ar–<u>H</u>), 7.29-7.80 (br m, 8H, Ar–<u>H</u>). ^{19}F NMR (282 MHz, C_6D_6) δ 9.8 (apparent t, $^3J_{FP}$ = 31 Hz). $^{31}P\{^1H\}$ NMR (121 MHz, C_6D_6) δ 59.9 (br apparent s, $\omega_{1/2}$ = 190 Hz, 1P), 78.2 (br apparent s, $\omega_{1/2}$ = 190 Hz, 1P). Anal. Calc. for $C_{29}H_{24}CoF_3O_2P_2$: C, 59.81; H, 4.15. Found: C, 59.35, H, 4.05. Crystals suitable for X-ray analysis were grown from hexanes/toluene at –35°C.

Synthesis of Co(CF$_3$)(CO)(P$_3$) [P$_3$ = (Ph$_2$PCH$_2$CH$_2$)$_2$PPh] (4). P$_3$ (352 mg, 0.658 mmol) was added to a THF solution of **1** (0.33 M, 2.0 mL, 0.66 mmol) and the mixture was heated to reflux under nitrogen (vented to an oil bubbler to allow CO to escape) for 72 h. The color of the solution changed from yellow to green and eventually became yellow again with bright yellow precipitate. The vessel was allowed to cool to RT. Hexanes (5 mL) were added and the mixture was cooled at –35°C overnight. The bright yellow solid was recovered by filtration, washed with hexanes (~1 mL x 3) and dried under vacuum. Yield: 408 mg, 0.591 mmol, 90% based on **1**. IR (neat, Nexus 6700 instrument) 542 (m), 618 (w), 634 (m), 651 (m), 673 (m), 691 (s), 738 (m), 751 (m), 800 (m), 818 (m), 845 (w), 867 (m), 884 (w), 914 (sh), 926 (m), 944 (s), 956 (m), 973 (m), 999 (w), 1035 (s), 1091 (m), 1106 (w), 1309 (w), 1414 (w), 1434 (m), 1484 (m), 1571 (w), 1586 (w), 1862(w), 1901(s), 2810-3130 (w) cm^{-1}. ^{1}H NMR (300 MHz, $CDCl_3$) δ 1.78-2.13 [ov m, 4H, C(sp^3)–H of P$_3$ ligand], 2.14-2.62 [ov m, 4H, C(sp^3)–H of P$_3$ ligand], 7.08-7.31 (ov m, 11H, Ar–<u>H</u>), 7.32-7.43 (ov m, 9H, Ar–<u>H</u>), 7.80-7.93 (ov m, 5H, Ar–<u>H</u>). ^{19}F NMR (282 MHz, $CDCl_3$) δ 11.3 (dt, $^3J_{FP}$ = 24 Hz, $^3J_{FP}$ = 39 Hz, C<u>F</u>$_3$). $^{31}P\{^1H\}$ NMR (121 MHz, $CDCl_3$) δ 64.4 (br apparent s, $\omega_{1/2} \approx$ 90 Hz, 2P, <u>P</u>Ph$_2$), 106.8 (m, 1P, R$_2$<u>P</u>Ph). Anal. Calc. for $C_{36}H_{33}CoF_3OP_3$: C, 62.62, H, 4.78. Found: C, 62.67, H, 4.78. Crystals suitable for X-ray analysis were grown from DCM/DEE at RT.

Synthesis of Co(CF$_3$)(CO)$_3$(SIPr) (5). Co(CF$_3$)(CO)$_3$(PPh$_3$) (500 mg, 1.05 mmol) and SIPr (617 mg, 1.58 mmol) were dissolved in THF (3.5 mL) and the yellow solution was heated to reflux for 5 days, causing the solution to become brown with light colored precipitate. The vessel was allowed to come to room temperature and the solvent volume was reduced by ~25% under vacuum. Hexanes (~12 mL) were added. The suspension was cooled at –35°C overnight before recovering the light brown solid by filtration, washing with hexanes (~3 mL x 3) and drying under vacuum. Yield: 400 mg, 0.664 mmol, 63% yield based on Co(PPh$_3$)(CO)$_3$(CF$_3$). IR (neat, Nexus 6700 instrument) 574 (m), 699 (w), 762 (m), 807 (m), 902 (w), 935 (w), 1000 (s), 1013 (sh), 1040 (s), 1107 (w), 1181 (w), 1240 (m), 1267 (m), 1323 (w), 1366 (w), 1386 (w),

1411 (sh), 1423 (m), 1451 (m), 1460 (sh), 1476 (m), 1590 (w), 1625 (w), 1949(sh), 1975 (s), 1990(sh), 2061(w), 2871 (w), 2936 (w), 2967 (m), 3026 (w), 3068 (w) cm^{-1}. ^{1}H NMR (300 MHz, C_6D_6) δ 1.06 (d, $^{3}J_{HH}$ = 7 Hz, 12H, C<u>H</u>$_3$), 1.45 (d, $^{3}J_{HH}$ = 7 Hz, 12H, C<u>H</u>$_3$), 3.08 [septet, $^{3}J_{HH}$ = 7 Hz, 4H, C<u>H</u>$(CH_3)_2$], 3.31 (s, 4H, C<u>H</u>$_2$C<u>H</u>$_2$), 7.07 (m, 4H, Ar–<u>H</u>), 7.23 (m, 2H, Ar–<u>H</u>). ^{19}F NMR (282 Hz, C_6D_6) δ 2.6 (s). Anal. Calc. for $C_{31}H_{38}CoF_3N_2O_3$: C, 61.79, H, 6.36, N, 4.65. Found: C, 62.26, H, 6.56, N, 4.71. Crystals suitable for X-ray analysis were grown from hexanes/toluene at RT.

Synthesis of [Co(CO)$_2$(=CF$_2$)(DPPE)](OTf) (6). Me_3SiOTf (112 μL, 138 mg, 0.621 mmol), dissolved in DCM (1 mL), was added to a solution of **3** (300 mg, 0.515 mmol) in DCM (4 mL), with stirring, producing dark orange solution. Stirring at RT was continued for 1 h and then the solvent/volatiles were removed under vacuum, producing oily solid. This material was dissolved in DCM (~3 mL); hexanes (~7 mL) were added and the suspension was cooled (–35^{o}C) overnight. The orange solid was recovered by filtration, washed with DEE (1.5 mL x 3) and dried under vacuum. Yield: 305 mg, 0.428 mmol, 83% based on **3**. IR (neat, Nexus 6700 instrument) 541 (m), 571 (m), 634 (s), 655 (w), 678 (m), 692 (s), 697 (s), 747 (s), 805 (m), 850 (w), 879 (w), 930 (w), 999 (m), 1027 (s), 1074 (w), 1099 (s), 1152 (s), 1177 (s), 1221 (s), 1237 (s), 1263 (m), 1269 (m), 1300 (m), 1409 (w), 1485 (w), 1574 (w), 1587 (w), 1943(w), 2012 (s), 2033 (s), 2078 (s), 2936 (w), 3062 (w), 3177 (w, br) cm^{-1}. ^{1}H NMR (300 MHz, $CDCl_3$) δ 3.14 (m, 4H, C<u>H</u>$_2$C<u>H</u>$_2$), 7.48-7.68 (ov m, 20H, Ar–<u>H</u>). ^{19}F NMR (282 Hz, $CDCl_3$) δ –78.6 (br s, 3F, SO_2C<u>F</u>$_3$), 119.8 (t, $^{3}J_{FP}$ = 26 Hz, 2F, C<u>F</u>$_2$). $^{31}P\{^{1}H\}$ NMR (121 MHz, $CDCl_3$) δ 78.4 (br m, 2P, CoP_2). Anal. Calc. for $C_{30}H_{24}CoF_5O_5P_2S$: C, 50.58, H, 3.40, S, 4.50. Found: C, 50.08, H, 3.47, S, 4.90.

Synthesis of [Co(CO)(=CF$_2$)(P$_3$)](OTf) (7). The procedure described above was followed, on approximately the same scale (345 mg, 0.500 mmol of **4**). Yield: 365 mg, 0.445 mmol, 89% based on **4**. IR (neat, Nexus 6700 instrument) 529 (w), 555 (m), 571 (m), 592 (m), 635 (s), 676 (s), 690 (s), 705 (s), 727 (m), 747 (s), 802 (m), 820 (m), 847 (w), 872 (m), 885 (w), 975 (w), 999 (m), 1029 (s), 1051 (s), 1097 (m), 1146 (s), 1190 (m), 1225 (m), 1263 (s), 1308 (w), 1401 (w), 1422 (w), 1436 (m), 1485 (w), 1573 (w), 1905 (w), 1976(m), 2019(s), 2085 (w), 2880-3120 (w). ^{1}H NMR (300 MHz, $CDCl_3$) δ 2.18-2.40 [ov m, 2H, C(sp^3)–H of P_3 ligand], 2.79 [m, 1H, C(sp^3)–H of P_3 ligand], 2.85-3.09 [ov m, 3H, C(sp^3)–H of P_3 ligand], 3.12-3.49 [ov m, 2H, C(sp^3)–H of P_3 ligand], 7.01-7.20 (ov m, 8H, Ar–<u>H</u>), 7.22-7.39 (ov m, 6H, Ar–<u>H</u>), 7.42-7.57 (ov

m, 7H, Ar–H), 7.58-7.69 (ov m, 4H, Ar–H). ^{19}F NMR (282 Hz, $CDCl_3$) δ –78.4 (br s, 3F, SO_2CF_3), 99.2 (m, 2F, CF_2). ^{19}F NMR (282 Hz, THF with C_6D_6 capillary) δ –78.6 (br s, 3F, SO_2CF_3), 96.0 (td, $^3J_{FP}$ = 30 and 12 Hz, 2F, CF_2). $^{31}P\{^1H\}$ (121 MHz, $CDCl_3$) δ 71.4 (br m, 2P, Ph_2PR), 108.8 (br m, 1P, R_2PPh). Anal. Calc. for $C_{37}H_{33}CoF_5O_4P_3S$: C, 54.16; H, 4.05; S, 3.91. Found: C, 53.91, H, 4.06, S, 3.85. Crystals suitable for X-ray analysis were grown from benzene/hexanes at RT.

Reaction of 4 with 6 to yield 3 and 7 ([Co]–CF_3/[Co]=CF_2 exchange). Compounds **4** (50 mg, 0.072 mmol) and **6** (52 mg, 0.072 mmol) were combined as solids and dissolved in DCM (3 mL), with stirring, producing dark orange solution. The mixture was stirred at RT for 1 h. An aliquot (0.5 mL) was removed for NMR analysis. ^{19}F and ^{31}P NMR data showed quantitative (relative to known BTB) conversion to **3** and **7**. ^{19}F (282 MHz) and $^{31}P\{^1H\}$ (121 MHz) NMR data in DCM with a C_6D_6 capillary: **3**: ^{19}F δ 8.8 (apparent t, $^3J_{FP}$ = 30 Hz). $^{31}P\{^1H\}$ δ 63.0 (br apparent s, $\omega_{1/2}$ = 180 Hz, 1P), 81.2 (br apparent s, $\omega_{1/2}$ = 180 Hz, 1P). **7**: ^{19}F δ –78.9 (br s, 3F, SO_2CF_3), 99.6 (m, 2F, CF_2). $^{31}P\{^1H\}$ δ 74.4 (br m, 2P, Ph_2PR), 112.4 (br m, 1P, R_2PPh).

2.2.3 Supplemental

Details for X-ray Crystallography. For 2, 3, 4, 5 and 7: samples were mounted on thin glass fibers using paraffin oil and were cooled to 200°K prior to data collection. Data were collected on a Bruker AXS KAPPA single crystal diffractometer equipped with a sealed Mo tube source (wavelength 0.71073Å) APEX II CCD detector. Raw data collection and processing were performed with APEX II software package from BRUKER AXS.15 Diffraction data were collected with a sequence of 0.5° ω scans at 0, 90, 180, and 270° in φ. Initial unit cell parameters were determined from 60 data frames collected at the different sections of the Ewald sphere. Semi-empirical absorption corrections based on equivalent reflections were applied. Systematic absences in the diffraction data set and unit-cell parameters were consistent with triclinic systems. Solutions in centrosymmetric space group yielded chemically reasonable and computationally stable results of refinement. The structures were solved by direct methods, completed with difference Fourier synthesis, and refined with full-matrix least-squares procedures based on F2. In the structure, compound molecules are situated in the general position. All non-hydrogen atoms were refined anisotropically with satisfactory thermal

parameters values. Additional crystallographic data and selected data collection parameters are reported below.

$Co(CF_3)(CO)_3[P(O\text{-}o\text{-}Tol)_3]$ (2): Empirical formula: $C_{25}H_{21}CoF_3O_6P$; FW = 564.32; Crystal size: 0.170 x 0.150 x 0.100 mm^3; Crystal system: monoclinic; Space group: P21/c (No14); Z = 4; a = 10.9801(2) Å, b = 13.0816(3) Å, c = 17.8831(4) Å, α = 90°, β = 102.5792(13)°, γ = 90°; Volume = 2507.02(9) Å3; Calculated density = 1.495 Mg/m^3; Absorption coefficient = 0.809 mm-1; F(000) = 1152; Θ range for data collection: 1.900 to 28.302°; Limiting Indices: -14≤h≤14, -13≤k≤17, -22≤l≤23: Reflections collected / unique: 18671/6162; R(int) = 0.0253; Completeness to Θ = 25.242°: 98.9%; Max. and min. transmission: 0.7457 and 0.6703; Data / restraints / parameters: 6162 / 0 / 325; Goodness-of-fit on F2: 1.016; Final R indices [I>2σ(I)]: R1 = 0.0348, wR2 = 0.0872; R indices (all data): R1 = 0.0493, wR2 = 0.0956; Largest diff. peak/hole: 0.438 / -0.328 e.Å-3.

$Co(CF_3)(CO)_2(DPPE)$ (3): Empirical formula: $C_{32.50}H_{28}CoF_3O_2P_2$; FW = 628.42; Crystal size: 0.150 x 0.110 x 0.090 mm^3; Crystal system: monoclinic; Space group: P21/c (No14); Z = 4; a = 15.8852(3) Å, b = 12.0588(2) Å, c = 15.3725(3) Å, α = 90°, β = 96.6240(9)°, γ = 90°; Volume = 2925.04(9) Å3; Calculated density = 1.427 Mg/m^3; Absorption coefficient = 0.744 mm-1; F(000) = 1292; Θ range for data collection: 2.126 to 28.327°; Limiting Indices: -16≤h≤21, -16≤k≤15, -20≤l≤20: Reflections collected / unique: 29290 / 7244; R(int) = 0.0188;Completeness to Θ = 25.242°: 99.0 %; Max. and min. transmission: 0.7457 and 0.6814; Data / restraints / parameters: 7244 / 139 / 377; Goodness-of-fit on F2: 1.024; Final R indices [I>2σ(I)]: R1 = 0.0297, wR2 = 0.0781; R indices (all data): R1 = 0.0349, wR2 = 0.0817; Largest diff. peak/hole: 0.750 / -0.360 e.Å-3. Co(P3)(CO)(CF3) (4): Empirical formula: C36H33CoF3OP3; FW = 690.46; Crystal size: 0.280 x 0.080 x 0.060 mm3; Crystal system: Orthorhombic; Space group: P212121 (No19);Z = 4;a = 7.9032(5) Å, b = 19.0147(14) Å, c = 21.3182(14) Å, α = 90°, β = 90°, γ = 90°; Volume = 3203.6(4) Å3; Calculated density = 1.432 Mg/m3; Absorption coefficient = 0.732 mm-1; F(000) = 1424; Θ range for data collection: 2.142 to 28.381°; Limiting Indices: -10≤h≤10, -25≤k≤25, -28≤l≤24: Reflections collected /unique: 26231 / 7908; R(int) = 0.0595; Completeness to Θ = 25.242°: 99.8 %; Max. and min. transmission: 0.7457 and 0.6475; Data / restraints / parameters: 7908 / 0 / 397; Goodness-of-fit on F2: 1.011; Final R indices [I>2σ(I)]: R1 = 0.0405, wR2 = 0.0689; R indices (all data): R1 = 0.0626, wR2 = 0.0757; Largest diff. peak/hole: 0.342 / -0.281 e.Å-3.

$Co(CF_3)(CO)_3(SIPr)$ (5): Empirical formula: $C_{38}H_{46}CoF_3N_2O_3$; FW = 694.70; Crystal size: 0.260 x 0.040 x 0.020 mm^3; Crystal system: Monoclinic; Space group: P21/n (No14); Z = 4; a = 17.7173(9) Å, b = 9.8573(5) Å, c = 21.8664(11) Å, α = 90°, β = 104.749(2)°, γ = 90°; Volume = 3693.0(3) Å3; Calculated density = 1.249 Mg/m3; Absorption coefficient = 0.516 mm-1; F(000) = 1464; Θ range for data collection: 1.710 to 28.324°; Limiting S2 Indices: -23≤h≤22, -12≤k≤13, -29≤l≤28: Reflection collected / unique: 38468 / 9111; R(int) = 0.0426; Completeness to Θ = 25.242°: 99.3 %; Max. and min. transmission: 0.7457 and 0.6781; Data / restraints / parameters: 9111 / 0 / 424; Goodness-of-fit on F2: 1.013; Final R indices [I>2σ(I)]: R1 = 0.0456, wR2 = 0.1047; R indices (all data): R1 = 0.0756, wR2 = 0.1166; Largest diff. peak/hole: 0.388 / -0.271 e.Å-3. [Co(P3)(CO)(=CF2)](OTf) (7): Empirical formula: C43H39CoF5O4P3S; FW = 898.64; Crystal size: 0.480 x 0.260 x 0.080 mm3; Crystal system: triclinic; Space group: P-1 (No2); Z = 2; a = 10.6178(6) Å, b = 13.4897(5) Å, c = 16.3442(8) Å, α = 70.515(2)°, β = 89.133(3)°, γ = 70.588(2)°; Volume = 2069.37(18) Å3; Calculated density = 1.442 Mg/m3; Absorption coefficient = 0.645 mm-1; F(000) = 924; Θ range for data collection: 2.334 to 28.433°; Limiting indices: -11≤h≤14, -17≤k≤18, -21≤l≤21: Reflections collected / unique: 15807 / 10061; R(int) = 0.0264;Completeness to Θ = 25.242°: 98.9 %; Max. and min. transmission: 0.7457 and 0.6047; Data / restraints / parameters: 10061 / 228 / 556; Goodness-of-fit on F2: 1.029; Final R indices [I>2σ(I)]: R1 = 0.0484, wR2 = 0.1204; R indices (all data): R1 = 0.0734, wR2 = 0.1340; Largest diff. peak/hole: 0.884 / -0.512 e.Å-3.

IR Data:

IR spectra:

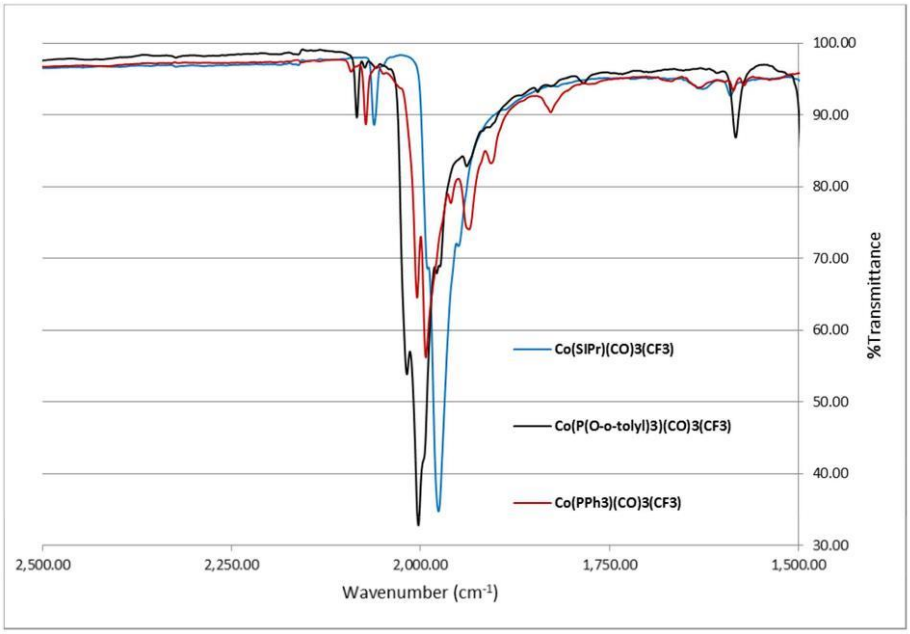

Figure 2.0.3: FT-IR spectra (Nicolet Nexus 6700 instrument, neat/solid samples) for tri-carbonyl/trifluoromethyl complexes $Co(PPh_3)(CO)_3(CF_3)$,$Co[P(O\text{-}o\text{-}Tol)_3](CO)_3(CF_3)$ (**2**) and $Co(SIPr)(CO)_3(CF_3)$ (**5**) (metal carbonyl region).

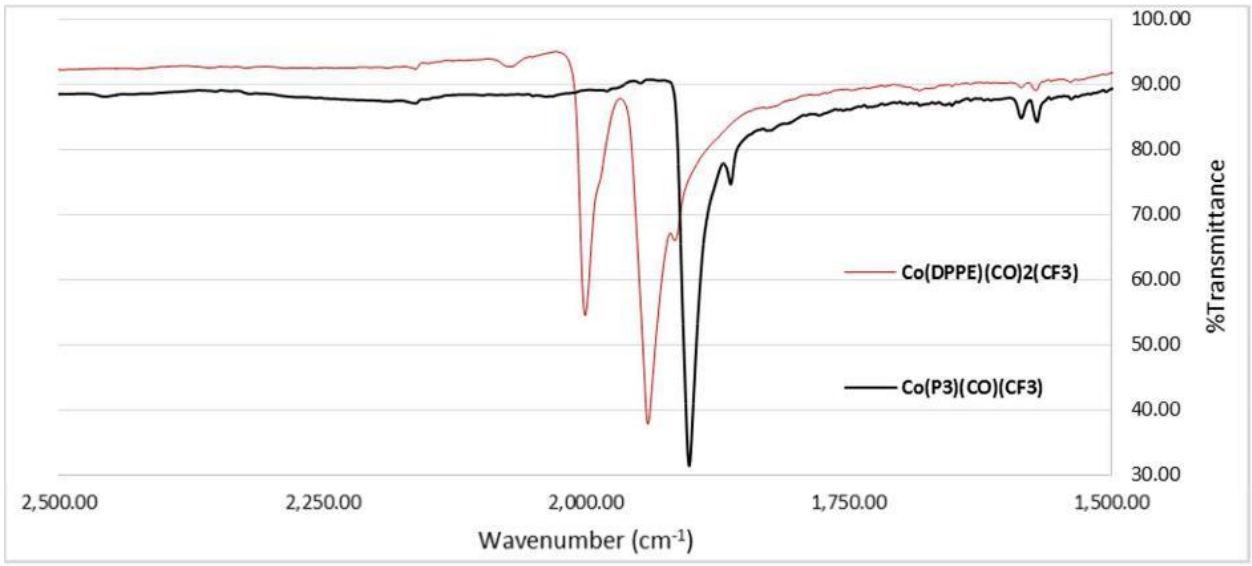

Figure 2.0.4: FT-IR spectra (Nicolet Nexus 6700 instrument, neat/solid samples) for di- and mono-carbonyl/trifluoromethyl complexes $Co(DPPE)(CO)_2(CF_3)$ (**3**) and $Co(P_3)(CO)_3(CF_3)$ (**4**) (metal carbonyl region).

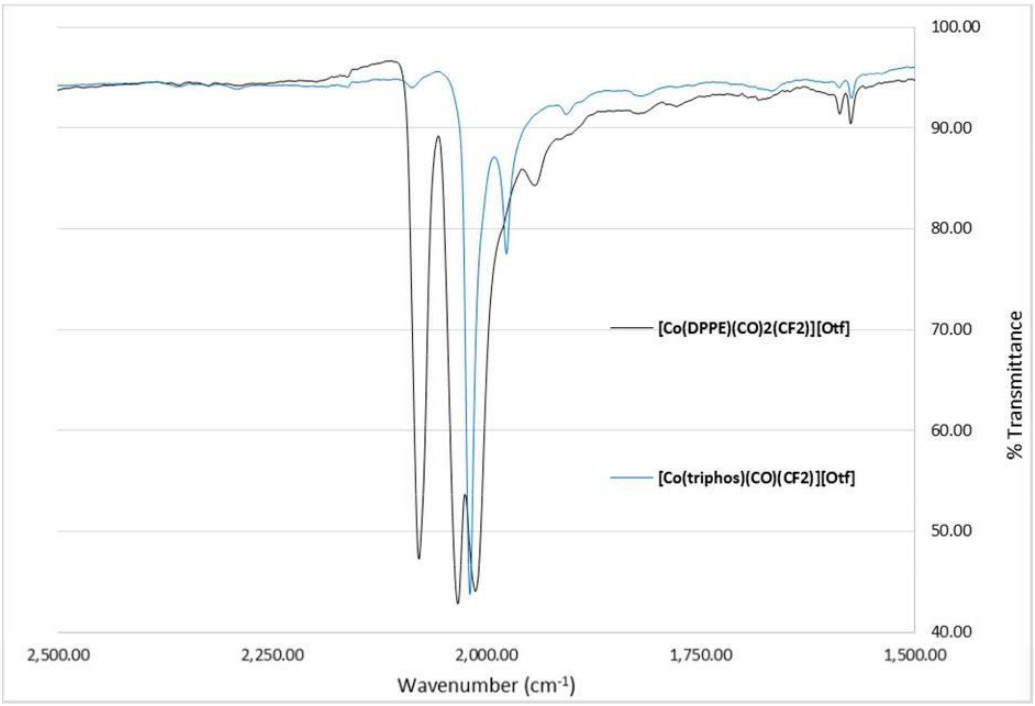

Figure 2.0.5: FT-IR spectra (Nicolet Nexus 6700 instrument, neat/solid samples) for di- and mono-carbonyl/difluorocarbene complexes $[Co(DPPE)(CO)_2(=CF_2)](OTf)$ (**6**) and$[Co(P_3)(CO)(=CF_2)](OTf)$ (**7**) (metal carbonyl region).

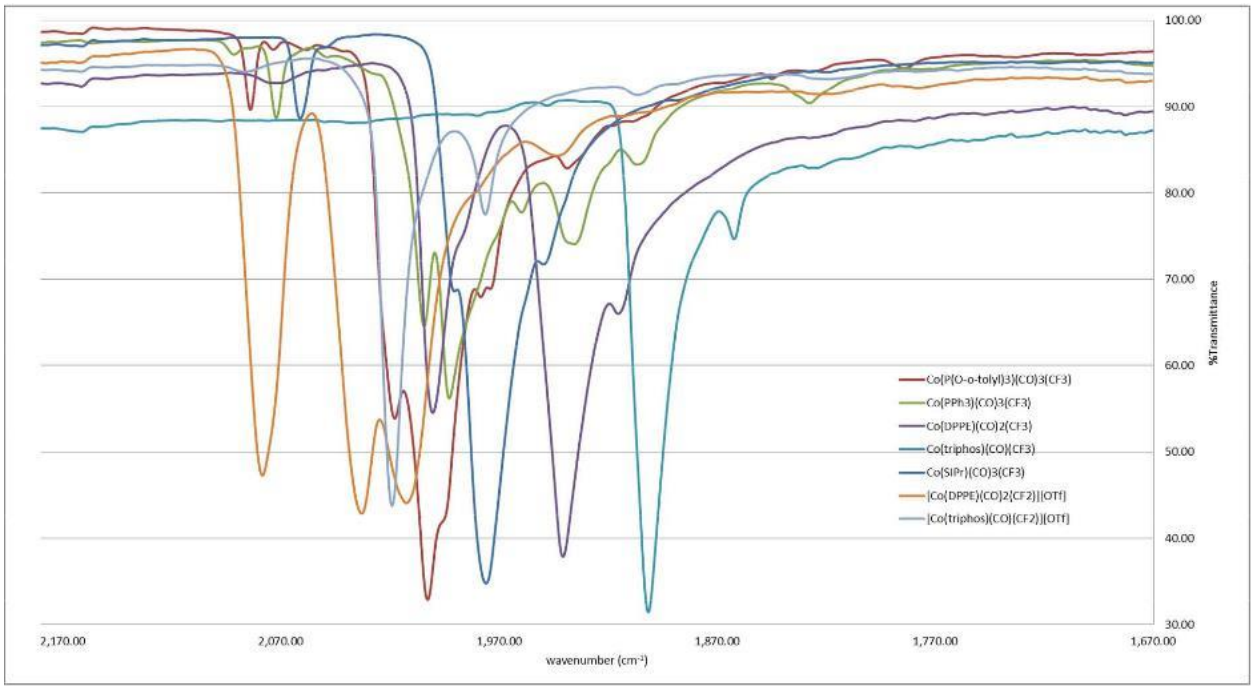

Figure 2.0.6: FT-IR spectra (Nicolet Nexus 6700 instrument, neat/solid samples) for all new compounds and $Co(PPh_3)(CO)_3(CF_3)$.

Determination of ΔG‡ for axial/equatorial (P/P') exchange for $Co(DPPE)(CO)_2(CF_3)$ (3).[35]

Complex 3 (0.034 M in $CDCl_3$), in a screw-cap NMR tube, was examined by ^{19}F NMR (282 MHz, ceramic spinner) at the following temperatures (^oC): 20, 10, 5, 0, –2.5 (T_c), –5, –7.5, –10, –20 and –40 (see below for stacked spectra). The coalescence temperature (T_c) was –2.5 ^oC (270.5 K). The greatest separation of peaks was $\Delta\nu$ = 39 Hz ($\Delta\nu$ did not change below –40 ^oC); these values were used to calculate $\Delta G^‡$ for P/P' exchange, according to: $\Delta G^‡ = a\ T_c\ [9.972 + \log(T_c/K_c)]$ T_c = 270.5 K $\Delta\nu$ = 39 Hz $K_c = 2–1/2\ \pi\ \Delta\nu$ = 86.6 a = 0.004575 kcal K^{-1} mol^{-1} $\Delta G^‡$ = (0.004575)(270.5)[9.972 + log(270.5/86.6)] = 13.0 ± 0.3 kcal mol^{-1}. Standard deviation was calculated using the partial derivative method: With $\sigma(T_c)$ = 5K and $\sigma(\Delta\nu)$ = 2 Hz $\partial\Delta G^‡/\partial Tc$ = a

[log (T_c/K_c) + 10.972] = (0.004575)[log(270.5/39) + 10.972] = 0.054 $\partial\Delta G^{\ddagger}/\partial\Delta\nu$ = – a T_c $\Delta\nu$–1 = – (0.004575)(270.5)(39)–1 = – 0.032 $\sigma(\Delta G^{\ddagger})$ = $\{(\partial\Delta G^{\ddagger}/\partial T_c)^2[\sigma(T_c)]^2 + (\partial\Delta G^{\ddagger}/\partial\Delta\nu)^2[\sigma(\Delta\nu)]^2\}^{1/2}$ = $\{(0.054)^2(5)^2 + (– 0.032)^2(2)^2\}^{1/2}$ = 0.3 kcal mol^{-1}. Note that other VT-NMR data for complexes $Co(PPh_3)(CO)_3(CF_3)$, **4** and **6**, were collected in $CDCl_3$ in the 0.03-0.05 M concentration range in screw-cap NMR tubes.

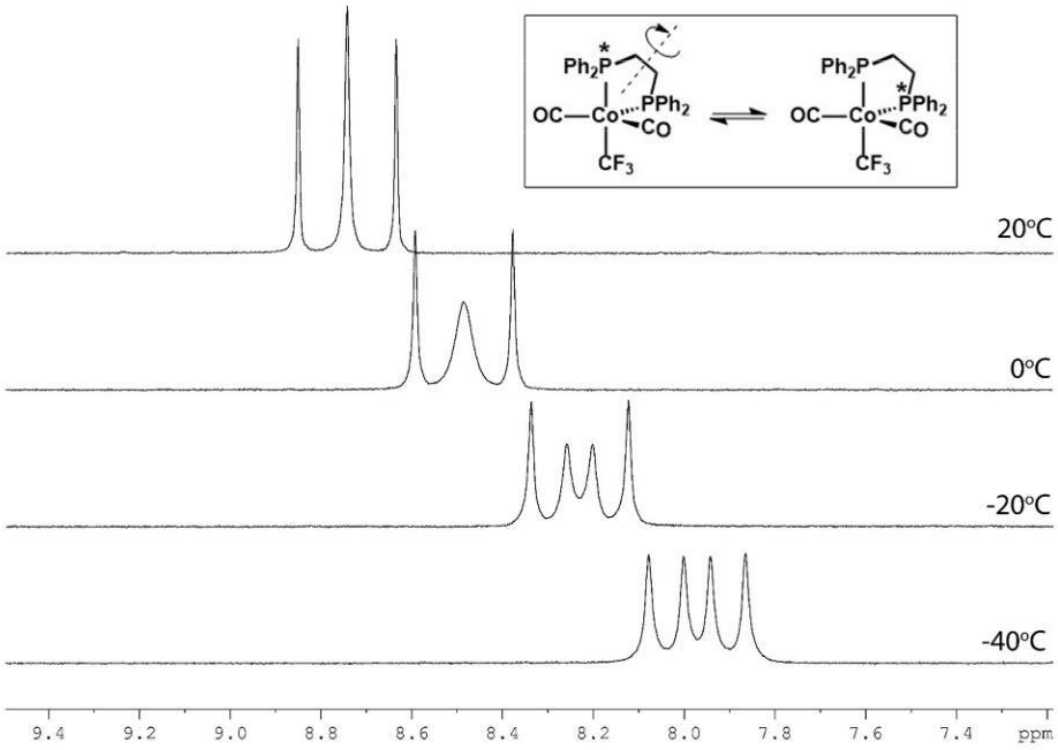

Figure 2.0.7: Variable-temperature (–40 to 20°C) ^{19}F NMR (282 MHz, $CDCl_3$) spectra of **3**. The inset illustrates the proposed exchange process.

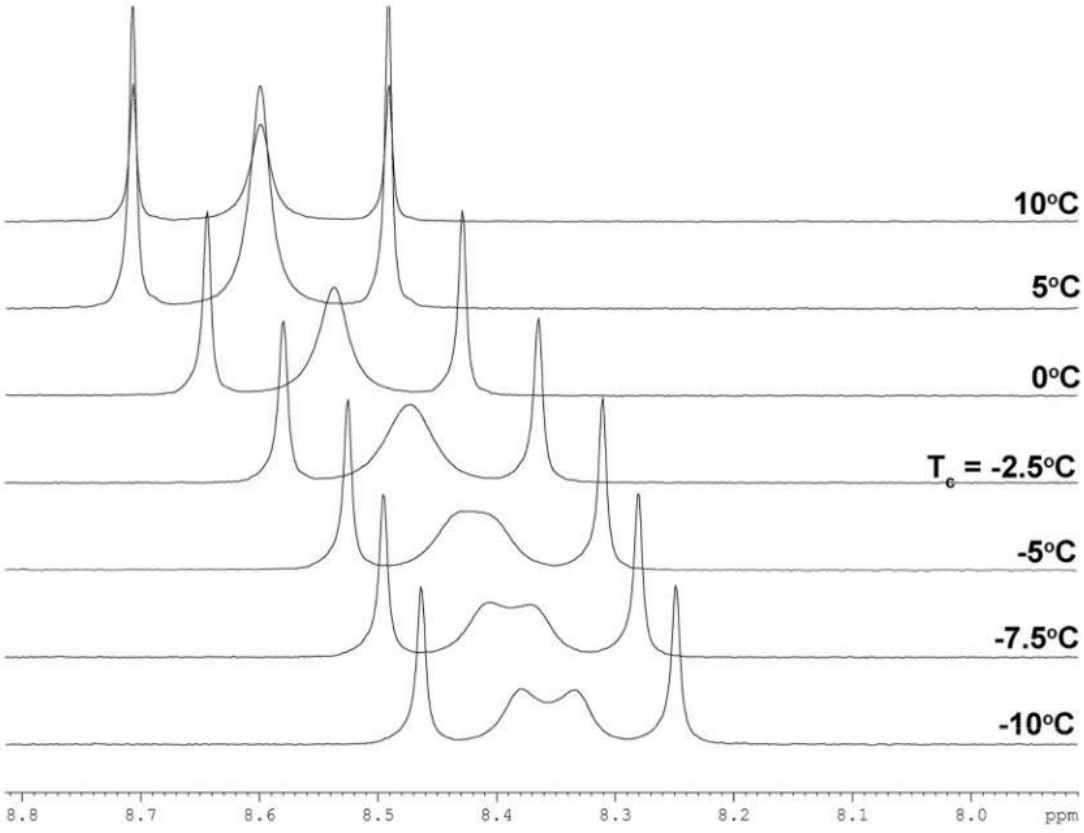

Figure 2.0.8: Variable-temperature (–10 to 10 °C) ^{19}F NMR (282 MHz, $CDCl_3$) spectra of **3**.

REFERENCES

(1) (a) Steinborn, D. *Fundamentals of organometallic catalysis*; Wiley-VCH: Weinheim, 2012. (b) Metal-Catalysis in Industrial Organic Processes; Chiusoli, G. P.; Maitlis, P. M., Eds.; RSC Publishing: Cambridge, 2006.

(2) (a) Taw, F. L.; Clark, A. E.; Mueller, A. H.; Janicke, M. T.; Cantat, T.; Scott, B. L.; Hay, P. J.; Hughes, R. P.; Kiplinger, J. L. *Organometallics* **2012**, *31*, 1484-1499. (b) Hughes, R. P. *Adv. Organomet. Chem.* **1990**, *31*, 183-267. (c) Brothers, P. J.; Roper, W. R. *Chem. Rev.* **1988**, *88*, 1293-1326.

(3) (a) Ojima, I. *Fluorine in Medicinal Chemistry and Chemical Biology*; Blackwell: Chichester, U.K., 2009. (b) Chambers, R. D. *Fluorine in Organic Chemistry*; Blackwell: Oxford, 2004. (c) Kirsch, P. *Modern Fluoroorganic Chemistry: Synthesis, Reactivity, Applications*; Wiley-VCH: Weinheim, 2004.

(4) (a) Alonso, C.; de Marigorta, E. M.; Rubiales, G.; Palacios, F. *Chem. Rev.* **2015**, *115*, 1847-1935. (b) Wang, J.; Sánchez-Roselló, M.; Aceña, J. L.; del Pozo, C.; Sorochinsky, A. E.; Fustero, S.; Soloshonok, V. A.; Liu, H. *Chem. Rev.* **2014**, *114*, 2432-2506. (c) Zhu, W.; Wang, J.; Wang, S.; Gu, Z.; Aceña, J. L.; Izawa, K.; Liu, H.; Soloshonok, V. A. *J. Fluorine Chem.* **2014**, *167*, 37-54. (d) Müller, K.; Faeh, C.; Diederich, F. *Science* **2007**, *317*, 1881-1886. (e) Jeschke, P. *ChemBioChem* **2004**, *5*, 570-589. See also ref. 3a.

(5) McCoy, M. *Chem. Eng. News* **2013**, *91(50)*, 8.

(6) (a) Panferova, L. I.; Miloserdov, F. M.; Lishchynskyi, A.; Martinez Belmonte, M.; Benet-Buchholz, J.; Grushin, V. V. *Angew. Chem. Int. Ed.* **2015**, 54, 5218-5222. (b) Konovalov, A. I.; Lishchynskyi, A.; Grushin, V. V. *J. Am. Chem. Soc.* **2014**, *136*, 13410-13425. (c) Morimoto, H.; Tsubogo, T.; Litvinas, N. D.; Hartwig, J. F. *Angew. Chem. Int. Ed.* **2011**, *50*, 3793-3798. (d) Dubinina, G. G.; Furutachi, H.; Vicic, D. A. *J. Am. Chem. Soc.* **2008**, *130*, 8600-8601. (e)

Wiemers, D. M.; Burton, D. J. *J. Am. Chem. Soc.* **1986**, *108*, 832-834. (f) McLoughlin, V. C. R.; Thrower, J. *Tetrahedron* **1969**, *25*, 5921-5940.

(7) Metal-catalyzed perfluoroalkyl transfer involving probable [M]–R^F intermediates: (a) Ohashi, M.; Shirataki, H.; Kikushima, K.; Ogoshi, S. *J. Am. Chem. Soc.* **2015**, *137*, 6496-6499. (b) Knauber, T.; Arikan, F.; Röschenthaler, G.-V.; Gooßen, L. J. *Chem. Eur. J.* **2011**, *17*, 2689-2697. (c) Cho, E. J.; Senecal, T. D.; Kinzel, T.; Zhang, Y.; Watson, D. A.; Buchwald, S. L. *Science* **2010**, *328*, 1679-1681. (d) Wang, X. Truesdale, L.; Yu, J.-Q. *J. Am. Chem. Soc.* **2010**, *132*, 3648-3649. (e) Oishi, M.; Kondo, H.; Amii, H. *Chem. Commun.* **2009**, 1909-1911. See also ref. 4c.

(8) Trifluoromethylation by photoredox catalysis with metal-containing photosensitizers: (a) Choi, W. J.; Choi, S.; Ohkubo, K..; Fukuzumi, S.; Cho, E. J.; You, Y. *Chem. Sci*. **2015**, *6*, 1454-1464. (b) Nagib, D. A.; MacMillan, D. W. C. *Nature* **2011**, *480*, 224−228.

(9) (a) Kress, S.; Blechert, S. *Chem. Soc. Rev.* **2012**, *41*, 4389-4408. (b) Handbook of Metathesis; Grubbs, R. H., Ed.; Wiley-VCH: Weinheim, Germany, 2003.

(10) Takahira, Y.; Morizawa, Y. *J. Am. Chem. Soc.* **2015**, *137*, 7031-7034.

(11) Harrison, D. J.; Lee, G. M.; Leclerc, M. C.; Korobkov, I.; Baker, R. T. *J. Am. Chem. Soc.* **2013**, *135*, 18296-18299.

(12) Harrison, D. J.; Gorelsky, S. I.; Lee, G. M.; Korobkov, I.; Baker, R. T. *Organometallics* **2013**, *32*, 12-15.

(13) (a) Yuan, J.; Hughes, R. P.; Golen, J. A.; Rheingold, A. L. *Organometallics* **2010**, *29*, 1942-1947. (b) Trnka, T. M.; Day, M. W.; Grubbs, R. H. *Angew. Chem., Int. Ed.* **2001**, *40*, 3441-3444.

(14) Huang, Y.; Li, J.; Zhou, J.; Wang, Q.; Gui, M. *J. Organomet. Chem.* **1981**, *218*, 169-175.

(15) Ivin, K. J.; Rooney, J. J.; Stewart, C. D.; Green, M. L. H.; Mahtab, R. *J. Chem. Soc., Chem. Commun.* **1978**, 604-606.

(16) Boday, D. J. The State of Fluoropolymers. In *Advances in Fluorine Containing Polymers*; American Chemical Society: Washington, 2012.

(17) Syntheses of **1** and related compounds: (a) Hieber, W.; Beck, W.; Lindner, E. *Z. Naturforsch* **1961**, *16b*, 229-23. (b) McClellan, W. R. *J. Am. Chem. Soc.* **1961**, *83*, 1598-1600. (c) Udovich, C. A.; Clark, R. J. *Inorg. Chem.* **1968**, *8*, 938-944. (d) Berg, G. C. V. D.; Oskam, A.; Vrieze, K. *J. Organomet. Chem.* **1974**, *69*, 169-177.

(18) Deng, J.; Li, Q.; Xie, Y.; King, R. B. *J. Fluorine Chem.* **2013**, *146*, 37-45.

(19) The reaction between $Co_2(CO)_8$ and CF_3I affords **1** in 6% yield: Beveridge, A. D.; Clark, H. C. *J. Organomet. Chem.* **1968**, *11*, 601-614.

(20) The related trifluoroacyl complex $Co(CO)_4[C(O)CF_3)]$ reacts with PPh_3 to give $Co(PPh_3)(CO)_3[C(O)CF_3)]$, which can be converted to $Co(PPh_3)(CO)_3(CF_3)$: Heck, R. F.; Beslow, D. S. *J. Am. Chem. Soc.* **1962**, *84*, 2499-2502.

(21) Edgell, W. F.; Lyford IV, J. *Inorg. Chem.* **1970**, *9*, 1932-1933.

(22) Trifluoroacylation of dienes with $Co(CO)_4[C(O)CF_3]$: Kohn, B. L.; Rovis, T. *Chem. Sci.* **2014**, *5*, 2889-2892.

(23) Synthesis of $Zn[Co(CO)_4]_2$ at high temperature (200 ^oC) under CO pressure (> 4500 psi or 210 atm) in toluene: Schrauzer, G. N.; Bastian, B. N.; Fosselius, G. A. *J. Am. Chem. Soc.* **1966**, *88*, 4890-4894.

(24) Compounds **1** and $Co(CO)_4[C(O)CF_3]$ can be obtained in pure form (i.e., solvent-free) if the reaction with the trifluoromethyl anhydride is conducted in very low-boiling solvent (e.g., Me_2O or Et_2O), which can be separated from the volatile products, albeit with low or unreported yields (see refs. 17a,c).

(25) The concentration/yield of **1** was determined by ^{19}F NMR integration (9 s delay time) relative to a known amount of 1,3-bis(trifluoromethyl)benzene.

(26) Mullica, D. F.; Sappenfield, E. L.; Gipson, S. L.; Wilkinson, C. C. *Acta Crystallogr. Sect. C.* **1997**, *C53*, 572-574.

(27) Llewellyn, S. A.; Malcolm, L. H.; Cowley, G.; Cowley, A. R. *Dalton Trans*. **2006**, *34*, 4164-4168.

(28) The Co-C-O angles (deg) for the Co–CO groups of **5**: 170.68(19), 171.02(19), 177.0(2); cf. compound **2**: 178.51(18), 178.54(19), 179.10(19).

(29) $[Cp^*Mo(CO)_3(=CF_2)](OTf)$: Koola, J. D.; Roddick, D. M. *Organometallics* **1991**, *10*, 591-597.

(30) Terminal first-row metal difluorocarbenes: (a) Richmond, T. G.; Crespi, A. M.; Shriver, D. F. *Organometallics* **1984**, *3*, 314-319. (b) Crespi, A. M.; Shriver, D. F. *Organometallics* **1985**, *4*, 1830--1835.

(^{31}) DFT analysis of $CpCo(PPh_3)(=CFR)$ (R = F or CF_3) supports a formal Co^I oxidation state and neutral carbene ligands (see ref. 12).

(32) Thermal conditions: 48 h, 50 ^oC in THF. Photolytic: 160 W medium pressure Hg lamp, quartz reactor, 3 h, $\leq$ 60 ^oC in THF.

(33) Kuhn, K. M.; Grubbs, R. H. *Org. Lett.* **2008**, *10*, 2075-2077.

(34) Armarego, W. L. F.; Perrin, D. D. *Purification of Laboratory Chemicals,* 4th ed.; Butterworth-Heinemann: Oxford, 1996; p. 452.

(35) Martin, M. L.; Martin, G. J.; Delpeuch, J.-J. Practical NMR Spectroscopy; Heyden: Philadelphia, 1980.

3 Chapter 3: d^{10} Nickel Difluorocarbenes and their Cycloaddition Reactions with Tetrafluoroethylene

"Faithless is he that says farewell when the road darkens."

— J.R.R. Tolkien, The Fellowship of the Ring

3.1 Context

The lack of reactivity of the cationic d^8 $[Co]=CF_2]^+$ complexes as well as the slow cycloaddition reactions of the neutral $[Co]=CF_2$ half-sandwich systems described in the introduction led us to pursue different avenues to achieve our goals towards developing a catalyst for the metathesis of fluorinated alkenes. The focus of this chapter is the synthesis and reactivity of the first examples of stable d^{10} nickel(0) difluorocarbenes.

The previous chapter identified the importance of the electron density of the metal towards metal difluorocarbene reactivity with TFE. In this chapter we introduce the synthesis of two new d^{10} $[Ni]=CF_2$ complexes along with their full characterization. It will be shown that the increased electron density on the metal increases the overall reactivity of these types of complexes with fluoroalkenes, while also occurring through a different mechanism than previous cobalt examples.

These $[Ni]=CF_2$ complexes, although more reactive towards production of metallacyclobutanes, were not capable of producing the desired metathesis products. Attempts to destabilize the metallacycle product using both Lewis and Brønsted acids produced a nickel vinyl species and a ring-contracted nickel metallacyclopropane respectively.

3.1.1 Published Contribution

Harrison, D. J.; Daniels, A. L.; Korobkov, I.; Baker, T. *Organometallics*. **2015**, *34*, 5683-5686.

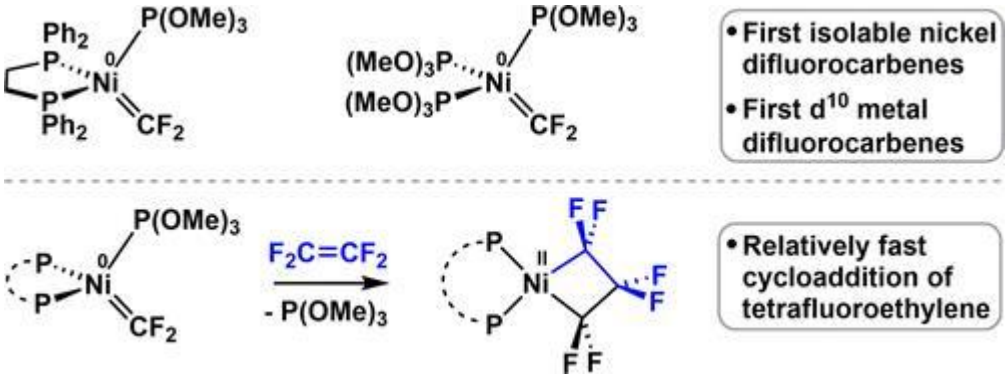

We report the first isolable nickel difluorocarbene complexes {Ni(=CF_2)P_2[$P(OMe)_3$]; P_2 = $Ph_2P(CH_2)_2PPh_2$ (**1**); P_2 = 2 $P(OMe)_3$ (**2**)}, which are also the only examples of formally d^{10} metal fluorocarbenes. These electron-rich [Ni^0]=CF_2 complexes react with tetrafluoroethylene (TFE) to yield rare perfluorometallacyclobutanes [Ni(κ^2-$CF_2CF_2CF_2$-)P_2,**3** and **4**], with potential relevance to fluoroalkene metathesis and polymerization. Kinetic experiments establish that the reactions of the new [Ni]=CF_2 compounds with TFE are considerably faster than the analogous reactions of their previously reported [Co]=CF_2 counterparts. Further, we show that TFE addition to **2** is a dissociative process, in contrast to [Co]=CF_2, which reacts with TFE in an associative fashion. Finally, preliminary reactivity of a [Ni](κ^2-$CF_2CF_2CF_2$-) complex (**3**) is described.

Author contributions: The manuscript was written by DJH with contributions and editing by ALD and RTB. DJH was responsible for the synthesis and characterization of complexes **1** and **2**. ALD performed reactivity studies of complexes **1** and **2** and was responsible for SI. IK performed X-ray crystallography.

3.2 Introduction

Metal alkylidenes ([M]=CRR$'$; R, R$'$ = H, alkyl, aryl) participate in a variety of catalytic transformations, most notably in alkene metathesis.[1] Fluorocarbenes ([M]=CFR^F, R^F = F or perfluoroalkyl), on the other hand, are quite rare[2,3] and have only recently been utilized in catalysis. Takahira and Morizawa reported (2015) cross metathesis between fluoroalkenes and *electron-rich* alkenes (CH_2=CHOR), with [Ru]=CF_2 and [Ru]=CHOR intermediates, in the first examples of metal-catalyzed CF_2 transfer.[4] Catalysis involving fluorinated alkenes/metal fluorocarbenes is inherently challenging,[1,4,9,13] but has tremendous potential in the technologically important area of fluoro-organic synthesis.[5,6,7]

We are examining the viability of *first-row* (non-precious) metal fluorocarbenes as initiators for catalytic perfluoroalkene metathesis or polymerization, as outlined in Scheme 3.1. The metathesis mechanism is identical to the one established for non-fluorinated olefins (*i.e.*, the Chauvin mechanism)[9b] and our approach to fluoroalkene polymerization is inspired by the Green-Rooney mechanism, originally proposed to describe the polymerization of non-fluorinated alkenes.[8] The fluoro-Green-Rooney mechanism avoids migratory alkene insertion into unreactive metal-perfluoroalkyl bonds,[9] in contrast to the more familiar Cossee-Arlman pathway (detailed analysis chapter 6, Scheme 6.1),[10] and the metal-perfluoroalkyl bonds of the metallacyclobutane intermediates are expected to be destabilized by ring-strain.

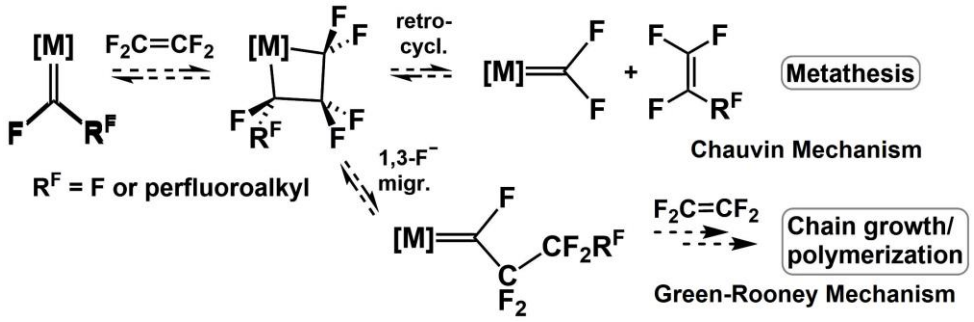

Scheme 3. 1

We recently reported the reactions of tetrafluoroethylene (CF_2=CF_2, TFE) with cobalt(I) fluorocarbenes ([Co]=CFR^F, R^F = F or CF_3) to yield metallacyclobutanes (Scheme 3.2): the first examples of formal [2+2] cycloadditition between perfluorinated alkene and metal carbene reactants.[11] However, the perfluorocobaltacyclobutanes [*i.e.*, cobalt(III) bis(perfluoroalkyl) complexes] are decidedly more stable than the free cobalt perfluorocarbenes and tetrafluoroethylene (ΔG_{cycl} = –25.3 kcal mol^{-1} for R^F = F, from DFT/M06/def2-TZVP calculations[12]), despite the destabilizing ring-strain in the four-membered metallacycle. The strong M–R^F bonds[2,9] of the metallacyclobutanes and the weak *singlet* carbene-metal interaction (and the related weak C=C bonds of fluoroalkenes)[13,14] contribute to ΔG_{cycl}, which is sufficiently large to preclude catalysis with our [Co]=CFR^F/[Co](κ^2-$CF_2CF_2CFR^F$-) systems.

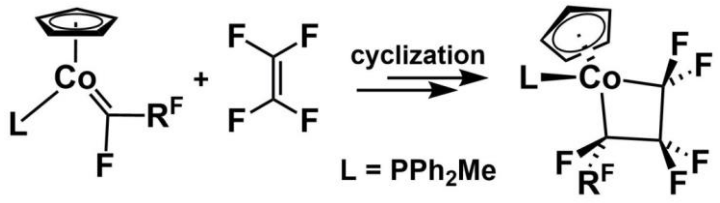

Scheme 3. 2

Considering the limitations of the cobalt system (*i.e.*, slow reactions with TFE and large ΔG_{cycl}), we turned our attention to new metal/ligand combinations. We now report the first persistent perfluorocarbene complexes of nickel. These compounds are also the first metal perfluorocarbenes with a formal d^{10} electron configurations.[15] The cycloaddition reactions of the [Ni]=CF_2 complexes with TFE are described, along with preliminary reactivity of the metallacycles.

3.2.1 Results and Discussion

Following the method developed by Hughes and co-workers for making iridium fluorocarbenes,[16] two-electron reduction of Ni(CF_3)(OC(O)CF_3)(DPPE) [DPPE = $Ph_2P(CH_2)_2PPh_2$][17] with potassium graphite, in the presence of $P(OMe)_3$, gives Ni(=CF_2)(DPPE)[$P(OMe)_3$] (**1**) in 69% isolated yield (Scheme 3.3A).[18] The molecular structure is depicted in Figure 3.1. The nickel-carbene bond distance is 1.771(4) Å, compared with Co=CFR^F (R^F = F, CF_3; four examples) distances of 1.740(1)-1.758(5) Å, and with Ni–CO bond lengths of 1.785(2) and 1.778(2) Å in Ni($CO)_2$(DPPE).[19] To gain deeper insight into this new class of metal carbene, we prepared another example, Ni(=CF_2)[$P(OMe)_3]_3$ (**2**), by treating **1** with $P(OMe)_3$ in the presence of CuCl to sequester the DPPE ligand (Scheme 3.3B; 68% isolated yield).

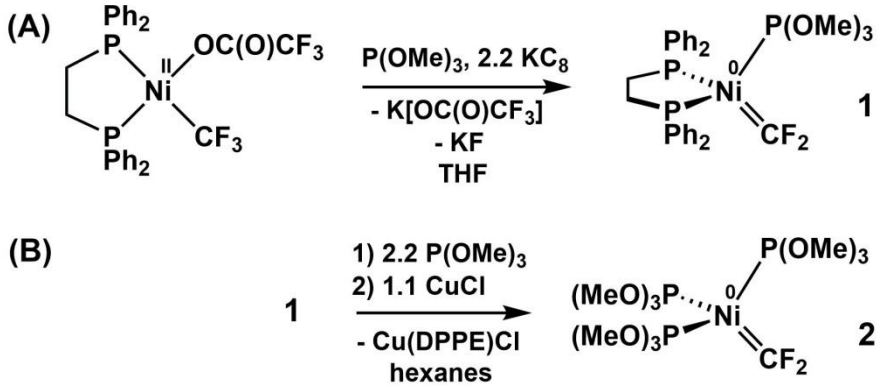

Scheme 3. 3

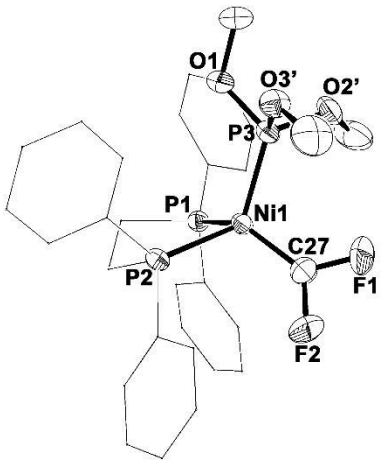

Figure 3.1: ORTEP representation of the X-ray crystal structure of **1** with 50% probability thermal ellipsoids. Hydrogen atoms are omitted and the carbon framework of the DPPE ligand is depicted as a wire cage structure for clarity. One orientation is shown for the disordered (over two positions) oxygen atoms, O2' and O3'. Selected bond distances [Å]: Ni1–C27 = 1.771(4), Ni1–P1 = 2.183(1), Ni1–P2 = 2.2100(9), Ni1–P3 = 2.148(1), C27–F1 = 1.340(5), C27–F2 = 1.327(5).

Fluorocarbene complexes of group 10 metals are extremely uncommon. Examples are limited to transient $[M]=CF_2$ species generated in the gas phase[14,20] and, in one case, the existence of $[Pt^{II}]=CF_2$ was inferred from its pyridine adduct ($[[Pt^{II}]–CF_2–pyr$).[21] Group 10 metal difluorocarbenes with d^8 electron configurations (M^{II}) are expected to be very electrophilic, with the π bond polarized toward the metal and thus unsuitable for reactions with electron-poor fluoroalkenes. Compounds **1** and **2** are the first metal fluorocarbenes with a d^{10} electron counts[15] and tetrahedral geometry at the metal centers,[22,23] and should have vastly different reactivity than d^8 systems. To illustrate, Roper *et al.* found that $[Ru^{II}]=CF_2$ (d^6) complexes are potent electrophiles but $[Ru^0]=CF_2$ (d^8) is nucleophilic[2,24,25] and we have noted previously the need for electron-rich metal fluorocarbenes for reactions with electrophilic fluoroalkenes.[11]

Complexes **1** and **2** react with TFE ($CF_2=CF_2$) to yield the first examples of perfluoronickelacyclobutanes (**3** and **4**) (Scheme 3.4A; 87% isolated yield for **3**; 94% ^{19}F NMR yield for **4**): the first step in a perfluoroalkene/metal perfluorocarbene metathesis or fluoro-Green-Rooney mechanism (Scheme 3.1). Although the bis(phosphite) metallacycle, **4**, is produced in high yield by NMR, attempts to isolate this compound resulted in partial

isomerization to the alkene complex, Ni(η^2-CF_2=$CFCF_3$)[$P(OMe)_3$]$_2$ (more details on metallacycle reactivity below). Therefore, in order to synthesize suitable crystals for XRD complex **4** was treated with DPPE which readily formed complex **3** with high purity.

The reactions of **1** and **2** with TFE, to give metallacycles **3** and **4**, are fast compared to CoCp(=CF_2)(PPh_2Me).[11a,26] For **1**, the mechanism is complicated by the formation of small amounts of Ni(=CF_2)[$P(OMe)_3$]$_3$ (**2**) as metallacycle **3** is produced and $P(OMe)_3$ is liberated (Scheme 3.4B; K_{eq} = 4.2 L mol^{-1} at 23^{o}C).[27] Nonetheless, the growth of **3** is reasonably modeled by a first-order rate law (excess TFE), affording a rate constant of 0.34 h^{-1}. The first-order rate constant for the formation of **4** is 0.50 h^{-1}, *versus* <0.033 h^{-1} for Co(κ^2-$CF_2CF_2CF_2$-)(Cp)(PPh_2Me) [11a] under the same conditions[26] (time traces in the Supporting Information). Free $P(OMe)_3$ (20 equiv) caused a significant decrease in the rate of TFE addition **2** (to <0.047 h^{-1}),[28] in contrast to CoCp(=CF_2)(PPh_2Me), for which only marginal rate-suppression was observed when 20 equiv of PPh_2Me was present.[11a] Thus, TFE addition to the nickel fluorocarbene **2** (and likely **1**) follows a dissociative mechanism, while TFE reacts with [Co]=CF_2 in an associative fashion.[11a,12]

Prior to our cobalt-containing fluorocarbenes, only one perfluorometallacyclobutane had been reported [Fe(κ^2-$CF_2CF_2CF_2$-)$(CO)_4$, made by decarbonylation of the bis(acyl) precursor[29]]. Very recently, two Pt(κ^2-$CF_2CF_2CF_2$-)L_2complexes (L_2 = 1,5-COD or 2 pyridine; COD = cyclooctadiene) were disclosed, derived from Pt(1,5-COD)Me_2 and I$(CF_2)_3$I.[30] The molecular structure of **3** is shown in Figure 3.2. The NiP_2C_2 substructure is almost perfectly planar[31] but the C27–Ni1–C29 angle is significantly compressed (71^o), as observed in our cobalt perfluorometallacyclobutanes[11a] and the Pt-containing examples mentioned above.

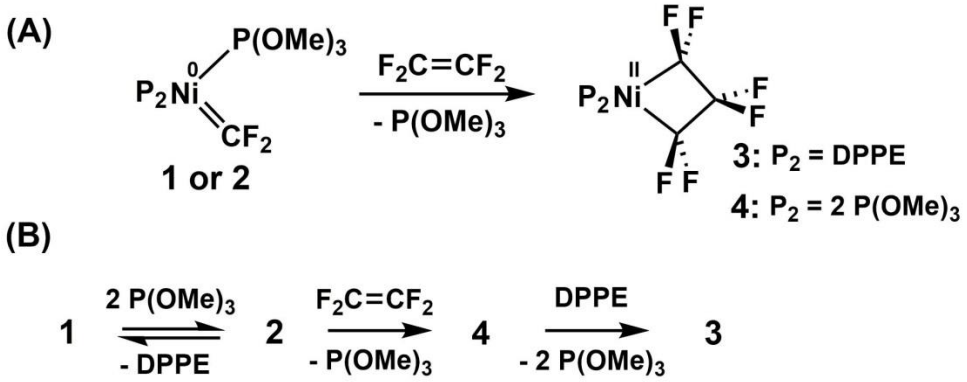

Scheme 3. 4

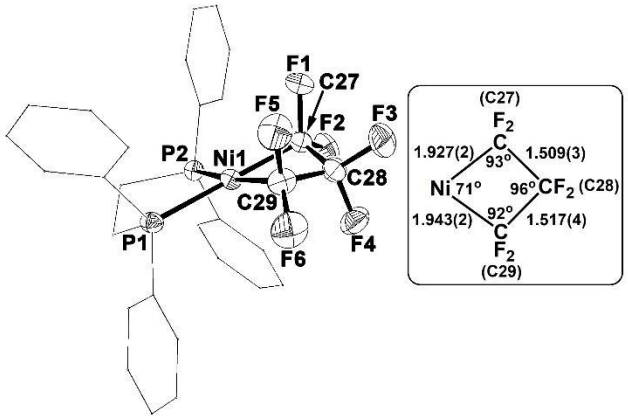

Figure 3.2: ORTEP representation of the X-ray crystal structure of **3** with 50% probability thermal ellipsoids. Hydrogen atoms are omitted and the carbon framework of the DPPE ligand is depicted as a wire cage structure for clarity. Selected bond distances [Å]: Ni1–P1 = 2.1861(6), Ni1–P2 = 2.1701(5), C27–F1 = 1.383(3), C27–F2 = 1.377(3), C28–F3 = 1.368(3), C28–F4 = 1.356(3), C29–F5 = 1.388(3), C29–F6 = 1.367(3). Additional distances and angles are displayed in the inset.

Preliminary reactivity studies on perfluorometallacyclobutane **3** establish trends similar to those seen for the cobalt analogs. Fluoride-abstraction using Me_3SiOTf (Tf = SO_2CF_3) yields the ring-opened vinyl product Ni(DPPE)(*cis*- and *trans*-CF=CFCF$_3$)(OTf) (**5**) (Scheme 3.5A; ^{19}F NMR yield for both isomers: 82%). Note that Co(κ^2-$CF_2CF_2CF_2$-)(Cp)(PPh_2Me) gave exclusively the *trans*-vinyl species under similar conditions. Further, catalytic $HNTf_2$ induces isomerization/ring-contraction to hexafluoropropylene complex **6** (Scheme 3.5B; ^{19}F NMR yield: 85%), as observed with the cobalt systems.

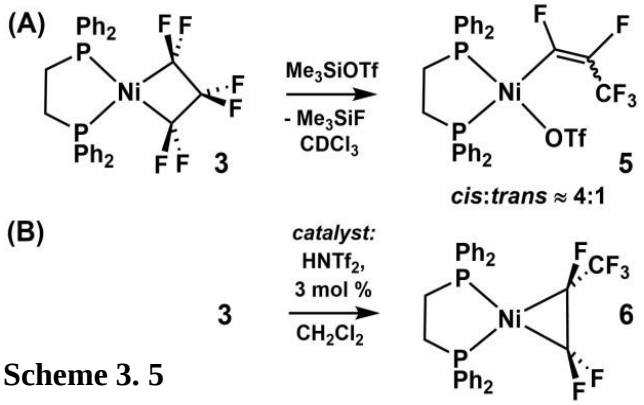

Scheme 3. 5

These reactions likely proceed by β-fluoride activation and a cationic π-bound perfluoroallyl complex {[Ni](η^2 or η^3-C_3F_5)$^+$}.[11a,32]

3.2.2 Conclusion

In summary, we have described the first isolable nickel difluorocarbenes and the only examples of CF_2 ligands bound to d^{10} metals (**1** and **2**). The electron-rich [Ni]=CF_2 bonds undergo cycloaddition reactions with TFE to produce rare perfluorometallacyclobutanes (**3** and **4**). These results are pertinent to metal-mediated metathesis of perfluoroalkenes or perfluoroalkene polymerization *via* a modified Green-Rooney mechanism (Scheme 3.1). TFE addition to **1** or **2** proceeds with pseudo-first-order rate constants at least an order of magnitude greater than previously reported CoCp(=CF_2)(PPh_2Me),[11a] which is encouraging for possible catalytic applications. Interesting, the reaction of TFE with **2** is inhibited by free $P(OMe)_3$, pointing to a dissociative process, whereas TFE addition to CoCp(=CF_2)(PPh_2Me) does not require ligand dissociation.[12] We have now identified two classes of first-row metal fluorocarbenes ([Co]=CFR^F and [Ni]=CF_2) that react with tetrafluoroethylene to give perfluorometallacyclobutanes. The new nickel systems will provide greater opportunities for tuning the electronic environment at the metal through variation of the ancillary ligands, compared to the cobalt fluorocarbenes. Complexes **2** and **4**, with labile phosphite ligands, will be especially useful in this regard. Fluoride-abstraction from metallacycle **3** produces the nickel perfluorovinyl compound **5** as *cis* and *trans* isomers. In the presence of catalytic $HNTf_2$, **3** is converted to the perfluoroalkene complex **7**. This reactivity is similar to that seen for the related cobalt systems we reported previously.[11a] So far, however, we have not observed retro-cycloaddition to afford a new alkene/carbene, as required by the Chauvin metathesis mechanism, or the 1,3-fluoride shift needed for alkene polymerization. Ongoing work seeks to address these challenges and an ongoing computational collaboration is investigating the thermodynamics of TFE addition to the [Ni^0]=CF_2 complexes.

3.2.3 Experimental Section

General. Experiments were conducted under nitrogen, using Schlenk techniques or an MBraun glove box. All solvents were deoxygenated by purging with nitrogen. Toluene, hexanes, diethyl ether (DEE) and tetrahydrofuran (THF) were dried on columns of activated alumina using a J. C. Meyer (formerly Glass Contours) solvent purification system. C_6D_6 was dried over activated

alumina (heated at 300°C for > 8 h under vacuum) (10 wt. %). Toluene-d_8 was dried over sodium/benzophenone and vacuum transferred prior to use. $CDCl_3$ and dichloromethane (CH_2Cl_2) were dried by refluxing over CaH_2, distillation and filtration through activated alumina (5 wt. %). All solvents were stored over activated (heated at ~ 250°C for >8 h under vacuum) 4 Å molecular sieves. Glassware was oven-dried at 150°C for >2 h. Commercial chemicals: CuCl (Strem, 99.99%), bis(cyclooctadiene)nickel(0) [$Ni(COD)_2$, Strem, 98%], 1,2-bis(diphenylphosphino)ethane (DPPE) (Strem, 99%), trifluoroacetic anhydride (Aldrich, >99%), graphite powder (synthetic, 7-11 micron, Alfa Aesar, 99%), potassium (Aldrich, 99.5%, cubes in mineral oil), trimethylsilyl trifluoromethanesulfonate (Me_3SiOTf, Aldrich, 99%), bis(trifluoromethanesulfonyl)imide ($HNTf_2$, Fluka, ≥95%). Deuterated (≥99.5%) NMR solvents were purchased from Cambridge Isotopes Labs. Tetrafluoroethylene (TFE) was made by depolymerizing polytetrafluoroethylene (Scientific Polymer Products, powdered) under vacuum, using a slightly modified literature procedure[33] [10-20 mTorr, 650°C, 15-20 g scale, product stabilized with ~ 0.3 wt. % R(+)-limonene (Aldrich, 97%)], giving TFE of ≥97% purity. ^1H, ^{19}F and $^{31}P\{^1H\}$NMR spectra were recorded on 300 MHz Bruker Avance or AvanceII instruments at room temperature (RT, 23±1°C), except where noted. ^1H NMR spectra were referenced to the residual proton peaks associated with the deuterated solvents (C_6D_6: 7.16 ppm; $CDCl_3$: 7.26 ppm; toluene-d_8: 2.09 ppm). ^{19}F NMR spectra were referenced to internal 1,3-bis(trifluoromethyl)benzene (BTB) (Aldrich, 99%, deoxygenated by purging with nitrogen, stored over activated 4 Å molecular sieves), set to –63.5 ppm. ^{19}F NMR yields were obtained from the relative integrations of quantitative BTB and product peaks, using a delay time of 10 s. $^{31}P\{^1H\}$NMR data were referenced to external H_3PO_4 (85% aqueous solution), set to 0.0 ppm. UV-vis spectra were recorded on a Cary 100 instrument, using sealable quartz cuvettes (1.0 cm pathlength). Elemental analyses were performed at the University of Montreal (Montreal, Quebec, Canada).

Synthesis of potassium graphite (KC_8) (adapted from ref. 34). Graphite powder (4.00 g, 0.333 mol) was heated (>300°C) in a sand bath under vacuum (<20 mTorr) for 2 h. In glove box: potassium metal (freshly cut lump, surface contamination removed) (1.70 g, 0.0434 mol) was added to the flask containing the graphite, along with glass-covered stir bar. The flask was sealed under vacuum (<20 mTorr) and heated at 170°C with stirring for 2.5 h until the potassium

was consumed and brown-bronze homogeneous powder was obtained. This material was stored in the under nitrogen at –35°C.

Synthesis of $Ni(CF_3)(OC(O)CF_3)(PPh_3)_2$ (adapted from ref. 35). The published procedure was followed with minor modifications: $Ni(COD)_2$ was added, by solid addition funnel, to a vigorously stirred solution of PPh_3 in THF. The dark red mixture was stirred at RT for *5 min* (instead of 15 min), before cooling in an acetone/dry ice. The shorter mixing time gave better yields (65-70%) in our hands. ^1H, ^{19}F, $^{31}P\{^1H\}$ NMR data were consistent with those reported, except for a minor impurity observed by ^{19}F NMR {(282 MHz, $CDCl_3$) δ –21.1 (apparent s), <5% of total integration by ^{19}F NMR}.

Synthesis of $Ni(CF_3)(OC(O)CF_3)$(DPPE) (adapted from ref. 36). We performed this reaction on a larger scale than reported and modified to the procedure to avoid the use of CH_2Cl_2 solvent, as follows. $Ni(CF_3)(OC(O)CF_3)(PPh_3)_2$ (3.00 g, 3.92 mmol) and DPPE (1.57 g, 3.95 mmol) were combined as solids and DEE (150 mL) was added with stirring, giving an orange-yellow suspension. The flask was sealed and stirred at RT for ~ 12 h, affording a new yellow suspension (very similar in appearance to the original mixture). The yellow solid was recovered by filtration, washed with DEE (~ 5 mL x 3) and dried under vacuum. Yield: 2.38 g, 3.72 mmol (MW: 639.1), 90% based on $Ni(CF_3)(OC(O)CF_3)(PPh_3)_2$. ^1H, ^{19}F, $^{31}P\{^1H\}$ NMR data were consistent with those reported and indicated pure material.

Synthesis of $Ni(CF_2CF_3)(OC(O)CF_2CF_3)$(DPPE)(adapted from ref. 36). The published procedure was followed [3.64 mmol scale, in $Ni(COD)_2$] with the modification noted above for the synthesis of $Ni(CF_3)(OC(O)CF_3)(PPh_3)_2$ (i.e., 5 min mixing time at RT for the $Ni(COD)_2/PPh_3$ solution before cooling). Yield: 1.89 g (bright yellow powder), 2.56 mmol (MW: 739.2) 70% (crude) based on $Ni(COD)_2$. ^1H, ^{19}F, $^{31}P\{^1H\}$ NMR data in $CDCl_3$ were consistent with those reported except for minor impurities observed by ^{19}F {(282 MHz, $CDCl_3$) δ –92.5 (d, J = 37 Hz), –80.6 (s), 4% of total integration; $^{31}P\{^1H\}$ NMR (121 MHz, $CDCl_3$) δ 39.6 (s)].

Synthesis of 1 $Ni(=CF_2)$(DPPE)$(P(OMe)_3)$. $Ni(CF_3)(OC(O)CF_3)$(DPPE) (1.00 g, 1.56 mmol) was combined with THF (30 mL), giving yellow-orange solution. With stirring, $P(OMe)_3$ (192 μL, 202 mg, 1.63 mmol) was added, causing the mixture to become slightly darker orange. Within 5 min of adding the phosphite, the vessel was placed in an acetone/dry ice bath and

allowed to cool to ~ –80°C over 20 min, with stirring. KC_8 (470 mg, 3.48 mmol, 2.2 equiv) was added in portions to the cooled mixture over 5 min. A dark brown-orange suspension was obtained, which was stirred at ~ –80°C for 5 min after the addition of the KC_8 was finished and then the vessel was allowed to warm to 10°C over 50 min. The solvent/volatiles were removed under vacuum at or below RT. The residue was extracted with DEE (10 mL x 4) and the extracts were filtered through Celite (~ 1 cm in a 15 mL medium fritted funnel). The dark orange-red filtrate was concentrated to ~ 5-10 mL under vacuum, causing red-orange solid to form. Hexanes (~ 40 mL) were added and the suspension was cooled (–35°C) for ~ 20 h. While the mixture was still cold, the solid was recovered by filtration; the red solid was washed with hexanes (~ 1.5 mL x 5) and then dried under vacuum. Yield: 682 mg, 1.08 mmol (MW: 631.2), red crystalline powder, 69% based on Ni(DPPE)[OC(O)CF_3](CF_3), stored at –35°C. UV-vis (0.6 mM in CH_2Cl_2): $\lambda_{max}(\varepsilon)$ = 430 (1200). ^{1}H NMR (300 MHz, C_6D_6) δ 1.92 (m, 2H, PC$\underline{H}^A$H^{B}C$\underline{H}^A$H^{B}P), 2.24 (m, 2H, PCH$^A\underline{H}^B$CH$^A\underline{H}^B$P), 3.26 (d, $^3J_{HP}$ = 12 Hz, 9H, OCH_3), 7.00-7.19 (ov m, 12H, Ar-H), 7.42 (m, 4H, Ar-H), 7.92 (m, 4H, Ar-H). ^{19}F NMR (282 Hz, C_6D_6) δ 92.0 (dt, $^3J_{FP}$ = 61 Hz and 42 Hz, 2F, Ni=CF_2). ^{31}P{^{1}H} (121 MHz, C_6D_6) δ 46.2 [dt, $^2J_{PP}$ = 31 Hz, $^3J_{PF}$ = 42 Hz, 2P, Ni(DPPE)], 161.5 [apparent septet, tt, $^2J_{PP}$ = 31 Hz, $^3J_{PF}$ = 61 Hz, 1P, P$(OMe)_3$]. Anal. Calc. for $C_{30}H_{33}F_2NiO_3P_3$: C, 57.09, H, 5.27. Found: C, 56.90, H, 5.20. Single crystals suitable for X-ray diffraction were grown from hexanes/toluene (~ 5:1 v/v) at –35°C (see below for additional crystallographic details).

Attempted synthesis of Ni(=CFCF_3)(DPPE)(P$(OMe)_3$). The procedure described above for the synthesis of **1** was followed, using Ni(DPPE)X(CF_2CF_3) [X = $CF_2CF_3C(O)O$ or Br] (0.37 mmol scale), to the point that the THF solution warmed to RT. A portion of this solution was removed from the bulk reaction mixture, filtered through Celite (1 cm in a Pasteur pipet) and the filtrate was collected in an NMR tube containing a C_6D_6 capillary (BTB added for ^{19}F NMR reference). ^{19}F and ^{31}P{^{1}H} NMR data showed numerous products but no evidence for the target nickel fluorocarbene complex. A similar approach, using Na(Hg) (2.2 equiv) in THF as the reductant, also failed to yield Ni(DPPE)[P$(OMe)_3$][=CF(CF_3)].

Synthesis of 2 {Ni(=CF_2)(P$(OMe)_3)_3$}. Compound **1** (200 mg, 0.317 mmol) was combined with hexanes (2.5 mL) and P$(OMe)_3$ (83 µL, 87 mg, 0.70 mmol) was added with stirring (orange-red suspension). After 10 min, CuCl (35 mg, 0.35 mmol) was added. The vial was protected from light and vigorous stirring was continued for 14 h (at ~ 27°C in the glove box); during this time,

the color of the supernatant solution and the suspended solid became lighter orange. The suspension was filtered through Celite (~ 1 cm in a Pasteur pipet) to remove hexanes-insoluble Cu(DPPE)Cl; the origin vial/Celite mini-filter were washed with hexanes (~ 0.3 mL x 3) and these washings were collected with the rest of the orange filtrate. The solvent/volatiles were removed from the filtrate under vacuum. The product was sublimed (5-10 mTorr, 30°C; the condensation probe was cooled with dry ice/acetone slurry). The orange material was washed from the sublimation probe with DEE into a pre-weighed vial. Removal of solvent under vacuum gave **2** as orange waxy semi-solid. Yield: 104 mg, 0.216 mmol (MW: 480.9), 68% based on **1**, stored at –35°C. Note: the purity of the crude product, before sublimation, is >95% by ^{1}H, ^{19}F and ^{31}P NMR. UV-vis (0.6 mM in CH_2Cl_2): $\lambda_{max}(\varepsilon)$ = 397 (1200). ^{1}H NMR (300 MHz, C_6D_6) δ 3.54 (m, 27H, OC<u>H</u>$_3$). ^{19}F NMR (282 Hz, C_6D_6) δ 102.5 (q, $^{3}J_{FP}$ = 59 Hz, 2F, Ni=CF_2). ^{31}P{^{1}H} (121 MHz, C_6D_6) δ 162.8 (t, $^{3}J_{PF}$ = 59 Hz). Anal. Calc. for $C_{10}H_{27}F_2NiO_9P_3$: C, 24.97, H, 5.66. Found: C, 24.75, H, 5.74.

Synthesis of 3 [Ni(κ^2-$CF_2CF_2CF_2$-)(DPPE)]. Compound **1** (300 mg, 0.475 mmol) was combined with THF (5 mL) in a 50 mL Pyrex® tube, sealable with a single Teflon® valve (i.e., a "bomb"), affording a dark orange-red solution. The bomb was degassed with three freeze-pump-thaw cycles. TFE (2 atm) was added to the evacuated bomb, which was sealed under TFE pressure. The mixture was stirred at RT for ~ 25 h (color changed from orange-red to yellow). The TFE pressure was vented and the solution was transferred to a 25 mL round-bottom flask, which was sealed with a vacuum adaptor. Removal of the solvent/volatiles under vacuum gave yellow solid; toluene (~ 3 mL) was added to the residue, giving a yellow suspension, and was removed under vacuum (to remove the phosphite by-product, which otherwise appears in the product). Toluene (3 mL) was added to the residue and, after stirring the resulting suspension for 5 min, hexanes (20 mL) were added. The flask was sealed and cooled (–35°C) for ~ 16 h. The yellow solid was recovered by filtration while cold, washed with hexanes (~ 3 mL x 4) and dried under vacuum. Yield: 252 mg, 0.415 mmol (MW: 607.1), 87% yield based on Ni, stored at –35°C. UV-vis (0.8 mM in CH_2Cl_2): $\lambda_{max}(\varepsilon)$ = 370-470 (tailing signal overlapping with off-scale absorbances in the UV region) (ε = 250 L mol^{-1} cm^{-1} at 400 nm). ^{1}H NMR (300 MHz, $CDCl_3$) δ 2.19 (m, 4H, C<u>H</u>$_2$C<u>H</u>$_2$), 7.39-7.55 (ov m, 12H, Ar–<u>H</u>), 7.61-7.77 (ov m, 8H, Ar–<u>H</u>). ^{19}F NMR (282 Hz, $CDCl_3$) δ –124.5 (m, 2F, β-CF_2), –117.1 [apparent triplet, $^{3}J_{FP}$ (avg) = 21 Hz, 4F, α-CF_2]. ^{31}P{^{1}H} (121 MHz, $CDCl_3$) δ 44.9 [quintet of triplets, $^{3}J_{PF}$ (avg) = 21 Hz, $^{4}J_{PF}$ = 6 Hz].

Anal. Calc. for $C_{29}H_{24}F_6NiP_2$: C, 57.37, H, 3.98. Found: C, 57.30, H, 4.01. Single crystals suitable for X-ray diffraction were grown from toluene/THF (~ 1:8 v/v) at –35°C (see below for additional crystallographic details).

Synthesis of 4 {Ni(κ^2-$CF_2CF_2CF_2$-)[P(OMe)$_3$]$_2$} for NMR characterization. A 0.080 M solution of **2** in C_6D_6 (0.5 mL), in a J. Young NMR tube with a known quantity of BTB, was degassed with three freeze-pump-thaw cycles. TFE was added (1.7 atm) to the evacuated tube, allowing >1 min for the gas to saturate the solution/headspace. The tube was sealed under TFE pressure and left to stand at RT for 20 h before collecting NMR data. Compound **2** was completely consumed and the yield of **4**, from ^{19}F NMR integration relative to BTB, was >92% (three trials). Aside from unreacted TFE, the only contaminant was trace (<3%) of Ni[P(OMe)$_3$]$_2$(η^2- CF_2=$CFCF_3$) (**6**). ^{1}H NMR (300 MHz, C_6D_6) δ 3.45 [d, $^3J_{HP}$ = 11 Hz, $POCH_3$ free/Ni-bound P(OMe)$_3$]. ^{19}F NMR (282 Hz, C_6D_6) δ –132.5 (s, unreacted TFE), –122.1 (quintet, $^3J_{FF}$ = 3 Hz, 2F, β-CF_2), –103.9 (apparent s, 4F, α-CF_2). ^{31}P{^{1}H} (121 MHz, C_6D_6) δ 133.1 [s, free/Ni-bound P(OMe)$_3$]. Note (i): Attempts to purify **4**, by removing solvent, washing with cold hexanes, and drying in vacuo, resulted in greater amounts of **6** as a contaminant. Note (ii): **4** is quantitatively converted to **3** by treatment with DPPE (1 equiv) with loss of P(OMe)$_3$ (2 equiv).

Synthesis of 5 [Ni(DPPE)(OTf)(cis- and trans-CF=$CFCF_3$)] for NMR characterization. Complex **4** (36 mg, 0.059 mmol) was partially dissolved in $CDCl_3$ (0.9 mL) in a vial with a stir bar. The vial/yellow suspension was cooled to –35°C in the glove box freezer and, immediately upon removal from the freezer, Me_3SiOTf (11 µL, 13 mg, 0.060 mmol) was added and the mixture was stirred at RT for 20 min. The yellow suspension became homogeneous and darkened to orange-yellow upon adding the silyl triflate; after 10-15 min, crystalline precipitate had formed. The solvent/volatiles were removed under vacuum to give yellow solid. The solid was dissolved in 1.50 mL of CH_2Cl_2 and BTB (6.3 µL, 8.7 mg, 0.041 mmol) was added. A portion (0.6 mL) was removed for ^{19}F and ^{31}P{^{1}H} NMR analysis. The ^{19}F NMR yield of **5** (cis and trans isomers) was 82% (cis/trans ≈ 4:1). For ^{1}H NMR data, the solvent was removed under vacuum from the above solution and a portion of the residue was dissolved in $CDCl_3$ (sparingly soluble). **5** (cis): ^{19}F NMR (282 Hz, CH_2Cl_2 with C_6D_6 capillary) δ –142.6 [doublet of quartets, $^3J_{FF}$ = 17 Hz, $^4J_{FP}$ = 14 Hz, 1F, CF=C<u>F</u>(CF_3)], –103.9 [doublet of quartets, $^3J_{FP}$ = 31 Hz, $^4J_{FF}$ = 7 Hz, 1F, C<u>F</u>=CF(CF_3)], –78.8 (s, 3F, $SO_2C\underline{F}_3$), –68.7 [ddd, $^3J_{FF}$ = 17 Hz, $^4J_{FF}$ = 7 Hz, $^5J_{FP}$ = 3 Hz, 3F, CF=CF(C<u>F</u>$_3$)]. ^{31}P{^{1}H} (121 MHz, CH_2Cl_2 with C_6D_6 capillary) δ 42.7 (ddd, $^2J_{PP}$ = 50 Hz,

$^{3}J_{PF}$ = 31 Hz, $^{4}J_{PF}$ = 14 Hz, 1P, Ni–P^{A}), 53.7 (dm, $^{2}J_{PP}$ = 50 Hz, $^{5}J_{PF}$ cannot be discerned, 1P, Ni–P^{B}). **5** (trans): ^{19}F NMR (282 Hz, CH_2Cl_2 with C_6D_6 capillary) δ –175.0 [doublet of quartets, $^{3}J_{FF(trans)}$ = 117 Hz, $^{3}J_{FF}$ = 13 Hz, 1F, CF=C<u>F</u>(CF_3)], –120.1 [dm, $^{3}J_{FF(trans)}$ = 117 Hz, $^{3}J_{FP}$ = 34 Hz, $^{3}J_{FF}$ = 21 Hz, 1F, C<u>F</u>=CF(CF_3)], –68.6 (dd, $^{3}J_{FF}$ = 21 Hz, $^{3}J_{FF}$= 13 Hz, 3F, CF=CF(C<u>F</u>$_3$), overlapping with CF_3 peak of cis isomer). $^{31}P\{^{1}H\}$ (121 MHz, CH_2Cl_2 with C_6D_6 capillary) δ 41.6 (dd, $^{2}J_{PP}$ = 47 Hz, $^{3}J_{PF}$ = 34 Hz, 1P, Ni–P^{A}), 53.9 (dm, $^{2}J_{PP}$ = 47 Hz, 1P, overlapping with P signal of cis isomer, Ni–P^{B}). ^{1}H NMR (300 MHz, $CDCl_3$) for cis <u>and</u> trans isomers: δ 0.07 (s, trace silicone grease), 1.46-1.68 (ov m, 4H, C<u>H</u>$^{A}_2$C<u>H</u>$^{B}_2$, minor trans isomer), 2.18-2.60 (ov m, 4H, C<u>H</u>$^{A}_2$C<u>H</u>$^{B}_2$, major cis isomer), 5.30 (trace CH_2Cl_2), 7.22-7.76 (ov m, Ar–<u>H</u>, cis and trans isomers), 7.76-7.97 (ov m, Ar–<u>H</u>, cis and trans isomers), 8.03 (m, 2H, Ar–<u>H</u>, cis isomer), 8.48 (m, 2H, Ar–<u>H</u>, cis isomer). The ^{1}H NMR spectrum also showed a symmetrical multiplet (2.00 ppm; integration ≈ 20% relative to the overlapping C<u>H</u>$^{A}_2$C<u>H</u>$^{B}_2$ peaks of the major cis isomer), apparently belonging to the $CH^{A}_2CH^{A}_2$ substructure of Ni(DPPE)X_2. It is possible that X = OTf, although the ^{1}H chemical shift of the $CH^{A}_2CH^{A}_2$ multiplet does not match the literature value (2.32 ppm) for this known compound and the corresponding ^{31}P NMR signal was not observed, possibly due to isomerism with the paramagnetic tetrahedral form.[36] The ^{19}F and $^{31}P\{^{1}H\}$ NMR spectra of the cis-/trans-vinyl mixture are shown below.

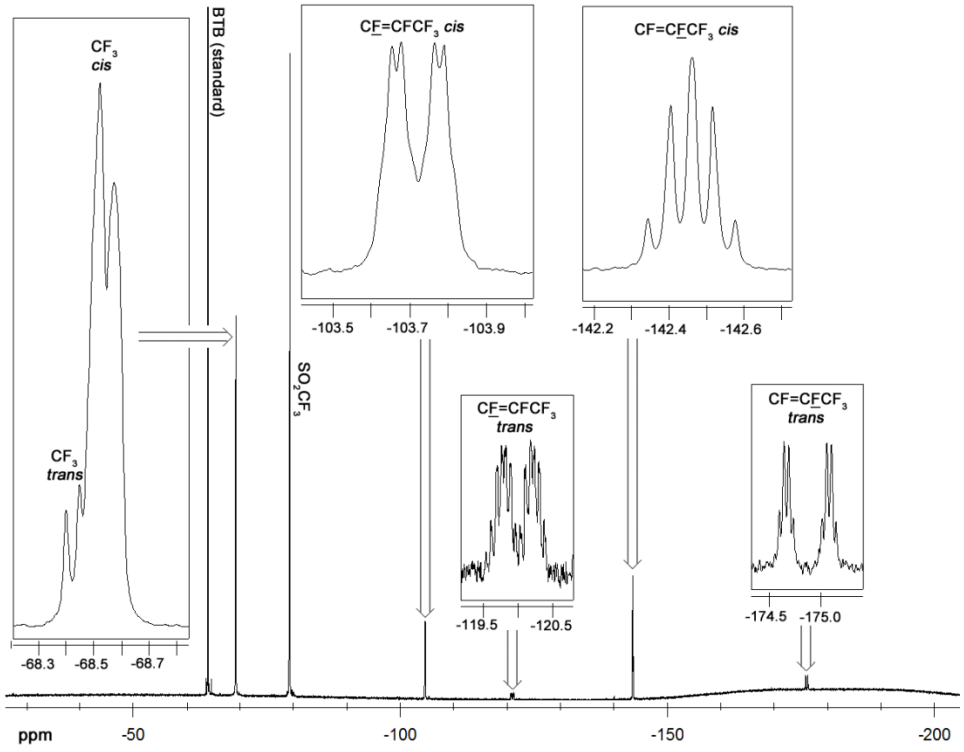

Figure 3.3: ^{19}F NMR (282 MHz, CH_2Cl_2 with C_6D_6 capillary) spectrum of **5** [Ni(DPPE)(OTf)(cis- and trans-$CF=CFCF_3$)]. The product peaks are expanded in the insets. Note that the top of the BTB peak is off-scale.

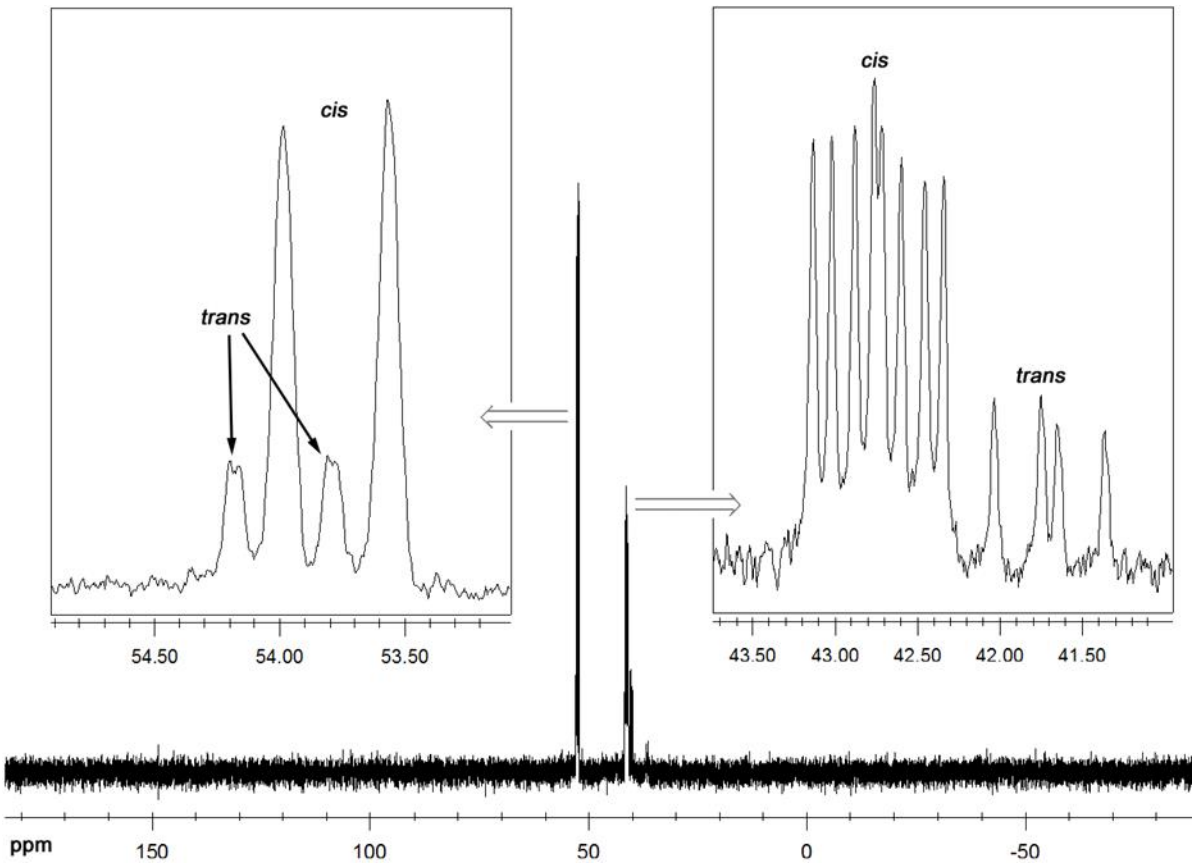

Figure 3.4: $^{31}P\{^{1}H\}$ NMR (121 MHz, CH_2Cl_2 with C_6D_6 capillary) spectrum of **5** [Ni(DPPE)(OTf)(cis- and trans-CF=CFCF$_3$)]. The product peaks are expanded in the insets. Minor contaminants are not labeled.

Synthesis of 6 [Ni(η^2- CF_2=CFCF$_3$**)(DPPE)] for NMR characterization.** Complex **3** [0.60 mL of 0.083 M solution in CH_2Cl_2 (0.050 mmol) with BTB (0.032 M, 0.019 mmol)] was treated with $HNTf_2$ [30 µL of 0.050 M solution in CH_2Cl_2 (0.0015 mmol), 3 mol %] in a screw-cap NMR tube containing a C_6D_6 capillary at RT. Upon mixing, the color changed slightly from yellow to deeper/more intense yellow. ^{19}F and $^{31}P\{^{1}H\}$ NMR data was obtained 30-40 min after adding the acid and showed complete consumption of **3** and the production of **6** as the primary product (>85% by ^{19}F NMR, 3 trials). NMR data for **6**: ^{19}F (282 Hz, CH_2Cl_2 with C_6D_6 capillary) δ –212.4 [dm, $^{3}J_{FF(trans)}$ = 81 Hz, $^{3}J_{FP}$ = 10 Hz, 1F, C$\underline{F}$CF$_3$], –117.1 [m, $^{2}J_{FF}$ = 188 Hz, $^{3}J_{FF(trans)}$ = 81 Hz, $^{3}J_{FP}$ = 45 Hz, C$\underline{F}^{A}F^{B}$, trans to CF$_3$], –110.0 (m, $^{2}J_{FF}$ = 188 Hz, $^{3}J_{FP}$ = 36 Hz, $CF^{A}\underline{F}^{B}$, cis to

CF_3), –65.7 (m, 3F, CF_3). $^{31}P\{^1H\}$ NMR (121 Hz, CH_2Cl_2 with C_6D_6 capillary) δ 38.1 (m, $^2J_{PP}$ = 46 Hz, $^3J_{PF}$ = 45, 36 and 10 Hz, 1P, Ni-P^A), 42.7 (m, $^2J_{PP}$ = 46 Hz, 1P, Ni-P^B). Removal of the solvent under vacuum gave yellow solid residue, which was dissolved in $CDCl_3$ to obtain ^1H NMR data. ^1H NMR (300 Hz, $CDCl_3$) δ 1.87-2.73 (ov m, 4H, $C\underline{H}^B{}_2C\underline{H}^A{}_2$), 7.10-7.59 (ov m, 12H, Ar–H), 7.59-8.14 (ov m, 8H, Ar–H). The ^{19}F and $^{31}P\{^1H\}$ NMR spectra of **6** are shown below.

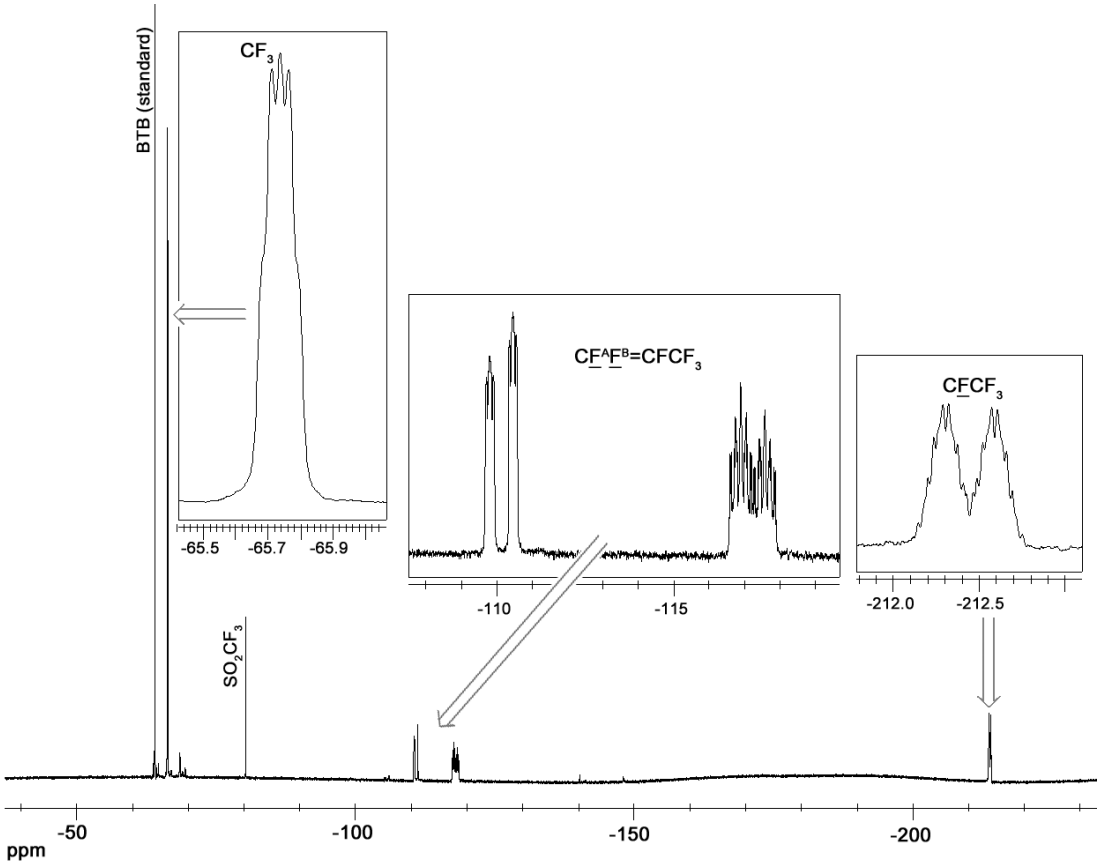

Figure 3.5: ^{19}F NMR (282 MHz, CH_2Cl_2 with C_6D_6 capillary) spectrum of **6** [Ni(DPPE)(η^2-CF_2=$CFCF_3$)]. The product peaks are expanded in the insets. Minor contaminants are not labeled. Note that the top of the BTB peak is off-scale.

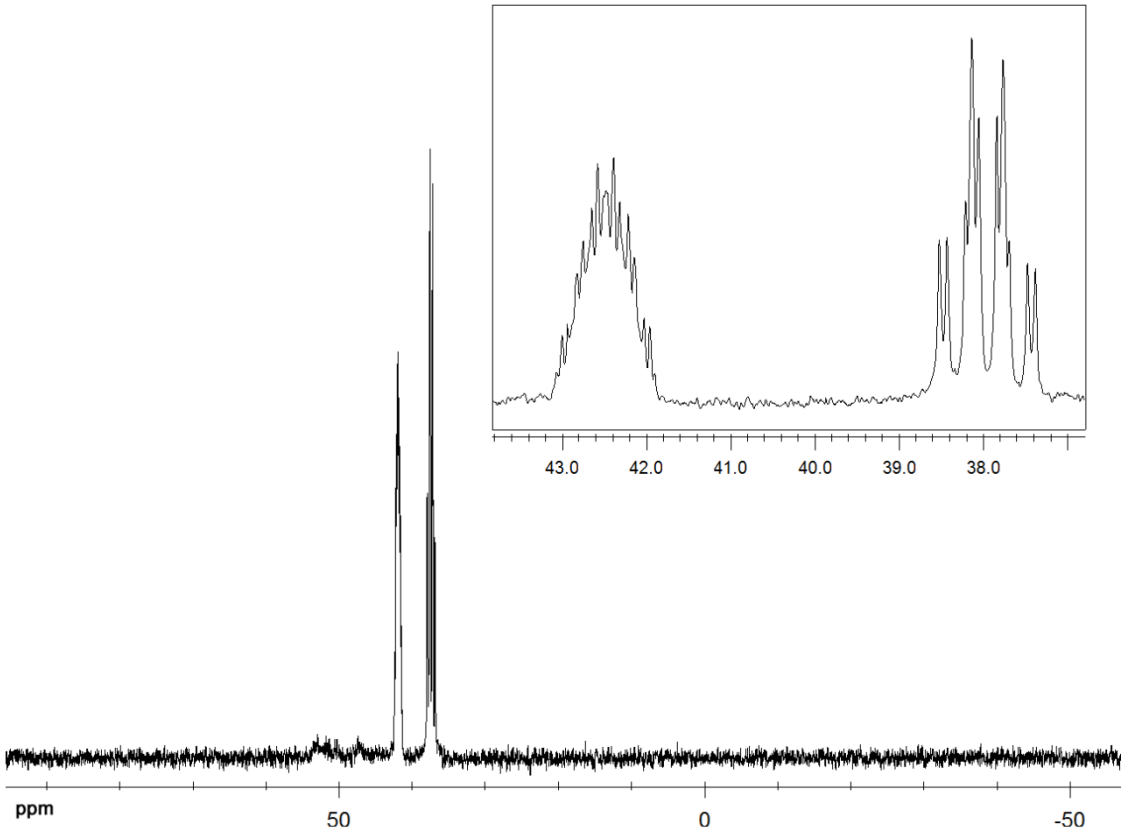

Figure 3.6: $^{31}P\{^{1}H\}$ NMR (121 MHz, CH_2Cl_2 with C_6D_6 capillary) spectrum of **6** [Ni(DPPE)(η^2-CF_2=$CFCF_3$)]. The product peaks are expanded in the insets. Minor contaminants are not labeled.

Calculation of K_{eq} for 1 + 2 $P(OMe)_3$ ⇌ 2 + DPPE. Complex **2** (19 mg, 0.040 mmol), DPPE (16 mg, 0.040 mmol) and a known quantity of BTB were dissolved in C_6D_6 (0.50 mL) (0.080 M total [Ni]=CF_2 concentration). After shaking the mixture in a small vial, orange solution was obtained, which was placed in a screw-capped NMR tube. The first NMR data were collected ~ 20 min after mixing and ~ 15 min after placing the NMR tube into the probe (23°C). NMR experiments established that equilibrium was reached in <15 min at RT. The equilibrium concentrations were obtained by integration of the ^{19}F NMR signals of the carbenes (**1** and **2**) relative to known BTB. Note that ^{1}H, ^{19}F and $^{31}P\{^{1}H\}$ showed only **1**, **2**, $P(OMe)_3$ and DPPE.

Equilibrium concentrations at 23°C in C_6D_6:

[**1**] = 0.045 M; [$P(OMe)_3$] = 2*[**1**] = 0.090 M; [**2**] = 0.039 M; [DPPE] = [**2**] = 0.039 M.

K_{eq} = {[**2**][DPPE]}/{[**1**][$P(OMe)_3$]^2} = $0.039^2/(0.045*0.090^2)$ = 4.2 L mol^{-1}

Kinetic experiments: reactions of 1 and 2 with excess TFE. A toluene-d_8 solution (0.50 mL) containing **1** or **2** (0.080 M) and a known quantity of BTB, in a J. Young NMR tube, was degassed with three freeze-pump-thaw cycles. TFE was added to the evacuated tube (1.7 atm) at RT (~ 23^{o}C), allowing ~ 1 min to ensure the solution/headspace were saturated, and then tube was sealed. Within 2 min of adding the TFE, the NMR tube was placed in the NMR (AVANCE 300II) probe (preheated to 30.0^{o}C). Spectra were collected with delay times (D1) of 10 s, using 16 scans for each spectrum (acquisition time = 172 s per spectrum), with 728 s intervals between the spectra (1 spectrum per 15 min or 900 s). Data collection on the first spectrum in the kinetic series was collected 10 min (600 s) after inserting the sample in the probe. Starting material and product concentrations were obtained by integration relative to BTB. The ^{19}F NMR yields of **3** and **4** were >90%. Time traces and rate constant analyses can be found below.

Kinetic experiment: reaction of 2 with excess TFE and 20 equiv of $P(OMe)_3$. The experimental setup was identical to above, except $P(OMe)_3$ (94 µL, 99 mg, 0.80 mmol) was added to the NMR sample ~ 15 min before commencing freeze-pump-thaw cycles. A 7026 s interval between spectra was used (7026 + 174 = 7200 s or 2 h; one spectrum per 2 h). The ^{19}F NMR yield of **4** was considerably lower (60%) in the presence of excess phosphite and other unknown products were observed (several broad peaks between –65 and –75 ppm; ~ 20% of the total integration of the metallacycle, **4**). Time traces and rate constant analyses can be found below.

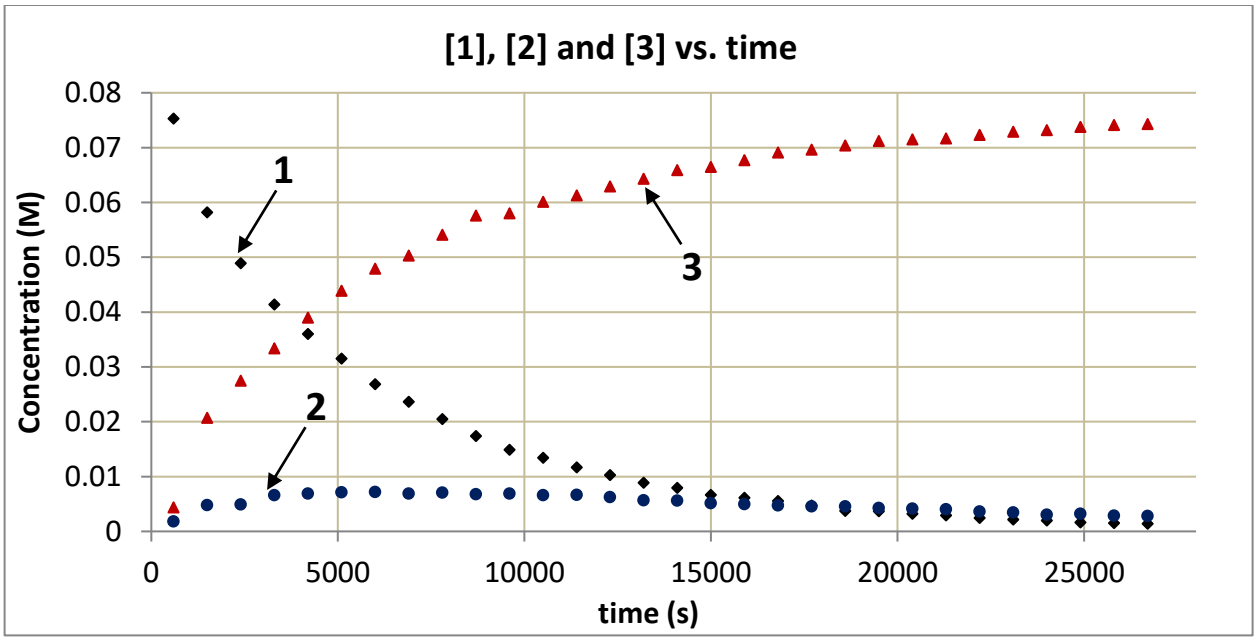

Figure 3.7: Reaction of **1** with excess TFE: Ni(=CF_2)(DPPE)($P(OMe)_3$) [**1**], Ni(=CF_2)($P(OMe)_3$)$_3$ [**2**] and Ni(κ^2-$CF_2CF_2CF_2$-)(DPPE)] [**3**] vs. time. $[\mathbf{1}]_o$ = 0.080 M in toluene-d_8; P_{TFE} = 1.7 atm; T = 30.0°C.

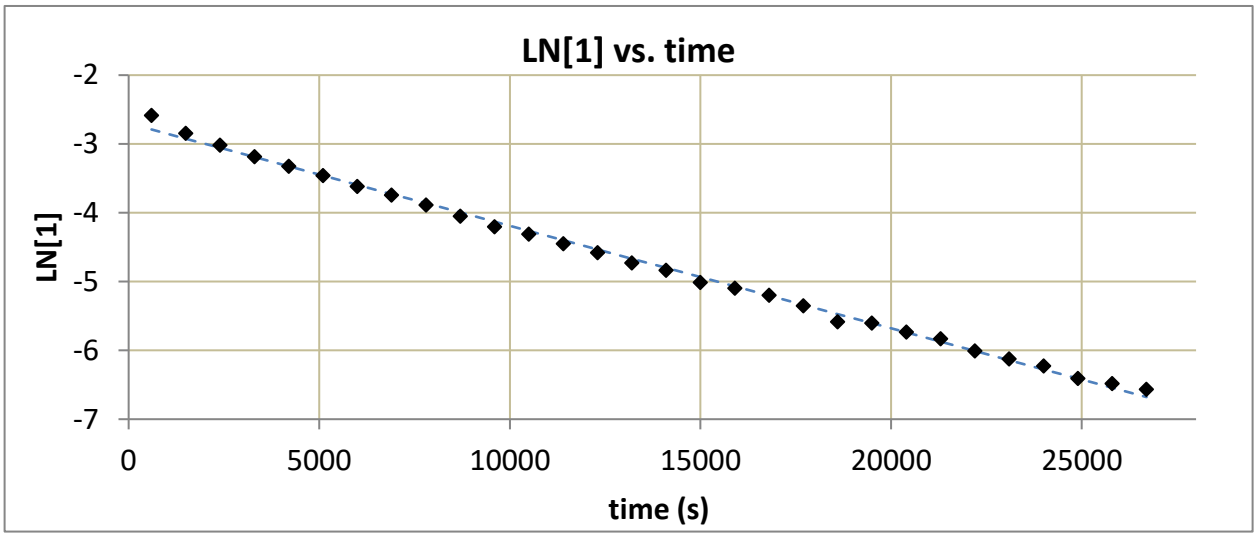

Figure 3.8: Ln[**1**] vs. time. The linear least-squares best fit (y = 1.49*10–4*x – 2.70; R2 = 0.9972, S = 0.06359) is displayed as a dotted line, corresponding to k = 1.5*10–4 s–1 (0.54 h–1) for the decay of Ni(=CF_2)(DPPE)($P(OMe)_3$) **1**.

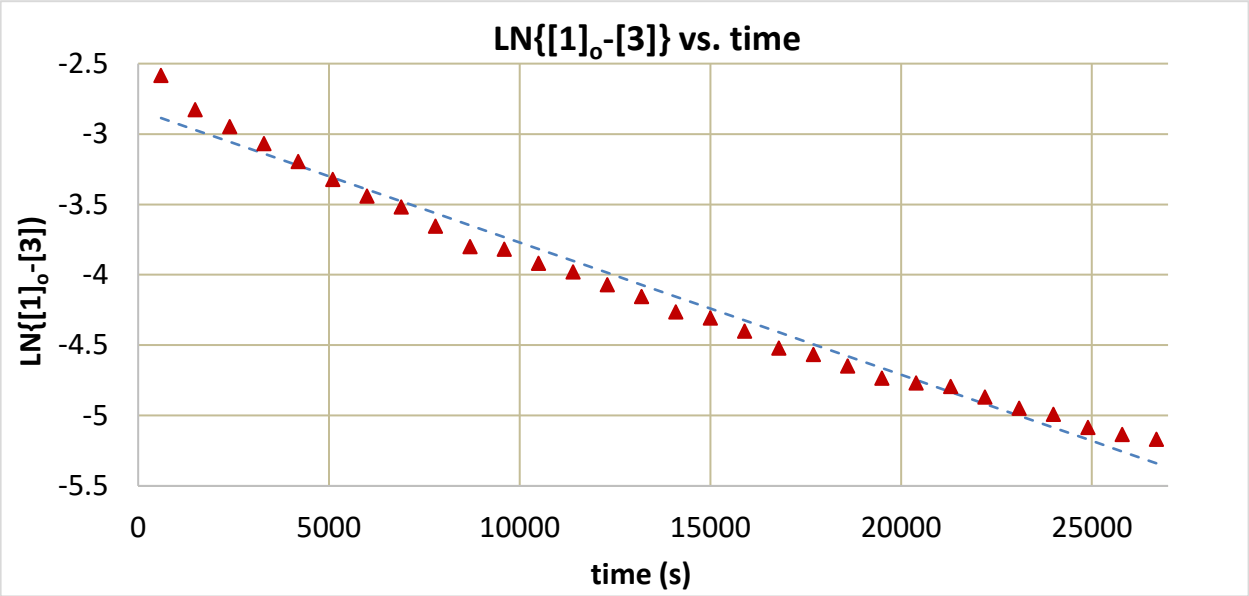

Figure 3.9: Ln{[**1**]o – [**3**]} vs. time. The linear least-squares best fit (y = 9.40*10–5*x – 2.83; R2 = 0.9805, S = 0.1069) is displayed as a dotted line, corresponding to k = 9.4*10–5 s–1 (0.34 h–1) for the growth of Ni(κ^2-$CF_2CF_2CF_2$-)(DPPE)] (**3**).

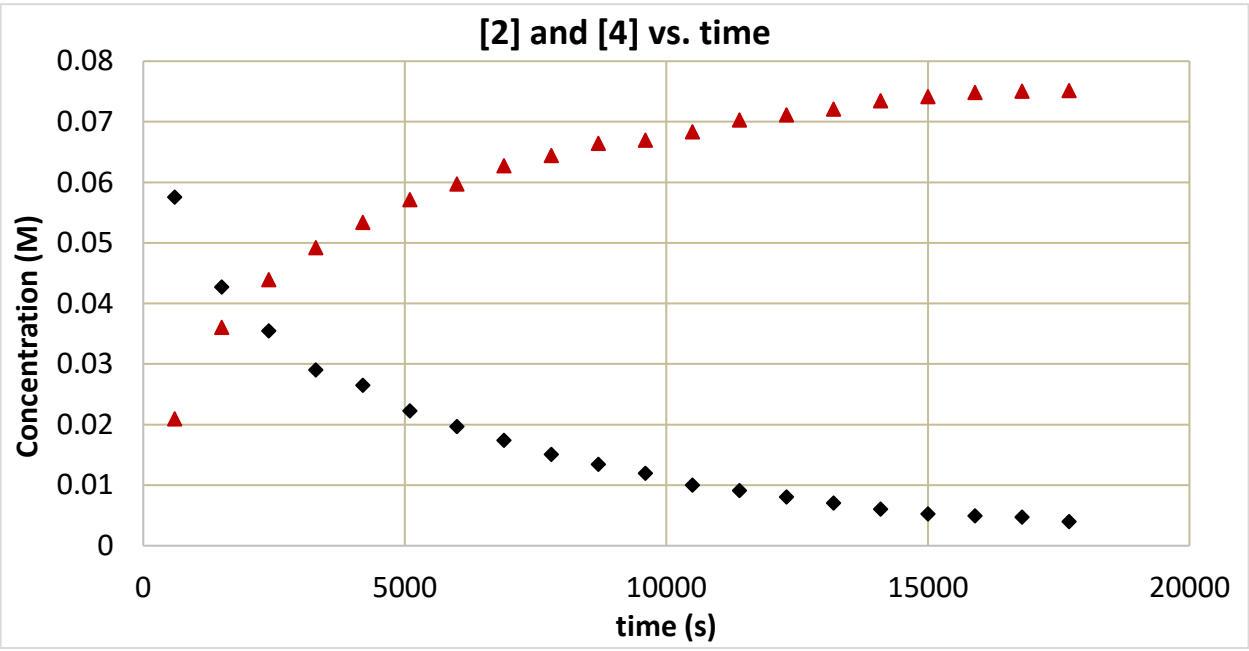

Figure 3.10: Reaction of Ni(=CF_2)($P(OMe)_3$)$_3$ (**2**) with excess TFE: [**2**] and Ni(κ^2-$CF_2CF_2CF_2$-)[$P(OMe)_3$]$_2$ [**4**] vs. time. [**2**]^o = 0.080 M in toluene-d^8; PTFE = 1.7 atm; T = 30.0^{o}C.

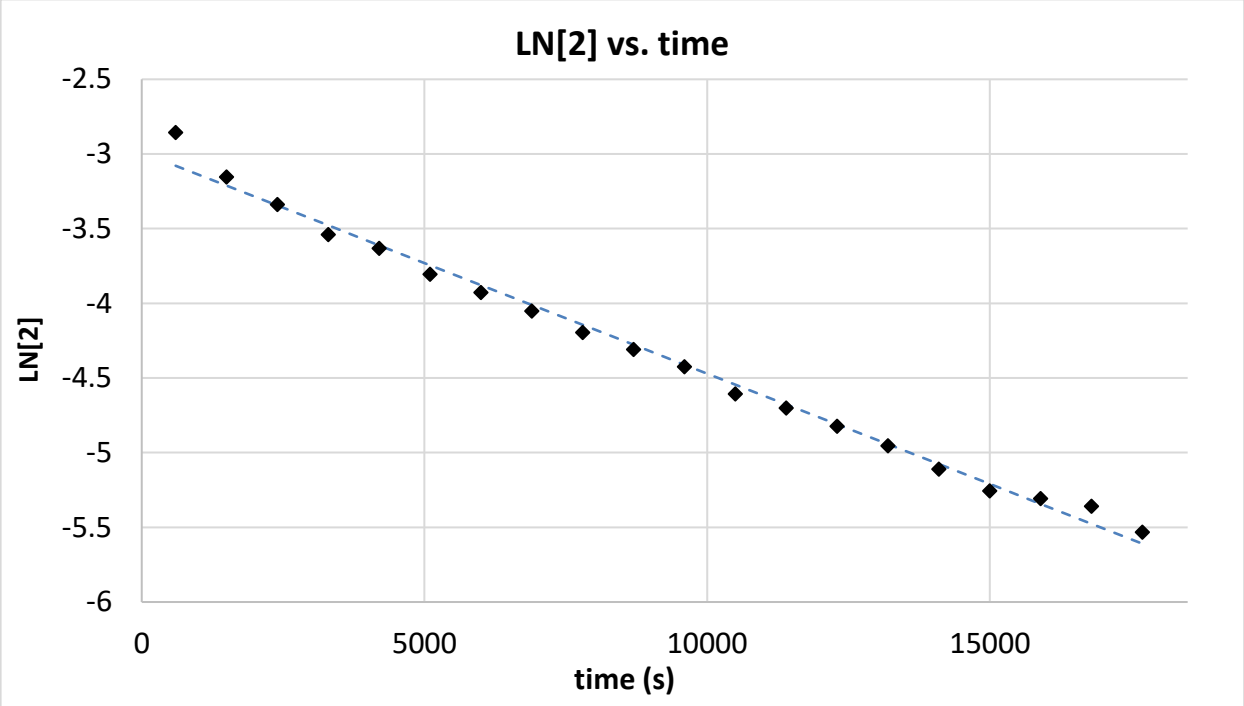

Figure 3.11: Ln[2] vs. time. The linear least-squares best fit (y = 1.48*10–4*x – 2.99; R2 = 0.9918, S = 0.07389) is displayed as a dotted line, corresponding to k = 1.5*10–4 s–1 (0.54 h–1) for the decay of $Ni(=CF_2)(P(OMe)_3)_3$ (**2**).

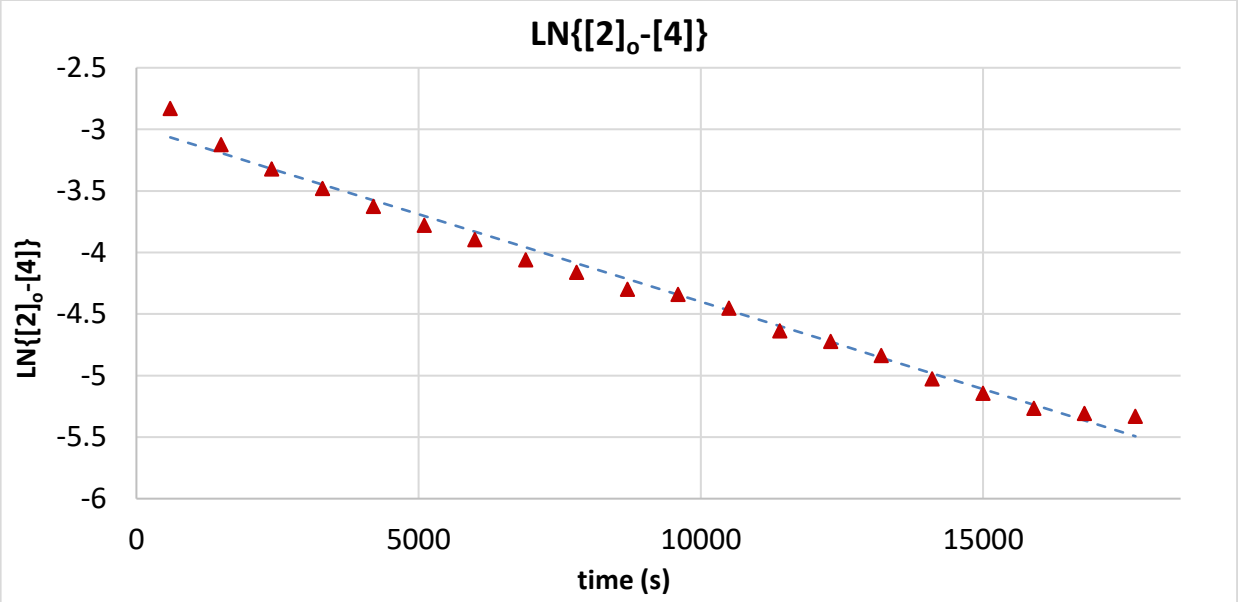

Figure 3.12: Ln{[**2**]o – [**4**]} vs. time. The linear least-squares best fit (y = 1.42*10–4*x – 2.98; R2 = 0.9881, S = 0.08526) is displayed as a dotted line, corresponding to k = 1.4*10–4 s–1 (0.50 h–1) for the growth of Ni(κ^2-$CF_2CF_2CF_2$-)[$P(OMe)_3$]$_2$ (**4**).

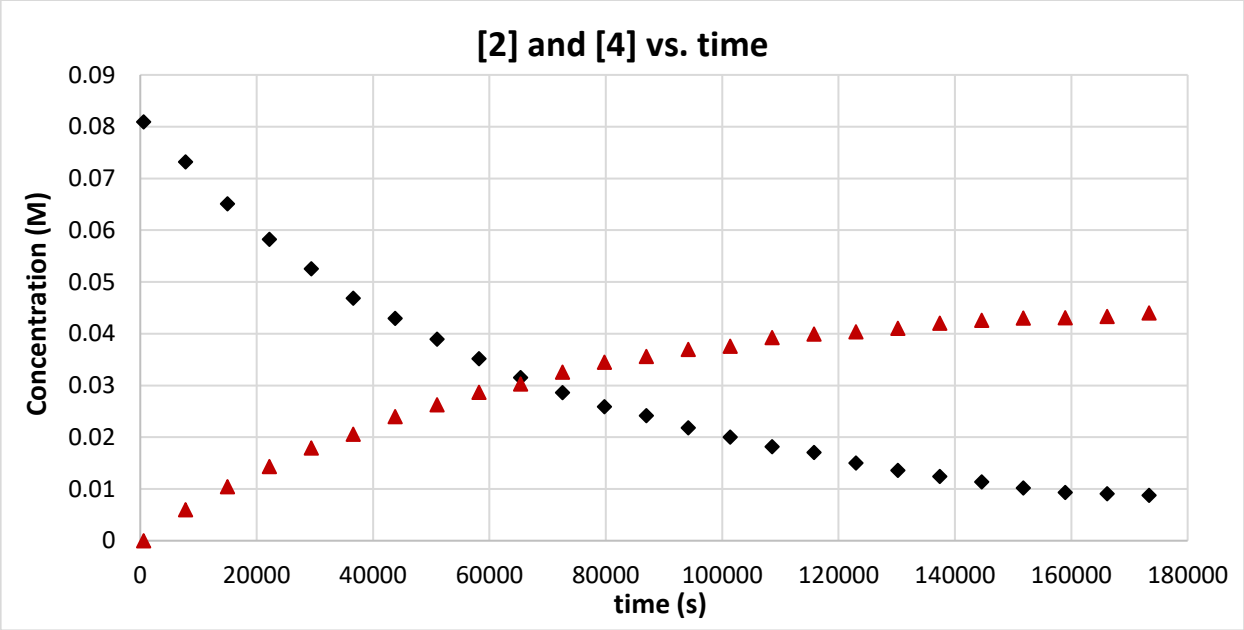

Figure 3.13: Reaction of Ni(=CF_2)($P(OMe)_3$)$_3$ (**2**) with excess TFE and 20 equiv of $P(OMe)_3$: [**2**] and [**4**] vs. time. [**2**]o = 0.080 M; $[P(OMe)_3]_o$ = 1.6 M in toluene-d_8; PTFE = 1.7 atm; T = 30.0^{o}C.

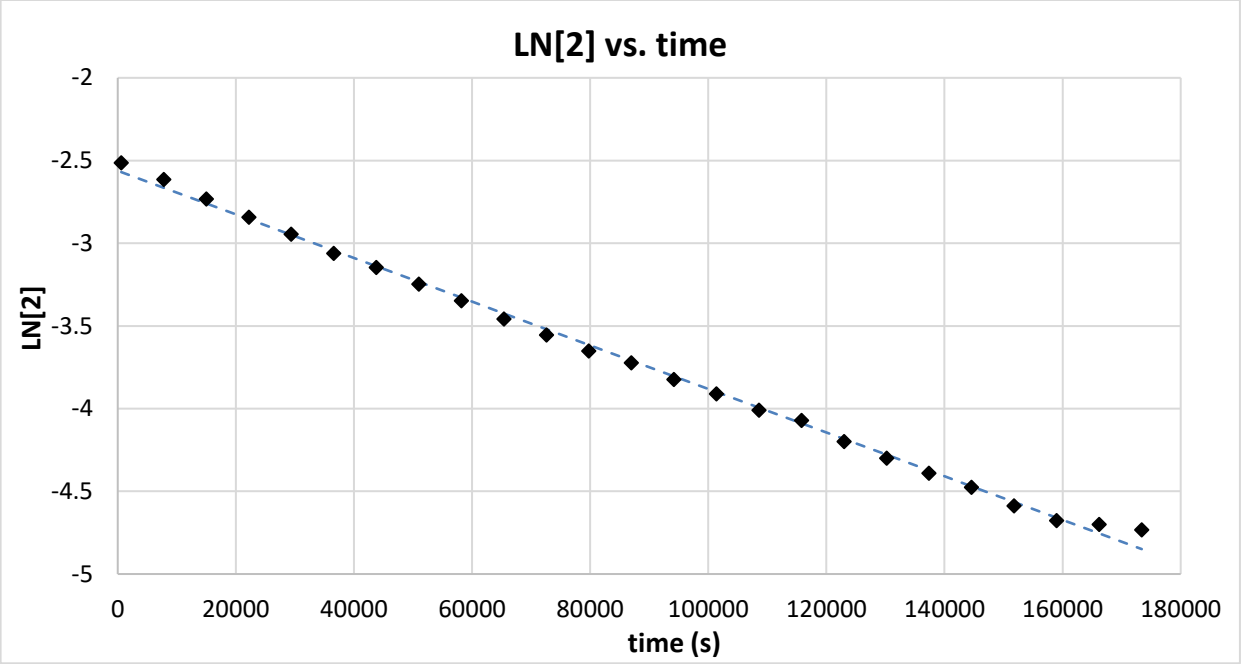

Figure 3.14: Ln[**2**] vs. time [with 20 equiv of $P(OMe)_3$]. The linear least-squares best fit (y = 1.32*10–5*x – 2.56; R2 = 0.9974, S = 0.03634) is displayed as a dotted line, corresponding to k = 1.3*10–5 s–1 (0.047 h–1) for the decay of Ni(=CF_2)($P(OMe)_3$)$_3$ (**2**).

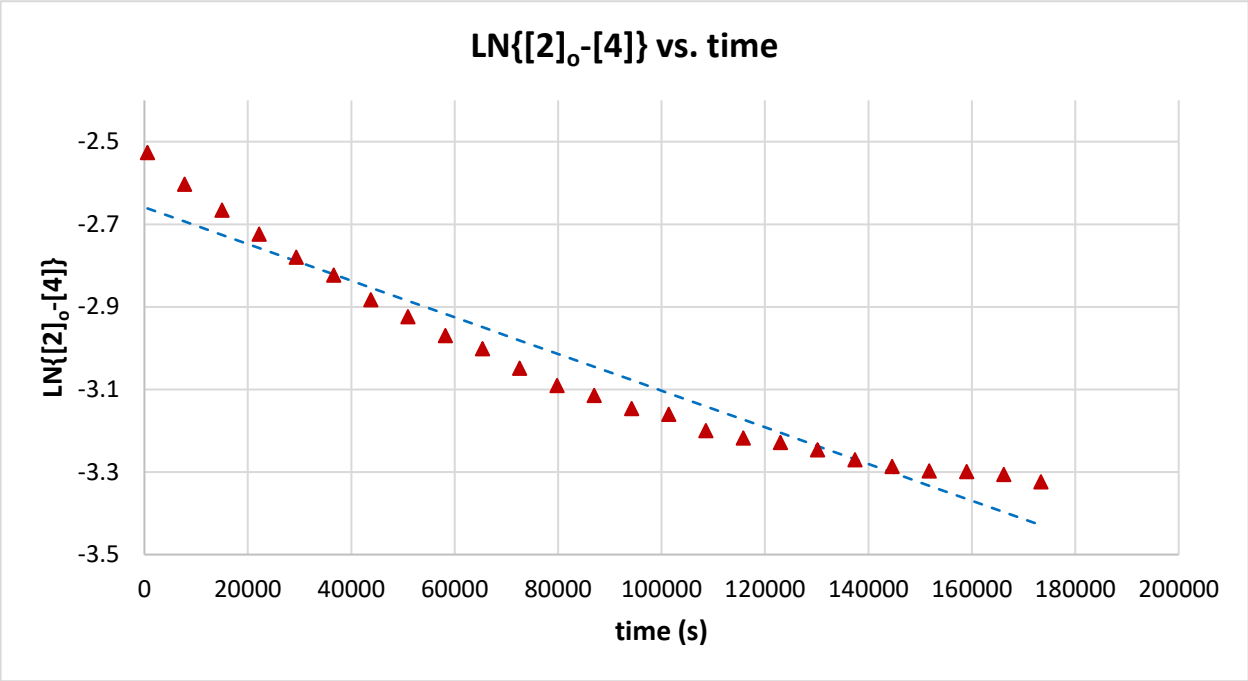

Figure 3.15: Ln{[**2**]o – [**4**]} vs. time [with 20 equiv of $P(OMe)_3$]. The linear least-squares best fit (y = 4.44*10–6*x – 2.66; R2 = 0.9347, S = 0.06352) is displayed as a dotted line, corresponding to k = 4.4*10–6 s–1 (0.016 h–1) for the growth of Ni(κ^2-$CF_2CF_2CF_2$-)$[P(OMe)_3]_2$ (**4**)

Crystallographic details for 1 {Ni(DPPE)[$P(OMe)_3$](=CF_2)} and 3 [Ni(DPPE)(κ^2-$CF_2CF_2CF_2$-)]. Samples were mounted on thin glass fibers using paraffin oil and were cooled to 200°K prior to data collection. Data were collected on a Bruker AXS KAPPA single crystal diffractometer equipped with a sealed Mo tube source (wavelength 0.71073 Å) APEX II CCD detector. Raw data collection and processing were performed with APEX II software package from BRUKER AXS.[37] Diffraction data were collected with a sequence of 0.5° ω scans at 0, 90, 180, and 270° in ϕ. Initial unit cell parameters were determined from 60 data frames collected at the different sections of the Ewald sphere. Semi-empirical absorption corrections based on equivalent reflections were applied. Solutions in centrosymmetric space group yielded chemically reasonable and computationally stable results of refinement. The structures were solved by direct methods, completed with difference Fourier synthesis, and refined with full-matrix least-squares procedures based on F^2. In the structure, compound molecules are situated

in the general position. All non-hydrogen atoms were refined anisotropically with satisfactory thermal parameters values. To achieve satisfactory thermal parameters, it was not necessary to use constraints. Additional crystallographic data and selected data collection parameters are reported below. The cif files for the following structures are available as Supporting Information.

1: Empirical formula: $C_{30}H_{33}F_2NiO_3P_3$; FW = 631.18; Crystal size: 0.130 x 0.080 x 0.060 mm^3; Crystal system: orthorhombic; Space group: $P2_12_12_1$; Z = 4; a = 10.4679(3) Å, b = 11.6610(3) Å, c = 24.7749(8) Å; α = 90°, β = 90°, γ = 90°; Volume = 3024.18(15) $Å^3$; Calculated density = 1.386 Mg/m^3; Absorption coefficient = 0.842 mm^{-1}; F(000) = 1312; Θ range for data collection: 1.644 to 28.301°; Limiting indices: -13<=h<=12, -15<=k<=15, -33<=l<=33; Reflections collected / unique: 33985 / 7446; R(int) = 0.0603; Completeness to Θ = 25.242°: 99.6 %; Max. and min. transmission: 0.7457 and 0.6763; Data / restraints / parameters: 7446 / 0 / 370; Goodness-of-fit on F^2: 1.016; Final R indices [I>2σ(I)]: R1 = 0.0396, wR2 = 0.0716; R indices (all data): R1 = 0.0644, wR2 = 0.0780; Largest diff. peak/hole: 0.442 and -0.256 e.$Å^{-3}$.

3: Empirical formula: $C_{29}H_{24}F_6NiP_2$; FW = 607.13; Crystal size: 0.230 x 0.190 x 0.170 mm^3; Crystal system: monoclinic; Space group: $P2_1$; Z = 2; a = 9.6422(6) Å, b = 15.7842(10) Å, c = 9.7038(6) Å; α = 90°, β = 116.7491(11)°, γ = 90°; Volume = 1318.82(14) $Å^3$; Calculated density = 1.529 Mg/m^3; Absorption coefficient = 0.917 mm^{-1}; F(000) = 620; Θ range for data collection: 2.350 to 28.358°; Index ranges: -12<=h<=11, -17<=k<=20, -12<=l<=12; Reflections collected / unique: 11497 / 5513; R(int) = 0.0133; Completeness to Θ = 25.242°, 99.1 %; Max. and min. transmission: 0.7457 and 0.6789; Data / restraints / parameters: 5513 / 73 / 343; Goodness-of-fit on F^2: 1.008; Final R indices [I>2σ(I)]: R1 = 0.0201, wR2 = 0.0493; R indices (all data): R1 = 0.0209, wR2 = 0.0496; 0.270 and -0.190 e.$Å^{-3}$.

Reference

([1]) (a) Olefin Metathesis: Theory and Practice; Grela, K., Ed.; John Wiley & Sons: Hoboken, NJ, 2014. (b) Handbook of Metathesis; Grubbs, R. H., Ed.; Wiley-VCH: Weinheim, Germany, 2003. (c) Fustero, S.; Simón-Fuentes, A.; Barrio, P.; Haufe, G. *Chem. Rev.* **2015**, *115*, 871-930.

([2]) Brothers, P. J.; Roper, W. R. *Chem. Rev.* **1988**, *88*, 1293-1326.

([3]) (a) Yuan, J.; Hughes, R. P.; Golen, J. A.; Rheingold, A. L. *Organometallics* **2010**, *29*, 1942-1947. (b) Trnka, T. M.; Day, M. W.; Grubbs, R. H. *Angew. Chem., Int. Ed.* **2001**, *40*, 3441-3444.

([4]) Takahira, Y.; Morizawa, Y. *J. Am. Chem. Soc.* **2015**, *137*, 7031-7034.

([5]) (a) Ojima, I. *Fluorine in Medicinal Chemistry and Chemical Biology*; Blackwell: Chichester, U.K., 2009.

([6]) (a) Wang, J.; Sánchez-Roselló, M.; Aceña, J. L.; del Pozo, C.; Sorochinsky, A. E.; Fustero, S.; Soloshonok, V. A.; Liu, H. *Chem. Rev.* **2014**, *114*, 2432-2506. (b) Zhu, W.; Wang, J.; Wang, S.; Gu, Z.; Aceña, J. L.; Izawa, K.; Liu, H.; Soloshonok, V. A. *J. Fluorine Chem.* **2014**, *167*, 37-54. (c) Jeschke, P. *ChemBioChem* **2004**, *5*, 570-589.

([7]) Im, J.; Walshe-Langford, G. E.; Moon, J.-W.; Löffler, F. E. *Environ. Sci. Technol.* **2014**, *48*, 13181-13187.

([8]) Ivin, K. J.; Rooney, J. J.; Stewart, C. D.; Green, M. L. H.; Mahtab, R. *J. Chem. Soc., Chem. Commun.* **1978**, *14*, 604-606.

([9]) (a) Taw, F. L.; Clark, A. E.; Mueller, A. H.; Janicke, M. T.; Cantat, T.; Scott, B. L.; Hay, P. J.; Hughes, R. P.; Kiplinger, J. L. *Organometallics* **2012**, *31*, 1484-1499. (b) Hughes, R. P. *Adv. Organomet. Chem.* **1990**, *31*, 183-267.

([10]) (a) Cossee, P. *J. Catal.* **1964**, *3*, 80-89. (b) Arlman, E. J.; Cossee, P. *J. Catal.* **1964**, *3*, 99-104. (c) Brookhart, M.; Green, M. L. H. *J. Organomet. Chem.* **1983**, *250*, 395-408. (d) Clawson, L.; Soto, J.; Buchwald, S. L.; Steigerwald, M. L.; Grubbs, R. H. *J. Am. Chem. Soc.* **1985**, *107*, 3377-3378.

([11]) (a) Harrison, D. J.; Lee, G. M.; Leclerc, M. C.; Korobkov, I.; Baker, R. T. *J. Am. Chem. Soc.* **2013**, *135*, 18296-18299. (b) Harrison, D. J.; Gorelsky, S. I.; Lee, G. M.; Korobkov, I.; Baker, R. T. *Organometallics* **2013**, *32*, 12-15.

([12]) Fuller, J. T.; Harrison, D. J.; Leclerc, M. C.; Baker, R. T.; Ess, D. H.; Hughes, R. P. *Organometallics*. **2015**, *34*, 5210-5213.

([13]) Vasiliu, M.; Arduengo, A. J., III; Dixon, D. A. *J. Phys. Chem. C* **2014**, *118*, 13563-13577.

([14]) Transient $[Ni{=}CF_2]^+$ and $[Ni{=}CH_2]^+$: *Halle, L. F.; Armentrout, P. B.; Beauchamp, J. L. Organometallics* **1983,** *2*, 1829-1833.

([15]) Here, carbene ligands are formulated as neutral two-electron donors and d-electron counts are calculated accordingly, consistent with the DFT analysis of the cobalt-fluorocarbene bonding. See ref. 11b.

([16]) (a) Hughes, R. P.; Laritchev, R. B.; Yuan, J.; Golen, J. A.; Rucker, A. N.; Rheingold, A. L. *J. Am. Chem. Soc.* **2005**, *127*, 15020-15021. (b) Bourgeois, C. J.; Hughes, R. P.; Yuan, J.; DiPasquale, A. G.; Rheingold, A. L. *Organometallics* **2006**, *25*, 2908-2910. (c) Yuan, J.; Hughes, R. P.; Rheingold, A. L. *Eur. J. Inorg. Chem.* **2007**, 4723-4725.

([17]) Maleckis, A.; Sanford, M. S. *Organometallics* **2014**, *33*, 3831-3839.

([18]) Attempts to make $Ni[{=}CF(CF_3)](DPPE)[P(OMe)_3]$ from $Ni(CF_2CF_3)(DPPE)[OC(O)CF_2CF_3]$, as outlined in Scheme 3.3A [*i.e.*, treatment with $P(OMe)_3$ and KC_8], were unsuccessful. See the Supporting Information.

([19]) Ariyananda, P. W. G.; Kieber-Emmons, M. T.; Yap, G. P. A.; Riordan, C. G. *Dalton Trans.* **2009**, 4359-4369.

([20]) Transient Pt(=CF_2)X_2: Cho, H.-G.; Andrews, L. *J. Am. Chem. Soc.* **2008**, *130*, 15836-15841.

([21])Martínez-Salvador, S.; Menjón, B.; Forniés; J.; Martín, A.; Usón, I. *Angew. Chem. Int. Ed.* **2010**, *49*, 4286-4289.

([22]) Computed [Ni^0]=CF_2: Dalmázio, I.; Duarte, H. A. *J. Chem. Phys.* **2001**, *115*, 1747-1756.

([23]) Computed M(=CF_2)$(CO)_3$ (M = Ni, Pd, Pt): Ehlers, A. W.; Dapprich, S.; Vyboishchikov, S. F.; Frenking, G. *Organometallics* **1996,** *15*, 105-117.

([24]) Electrophilic [Ru^{II}]=CF_2: Clark, G. R.; Hoskins, S. V.; Roper, W. R. *J. Organomet. Chem.* **1982**, *234*, C9-C12.

([25]) Nucleophilic [Ru^0]=CF_2: Clark, G. R.; Hoskins, S. V.; Jones, T. C.; Roper, W. R. *J. Chem. Soc., Chem. Commun.* **1983**, 719-721.

([26]) Conditions for kinetic experiments: 30.0°C, P_{TFE} = 1.7 atm, $[M{=}CF_2]_o$ = 0.080 M.

([27]) In C_6D_6; total [Ni=CF_2] = 0.080 M; equilibrium was reached in <15 min at RT. See the Supporting Information for more details.

([28]) The reaction of **2** with TFE in the presence of excess $P(OMe)_3$ at 30°C (i.e., the conditions used for kinetic runs) gives **4** in 60% yield by ^{19}F NMR (see the Supporting Information).

([29]) Karel, K. J.; Tulip, T. H.; Ittel, S. D. *Organometallics* **1990**, *9*, 1276-1282.

([30]) Xu, L.; Solowey, D. P.; Vicic, D. A. *Organometallics*, **2015**, *34*, 3474-3479.

([31]) ∑ bond angles around Ni1 = 360.0(1)°.

([32]) Ohashi, M.; Shibata, M.; Ogoshi, S. *Angew. Chem. Int. Ed.* **2014**, *53*, 13578-13582.

([33]) Hunadi, R. J.; Baum, K. *Synthesis* **1982**, *39*, 454.

([34]) Lalancette, J.-M.; Rollin, G.; Dumas, P. *Can. J. Chem.* **1972**, *50*, 3058-3062.

([35]) Maleckis, A.; Sanford, M. S. *Organometallics* **2014**, *33*, 3831-3839.

([36]) Fochi, F.; Jacopozzi, P.; Wegelius, E.; Rissanen, K.; Cozzini, P.; Marastoni, E.; Fisicaro, E.; Manini, P.; Fokkens, R.; Dalcanale, E. *J. Am. Chem. Soc.* **2001**, *123*, 7539-7552.

([37]) APEX Software Suite v.2010; Bruker AXS: Madison, WI, 2005.

4 Nickel Fluorocarbene Metathesis with Fluoroalkenes

"Boldness be my friend" ~ William Shakespeare

4.1 Context

As shown in Chapter 3, when moving to a more electron-rich metal like nickel(0) there was a marked increase in reactivity with TFE. For example, the nickel was capable of performing the first step of the Chauvin mechanism, metallacyclobutane formation, within hours as opposed to previous examples which took days to go to completion. Unfortunately, no metathesis products were formed. In an effort to coerce this type of reactivity out of nickel, instead of modifying the [NiP_3] metal fragment we focused on modifying the carbene fragment.

In this chapter we focus on the synthesis and reactivity of novel d^{10} [Ni]=CF(CF_3) carbenes. By removing a heteroatom from the carbene fragment it should stabilize the triplet state, giving the transition metal carbene bond more covalent character. The substrates utilized within this chapter are various fluorinated alkenes such as: TFE, vinylidene fluoride (VDF; CF_2=CH_2) and trifluoroethylene (T^rFE; CF_2=CFH). These new transition metal fluorocarbenes react with these substrates to produce both metallacycle and metathesis products. The observation that no interconversion takes place between the metallacycle and metathesis products suggested two separate pathways which are discussed in detail. This chapter also shows unique reactivity of metallacycles containing CHF moieties. Additionally, steric and electronic effects will be analyzed in regards to regio-/stereo-selectivity of the products.

4.1.1 Published Contribution

Harrison, D. J.;[#] Daniels, A. L.;[#] Guan, J.;[#] Gabidullin, B. M.; Hall, M. B.; Baker, R. T. *Angew. Chem. Int. Ed*. **2018**, *57*, 5772-5776.

[#] These authors contributed equally.

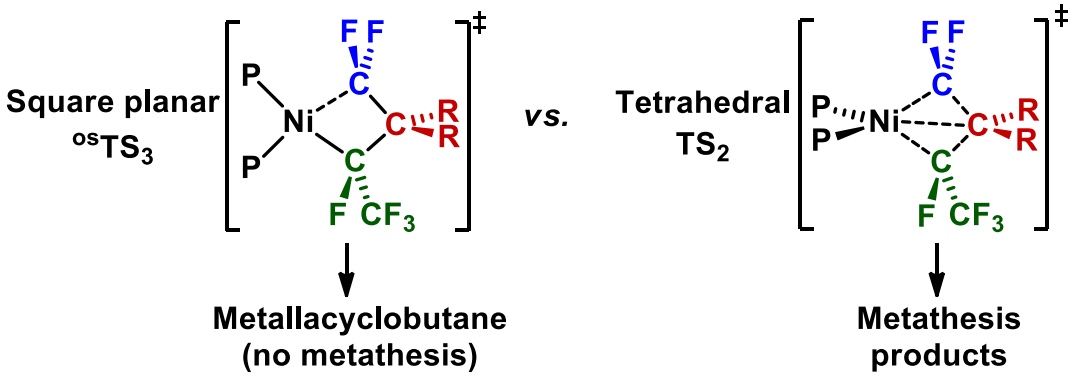

Alkene metathesis with directly fluorinated alkenes is challenging, limiting its application in the burgeoning field of fluoro-organic chemistry. A new nickel tris(phosphite) fluoro-(trifluoromethyl)carbene, $P_3Ni{=}CFCF_3$, reacts with $CF_2{=}CF_2$ (TFE) or $CF_2{=}CH_2$ (VDF) to yield both metallacyclobutane and perfluorocarbene metathesis products, $P_3Ni{=}CF_2$ and $CR_2{=}CFCF_3$ (R = F, H; P = $P(OMe)_3$, $P(O^iPr)_3$). The reaction of $P_3Ni{=}CFCF_3$ with trifluoroethylene also yields metathesis products, $P_3Ni{=}CF_2$ and cis/trans-$CFCF_3{=}CFH$. However, unlike reactions with TFE and VDF, this reaction forms metallacyclopropanes and fluoronickel alkenyl species, resulting presumably from instability of the expected metallacyclobutanes. Density functional theory calculations (DFT-M06) and experimental evidence establish that the observed metallacyclobutanes are *not* intermediates to the observed metathesis products, highlighting a novel variant of the Chauvin mechanism enabled by the disparate four coordinate transition states.

Author Contributions: DJH, ALD and JG were equal contributors to experimentation, authorship, and editing of manuscript with help from RTB and MBH. Complex synthesis and characterization were performed by DJH and ALD. Experiments with all substrates other than TFE were done by ALD, including product characterization. JG provided DFT calculations.

4.2 Introduction

Metal-catalyzed alkene metathesis is an immensely valuable C–C bond-forming method in organic synthesis.[1] This process involving fluoroalkenes could be an appealing option for obtaining new hydrofluoroalkenes which have recently been identified as low global warming potential refrigerants and blowing agents.[2] Metathesis traditionally produces new alkenes,

polymers and organic compounds through the widely accepted [2+2] cycloaddition/retro-cycloaddition pathway (Chauvin mechanism; Scheme 4.1).[1] Computational studies suggest that this mechanism would be problematic for fluoroalkenes using typical Ru catalysts, as confirmed experimentally.[3,4] Although recent elegant work has shown that cross-metathesis of fluoroalkenes and electron-rich alkenes can be accomplished with both Ru and Group 6 catalysts[5,6], addition of metal fluorocarbenes to electron-poor fluoroalkenes will likely require the former to be more strongly nucleophilic. In light of the strong M-C^F bonds formed by second and third row transition metals, we have targeted nucleophilic first row metal fluorocarbenes and recently demonstrated their [2+2] cycloaddition to fluoroalkenes.[7,8,9]

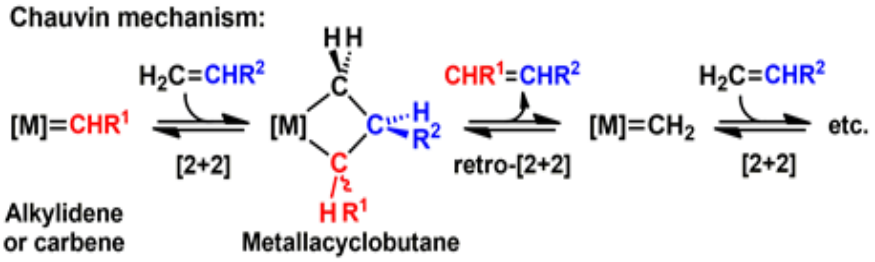

Scheme 4.1

In fact, early gas phase work by Beauchamp et al. suggested that d^9 $[Ni=CF_2]^+$ may effect selected fluoroalkene metathesis reactions depending on the thermodynamic stability of the resulting fluoroalkene and Ni fluorocarbene partners.[10,11] We recently reported the first examples of d^{10} Ni fluorocarbenes and their much faster (vs. Co) cycloaddition reactions with tetrafluoroethylene (TFE).[8,9] We now report the first Ni=CF(CF_3) carbene complexes and show their reactivity towards fluoro-alkenes.

The Chauvin mechanism (Scheme 4.1), involving a high-energy metallacyclobutane intermediate, has been the mainstay for our understanding of metathesis activity and selectivity using both homogeneous and heterogeneous catalysts.[1,3] In contrast, we have demonstrated that the cycloaddition reaction of Co fluorocarbene complexes with TFE involves a high-energy diradical intermediate followed by formation of a very stable metallacyclobutane (ca. 30 kcal/mol below starting materials).[12] The difference in energy between [M]=CF_2/TFE reactants (M = Co, Ni) and the metallacyclic products is sufficiently large that metathesis reactions following the Chauvin mechanism are likely unfeasible for these systems. In this work we show that a similar mechanism is in play for the Ni=CF(CF_3) carbene and several fluoro-alkenes

($CR_2=CF_2$; R = H, F) to from stable metallacyclobutanes, whereas a novel, parallel reaction pathway affords the metathesis products $Ni=CF_2$ + $R_2C=CF(CF_3)$. In addition, analogous reactions of trifluoroethylene (TrFE) afford both metathesis products and products derived presumably from unstable metallacyclobutanes. The thermodynamics and mechanistic pathways of these unprecedented transformations have been examined by density functional theory (DFT) methods (M06).

4.2.1 Results and Discussion

The new fluoro(trifluoromethyl)carbene complex $Ni(=CFCF_3)(P(O\text{-}i\text{-}Pr)_3)_3$ (**1**) was obtained from the reaction of $Ni[P(O\text{-}i\text{-}Pr)_3]_4$ with $Cd(CF_2CF_3)_2$·DME (DME = 1,2-dimethoxyethane)[13,14] (Scheme 4.2; ~40% isolated yield).[15,16] Our synthetic approach is similar to that developed by Roper and coworkers for making precious metal difluorocarbenes $[M^0]=CF_2$; M = Ru, Os).[10c,17] Analogous reactions with other NiL_4 complexes {L = PPh_3, $P(OMe)_3$, $P(OPh)_3$, CN[2,6-$Me_2(C_6H_3)$], CO} failed to give the corresponding $NiL_3(=CFCF_3)$ compounds in greater than trace amounts.

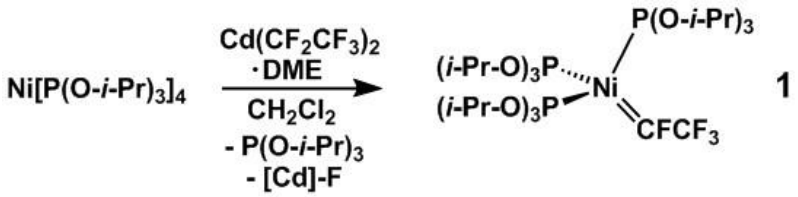

Scheme 4. 3

Complex **1** reacts with TFE (1.6 equiv, room temperature in C_6D_6, < 20 min) to yield trifluoromethyl-substituted perfluoro-nickelacyclobutane **2** (Scheme 4.3). Significantly, $CFCF_3/CF_2$ metathesis products are also observed in the same reaction mixture; specifically, hexafluoropropylene (HFP) and a new nickel difluorocarbene (**3**). The ratio of metallacycle to $[Ni]=CF_2$ is ~ 9:1 for this system. Additionally, the reaction is significantly retarded upon addition of excess phosphite without affecting the product ratio, suggesting that both products are formed via a dissociative mechanism.

To assess the effect of hydrogen substitution on the alkene, we showed that reaction of **1** with 1,1-difluoroethylene (CF_2=CH_2, VDF) also gives metathesis and metallacyclobutane products (Scheme 4.3; R = H).[24] Note that the alkene generated by the metathesis pathway, CH_2=$CFCF_3$, is the industrially relevant refrigerant HFO-1234yf.[18] Compared to the TFE reaction, metathesis products now constitute a larger proportion of the product mixture (**2b**:**3** ≈ 5:1), illustrating the sensitivity of the product distribution to the alkene substituents. For both reactions, the mass balance is near-quantitative: the metallacycle (**2a** or **2b**) and nickel difluorocarbene (**3**) account for >95% of **1**. Further, the ratio of metallacycle to metathesis products does not change with time, suggesting that the former is not an intermediate *en route* to the latter.[19] This observation points to a non-traditional Chauvin mechanism for these metathesis reactions (see below).

Interestingly, the cycloaddition reaction of **1** with VDF produced a single regioisomer with the methylene fragment in the β-position of the metallacycle. This may be due to steric effects where the carbon with smaller substituents (CH_2 vs. CF_2) can approach the large Ni=$CFCF_3$ fragment more easily. However, if the metallacycle is derived primarily through the diradical mechanism of the cycloaddition reaction shown previously for Co,[12] it is also possible that the obtained regioisomer results from added stabilization of the diradical intermediate.[20]

We further probed the effect of fluoroalkene substituents through reaction of **1** with 1,1,2-trifluoroethylene (TrFE) which again produced the expected metathesis products Ni=CF_2 and *cis/trans*-CHF=$CFCF_3$. However the expected metallacyclobutane products were not observed by ^{19}F, ^{31}P and ^{1}H NMR; instead metallacyclopropanes and fluoronickel alkenyl species

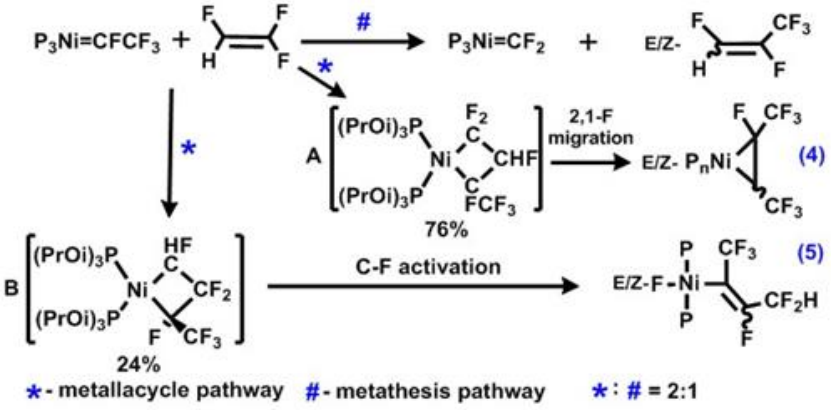

Scheme 4. 4

were observed (Scheme 4.4). Assuming initial formation of the two regioisomeric metallacyclobutanes, we propose two routes for their further conversion. For major isomer **A** a 2,1-fluoride migration results in ring contraction to form the *E/Z*-isomers of (**4**) in a similar reaction to that reported previously for the Co perfluorinated variant using a Brønsted acid catalyst.[7]

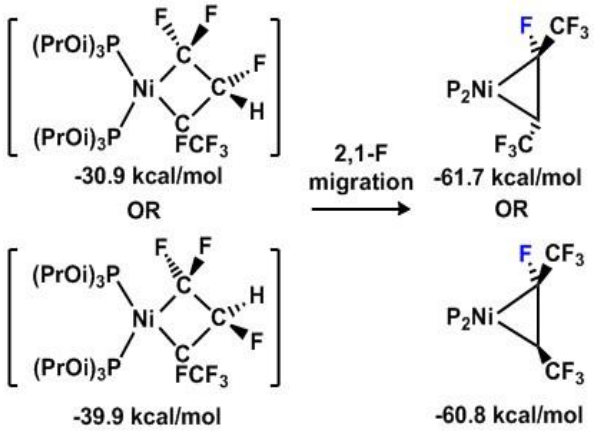

Scheme 4. 6

The driving force for these reactions is presumably formation of stable CF_3 groups (Scheme 4.5).[21] In contrast, minor isomer **B** undergoes C-F bond activation by the Ni center, forming the *E/Z*-fluoronickel alkenyl isomers (**5**). Based on our previous work involving fluoride abstraction from fluorometalla-cyclobutanes[9] and recent DFT studies on Ru carbenes[22] a plausible mechanism for the formation of (5) is a β-fluoride abstraction from metallacycle B forming a Ni-F allyl complex, followed by a 1,3-fluoride shift (Figure 4.33, Page 146). The detailed reaction pathway for this transformation is still under investigation. Although metallacycles **A** and **B** are not observed, calculations confirm their intermediate thermodynamic stability between those derived from TFE and VDF (see experimental section). In addition, the absence of products like **4** and **5** from reactions of **1** with either TFE or VDF[23] suggests that the presence of a CHF moiety in the metallacyclobutanes allows for a lower energy transition state for the 2,1-F migration and C-F activation pathways. Assuming intermediate formation of **4** and **5,** the metathesis products constitute almost 50% of the fluorine [(**4** + **5**):**3** ≈ 2:1].

A related Ni fluorocarbene complex, $Ni[P(OMe)_3]_3(=CFCF_3)$ (**6**), was synthesized through two-electron reduction[8a,24] of a mixture of $Ni(PPh_3)_2(CF_2CF_3)Br$ and $P(OMe)_3$ albeit with PPh_3 and other minor contaminants (^{19}F NMR yield: 17%; Scheme 4.6).

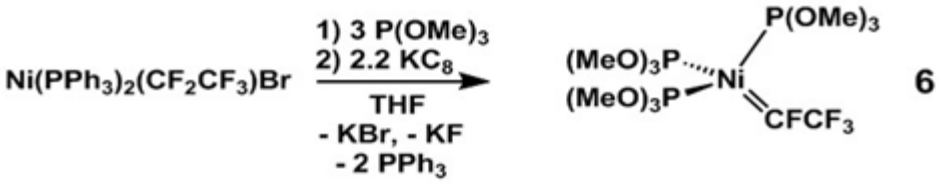

Scheme 4. 7

Treatment of **6** with TFE afforded metathesis and metalla-cyclobutane products in a 1:1.4 ratio, demonstrating a significant ancillary ligand effect. In contrast, reaction of Ni(tripod)=CF(CF_3) complex (**7**)[16] with TFE gave metallacycle with no metathesis products ([tripod = $MeC(CH_2PPh_2)_3$]; see section 4.2.4).

To further understand these observations, we investigated these reactions in more detail using density functional theory (DFT) approaches employing the M06 functional.[21,25,26,27,28,29] In the reaction between TFE and **1** both reactants have singlet ground states, and the ancillary ligand

P(O-*i*-Pr)$_3$ has a low free energy of dissociation of 0.5 kcal/mol from Ni(=CFCF$_3$)[P(O-*i*-Pr)$_3$]$_3$. Hence we propose that the reaction initiates with loss of P(O-*i*-Pr)$_3$ and subsequent interaction of Ni(=CFCF$_3$)[P(O-*i*-Pr)$_3$]$_2$with TFE (Figure 4.1).[30] The calculated results reveal two independent pathways under experimental conditions, which can lead to metathesis and metallacycle products, respectively.

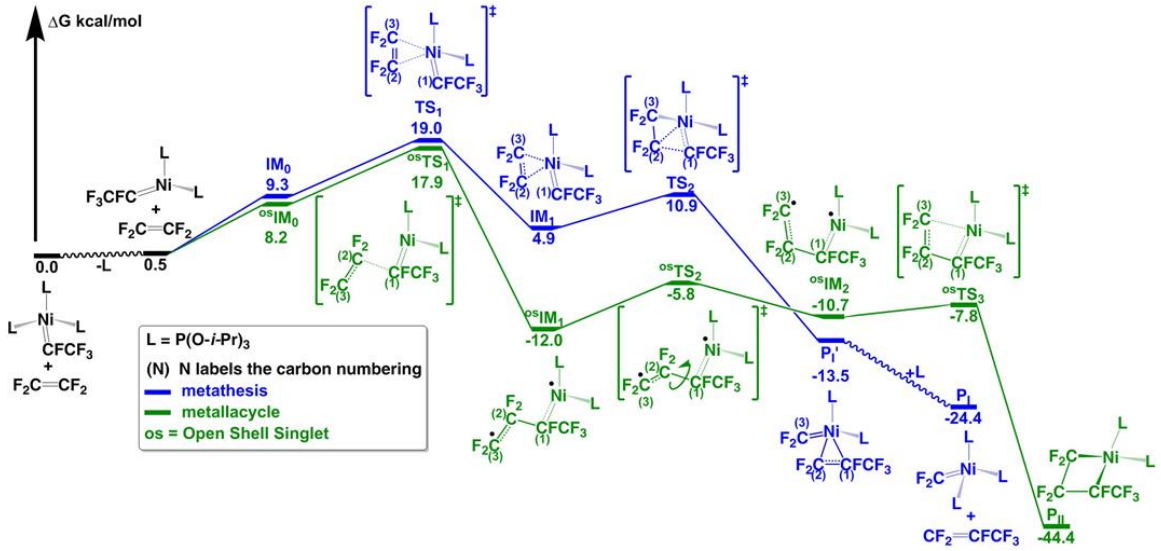

Figure 4.1: Reaction coordinate for reaction of **1** with TFE

In the metathesis pathway (blue in Figure 4.1), TFE binds weakly to the nickel center in IM_0 through both C atoms leading to transition state TS_1, located 19.0 kcal/mol above the reactants, and intermediate IM_1, about 4.9 kcal/mol higher than the reactants, in which the TFE C2–C3 bond is elongated by back-bonding from the electron-rich Ni center. Further elongation of the C2–C3 bond that accompanies formation of bicyclic transition state TS_2 (about 10.9 kcal/mol above the reactants) occurs in a plane that is *perpendicular* to that of the ancillary phosphite ligands. This unusual strained bicyclic intermediate is high enough in energy to prevent the complex from going through the highly downhill formation of the metallacycle, *vide infra*. The C2–C3 bond in TFE is then cleaved, with one $–CF_2$ residue bound to the Ni, while the other $–CF_2$ residue binds to carbene carbon C1 to produce P_I' (ΔG = -13.5 kcal/mol). Finally, metathesis products HFP and $Ni(=CF_2)[P(O\text{-}i\text{-}Pr)_3]_3$ (P_I) are formed by exchange between the ancillary ligand and $CF_2=CFCF_3$, a process that is energetically favorable by 10.9 kcal/mol.

The unproductive metallacycle pathway (green in Figure 4.1), commences with the formation of an open-shell singlet diradical intermediate ($^{os}IM_0$) via one C atom of TFE weakly bonding with the carbene C atom, without the direct involvement of the metal. Formation of the C1–C2 σ bond (1.529 Å), through $^{os}TS_1$ (ΔG = 17.9 kcal/mol) followed by low-energy rotation through $^{os}TS_2$ (ΔG = -5.8 kcal/mol) around the newly-formed C1–C2 bond affords $^{os}IM_2$, another diradical intermediate that is slightly less stable than $^{os-1}IM_1$. Finally, metallacycle product P_{II} results from the C3–Ni diradical of $^{os}TS_3$ (ΔG = -7.8 kcal/mol) with formation of the C3–Ni bond *in the same plane as the ancillary ligands* (see Table S1 for spin densities of the open-shell singlet species). The metallacycle and metathesis products both exhibit remarkably low energies (-44.4 kcal/mol and -24.4 kcal/mol, respectively) relative to the starting materials; thus, the pathways leading to metathesis products and metallacycle are too exothermic to be reversible. Since the rate-controlling transition states in both Pathways, TS_1 and $^{os-1}TS_1$, have comparable barriers (19.0 vs 17.9 kcal/mol), the product ratio will be determined by subtle differences in these transition states, as shown with the observed increases of metathesis products with ancillary ligand and upon replacement of C-F bonds (with C-H) from the metathesis partner. Moreover, to eliminate the possibility of this transformation progressing via a triplet state, it was calculated that for the rate-determining barrier, TS_1, the open-shell singlet is significantly lower in energy than the closed-shell singlet (17.9 kcal/mol vs 22.6 kcal/mol), which is lower in turn than the triplet state (22.6 kcal/mol vs 24.1 kcal/mol). At the key intermediate IM_1, the closed-shell singlet state is

very unstable, while the open-shell singlet is still more stable than the triplet. After IM_1, the open-shell singlet and triplet are close in energy until the product, which is much more stable as the singlet, confirming that the diradical mechanism is the most probable. (see section 4.2.4)

4.2.2 Conclusion

To summarize, we have demonstrated the first examples of metal fluorocarbene metathesis with fluoroalkenes, occurring either through a novel variant of the Chauvin mechanism enabled by a tetrahedral four-coordinate transition state or a non-productive metallacycle pathway occurring through a diradical mechanism enabled by a square planar transition state. These results extend our understanding of metathesis mechanisms beyond the original Chauvin postulate, in which the metallacycle is an intermediate en route to metathesis products.[1] Despite the important advances described herein, considerable challenges still face metal-mediated polyfluoroalkene metathesis. First, a more general source of nucleophilic metal carbenes is needed.[31] Second, ground state energy differences between the $Ni{=}CF_2$ and $Ni{=}CFCF_3$ carbene complexes introduce additional barriers to efficient metal-catalyzed fluoroalkene metathesis that will require careful selection of the carbene/fluoroalkene partners. Ongoing experimental and computational efforts are focused on finding more systems that favor the metathesis pathway.

4.2.3 Experimental Section

General: Experiments were conducted under nitrogen, using Schlenk techniques or an MBraun glove box. All solvents were deoxygenated by purging with nitrogen. Toluene, hexanes, diethyl ether (Et_2O), 1,2-dimethoxyethane (DME) and tetrahydrofuran (THF) were dried on columns of activated alumina using a J. C. Meyer (formerly Glass Contours) solvent purification system. C_6D_6 was dried over activated alumina (heated at 300 ^oC for > 6 h under vacuum) (10 wt. %). MeCN, CH_2Cl_2 and CD_2Cl_2 were distilled from CaH_2 and then passed through activated alumina (10 wt. %). Toluene-d_8 was dried over sodium/benzophenone and vacuum-transferred from the deep purple ketyl solution before use. All solvents were stored over activated (heated at ~ 250 ^oC for > 6 h under vacuum) 4 Å molecular sieves. Glassware was oven-dried at 150 ^oC for > 2 h. Commercial chemicals: $P(OMe)_3$ (Aldrich, 97%), $P(O\text{-}i\text{-}Pr)_3$ (Aldrich, 95%), $MeC(CH_2PPh_2)_3$ (Strem, 97%); deuterated (≥99.5%) NMR solvents (Cambridge Isotopes Labs). Tetrafluoroethylene ($CF_2{=}CF_2$, TFE) was obtained by pyrolysis of polytetra-fluoroethylene (Scientific Polymer Products, powdered) under vacuum, using a slightly modified literature

procedure[32] [10-20 mTorr, 650 °C, 15-20 g scale, product stabilized with ~ 0.3 wt. % R(+)-limonene (Aldrich, 97%)], giving TFE of ≥ 97% purity. The following chemicals were made following literature procedures: $Ni(PPh_3)_4$,[33] NiP_4 [P = $P(OMe)_3$, $P(O\text{-}i\text{-}Pr)_3$, $P(OPh)_3$][34], KC_8[5] and $Cd(CF_2CF_3)_2$·DME (DME = 1,2-dimethoxyethane).[35] ^1H, ^{19}F and $^{31}P\{^1H\}$ NMR spectra were recorded on a 300 MHz Bruker Avance or AvanceII instrument at room temperature (RT, 23 ± 1°C), except where noted. ^1H NMR spectra were referenced to the residual proton peaks associated with the deuterated solvents (C_6D_6: 7.16 ppm; CD_2Cl_2: 5.32 ppm; toluene-d_8: 2.09 ppm). $^{13}C\{^1H\}$ spectra in toluene-d_8 were referenced to the methyl carbon peak at 20.43 ppm. ^{19}F NMR spectra were referenced against internal 1,3-bis(trifluoromethyl)benzene (BTB) (Aldrich, 99%, deoxygenated by purging with nitrogen, stored over activated 4 Å molecular sieves), set to –63.5 ppm. ^{19}F NMR yields were obtained from the relative integrations of quantitative BTB and product peaks, using 5 s delay times. $^{31}P\{^1H\}$ NMR data were referenced against external H_3PO_4 (85% aqueous solution), set to 0.0 ppm. UV-vis spectra were recorded on a Cary 100 instrument, using sealable quartz cuvettes (1.0 cm pathlength). Elemental analyses were performed by Canadian Microanalytical Services Ltd. (Delta, British Columbia, Canada).

Synthesis of {Ni(=CFCF$_3$)[P(O-*i*-Pr)$_3$]$_3$} (1). $Ni[P(O\text{-}i\text{-}Pr)_3]_4$ (100 mg, 0.11 mmol) and $Cd(CF_2CF_3)_2$·DME (59 mg, 0.13 mmol) were combined as solids and 2 mL of CH_2Cl_2 were added with stirring; within 1 min, the solution was deep purple and homogeneous. Stirring at ambient temperature was continued for 15 min. The solvent was removed under vacuum to yield an amorphous purple residue. The residue was extracted with hexanes (~0.5 mL x 3) and the purple extracts were filtered through Celite (~1 cm in a Pasteur pipet). Note: Extraction left behind amorphous, slightly yellow-brown material. The purple hexanes solution was then extracted with MeCN (~0.5 mL x 3). The layers were separated with a Pasteur pipet and the orange-brown MeCN washings were discarded. The solvent was removed under vacuum from the purple hexanes solution, affording a purple oil. The purity of product at this stage was ~95 %, by ^1H, ^{19}F and $^{31}P\{^1H\}$ NMR; the only significant contaminant was $Ni[P(O\text{-}i\text{-}Pr)_3]_4$. The yield was 35-40 % based on $Ni[P(O\text{-}i\text{-}Pr)_3]_4$, determined gravimetrically and by quantitative ^{19}F NMR spectroscopy. Sublimation at RT ($2\cdot10^{-3}$ mTorr; probe cooled with dry ice/acetone slurry) gave an oily purple product of marginally increased purity {i.e., < 2% $Ni[P(O\text{-}i\text{-}Pr)_3]_4$} but significantly diminished yield (25-30 %). This compound is extremely sensitive to air and is unstable at RT in solution (> 90% decomposition, 20 h in C_6D_6 at RT). UV-vis (2.5 mM in

hexanes): λ_{max} (ε) = 534 (420), 750 (90) (shoulder). ^{1}H NMR (300 MHz, C_6D_6) δ 1.27 [d, $^{3}J_{HH}$ = 6 Hz, 54H, CH(C<u>H</u>$_3$)$_2$], 4.72 [m, 9H, C<u>H</u>(CH$_3$)$_2$]. ^{19}F NMR (282 MHz, C_6D_6) δ –74.2 (d, $^{3}J_{FF}$ = 13 Hz, 3F, CFC<u>F</u>$_3$), 24.6 [very broad apparent s (barely distinguishable from baseline at RT), $\omega_{1/2}$ ≈ 2000 Hz, 1F, C<u>F</u>CF$_3$). ^{31}P{^{1}H} NMR (121 MHz, C_6D_6) δ 151.1 {br apparent s, overlapping with minor/sharp s of Ni[P(O-*i*-Pr)$_3$]$_4$ (see below), $\omega_{1/2}$ ≈ 400 Hz, 3P, Ni–<u>P</u>}. NMR data for Ni[P(O-*i*-Pr)$_3$]$_4$ contaminants (~5 % before sublimation, <2 % after): ^{1}H NMR (300 MHz, C_6D_6) δ 1.32 [d, $^{3}J_{HH}$ = 6 Hz, 72H, CH(C<u>H</u>$_3$)$_2$], 4.84 [m, 12H, C<u>H</u>(CH$_3$)$_2$]. ^{31}P{^{1}H} NMR (121 MHz, C_6D_6) δ 152.1 (s, 4P, Ni Ni–<u>P</u>). Low-temperature NMR data for **1**: ^{13}C{^{1}H} (75 MHz, toluene-d_8, –35°C) δ 24.8 [s, 18C, CH(<u>C</u>H$_3$)$_2$], 67.1 [s, 9C, <u>C</u>H(CH$_3$)$_2$], 225.6 [doublet of multiplets (weak, poorly resolved), $^{1}J_{CF}$ = 420 Hz, <u>C</u>FCF$_3$]; note that <u>C</u>F$_3$ peak was not observed, possibly because it was obscured under the under toluene-d_8 aromatic peaks. Also, weak ^{13}C{^{1}H} signals were observed for Ni[P(O-*i*-Pr)$_3$]$_4$ at 25.6 and 65.7 ppm. ^{19}F NMR (282 MHz, toluene-d_8, –45°C) δ –77.4 (m, 3F, CFC<u>F</u>$_3$), 34.2 (quartet of quartets, $^{3}J_{FP}$ = 102 Hz, $^{3}J_{FF}$ = 13 Hz, 1F, C<u>F</u>CF$_3$). ^{31}P{^{1}H} NMR (121 MHz, toluene-d_8, –45 °C) δ 156.0 (dq, $^{3}J_{PF}$ = 102 Hz, $^{4}J_{PF}$ = 23 Hz, 3P, Ni–<u>P</u>). See below for NMR spectra.

Attempted synthesis of Ni(=CFCF$_3$)P$_3$from NiP$_4$ and Cd(CF$_2$CF$_3$)$_2$·DME [P = PPh$_3$, P(OMe)$_3$, P(OPh)$_3$]. The NiP_4 compounds were treated with Cd(CF$_2$CF$_3$)$_2$·DME, as described above for the synthesis of **1**; in each case CH_2Cl_2 and hexanes were screened as solvents (i.e., the best-performing solvents for making **1**). Trace Ni[P(OMe)$_3$]$_3$(=CFCF$_3$) (> 2 % yield) was observed, 0.5 h after combining the reagents, in the reaction between Ni[P(OMe)$_3$]$_4$ and Cd(CF$_2$CF$_3$)$_2$·DME but otherwise fluorocarbene products were not observed.

Reaction of 1 with CF$_2$=CF$_2$ (TFE) to yield {Ni[-CF(CF$_3$)CF$_2$CF$_2$-][P(O-*i*-Pr)$_3$]$_2$} (2), {Ni(=CF$_2$)[P(O-*i*-Pr)$_3$]$_3$} (3) and HFP (CF$_2$=CFCF$_3$). A C_6D_6 solution (0.60 mL) containing **1** (57 mM) and BTB (32 mM) {with trace Ni[P(O-*i*-Pr)$_3$]$_4$ contaminant, ca. 2% relative to **1**}, prepared as described above and purified by sublimation, was placed in a septum-capped NMR tube (homogeneous dark purple solution). TFE (1.3 mL at 23 °C and 1 atm; 0.053 mmol) was added to the tube, through the septum via a syringe needle; mixing was achieved by shaking the tube. Within 3 min of adding the TFE, the purple solution had changed color to orange-yellow (homogeneous). ^{19}F, ^{31}P{^{1}H} and ^{1}H NMR data were collected (at 23°C) over 7 min (in the order listed), starting 10 min after adding the TFE. Note: NMR and other data for related nickel difluorocarbenes ([Ni]=CF$_2$) and perfluorocyclobutanes {[Ni](-CF$_2$CF$_2$CF$_2$-)} can be found in

reference 36. NMR data for **2**: ^{1}H NMR (300 MHz, C_6D_6) δ 1.20 {d, $^{3}J_{HH}$ = 6 Hz, 36H, Ni-$P^{A\&B}[OCH(C\underline{H}_3)_2]_3$, overlapping with $CH(C\underline{H}_3)_2$ signal from free phosphite}, 4.76 {m, 3H, Ni-$P^{A}[OC\underline{H}(CH_3)_2]_3$, overlapping with Ni-$P^{B}[OC\underline{H}(CH_3)_2]_3$ and $C\underline{H}(CH_3)$ signal from free phosphite}, 4.86 {m, 3H, Ni-$P^{B}[OC\underline{H}(CH_3)_2]_3$, overlapping with Ni-$P^{A}[OC\underline{H}(CH_3)_2]_3$ and $C\underline{H}(CH_3)$ signal from free phosphite}. ^{19}F NMR (282 MHz, C_6D_6) (see Figure 4.2 for fluorine labeling scheme) δ –209.6 (m, 1F, F^{B}), –122.8 (dm, $^{2}J_{FF}$ = 217 Hz, 1F, $F^{C\text{ or }D}$), –119.8 (dm, $^{2}J_{FF}$ = 244 Hz, 1F, $F^{E\text{ or }F}$), –113.7 (dm, $^{2}J_{FF}$ = 244 Hz, 1F, $F^{E\text{ or }F}$), –99.9 (dm, $^{2}J_{FF}$ = 217 Hz, 1F, $F^{C\text{ or }D}$), –65.1 (m, 3F, F^{A}). ^{31}P{^{1}H} NMR (121 MHz, C_6D_6) δ 119.9-123.4 (overlapping multiplets, 2P, Ni–P^{A} and Ni–P^{B}). NMR data for **3**: ^{1}H NMR (300 MHz, C_6D_6) δ 1.33 [d, $^{3}J_{HH}$ = 6 Hz, 54H, $CH(C\underline{H}_3)_2$], 4.63 {m, 9H, $C\underline{H}(CH_3)_2$, largely obscured by $C\underline{H}(CH_3)_2$ peaks from free phosphite, $Ni[P(O\text{-}i\text{-}Pr)_3]_4$ and **2**}. ^{19}F NMR (282 MHz, C_6D_6) δ 93.7 (q, $^{3}J_{FP}$ = 60 Hz, 2F, $Ni{=}C\underline{F}_2$). ^{31}P{^{1}H} NMR (121 MHz, C_6D_6) δ 155.5 (t, $^{3}J_{PF}$ = 60 Hz, $Ni\underline{P}_3$). NMR data for $P(O\text{-}i\text{-}Pr)_3$: ^{1}H NMR (300 MHz, C_6D_6) δ 1.20 {d, $^{3}J_{HH}$ = 6 Hz, 18H, $CH(C\underline{H}_3)_2$, overlapping with signals from Ni-$P^{A\&B}[OCH(C\underline{H}_3)_2]_3$}, 4.45 [m, 3H, $C\underline{H}(CH_3)_2$]. ^{31}P{^{1}H} NMR (121 MHz, C_6D_6) δ 135.6 (br s, 1P, P of free phosphite). NMR data for $Ni[P(O\text{-}i\text{-}Pr)_3]_2(\text{-}CF_2CF_2CF_2\text{-})$ {0.03 molar equiv. relative to **2**; formed by the reaction of $Ni[P(O\text{-}i\text{-}Pr)_3]_4$ or **3** with TFE}: ^{19}F NMR (282 MHz, C_6D_6) δ –116.7 (s, 2F, $\text{-}CF_2C\underline{F}_2CF_2\text{-}$), –124.7 (s, 4F, $\text{-}C\underline{F}_2CF_2C\underline{F}_2\text{-}$). Note that the ^{1}H and ^{31}P{^{1}H} peaks associated with $Ni[P(O\text{-}i\text{-}Pr)_3]_2(\text{-}CF_2CF_2CF_2\text{-})$ were obscured by the signals from other species in the mixture. NMR data for unreacted TFE (0.07 molar equiv relative to **2**): ^{19}F NMR (282 MHz, C_6D_6) δ –132.5 (s, 4F). NMR data for $CF_2{=}CFCF_3$ (HFP) (0.08 molar equiv relative to **2**): ^{19}F NMR (282 MHz, C_6D_6) δ –69.2 (m, 3F, $C\underline{F}_3$), –91.4 (m, 1F, $C\underline{F}^{A}F^{B}$ cis to CF_3), –105.8 (m, 1F, $CF^{A}\underline{F}^{B}$ trans to CF_3), –192.8 (m, 1F, $C\underline{F}CF_3$). See below for NMR spectra.

Reaction of 1 with $CF_2{=}CH_2$ (VDF). A C_6D_6 solution (0.60 mL) containing **1** (57 mM) and BTB (32 mM) {with trace $Ni[P(O\text{-}i\text{-}Pr)_3]_4$ contaminant, ca. 2% relative to **1**}, prepared as described above was placed in a septum-capped NMR tube (homogeneous dark purple solution). VDF (1.3 mL at 23ºC and 1 atm; 0.082 mmol) was added to the tube, through the septum via a syringe needle; mixing was achieved by shaking the tube. Within 1 min of adding the VDF, the purple solution had changed color to orange (homogeneous). As for the TFE reaction, the metallacycle and nickel difluorocarbene products account for >95% of **1**. ^{19}F NMR resonances were assigned to the various species in solution from the ^{19}F COSY and ^{1}H-^{19}F HMBC NMR spectra (Figs. S17 and S24). Notably, the metallacycle CF_2 resonances did not exhibit well-

defined germinal F-F coupling due to the similarity of their chemical shifts. Their inequivalence was demonstrated, however, at low temperatures (Fig. S18). NMR data for metallacycle: ^{1}H NMR (300 MHz, C_6D_6) δ 1.26 (m, CH(C$\underline{H}_3$)$_2$), 3.7 (m, 1H, -CF2C$\underline{H}_A$H$_B$CFCF$_3$-), 4.0 {m, 1H, -CF$_2$CH$_A\underline{H}_B$CFCF$_3$-), 4.8 ppm (m, C$\underline{H}$(CH$_3$)$_2$, largely obscured by C$\underline{H}$(CH$_3$)$_2$ peaks from free phosphite, Ni[P(O-*i*-Pr)$_3$]$_4$ and **3**}.^{19}F NMR (282 MHz, C_6D_6) δ -181.6 (m, 1F, C$\underline{F}$CF$_3$), -82.1 (overlapping m, 2F, -CFCF$_3$CH$_2$C$\underline{F}_2$-), -73.2 ppm (m, 3F, CFC$\underline{F}_3$). ^{31}P{^{1}H} NMR (121 MHz, C_6D_6) δ 125.7 {m, Ni[P(OiPr)$_3$]$_2$}, 152.2 ppm (s, NiP$_4$; P = P(OiPr)$_3$). ^{19}F and ^{31}P{^{1}H} NMR data for Ni=CF$_2$ and hydrofluoroalkene: ^{19}F NMR (282 MHz, C_6D_6) δ -124.9 (m, 1F, C$\underline{F}$CF$_3$=CH$_2$), -74.0 (d, 3F, $^{3}J_{FF}$ = 11 Hz, CFC$\underline{F}_3$=CH$_2$), 93.8 ppm (quart, 2F, $^{3}J_{FP}$ = 60 Hz, Ni=C$\underline{F}_2$). ^{31}P{^{1}H} NMR (121 MHz, C_6D_6) δ 155.7 ppm (t, $^{3}J_{PF}$ = 60 Hz, $\underline{P}_3$Ni=CF$_2$). See below for NMR spectra.

Reaction of 1 with CF$_2$=CFH (TrFE) to yield {Ni(=CF$_2$)[P(O-*i*-Pr)$_3$]$_3$} (3), cis/trans-(CFH=CFCF$_3$), cis/trans-{Ni[-CF(CF$_3$)=CH(CF$_3$)-][P(O-*i*-Pr)$_3$]$_2$} (E/Z-4), and E/Z-P$_2$Ni{-CCF$_3$=CF(CF$_2$H)} (E/Z-5). A C_6D_6 solution (0.50 mL) containing **1** (46mM) {with trace Ni[P(O-*i*-Pr)$_3$]$_4$ contaminant, ca. 2% relative to **1**}, prepared as described above was placed in a septum-capped NMR tube (homogeneous dark purple solution). HTFE (1.0 mL at 23°C and 1 atm; 0.041 mmol; 1.3 equiv.) was added to the tube, through the septum via a syringe needle; mixing was achieved by shaking the tube. Within 1 min of adding the HTFE, the purple solution had changed color to orange (homogeneous). As for the TFE reaction, the metallacycle and nickel difluorocarbene products account for >95% of **1**. ^{19}F NMR resonances were assigned to the various species in solution from the ^{19}F COSY NMR spectra (Figs. SXX). NMR data for **cis/trans-(CFH=CFCF$_3$)**: ^{1}H NMR (300 MHz, C_6D_6) δ 5.7 (dd, $^{2}J_{HF}$ = 1.26, 68 Hz, $^{3}J_{HF}$ = 14 Hz, cis-CFCF$_3$=CF$\underline{H}$), 5.6 ppm (dd, $^{2}J_{HF}$ = 70 Hz, $^{3}J_{HF}$ = 5 Hz, trans-CFCF$_3$=CF$\underline{H}$) ^{19}F NMR (282 MHz, C_6D_6) δ -69.2 (dd, $^{3}J_{FF}$ = 20 Hz, $^{4}J_{FF}$ = 11 Hz, trans-CFC$\underline{F}_3$=CFH), -72.1(dd, $^{3}J_{FF}$ = 14 Hz, $^{4}J_{FF}$ = 5 Hz, cis-CFC$\underline{F}_3$=CFH), -153.9 (ddquart, $^{2}J_{FH}$ = 68 Hz, $^{3}J_{FF}$ = 9 Hz, $^{4}J_{FF}$ = 5 Hz, cis-CFCF$_3$=C$\underline{F}$H), -159.9 (qd, $^{3}J_{FF}$ = 14 Hz, $^{4}J_{FF}$ = 9 Hz, cis-C$\underline{F}$CF$_3$=CFH), -164.6 (ddquart, $^{3}J_{FF}$ = 135 Hz, $^{2}J_{FH}$ = 70 Hz, $^{4}J_{FF}$ = 20 Hz, trans-CFCF$_3$=CH$\underline{F}$), -180 ppm (dquartd, $^{3}J_{FF}$ = 135 Hz, $^{3}J_{FF}$ = 11 Hz, $^{3}J_{FH}$ = 5 Hz, trans-CFCF$_3$=C$\underline{F}$H). NMR data for **P$_3$Ni=CF$_2$**: ^{19}F NMR (282 MHz, C_6D_6) δ 93.7 ppm (quart, $^{3}J_{FP}$ = 60 Hz, Ni=CF$_2$). ^{31}P{^{1}H} NMR (121 MHz, C_6D_6) δ 155.5 ppm (t, $^{3}J_{PF}$ = 60 Hz). NMR data for **E/Z-4**: ^{1}H NMR (300 MHz, C_6D_6) δ 3.2 (dq, $^{3}J_{HP}$ = 11 Hz, $^{3}J_{HF}$ = 30 Hz; cis-P$_2$Ni←C$\underline{H}$CF$_3$=CFCF$_3$), 2.7 ppm (dq, $^{3}J_{HP}$ = 10, $^{3}J_{HF}$ = 22 Hz; trans-

$P_2Ni\leftarrow C\underline{H}CF_3=CFCF_3$) ^{19}F NMR (282 MHz, C_6D_6) δ -48.6 (ddt, $^3J_{FH}$ = 5 Hz, $^4J_{FF}$ = 15 Hz, $^4J_{FP}$ = 9.18 Hz; cis-$P_2Ni\leftarrow CH\underline{CF_3}=CFCF_3$), -50.7 (dd, $^3J_{FH}$ = 11 Hz, $^4J_{FF}$ = 10 Hz, trans-$P_2Ni\leftarrow CH\underline{CF_3}=CFCF_3$), -66.0 (dq, J = 14 Hz, J = 10 Hz; cis-$P_2Ni\leftarrow CHCF_3=CF\underline{CF_3}$), -69.5 (d, 3JFF = 12 Hz, trans-$P_2Ni\leftarrow CHCF_3=CF\underline{CF_3}$), -166.3 (mult, cis-$P_2Ni\leftarrow CHCF_3=C\underline{F}CF_3$), -191.3 ppm (br mult, trans-$P_2Ni\leftarrow CHCF_3=C\underline{F}CF_3$) $^{31}P\{^1H\}$ NMR (121 MHz, C_6D_6) δ 142.0 (unresolved dqq, trans-$\underline{P_2}Ni\leftarrow CHCF_3=C\underline{F}CF_3$), 142.4 ppm (unresolved ddq, cis-$\underline{P_2}Ni\leftarrow CHCF_3=C\underline{F}CF_3$). NMR data for **cis/trans-5**: ^1H NMR (300 MHz, C_6D_6) δ 6.1 (mult, cis-P_2Ni-$CCF_3=CFCF_2\underline{H}$), 5.8 ppm (dt, $^3J_{HF}$ = 33.9 Hz, $^2J_{HF}$ = 13.2 Hz, trans-P_2Ni-$CCF_3=CFCF_2\underline{H}$) ^{19}F NMR (282 MHz, C_6D_6) δ -63.2 (mult, trans-P_2Ni-$CCF_3=CFC\underline{F_2}H$), -72.7 (dt, $^4J_{FF}$ = 12 Hz, $^4J_{FP}$ = 3 Hz, trans-P_2Ni-$C\underline{CF_3}=CFCF_2H$), -132.7 ppm (dtq, $^3J_{FH}$ = 21 Hz, $^3J_{FF}$ = 19 Hz, $^4J_{FF}$ = 12 Hz).

Synthesis of {Ni(Br)(CF_2CF_3)(PPh_3)$_2$}. A round bottom Schlenk was charged with PPh_3 (420 mg, 1.6 mmol, 2.2 equiv.) which was dissolved with THF (10 mL). $Ni(COD)_2$ (200 mg, 0.73 mmol) was added to a solid addition funnel and the glassware was assembled. Addition of $Ni(COD)_2$ yielded a dark red solution that was stirred at RT for 10 minutes. The solution was cooled using an acetone/dry ice bath (-78°C) for 10 minutes. PFPA (0.26 mL, 1.3 mmol, 1.8 equiv.) was added dropwise to this solution via syringe over 5 minutes and the solution was stirred at -78°C for 10 minutes after the addition was complete. The solution was removed from the acetone/dry-ice bath and was allowed to warm to RT over 0.5 h. The solution was removed under vacuum leaving a dark orange foamy solid. The solid was dissolved in THF (6 mL) and LiBr (50 mg, 0.58 mmol) was added to the solution which immediately became heterogeneous and dark purple. The solution was stirred for 0.5 h and the solvent was removed under vacuum affording dark purple, sticky, semi-solid. The residue was dissolved in a minimum of Et_2O and the solution was filtered through celite. The remaining purple residue was extracted with Et_2O (3x1mL) and the extracts were filtered through celite. The filtrates were combined and the solvent was concentrated to 1 mL. Hexanes (10 mL) was added causing significant purple precipitate to form. The solution was cooled in freezer (-35°C) for 2 h before recovering the purple precipitate on a glass frit (15 mL, M) and drying in vacuo. Yield: 360 mg. Note: Compound appears to be paramagnetic and unobservable by NMR therefore the quantitative conversion to Ni(Br)(CF_2CF_3)(DPPE)will be used to confirm the synthesis of Ni(Br)(CF_2CF_3)(PPh_3)$_2$.

Reaction of Ni(Br)(CF_2CF_3)(PPh_3)$_2$ with DPPE to confirm the identity and purity of {Ni(Br)(CF_2CF_3)(PPh_3)$_2$}. A glass vial was charged with [Ni(Br)(CF_2CF_3)(PPh_3)$_2$] (50 mg, 0.06 mmol). The solid was dissolved in THF (ca. 1.0 mL). To this purple solution was added DPPE (25 mg, 0.06 mmol) which became a dark orange immediately after the addition. The orange solution was stirred under nitrogen at RT for 1.0 h. The solution was concentrated to 0.25 mL and hexanes (10 mL) was added causing the formation of significant orange precipitate. The solution was placed into glove box freezer (-35oC) overnight (20h). The precipitate was collected on a glass frit (15mL, F) and dried under vacuum leaving a bright orange powder: Ni(Br)(CF_2CF_3)(DPPE). Yield: 38 mg, 97% yield. ^{19}F NMR (282 Hz, $CDCl_3$) δ – 89.5 ppm (apparent dd, $^3J_{FPcis}$ = 27.2 Hz, $^3J_{FPtrans}$ = 37.5 Hz, 2F, CF_2), - 77.7 ppm (m, 3F, CF_3). $^{31}P\{^1H\}$ NMR (121 Hz, $CDCl_3$) δ 43.6 ppm (dt, $^2J_{PP}$ = 46 Hz, $^3J_{PFcis}$ = 27.2 Hz, 1P) 61.2 ppm (dt, $^2J_{PP}$ = 46 Hz, $^3J_{PFtrans}$ = 37.5 Hz, 1P). ^{1}H NMR (300 MHz, $CDCl_3$) δ 2.0 (ov m, 4H, non-equivalent overlapping CH_2 signals) 7.4 – 8.1 ppm (m, 20H, phenyl residues).

Synthesis of {Ni(=CFCF_3)[P(OMe)$_3$]$_3$ } (6). A glass vial was charged with Ni(PPh_3)$_2$(Br)(CF_2CF_3) (53 mg, 0.07 mmol) and dissolved in toluene/THF (1:1; 3 mL). P(OMe)$_3$ (24 μL, 0.2 mmol) was added via microliter syringe causing the solution to go from purple to yellow-orange. KC_8 (20 mg, 0.15 mmol) was added causing an immediate color change from yellow-orange to dark purple. The solution was passed through Celite (filter pipette) and the solution was removed under vacuum yielding a purple semi-solid. This solid was dissolved in a minimum of toluene (ca. 1 mL), the solution was passed through Celite (filter pipette) and the filtrate was removed in vacuo leaving a purple oil. Yield: 30 mg, impure. ^{19}F NMR (282 Hz, C_6D_6) δ -84, - 76 (unidentified impurities), -74.9 (m, 3F, CFC<u>F</u>$_3$), -74.3 (br s, unidentified impurity), -63.5 (s, BTB), -40.9 (s, unidentified impurity), -38.5 (s, unidentified impurity), 48.0 ppm (quartet of quartets, $^3J_{FP}$ = 102 Hz, $^3J_{FF}$ = Hz, 1F, C<u>F</u>CF_3). $^{31}P\{^1H\}$ NMR (121 Hz, C_6D_6) δ -8.1 ppm (s, free phosphine remnants from synthesis of **2**), 155.6 (d, unidentified impurity), 161.1 (s, NiP_4; P = P(OMe)$_3$), 163.0 ppm (dq, $^3J_{PF}$ = 102 Hz, $^4J_{PF}$ = 23 Hz, Ni<u>P$_3$</u>CFCF_3). ^{1}H NMR (300 MHz, C_6D_6) δ 3.11 – 3.45 (ov m, CH_3 residues of free P(OMe)$_3$/Ni(P)$_4$/Ni[P]$_3$($CFCF_3$); P = P(OMe)$_3$), 6.55 – 7.00 (ov m, free PPh_3/Ni(PPh_3)(P)$_3$; P = P(OMe)$_3$).

Reaction of impure {Ni(=CFCF_3)[P(OMe)$_3$]$_3$} (6) with CF_2=CF_2 (TFE) to yield {Ni(κ^2-CFCF_3CF_2CF_2-)[P(OMe)$_3$]$_2$}, Ni(=CF_2)[P(OMe)$_3$]$_3$ (6b), and CF_2=CFCF_3 (HFP). A C_6D_6

solution (0.60 mL) containing **2** (98 mM; with impurities described above) and BTB (19 mmol), was placed in a septum-capped NMR tube (homogeneous dark purple solution). TFE (1.5 mL at 23°C and 1 atm; 0.061 mmol) was added to the tube, through the septum via a syringe needle; mixing was achieved by shaking the tube. ^{19}F, $^{31}P\{^{1}H\}$, and ^{1}H NMR was taken within 5 minutes of adding the TFE. Note: Experiment was performed four times. NMR was taken immediately after TFE addition and after 6 hours. Impurity concentration was shown to not decrease over the course of the reaction and therefore do not appear to participate in the desired reactivity of the carbene. Additionally, the ratio of carbene to metallacycle was observed to be 1:1 throughout the reaction. NMR data for **{ Ni(κ^2-CFCF$_3$CF$_2$CF$_2$-)[P(OMe)$_3$]$_2$}**: ^{19}F NMR (282 Hz, C_6D_6) δ -209.7 (m, 1F, C – F), -121.8 (m, 1F, $^{2}J_{FF}$ = 224.7 Hz, C – F), -120.3 (m, 1F, $^{2}J_{FF}$ = 244.5 Hz, C – F), -115.2 (m, 1F, $^{2}J_{FF}$ = 244.5 Hz, C – F), -101.2 (m, 1F, $^{2}J_{FF}$ = 224.5 Hz, C – $F^{C\text{ or }D}$), -66.2 ppm (m, 3F, C – CF_3^E). $^{31}P\{^{1}H\}$NMR (121 Hz, C_6D_6) δ 132.7 ppm (overlapping multiplets, 2P, Ni[$\underline{P}$(OMe)$_3$]$_2$). ^{1}H NMR (300 Hz, C_6D_6) δ 3.08 (m, 9H, Ni[(P(OMe)$_3$]$_3$) NMR data for **6b**: ^{19}F NMR (282 Hz, C_6D_6) δ 102.5 ppm (q, $^{2}J_{FF}$ = 59.1 Hz, Ni=C$\underline{F}_2$). $^{31}P\{^{1}H\}$(121 Hz, C_6D_6) NMR δ 164.3 ppm (t, $^{3}J_{PF}$ = 59 Hz). ^{1}H NMR (300Hz, C_6D_6) δ 3.26 – 3.45 (ov m, 9H, Ni[(PO$\underline{Me}$)$_3$]$_3$). NMR data for **HFP**: ^{19}F NMR (282 Hz, C_6D_6) δ -192.8 (m, 1F, C$\underline{F}$CF$_3$), -105.8 (m, 1F, $CF^A\underline{F}^B$ trans to CF_3), -91.4 ppm (m, 1F, m, 1F, C$\underline{F}^AF^B$ cis to CF_3), -69.2 ppm (m, 3F, C$\underline{F}_3$). NMR data for unreacted **6**: ^{19}F NMR {282 Hz, C_6D_6) δ -84 - - 76 (unidentified impurities from synthesis of **6**), -74.9 (m, 3F, CFC$\underline{F}_3$), -74.3 (br s, unidentified impurity from synthesis of **6**), -40.9 (s, unidentified impurity from synthesis of **6**), -38.5 (s, unidentified impurity from synthesis of **6**), 48.0 ppm (quartet of quartets, $^{3}J_{FP}$ = 102 Hz, $^{3}J_{FF}$ = Hz, 1F, C$\underline{F}$CF$_3$). $^{31}P\{^{1}H\}$ NMR (121 Hz, C_6D_6) δ -8.1 ppm (s, free phosphine remnants from synthesis of **6**), 155.6 (d, unidentified impurity), 161.1 (s, NiP_4; P = P(OMe)$_3$), 163.0 ppm (dq, $^{3}J_{PF}$ = 102 Hz, $^{4}J_{PF}$ = 23 Hz, Ni$\underline{P}_3$CFCF$_3$), $^{31}P\{^{1}H\}$ NMR (121 Hz, C_6D_6) δ 3.11 – 3.45 (ov m, CH_3 residues of free P(OMe)$_3$/Ni(P)$_4$/Ni[P]$_3$(CFCF$_3$); P = P(OMe)$_3$). NMR data for unreacted **TFE**: ^{19}F NMR (282 Hz, C_6D_6) δ -132.5 ppm (s, 4F, C$\underline{F}_2$=C$\underline{F}_2$).

Synthesis of Ni(=CFCF$_3$)(P$_3$)[(7); P$_3$ = MeC(CH$_2$PPh$_2$)$_3$]. A stirred solution of **1** (55 mg, 0.070 mmol) in toluene (ca. 1 mL), prepared as described above (purified by sublimation), was treated with P_3 (47 mg, 0.075 mmol) at RT. A purple solid formed immediately (supernatant solution was faintly yellow). The mixture was stirred for 10 min before adding hexanes (ca. 1 mL). After allowing the mixture to stand at RT for 1 h, the resulting purple solid was recovered

by filtration (pre-weighed 2 mL medium porosity frit), washed with toluene (ca. 1.5 mL x 3) and Et_2O (ca. 1.5 mL x 3) and dried under reduced pressure. Yield: 48 mg, 0.061 mmol, 87 % based on **1**. Note that the solubility of this compound is generally poor in organic solvents (e.g., benzene, toluene, hexanes, Et_2O, DME); it is most soluble in CH_2Cl_2 and THF. UV-vis (1.6 mM in CH_2Cl_2): $\lambda_{max}(\varepsilon)$ = 506.25. ^{1}H NMR (300 MHz, CD_2Cl_2) δ 1.53 (quartet, $^4J_{HP}$ = 3 Hz, 3H, C<u>H</u>$_3$), 2.28 (d, $^2J_{HP}$ = 8 Hz, 6H, C<u>H</u>$_2$), 2.48 (s, water), 6.8 – 7.52 (ov m, Ar–<u>H</u>). ^{19}F NMR (282 MHz, CD_2Cl_2) δ –73.7 (apparent quintet, $^3J_{FF}$ = $^4J_{FP}$ = 19 Hz, 3F, CFC<u>F</u>$_3$), 26.7 ppm (quartet of quartets, $^3J_{FP}$ = 73 Hz, $^3J_{FF}$ = 19 Hz, 1F, C<u>F</u>CF$_3$). ^{31}P{^{1}H} NMR (121 MHz, CD_2Cl_2) δ 10.8 (doublet of quartets, $^3J_{PF}$ = 73 Hz, $^4J_{PF}$ = 19 Hz, 3P, Ni–<u>P</u>). ^{19}F and ^{31}P{^{1}H} NMR data for **2** in THF: ^{19}F NMR (282 MHz, THF with C_6D_6 capillary) δ –73.6 (apparent quintet, $^3J_{FF}$ = $^4J_{FP}$ = 19 Hz, 3F, CFC<u>F</u>$_3$), 30.5 (quartet of quartets, $^3J_{FP}$ = 73 Hz, $^3J_{FF}$ = 19 Hz, 1F, C<u>F</u>CF$_3$). ^{31}P{^{1}H} NMR (121 MHz, THF with C_6D_6 capillary) δ 14.4 (doublet of quartets, $^3J_{PF}$ = 73 Hz, $^4J_{PF}$ = 19 Hz, 3P, Ni–<u>P</u>). Anal. Calc. for $C_{43}H_{39}F_4NiP_3$: C, 65.93; H, 5.02. Found: C, 65.67; H, 5.36. Crystals suitable for X-ray analysis were grown by diffusion of Et_2O vapor into a THF solution of **7** at –35 °C. NMR spectra and crystallographic details can be found below.

Reaction of 7 with CF_2=CF_2 (TFE). TFE (1.3 mL, 0.053 mmol, excess) was added by syringe to a saturated solution of **2** in THF (0.60 mL, 14 mM) in a septum-capped NMR tube containing a C_6D_6 capillary and BTB (32 mM). Mixing was achieved by inverting the tube several times. After 35 min at RT, ^{19}F NMR data showed that 14% of **7** had been consumed (concentration: 12 mM) to give ~1 mM of a product having the characteristic ^{19}F NMR signature associated with the Ni[-CF(CF_3)CF_2CF_2-] substructure, which we tentatively assign as Ni(κ^2-P_3)[-CF(CF_3)CF_2CF_2-] [P_3 = MeC(CH_2PPh_2)$_3$]. The NMR sample was allowed to stand at RT for another 45 min, then heated at 50 °C for 1 h 20 min before collecting ^{19}F and ^{31}P{^{1}H} NMR data. ^{19}F NMR data showed that 70% of **7** had been consumed (concentration: 4 mM) to give primarily the species assigned as Ni(κ^2-P_3)[-CF(CF_3)CF_2CF_2-] (8 mM) and other unidentified products. Metathesis products, Ni(P_3)(=CF_2) and CF_2=CFCF_3, were not observed but further heating generated additional uncharacterized products. NMR data for putative Ni(κ^2-P_3)[-CF(CF_3)CF_2CF_2-]: ^{19}F NMR (282 MHz, THF with C_6D_6 capillary) (see Figure 4.2 for fluorine labeling scheme) δ 208.0 (m, 1F, F^B), –121.8 (dm, $^2J_{FF}$ = 247 Hz, 1F, $F^{F\text{ or }E}$), –119.9 (dm, $^2J_{FF}$ = 216 Hz, 1F, $F^{C\text{ or }D}$), –114.5 (dm, $^2J_{FF}$ = 247 Hz, 1F, $F^{F\text{ or }E}$), –101.1 (dm, $^2J_{FF}$ = 216 Hz, 1F, $F^{C\text{ or}}$

^{D}), –65.8 (m, 3F, F^{A}). $^{31}P\{^{1}H\}$ NMR (121 MHz, THF with C_6D_6 capillary) δ –2.1 (br apparent singlet, $\omega_{1/2} \approx 240$ Hz, 3P, non-equiv P atoms of κ^2-P_3).

Qualitative experiment to determine if reaction of 1 with TFE occurs via a dissociative vs. associative mechanism. Two C_6D_6 solutions (0.50 mL) containing **1** (54 mM) {with trace $Ni[P(O\text{-}i\text{-}Pr)_3]_4$ contaminant, ca. 2% relative to **1**} was placed in two septum-capped NMR tubes (homogeneous dark purple solution). Both NMR tubes had TFE (4.0 mL at 23 °C and 1 atm; 0.16 mmol; 6 equiv.) added to the tube, through the septum via a syringe needle; one of the two NMR tubes contained excess $P(O^{i}Pr)_3$ (0.55 mmol; 20 equiv.). The ^{19}F NMR (282 MHz) revealed that the reaction with excess phosphite showed product formation after 10 min. (vs. 2 min without phosphite) and did not go to completion even after 1 hour (unlike the reaction without phosphite). NMR spectra can be found below.

^{1}H NMR, ^{19}F NMR and ^{31}P NMR Spectra

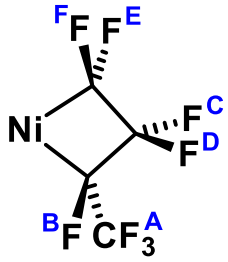

Figure 4.2: Fluorine labeling scheme for complex **2a**,**c** and $Ni(\kappa^2\text{-}P_3)[\text{-}CF(CF_3)CF_2CF_2\text{-}]$ (**7**).

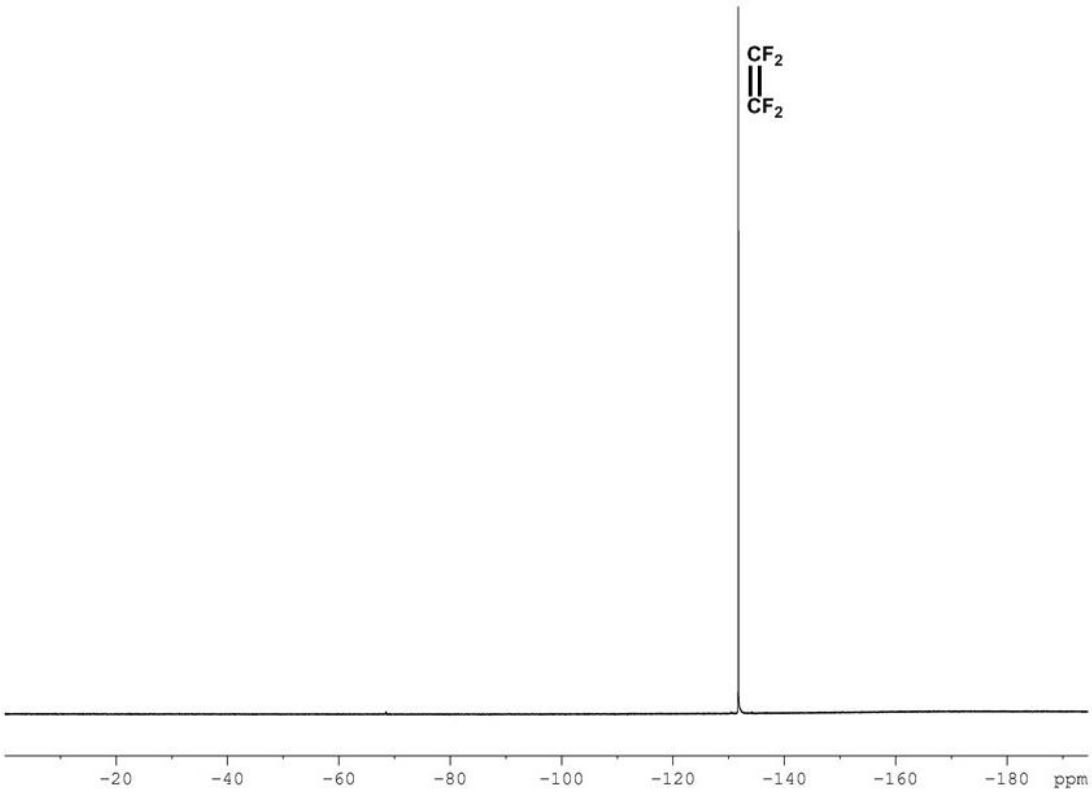

Figure 4.3: ^{19}F NMR (282 Hz, C_6D_6) spectrum of TFE from PTFE pyrolysis

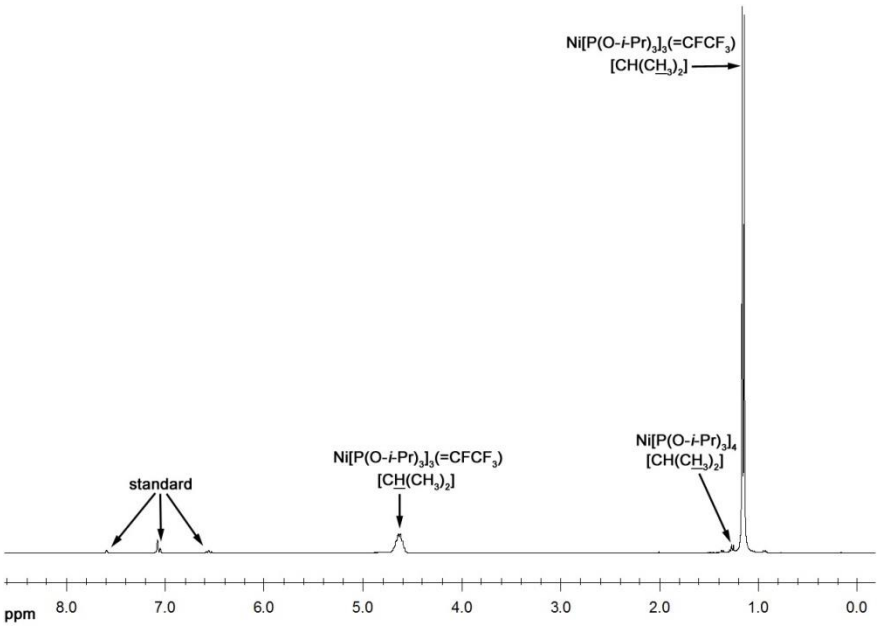

Figure 4.4: ^{1}H NMR (300 Hz, C_6D_6) spectrum for $Ni[P(O\text{-}i\text{-}Pr)_3]_3(=CFCF_3)$ (**1**, sublimed) at RT.

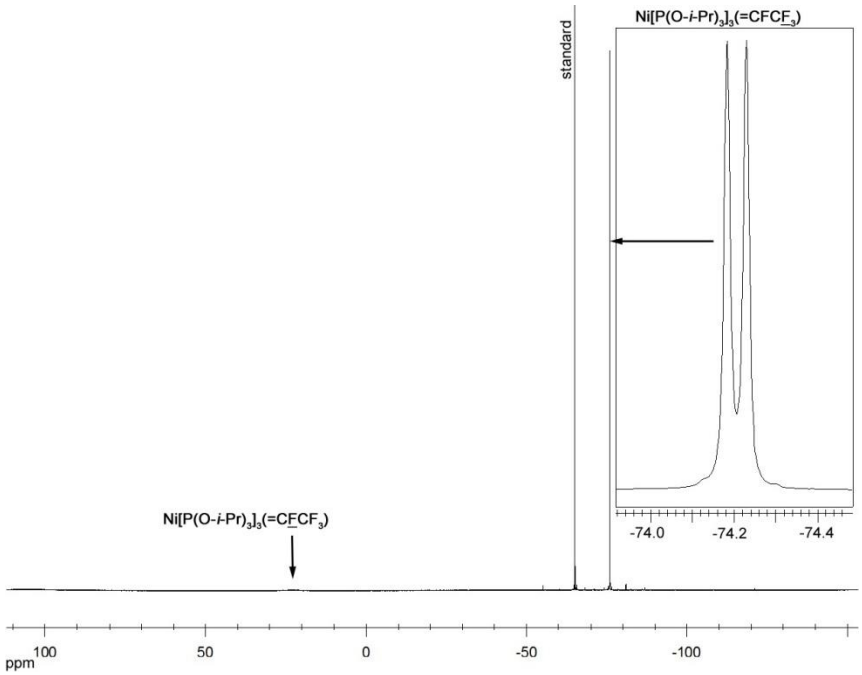

Figure 4.5: ^{19}F NMR (282 Hz, C_6D_6) spectrum for $Ni(=CFCF_3)[P(O\text{-}i\text{-}Pr)_3]_3$ (**1**, sublimed) at RT. The inset shows an expansion of the target CF_3 peak. Note that the $CFCF_3$ peak (24.6 ppm) is barely visible in this view. Also, F-F coupling is observed at RT but F-P co coupling is not. See below for the low-temperature spectrum.

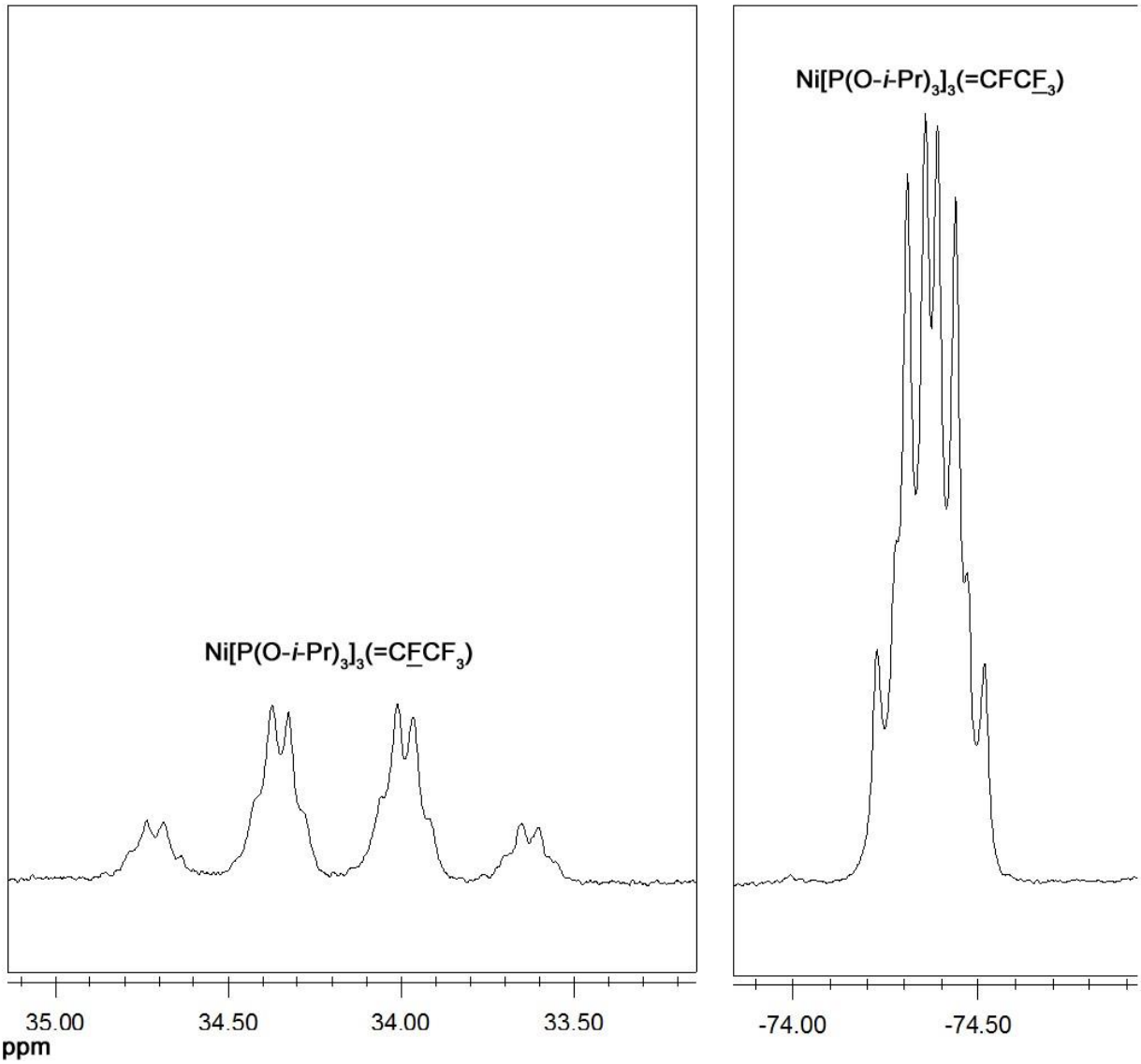

Figure 4.6: Partial ^{19}F NMR (282 Hz, toluene-d8) spectrum for $Ni[P(O\text{-}i\text{-}Pr)_3]_3(=CFCF_3)$ (**1**) at –45°C, showing the expanded $CFCF_3$ and $CFCF_3$ signals with F-P coupling.

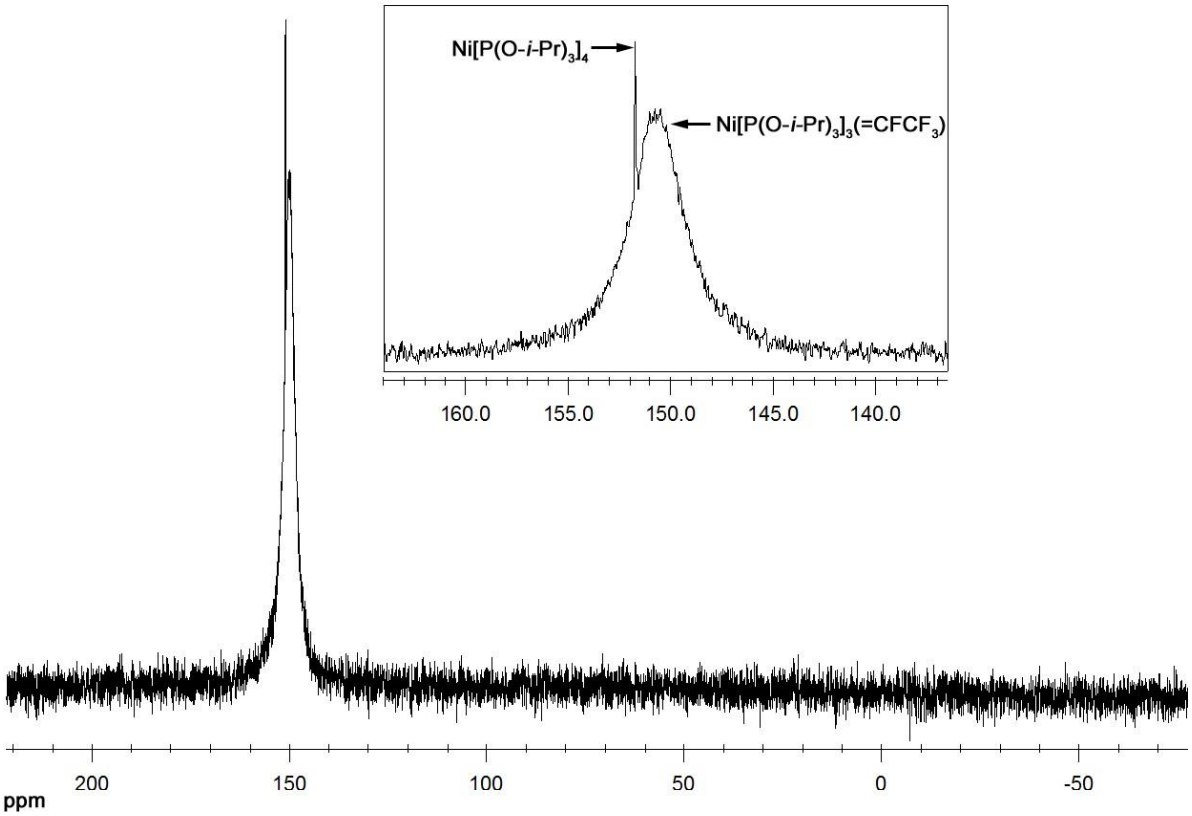

Figure 4.7: $^{31}P\{^{1}H\}$ NMR (121 MHz, C_6D_6) spectrum for $Ni(=CFCF_3)[P(O\text{-}i\text{-}Pr)]_3$ (**1**, sublimed) at RT. The inset shows an expansion of the target and minor contaminant {i.e., < 2% $Ni[P(O\text{-}i\text{-}Pr)_3]_4$} peaks.

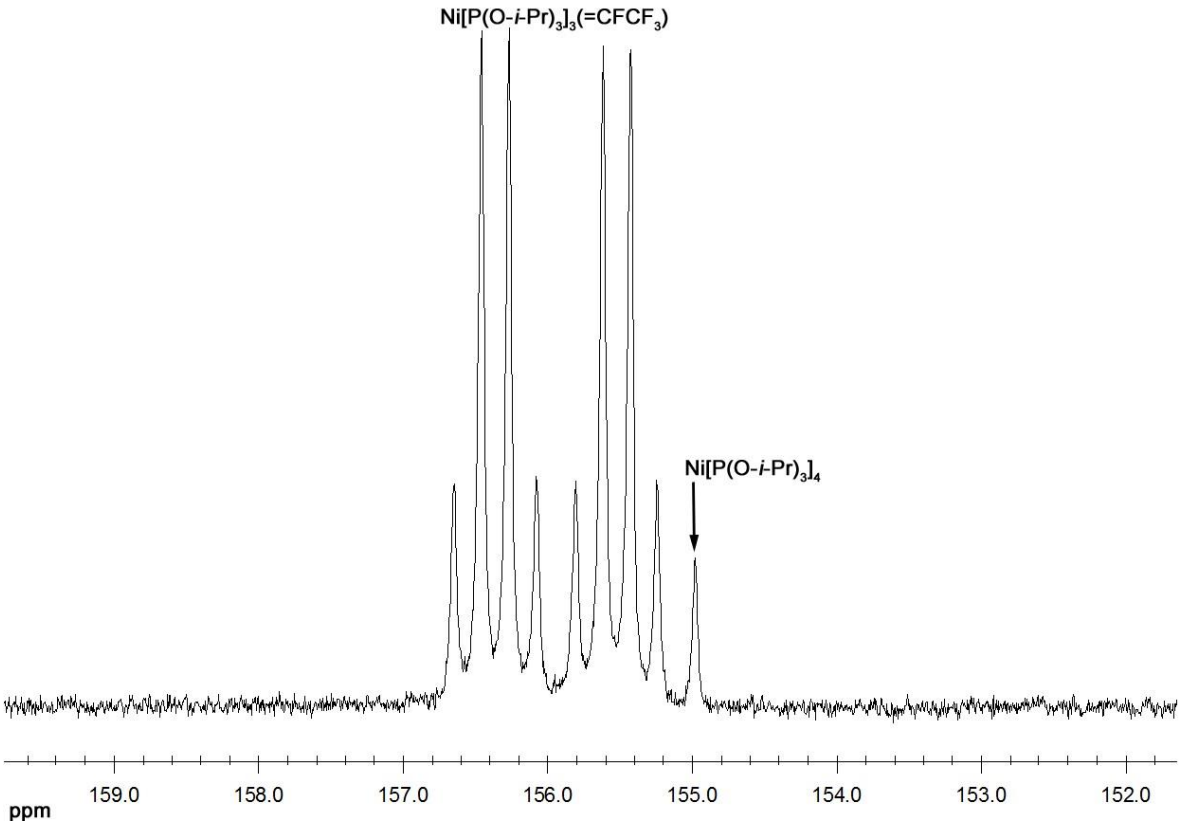

Figure 4.8: $^{31}P\{^{1}H\}$ NMR (121 MHz, toluene-d_8) spectrum for Ni(=$CFCF_3$)[P(O-i-Pr)]$_3$ (**1**) at –45 ^{o}C, showing P-F coupling.

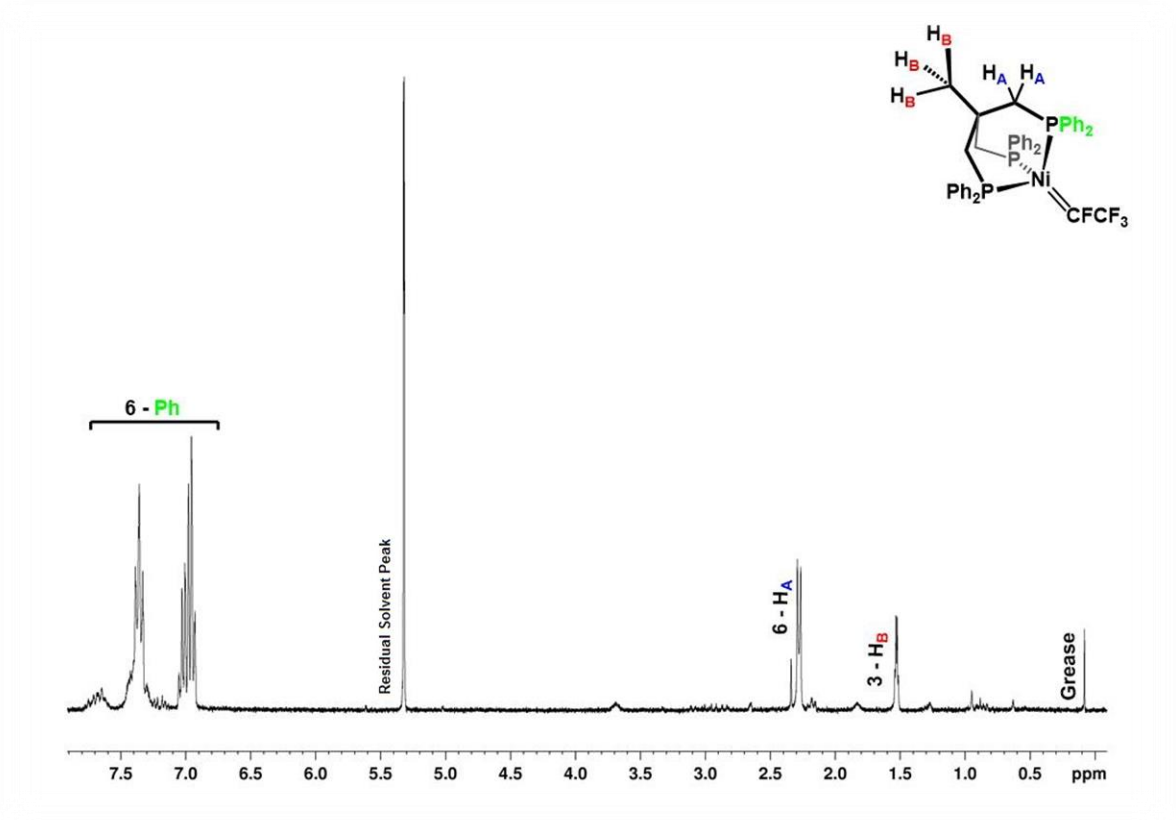

Figure 4.9: ^{1}H NMR (300 MHz, CD_2Cl_2) of $Ni(=CFCF_3)(P_3)[P_3 = MeC(CH_2PPh_2)_3]$ (**7**). The limited solubility of **7** accounts for the low signal/contaminant ratio.

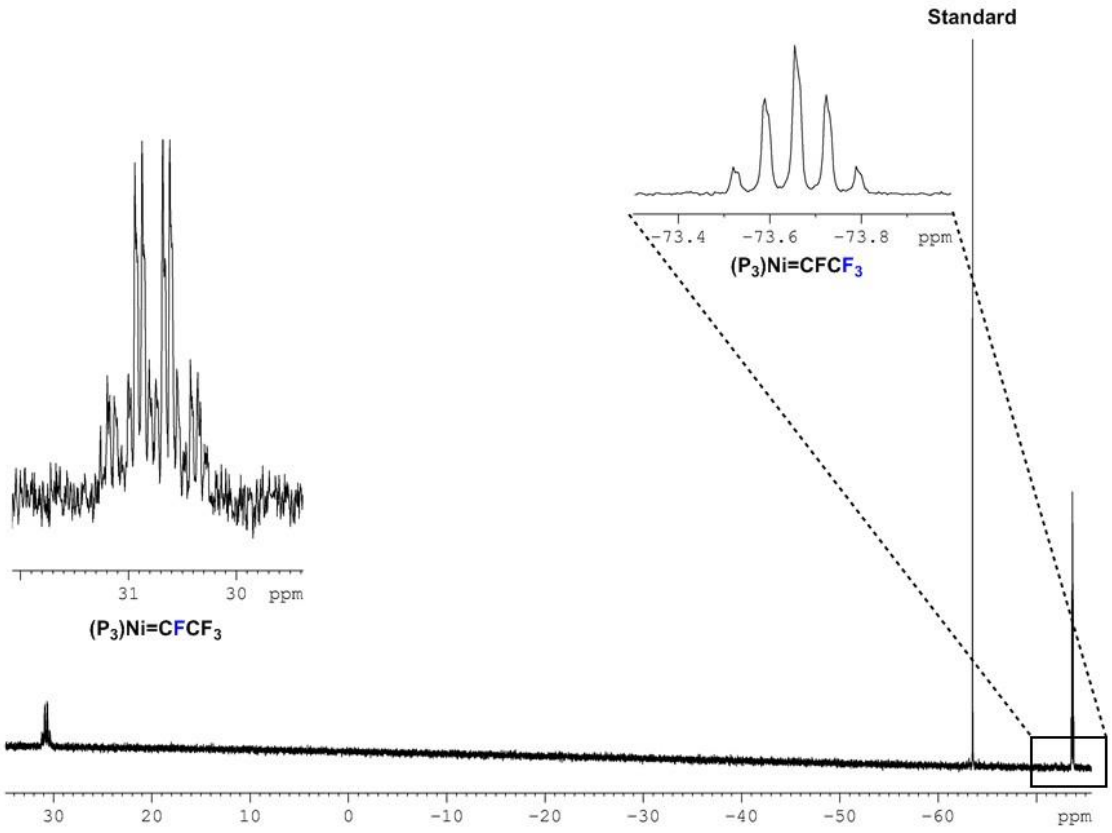

Figure 4.10: ^{19}F NMR (282 MHz, CD_2Cl_2) spectrum of Ni(=CFCF$_3$)(P$_3$) [P$_3$ = MeC(CH$_2$PPh$_2$)$_3$] (**7**).

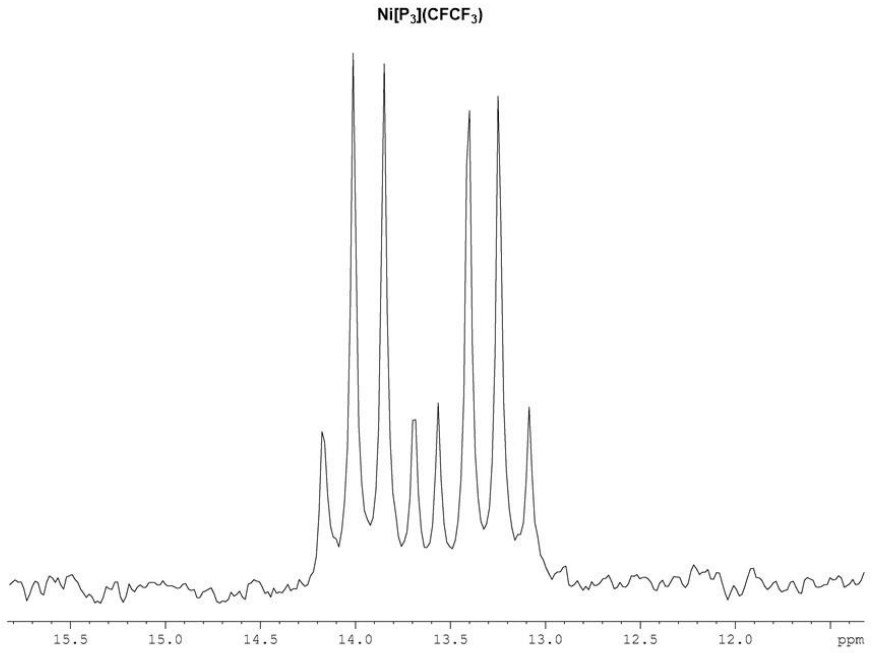

Figure 4.11: $^{31}P\{^{1}H\}$ NMR (121 MHz, CD_2Cl_2) spectrum of Ni(=$CFCF_3$)(P_3) [P_3 = $MeC(CH_2PPh_2)_3$] (**7**).

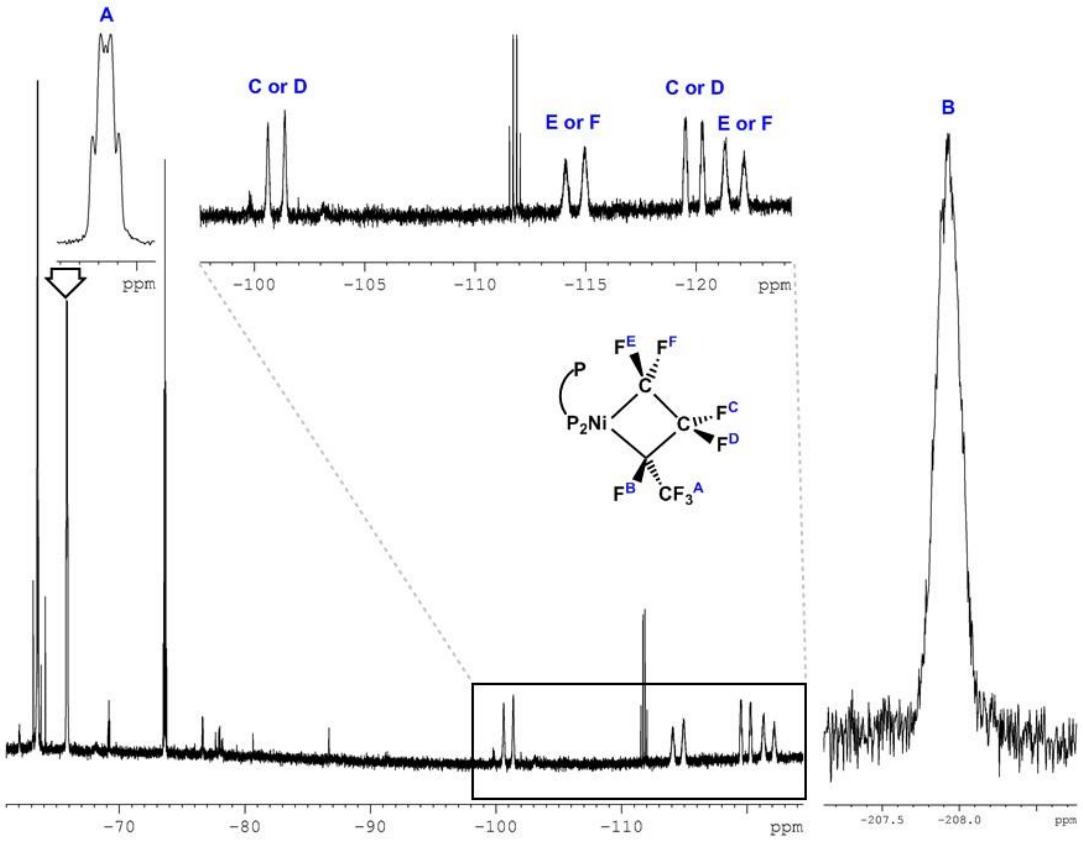

Figure 4.12: ^{19}F NMR (282 MHz, THF with C_6D_6 capillary) spectrum for the reaction of $Ni(=CFCF_3)(P_3)$ (**7**) with TFE. [$P_3 = MeC(CH_2PPh_2)_3$]

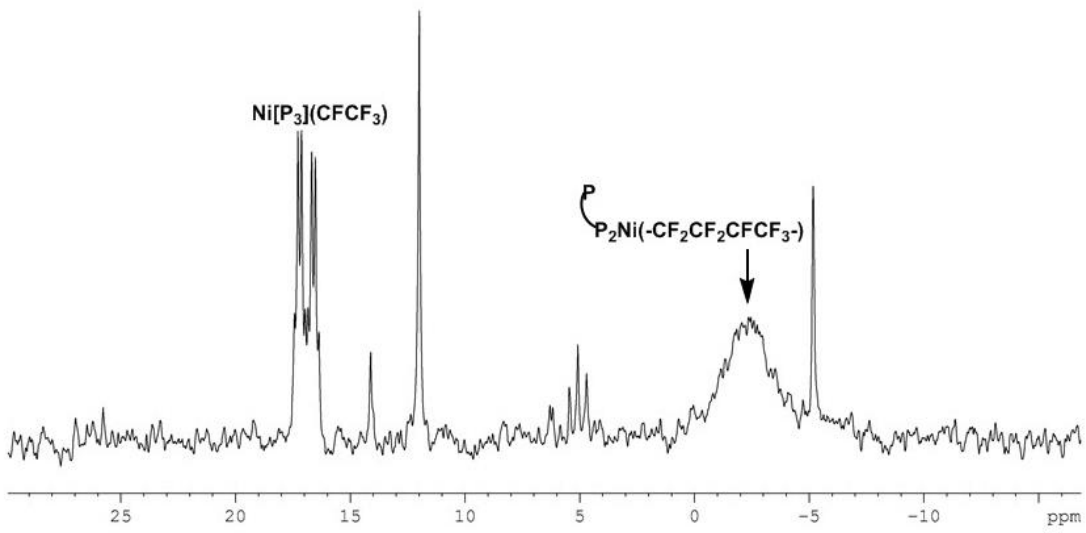

Figure 4.13: ^{31}P NMR (121 MHz, THF with C_6D_6 capillary) spectrum for the reaction of $Ni(=CFCF_3)(P_3)$ (**7**) with TFE. [P_3 = $MeC(CH_2PPh_2)_3$].

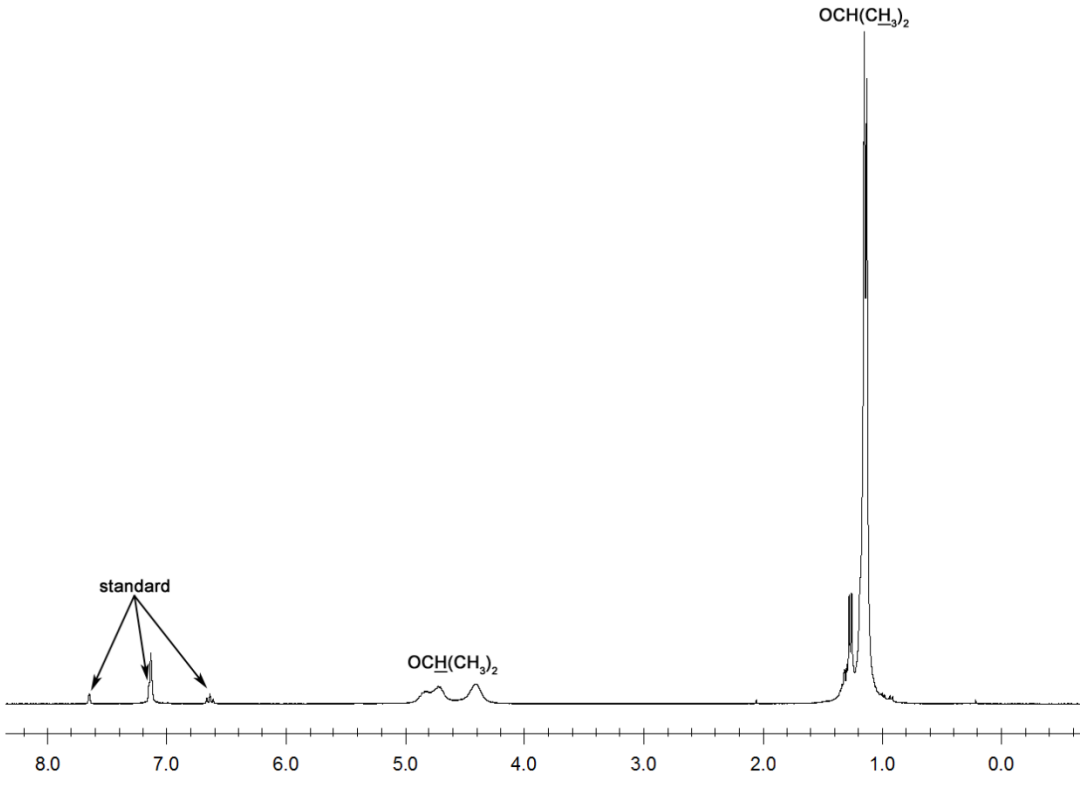

Figure 4.14: ^{1}H NMR (300 MHz, C_6D_6) spectrum for the reaction of $Ni(=CFCF_3)[P(O\text{-}i\text{-}Pr)_3]_3$ (**1**) with TFE.

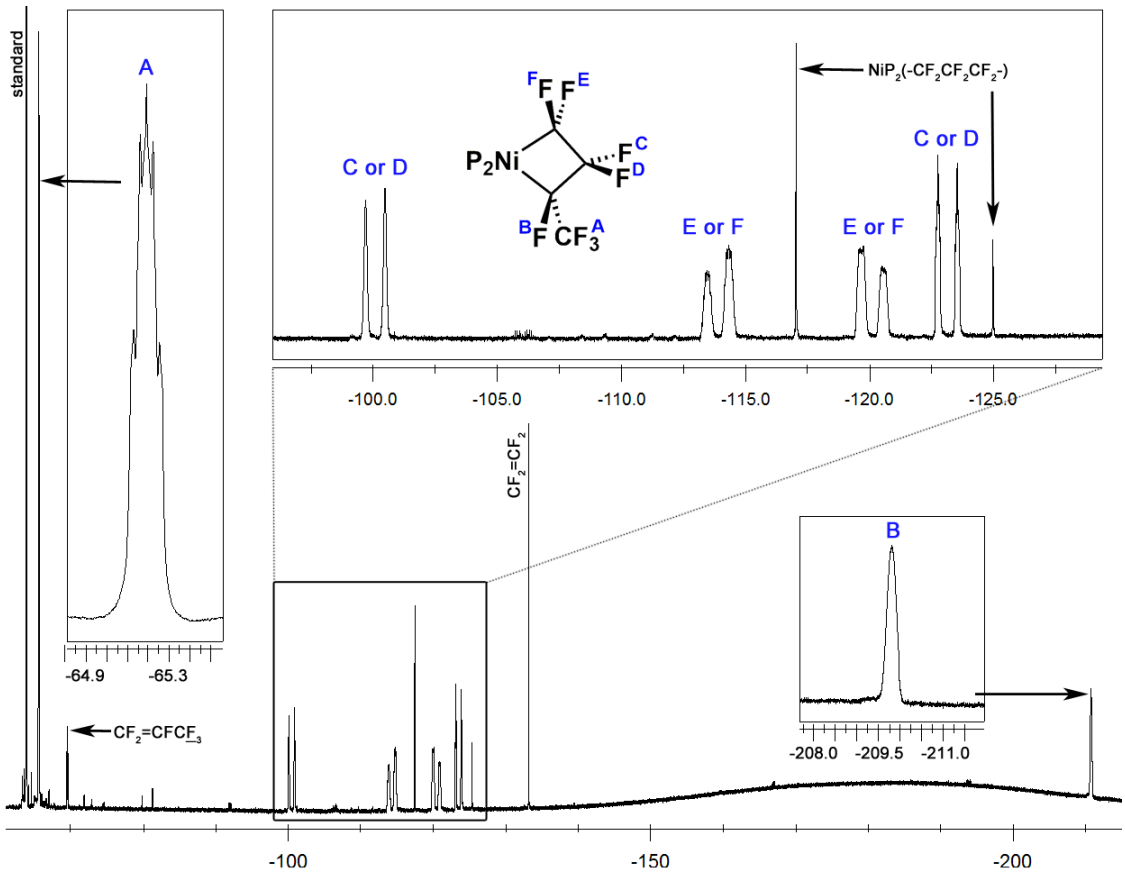

Figure 4.15: ^{19}F NMR (282 MHz, C_6D_6) spectrum (upfield) for the reaction of Ni(=CFCF$_3$)[P(O-i-Pr)$_3$]$_3$ (**1**) with TFE. The insets show expanded spectral regions and the labeling scheme.

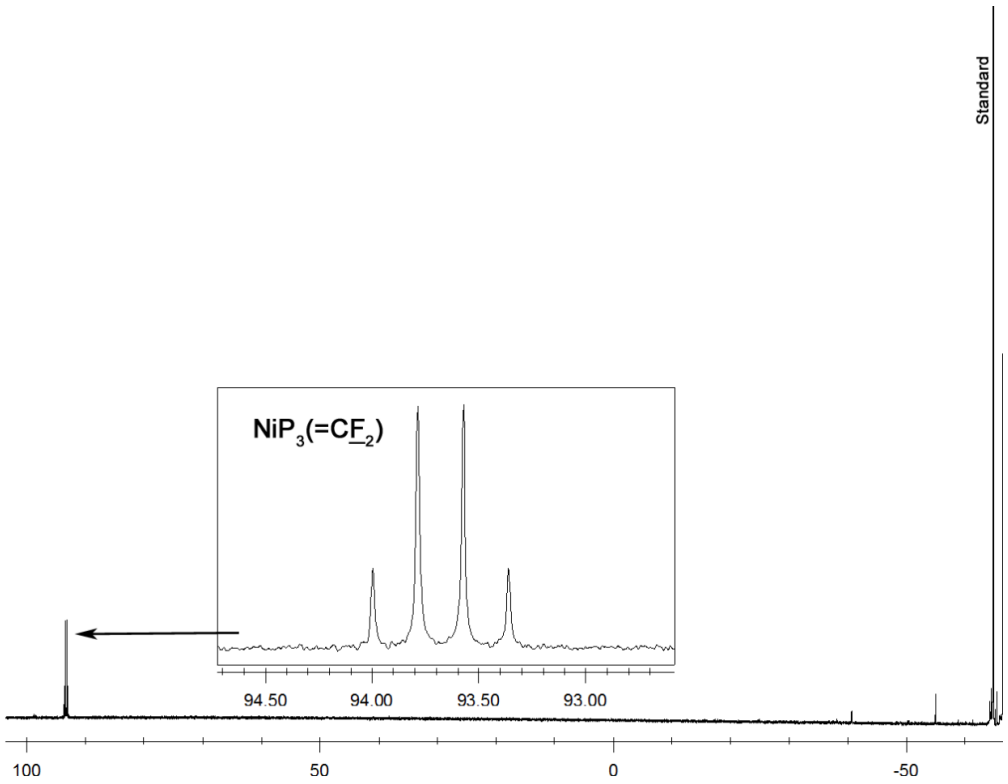

Figure 4.16: ^{19}F NMR (282 MHz, C_6D_6) spectrum (downfield) for the reaction of $Ni(=CFCF_3)[P(O\text{-}i\text{-}Pr)_3]_3$ (**1**) with TFE. The inset shows expanded $Ni=C\underline{F}_2$ region.

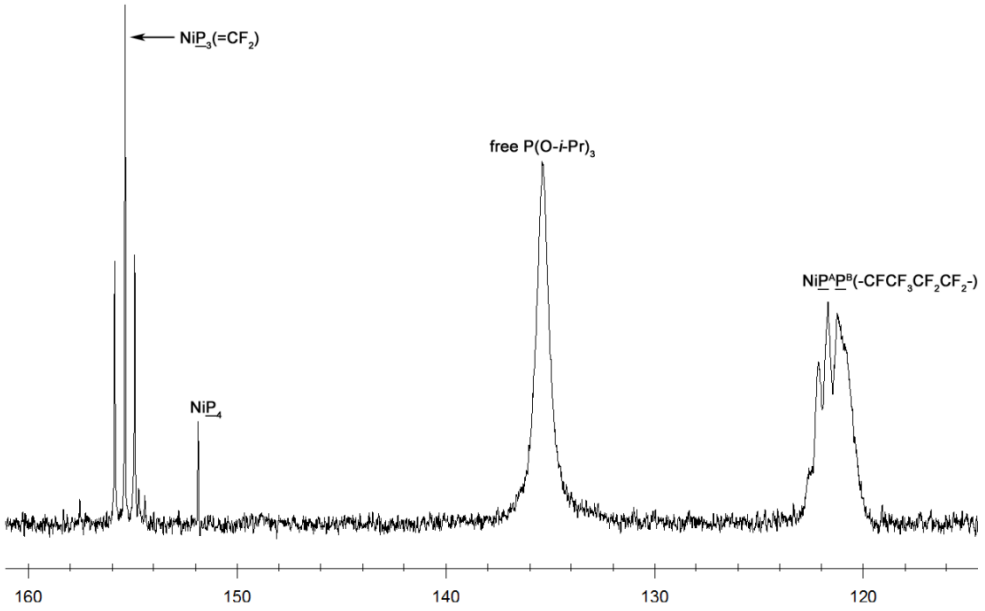

Figure 4.17: $^{31}P\{^1H\}$ NMR (121 MHz, C_6D_6) spectrum for the reaction of $Ni(=CFCF_3)[P(O\text{-}i\text{-}Pr)_3]_3$ (**1**) with TFE.

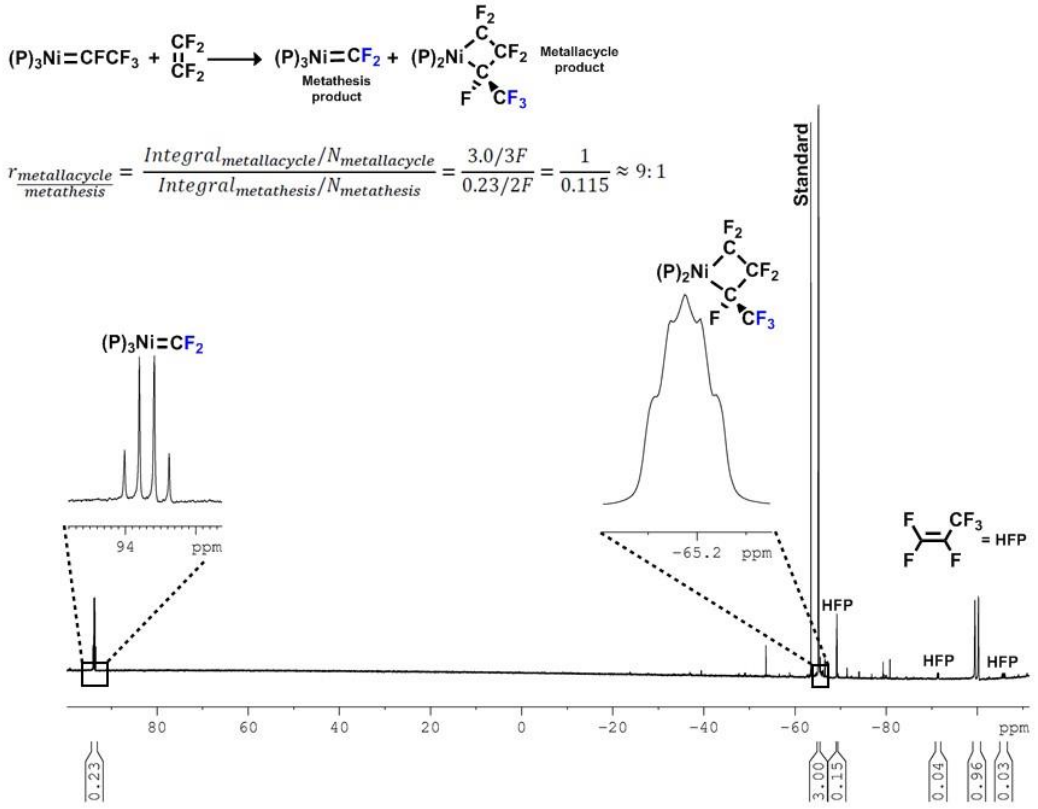

Figure 4.18: ^{19}F NMR (282 MHz, C_6D_6) spectrum (downfield) for the reaction of $Ni(=CFCF_3)[P(O\text{-}i\text{-}Pr)_3]_3$ (**1**) with TFE. Spectrum includes the calculation of the metallacycle/metathesis ratio.

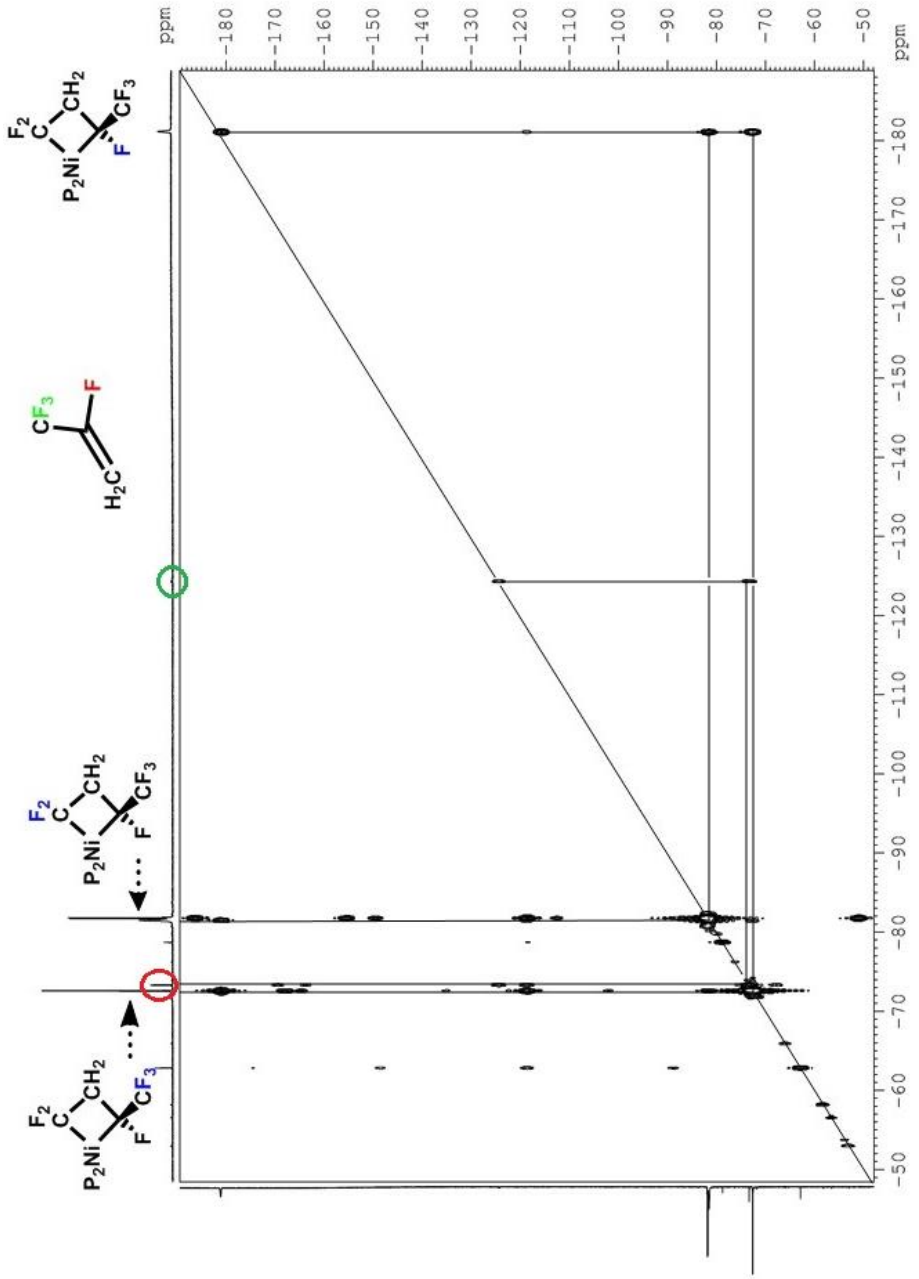

Figure 4.19: Two-dimensional ^{19}F COSY experiment in C_6D_6 to help in the assignment of the hydrofluoroalkene metathesis peaks and the CF_2 peaks of the metallacycle product.

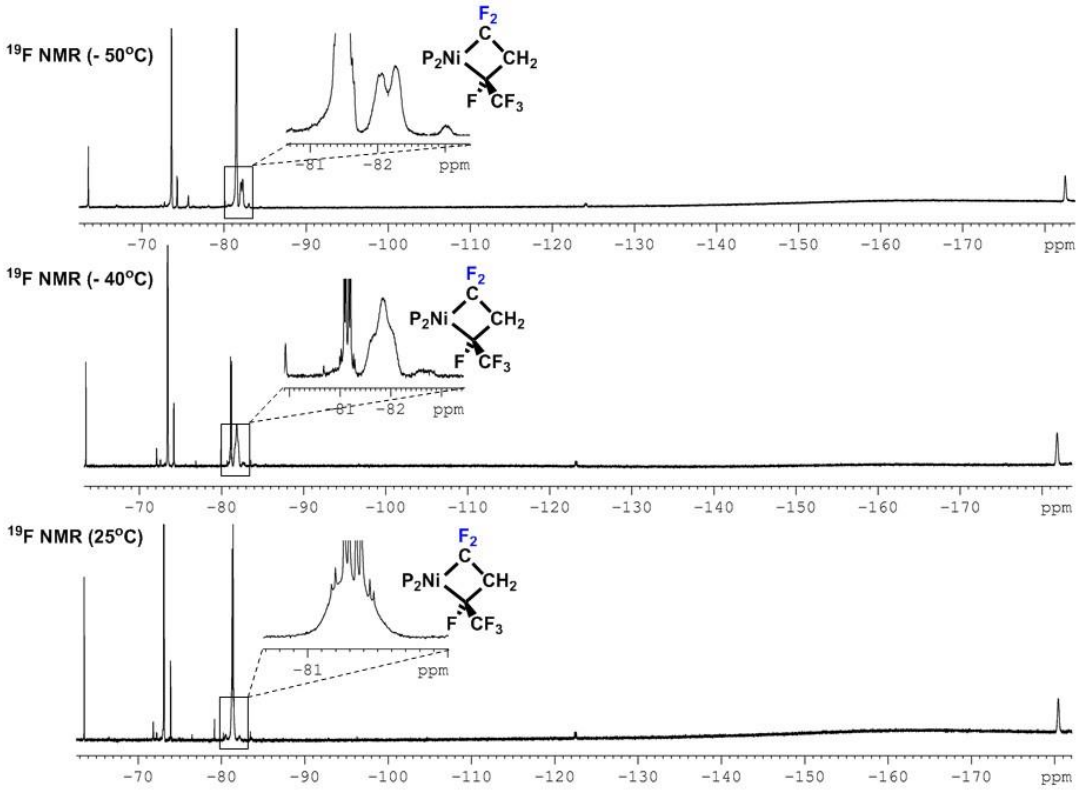

Figure 4.20: Low temperature ^{19}F NMR (282 MHz, C_6D_6) spectra of metallacycle product formed from $Ni(=CFCF_3)[P(O\text{-}i\text{-}Pr)_3]_3$ **1** and VDF showing inequivalent CF_2 resonances overlapped with that due to excess VDF.

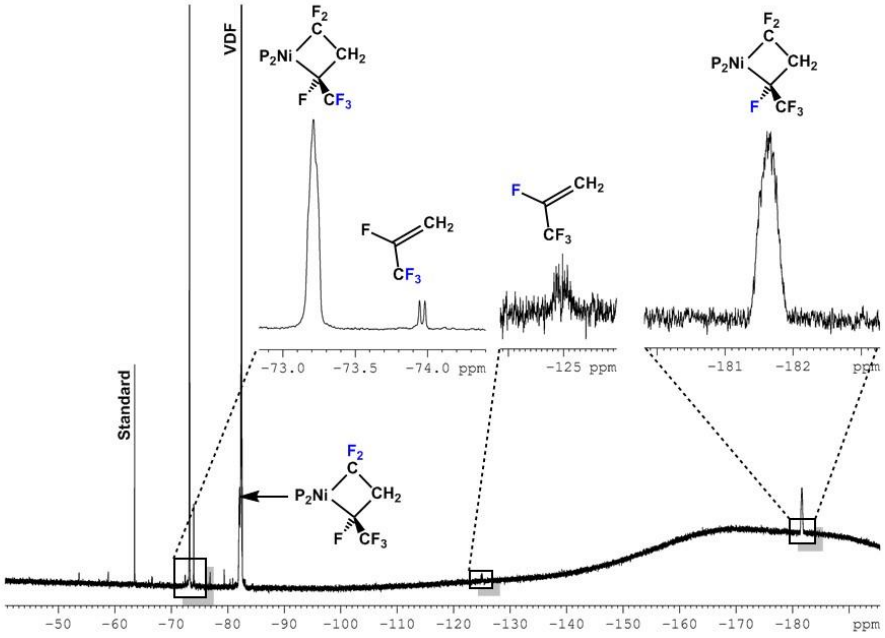

Figure 4.21: ^{19}F NMR (282 MHz, C_6D_6) spectrum (upfield) for the reaction of $Ni(=CFCF_3)[P(O\text{-}i\text{-}Pr)_3]_3$ (**1**) with VDF.

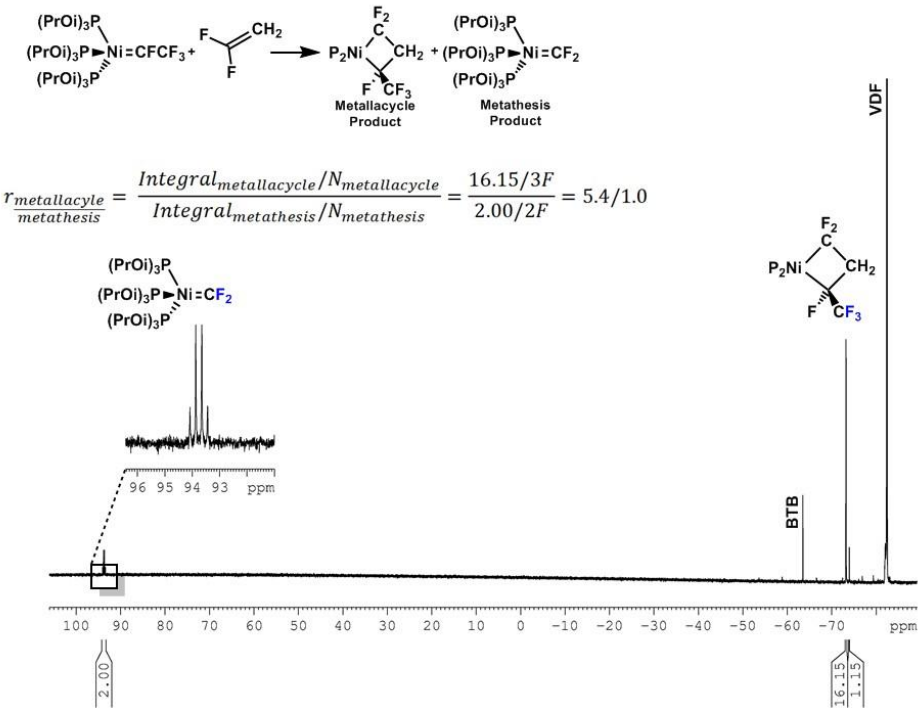

Figure 4.22: ^{19}F NMR (282 MHz, C_6D_6) spectrum (downfield) for the reaction of $Ni(=CFCF_3)[P(O\text{-}i\text{-}Pr)_3]_3$ (**1**) with VDF. Spectrum includes the calculation of the metallacycle/metathesis ratio.

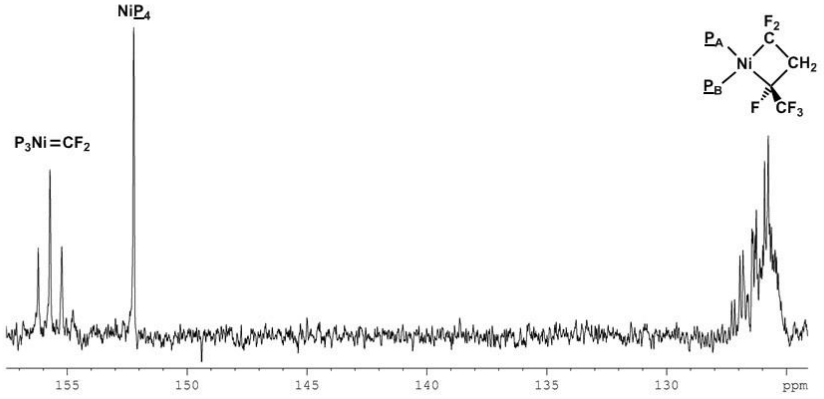

Figure 4.23: $^{31}P\{^1H\}$ NMR (121 MHz, C_6D_6) spectrum for the reaction of $Ni(=CFCF_3)[P(O\text{-}i\text{-}Pr)_3]_3$ (**1**) with VDF.

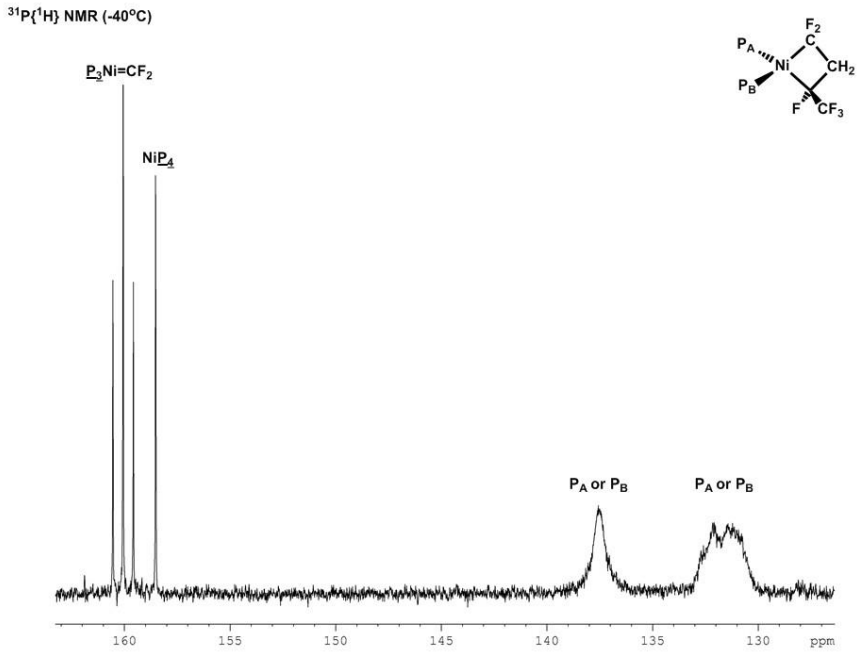

Figure 4.24: $^{31}P\{^{1}H\}$ NMR (121 MHz, C_6D_6) low temperature (-40°C) spectrum for the reaction of $Ni(=CFCF_3)[P(O\text{-}i\text{-}Pr)_3]_3$ (**1**) with VDF.

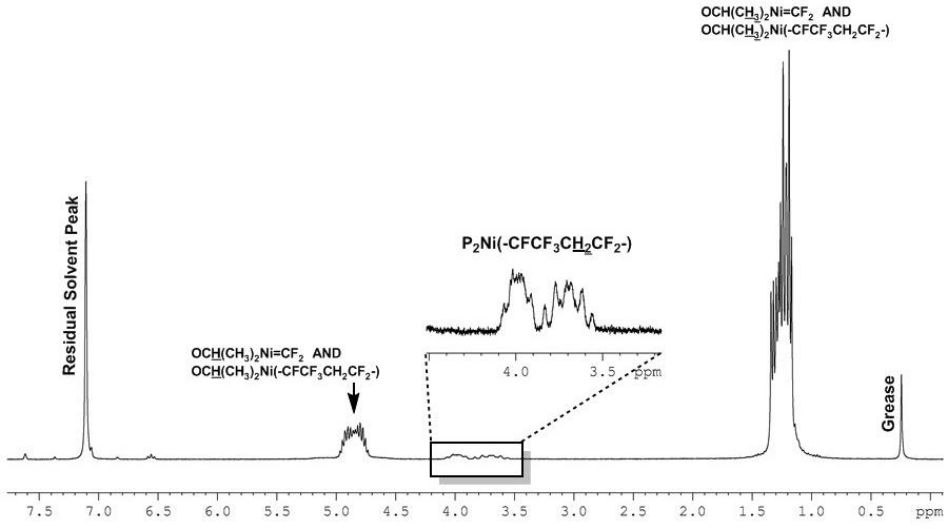

Figure 4.25: ^{1}H NMR (300 MHz, C_6D_6) spectrum for the reaction of $Ni(=CFCF_3)[P(O\text{-}i\text{-}Pr)_3]_3$ (**1**) with VDF.

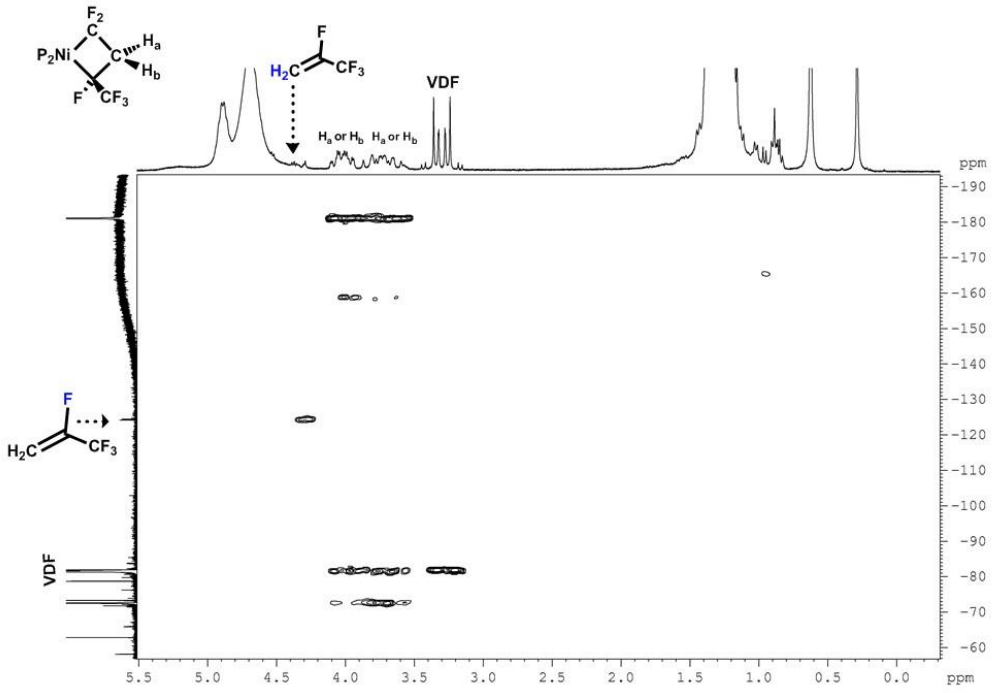

Figure 4.26: Two dimensional (^{1}H - ^{19}F) HMBC spectrum for the reaction of Ni(=CFCF$_3$)[P(O-i-Pr)$_3$]$_3$ (**1**) with VDF

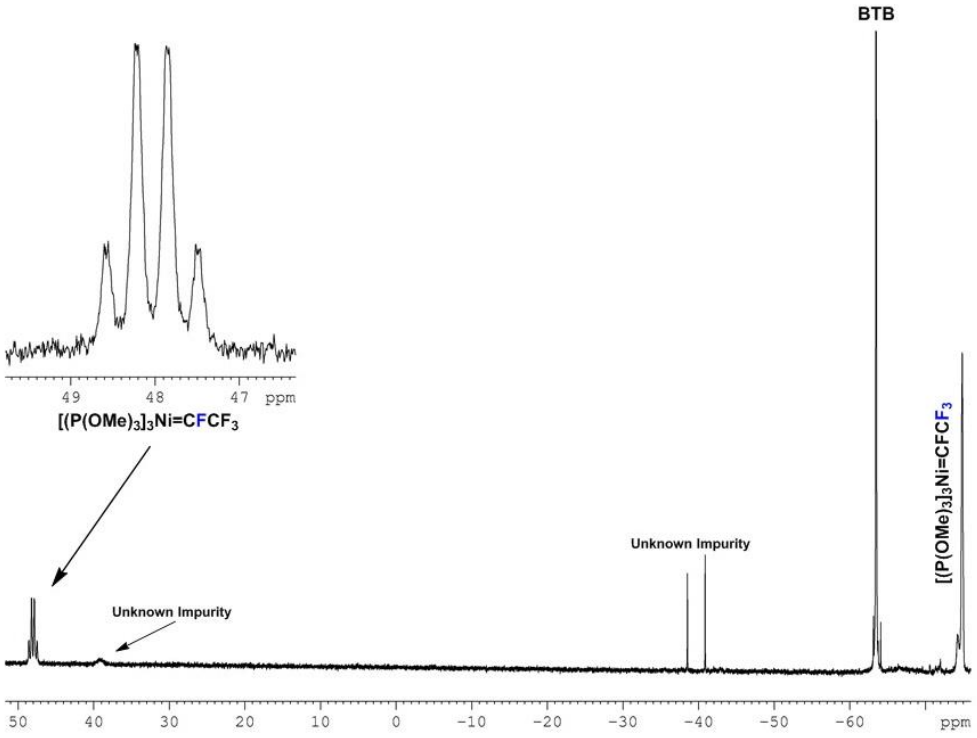

Figure 4.27: ^{19}F NMR (282 MHz, C_6D_6) spectrum of $Ni(=CFCF_3)[P(OMe)_3]_3$ (**6**).

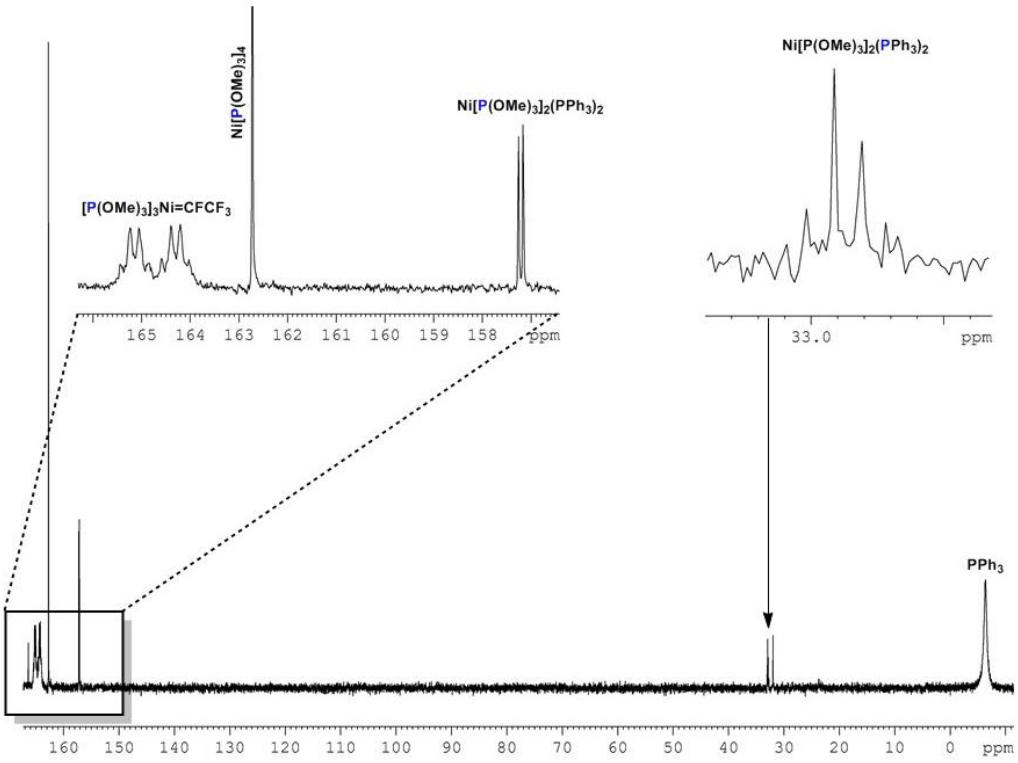

Figure 4.28: $^{31}P\{^{1}H\}$ NMR (121 MHz, C_6D_6) spectrum of $Ni(=CFCF_3)[P(OMe)_3]_3$ (**4**).

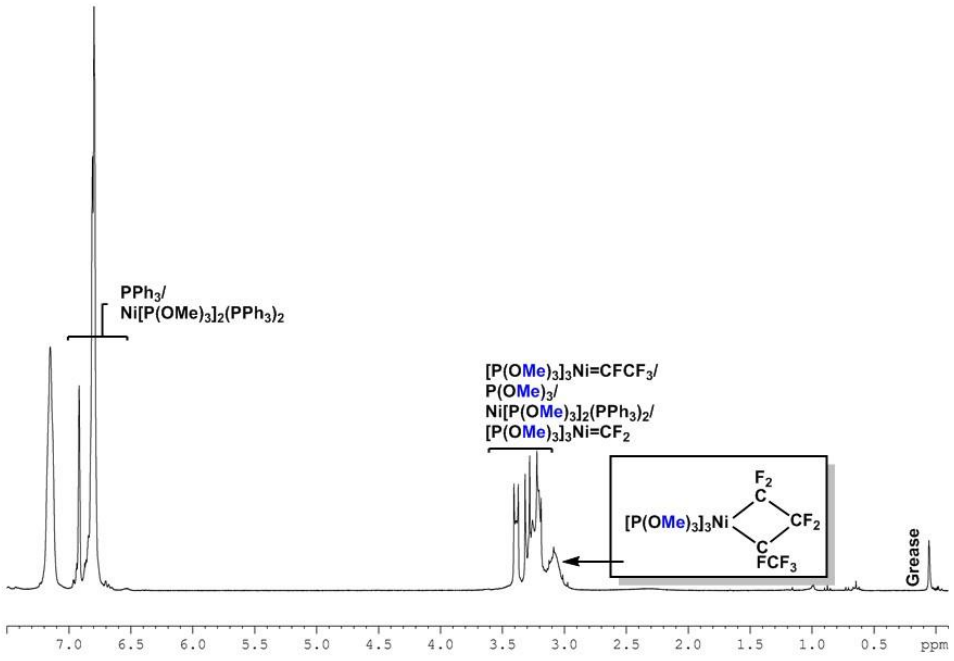

Figure 4.29: ^{1}H NMR (300 MHz, C_6D_6) spectrum of$Ni(=CFCF_3)[P(OMe)_3]_3$ (**6**)).

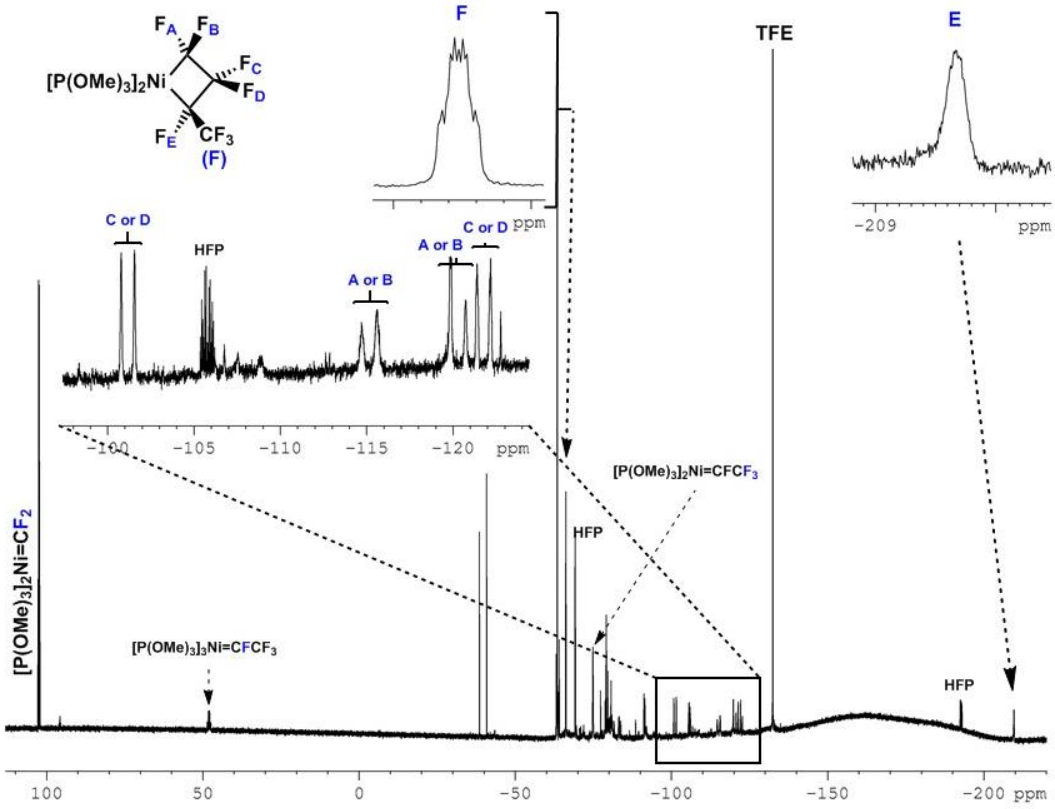

Figure 4.30: ^{19}F NMR (282 MHz, C_6D_6) spectrum for the reaction of $Ni(=CFCF_3)[P(OMe)_3]_3$ (**6**)with TFE.

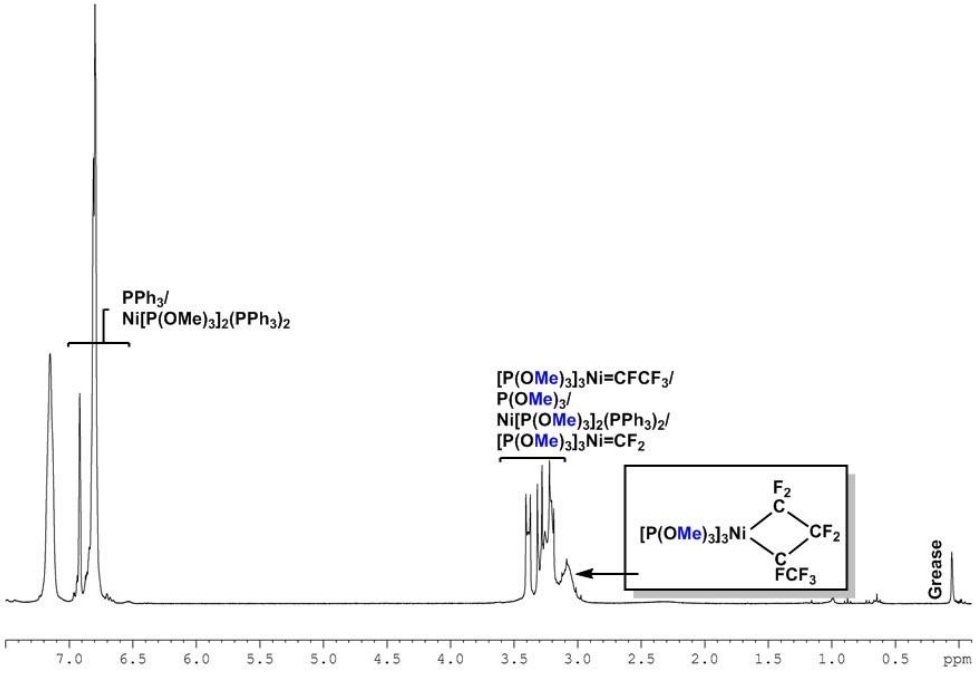

Figure 4.31: ^{1}H NMR (300 MHz, C_6D_6) spectrum for the reaction of Ni(=CFCF$_3$)[P(OMe)$_3$]$_3$ (**6**)with TFE.

$$Ratio_{\frac{metallacycle}{metathesis}} = \frac{Integral_{metallacycle}}{N} \Big/ \frac{Integral_{metathesis}}{N} = \frac{4.16}{3} \Big/ \frac{2}{2} = 1.4/1$$

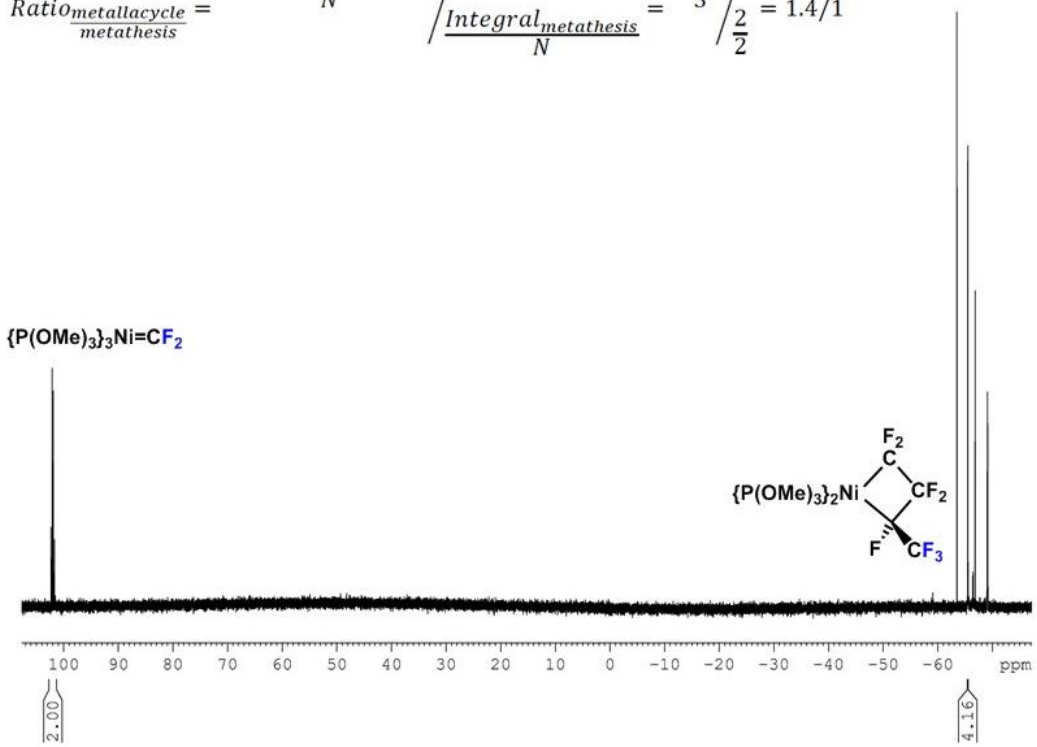

Figure 4.32: ^{19}F NMR (282 MHz, C_6D_6) spectrum for the reaction of $Ni(=CFCF_3)[P(OMe)_3]_3$ (**6**)with TFE showing the integrations of the $Ni=CF_2$ peak and the $Ni(-CFCF_3-CF_2-CF_2-)$ used to calculate the metallacycle/metathesis ratio.

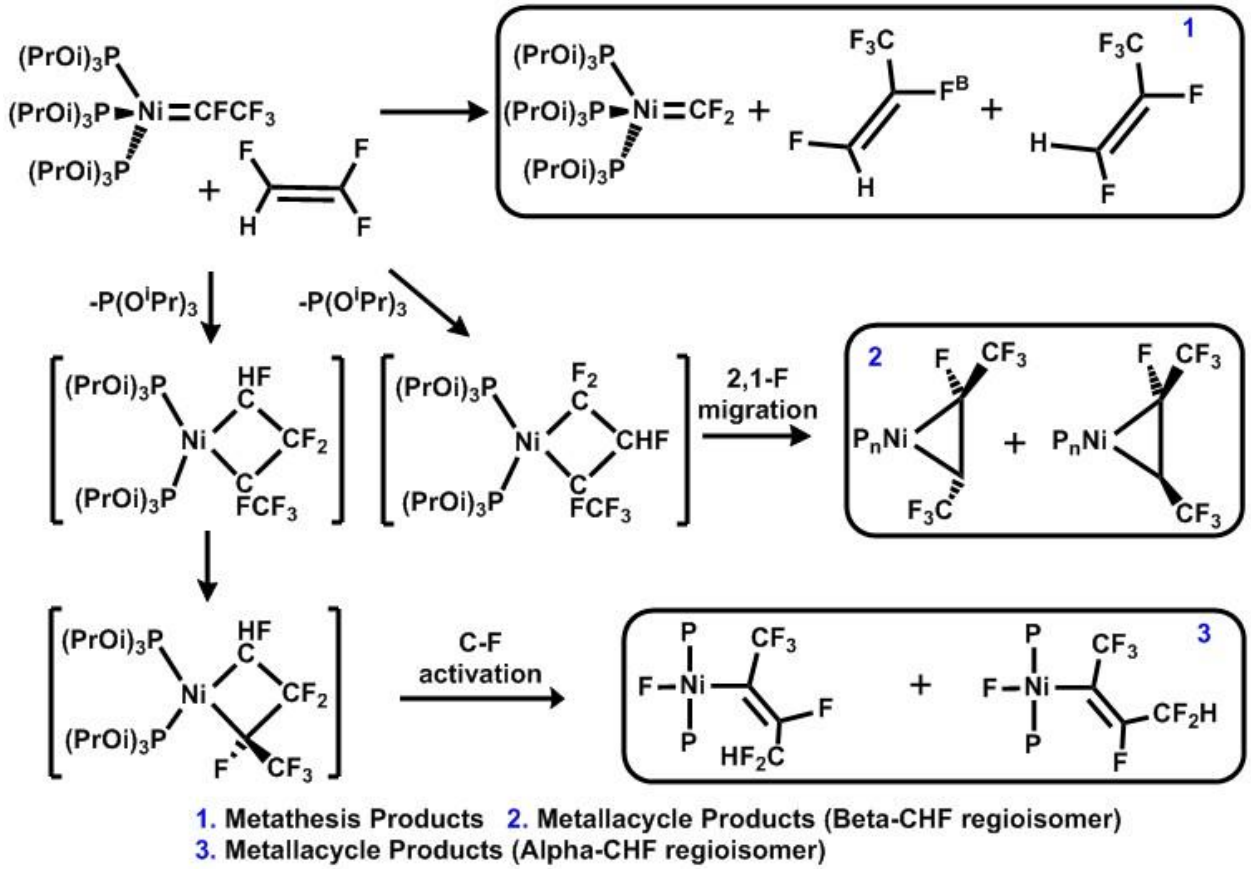

Figure 4.33: Proposed reaction mechanism for the reaction of **1** with TrFE

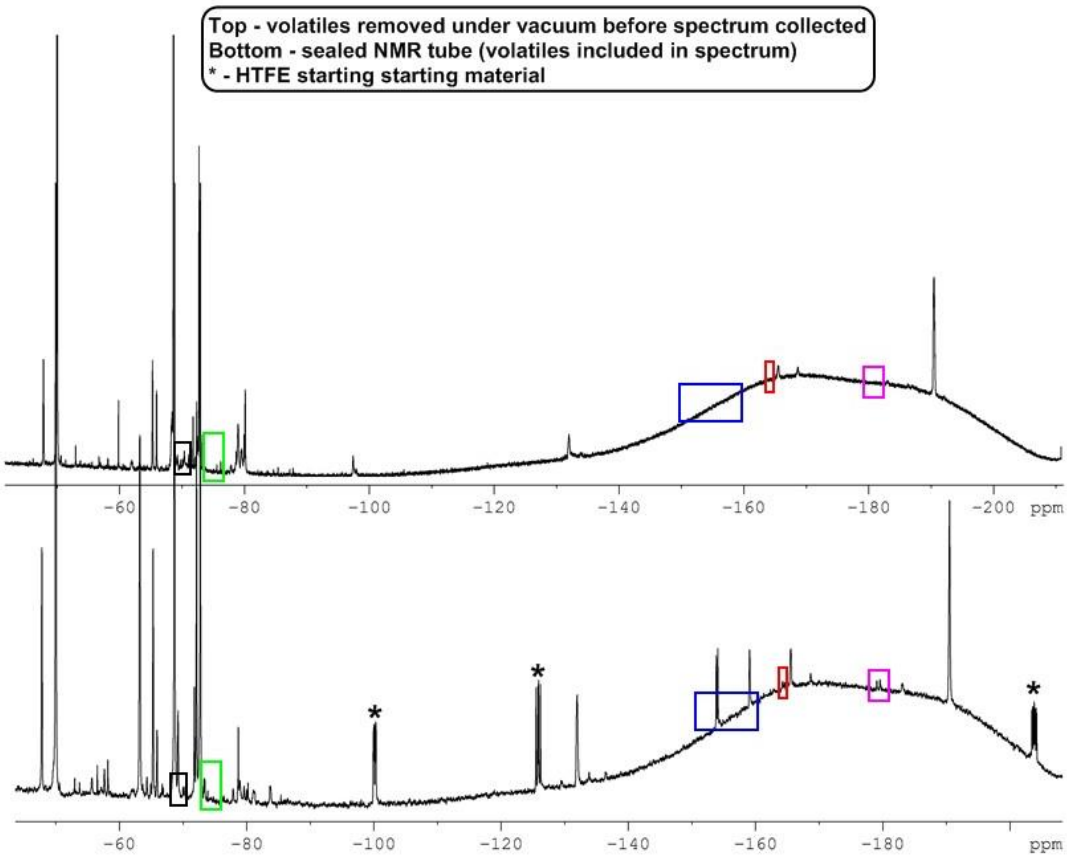

Figure 4.34: Stacked ^{19}F NMR (282 MHz, C_6D_6) spectra for the reaction of **1** with $CFH=CF_2$ showing the reaction before the solvent was removed and after showcasing the formation of several volatile fluorinated products.

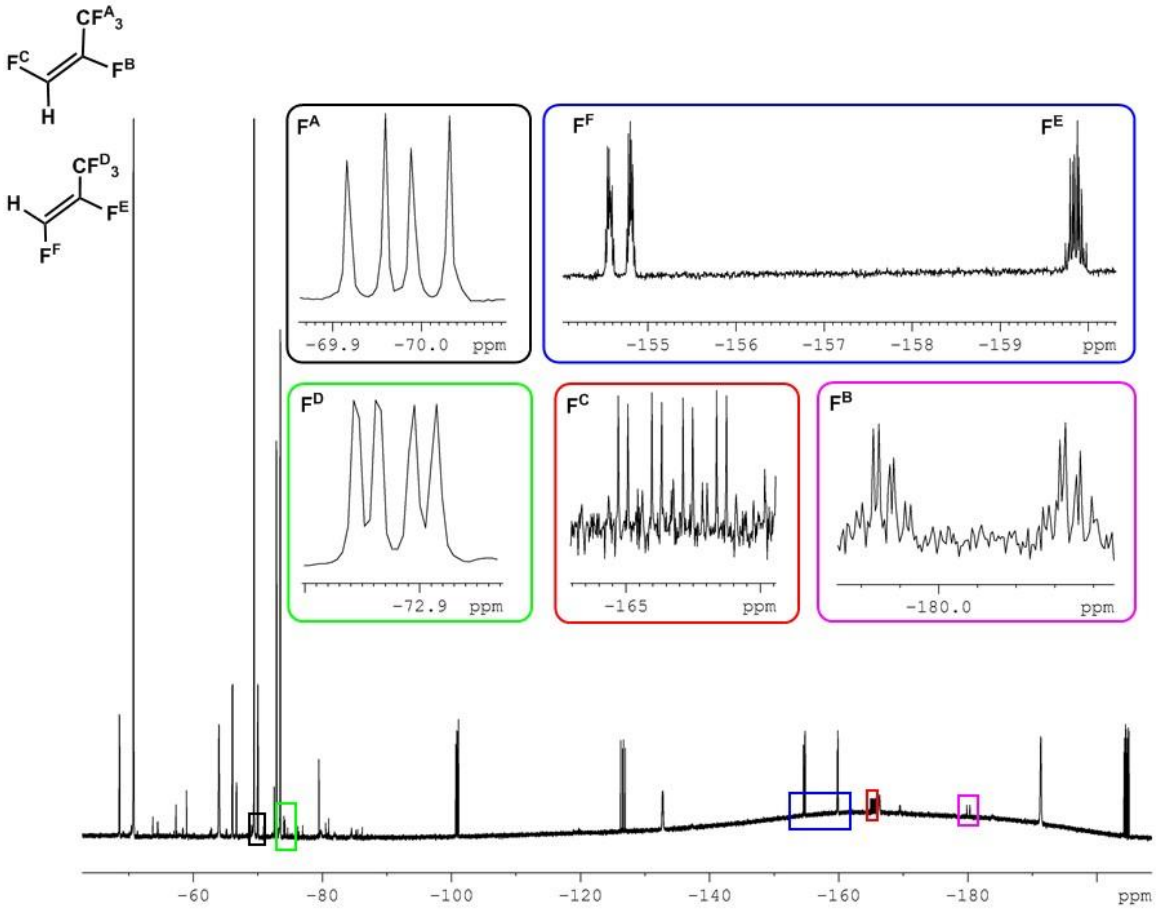

Figure 4.35: ^{19}F NMR (282 MHz, C_6D_6) spectrum for the reaction of **1** with $CHF=CF_2$ focusing on the peaks associated with volatile fluorinated compounds.

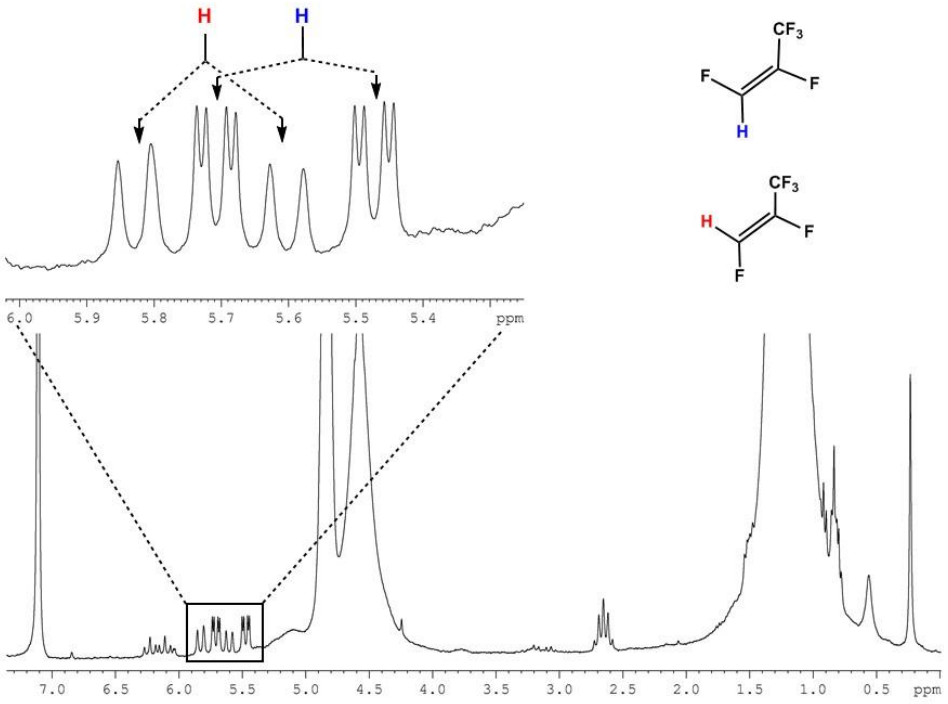

Figure 4.36: ^{1}H NMR (300 MHz, C_6D_6) spectrum for the reaction of **1** with $CHF=CF_2$ focusing on the olefinic region of the spectrum where the compounds cis/trans-$CHF=CFCF_3$ are observed.

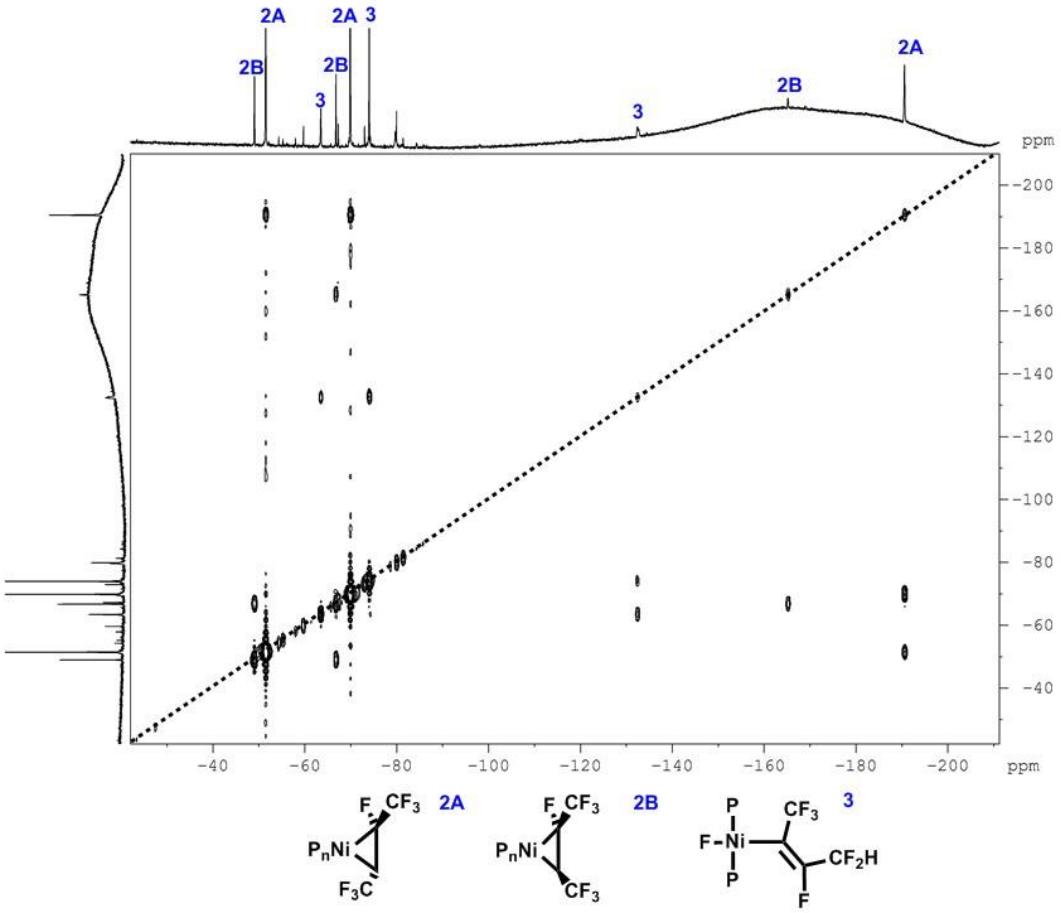

Figure 4.37: Two-dimensional ^{19}F COSY experiment of the reaction mixture of **1** with $CFH=CF_2$ after the volatiles were removed in C_6D_6 to help in the assignment of the major products from the non-metathesis pathways.

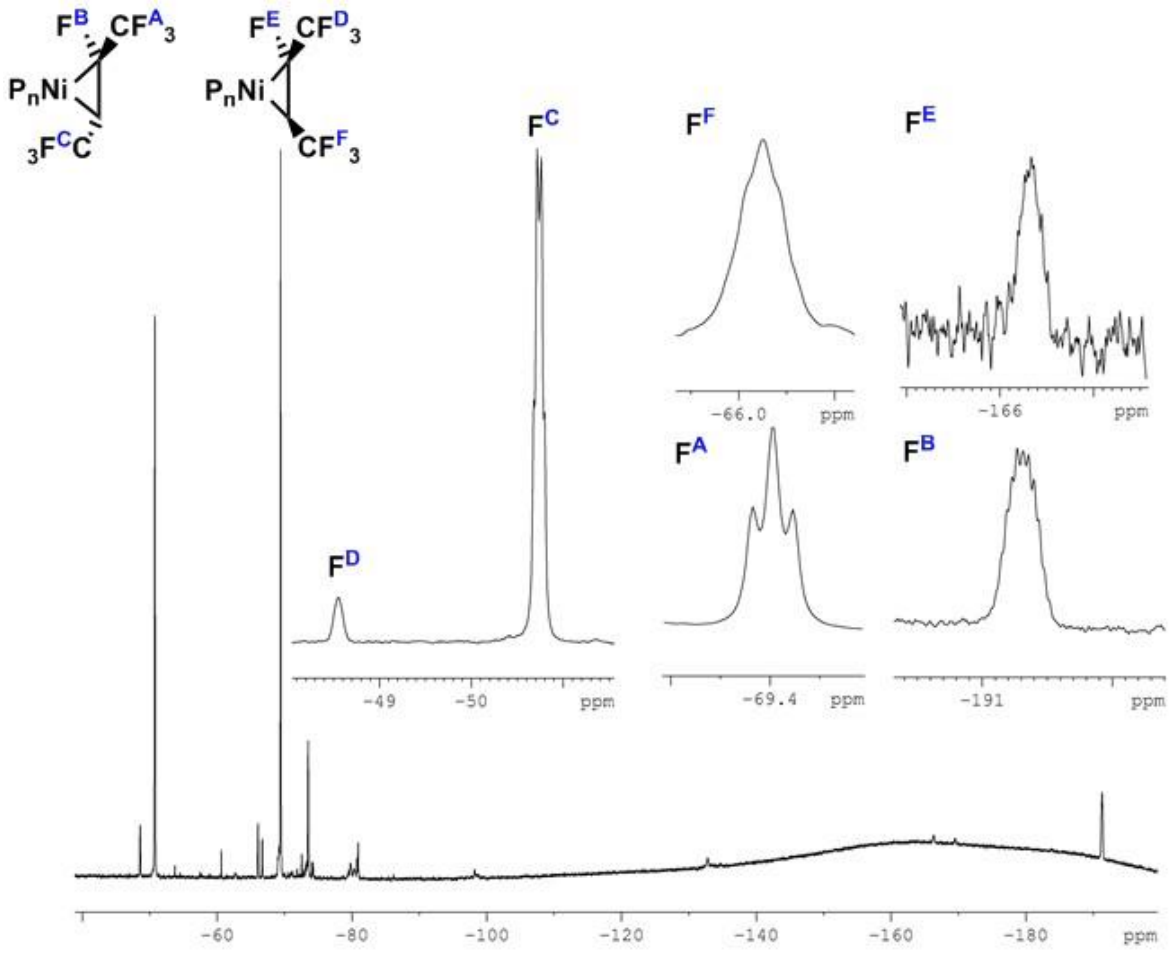

Figure 4.38: ^{19}F NMR (282 MHz, C_6D_6) spectrum for the reaction of **1** with $CHF=CF_2$ after the solvent was removed focusing on the peaks associated with E/Z-4

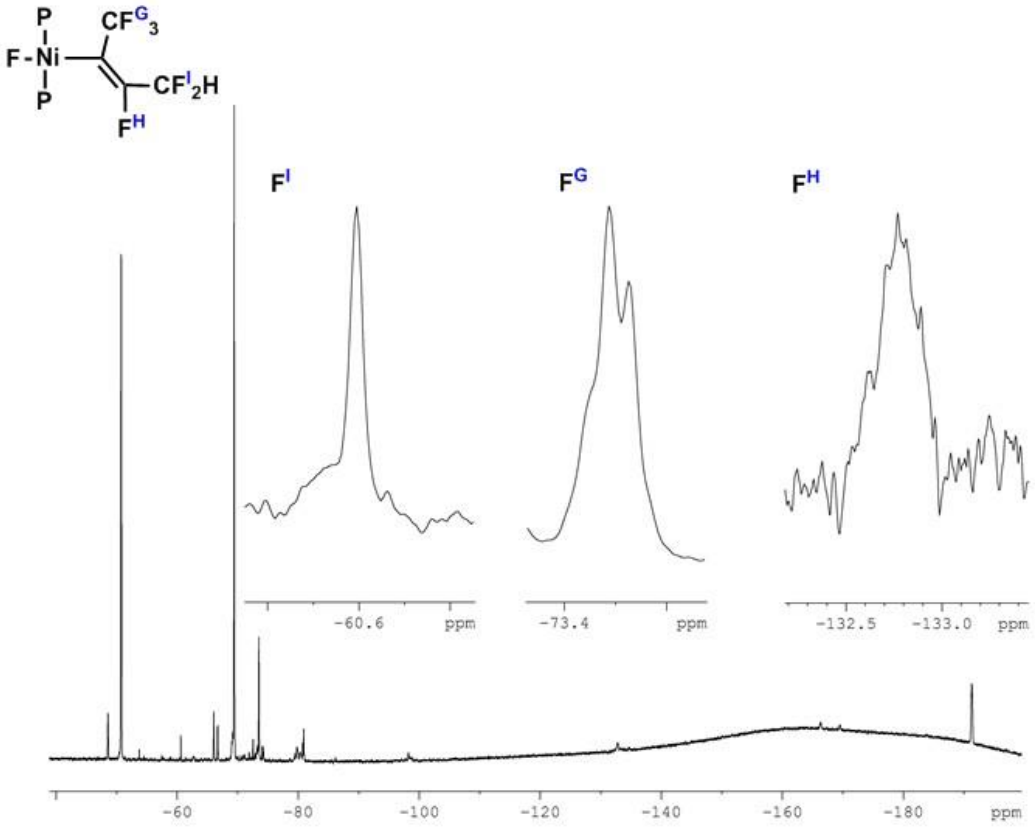

Figure 4.39: ^{19}F NMR (282 MHz, C_6D_6) spectrum for the reaction of **1** with $CHF=CF_2$ after the solvent has been removed focusing on the peaks associated with cis isomer of 5.

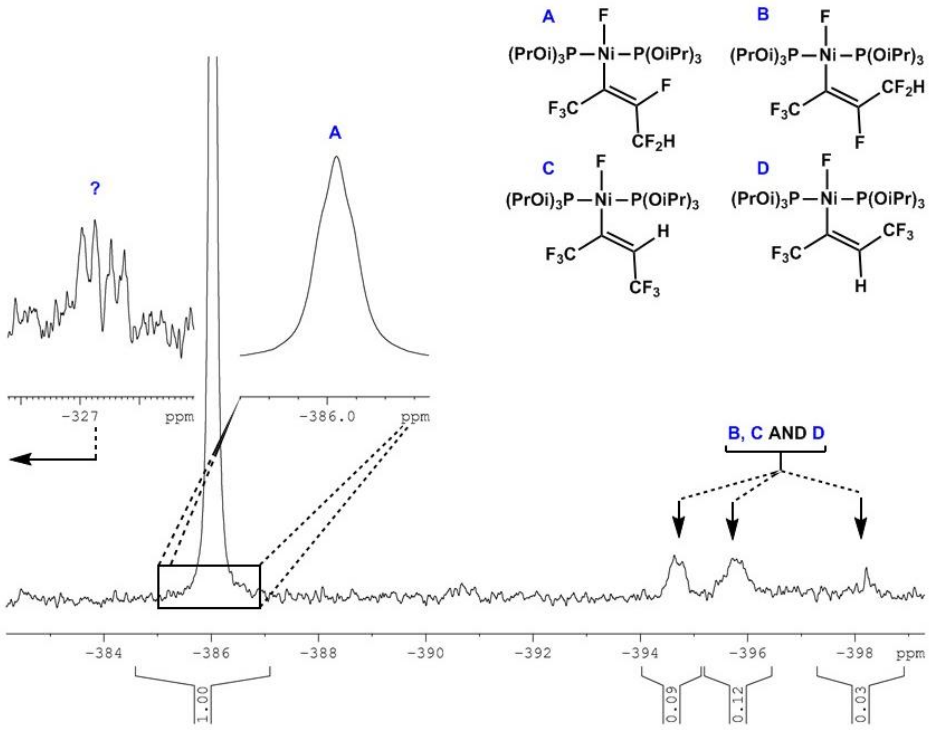

Figure 4.40: ^{19}F NMR (282 MHz, C_6D_6) upfield spectrum for the reaction of **1** with $CHF=CF_2$ focusing on Ni-F peaks. Nickel vinyl compounds A and B are the major products of this reaction while compound C and D are predicted to be formed through a 2,1 fluoride shift of the β-CHF metallacycle pathway (Fig. 4.33) however could not be fully characterized.

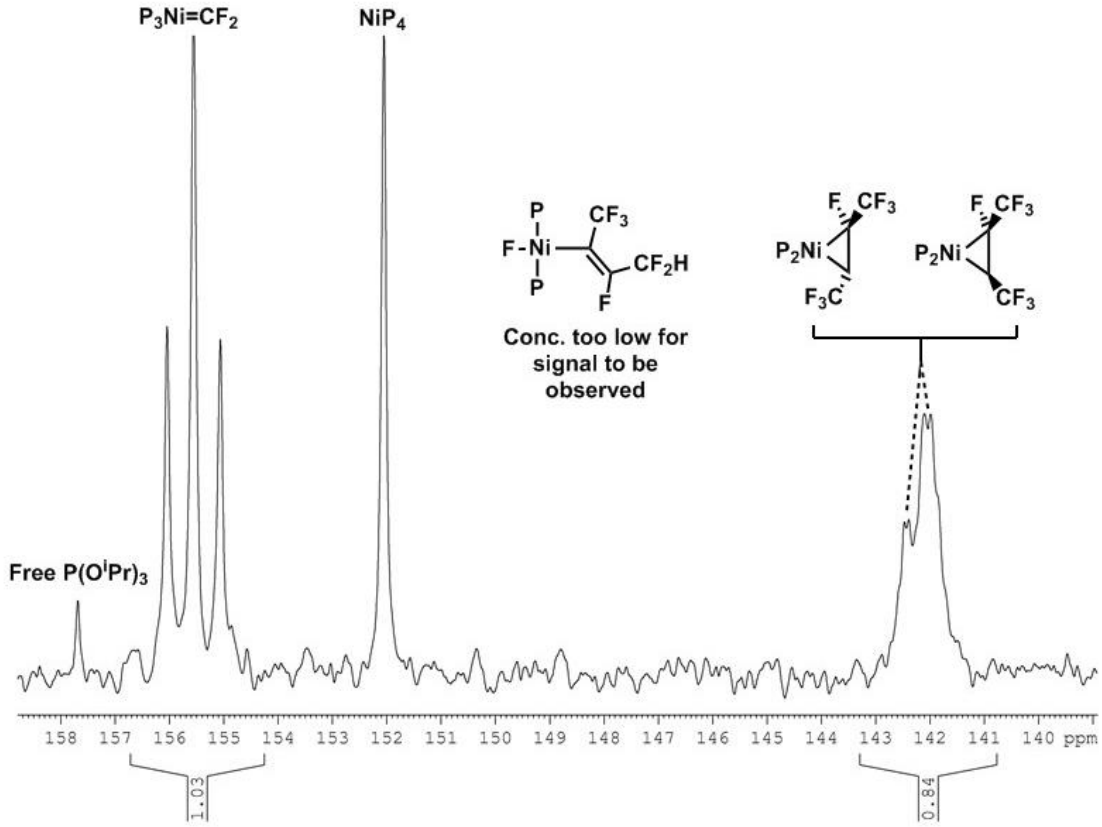

Figure 4.41: $^{31}P\{^{1}H\}$ NMR (121 MHz, C_6D_6) of the reaction of **1** with HTFE after the volatiles had been removed

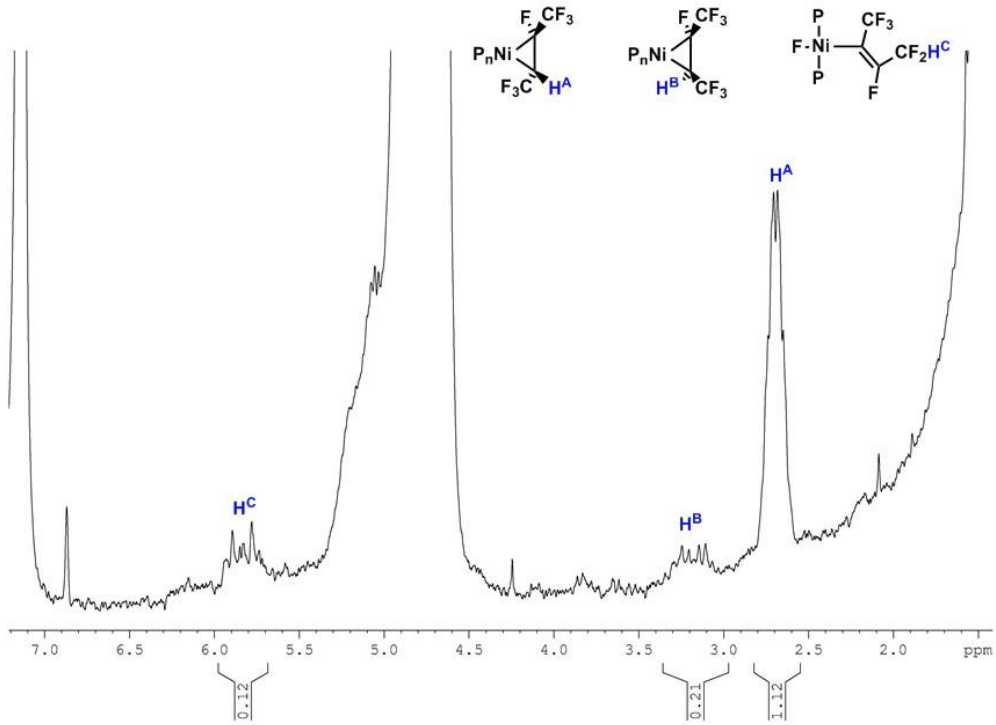

Figure 4.42: ^{1}H NMR (300 MHz, C_6D_6) spectrum for the reaction of **1** with $CHF{=}CF_2$ after the removal of volatiles.

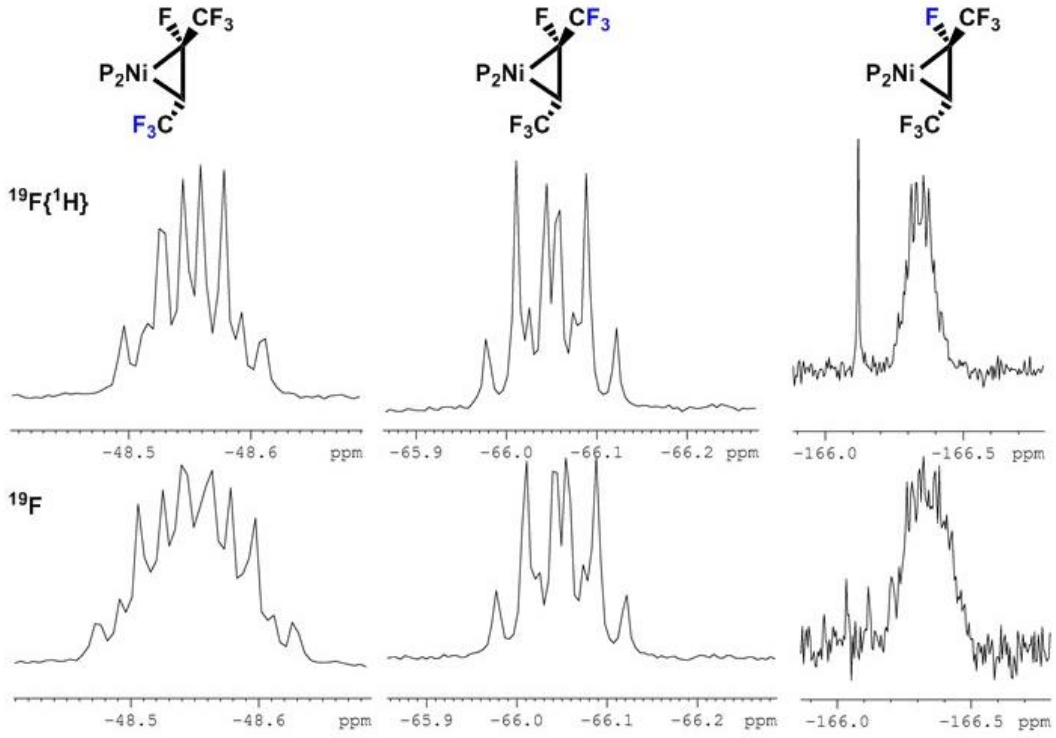

Figure 4.43: ^{19}F NMR Overlapped with $^{19}F\{^{1}H\}$ NMR (282 MHz, C_6D_6) showing the proton coupling of E-4

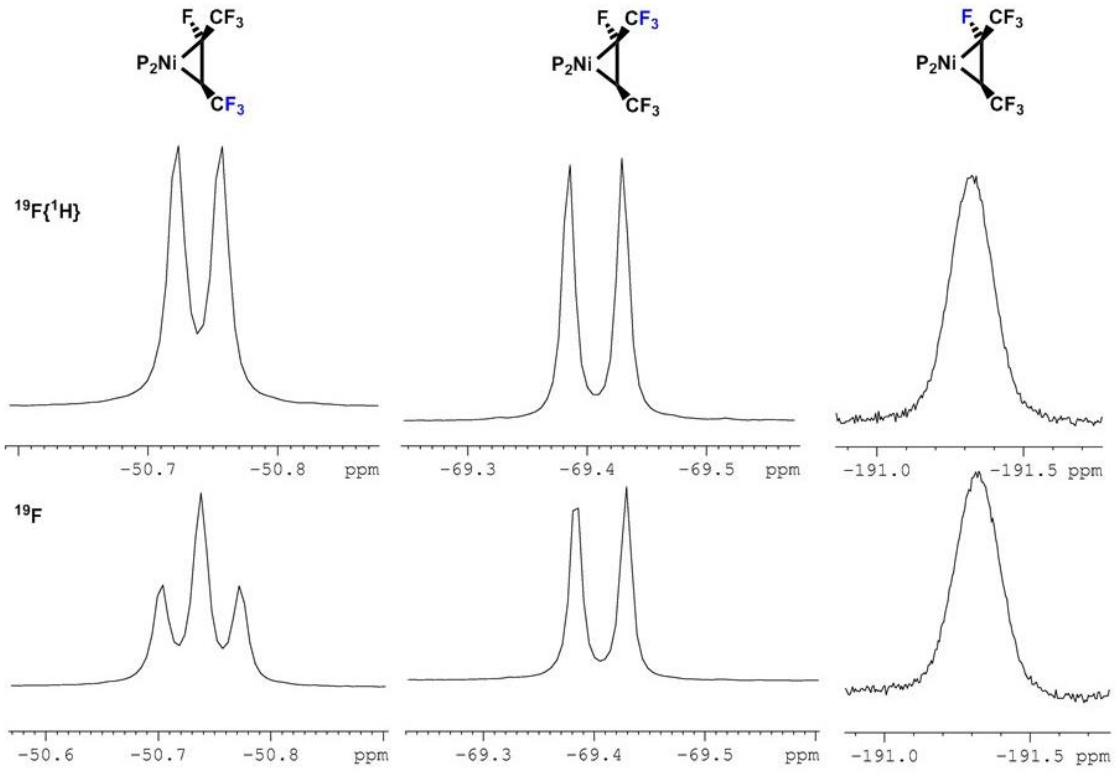

Figure 4.44: ^{19}F NMR Overlapped with $^{19}F\{^{1}H\}$ NMR (282 MHz, C_6D_6) showing the proton coupling of Z-4

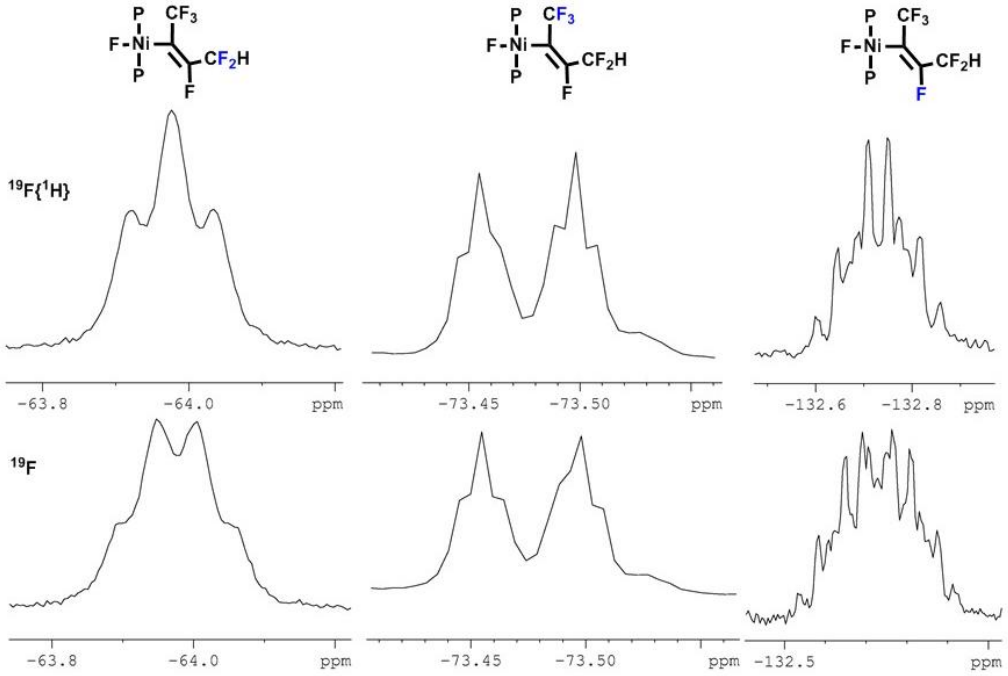

Figure 4.45: ^{19}F NMR Overlapped with $^{19}F\{^1H\}$ NMR (282 MHz, C_6D_6) showing the proton coupling of Z-5

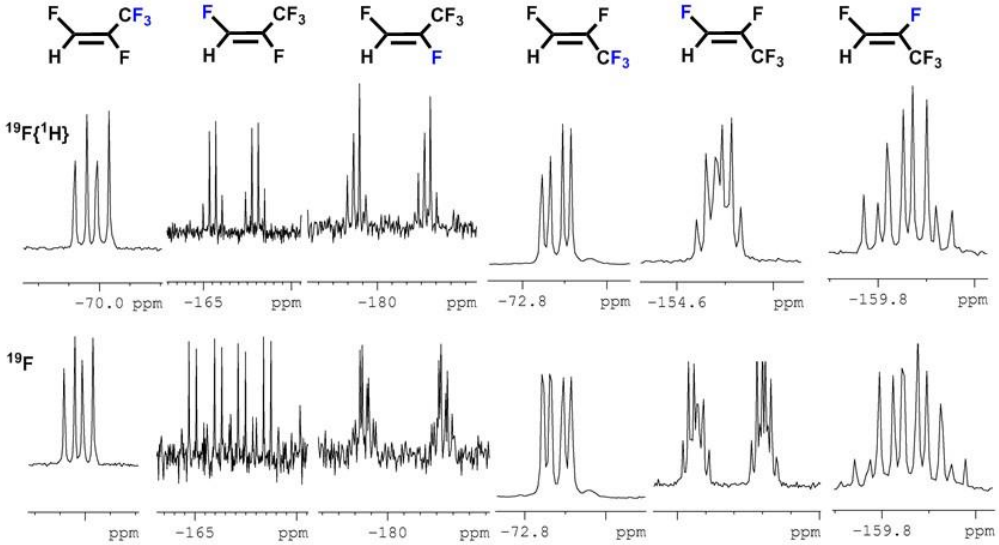

Figure 4.46: ^{19}F NMR Overlapped with $^{19}F\{^1H\}$ NMR (282 MHz, C_6D_6) showing the proton coupling of the E/Z- 1,2,3,3,3-pentafluoro-1-propene.

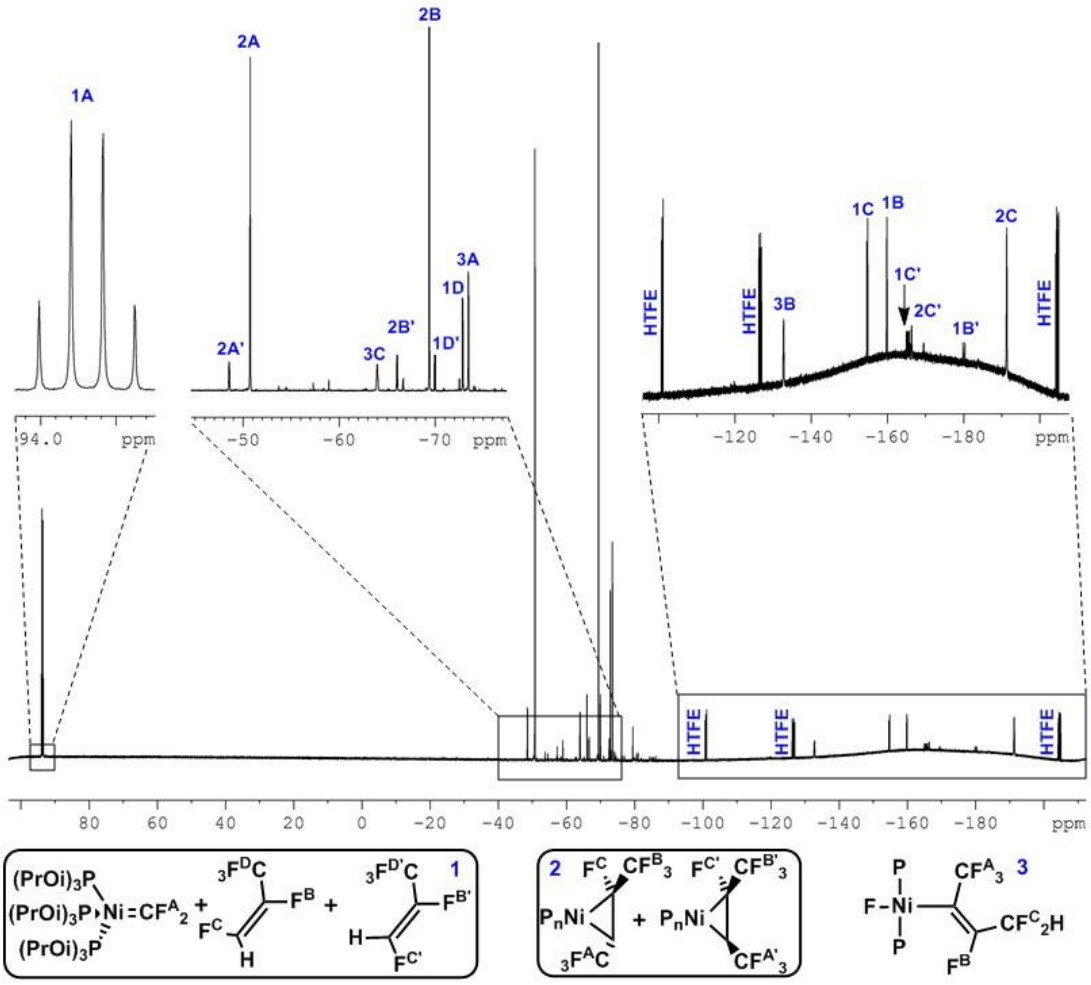

Figure 4.47: ^{19}F NMR (282 MHz, C_6D_6) full spectrum for the reaction of **1** with $CHF=CF_2$ including F-labelling of all major products. Structural isomers of compound **3** were not capable of being fully characterized.

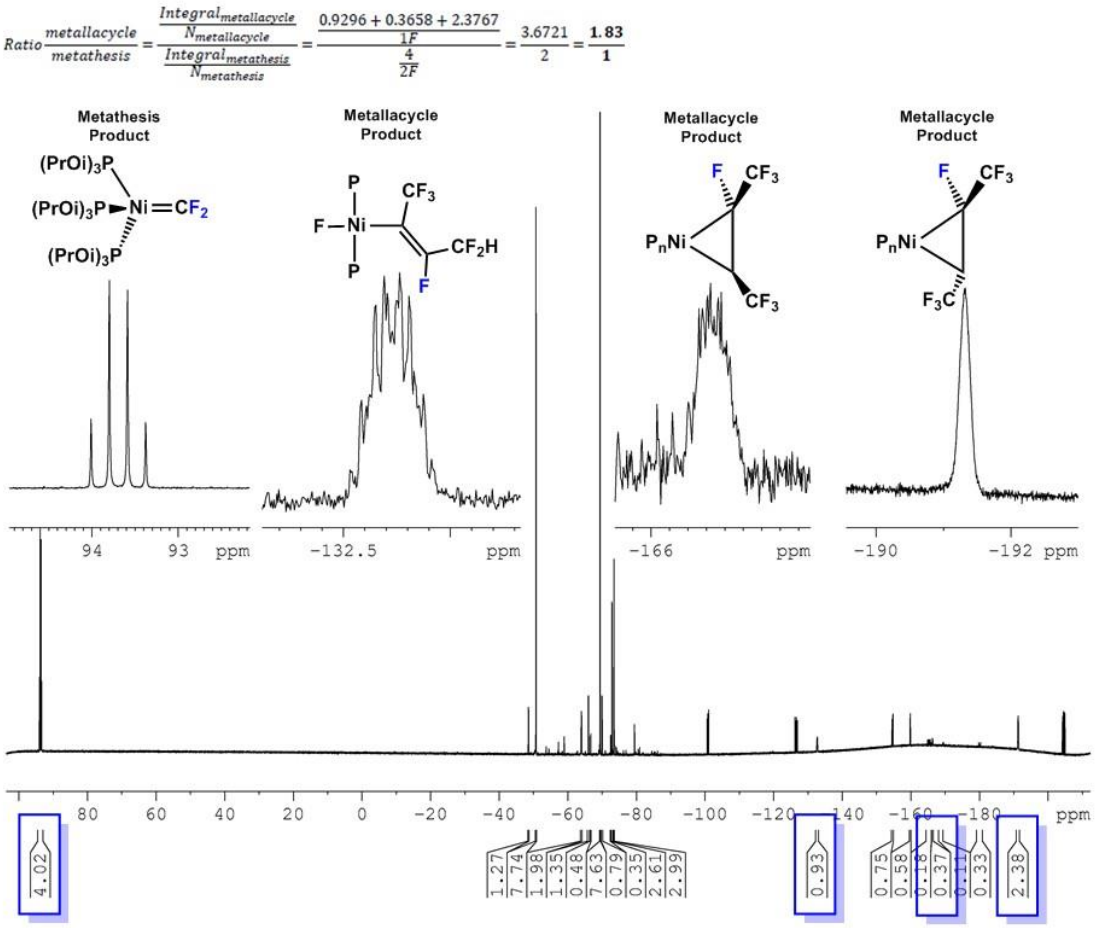

Figure 4.48: ^{19}F NMR (282 MHz, C_6D_6) full spectrum for the reaction of **1** with $CHF=CF_2$. Included is the calculation used to determine the ratio of metathesis versus metallacycle formation.

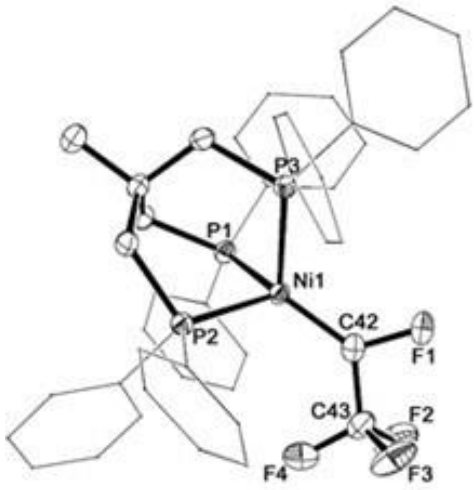

Figure 4.49: ORTEP molecular structure of **7** with 50% probability thermal ellipsoids. Hydrogen atoms are not shown, and the phenyl groups are depicted as wire cage structures for clarity.

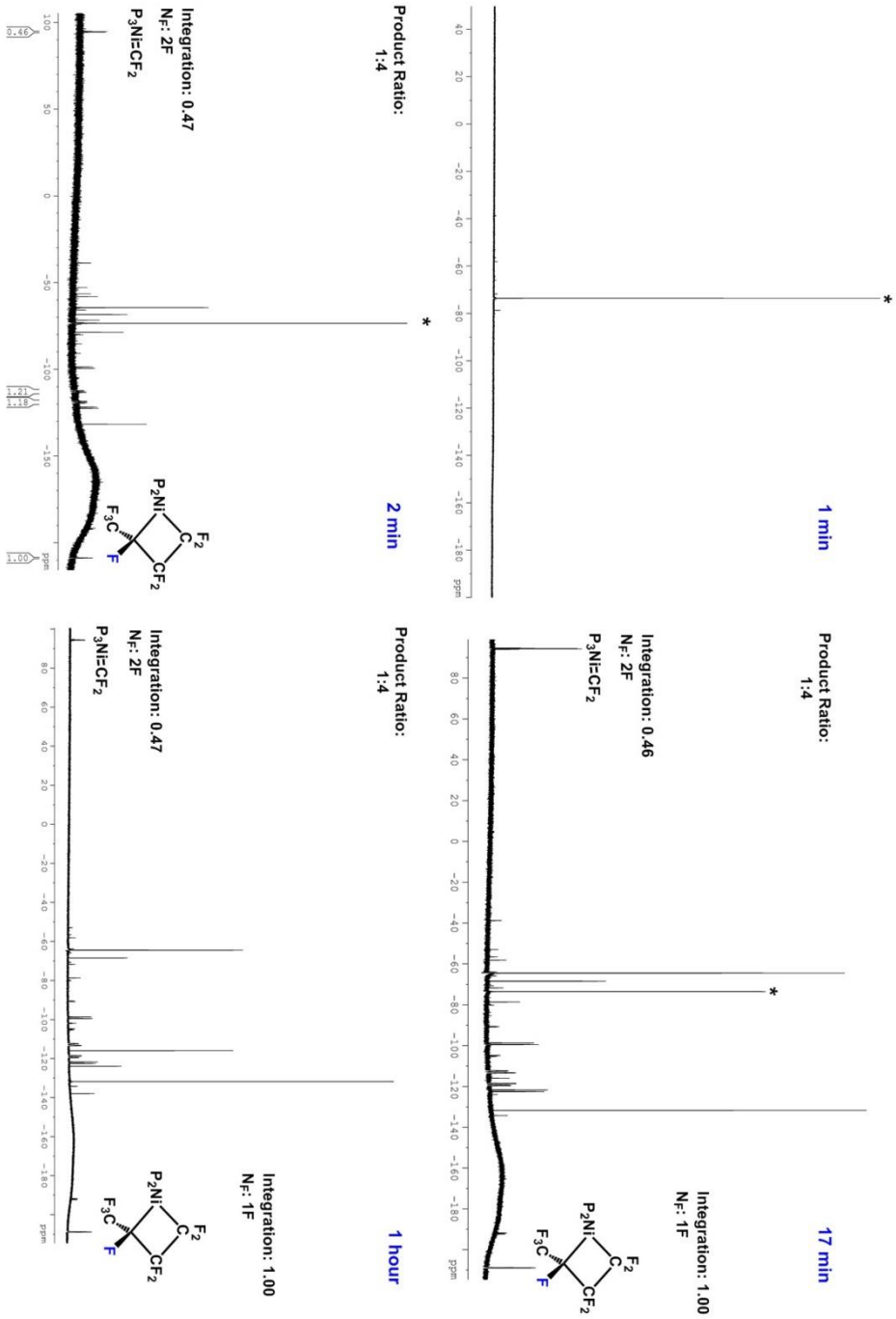

Figure 4.50: Qualitative kinetic experiment between complex **1** (labelled in NMR with an asterisk) and excess TFE showing the progression of the reaction over an hour at room temperature. Spectra shows the product ratio remaining relatively unchanged throughout the course of the reaction. Reaction is complete within an hour.

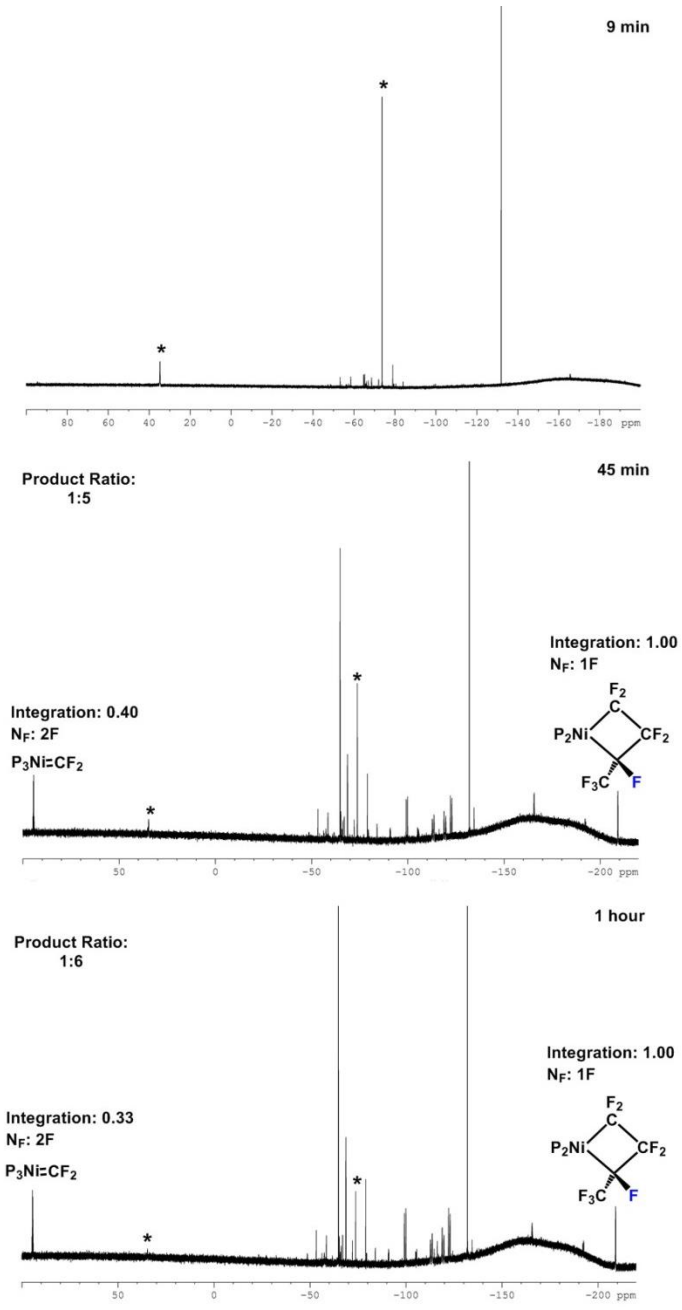

Figure 4.51: Qualitative Kinetics experiment between complex **1** (labelled in NMR with an asterisk) and excess TFE in the presence of 20 equiv. of $P(O^iPr)_3$. Experiment shows the product ratio remaining relatively unchanged throughout the course of the reaction. Unlike the same experiment without excess phosphite the reaction only begins to form products after 10 min. and the starting material (**1**) is still present after an hour of reaction time at room temperature.

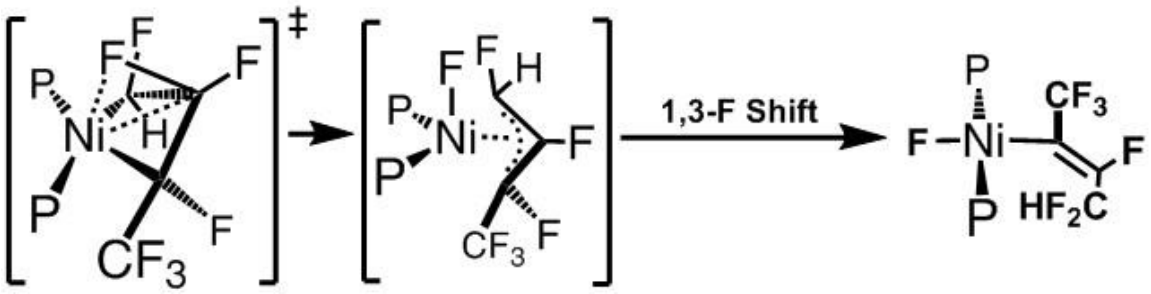

Figure 4.52: Proposed mechanism in the formation of (**5**) via β-Fluoride abstraction of metallacyclobutane B forming Ni-F allyl complex followed by 1,3 F-shift leading to the observed product.

Crystallographic information for Ni(P_3)(=CFCF_3) [(2); P_3 = MeC(CH_2PPh_2)$_3$] The sample was mounted on thin glass fibers using paraffin oil and was cooled to 200 K prior to data collection. Data were collected on a Bruker AXS KAPPA single crystal diffractometer equipped with a sealed Mo tube source (wavelength 0.71073 Å) APEX II CCD detector. Raw data collection and processing were performed with APEX II software package from BRUKER AXS.[6] Diffraction data were collected with a sequence of 0.5 ° ω scans at 0, 90, 180, and 270 ° in ϕ. Initial unit cell parameters were determined from 60 data frames collected at the different sections of the Ewald sphere. Semi-empirical absorption corrections based on equivalent reflections were applied. Systematic absences in the diffraction data set and unit-cell parameters were consistent with orthorhombic systems. Solutions in centrosymmetric space group yielded chemically reasonable and computationally stable results of refinement. The structures were solved by direct methods, completed with difference Fourier synthesis, and refined with full-matrix least-squares procedures based on F^2. In the structure, compound molecules are situated in the general position. All non-hydrogen atoms were refined anisotropically with satisfactory thermal parameters values. To achieve satisfactory thermal parameters, it was not necessary to use constraints. Additional crystallographic data and selected data collection parameters are reported below. The cif file, atomic coordinates, etc., are available as Supporting Information.

Empirical formula: $C_{43}H_{39}F_4NiP_3$; FW = 783.36; Crystal size: 0.326 x 0.169 x 0.123 mm3; Crystal system: orthorhombic; Space group: P n a 21; a = 20.8829(5) Å, b = 10.2812(2) Å, c = 17.3573(4) Å; α = 90°, β = 90°, γ = 90°; Volume = 3726.63(14) Å3; Calculated density = 1.396 Mg/m3; Absorption coefficient = 0.700 mm^{-1}; F(000) = 1624; Θ range for data collection: 1.950

to 27.924°; Limiting indices: -27<=h<=27, -13<=k<=13, -22<=l<=22: Reflections collected / unique: 45666 / 8928; R(int) = 0.0446; Completeness to Θ = 25.242°: 100.0 %; Data / restraints / parameters: 8928 / 1 / 461; Goodness-of-fit on F^2: 0.953; Final R indices [I>2σ(I)]: R1 = 0.0324, wR2 = 0.0711; R indices (all data): R1 = 0.0485, wR2 = 0.0793; Largest diff. peak/hole: 0.364 and -0.261 e.Å-3.

References

([1]) (a) *Olefin Metathesis: Theory and Practice*; Grela, K., Ed.; John Wiley & Sons: Hoboken, NJ, 2014. (b) Handbook of Metathesis; R. H. Grubbs, Ed.; Wiley-VCH: Weinheim, Germany, 2003.

([2]) (a) S. F. Yana Motta, E. D. Vera Bercerra, M. W. Spatz, *Analysis of LGWP Alternatives for Small Refrigeration (Plugin) Applications;* International Refrigeration and Air Conditioning Conference; Purdue University: West Lafayette, IN, 2010; Paper 1149. (b) A. Mota-babiloni, P. Makhnatch, R. Khodabandeh, *Intl. J. Refrig*. **2017**, *82*, 288-301.

([3]) (a) S. Fomine, M. A. Tlenkopatchev, *Appl. Catal., A.* **2009**, *355*, 148-155. (b) M. Vasiliu, A. J. Arduengo, III, D. A. Dixon, *J. Phys.Chem. C* **2014**, *118*, 13563-13577.

([4]) T. M. Trnka, M. W. Day, R. H. Grubbs, *Angew. Chem. Int. Ed*. **2001**, *40*, 3441-3444.

([5]) Y. Takahira, Y. Morizawa, *J. Am. Chem. Soc.* **2015**, *137*, 7031-7034.

([6]) (a) M. J. Koh, T. T. Nguyen, H. Zhang, R. R. Schrock, A. H. Hoveyda, *Nature* **2016**, *531*, 459-465. (b) T. T. Nguyen, M. J. Koh, X. Shen, F. Romiti, R. R. Schrock, A. H. Hoveyda, *Science* **2016**, *352*, 569-574. (c) M. J. Koh, T. T. Nguyen, J. K. Lam, S. Torker, J. Hyvl, R. R. Schrock, A. H. Hoveyda, *Nature*. **2017**, *542*, 80-86.

([7]) D. J. Harrison, G. M. Lee, M. C. Leclerc, I. Korobkov, R. T. Baker, *J. Am. Chem. Soc.* **2013**, *135*, 18296-18299.

([8]) D. J. Harrison, S. I. Gorelsky, G. M. Lee, I. Korobkov, R. T. Baker, *Organometallics*, **2013**, *32*, 12-15.

([9]) D. J. Harrison, A. L. Daniels, I. Korobkov, R. T. Baker, *Organometallics* **2015**, *34*, 5683–5686.

([10]) L. F. Halle, P. B. Armentrout, J. L. Beauchamp, *Organometallics*. **1983**, *2*, 1829-1833.

([11]) For a unique example of apparent Ni-mediated alkene metathesis see: F. G. N. Cloke, P. B. Hitchcock, M. F. Lappert, C. MacBeath, G. O. Mepsted, *J. Chem. Soc., Chem. Commun*., **1995**, 87-88.

([12]) J. T. Fuller, D. J. Harrison, M. C. Leclerc, R. T. Baker, D. H. Ess, R. P. Hughes, *Organometallics* **2015**, *34*, 5210-5213.

([13]) S. D. Ittel, *Inorg. Synth.* **1990**, *28*, 98-104.

([14]) H. Lange, D. Naumann, *J. Fluorine Chem.* **1984**, *26*, 1-18.

([15]) Complex **1** was obtained in ~95% purity with the only NMR-visible contaminant being the starting material, $Ni[P(O\text{-}i\text{-}Pr)_3]_4$. Sublimation gave marginally improved purity but significantly diminished yield. See the Supporting Information.

([16]) The [Ni]=$CFCF_3$ sub-structure was confirmed by synthesizing $Ni(P_3)(=CFCF_3)$, **7** [P_3 = $MeC(CH_2PPh_2)_3$] from **1**, by phosphite-substitution, to obtain a crystalline derivative suitable for X-ray structural determination (see SI).

([17]) G. R. Clark, S. V. Hoskins, T. C. Jones, W. R. Roper, *J. Chem. Soc., Chem. Commun.* **1983**, 719-721.

([18]) M. Reisch, *Chem. Eng. News* **2010**, *88*, 23.

([19]) Complex **3** does not react with excess HFP (24h, 50°C).

([20]) J. Clayden, N. Greeves, S. Warren, P. Wothers. Radical stability. In *Organic Chemistry*; Oxford: New York, **2004**; pp. 1026-1028.

([21]) D. O'Hagan, Chem. Soc. Rev. **2008**, *37*, 308-319.

([22]) W. Janse van Rensburg, P. J. Steynberg, W.H. Meyer, M. M. Kirk, G.S. Forman, *J. Am. Chem. Soc*. **2004**, *126*, 14332-14333.

([23]) DFT calculations for the stability of the metallacyclobutanes/-propanes formed from reactions of 1 with TFE and VDF are shown in the computational SI.

([24]) (a) R. P. Hughes, R. B. Laritchev, J. Yuan, J. A. Golen, A. N. Rucker, A. L. Rheingold, *J. Am. Chem. Soc.* **2005**, *127*, 15020-15021. (b) C. J. Bourgeois, R. P. Hughes, J. Yuan, A. G. DiPasquale, A. L. Rheingold, *Organometallics* **2006**, *25*, 2908-2910. (c) J. Yuan, R. P. Hughes, A. L. Rheingold, *Eur. J. Inorg. Chem.* **2007**, 4723-4725.

([25]) (a) The density functional theory (DFT) calculations were performed with the Gaussian 09 Suite of programs: Gaussian 09, revision D. 01, M. J. Frisch, et al. Gaussian, Inc.: Wallingford, CT. 2013 (see SI for full reference). (b) The M06 functional (see ref. 26) was employed with the 6-311+G* basis set for the C, H, O, F, and P atoms, and the Stuttgart quasi-relativistic basis set and effective core potential (see ref. 29) for Ni. Each species was optimized in the gas phase on an ultrafine grid. Analytical frequency calculations were performed on all optimized structures to ensure that either a minimum or a first-order saddle point was achieved, and to obtain the thermal Gibbs free energy corrections. Further single point calculations were carried out on the basis of the optimized geometries with the continuum solvation model SMD (see ref. 28) at the same level of theory to account for solvent effects, where THF (tetrahydrofuran) was employed as the solvent. The reported energies (ΔG) in this work include the electronic energy, DFT-D3 empirical dispersion corrections proposed by Grimme et al. (see ref. 29), the gas-phase thermal correction for the Gibbs free energy and SMD solvation corrections. The bond energy of the ancillary ligand L (L = $P(O\text{-}i\text{-}Pr)_3$) from the nickel carbene complex was calculated from the following equation: $NiL_3(=CFCF_3) \rightarrow NiL_2(=CFCF_3) + L$.

([26]) Y. Zhao, D. G. Truhlar, *Theor. Chem. Acc.* **2008**, *120*, 215-241.

([27]) (a) M. Dolg, U. Wedig, H. Stoll, H. Preuss, *J. Chem. Phys.* **1987**, *86*, 866-872. (b) J. M. L. Martin, A. Sundermann, *J. Chem. Phys.* **2001**, *114*, 3408-3420.

([28]) A. V. Marenich, C. J. Cramer, D. G. Truhlar, *J. Phys. Chem. B* **2009**, *113*, 6378-6396.

([29]) S. Grimme, J. Antony, S. Ehrlich, H. Krieg, *J. Chem. Phys.* **2010**, *132*, 154104-1-154104-19.

([30]) That the prior dissociation energy of a phosphine adds to this reaction barrier is confirmed through treatment of complex **7** with TFE which shows little reactivity until the solution is heated to 60^{o}C (more details in SI).

([31]) G. M. Lee, D. J. Harrison, I. Korobkov, R. T. Baker. *Chem. Commun*., **2014**, *50*, 1128.

([1]) Hunadi, R. J.; Baum, K. *Synthesis* **1982**, *39*, 454.

([33]) Smeets, A.; Van den Bergh, K.; De Winter, J.; Gerbaux, P.; Verbiest, T.; Koeckelberghs, G. *Macromolecules* **2009**, *42*, 7638-7641.

([34]) Ittel, S. D. *Inorg. Synth.* **1990**, *28*, 98-104.

([35]) Lange, H.; Naumann, D. *J. Fluorine Chem.* **1984**, *26*, 1-18.

([36]) For Ni[P(OMe)$_3$]$_3$(=CF$_2$) and Ni[P(OMe)$_3$]$_2$(-CF$_2$CF$_2$CF$_2$-), see: Harrison, D. J.; Daniels, A. L.; Korobkov, I.; Baker, R. T. *Organometallics* **2015**, *34*, 5683-5686.

([6]) APEX Software Suite v.2010; Bruker AXS: Madison, WI, **2005**.

5 Metathesis and Metallacycle Reactivity of $P_3Ni{=}CF(CF_3)$ with Alkenes [P = $P(O^iPr)_3$]

"What on earth would a man do with himself, if something did not stand in his way?"

~ H. G. Wells

5.1 Context

In the previous chapter we had taken our first large strides with fluoro-metathesis through the discovery of not only the nickel carbene capable of such a difficult transformation but also the illuminating mechanism that made it possible while simultaneously showing us another hurdle, which was the existence of two pathways towards metallacycle formation and metathesis. Subtle differences between the two mechanisms such as geometry of the intermediates [Square planar (metallacycle) vs. tetrahedral (metathesis)] as well as activation barriers of the formation of the coordination complex ('inner sphere' metathesis mechanism) and singlet diradical mechanism ('outer sphere' metallacycle mechanism) meant that for the substrates attempted (TFE, VDF, T^tFE) only substoichiometric amounts of the desired metathesis products could be formed due to the consumption of the nickel complex to form the more stable metallacycle product. This chapter attempts to broaden the substrate scope to increase our understanding of fluoro-metathesis in general but also to determine if the metallacycle mechanism can be subdued by modifying the electronic, steric or physical properties such as ring strain of the selected substrates.

This chapter probes the fluoro-metathesis process by taking the $P_3Ni{=}CFCF_3$ complexes (P = $P(O^iPr)_3$ (**1**), $P(OMe)_3$ (**2**)) utilized in Chapter 4 and discerning which modifications will yield more favorable results. Previous research by Grubbs, Schrock, Takahira and Morizawa showed that unfavorable metathesis reactions could be enhanced by modifying the carbene formed after a single turnover whereas our research revealed an increase in metathesis products with decreasing numbers of fluorines for C2 alkenes. As such, substrates such as $CF_2{=}CF(OCF_3)$, $CH_2{=}CH_2$, and $ArH{=}CH_2$ were used to afford more destabilized $Ni{=}CF(OCF_3)$ or $Ni{=}CR_2$ alkylidenes. Sequentially more strained cyclic alkenes such as perfluoro-cyclobutene, cyclopentene and norbornenes were also utilized with the intention of destabilizing the metallacycle product while

simultaneously forming a reactive carbene which would allow us to access desirable ROMP techniques already employed with great success in traditional metathesis reactions.

Several of the substrates did indeed produce the desired metathesis products; however, metallacycle formation was dominant. In the case of non-fluorinated substrates the metallacycle was the exclusive product, leading to a reevaluation of the possible mechanism for this process that may allow for a greater level of control via the ancillary ligands.

Published Contribution

Daniels, A. L; Guan, J.; Hall, M. B.; Baker, R. T. **2019** (Submitted).

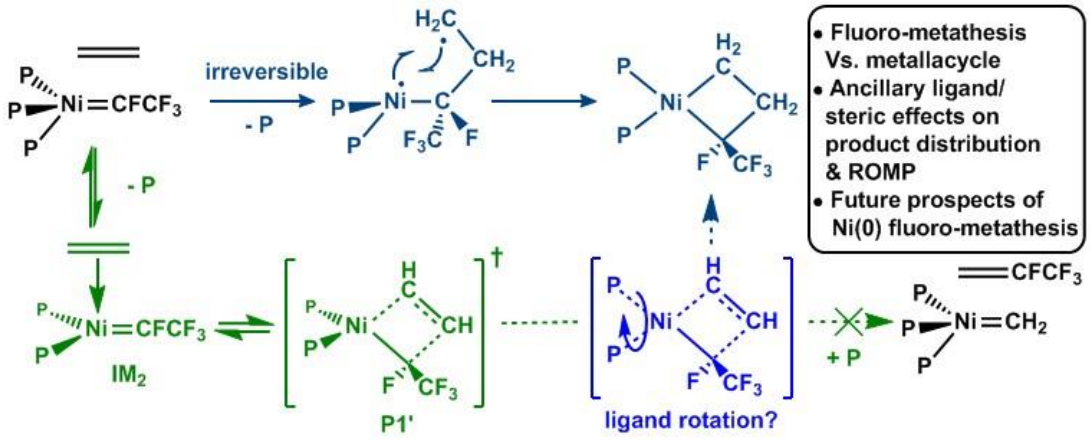

Metathesis of electrophilic fluoroalkenes is complicated by the need for a *nucleophilic* metal fluorocarbene that is capable of binding the substrate. In previous work we showed that d^{10} metal fluorocarbene complex, $P_3Ni{=}CF(CF_3)$ [P = $P(O^iPr)_3$] **1**, reacts with fluoroalkenes to produce both 4-membered metallacycles and metathesis products via separate reaction pathways. Herein we utilize computational and experimental results to determine the reactivity of this heteroatom-stabilized carbene with a variety of alkene substrates. Reaction of **1** with trifluoromethyl trifluorovinyl ether, $CF_2{=}CF(OCF_3)$, produced both metallacycle and metathesis products, with preferential formation of the more stabilized difluorocarbene [$P_3Ni{=}CF_2$ vs. [$P_3Ni{=}CF(OCF_3)$], and a higher ratio of metathesis to metallacycle products than previous examples using tetrafluoroethylene and vinylidene difluoride. In contrast, reactions with hexafluoropropene gave a single metallacycle, taking advantage of the previously proposed diradical mechanism that does not require coordination of this bulky alkene to the nickel center. Surprisingly, both ethylene and styrene derivatives gave metallacycles although some evidence was obtained for alkene

coordination to nickel; computational studies are presented to identify the origin of these observations. Finally, attempts to form fluoropolymers via ring-opening metathesis polymerization of perfluorocyclobutene were thwarted by preferential intramolecular back-biting of the ring-opened metathesis product, followed by a fluoride shift to afford a spiro-nickelacyclobutane product. Further efforts on metallacycle destabilization via ring strain using both cyclopentene and methyl 5-norbornene 2-carboxylate also afforded metallacycles exclusively.

Author contributions: The manuscript was written by ALD and RTB. ALD was responsible for the synthesis and characterization of all complexes. ALD performed reactivity studies of complexes **1** and **2** and was responsible for SI. JG performed DFT analysis and MBH helped write the DFT section.

5.2 Introduction

Metal alkylidenes are well known for their use in the invaluable metathesis transformation of alkenes.[1] However, this same transformation of fluoroalkenes is limited to a few notable examples of cross-metathesis[2] and ring-closing metathesis of monofluoro-substituted alkenes.[3] Catalytic fluoroalkene self-metathesis is particularly appealing in that it could allow direct access to industrially relevant products such as low global warming hydrofluoroalkene refrigerants and blowing agents, new fluorinated monomers and polymers, and cyclic structures for use in pharmaceuticals and agrochemicals.[4] Unfortunately, the unfavorable electronic properties of metal fluorocarbenes have hindered this development, as shown previously in reactions of $CH_2{=}CF_2$ with Grubbs-type catalysts that afford the stable [Ru]=CF_2 complex.[2a,5] Catalytic fluoroalkene cross-metathesis has been achieved through ingenious workarounds. Takahira and Morizawa used electron-rich alkene partners with fluoroalkenes, although the reactions are slow and achieve modest turnover numbers.[2b] Work by Hoveyda, Schrock and co-workers avoided the formation of stable metal carbenes altogether through careful substrate selection, giving the [M]=CFH intermediate which can then react further.[2c,d]

In contrast, metal *perfluoro*-carbenes such as [M]=CF(CF_3) are less common and have only recently been shown to afford metathesis products from fluoroalkenes, albeit stoichiometrically.[6]

We reported that d^{10} metal fluorocarbenes, $P_3Ni{=}CF(CF_3)$ [P = $P(O^iPr_3)_3$, **1**; $P(OMe)_3$, **2**] react with fluoroalkenes to produce both the expected (based on previous publications[7]) metallacyclobutanes as well as metathesis products. Proceeding through disparate 4-coordinate transition states, only the metathesis pathway involves alkene coordination to the nickel center, with C-C bond formation occurring in a plane perpendicular to the NiP_2 plane (Figure 5.1).

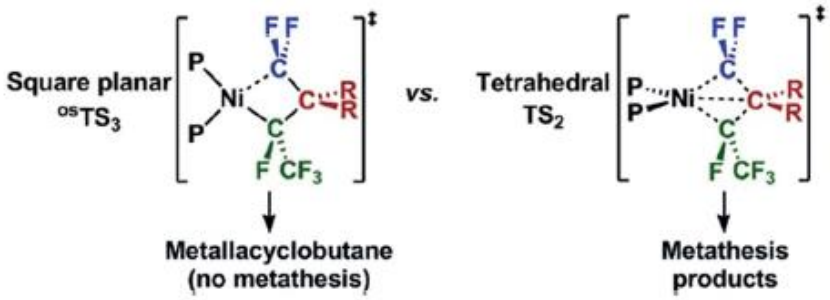

Figure 5.1: Transition states for formation of metallacycle vs. metathesis products from $P_3Ni{=}CF(CF_3)$ and fluoroalkenes.

Metallacycle formation, on the other hand, involves attack of the carbene carbon on the fluoroalkene carbon, generating a diradical intermediate with the new C-C bond formed in the NiP_2 plane, as determined by us previously with Co.[8] Similar reactions with analogous d^{10} $P_3Ni{=}CF_2$ complexes afford only metallacycles, even with electron-rich examples such as $(dppe)[P(OMe)_3]Ni{=}CF_2$. Thus, by replacing fluorine π-donors by CF_3 and lowering the triplet state energy of the carbene fragment, the reactivity of the metal carbene was significantly enhanced (Scheme 5.1). [9]

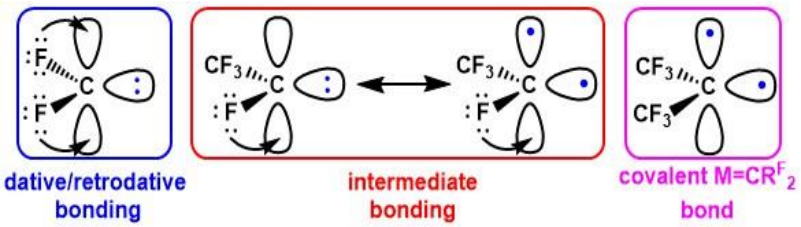

Scheme 5. 1

These observations support computational studies by Occhipinti and Jensen that show a correlation with the degree of electron-sharing between the ligated transition metal and carbene fragments and their electronic properties (nucleophilic vs. electrophilic) and reactivity (i.e., metallacycle intermediate leading to either metathesis products or cyclobutanes).[10] Typical

Schrock and Grubbs catalysts achieve this electron-sharing via access to triplet states of both the carbene and the transition metal fragments, leading to a $M=CR_2$ bond that has covalent character that can be classified as either nucleophilic or electrophilic (depending on the metal oxidation state and ancillary ligands) yet both being capable of metathesis reactivity with alkenes.[10,11] Fischer carbenes (both stabilized and unstabilized), on the other hand, are classified using more traditional dative/retrodative bonding (Figure 5.2) and typically behave sluggishly in alkene metathesis reactions. However, it should be noted that there are occasions when metal enforces spin state in the metal and vice versa (carbene to metal spin enforcement) as shown by Casey using $(CO)_5W=CPh_2$[12] where a ground state triplet carbene ($=CPh_2$) enforced a spin triplet state in the $TM=CAr_2$ alkylidene giving both cyclopropanation and metathesis products.[13] Where work by Grubbs showed that the spin triplet state of $Cl_2Ru=CR_2$ could encourage a triplet state in a the significantly stabilized singlet ground state of CR_2 with R =-OEt, -SEt and -N(carbazole) which could catalyze metathesis reactions with strained ring-systems albeit were significantly de-activated.[14]

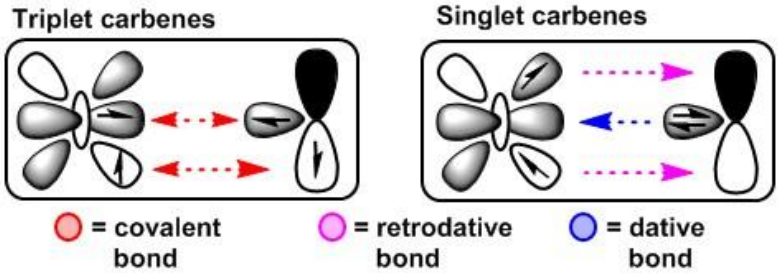

Figure 5.2: Constituent effect on the electronic state of a transition metal carbene

Metathesis reactivity using **1** with both tetrafluoroethylene (TFE) and vinylidene difluoride (VDF, $CF_2=CH_2$) to a single turnover due to formation of $P_3Ni=CF_2$, calculated to be 24.4 kcal/mol more stable than **1**. Herein we explore the reactivity of **1** with a wider range of alkene substrates with a view to formation of more reactive metal fluorocarbene intermediates required to achieve catalytic fluoroalkene metathesis.

In reactions of **1** with TFE, VDF and trifluoroethylene (T^rFE) the ratio of metathesis to metallacycle products increases as the fluorine content in the substrate decreases [VDF>T^rFE>TFE] although this order also reflects the decreasing steric bulk of the alkene. On the basis of early gas-phase studies, Beauchamp and co-workers speculated that metathesis of

fluoroalkenes with d^9 Ni^{i+} may be possible if the thermodynamic stability of the Ni fluorocarbene/fluoroalkene pairs was properly matched.[15] For example, research by Keefe and O'Ferall states that the difference in energy between a fully fluorinated ruthenium carbene versus a partially fluorinated carbene is a surprising 41.6 kcal/mol.[16] Therefore, for successful catalytic metathesis of fluoroalkenes to be realized, careful selection of substrates would be needed to give the reaction a thermodynamic driving force. This research looks to increase our understanding of first-row metal perfluoro-carbenes and their reactivity with various substrates to determine if the above requirements can be met and exploited for catalytic transformations.

5.3 Results

Reaction of **1** with trifluoromethyl trifluorovinyl ether [CF_2=$CF(OCF_3)$, Tr^FOCF_3] should give the less stable (vs. P_3Ni=CF_2) metal fluorocarbene, P_3Ni=$CF(OCF_3)$, as one of the metathesis products. In fact, the reaction in C_6D_6 produced a mixture of products including the expected isomeric metallacyclobutanes, **3-cis/trans)** and difluorocarbene P_3Ni=CF_2, **5** (Scheme 5.2; see supplementary for product characterization).

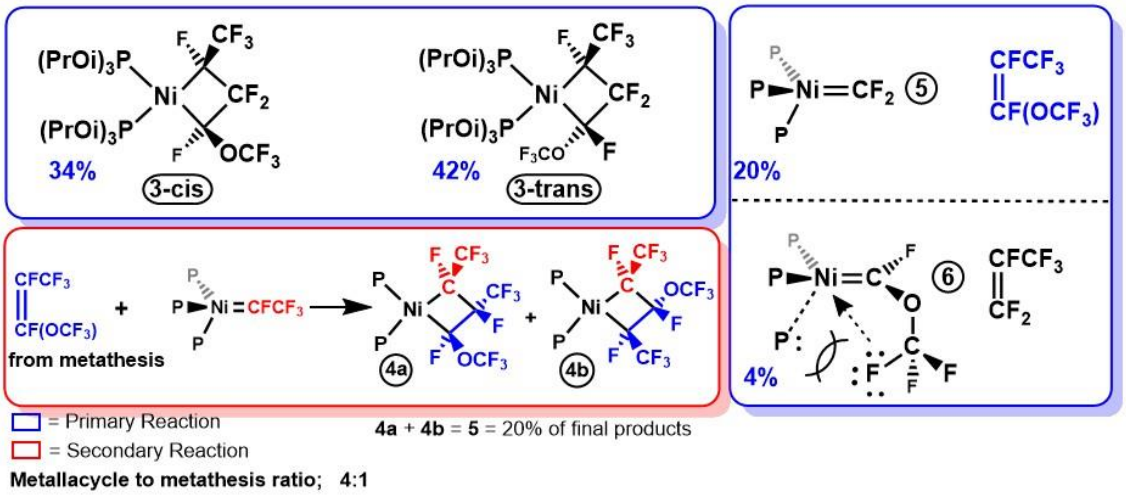

Scheme 5. 3

However, the expected new fluoroalkene, $CF(CF_3)$=$CF(OCF_3)$ was not observed as rapid reaction with remaining **1** gave metallacycle regioisomers **4a-b** with the same yield as co-product **5.** Further analysis of minor products showed the formation of a new carbene ^{19}F NMR pseudotriplet resonance at ca. 100 ppm ($^3J_{PF} \approx 50$ Hz) due to a unique P_2Ni fluorocarbene **6** (Scheme 2). The broad O-CF_3 resonance in **6** is consistent with a significant Ni--F interaction

that presumably prevents coordination of the third phosphite to Ni. Similar interactions have been observed in Ni BF_4 complexes.[17] The metallacycle to metathesis ratio (4:1) observed for Tr^FOCF_3 is lower than those for both TFE (9:1) and VDF (5.4:1) using **1**. This increase in the amount of metathesis products for both VDF and Tr^FOCF_3 compared to TFE suggests that electronics (R = H, OCF_3 good electron donor groups) play a role in the kinetics of the metathesis mechanism. The regioselectivity of the primary metallacycle products, **3**, on the other hand, is favored by both steric and electronic factors with the diradical intermediate[7b] more stabilized with the $CF(OCF_3)$ end group (vs. CF_2); Scheme 5.3).

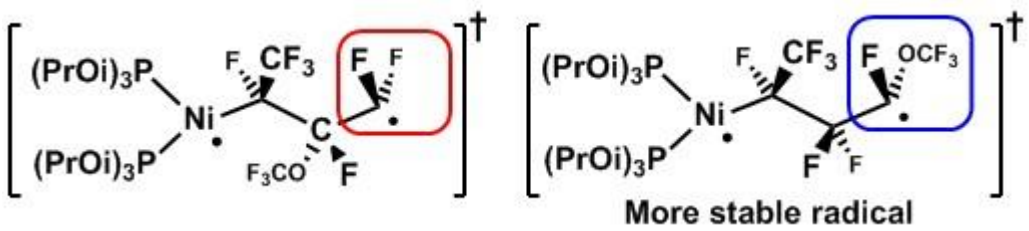

Scheme 5. 4

No selectivity is observed for the secondary metallacycle products (ca. 1:1) derived from intermediate alkene $CF(CF_3)=CF(OCF_3)$.

For the bulky, electrophilic fluoroalkene, hexafluoropropene (HFP), productive metathesis should be discouraged by both weak binding to Ni and steric repulsion between the two $CF(CF_3)$ groups. Indeed, reaction of **1** with HFP afforded a single metallacycle with trans-CF_3 substituents, $P_2Ni[\kappa^2\text{-}CF(CF_3)CF_2CF(CF_3)]$, **7** (Scheme 5.4; see supplemental section).

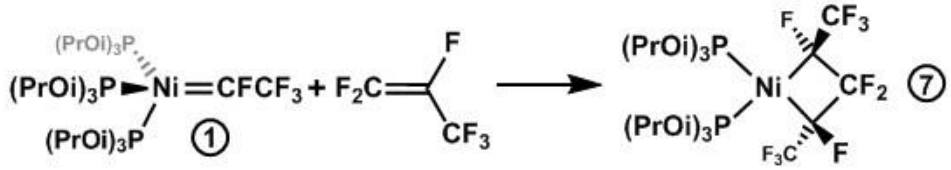

Scheme 5. 5

In keeping with the C2 alkene trend that showed a higher degree of metathesis products with decreasing fluorine substitution, we expected reaction of **1** with ethylene to give a high ratio of metathesis to metallacycle products. Instead, the reaction produced a single metallacycle,

$P_2Ni(\kappa^2\text{-}CFCF_3CH_2CH_2)$-, **8** perhaps due to a reluctance to undergo cycloreversion to high-energy $P_3Ni{=}CH_2$. We thus moved to access presumably more stable metal fluorocarbene, $P_3Ni{=}CHAr$ through reaction of **1** with styrene derivatives. With relatively electron-rich 4-methoxy-styrene, however, a single metallacycle $P_2Ni(\kappa^2\text{-}CFCF_3CH_2CH(Ar)\text{-})$, **9** was again obtained (Scheme 5.5).

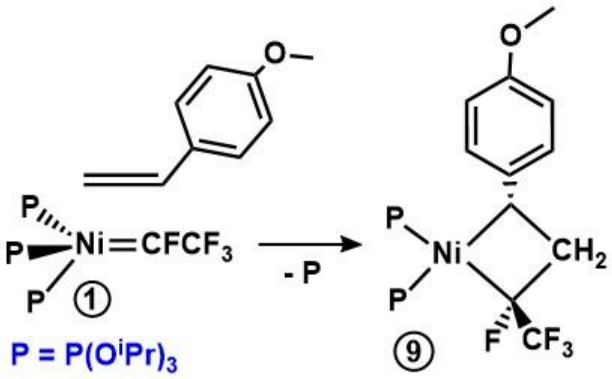

Scheme 5. 6

The observed regioselectivity is once more consistent with radical stabilization by the electron-rich aryl substituent substituent as evidenced by a similar reaction of **1** with electron-poor pentafluorostyrene that afforded both regioisomers in a 2:1 ratio (Scheme 5.6).

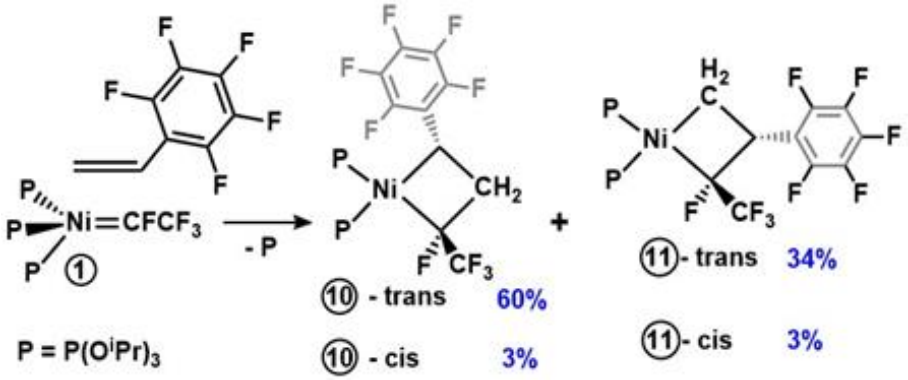

Scheme 5. 7

To further encourage the metathesis pathway that requires alkene binding, the reaction of 4-methoxystyrene with Ni fluorocarbene **2**, containing the smaller $P(OMe)_3$ ligand, was investigated. Surprisingly, both metallacycle regioisomers, **12**, **13 cis/trans** were formed in a 2:1 ratio (Scheme 5.7).

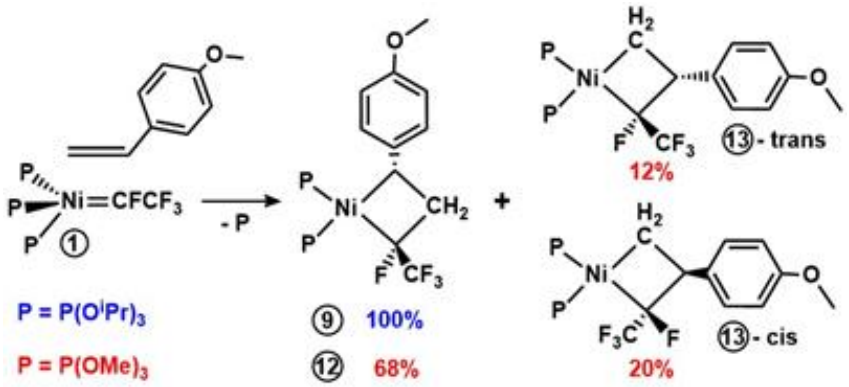

Scheme 5. 8

This result represents a contradiction to both the expected selectivity of the singlet di-radical mechanism (*vide infra*) as well as steric effects that should have led to higher regioselectivity with the bulkier phosphite ligand. As a change in regioselectivity would not be expected for the diradical metallacycle pathway, this result suggests a role for alkene binding, previously associated with the metathesis pathway (Scheme 5.8).

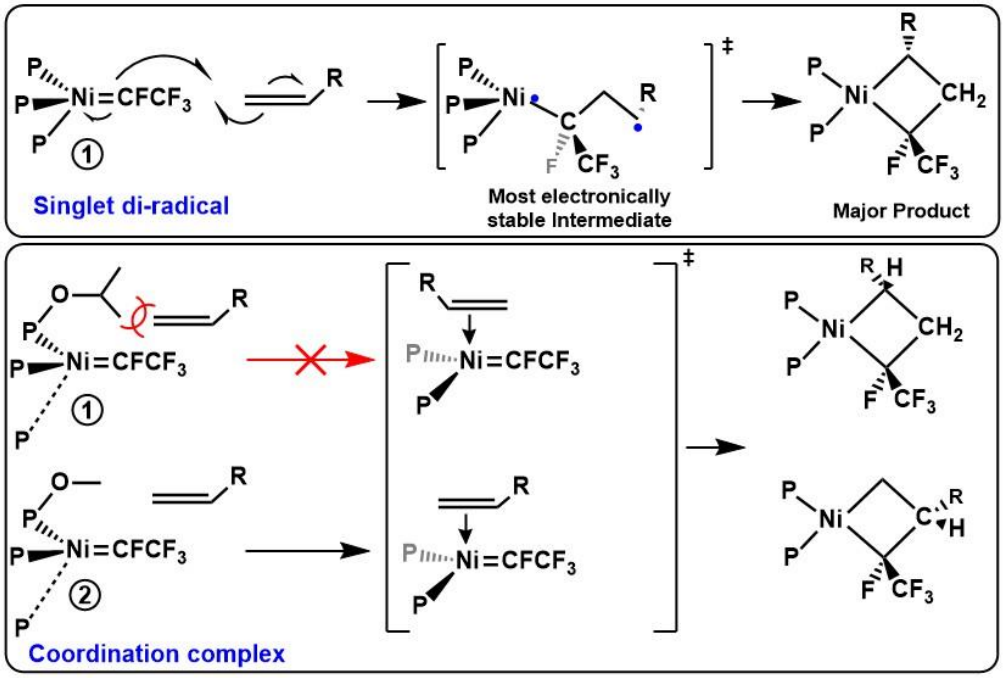

Scheme 5. 9

Given that a square planar geometry around the metal is necessary for the formation of metallacycle product (Figure 5.1) this led to a reevaluation of our previous results with ethylene.

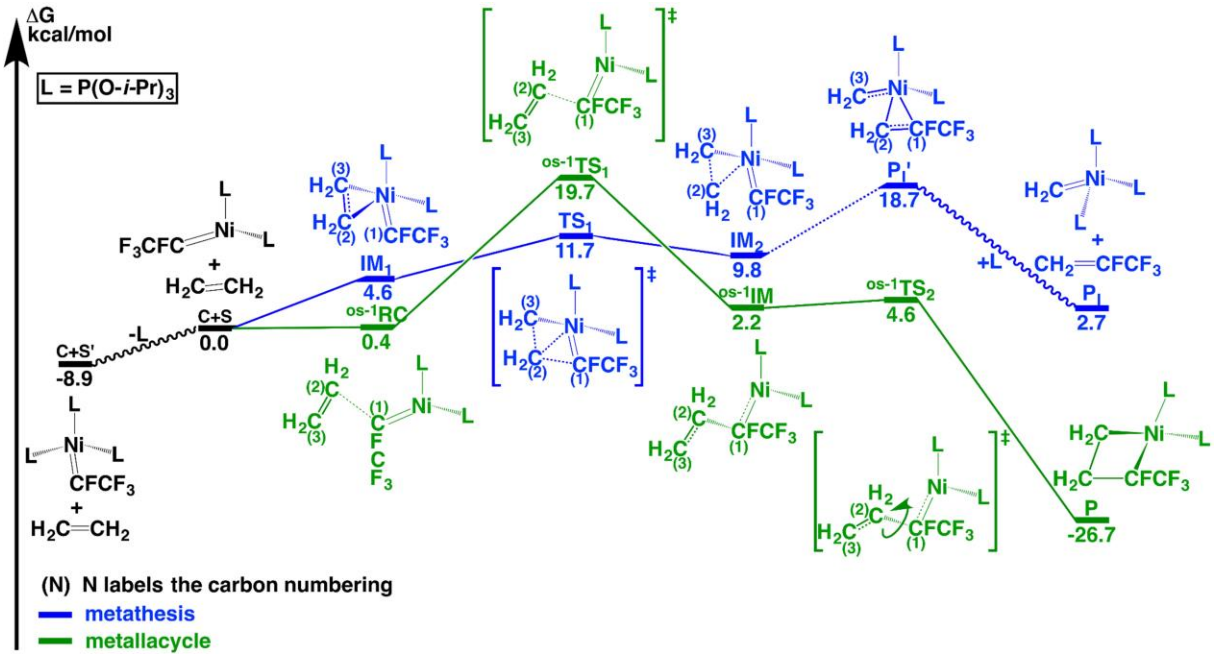

Figure 5.3: Reaction coordinate of **1** with ethylene showing the parallel reaction pathways for metallacycle formation (green) and metathesis (blue)

We surmised that a single product was observed due to formation of high energy $P_3Ni{=}CH_2$ so we employed DFT calculations to determine the reaction coordinate for both the metallacycle and metathesis pathways (Figure 5.3). As can be seen, the metathesis pathway (blue) has significantly lower energy intermediates than those of the metallacycle pathway (green). Additionally, no suitable intermediate could be found between IS1 and the final metathesis product, $Ni{=}CH_2$. This suggests an alternate pathway that would link together the metallacycle and metathesis pathways (Scheme 5.9), explaining the absence of any observed metathesis products even when monitoring the reaction by NMR.

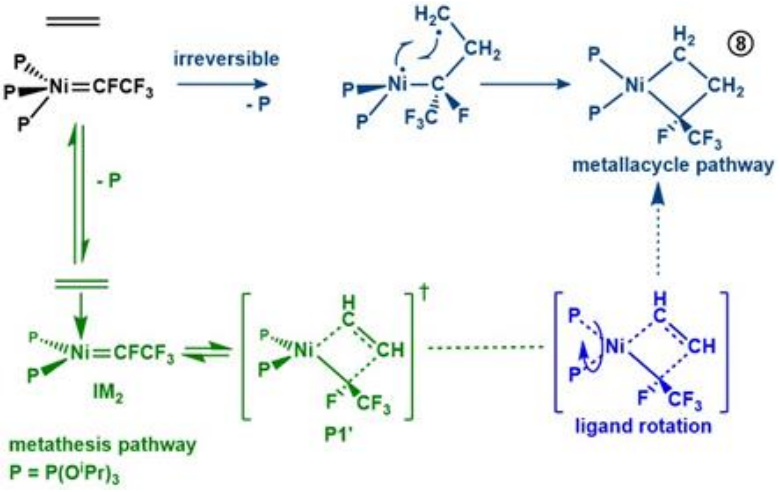

Scheme 5. 11

Additionally, the metallacycle stability compared to both starting material and $Ni=CH_2$ (-26.7 and -24.0 kcalmol^{-1} respectively) is such that it drives formation of the metallacycle exclusively.

In contrast, perfluorocyclobutene (PFCB) should be able to coordinate to Ni and afford a new thermodynamically favorable Ni fluorocarbene (4.3 kcal mol^{-1} more stable than **1**; Scheme 10]. Moreover, this would be the first example of metal-mediated fluoroalkene oligomerization via ring-opening metathesis polymerization (ROMP).

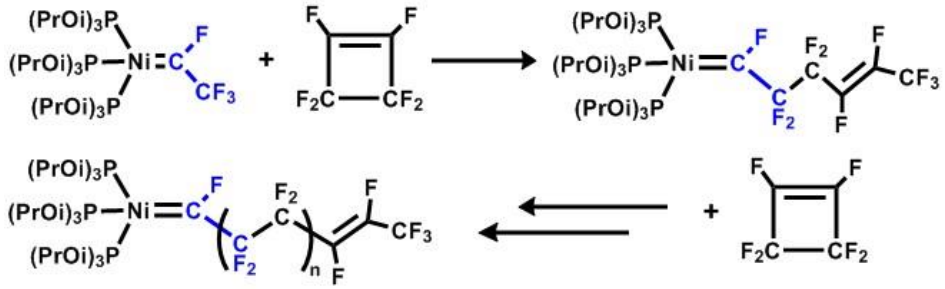

Scheme 5. 13

Monitoring the reaction of **1** and PFCB by ^{19}F NMR spectroscopy showed after 1 h formation of a new fluorocarbene (54 ppm, presumably $[P_3Ni=CF(CF_2)_2CF=CF(CF_3)]$) that slowly converted to metallacycle peaks over several hours at room temperature. Formation of linear fluorinated oligomers was never observed; suggesting that intramolecular back-biting of the 4-alkene unit with the carbene is favored over intermolecular reaction with another equivalent of PFCB (Scheme 5.11), even when excess of the latter was utilized. Indeed, a single metallacycle product **14** was observed upon reaction completion.

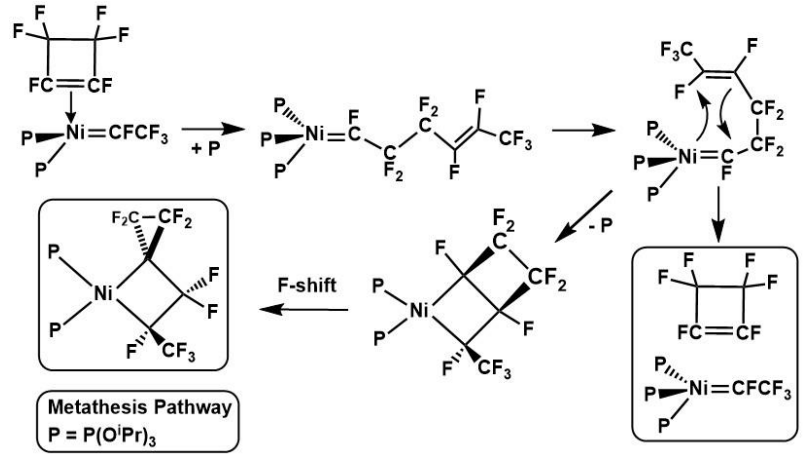

Scheme 5. 14

Analysis of **14** by ^{19}F and ^{31}P NMR spectroscopy showed several characteristic resonances for a fluorinated metallacycle such as geminally-coupled fluorines ($^{2}J_{FF}$ > 200 Hz), and a fluorine on the same carbon as a CF_3 moiety ($\delta \approx$ -200 ppm). However, 2D F-F COSY experiments revealed two unique CF_2 resonances coupled only to each other,[18] consistent with the cyclopropyl-substituted nickelacyclobutane structure containing a spiro-carbon moiety. This structure could result from a fluoride shift, as proposed in Scheme 5.12 although details remain to be fully elucidated.

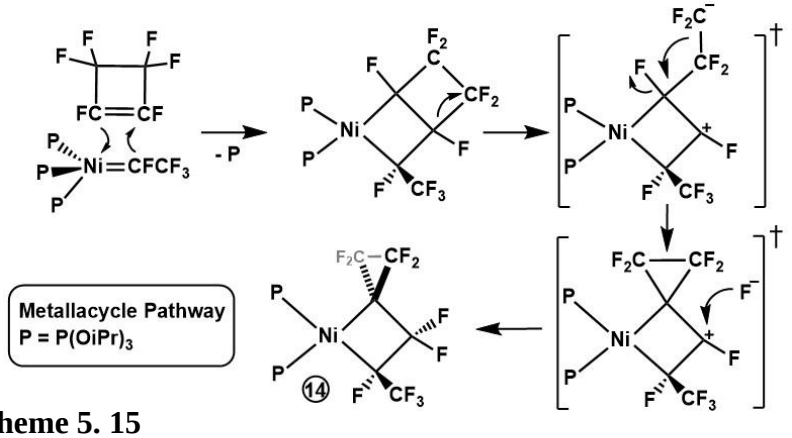

Scheme 5. 15

If this reaction follows a similar reaction pathway to ethylene it may even be possible that, due to the relative stability of the newly formed carbene [vs. $P_3Ni{=}CF(CF_3)$], the metathesis reaction is reversible, allowing time for the NiP_2 rotation mechanism to then form the stable metallacycle. A full DFT study of this phenomenon is in progress. The solubility of complex **14** and its DPPE analog in alkane solvents have so far prevented its structural confirmation by X-ray diffraction.

To further encourage the metathesis pathway, strained cyclic alkenes were utilized with a view to destabilizing the metallacycles through ring strain. While complex **1** reacted rapidly with cyclopentene, only two metallacycles were observed (**15-cis/trans)**, with a clear preference for the 15 trans isomer that has the bulky substituents on opposite sides of the metallacycle (Scheme 5.13).

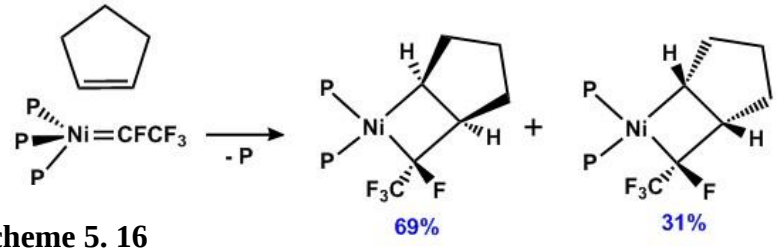

Scheme 5. 16

To increase the ring-strain further, a norbornene derivative was utilized, methyl 5-norbornene 2-carboxylate. However, even with this significantly strained bicyclic ring-system, reaction with **1** produced complexes **16-cis/trans** (Scheme 5.14).

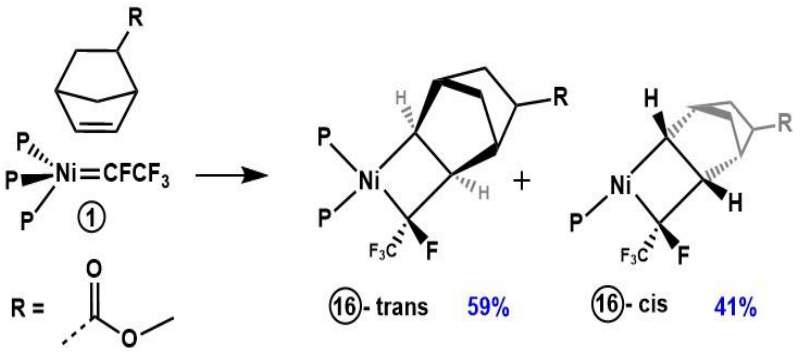

Scheme 5. 18

5.4 Conclusion

In this research we have shown that Ni=CF(CF_3) carbenes are capable of performing the stoichiometric fluoro-metathesis reaction. Catalytictransformations will require careful selection of substrates and catalyst design. Firstly, for new fluoroalkene synthesis, it is unclear whether a terminal CF_2-containing alkene can ever be pushed beyond a single turnover, due to the stability of the Ni=CF_2 unit. As a result, utilization of these substrates may be restricted to cross-metathesis with electron-rich alkenes. Instead, valuable substrates may include those which generate [Ni]=CFR^F or [Ni]=CHR^F carbenes. Second, for reactions that produce nearly isoenergetic metal fluorocarbenes such as PFCB, additional substrates should be tested to identify those not prone to back-biting and/or subsequent fluoride shifts. Indeed, preliminary experiments with perfluorocyclopentene afford additional products for which characterization is underway. Third, from a catalyst design perspective, ligands that enforce tetrahedral coordination may subdue the competing metallacycle pathway, leading to more productive metathesis. In order to obtain true catalytic fluoro-metathesis the metallacycle mechanism needs to be suppressed while also choosing substrates that prevent the formation of hetero-atom stabilized singlet carbenes and/or tailor the metal fragment geometry, electronic structure and ligand environment to favor a high spin-triplet state to further encourage covalent M=CR^F_2 behavior which may result in successful catalytic fluoro-metathesis. Further computational and experimental studies are underway.

5.5 Experimental Section

General: Experiments were conducted under nitrogen, using Schlenk techniques or an MBraun glove box. All solvents were deoxygenated by purging with nitrogen. Toluene, hexanes, diethyl ether (Et_2O), 1,2-dimethoxyethane (DME) and tetrahydrofuran (THF) were dried on columns of activated alumina using a J. C. Meyer (formerly Glass Contours) solvent purification system. C_6D_6 was dried over activated alumina (heated at 300 ^oC for > 6 h under vacuum) (10 wt. %). MeCN, CH_2Cl_2 and CD_2Cl_2 were distilled from CaH_2 and then passed through activated alumina (10 wt. %). Toluene-d_8 was dried over sodium/benzophenone and vacuum-transferred from the deep purple ketyl solution before use. All solvents were stored over activated (heated at ~ 250 ^oC for > 6 h under vacuum) 4 Å molecular sieves. Glassware was oven-dried at 150 ^oC for > 2 h. Commercial chemicals: $P(OMe)_3$ (Aldrich, 97%), $P(O\text{-}i\text{-}Pr)_3$ (Aldrich, 95%), $MeC(CH_2PPh_2)_3$ (Strem, 97%); deuterated (≥99.5%) NMR solvents (Cambridge Isotopes Labs). Complex **1** and **2** were made using our previously published procedures.[6] ^1H, ^{19}F and $^{31}P\{^1H\}$ NMR spectra were recorded on a 300 MHz Bruker Avance or AvanceII instrument at room temperature (RT, 23 ± 1^oC), except where noted. ^1H NMR spectra were referenced to the residual proton peaks associated with the deuterated solvents (C_6D_6: 7.16 ppm; CD_2Cl_2: 5.32 ppm; toluene-d_8: 2.09 ppm). $^{13}C\{^1H\}$ spectra in toluene-d_8 were referenced to the methyl carbon peak at 20.43 ppm. ^{19}F NMR spectra were referenced against internal 1,3-bis(trifluoromethyl)benzene (BTB) (Aldrich, 99%, deoxygenated by purging with nitrogen, stored over activated 4 Å molecular sieves), set to –63.5 ppm. ^{19}F NMR yields were obtained from the relative integrations of quantitative BTB and product peaks, using 5 s delay times. $^{31}P\{^1H\}$ NMR data were referenced against external H_3PO_4 (85% aqueous solution), set to 0.0 ppm. ^1H NMR assignments are focused exclusively on metallacycle protons as ligand protons are fully characterized in previous publications with only moderate change in chemical shift unless otherwise stated.

Reaction of (1) with trifluoromethyl-trifluorovinyl ether [CF_2=$CF(OCF_3)$] producing metallacycles: (3) $Ni(\kappa^2\text{-}CFCF_3CF_2CF(OCF_3)\text{-})(P)_2$**-cis/trans, (4a)** $Ni(\kappa^2\text{-}CFCF_3CFCF_3CF(OCF_3)\text{-})(P)_2$**, (4b)** $Ni(\kappa^2\text{-}CFCF_3CF(OCF_3)CFCF_3)(P)_2$**, and carbenes (5)** $P_3Ni{=}CF_2$ **and (6)** $P_2Ni{=}CF(OCF_3)$. A 0.092 M solution was prepared by dissolving **1** in C_6D_6 (0.5 mL) which was then added to a septum cap NMR tube. CF_2=$CF(OCF_3)$ was added (5 mL; excess) via syringe through the septum cap. Within 2 minutes at room temperature (RT) the solution went from deep purple to orange. The solution was left to stand at RT for 0.5 h before

collecting NMR data. Complex **1** was completely consumed. ^{1}H NMR (300 MHz, C_6D_6) ^{1}H NMR (300 MHz, C_6D_6) δ 5.0-4.1 (overlapping multiplets, 3H, P(O-C*H*-(CH_3)$_2$)$_3$), 1.6-0.9 ppm (overlapping multiplets, 18H, P(O-CH-(C*H*$_3$)$_2$)$_3$). ^{19}F NMR (282 MHz, C_6D_6): **Complex 3 - trans**: -208.7 (multiplet, C*F*CF_3, 1F), -136.4 (multiplet, C*F*OCF_3, 1F), -118.2 (unresolved doublet of multiplets, $^{2}J_{FF}$ = 220 Hz, C*F*(F), 1F), -92.8 (unresolved doublet of multiplets, $^{2}J_{FF}$ = 220 Hz, CF(*F*), 1F), -64.3 (unresolved multiplet, CF*CF*$_3$, 3F), -53.6 ppm (overlapping dd, $^{4}J_{FF}$ = 12.8 Hz, $^{5}J_{FF}$ = 8 Hz). **Complex 3 – cis**: -207.3 (multiplet, C*F*CF3, 1F), -132.7 (multiplet, C*F*OCF_3, 1F), -113.8 (doublet of multiplets ($^{2}J_{FF}$ = 218.6 Hz, C*F*(F), 1F), -94.5 (doublet of multiplets, $^{2}J_{FF}$ = 218.6 Hz, CF(*F*), 1F), -64.2 (multiplet, CFCF3, 3F), -53.2 ppm (multiplet, CF(OCF3), 3F). **Complex 4a**: -200.1 (multiplet, C*F*CF_3, 2F), -69.2 (dmult-, ^{3}JFF = 148 Hz, 1F, C*F*OCF_3), -65.3 (multiplet, 3F, CF*CF*$_3$), -54.7 ppm (broad overlapping dd, $^{4}J_{FF} \approx 11$, $^{5}J_{FF}$ = 9 Hz, 3F, CF{OCF3}). **Complex 4b:** -188.73 (multiplet, 1F, C*F*CF_3), -187.91 (multiplet, 1F, C*F*CF3), -68.5 (dmultiplets, 3F, CFC*F*$_3$}), -67.9 (unresolved dd-multiplets, 3F, CF{O*CF*$_3$}), -63.8 (unresolved multiplet, 3F, CFC*F*$_3$), **Complex 5**: 94.4 ppm (q, $^{3}J_{PF}$ = 60Hz, Ni=C*F*$_2$). **Complex 6**: 111.5 (dd, $^{3}J_{PF}$ = 54 Hz, 54 Hz, Ni=C*F*{OCF_3}), -59.4 ppm (singlet, 3F, CF{OC*F*$_3$}). ^{31}P{^{1}H} NMR (121 MHz, C_6D_6): **Complex 3-trans**: 147-143 ppm (broad multiplet, 2P). **Complex 3-cis**: 128-125 ppm (broad multiplet, 2P). **Complex 4a/4b**: 125-120 ppm (broad grouping of multiplets). **Complex 5**: 158.5 ppm (triplet, $^{4}J_{FP}$ = 60Hz).

Reaction of (1) with HFP to form complex (7) {Ni(κ^2-CFCF$_3$CF$_2$CFCF$_3$-)P$_2$} (P = P(O^{i}Pr)$_3$). A 0.092 M solution was prepared by dissolving **1** in hexanes (0.5 mL) which was then added to a septum cap NMR tube. CF_2=CF(OCF_3) was added (5 mL; excess) via syringe through the septum cap. Within 1 hour at room temperature (RT) the solution went from deep purple to light yellow. The solution was then poured into a glass vial and the solvent was evaporated under reduced pressure, producing an yellow semi-solid. The semi-solid was dissolved in C_6D_6 (0.5 mL) and an NMR was taken. ^{1}H NMR (300 MHz, C_6D_6) δ 5.0-4.1 (overlapping multiplets, 3H, P(O-C*H*-(CH_3)$_2$)$_3$), 1.6-0.9 ppm (overlapping multiplets, 18H, P(O-CH-(C*H*$_3$)$_2$)$_3$). ^{19}F NMR (282 MHz, C_6D_6): δ -207.6 (multiplet, 2F, C*F*-CF_3), -106.2 (multiplet, 2F, -CFCF_3-C*F*$_2$-CFCF_3-), -63.9 ppm (multiplet, 6F, CFCF_3). ^{31}P{^{1}H} NMR (121 MHz, C_6D_6) δ 136.3 ppm (overlapping multiplet, 2P).

Reaction of (1) with ethylene (CH_2=CH_2) to form complex (8) {Ni(κ^2-CH$_2$CH$_2$CFCF$_3$)P$_2$} (P = P(O^{i}Pr)$_3$). A 0.092 M solution was prepared by dissolving **1** in hexanes (0.5 mL) which was

then added to a septum cap NMR tube. CH_2=CH_2 was added (5 mL; excess) via syringe through the septum cap. Reaction was left to sit 0.5h at RT before NMR was taken. The solution changed from purple to yellow within 30 seconds. The solution was poured into a glass vial and the solvent was removed under reduced pressure leaving a yellow semi-solid. The residue was dissolved in C_6D_6 and an NMR was taken. ^{1}H NMR (300 MHz, C_6D_6) δ 3.8 (triplet of multiplets, $^3J_{HH}$ = 12 Hz), 3.3 ppm (sextet, J = 12 Hz). ^{19}F NMR (282 MHz, C_6D_6): -183.1 (ddq of multiplets. $^3J_{PF}$ = 55.5 Hz, $^3J_{PF}$ = 47.1 Hz, $^3J_{FF}$ = 10.8 Hz, 1F, C*F*CF_3), -71.8 ppm (ddm, $^3J_{FF}$ = 10.8 Hz, $^4J_{FP}$ = 5.2 Hz, 3F, CFC*F_3*). ^{31}P{^{1}H} NMR (121 MHz, C_6D_6): overlapping apparent doublets centered about 136.1 ppm ($^3J_{PF}$ = 55.5 Hz, $^3J_{FP}$ = 47.1 Hz).

Reaction of (1) with 4-methoxy-styrene [CH_2=CH(Ph-OMe)] forming complex (9) {Ni(κ^2-CH(Ar)CH_2CFCF_3-)P_2} (P = P(O^{i}Pr)$_3$; Ar = para-methoxy-benzene). A 0.092 M solution was prepared by dissolving **1** in C_6D_6 (0.5 mL) which was then added to an NMR tube. (-CF_2)CF=CF(CF_2-) was added (6 μL; excess). Reaction was left to sit 3 h at RT before NMR was taken. The solution changed from purple to red within 3 h. ^{1}H NMR (300 MHz, C_6D_6) δ *Peaks associated with starting material* [*7.2, 6.7, 6.6, 5.5, 5, 3.3 ppm*], 7.8 (dd, $^3J_{HH}$ = 8.8 Hz, $^4J_{HH}$ = 3.3 Hz; Aryl CH), 6.8 (dd, $^3J_{HH}$ = 8.8 Hz, $^4J_{HH}$ = 3.3 Hz; Aryl CH), 4.9-4.3 (OCH[CH_3]$_2$), 3.8 (multiplet,CH_CH_B-$CFCF_3$), 3.4 (multiplet, CH_CH_B-$CFCF_3$), 2.6 ppm (multiplet, -CH[Aryl]), 1.3 – 1.0 ppm (multiplets, OCH(CH_3)$_2$) ^{19}F NMR (282 MHz, C_6D_6): δ -70.9 (dd, $^4J_{FP}$ = 6.4 Hz, $^3J_{FF}$ = 11.7 Hz; $CFCF_3$), -179.8 ppm (ddq-mult, $^3J_{FP}$ = 78.8 Hz , 3J_{FP} = 40.75 Hz , $^3J_{FF}$ = 11.73 Hz; $CFCF_3$). ^{31}P{^{1}H} NMR (121 MHz, C_6D_6): 139.4 (dd, $^3J_{PF}$ = 40.8 Hz, $^3J_{PP}$ = 9.4 Hz), 130.4 ppm (ddq, $^3J_{PF}$ = 78.8 Hz, $^3J_{PP}$ = 9.4 Hz, $^4J_{PF}$ = 6.2 Hz).

Reaction of (1) with (1,2,3,4,5)-pentafluoro-styrene forming complex (10)-{Ni(κ^2-CHArCH_2CFCF_3-)P_2}-cis/trans and (11)-{Ni(κ2-CH2CHArCFCF3-)P2}-cis/trans (P = P(O^{i}Pr)$_3$; Ar = pentafluoro-benzene). A 0.092 M solution was prepared by dissolving **2** in C_6D_6 (0.5 mL) which was then added to an NMR tube. (-CF_2)CF=CF(CF_2-) was added (-CF_2)CF=CF(CF_2-) was added (6 μL; excess). Reaction was left to sit 3 h at RT before NMR was taken. The solution changed from purple to yellow within 2h. Note: Percentage of **cis-12/13** is too low to determine exact chemical shift both the ^{1}H and ^{31}P NMR due to significant overlapping resonances and poor resolution. ^{1}H NMR (300 MHz, C_6D_6): **10-trans**: δ 3.9 (multiplet, 1H, C*H*H'), 3.4 (overlapping multiplets, 1H, CH*H'*), 2.0 ppm (overlapping multiplets, 1H, C*H*Ar). **11-trans**: δ 3.7 (multiplet, 1H, C*H*Ar), 3.4 (overlapping multiplet, 1H,

C*H*H'), 2.1 ppm (overlapping multiplet, 1H, CH*H'*). ^{19}F NMR (282 MHz, C_6D_6): **10-trans**: δ -183.6 (ddq, $^3J_{HF}$ = 58 Hz ,$^3J_{HF}$ = 31.7 Hz , $^3J_{FF}$ = 10 Hz, 1F, C*F*CF_3), -71.4 ppm (dd, $^3J_{FF}$ = 10Hz, $^4J_{PF}$ = 7 Hz, 3F, CFC*F*$_3$). **10-cis**: δ -189.6 (multiplet, 1F, C*F*CF_3), -65.5 ppm (unresolved dblt of dblt, 3F, CFC*F*$_3$). **11-trans**: δ -178.0 (unresolved dblt of mult., $^3J_{HF} \approx 30$ Hz, 1F, C*F*CF3), -74.0 ppm (multiplet, 3F, CFC*F*$_3$). **11-cis**: δ -182.9 (multiplet, 1F, C*F*CF_3), -66.0 ppm (unresolved dd, $^4J_{PF} \approx 12$ Hz, $^4J_{PF} \approx 16$ Hz, 3F, CFC*F*$_3$). ^{31}P{^{1}H} NMR (121 MHz, C_6D_6): **10-cis**: 128.4 (unresolved dd, $^3J_{PF} \approx 42.3$, $^2J_{PP} \approx 30$ Hz, 1P, P^{AorB}), 126.9 ppm (unresolved overlapping dd, $^2J_{PP} \approx 30$Hz, $^3J_{FP} \approx 28$ Hz, 1P, P^{AorB}). **11-cis**: 126.8 (overlapping multiplet, 1P, P^{AorB}), 126.3 ppm (overlapping doublet, $^2J_{PP}$ = 29 Hz, 1P, P^{AorB}).

Reaction of (2) with 4-methoxy-styrene [CH_2=CH(Ph-OMe)] to form complex (9) {listed previously}, (12) and (13)-cis/trans. (^{19}F NMR comparison). A 0.092 M solution was prepared by dissolving **2** in C_6D_6 (0.5 mL) which was then added to an NMR tube. (-CF_2)CF=CF(CF_2-) was added (-CF_2)CF=CF(CF_2-) was added (6 μL; excess). Reaction was left to sit 3 h at RT before NMR was taken. The solution changed from purple to yellow/orange within 3 h. ^{19}F NMR (282 MHz, C_6D_6): **Complex 12**: δ -70.9 (dd, $^4J_{PF}$ = 6.4 Hz, $^3J_{FF}$ = 11.7 Hz; CFCF_3), -179.8 ppm (ddq-mult, $^3J_{FP}$ = 78.8 Hz , $3J_{FP}$ = 40.75 Hz , $^3J_{FF}$ = 11.73 Hz; CFCF_3). **Complex 13-trans**: -70.0 (dd, $^4J_{PF}$ = 9.3 Hz, 3F, CFC*F*$_3$), -177.4 ppm (multiplet, 1F, C*F*CF3). **Complex 13-cis**: -69.3 (broad doublet, 3F, CFC*F*$_3$), -174.5 ppm (multiplet, 1F, C*F*CF3).

Reaction of (1) with perfluorocyclobutene [(-CF_2)CF=CF(CF_2-)] forming complex (14)-{Ni(κ^2-C[κ^2-CF_2-CF_2-]CF_2CFCF_3)P_2 (P = P(O^{i}Pr)$_3$). A 0.092 M solution was prepared by dissolving **1** in C_6D_6 (0.5 mL) which was then added to a septum cap NMR tube. Perfluorocyclobutene (3 mL; excess) was added via syringe through the septum cap. Reaction was left to sit 3 h at RT before NMR was taken. Solution remained purple for 2h before fading to orange after 3 h. ^{1}H NMR (300 MHz, C_6D_6): δ 5.0-4.1 (overlapping multiplets, 3H, P(O-C*H*-(CH_3)$_2$)$_3$), 1.6-0.9 ppm (overlapping multiplets, 18H, P(O-CH-(C*H*$_3$)$_2$)$_3$). ^{19}F NMR (282 MHz, C_6D_6): -189.6 (multiplet, 1F, C*F*CF_3), -123.5 (2nd order dd, 2JFF = 200 Hz, 3JFF = 24 Hz, 1F, C*F*(F)), -117.8 (2nd order multiplet, 2F, C*F*$_2$), -114.8 (2nd order multiplet, 2F, C*F*$_2$), -93.1 ppm (2nd order doublet of multiplets, $^2J_{FF}$ = 200 Hz, 1F, CF(*F*)). ^{31}P{^{1}H} NMR (121 MHz, C_6D_6): 160-152 ppm (broad multiplet, 2P).

Reaction of (1) with perfluorocyclobutene [(-CF_2)CF=CF(CF_2-)] forming complex (14). Time resolved experiment. A 0.092 M solution was prepared by dissolving **1** in hexene (0.5 mL) which was added to an NMR tube containing C_6D_6 (≈ 5 μL) which was sealed using a septum cap. NMR sample was then used to lock and shim the NMR using the sample. A pre-prepared syringe containing perfluorocyclobutene (3 mL, excess) was then injected and a kinetic experiment (NS = 16, 1.0 min. scan time, 2 min. dummy scan, #of experiments: 25, elapsed time: 1.5h) was run within 1 min. of injection of perfluorocyclobutene to NMR tube.^{19}F NMR (282 MHz, C_6D_6) {note: the following peaks do not constitute an accepted structure, merely a suggestion as to what the likely product is}: 54.2 (broad multiplet, 1F, C*FC*F_2R). -39.4 (broad multiplet, 2F, -C*F*$_2$-CF_2-), -42.1 (broad multiplet, 2F, -CF_2-C*F*$_2$-), -100.1 (dt, $^3J_{FF}$ = 50 Hz, $^3J_{FF}$ = 18Hz, 1F, -C*F*=$CFCF_3$), -166.4 ppm (overlapping dq, $^3J_{FF}$ = 50 Hz, $^3J_{FF}$ = 20 Hz). $^{31}P\{^1H\}$ NMR (121 MHz, C_6D_6): 159.5 (multiplet, 1P), 157.9 ppm (multiplet, 1P).

Reaction of (1) with cyclopentene forming complex 15 cis/trans. A 0.092 M solution was prepared by dissolving **1** in C_6D_6 (0.5 mL) which was then added to a septum cap NMR tube. Cyclopentene was added (3.6 μL) and the reaction was left to sit 2 h at RT before NMR was taken. The solution changed from purple to yellow within 2 h. ^{1}H NMR (300 MHz, C_6D_6) δ ^{19}F NMR (282 MHz, C_6D_6): δ -70.0 (dd, $^4J_{FP}$ = 11 Hz, $^3J_{FF}$ = 6.75), -77.1 (dd, J = 6.6 Hz, J = 11.24 Hz), -199.5 (ddq, $^3J_{FP}$ = 74 Hz, $^3J_{FP}$ = 47.1 Hz, 3JFF = 11.35 Hz), -203.1 ppm (mult). $^{31}P\{^1H\}$ NMR (121 MHz, C_6D_6): 152.1 ppm (singlet, NiP_4),149.1 (very broad multiplet), 136.6 (dd, $^3J_{PF}$ = 47.1, $^3J_{PP}$ = 11.5 Hz), 132.2 ppm (broad doublet, $^3J_{FP}$ = 74.0 Hz).

Reaction of (1) with 5-norbornene 2-carboxylate forming complex (16)–cis/trans. A 0.092 M solution was prepared by dissolving **1** in C_6D_6 (0.5 mL) which was then added to a septum cap NMR tube. Perfluorocyclobutene (3 mL; excess) was added via syringe through the septum cap. Reaction was left to sit 3 h at RT before NMR was taken. Solution remained purple for 2 h before fading to dark yellow after 3 h. ^{1}H NMR (300 MHz, C_6D_6): δ ^{19}F NMR (282 MHz, C_6D_6): **15-trans**: δ -202.6 (ddq, $^3J_{PF}$ = 69 Hz, $^3J_{PF}$ = 37 Hz, $^3J_{FF}$ = 12 Hz, 1F, C<u>F</u>CF_3), -69.9 ppm (dd, $^3J_{FF}$ = 12 Hz, $^4J_{PF}$ = 6 Hz, 3F, CFC<u>F</u>$_3$). **15-cis**: δ -205.1 (ddq, $^3J_{PF}$ = 68 Hz, $^3J_{PF}$ = 38 Hz, $^3J_{FF}$ = 12 Hz, 1F, C<u>F</u>CF_3), -70.0 ppm (dd, $^3J_{FF}$ = 12 Hz, $^4J_{PF}$ = 7 Hz, 3F, CFC<u>F</u>$_3$). $^{31}P\{^1H\}$ NMR (121 MHz, C_6D_6): **15-trans**: δ 133.6 (dd, $^3J_{FP}$ = 37 Hz, $^2J_{PP}$ = 15 Hz, 1P), 129.1 ppm (ddq, $^3J_{FP}$ = 69 Hz, $^2J_{PP}$ = 15 Hz , $^4J_{FP}$ = 6 Hz, 1P). **15-cis**: δ 134.6 (dd, $^3J_{FP}$ = 38 Hz, $^2J_{PP}$ = 17 Hz, 1P), 130.8 ppm (ddq, $^3J_{FP}$ = 68 Hz, $^2J_{PP}$ = 17 Hz, $^4J_{FP}$ = 7 Hz, 1P).

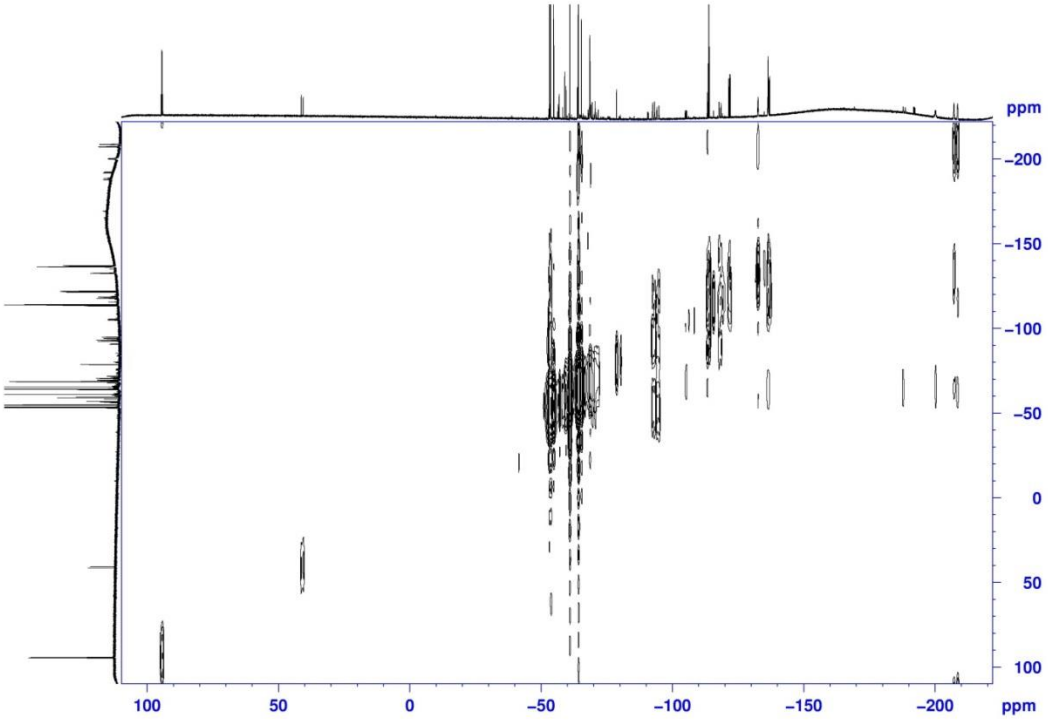

Figure 5.4: ^{19}F Cosy of reaction of **1** with $CF_2=CF(OCF_3)$ producing complex **3**, **4**, **5**, and **6**

5.6 Supplemental

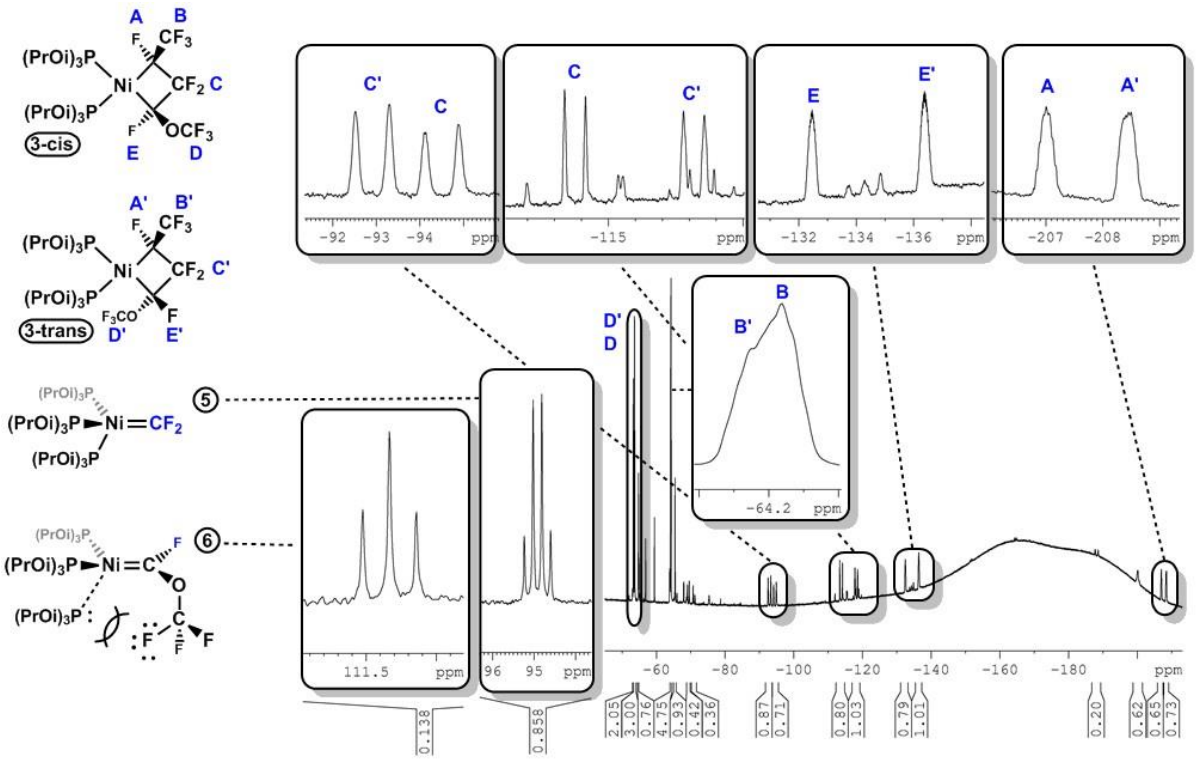

Figure 5.5: ^{19}F NMR of reaction between **1** with CF_2=CF(OCF_3). Close-up view of resonances associated with **3**-cis/tran, and nickel carbenes **5** and **6**.

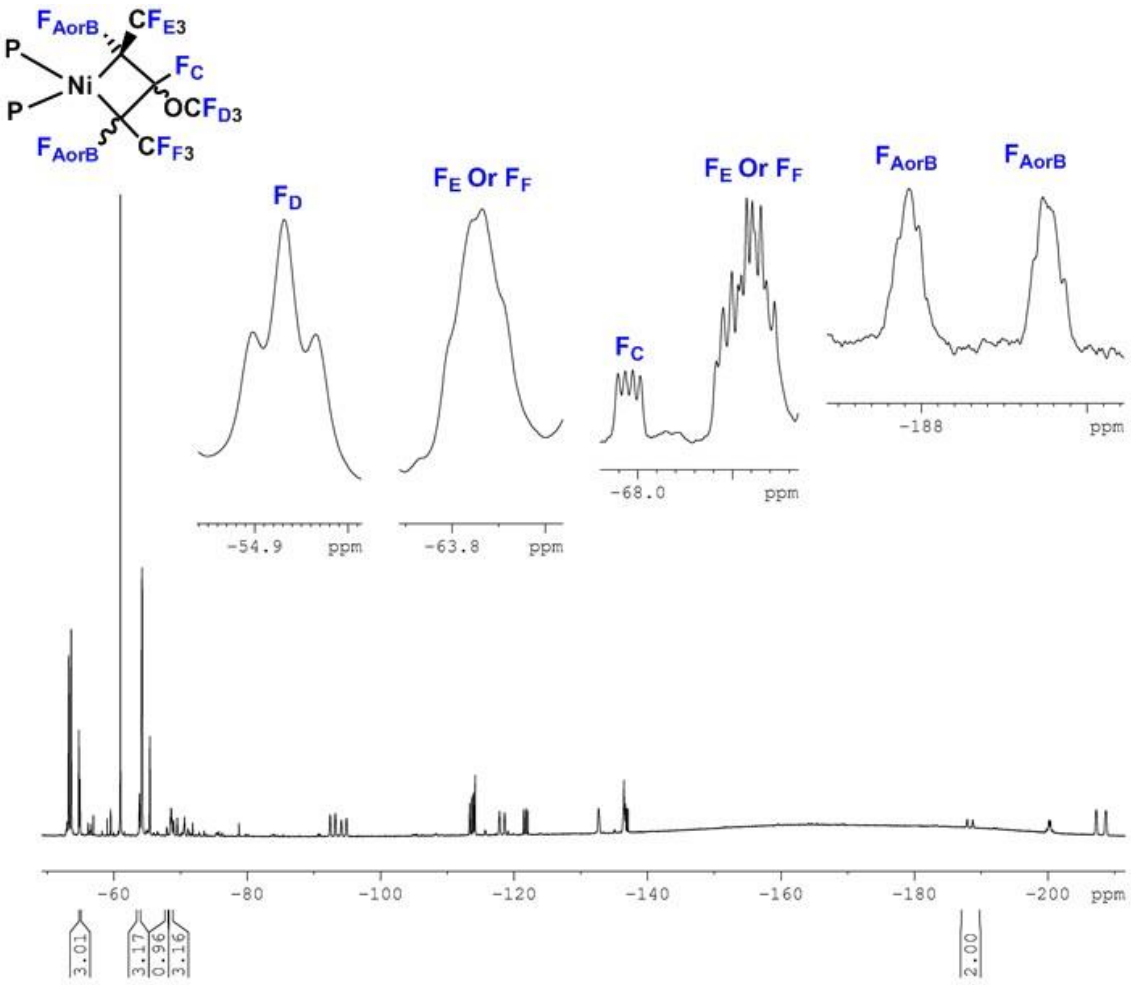

Figure 5.6: ^{19}F NMR of reaction between **1** with $CF_2=CF(OCF_3)$. Close-up view of resonances associated with complex **4b**

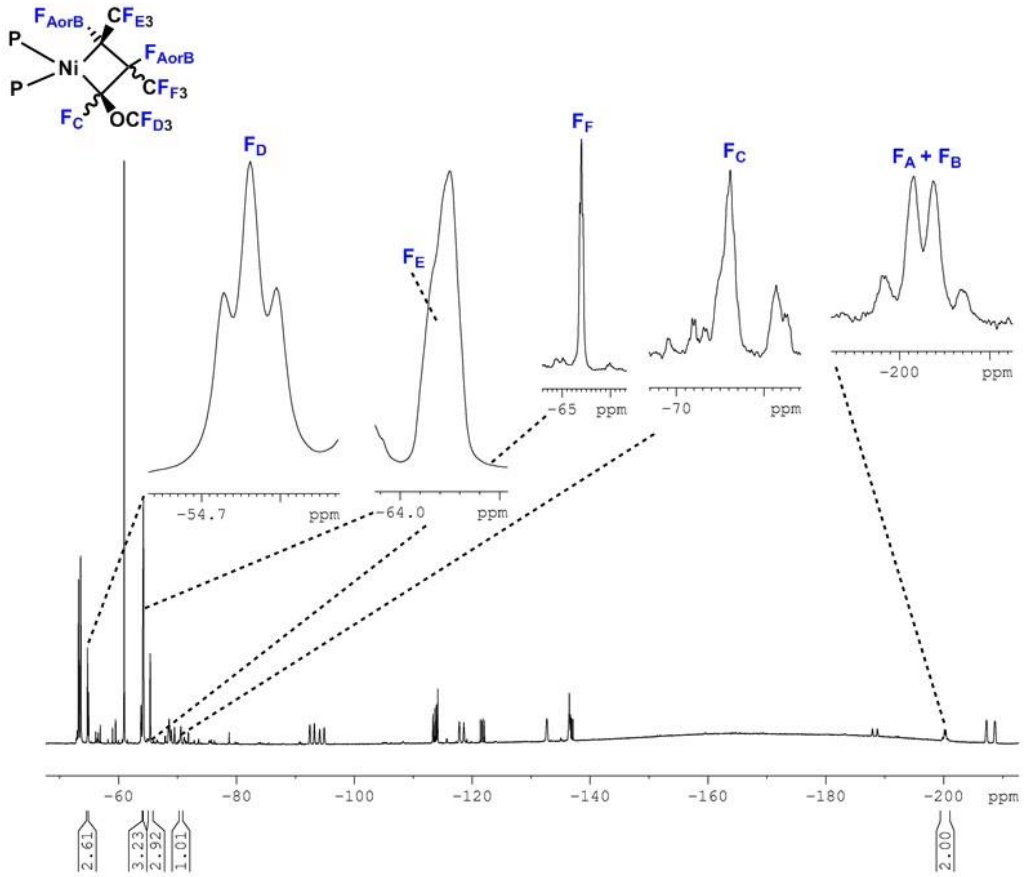

Figure 5.7: ^{19}F NMR of reaction between **1** with $CF_2=CF(OCF_3)$. Close-up view of resonances associated with complex **4a**.

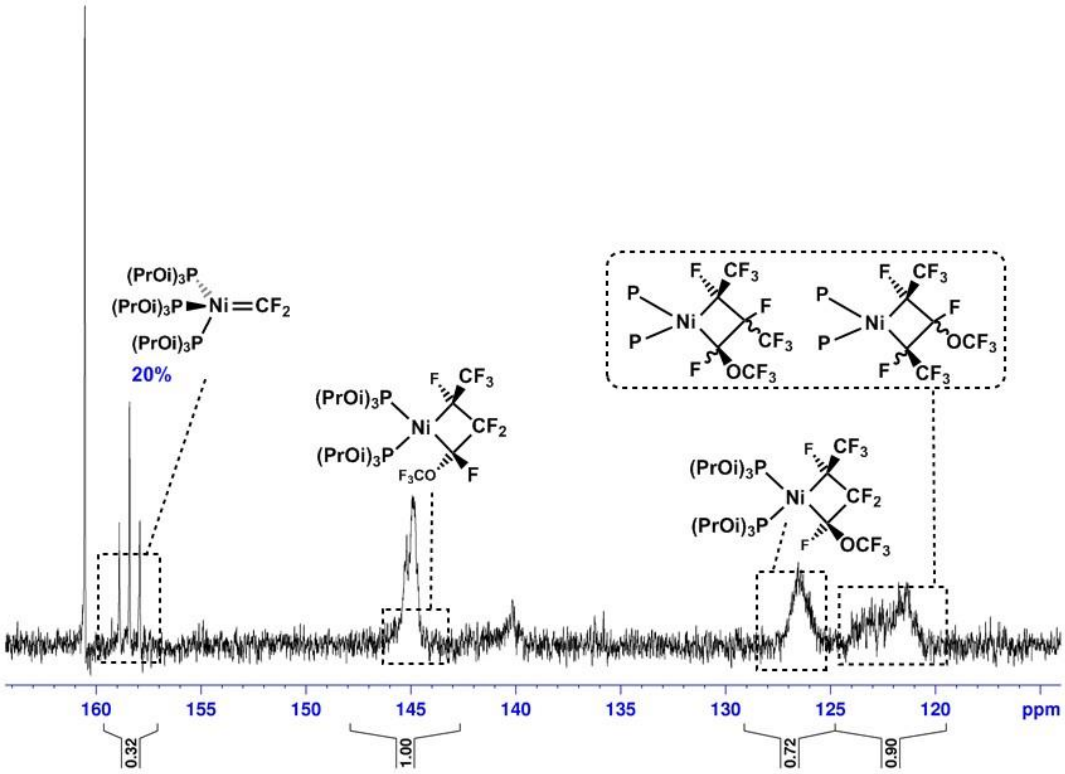

Figure 5.8: ^{31}P NMR of complex **1** reacted with CF_2=CF(OCF_3).

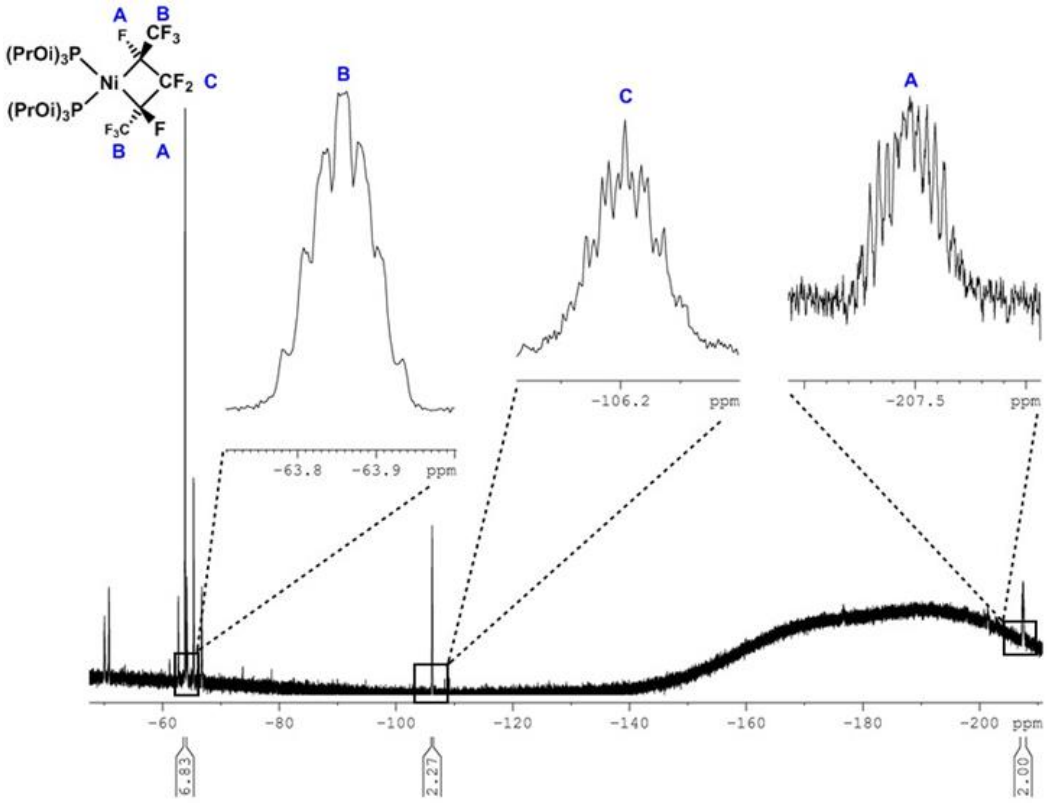

Figure 5.9: ^{19}F NMR of complex **7.**

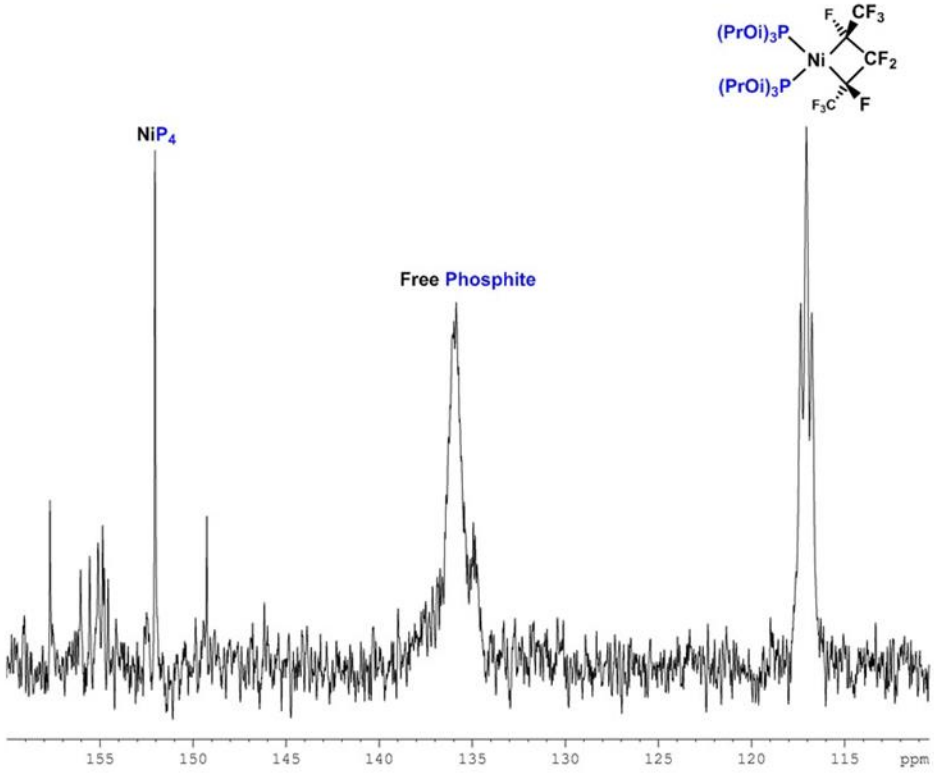

Figure 5.10: ^{31}P NMR of complex **7.**

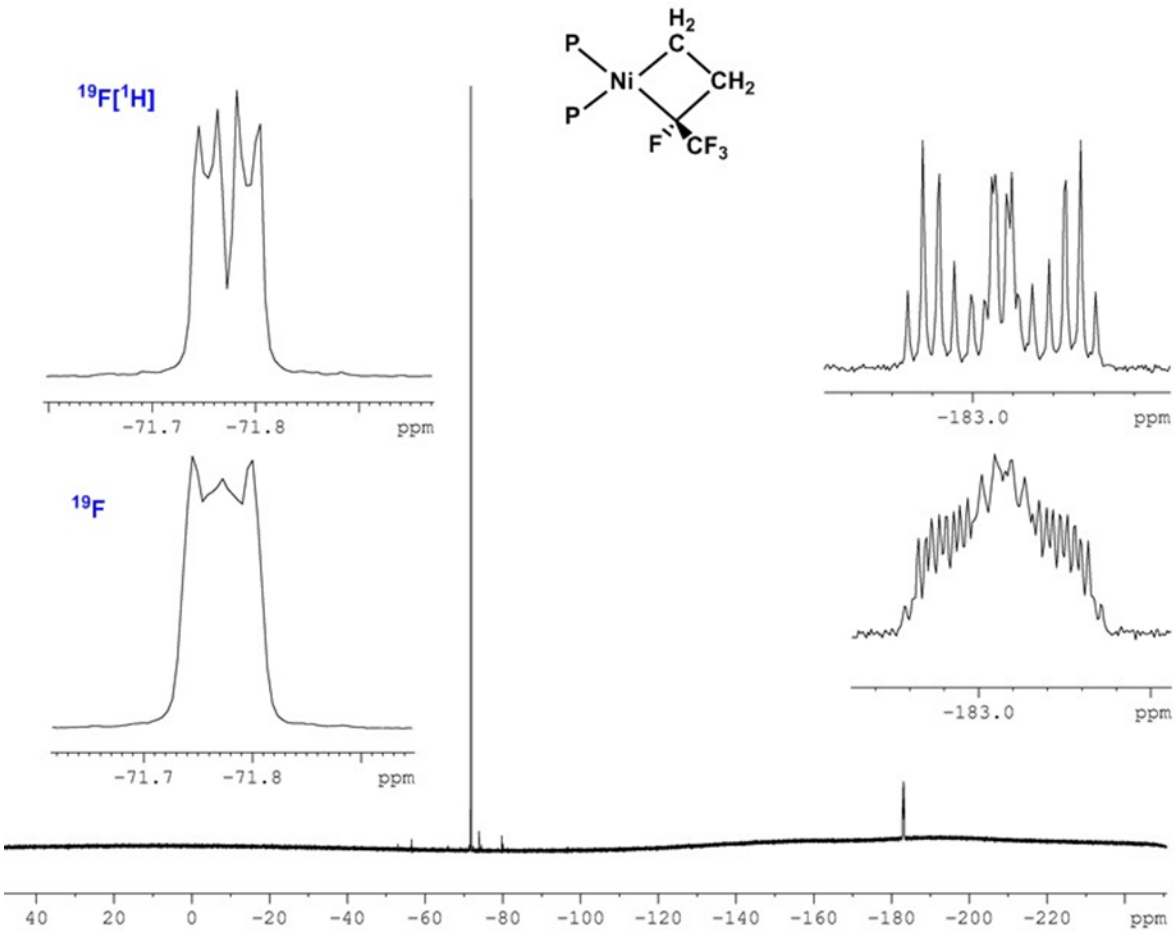

Figure 5.11: Stacked $^{19}F/^{19}F[^{1}H]$ NMR of complex **8**.

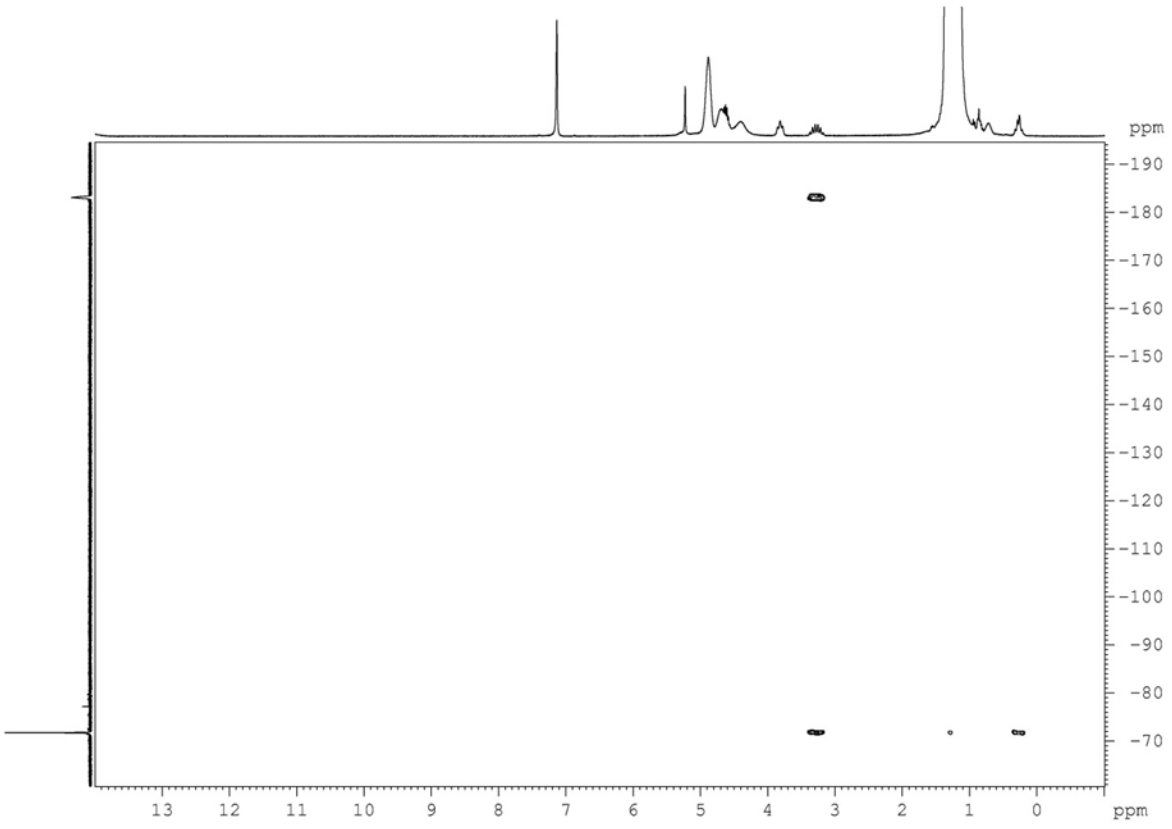

Figure 5.12: HMQC of Complex **8**.

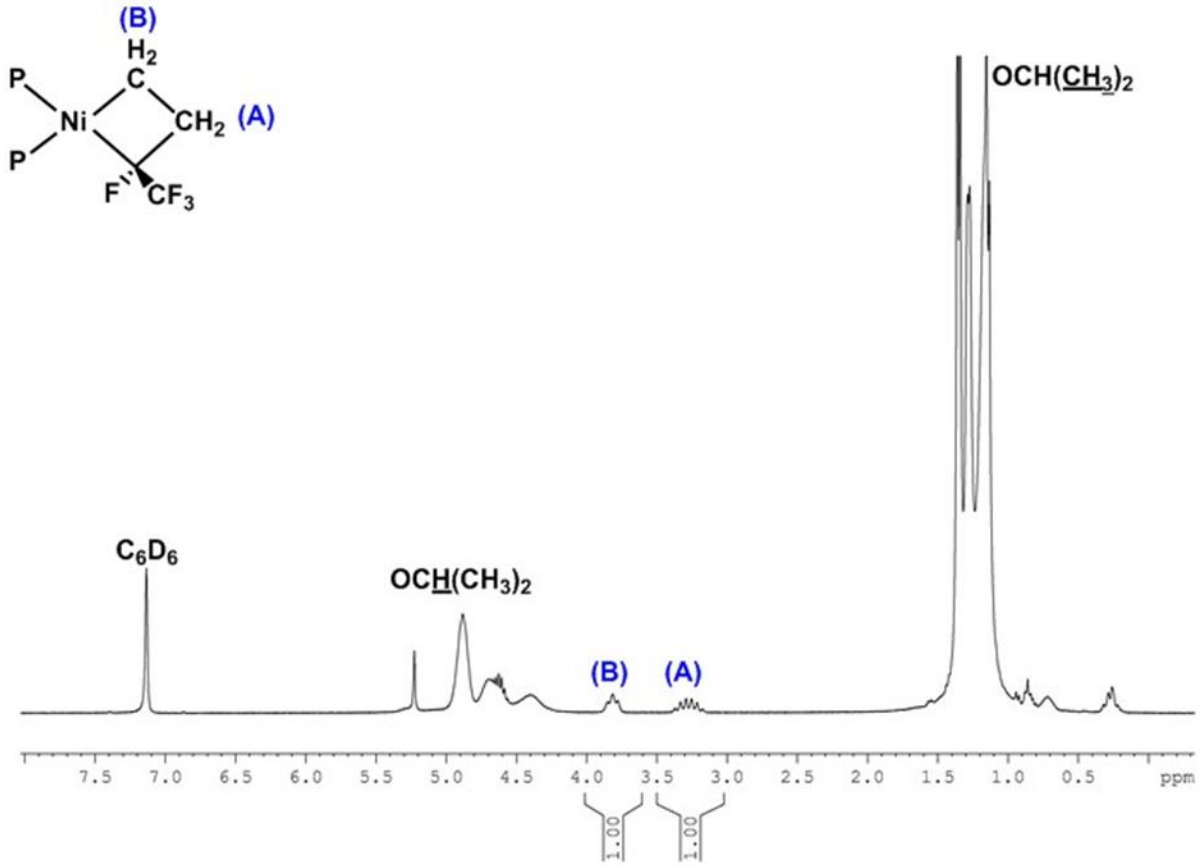

Figure 5.13: ^{1}H NMR of complex **8.**

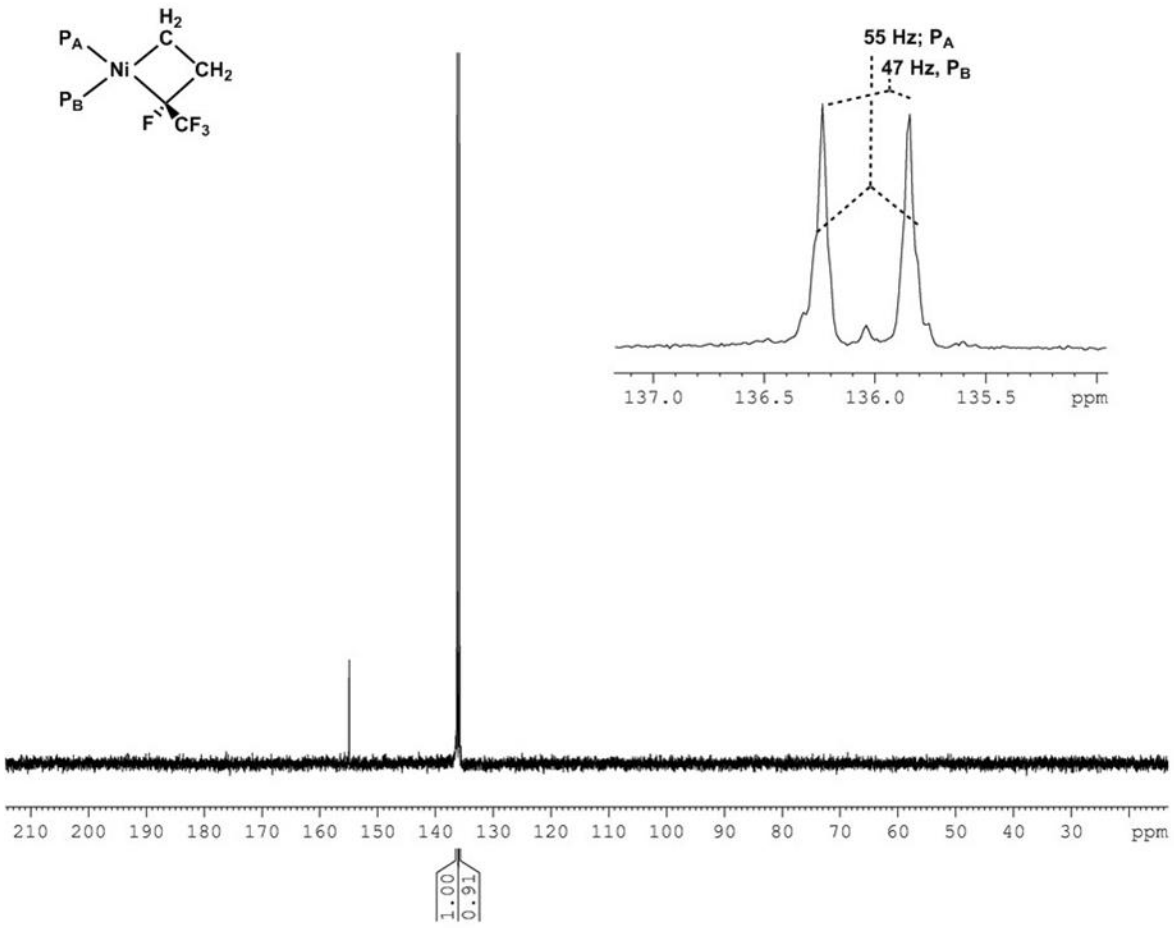

Figure 5.14: ^{31}P NMR of complex **8.**

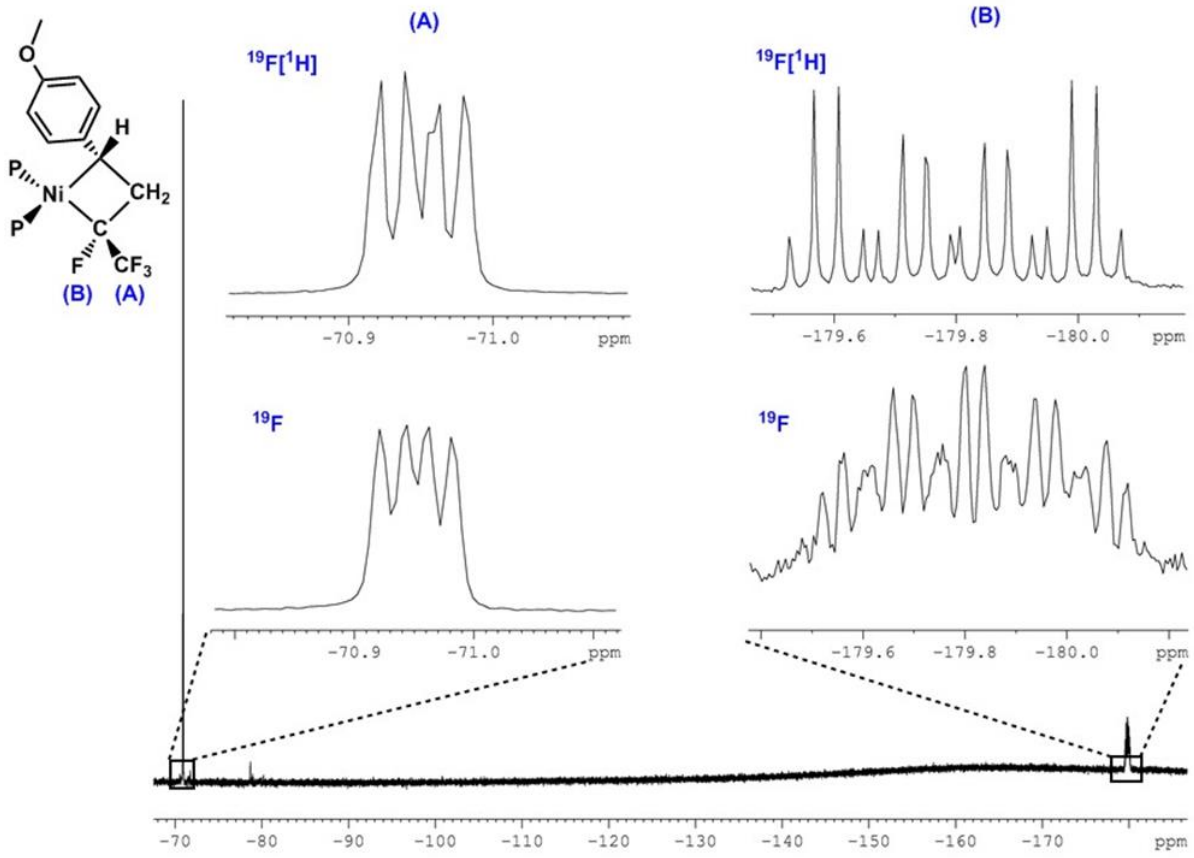

Figure 5.15: Stacked $^{19}F/^{19}F[^{1}H]$ NMR of complex **9.**

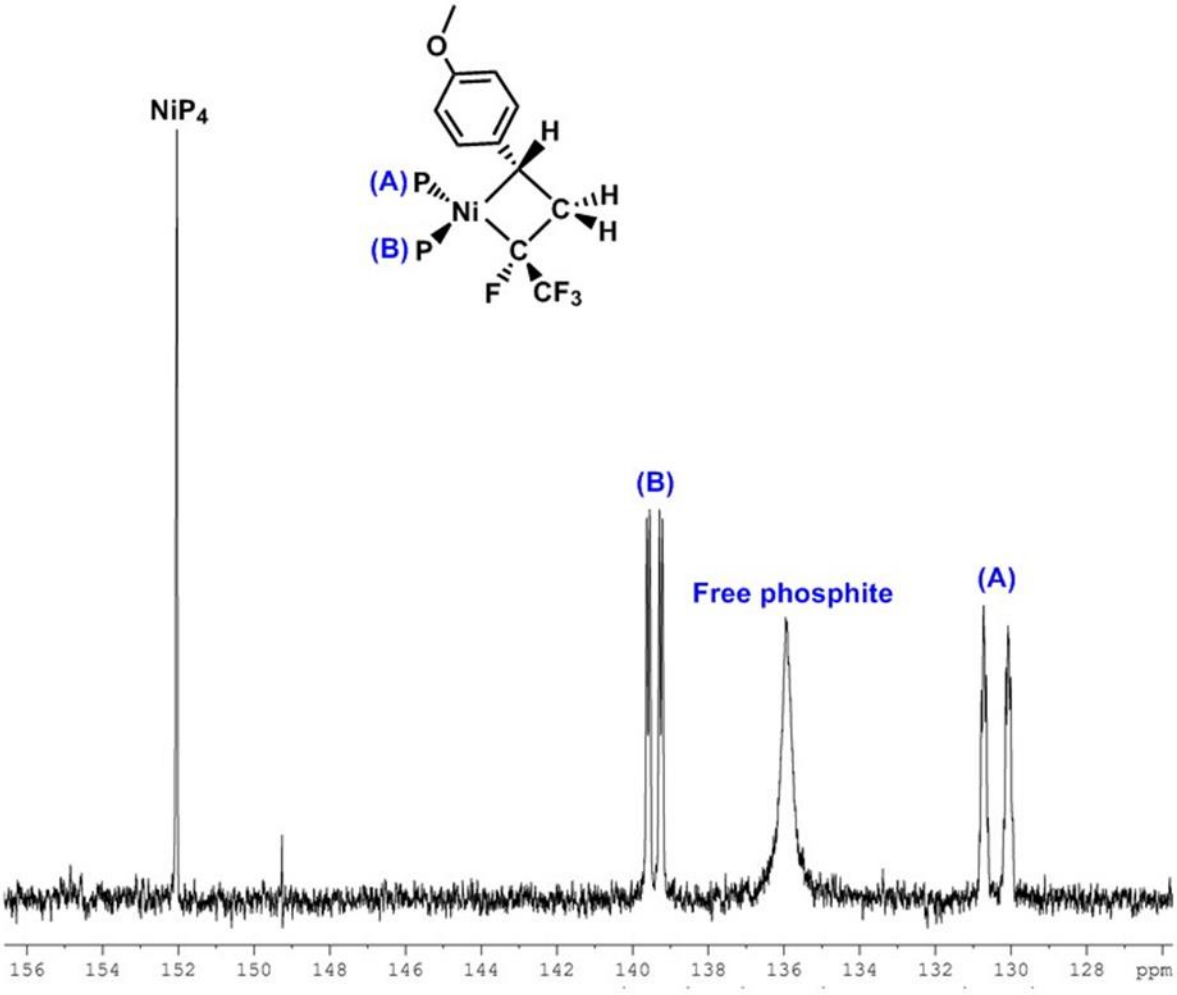

Figure 5.16: ^{31}P NMR of complex **9.**

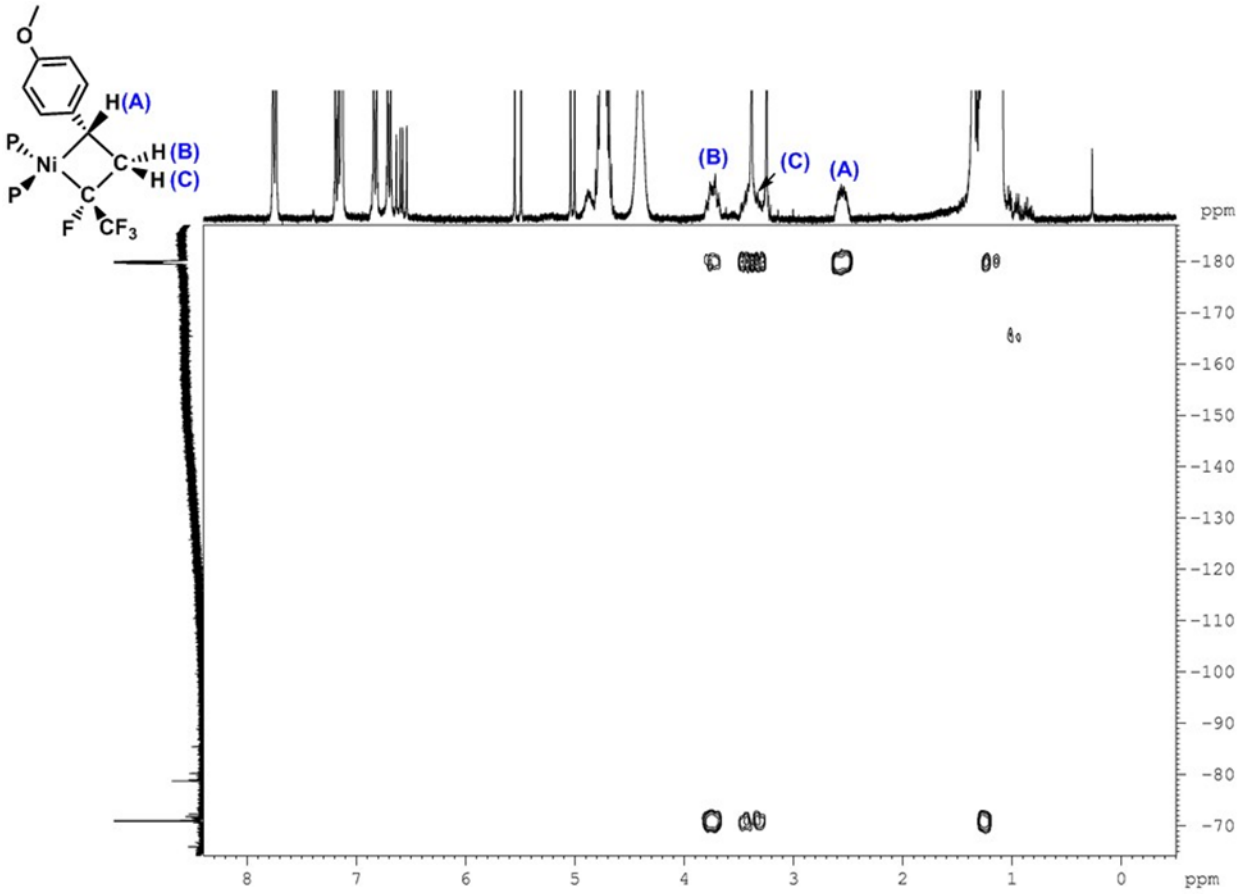

Figure 5.17: HMQC of complex **9** used to discern identity of metallacycle protons.

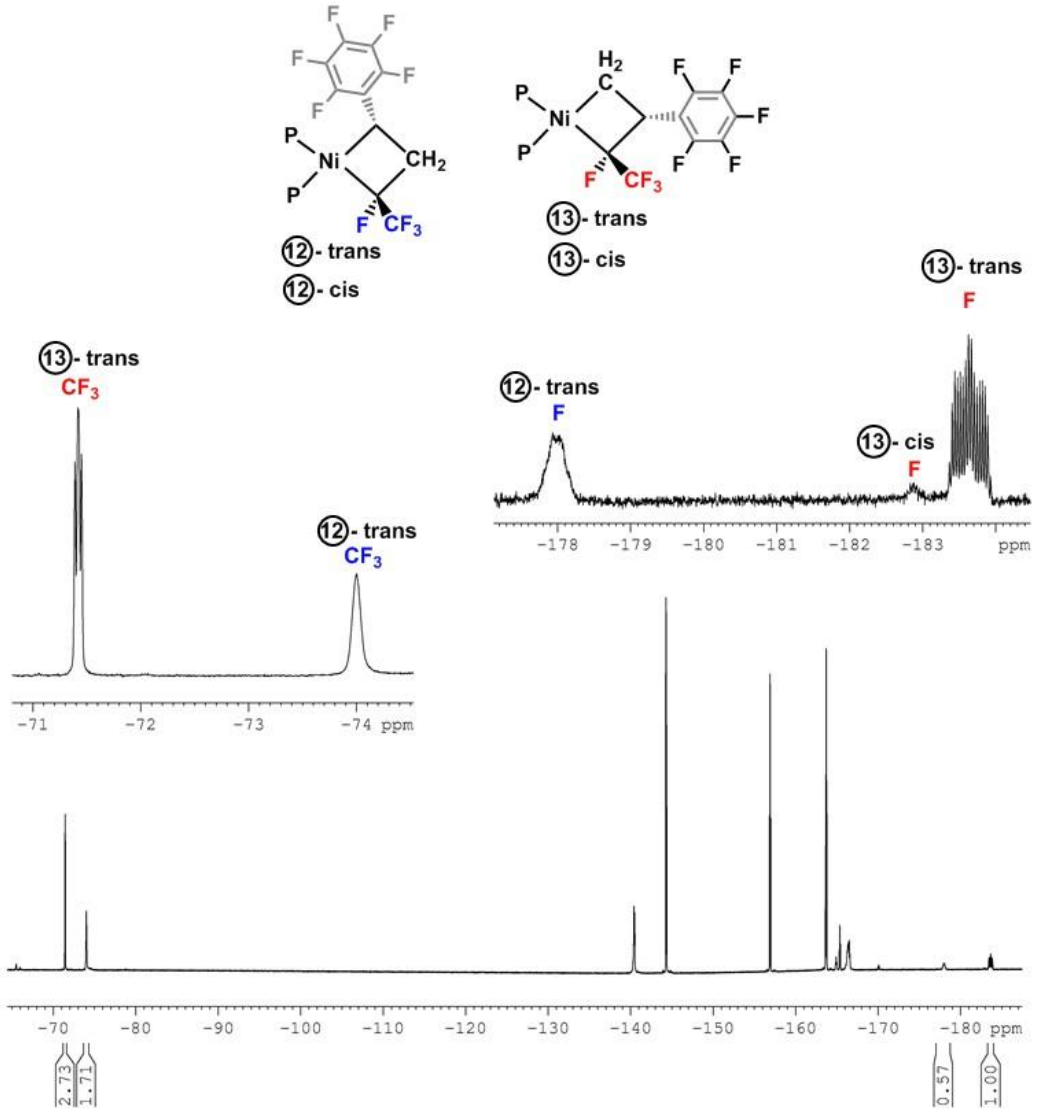

Figure 5.18: ^{19}F NMR of complex **12**, **13**.

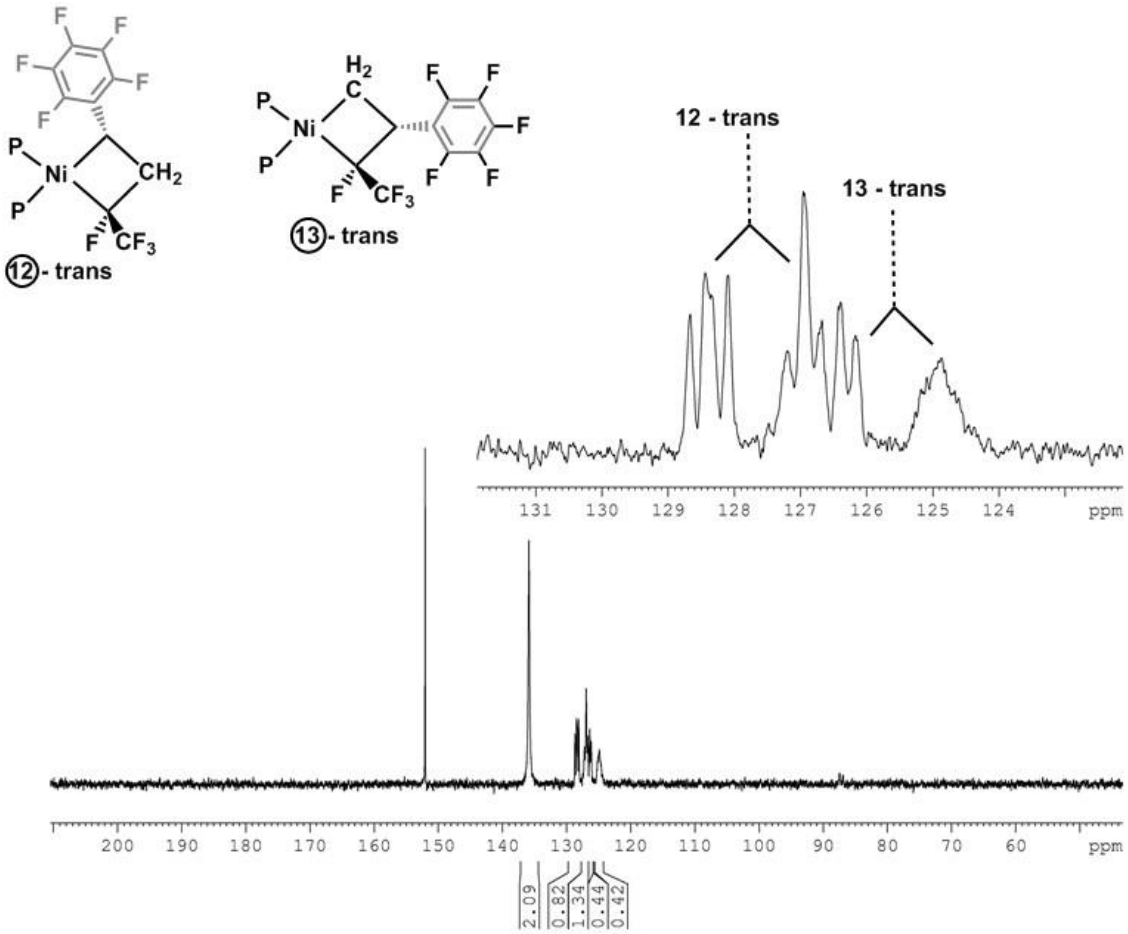

Figure 5.19: ^{31}P NMR of complex **12, 13.**

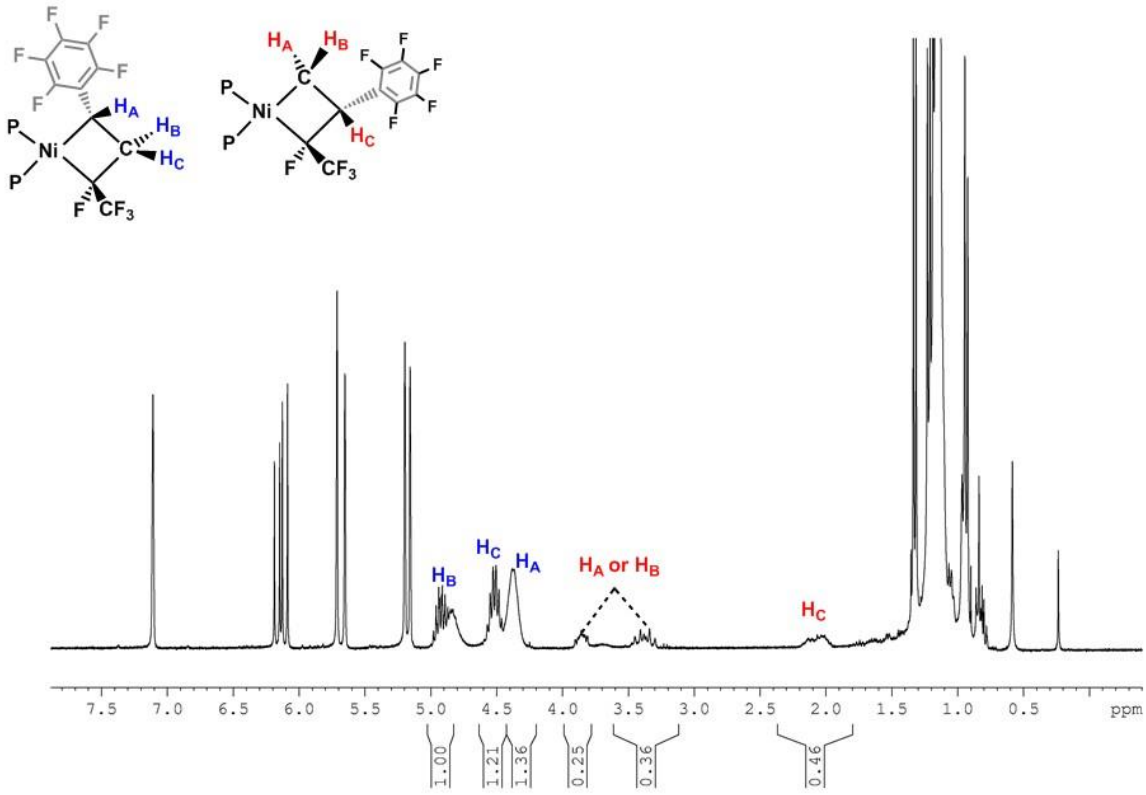

Figure 5.20: ^{1}H NMR of complex **12**, **13**.

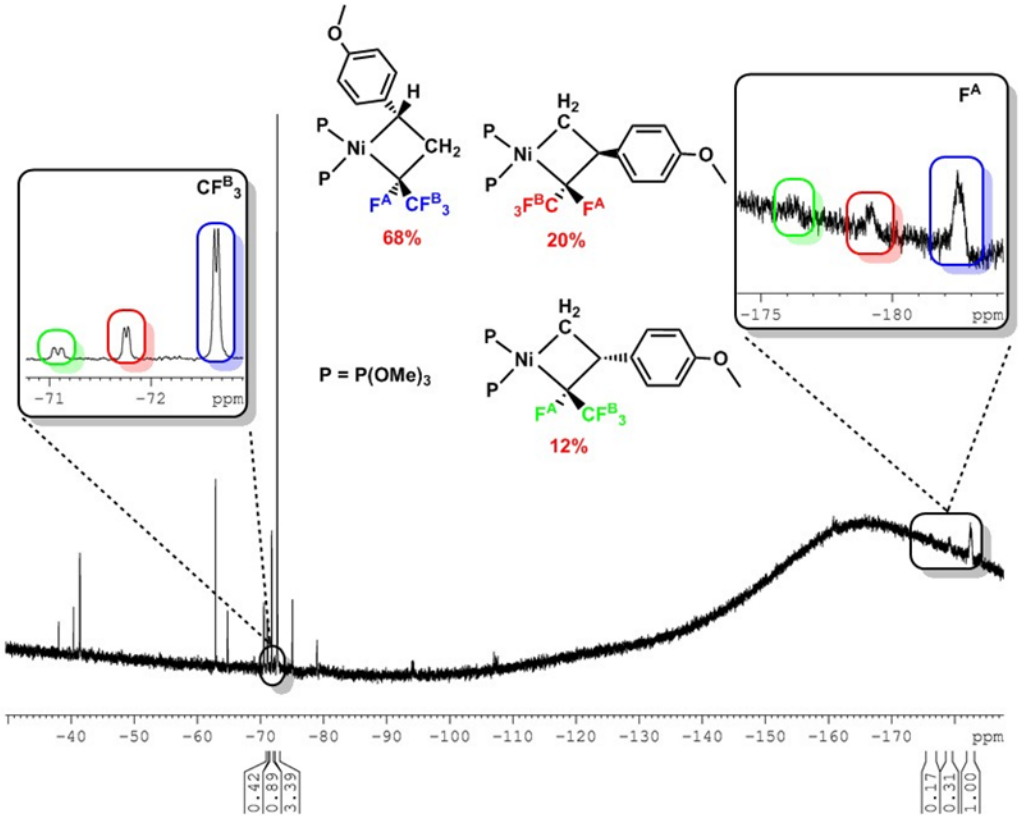

Figure 5.21: ^{19}F NMR of complex **2** reacting with 4-methoxy styrene showing how product distribution is dependent on sterics of ancillary ligands.

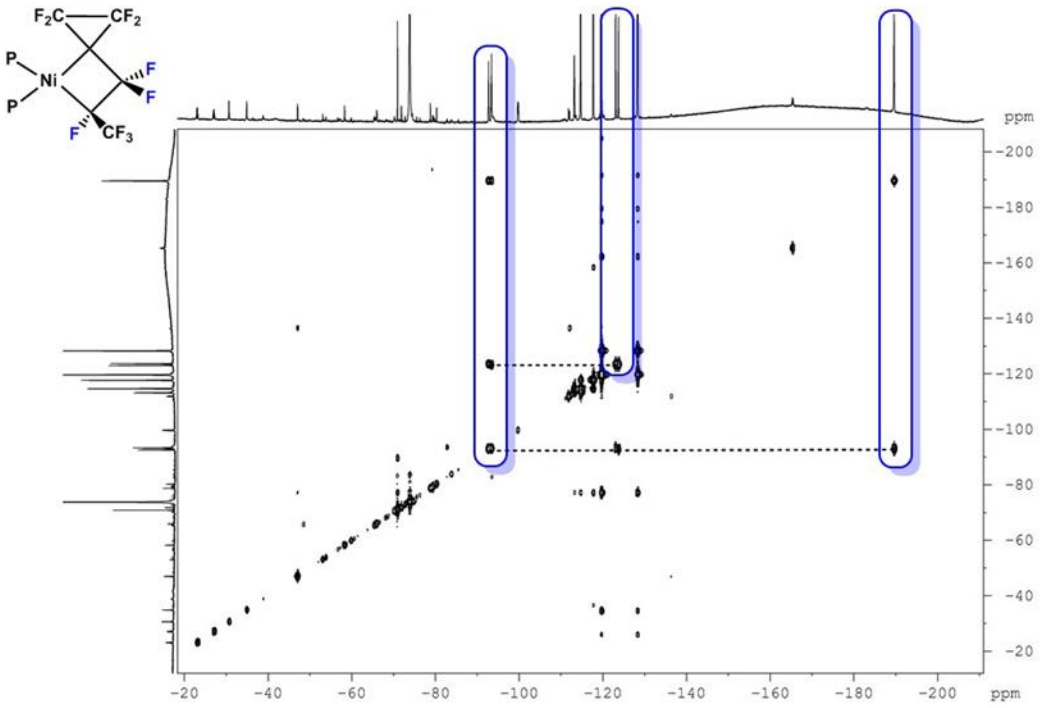

Figure 5.22: ^{19}F COSY showing correlation of α and β C - F of complex **14.**

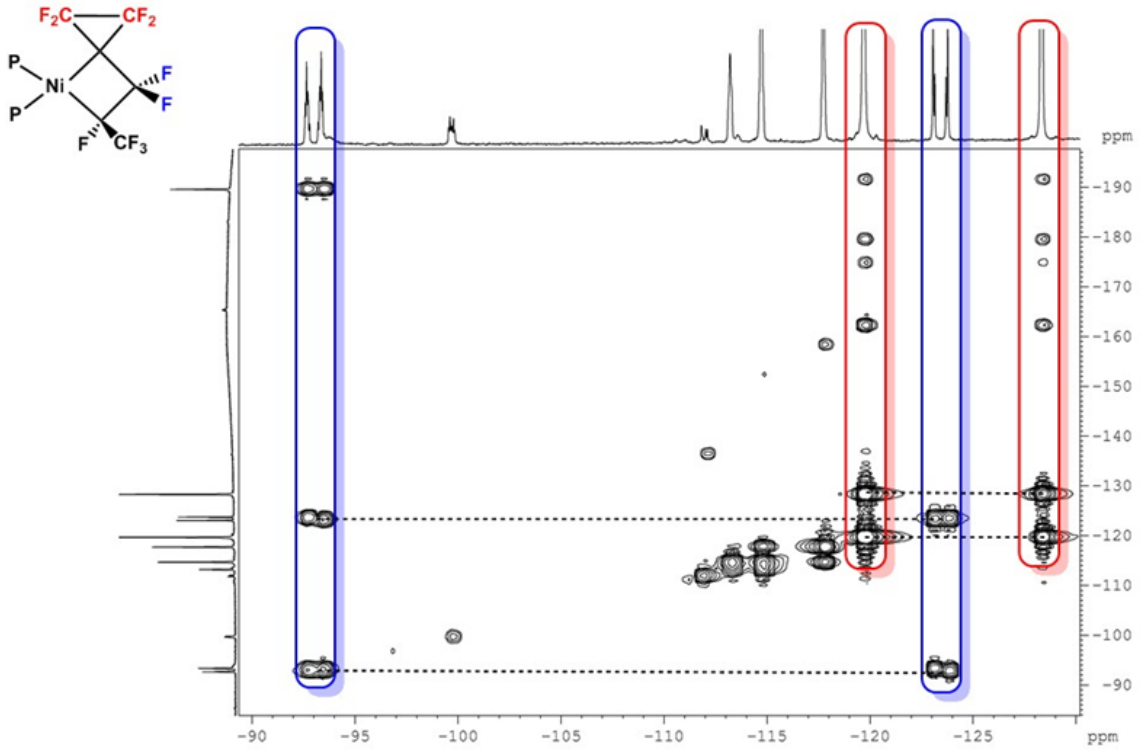

Figure 5.23: ^{19}F COSY showing β-C-F and CF_2 groups' viscinal to spyro-carbon of complex **14**.

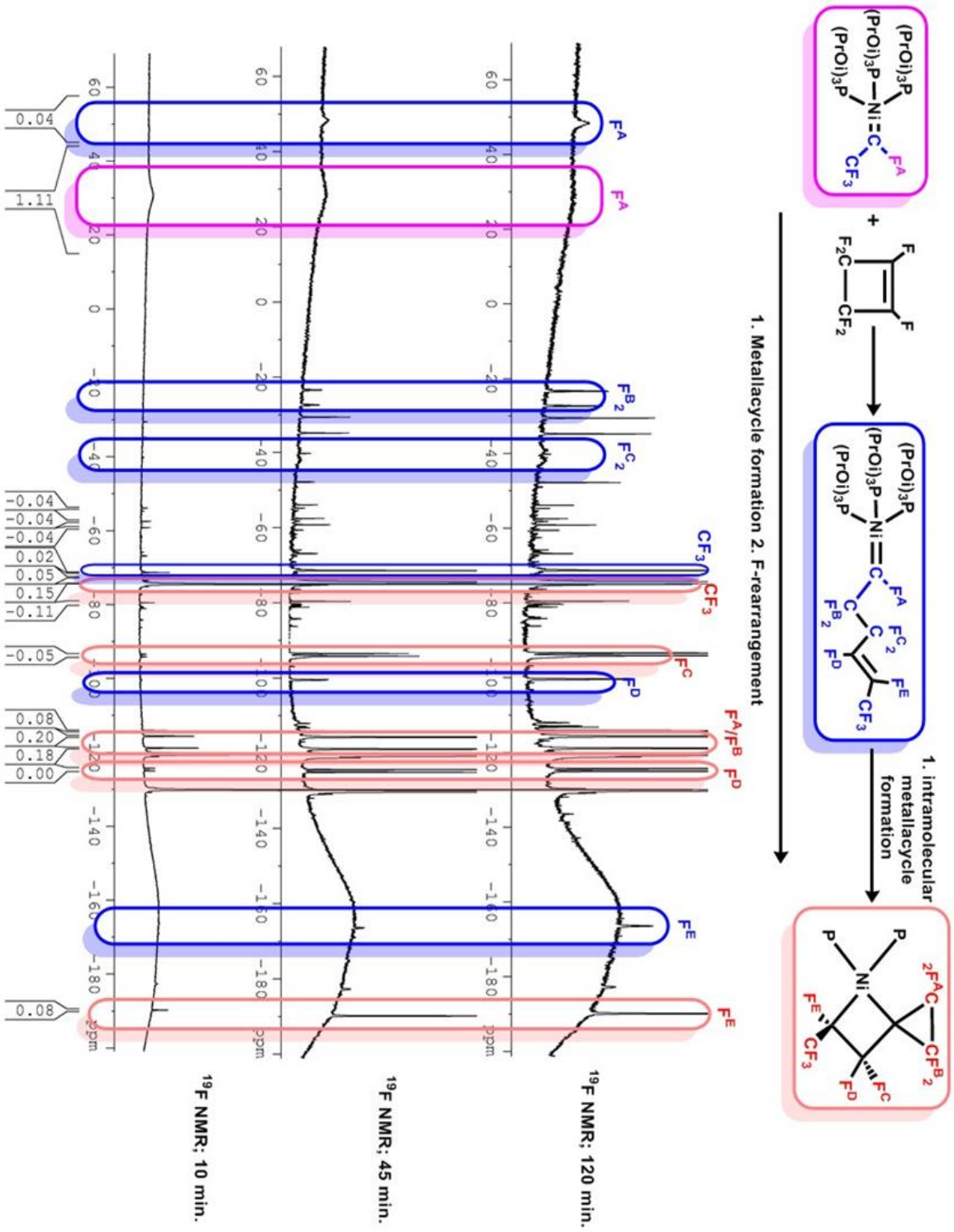

Figure 5.24: Time-resolved ^{19}F NMR of the reaction of **1** with perfluoro-cylobutene showing the formation of a new carbene (possible formation of ring opened carbene intermediate).

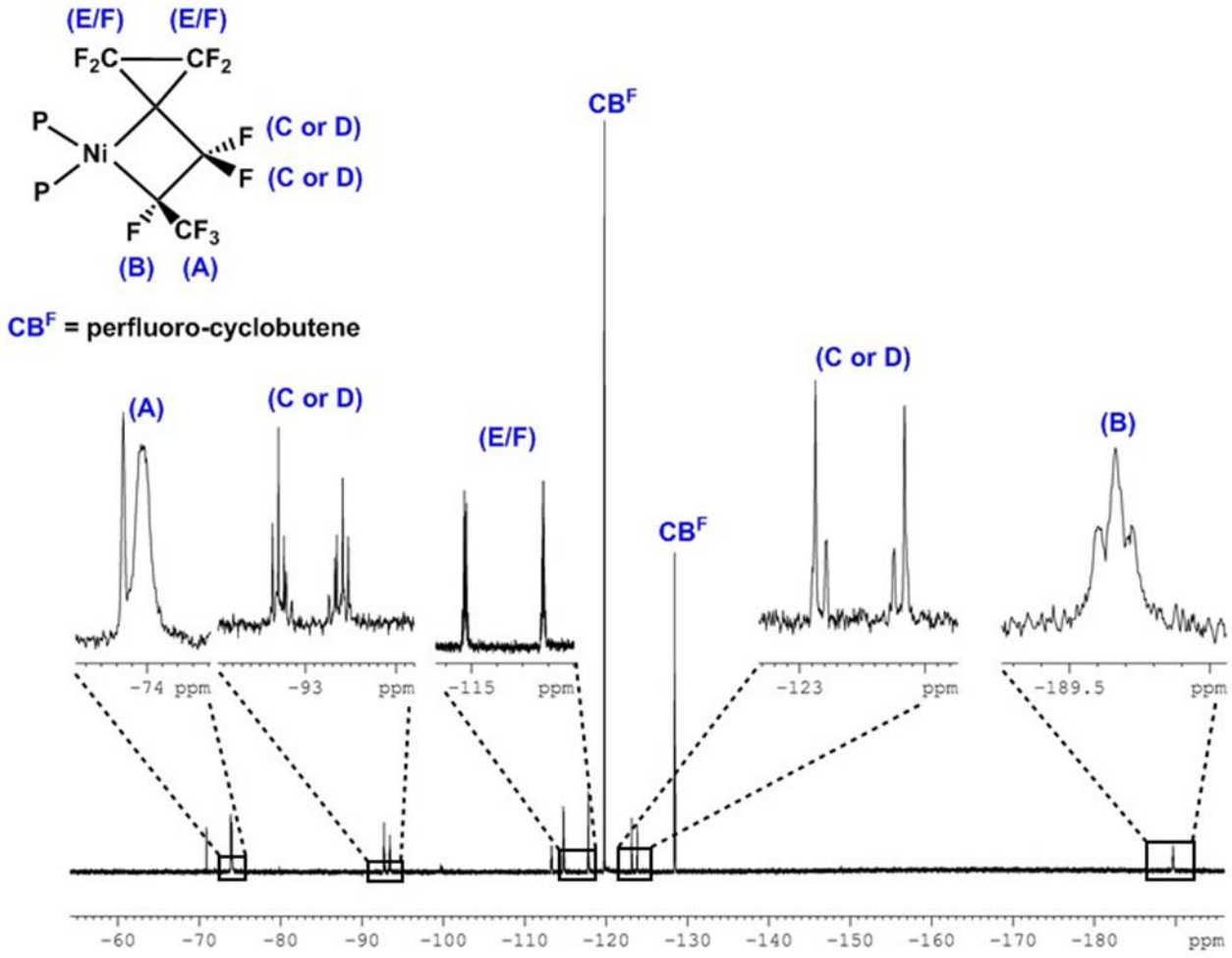

Figure 5.25: ^{19}F NMR of complex **14** with fluorine assignments.

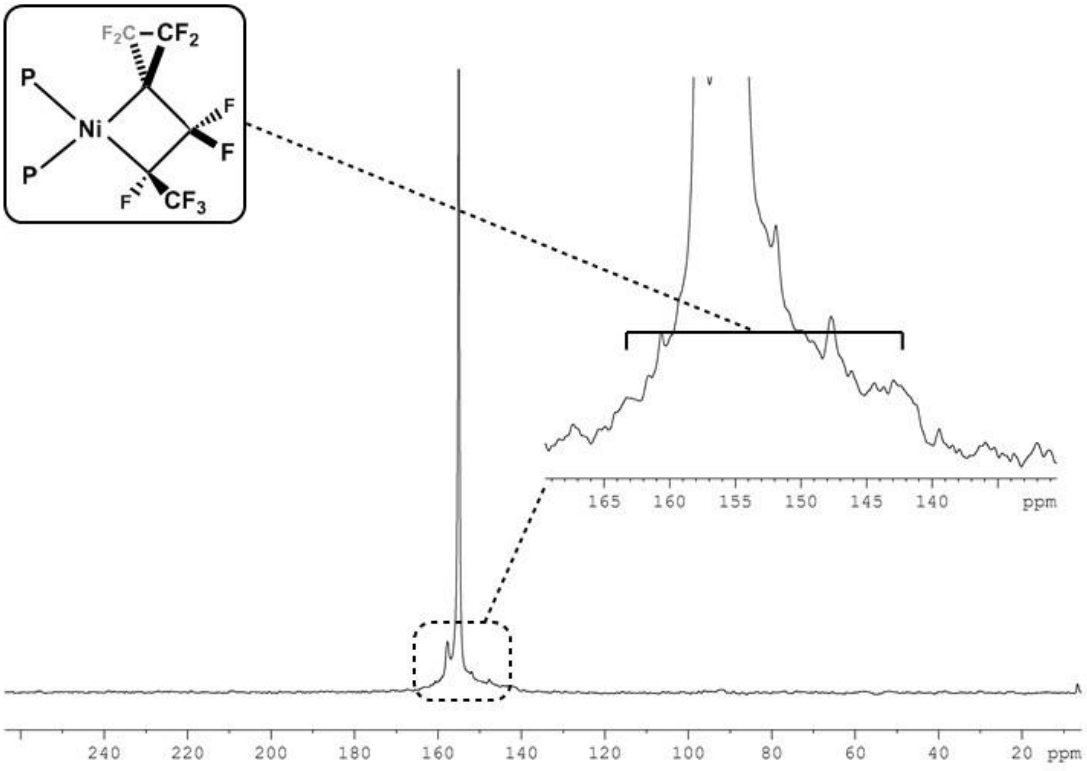

Figure 5.26: ^{31}P NMR of complex **14.**

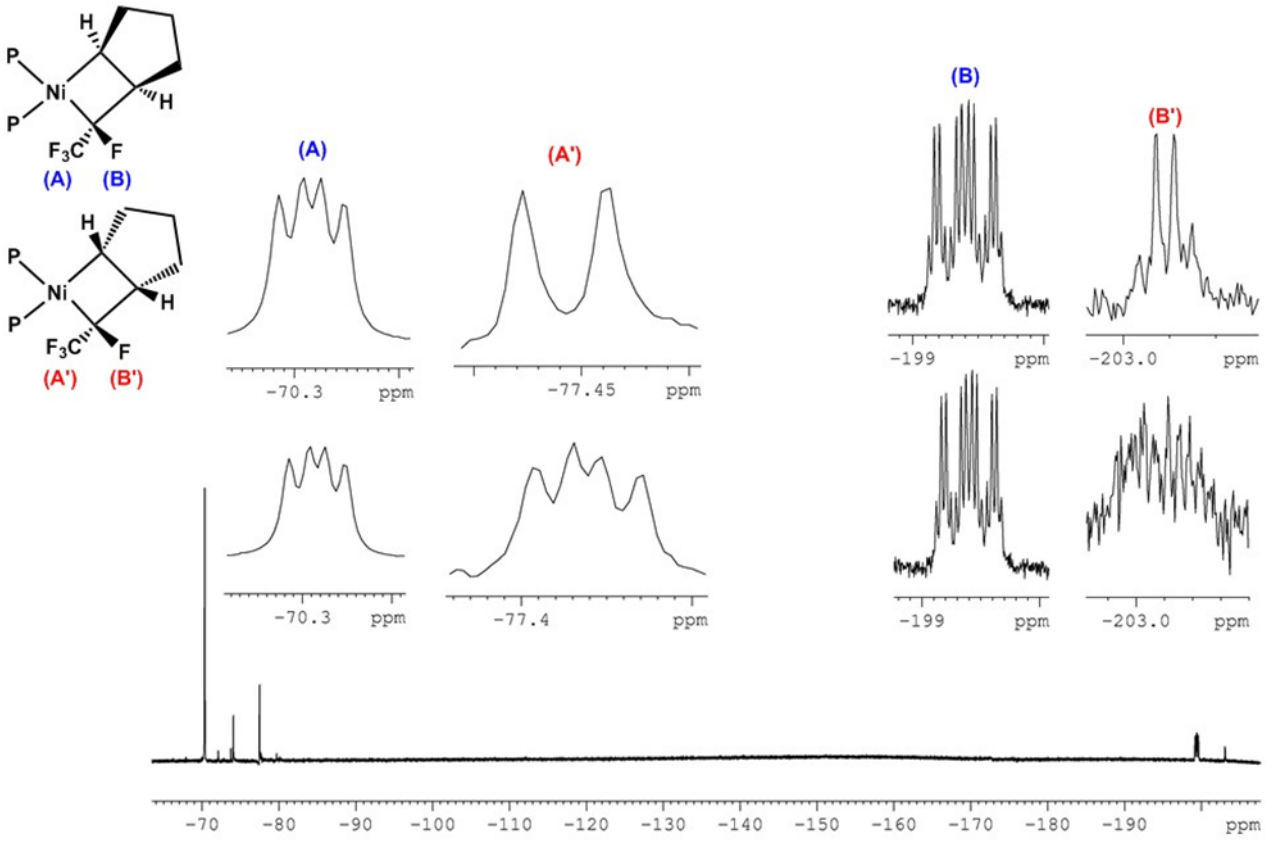

Figure 5.27: Stacked $^{19}F/^{19}F[^{1}H]$ spectra of complex **15** cis/trans.

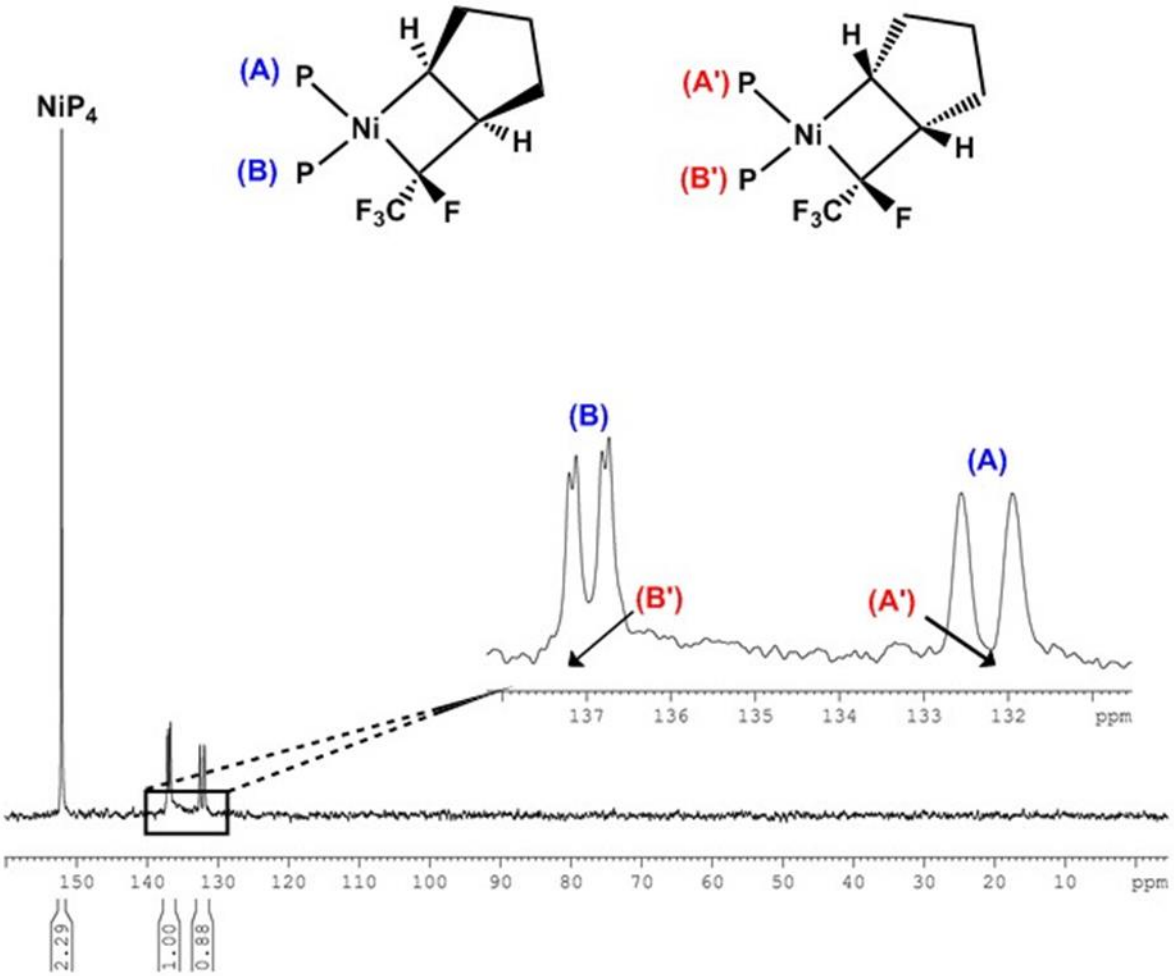

Figure 5.28: ^{31}P NMR of complex **15** cis/trans

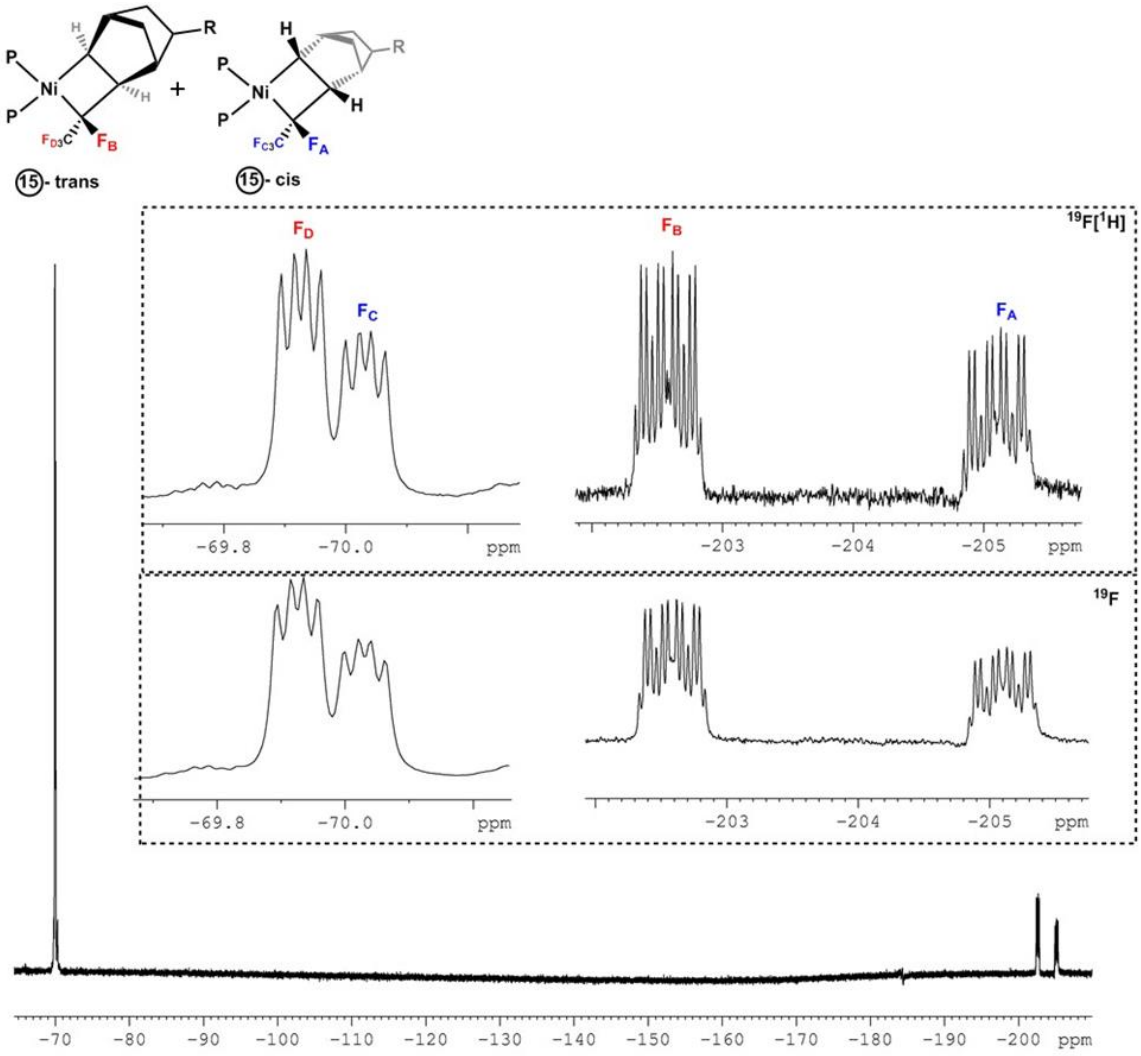

Figure 5.29: Stacked $^{19}F/^{19}F[^{1}H]$ spectra of complex **16**.

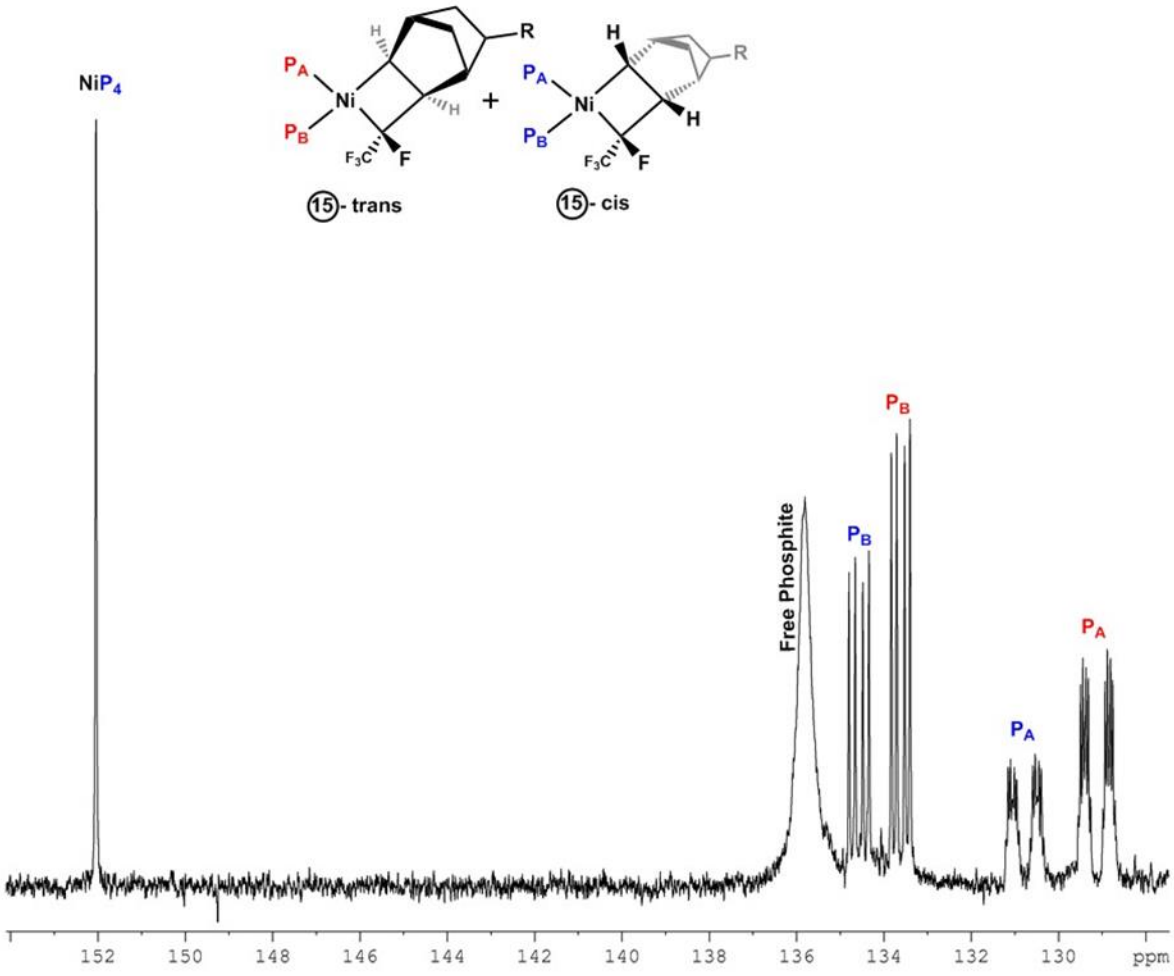

Figure 5.30: ^{31}P NMR of complex **16** with phosphine assignments.

[1] (a) Olefin Metathesis: Theory and Practice; Grela, K., Ed.; John Wiley & Sons: Hoboken, NJ, 2014. (b) Handbook of Metathesis; R. H. Grubbs, Ed.; Wiley-VCH: Weinheim, Germany, 2003

[2] (a) T. M. Trnka, M. W. Day, R. H. Grubbs, Angew. Chem. Int. Ed. 2001, 40, 3441-3444. (b) Y. Takahira, Y. Morizawa, J. Am. Chem. Soc. 2015, 137, 7031-7034. (c) M. J. Koh, T. T. Nguyen, H. Zhang, R. R. Schrock, A. H. Hoveyda, Nature 2016, 531, 459-465. (d) T. T. Nguyen, M. J. Koh, X. Shen, F. Romiti, R. R. Schrock, A. H. Hoveyda, Science 2016, 352, 569-574. (e) M. J. Koh, T. T. Nguyen, J. K. Lam, S. Torker, J. Hyvl, R. R. Schrock, A. H. Hoveyda, Nature. 2017, 542, 80-86.

[3] Poutsma, M. L. The Radical Stabilization Energy of a Substituted Carbon-Centered Free Radical Depends on Both the Functionality of the Substituent and the Ordinality of the Radical. *J. Org. Chem*. **2011**, *76*, 270-276. (b) Zipse H. Radical Stability—A Theoretical Perspective. In: Gansäuer A. (eds) Radicals in Synthesis I. Topics in Current Chemistry, vol 263. Springer, Berlin, Heidelberg

[4] (a) S. F. Yana Motta, E. D. Vera Bercerra, M. W. Spatz, *Analysis of LGWP Alternatives for Small Refrigeration (Plugin) Applications;* International Refrigeration and Air Conditioning Conference; Purdue University: West Lafayette, IN, 2010; Paper 1149. (b) A. Mota-babiloni, P. Makhnatch, R. Khodabandeh, *Intl. J. Refrig*. **2017**, *82*, 288-301. Muller, K., Faeh, C., Diederich, F. Science. 2007, 317, 1881-1886. (c) Jeschke, P. ChemBioChem. 2004, 5, 570-589. (d) Boday, D. J. The State of Fluoropolymers. In Advances in Fluorine Containing Polymers; American Chemical Society: Washington, 2012; Chapter 1, pp 1-5.

[5] S. Fomine, M. A. Tlenkopatchev, *Appl. Catal., A.* **2009**, *355*, 148-155. (b) M. Vasiliu, A. J. Arduengo, III, D. A. Dixon, *J. Phys.Chem. C* **2014**, *118*, 13563-13577.

[6] Harrison, D. J.; Daniels, A. L.; Guan, J.; Gabidullin, B. M.; Hall, M. B.; Baker, R. T. Nickel Fluorocarbene Metathesis with Fluoroalkenes. *Angew. Chem. Int. Ed*. **2018**, *57*, 5772-5776.

---

[7] (a) Harrison, D. J.; Lee, G. M.; Leclerc, M. C.; Korobkov, I.; Baker, R. T. *J. Am. Chem. Soc*. **2013**, *135*, 18296-18299. (b) Fuller, J. T.; Harrison, D. J.; Leclerc, M. C.; Baker, R. T.; Ess, D. H.; Hughes, R. P. *Organometallics*. **2015**, *34*, 5210-5213.

[8] Harrison, D. J.; Daniels, A. L.; Korobkov, I.; Baker, R. T. *Organometallics*. **2015**, 34, 4598.

[9] Frémont, P.; Marion, N.; Nolan, S. P. *Coord. Chem. Rev*. **2009**, *253*, 862-892.

[10] Occhipinti, G.; Jensen, V. R. *Organometallics*. **2011**, *30*, 3522-3529.

[11] Louie, J.; Grubbs, R. H. *Organometallics*. **2002**, *21*, 2153-2164.

[12] Casey, C. P.; Burkhardt, T. J. *J. Am. Chem. Soc*. **1974**, *96*, 7808-7809.

[13] Santamaria, J.; Aguilar, E. *Org. Chem. Front*. **2016**, *3*, 1561.

[14] Louie, J.; Grubbs, R. H. *Organometallics*, **2002**, *21*, 2153-2164.

[15] (a) L. F. Halle, P. B. Armentrout, J. L. Beauchamp, *Organometallics*. 1983, *2*, 1829-1833. (b) For a unique example of apparent Ni-mediated alkene metathesis see: F. G. N. Cloke, P. B. Hitchcock, M. F. Lappert, C. MacBeath, G. O. Mepsted, *J. Chem. Soc., Chem. Commun*., **1995**, 87-88.

[16] Gronert, S.; Keefe, J. R.; More O'Ferral, R. A. Stabilities of Carbenes: Independent Measures for Singlets and Triplets. *J. Am. Chem. Soc*. **2011**, *133*, 3381-3389.

[17] Burch, R. R.; Calabrese, J. C.; Ittel, S. D. *Organometallics*. **1988**, *7*, 1642.

[18] 2D spectra included in supporting information.

6 Synthesis and Reactivity of Mn–CF_3 Complexes

"If I have a thousand ideas and only one turns out to
be good, I am satisfied." ~ Alfred Nobel

6.1 Context

The previous chapters showed that both cobalt and nickel fluorocarbene complexes are capable of reacting with TFE to produce metallacyclobutanes. Our original goal posited that metal-mediated routes towards fluoropolymers may be possible via a Green-Rooney mechanism if a 1,3 fluoride shift could be effected within the metallacycle (i.e. by Lewis acid assistance) (Scheme 3.1; Chapter 3). Unfortunately, our research has shown that the Cβ-F bond is more reactive in these metallacycles and new strategies will be needed to preferentially access Cα-F reactivity. Returning then to the possibility of a fluoro-variant of the Cossee-Arlman mechanism utilizing M–CF_3 complexes, we reasoned that electron-rich Mn(II) complexes may offer the right balance of nucleophilicity (to attract the fluoroalkenes) and weak M-C bond (as Mn(II) has no crystal field stabilization). This chapter focuses on a modified synthesis towards new Mn–CF_3 complexes and their reactivity.

The methods developed in this chapter showcase the first new-examples of manganese trifluoromethyl complexes in over 50 years. These complexes exhibit longer bond-distances than similar Mn–CF_3 carbonyl complexes. For this reason, we were hopeful that with greater electron density and elongated M–CF_3 bonds that these would be ideal candidates towards the coordination and subsequent insertion of a fluoroalkene into this bond producing a growing fluoro-polymer chain. Unfortunately, none of the 4 new manganese trifluoromethyl complexes exhibited any reactivity with TFE. However, cyclic voltammetry did confirm that it may be possible to successfully reduce manganese to a $Mn^{(0)}$-CF_3 complex and abstraction of a fluoride using a Lewis acid led to the first examples of a $Mn^{(I)}$=CF_2 carbene.

6.1.1 Published Contribution

Daniels, A. L.; Da Gama, J. G.; Edjoc, R.; Gabidullin, B. M.; Baker, R. T. *Inorganics*. **2019**, *7*, 3.

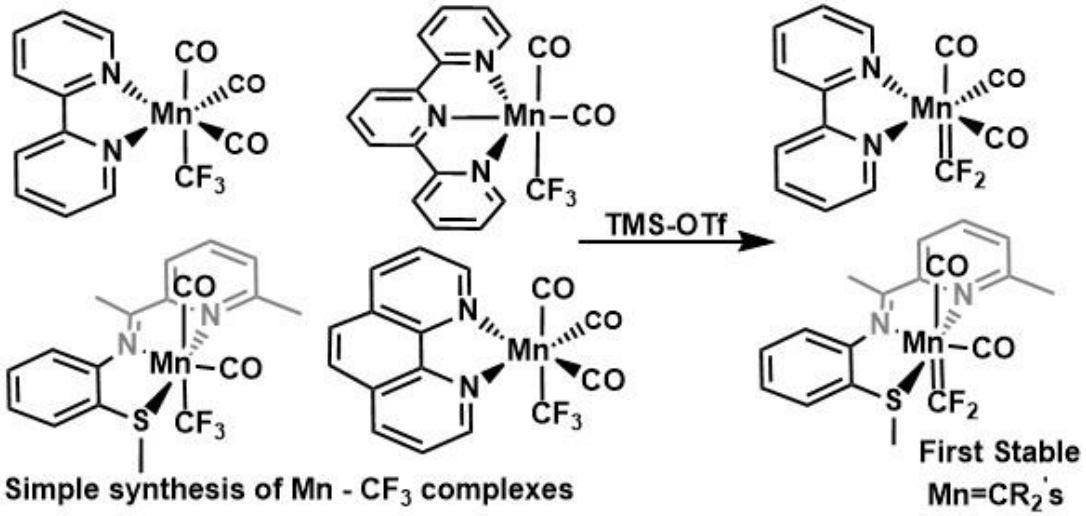

The synthesis, characterization and reactivity of several bi- and tridentate manganese carbonyl trifluoromethyl complexes are presented. These complexes exhibit elongated Mn–C_{CF3} bonds (vs $Mn(CF_3)(CO)_5$), suggesting a lability that could be utilized for the transfer or insertion of the CF_3 functional group into organic substrates. Unlike their Mn-X congeners (X = Cl, Br), these Mn–CF_3 complexes exhibit a preference for hard donor ancillary ligands, thus enabling the synthesis of 4 Mn–CF_3 complexes including a mixed-donor tridentate complex using an NNS Schiff base ([2-(methylthio)-N-(1-(pyridin-2-yl)ethylidene)aniline]). Although we have not yet identified efficient CF_3 transfer reactions, fluoride abstraction from the Mn-CF_3 complexes using trimethylsilyl triflate affords the first stable Mn fluorocarbenes as confirmed by ^{19}F NMR spectroscopy.

Author Contributions: Complex synthesis and characterization were performed by ALD with assistance from undergrads RE and JGD. Manuscript writing and editing were by ALD and RTB. BMG carried out the X-ray diffraction experiments.

6.2 Introduction

Organometallic compounds and especially metal alkyls (M–R) are immensely important players in catalysis.[1,2] Catalysis utilizing metal fluoroalkyl complexes, however, is less common due to the inherent stability of metal perfluoroalkyl bonds (M–R^F).[3,4,5] Nonetheless, these compounds

are useful to the increasingly important field of fluoro-organic synthesis.[6,7,8,9,10, 11,12,13,14] Prominent examples include [Cu]−R^F reagents for stoichiometric perfluoroalkyl transfer to organic substrates[15,16,17,18,19,20] and increasing numbers of transition metal (e.g., Cu, Ni, Pd) catalyzed C−R^F (where R^F is usually CF_3) bond-forming processes,[21,22] which can be used to obtain high-value fluorinated pharmaceuticals and agrochemicals.[6,8,8] One unsolved challenge, however, involves metal-catalyzed polymerization of fluoroalkenes via the Cossee-Arlman mechanism as commonly practiced with metallocene or Ziegler-Natta type catalysts (Scheme 6.1).

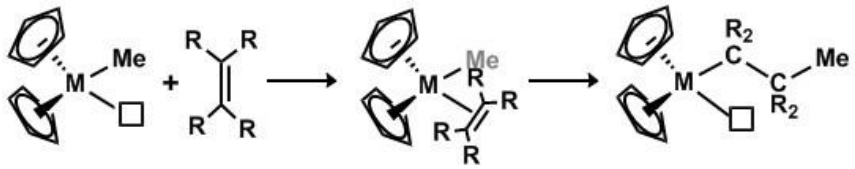

Scheme 6. 1

Early reports of metal-catalyzed alkene polymerization by Ziegler and coworkers using Et_2AlCl have evolved 5 decades later to a *tour de force* of organometallic chemistry with molecular control of polypropylene tacticity, living catalysts for block co-polymer formation, and late metal chain-walking as only three of many highlights.[23,24,25] In contrast, polymerization of fluoroalkenes traditionally utilizes radical processes, either in the gas phase or in aqueous emulsions. [7,26,27,28] As a result, the properties of fluoropolymers can be tuned by altering reaction conditions or changing the relative amounts of co-monomers, while attempts at molecular control have met with little success. Early work by Sianesi and Caporiccio reported the polymerization of hexafluoropropene (HFP) using a traditional Ziegler Natta catalytic system [$(Ti(O^iPr)_4$ + $Al(^iBu)_3$] over 15 days to produce a material thought to be low mol. wt. poly-HFP, but no follow-up investigations have appeared.[29] Similar work utilizing a chromium metallocene catalyst [$(Cr(C_6H_6)_2$] to produce dimers and trimers of HFP[30] purportedly through a metal-mediated process was later suggested to proceed via a soluble source of fluoride ion.[31,32] Finally, research by Kiplinger, Hughes and co-workers demonstrated that decomposition of the shock-sensitive $Cp_2TiF(CF_3)$ complex was capable of producing various insoluble oligomers in which both –(CF_2CF_2)- and –(CF_2CFH)- units were identified. The precise mechanism for the formation of these fluoro-oligomers including whether Ti nano-particles were involved was never determined.[3]

As can be seen from this previous research, metal-mediated formation of fluoro-oligomers and polymers only occurs under unusual conditions. This is certainly not unexpected as the best alkene polymerization catalysts are typically electrophilic. Moreover, attempts to use nucleophilic metal alkyl complexes typically result in stable fluoroalkene complexes that in some cases are better thought of as metallacyclopropanes due to extensive metal to alkene back-bonding. A rare well-characterized example involving insertion of a fluoroalkene into a metal alkyl was reported by Wilford and Stone (Equation 1).[33] Notably, they also observed that further insertion of TFE into the M-R^F bond did not occur.

$$M(CH_3)(CO)_5 + CF_2{=}CF_2 \rightarrow M(CF_2CF_2CH_3)(CO)_5 \quad (M = Mn, Re) \qquad \text{Eq. (1)}$$

Inspired by this work, we hypothesized that the half-filled d shell of a Mn(II) fluoroalkyl complex may contain a weak enough M-C_{RF} bond to allow for multiple alkene insertions. Indeed, Fujisawa, Nubika and co-workers showed that several tris(pyrazolyl)-borate and –methane-ligated $Mn^{(II)}$ halide complexes activated by $Al(i\text{-}Bu)_3$ and $[Ph_3C][B(C_6F_5)_4]$ are effective propylene polymerization catalysts.[34] For insertion of electron-poor fluoroalkenes, however, we would need a neutral Mn(II) complex with strongly electron-donating ligands. Computational studies of M–CF_3 vs. M–CH_3 show that CF_3 groups are significant σ-donors despite being considered a strong electron withdrawing group in organic chemistry. This, combined with their weak π-acceptor attributes, leads to significantly increased electron density on metal centers.[35] This research goes on to mention that while CF_3 groups tend to stabilize the metal d-orbitals, making them less reactive towards electrophiles, only group 7 complexes showed an increase in the overall negative natural charge on the metal center. For this reason we pursued the formation of Mn–CF_3 complexes to determine their reactivity towards fluoroalkenes. As Mn(II) prefers ‘hard’ ligands we initiated our study with typical N-donor ligands. After repeated unsuccessful attempts to install the CF_3 ligand on Mn(II) precursors, we prepared a variety of monovalent $Mn^{(I)}CF_3L_n(CO)_{5-n}$ (n = 1-3; L = bi- and tridentate N-donors) complexes with a view to eventual oxidation to Mn(II).

The few examples of Mn–CF_3 complexes are either derived from the original synthesis of $MnCF_3(CO)_5$, **1**, by McClellan in the 1960’s[36] or from a more recent route involving the treatment of $Mn(CO)_5Br$ with $AgPF_6$ and then $Cd(R^F)_2$ reagents.[37] The first synthesis of **1** involved treatment of $Na[Mn(CO)_5]$ with trifluoroacetic anhydride (TFAA) forming

$Mn(COCF_3)(CO)_5$.[38] Sublimation of this compound at 100°C not only separates it from the $Na[OCOCF_3]$ salt but also partially decarbonylates the Mn-$COCF_3$ unit, yielding a mixture of $Mn(COCF_3)(CO)_5$ and **1**.[39] Intriguingly, further workup was not necessary to form several N-ligated Mn–CF_3 complexes (*vide infra*). Here we report the synthesis characterization and reactivity of these complexes.

6.2.1 Results

Synthesis of $MnCF_3(CO)_5$, 1 Initial attempts at the formation of Mn-CF_3 complexes began with reactions of MnX_2 complexes (X = OAc, Br, Cl) with the Ruppert-Prakash reagent (trifluoro-methyltrimethylsilane [TMS-CF_3] + F^- source) in an attempt to synthesize Mn-CF_3 complexes directly. (Scheme 6.2) Unfortunately displacement of the X group by CF_3 proved difficult. Even after halide abstraction with Lewis acids such as $AgPF_6$, addition of CF_3 anions was unsuccessful. Moving to a Mn(I) source, $(CO)_5MnBr$, allowed for an easy exchange of CO groups with various ligands[40,41,42,43] but displacement of Br with CF_3 again was problematic, even after abstraction with $AgPF_6$.

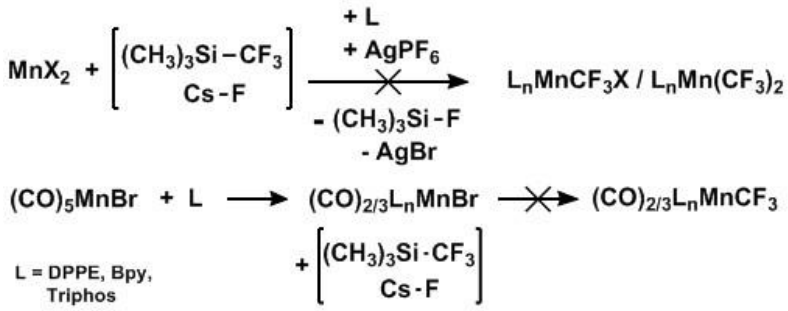

Scheme 6. 2

While we chose to avoid toxic and difficult to prepare $Cd(CF_3)_2$, this may offer an alternate route to Mn-CF_3 complexes with soft donors such as phosphines. Instead, we utilized the carbonyl Mn-CF_3 source, following the report of McClellan.[36] The initially obtained manganese perfluoroacyl/salt mixture was sublimed at 100°C in a static vacuum[39] affording light yellow crystals of $Mn(COCF_3)(CO)_5$ and **1** in a 4:6 ratio (by ^{19}F NMR) in 60% yield based on TFAA. Further workup was unnecessary as we found that ligand substitution on the acyl complex was accompanied by rapid decarbonylation at room temperature.

Substitution reactions of $Mn(COCF_3)(CO)_5$ to form new $Mn^{(I)}$–CF_3 complexes. Attempted reactions of the $MnCF_3(CO)_5$/$Mn(COCF_3)(CO)_5$mixture with various bi- and tridentate P-donor ligands[44] were unsuccessful as soft donor ligands appeared ineffective at displacing the strongly held carbonyls unlike the similar complexes $(CO)_5Mn$–X complexes (X = Br, I, Me) which have a rich coordination chemistry with soft ligands.[41] Hard donor ligands gave moderate success but reactions required harsh conditions (100 °C, 48 h reaction time) to afford partially formed mixtures of starting material and the desired products. As a result, we utilized a known method for the displacement of CO ligands via decarboxylation using trimethylamine N-oxide[45] which yielded relatively pure (≥ 90%) trimethylamine complexes, $Mn(CF_3)(NMe_3)_n(CO)_{5-n}$], **2**, **5** [Scheme 6.3] which were utilized directly for further syntheses. Reaction of **2** with bipyridine

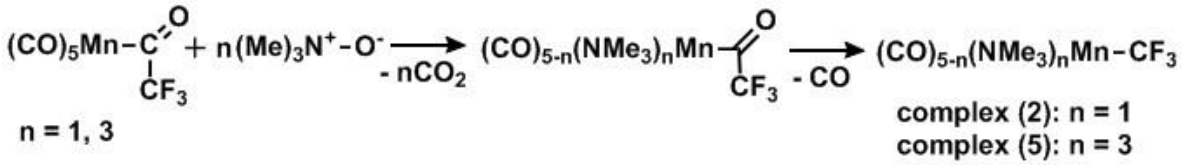

Scheme 6. 3

(Bpy) and phenanthroline (Phen) furnished complexes **3** and **4** respectively (50 °C, 12 h, Scheme 6.4). Formation of tridentate Mn–CF_3 complexes required a modifed synthesis. Three equivalents of Me_3NO were utilized to form $[Mn(CF_3)(Me_3N)_3(CO)_2]$, **5**, in toluene which was then refluxed with terpyridine (Tpy) (19 h, 100 °C) giving **6** in 60% yield.

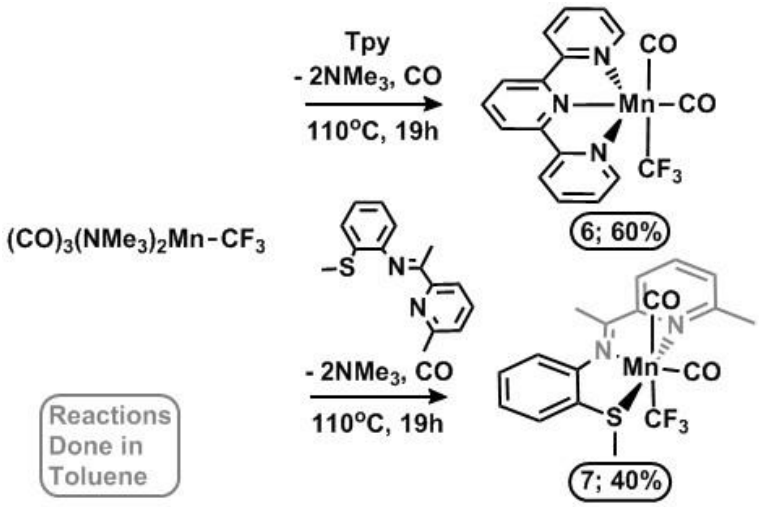

Scheme 6. 4

This method was also utilized with a tridentate mixed-donor NNS Schiff Base [2-(methylthio)-N-(1-(pyridin-2-yl)ethylidene)aniline] [40] to give **7** in 40% yield. (Scheme 6.5) In contrast, reactions of **2** and **5** with soft phosphine ligands gave mixtures of products, again showing the significant effect of the CF_3 group given that Mn–X complexes (X = Br, Cl) readily coordinate soft donors.[41,42,43]

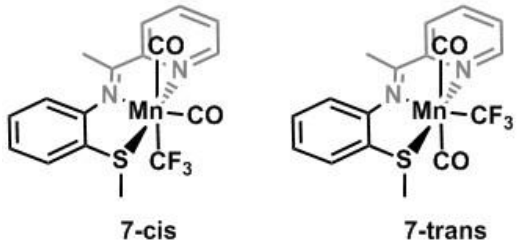

Scheme 6. 5

Solid state structures of new Mn–CF_3 complexes. The molecular structures of **3** and **6** determined by single crystal X-ray diffraction are shown in Figure 6.1 and selected bond lengths are compared to the known $Mn(CO)_5CF_3$ complex in Table 6.1.

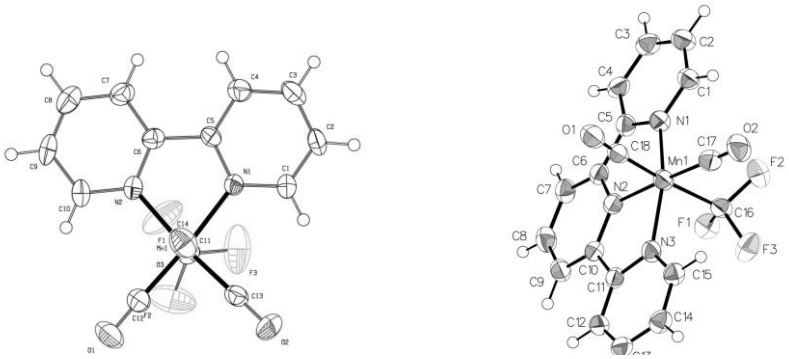

Figure 6.1: ORTEP structures of **3** and **6** with 50% ellipsoids.

Complex	Mn–C_{CF3}	Mn–C_{CO}	Mn-N
$Mn(CO)_5CF_3$ (**1**)	2.056(5)	NA 1.789(5) [cis]	NA
$Mn(CO)_3(Bpy)CF_3$(**3**)	2.039(7)	1.780(7) [cis] 1.823(1) [trans]	2.041(2) 2.034(8)
$Mn(CO)_2(Tpy)CF_3$(**6**)	2.096(1)	1.772(3) [cis] 1.818(9) [trans]	2.021(1),2.025(1) 1.959(2) [N2]

Table 6. 1: Selected bond lengths (Å) for Mn–CF_3 complexes

In both pseudo-octahedral structures, the CF_3 ligand is trans to CO. The elongation of the Mn–C_{CO} bond lengths trans to CF_3 (vs. those that are cis) is consistent with the strong trans influence of the CF_3 group.[4,31,46] The Mn–C_{CF3} bond distance in **3,** however, is significantly shorter than that in **1.** The reasoning for this observation may be due to more significant π-back bonding into the low-lying C–F σ*orbitals as the N-donor ligand adds more electron density to the metal center.[3] Research by Grushin and Macgregor however suggests that M-CF_3 bonding has little to no (< 8%) π-backbonding character. If significant ionic character is invoked for the Mn–C_{CF3} bond then the replacement of 2 CO ligands with 2 hard N donors would decrease the Lewis acidity at Mn increasing its interaction with the partial positive charge of the CF_3 carbon.[3,4] In contrast, the Mn–C_{CF3} bond distance in **6** is significantly *longer* than that in **1** in spite of the additional N-donors and one less CO ligand competing for the metal's π-back-donation. This may be due to more significant π-backbonding to the Tpy[47] and CO ligands which all display shorter bond lengths to Mn than those in **3** (Table 6.1). This would support the ionic interpretation of the bonding between manganese and the trifluoromethyl ligand as electron density is removed from the positive metal center thereby increasing repulsion with the partially positive CF_3 carbon.

NMR data for Mn–CF_3. The solution phase ^{19}F NMR data in CD_3CN for **2** – **4** are consistent with other M–CF_3 complexes (M = Fe, Co, Ni, Mn) with the CF_3 resonance between -15 and -30 ppm. The perfluoroacyl signal at ca. -90 ppm observed for $Mn(CO)_5(COCF_3)$ is not present after addition of any donor ligand that causes room temperature decarbonylation to form Mn–CF_3 complexes. The ^{19}F NMR spectrum of **7** shows two peaks at -19.88 and -20.43 ppm suggesting the presence of two different coordination isomers (presumably with the CF_3 cis- vs. trans- to CO;. Scheme 6.6). The alternate possibility of a hemilabile thioether donor [40] was discounted on the basis of variable temperature ^{19}F and ^{1}H NMR experiments that showed no changes in the intensities of the Mn–CF_3 or S-Me and N=C(CH_3) peaks, respectively. Addition of a coordinating solvent such as CD_3CN also had no effect on the integration of these resonances. The ^{19}F and ^{1}H NMR spectra for all Mn–CF_3 complexes are characteristically broad due to the 100% abundance of the quadrupolar ^{55}Mn nucleus[48] and ^{55}Mn NMR signals were not observed, presumably due to excessive quadruploar broadening.

IR data. Selected FT-IR data are listed in Table 6.2. As expected, the CO stretching frequencies shift to lower energies with increasing σ-donor strength of the ancillary ligands/electron density

on the metal centers, reaching a maximum electron density for the $MnCF_3(CO)_2(Tpy)$ and Mn(NNS)- $(CO)_2CF_3$ complexes. Again, ionic bonding in complex **6** could explain the longer M–C_{RF} bond distance despite having more electron density on the metal as discussed by Hughes.[4]

Complex	CO stretching frequencies (cm^{-})
$MnCF_3(CO)_5$ (**1**)	2140, 2040, 2010
$MnCF_3(Bpy)(CO)_3$ (**3**)	2020, 1910
$MnCF_3(CO)_3(Phen)$ (**4**)	2010, 1930
$MnCF_3(CO)_2(Tpy)$ (**6**)	2020, 1900, 1850
$MnCF_3(CO)_2(NNS)$ (**7**)	2020, 1910, 1900

Table 6. 2: Selected CO stretching frequencies for Mn–CF_3 complexes

Cyclic voltammetry data. Cyclic voltammetry (CV) was employed to determine if the Mn–CF_3 complexes could be successfully oxidized or reduced without decomposition. Complexes **3**, **4** and **7** were all subjected to CV between -2.5 and 2.5 V in a THF/electrolyte solution (0.1 M $[(Bu)_4N][BF_4]$ supporting electrolyte) with ferrocene as a reference. The cyclic voltammograms of **3**, **4** and **7** exhibited irreversible oxidation waves at 0.64 V, 0.66 V and 0.53 V (vs. ferrocene) respectively even when faster sweep rates (200 mV/s) were utilized. This suggests that the complexes decompose when oxidized from Mn(I) to Mn(II), most likely due to the loss of CO ligands by the coordinatively labile high spin d^5 complex due to the absence of ligand field stabilization. However, each of these complexes showed a quasi-reversible reduction at approximately -2.2 V.[49] Slower sweep rates of 50 mV/s were used to probe the stability of these reduced complexes and the quasi-reversible waves remained, suggesting the formation of stable $Mn^{(0)}$ species.

Mass spectrometry. Electron impact mass spectrometry (EI-MS) was attempted on complexes **3**, **4**, **6** and **7.**[50] Complexes **6** and **7** were too unstable to provide a useful MS spectrum but complexes **3**and **4** gave consistent fragmentation patterns suggesting the presence of the parent ions. The fragment observed for **3** was $[(N\text{-}N)(F)Mn{=}CF_2]^+$ (280.00375 Da, 0.2% int.; N-N = Bipy) derived from loss of all CO ligands followed by intramolecular α-F abstraction by the now

electron-rich Mn center. This was corroborated by the presence of both $[(N\text{-}N)Mn–CF_3]^+$ (303.99905 Da, 0.1 % int.) and $[(N\text{-}N)Mn–F]^+$ (254.00625 Da, 2.25% int.){N-N = Phen} fragment ions in the EI-MS of **4**.[51]

Reactivity. Due to the successful insertion of tetrafluoroethylene ($CF_2=CF_2$; TFE) into Mn–H and Mn–CH_3[33] and encouraged by the elongated M–CF_3 bonds possessed by our new complexes, we pursued reactions with fluoroalkenes such as vinylidene fluoride ($CF_2=CH_2$; VDF) and TFE. Unfortunately, even under 5 bar of VDF and higher temperatures (80^{o}C), these reactions failed to produce the desired insertion products. At first it was suspected that this may have been due to the inability to dissociate one of the remaining CO ligands, thus preventing coordination of the fluoroalkenes. For this reason we moved to the NNS complex **7** where displacement of the soft donor thiol group may allow for the coordination of olefins. This complex was still unable to coordinate the fluoroalkenes (TFE, VDF) even under forcing conditions. Attempts to labilize the CO ligands by oxidizing **3**/**4** to $Mn^{(II)}$ complexes utilizing $[Fe(Cp)_2][BF_4]$ was successful, but without crystal field stabilization, the newly formed high-spin d^5 Mn complex decomposed to form $[(N\text{-}N)_3Mn][BF_4]_2$ and other unidentified $Mn^{(II)}$ complexes as confirmed by cyclic voltammetry (*vide supra*). Additionally, as M–CF_3 complexes are known to stabilize higher oxidation states, we attempted to form Ar–CF_3 compounds through oxidative addition of Ar–I and subsequent reductive elimination of the desired compounds. However, reactions of aryl halides with complexes **3,4,6,7** showed no change by ^{19}F NMR regardless of reaction temperature or solvent.[52]

Finally, we investigated fluoride abstraction with a Lewis acid. Previous research invoked the formation of Mn=CF_2 carbenes as intermediates in C-halide exchange reactions but the $Mn(CO)_5$ unit was unable to stabilize the electron deficient CF_2 group.[53,54] In contrast, addition of trimethylsilyl triflate (TMS-OTf) to complex **4** gave a color change within minutes and the ^{19}F NMR spectrum revealed new resonances at 155.5 and 156.3 ppm suggesting formation of the first stable Mn=CF_2 carbene complex, cis/trans-{[(Phen)$(CO)_3$Mn=CF_2][OTf]}, **8** (Scheme 6.6). Given that this new carbene is cationic it is assumed that it will be strongly electrophilic unlike previous examples that our group has reported.[55,56,57]

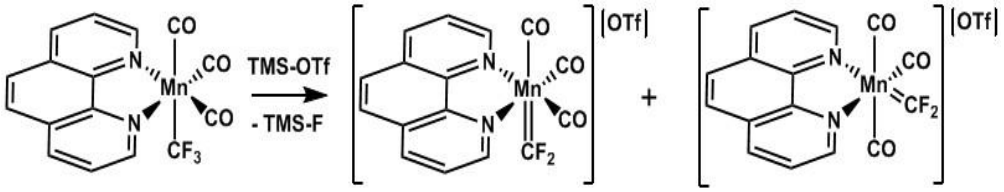

Scheme 6. 6

The above transformation serves as a general preparative method using various Mn-CF_3 complexes as ^{19}F NMR spectra revealed the formation of new carbenes (as isomeric mixtures) when complexes **3, 4** and **7** were subjected to fluoride abstraction via TMS-OTf.[58] Unfortunately, even with multiple N donors the carbene complexes tended to decompose over 24 h at room temperature, precluding us from obtaining elemental analyses. Given the rarity of first-row metal fluorocarbenes, preliminary reactivity studies were undertaken with ethylene. Monitoring the reaction of complex **8** with ethylene by ^{19}F NMR showed complete consumption of the carbene after 12 h at room temperature. Although several new resonances were observed, none could be assigned to the expected cyclopropanation product.[59,60] X-ray quality crystals obtained from the reaction solution revealed a new divalent product, $Mn(Phen)_2(OTf)_2$, **9** (Figure 6.2). Details of this redox reaction are as yet unclear and further reactivity investigations of **8** are underway.

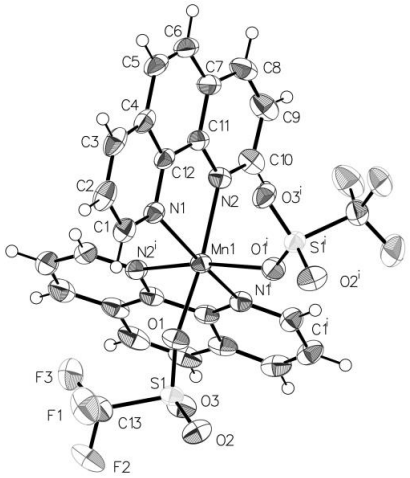

Figure 6.2: ORTEP structure of $Mn(Phen)_2(OTf)_2$, **9** (Mn-N1 = 2.2262, Mn-N2 = 2.2397 Å) with 50% ellipsoids.

6.2.2 Discussion/Conclusion

In summary, we have described a convenient synthesis for various bi- and tri-dentate N-ligated Mn–CF_3 carbonyl complexes in adequate to good yields. Our synthesis avoids the use of hazardous reagents such as $Cd(CF_3)_2$ used previously for the synthesis of $L_n(CO)_{5-n}Mn\text{-}CF_3$ {L = MeCN} complexes.[37] This will allow for more in depth computational/experimental studies of Mn–CF_3 electronic structure/reactivity. The structural data of these complexes show an unusual

elongation of the Mn–CF_3 bond when utilizing the terpyridine ligand and this may open the door towards CF_3 insertion or transfer utilizing similar ancillary ligands. Additionally, this publication has shown that Mn-CF_3 complexes undergo facile fluoride abstraction utilizing Lewis acids such as TMS-OTf to form hitherto unknown Mn=CF_2 carbenes. These cationic, presumably electrophilic carbenes react with electron-rich olefins and further reactivity studies are in progress.

6.2.3 Materials and Methods

General Procedures. Experiments were conducted under nitrogen, using Schlenk techniques or an MBraun glovebox. All solvents were deoxygenated by purging with nitrogen. Toluene, hexanes, diethyl ether (DEE), and tetrahydrofuran (THF) were dried on columns of activated alumina using a J. C. Meyer (formerly Glass Contours) solvent purification system. Dichloromethane (DCM) and $CDCl_3$ were dried by refluxing solution over calcium hydride (CaH_2) followed by distillation. C_6D_6 was dried over activated alumina (heated at 300 °C > 8 h under vacuum) (∼15 wt %). All solvents were stored over activated (heated at 250 °C for > 6 h under vacuum) 4 Å molecular sieves. Glassware was oven-dried at 150 °C for > 2 h. The following chemicals were obtained commercially: $Mn_2(CO)_{10}$ (Strem, 98%), trifluoroacetic anhydride (Aldrich, >99%), 2,2'-bipyridine (Strem, 98+%), 1,10-phenanthroline (Strem, anhydrous 99%), 2,2':6',2''-terpyridine (Aldrich, ≥98.5, trimethylsilyl triflate (Aldrich, 98%), C_6D_6/$CDCl_3$/CDCN (Cambridge Isotope Laboratories, d-99.5%). $Mn(CO)_5CF_3$ and the NNS ligand were prepared following literature procedures.[36,40] ^1H, ^{19}F, and $^{31}P\{^1H\}$ NMR spectra were recorded on 300 MHz Bruker Avance or AvanceII instruments at RT (21−23 °C). ^1H NMR spectra were referenced to the residual proton peaks (C_6D_6: 7.16 ppm; $CDCl_3$: 7.26 ppm). ^{19}F NMR spectra were referenced to internal 1,3-bis(trifluoromethyl)-benzene (BTB) (Aldrich, 99%), set to −63.5 ppm. ^{19}F NMR yields were calculated from product integration relative to a known quantity of BTB using 9 s delay times. $^{31}P\{^1H\}$ NMR data were referenced to external H_3PO_4, set to 0.0 ppm. IR data were obtained on a Nicolet NEXUS 670 FT-IR spectrometer using neat/solid samples by allowing a DCM solution of compounds **3,4,6,7** to evaporate on a NaCl plate under a stream of nitrogen. Elemental analyses were performed at the University of Ottawa. Electrochemical measurements were performed using a Princeton Applied Research (PAR) VersaSTAT 3 potentiostat/galvanostat/frequency response analyzer and V3-Studio electrochemical software version 1.0.281 (2008) (PAR) employing a three compartment glass

cell containing a 5 mmol THF/electrolyte solution of each complex (0.1M $[(Bu)_4N][BF_4]$). Mass spectroscopy was performed on a Kratos Analytical – Concept Magnetic sector Electron impact mass spectrometer.

Modified Synthesis of $MnCF_3(CO)_5$/$Mn(COCF_3)(CO)_5$.(1) Synthesis followed the procedure of McClellan and co-workers[36] but the complex was not further purified. All following preps utilized this starting material as a mixture of $MnCF_3(CO)_5$ and $Mn(COCF_3)(CO)_5$after sublimation. The complexes decarbonylated spontaneously following association of the N-donor ligand.

Synthesis of $MnCF_3(CO)_{5-n}(NMe_3)_n$ intermediates, n = 1 (2) and 3 (5). Me_3NO ([34 mg x n]; n = 1 or 3) was combined with a THF solution (3 mL; Preps **3** and **4**) or toluene (3 mL; Preps **6** and **7**) of $MnCF_3(CO)_5$/$Mn(COCF_3)(CO)_5$ (100 mg, 0.38 mmol) [Note: if the solids are combined without solvent a reaction occurs decomposing the two starting materials] once combined the solution changed colour from light yellow to orange and significant gas release was observed. The solution was stirred for 3 h at room temperature forming impure $MnCF_3(CO)_{5-n}(NMe_3)_n$ intermediates; Yield: 75% based on ^{19}F NMR. The preps for complexes **3,4,6,7** utilized these products directly without further workup.

Synthesis of 3. Bipy (59.4 mg, 0.38 mmol) was added to a THF solution (ca. 3 mL) of $MnCF_3(CO)_4(NMe_3)$ **2** and then heated at 50°C for 24 h. The suspension was cooled to -34°C overnight before the solid was collected by filtration and washed with hexanes (3 * 1.0 mL) followed by cold Et_2O (2 x 0.2 mL). The solid was then dried under reduced pressure giving a yellow solid. Yield: 73 mg, 53% based on $MnCF_3(CO)_5$/$Mn(COCF_3)(CO)_5$. IR (neat): 2360 (w), 2330 (w), 2020 (s), 1920 (s), 1620 (w), 1600 (w), 1470 (w), 1450 (w), 1320 (w), 1240(w), 1230(w), 1170 (w), 1130 (w), 1050(m), 953 (m), 889(w), 852 (w), 768(m) cm^{-1}. ^1H NMR (300 MHz, $CDCl_3$): □ 9 (unresolved multiplet, 2H), 8.3 (unresolved multiplet, 2H), 8.2 (unresolved multiplet, 2H), 7.6 (unresolved multiplet, 2H). ^{19}F NMR (282 MHz, $CDCl_3$): -21.1 ppm (br s, CF_3).

Synthesis of 4. Phen (68.5 mg, 0.38 mmol) was added to a THF solution (ca. 3 mL) of $MnCF_3(CO)_4(NMe_3)$ **2** and the solution was heated to 50°C for 19 h. Hexanes (8 mL) was added to the now yellow solution to induce precipitation. The suspension was cooled to -34°C overnight before the solid was collected by filtration and washed with hexanes (3 * 1.0 mL) followed by

cold Et_2O (2 x 0.2 mL). The solid was then dried under reduced pressure giving a yellow solid. Yield: 85 mg, 60% based on Phen. IR (neat): 2960 (w), 2920 (w), 2850 (w), 2010 (s), 1930 (s), 1650 (w), 1430 (m), 1350 (m), 1050 (m), 949 (m), 849 (w). ^{1}H NMR (300 MHz, $CDCl_3$): □ 9.42 (unresolved d, 2H), 8.43 (unresolved dd, 2H), 8.0 (multiplet, 2H), 7.8 ppm (unresolved d, 2H). ^{19}F NMR (282 MHz, $CDCl_3$): -20.9 ppm (br s, CF_3).

Synthesis of 6. NMe_3O (85.6 mg, 1.14 mmol; 3 equiv.) was added to a toluene solution (ca. 6 mL) of $MnCF_3(CO)_5$/$Mn(COCF_3)(CO)_5$(100 mg, 0.38 mmol) and the solution was stirred at RT for 2 h until the solution was light orange. Tpy (88.7 mg, 0.38 mmol) was added to the solution which was then refluxed under nitrogen at 110^{o}C for 4 h. The final solution was red. Hexanes was added to the solution to precipitate red crystals. The solution was cooled to -32 ^{o}C for 3 h before the solid was collected on a glass frit and washed with hexanes (3 * 1.5 mL) followed by Et_2O (3 * 1.0 ml) then dried under reduced pressure. Yield: 105 mg, 67% based on Tpy. IR (neat): 2970 (w), 2930 (w), 2850 (w), 2360 (w), 2330 (w), 2020 (s), 1900 (s), 1850 (s), 1600 (w), 1590 (w), 1560 (w), 1460 (w), 1430 (w), 1260 (w), 1050 (s), 953 (m), 769 cm^{-1} (m). ^{1}H NMR (300 MHz, CDCN): δ 9.3–8.5 (broad multiplets; 2H), 8.5–7.8 (broad multiplets, 6H), 7.8–7 ppm (broad multiplets, 3H). ^{19}F NMR (282 MHz, $CDCl_3$): -20.9 ppm (br s, CF_3).

Synthesis of 7-cis, 7-trans. NMe_3O (85.6 mg, 1.14 mmol; 3 equiv.) was added to a toluene solution (ca. 6 mL) of $MnCF_3(CO)_5$/$Mn(COCF_3)(CO)_5$ (100 mg, 0.38 mmol) and the solution was stirred at RT for 2 h until the solution was light orange. NNS (97 mg, 0.38 mmol) was added to the solution after 3 hours and the solution was refluxed at 110 ^{o}C overnight. After cooling, the solvent was removed under vacuum leaving an orange powder which was dissolved in a minimum of toluene and cooled to -32 ^{o}C overnight. The following day the solid was collected on a glass frit, washed with hexanes (3*1.5 mL) and dried under reduced pressure. Yield: 85 mg, 53% based on $MnCF_3(CO)_5$/$Mn(COCF_3)(CO)_5$. IR (neat): 2960 (m), 2930 (m), 2850 (m), 2020 (s), 1920 (s), 1910 (s), 1470 (w), 1440 (w), 1380 (w), 1330 (w), 1260 (w), 1050 (s), 970 (m), 943 (m), 775 (w), 748 (w), 681 cm^{-1} (w). ^{1}H NMR (300 MHz, CD_3CN): **7-trans**: δ 8.75 (broad singlet; 1H), , 7.4 - 6.23 ppm (overlapping multiplets; aryl-H's), 1.86 (broad singlet; 3H), 1.35 ppm (broad singlet; 3H); **7-cis**: 7.71 (broad multiplet; 1H), 7.4 – 6.23 (overlapping multiplets: aryl-H's), 3.55 (broad singlet; 3H), 1.62 (broad singlet; 3H). ^{19}F NMR (282 MHz, CD_3CN): **7-trans** -20.43 ppm (br singlet, CF_3); **7-cis**: -19.6 ppm (br s, CF_3).

Synthesis of cis/trans-[(Phen)(CO)$_3$Mn=CF$_2$][OTf], 8. A glass vial was charged with **3** (25 mg, 0.064 mmol) and dissolved in DCM (3 mL). To this solution was added TMS-OTf (12 μL, 0.064 mmol) and the reaction was stirred at RT for 1.5 hours (color changed from yellow to dark orange). The solvent was removed and the solid dried under reduced pressure for 2 h giving an orange solid. Yield: 28 mg, 84% yield. ^{1}H NMR (300 MHz, $CDCl_3$): δ 9.34 (broad singlet, 2H), 8.59 (broad singlet, 2H), 8.03 (broad singlet, 2H), 7.92 ppm (overlapping broad singlet, 2H). ^{19}F NMR (282 MHz, $CDCl_3$): major isomer: 155.6 (br s, Mn=CF_2), -77.7 ppm (br s, OTf); minor isomer: 156.3 (br s, Mn=CF_2), -78.2 ppm (br s, OTf).

Synthesis of [Mn=CF$_2$][OTf] complexes. The above preparation of complex **8** can be applied as a general synthesis to obtain the Mn=CF_2 adducts of several Mn-CF_3 complexes as can be seen from preliminary ^{19}F NMR spectra showing formation of new carbenes of complexes **3**, **4**, and **7** (see SI).[61]

Details for X-ray Crystallography. For **3**, **6**, and **9**: samples were mounted on thin glass fibers using paraffin oil and were cooled to 200K prior to data collection. Data were collected on a Bruker AXS KAPPA single crystal diffractometer equipped with a sealed Mo tube source (wavelength 0.71073Å) APEX II CCD detector. Raw data

collection and processing were performed with APEX II software package from BRUKER AXS.[ref] Diffraction data were collected with a sequence of 0.5° ω scans at 0, 90, 180, and 270° in φ. Initial unit cell parameters were determined from 60 data frames collected at different sections of the Ewald sphere. Semi-empirical absorption corrections based on equivalent reflections were applied. Systematic absences in the diffraction data set and unit-cell parameters were consistent with triclinic systems. Solutions in centrosymmetric space group yielded chemically reasonable and computationally stable results of refinement. The structures were solved by direct methods, completed with difference Fourier synthesis, and refined with full-matrix least-squares procedures based on F2. In the structure, compound molecules are situated in the general position. All non-hydrogen atoms were refined anisotropically with satisfactory thermal parameters values. Additional crystallographic data and selected data collection parameters are reported below.

$MnCF_3(Bipy)(CO)_3$ (**3**): Empirical Formula: $C_{14}H_8F_3MnN_2O_3$; FW = 364.16; Crystal size: 0.229 X 0.187 X 0.058 mm^3; Crystal System: Triclinic; Space Group: P_{-1}; Z = 2; a = 6.9984 (5) Å, b = 9.9870 (9) Å, c = 10.8023 (8), α = 88.652 (3)°, β = 71.277 (2)°, γ = 75.664 (2)°; Volume = 691.50 (0) $Å^3$; Calculated Density = 1.749 g/cm^3; Absorption Coefficient = 1.006 mm^{-1}; F(000) = 364.0; Θ range for data collection: 0.794 to 26.375°; Limiting indices: $-8\leq h\leq 8$, $-12\leq k\leq 12$, $-13\leq l\leq 13$: Reflections collected/unique: 8801/8801; R(int) = ?; Completeness to Θ = 25.242: 100%; Max and min transmission: Data / Restraint / parameters: 8801 / 0 / 209; Goodness-of-fit on F^2: 1.048; Final R indices [$I>2\sigma(I)$]: R1 = 0.0846, wR2 = 0.1213 ; R indices (all data): R1 = 0.1574, wR2 = 0.1456; largest diff. peak/hole: 0.773 / -0.640 $eÅ^{-3}$.

$MnCF_3(CO)_2(Tpy)$ (**4**): Empirical Formula: $C_{18}H_{11}F_3MnN_3O_2$; FW = 413.24; Crystal size: 0.11 X 0.05 X 0.03 mm^3; Crystal System: Monoclinic; Space Group: $P_{21/n}$; Z = 4; a = 9.0038 (3) Å, b = 13.9811 (5) Å, c = 13.4556 (5), α = 90.000(0)°, β = 107.861 (2)°, γ = 90.000 (0)°; Volume = 1612.20 (10) $Å^3$; Calculated Density = 1.702 g/cm^3; Absorption Coefficient = 4.890 mm^{-1}; F(000) = 832.0; Θ range for data collection: 0.746 to 56.026°; Limiting indices: $-11\leq h\leq 10$, $-17\leq k\leq 16$, $-16\leq l\leq 16$: Reflections collected/unique: 16611/3133; R(int) = ?; Completeness to Θ = 25.242: 98.4%; Max and min transmission: Data / Restraint / parameters: 3133 / 0 / 245; Goodness-of-fit on F^2: 1.037; Final R indices [$I>2\sigma(I)$]: R1 = 0.0574, wR2 = 0.1272 ; R indices (all data): R1 = 0.0893, wR2 = 0.1467; largest diff. peak/hole: 0.54 / -0.61 $eÅ^{-3}$.

$Mn(OTf)_2(Phen)_2$ (**9**): Empirical Formula: $C_{26}H_{16}F_6MnN_4O_6S_2$; FW = 713.49; Crystal size: 0.17 X 0.11 X 0.08 mm^3; Crystal System: Monoclinic; Space Group: $C_{2/c}$; Z = 4; a = 9.7736 (4) Å, b = 14.3565 (7) Å, c = 19.9052 (9), α = 90.000 (0)°, β = 95.585 (2)°, γ = 90.000 (0)°; Volume = 2779.70 (2) $Å^3$; Calculated Density = 1.705 g/cm^3; Absorption Coefficient = 4.115 mm^{-1}; F(000) = 1436.0; Θ range for data collection: 0.379 to 60.646°; Limiting indices: $-12\leq h\leq 12$, $-18\leq k\leq 18$, $-25\leq l\leq 25$: Reflections collected/unique: 20729/3208; R(int) = 0.0279; Completeness to Θ = 60.646: 100%; Max and min transmission: Data / Restraint / parameters: 3208/ 0/ 205; Goodness-of-fit on F^2: 1.102; Final R indices [$I>2\sigma(I)$]: R1 = 0.0357, wR2 = 0.0944 ; R indices (all data): R1 = 0.0366, wR2 = 0.0944; largest diff. peak/hole: 0.50 / -0.55 $eÅ^{-3}$.

6.2.4 IR Spectra

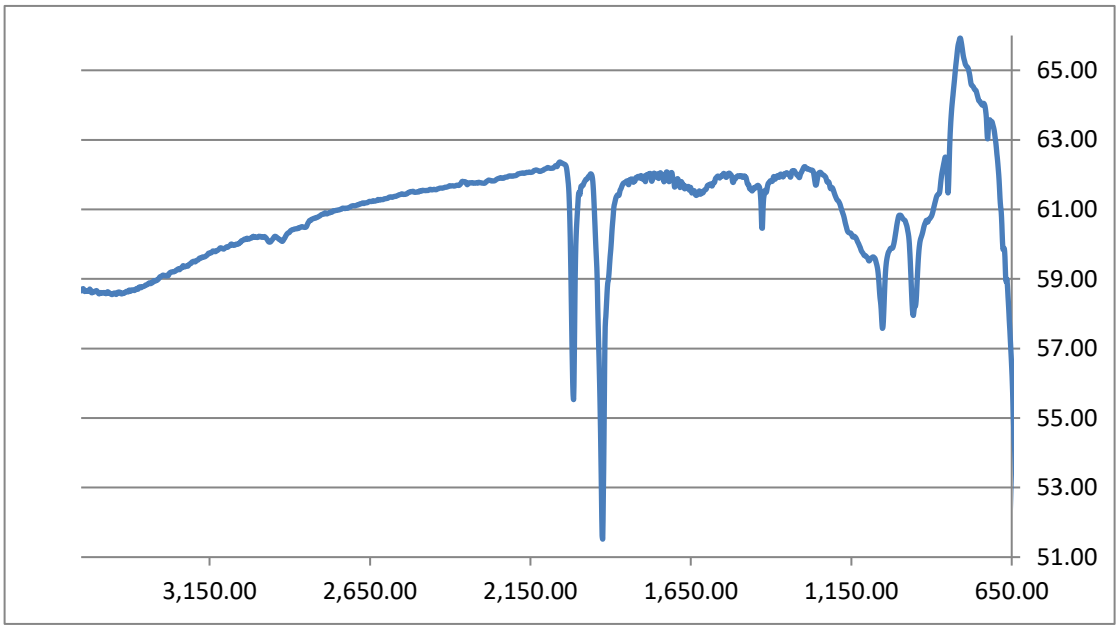

Figure 6.3: FT-IR spectra (Nicolet Nexus 670 instrument, neat/solid samples) for $MnCF_3(CO)_2(Phen)$ (**1**)

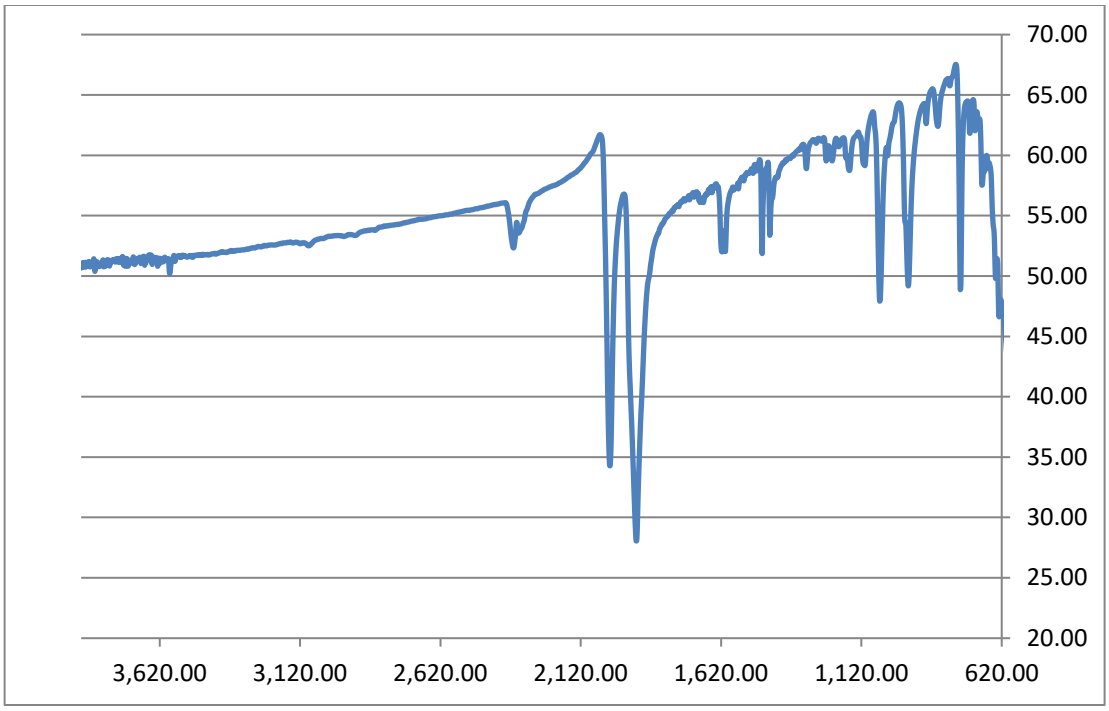

Figure 6.4: FT-IR spectra (Nicolet Nexus 670 instrument, neat/solid samples) for $MnCF_3(CO)_3(Bipy)$ (**2**).

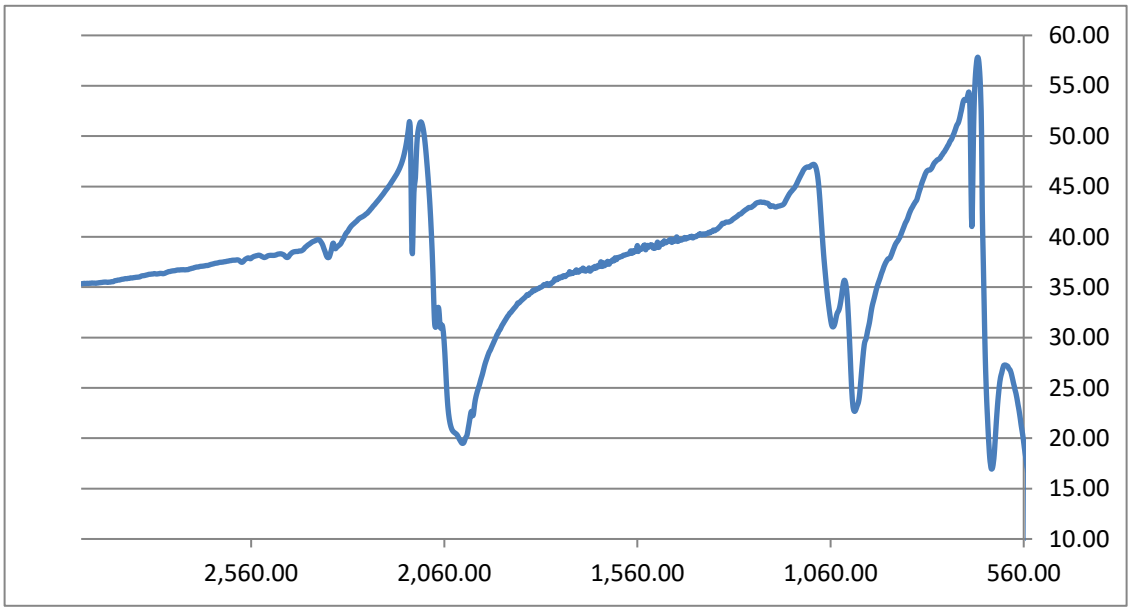

Figure 6.5: FT-IR spectra (Nicolet Nexus 670 instrument, neat/solid samples) for $MnCF_3(CO)_5$.

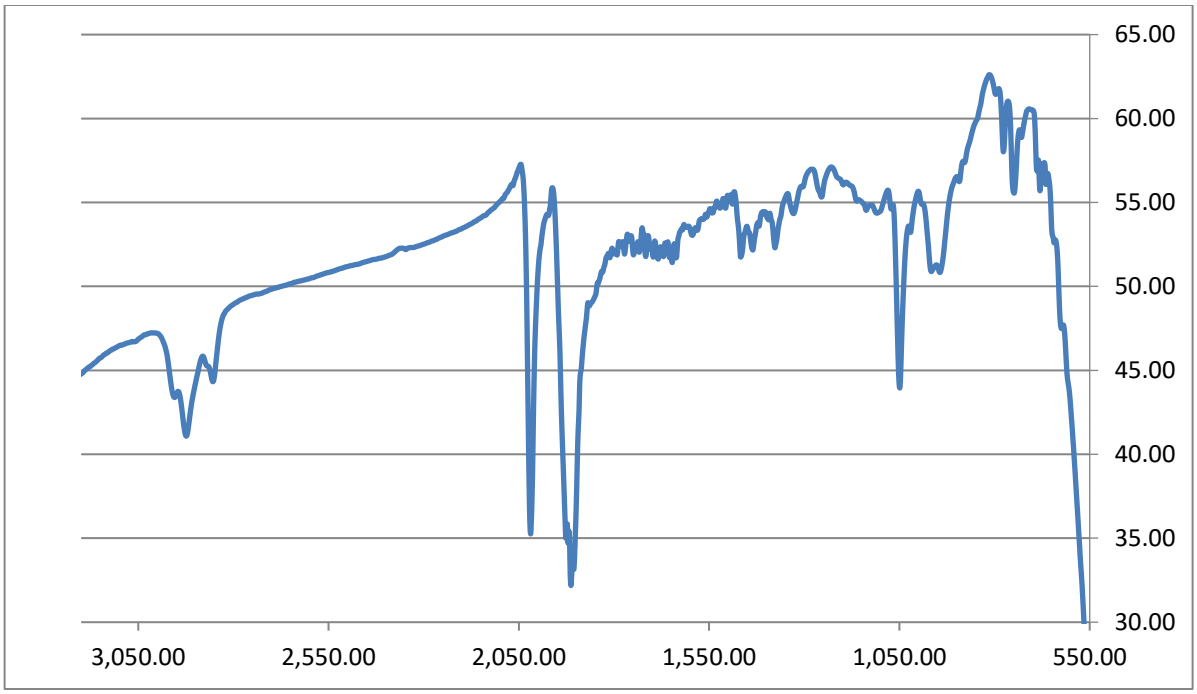

Figure 6.6: FT-IR spectra (Nicolet Nexus 670 instrument, neat/solid samples) for $MnCF_3(CO)_2(NNS)$ (**4**)

6.2.5 NMR Spectra

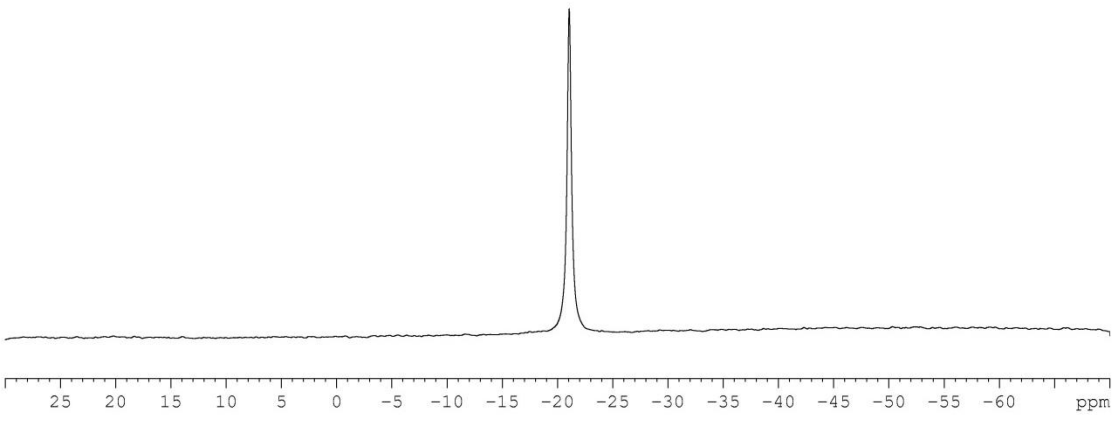

Figure 6.7: ^{19}F NMR (282 Mhz, CD_3CN) spectrum of $MnCF_3(Bipy)(CO)_3$ **3**.

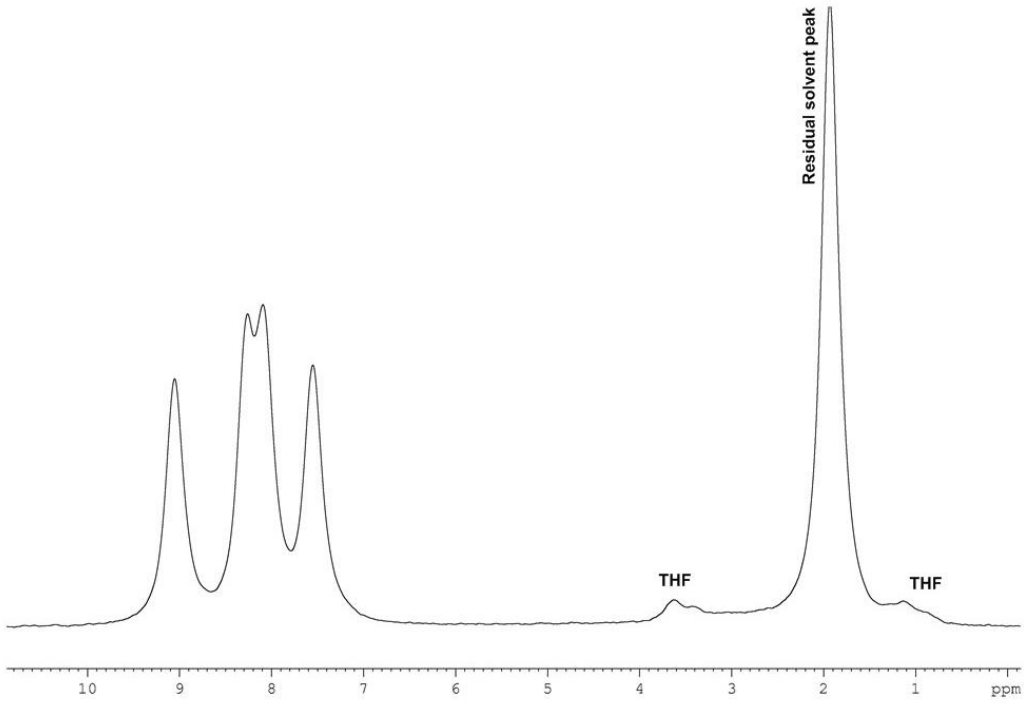

Figure 6.8: ^{1}H NMR (300 Mhz, CD_3CN) of $MnCF_3(Bipy)(CO)_3$ (**3**).

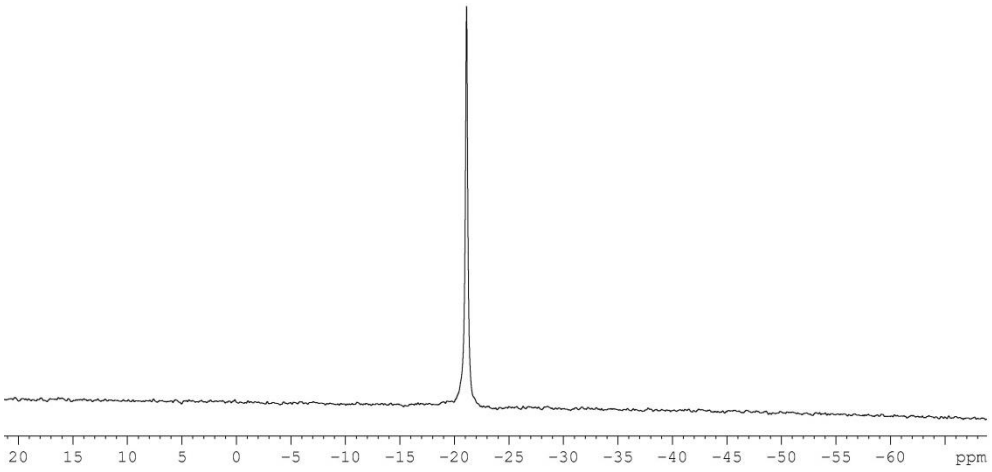

Figure 6.9: ^{19}F NMR (282 Mhz, $CDCl_3$) of $MnCF_3(CO)_2(Tpy)$ **4.**

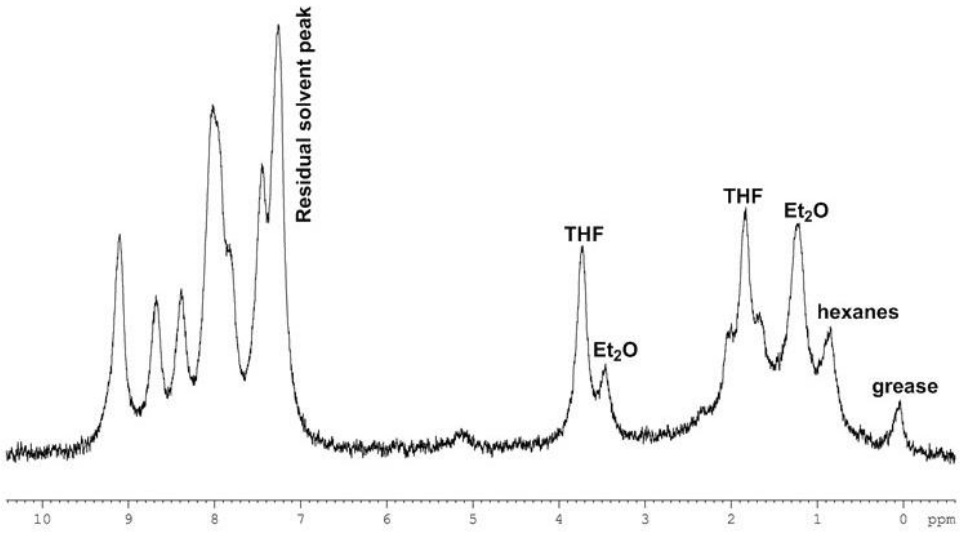

Figure 6.10: ^{1}H NMR (300 Mhz, $CDCl_3$) of $MnCF_3(CO)_2(Tpy)$ **4.**

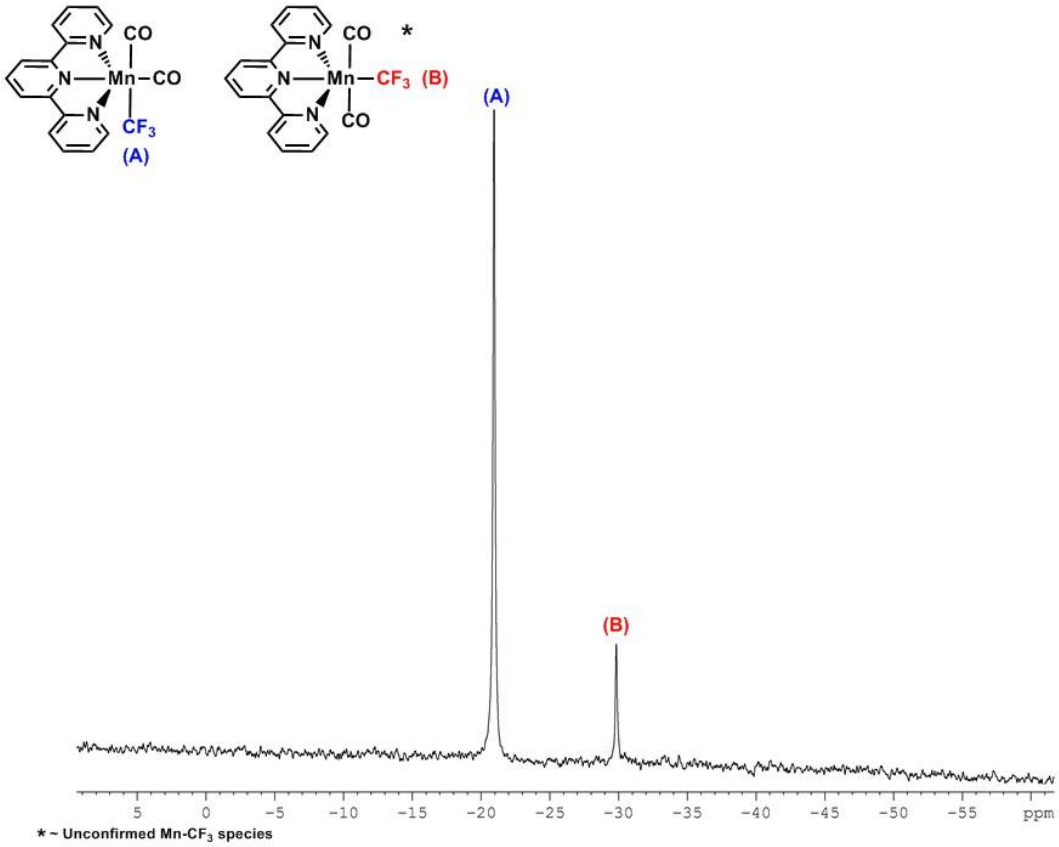

Figure 6.11: ^{19}F NMR (282 MHz, CD_3CN) spectrum of $MnCF_3(CO)_2Tpy$ (**6)**. Spectrum shows a minor Mn-CF_3 peak which is proposed to be the trans-Mn-CF_3 product.

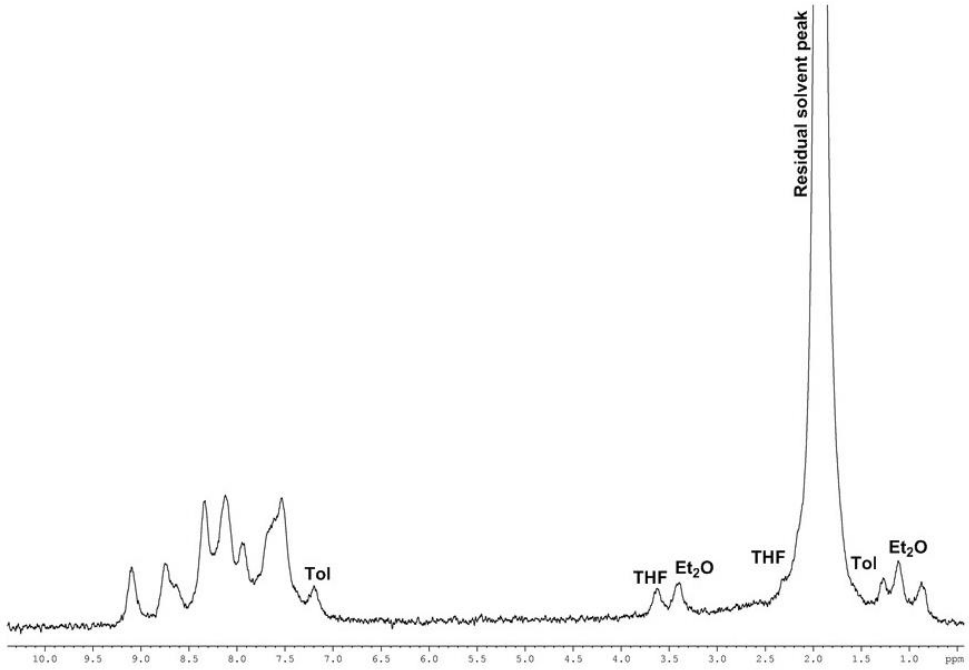

Figure 6.12: ^{1}H NMR (300 MHz, CD_3CN) spectrum of $MnCF_3(CO)_2Tpy$ **6**.

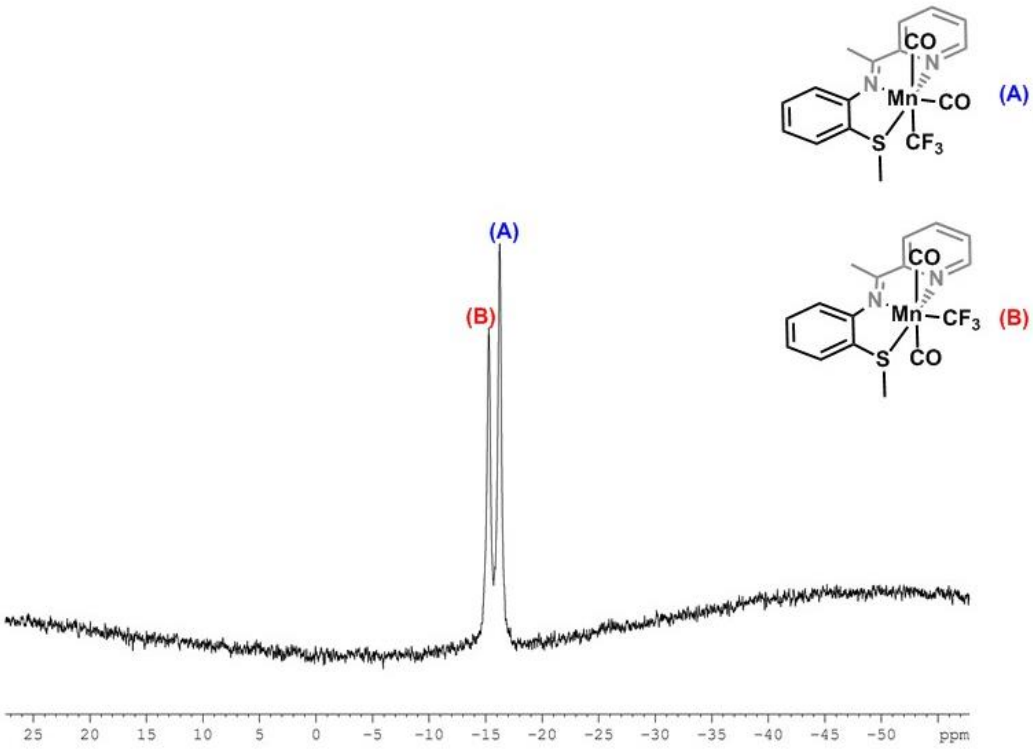

Figure 6.13: ^{19}F NMR (282 Mhz, CD_3CN) of complex $MnCF_3(CO)_2(NNS)$ (**7**).

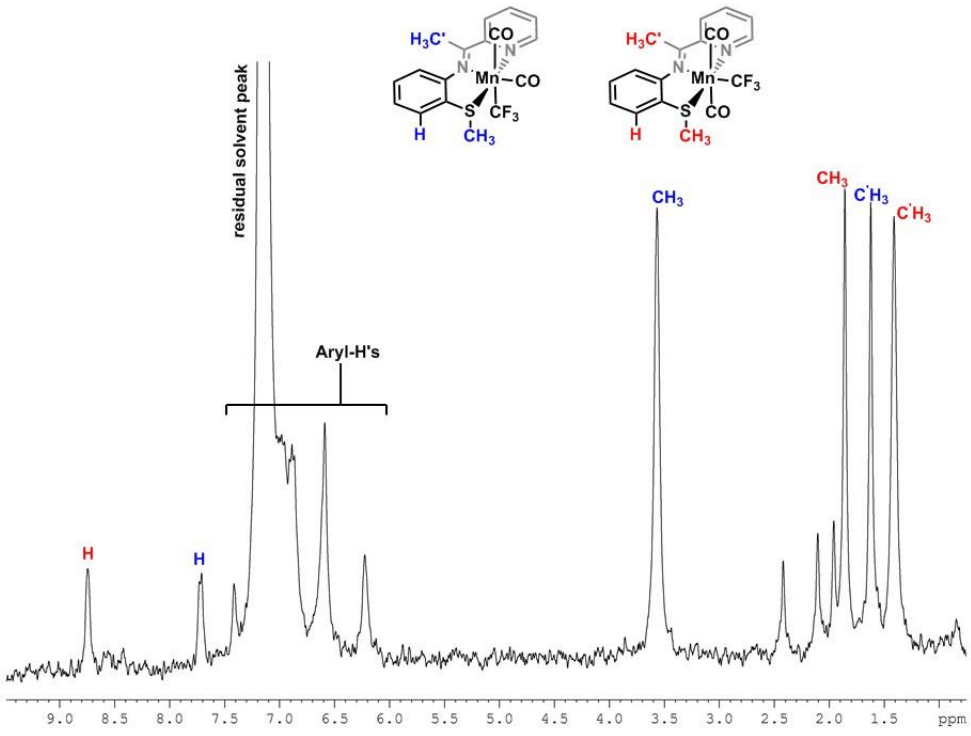

Figure 6.14: ^{1}H NMR (300 MHz, CD_3CN) spectrum of $MnCF_3(CO)_2(NNS)$ **(7)**.

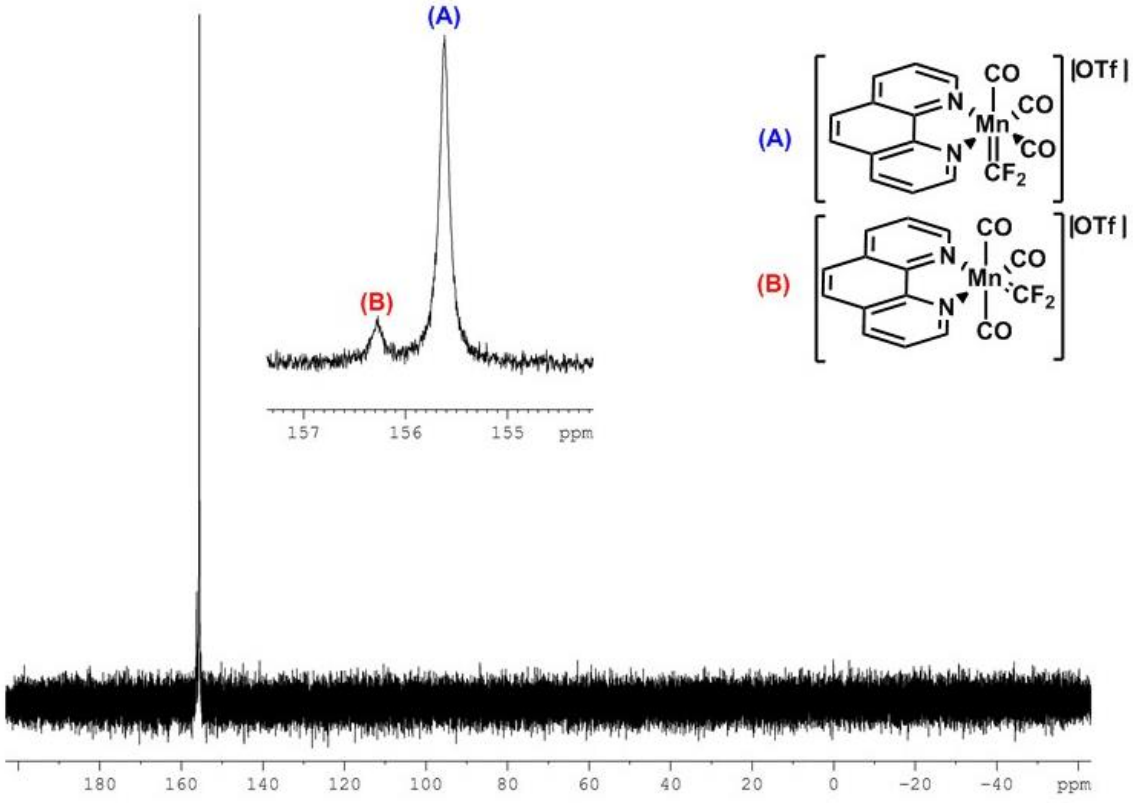

Figure 6.15: ^{19}F NMR (282 Mhz, C_6D_6) downfield spectrum of $[Mn(=CF_2)(CO)_3(Phen)][OTf]$ (**8**).

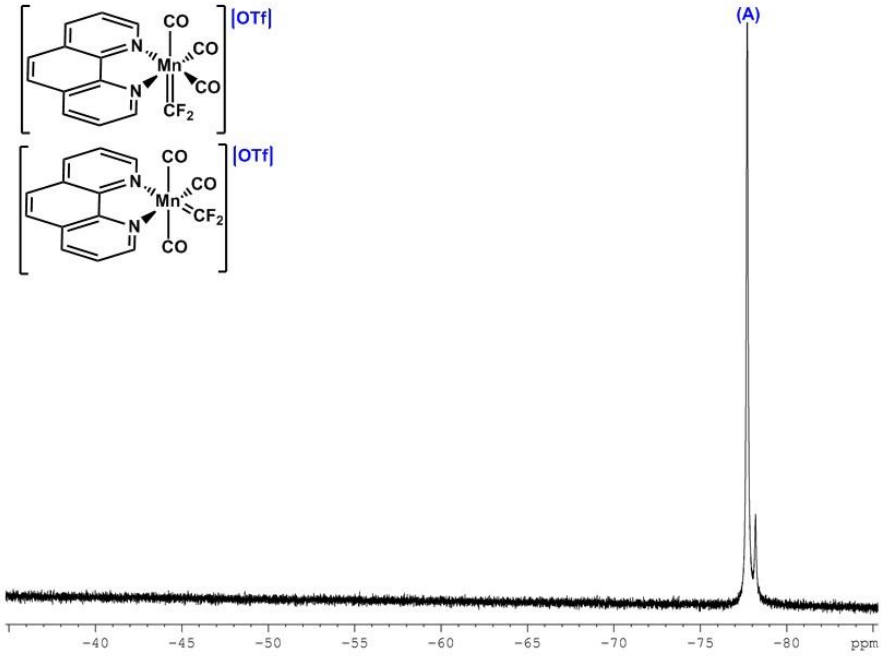

Figure 6.16: ^{19}F NMR (282 Mhz, C_6D_6) upfield spectrum of [Mn(=CF_2)(CO)$_3$(Phen)][OTf] (**8**).

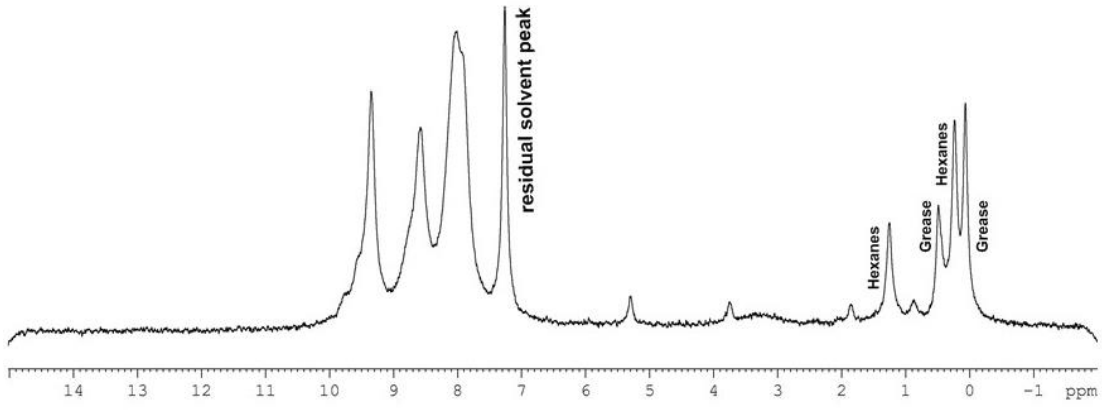

Figure 6.17: ^{1}H NMR (300 MHz, $CDCl_3$) spectrum of [Mn(=CF_2)(CO)$_3$(Phen)][OTf] (**8**).

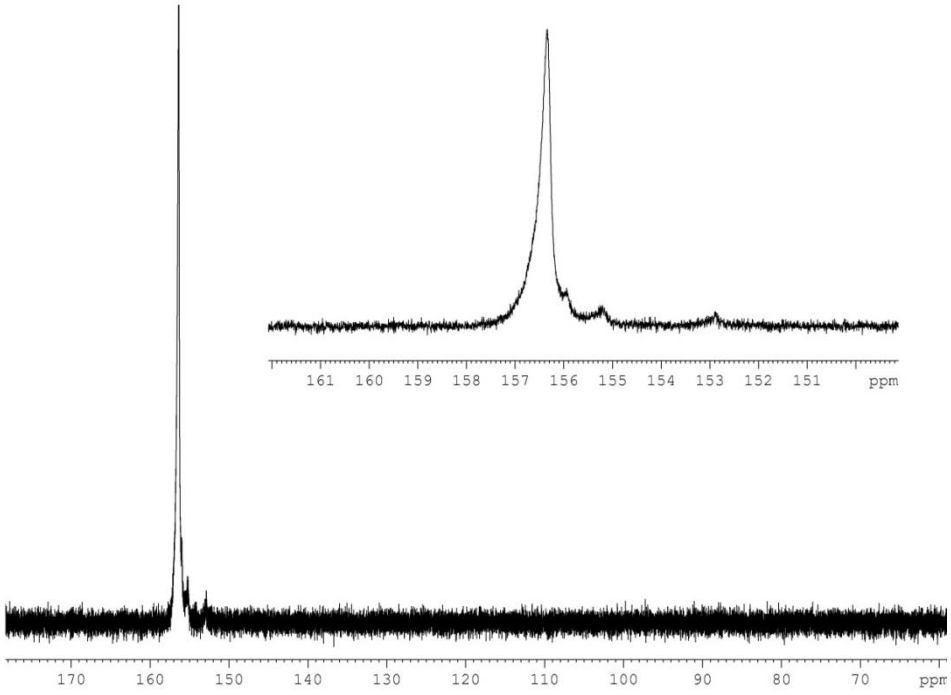

Figure 6.18: ^{19}F NMR (282 MHz, C_6D_6) downfield spectrum of $(NNS)(CO)_2Mn{=}CF_2$ complex.

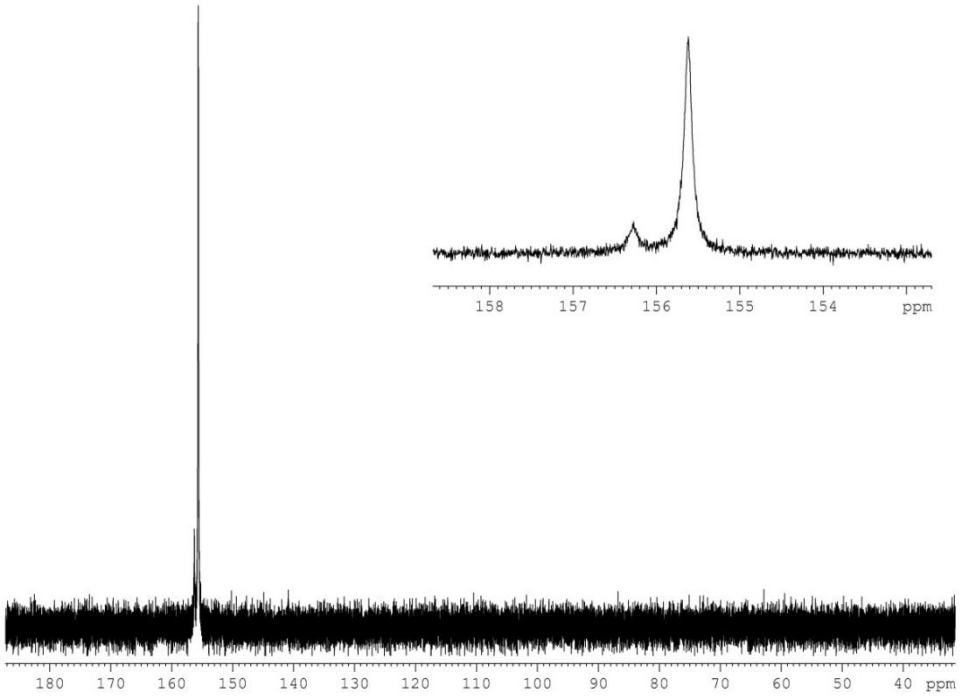

Figure 6.19: ^{19}F NMR (282 MHz, C_6D_6) downfield spectrum of $(Bpy)(CO)_3Mn{=}CF_2$ complex. Minor peak at 156.3 is proposed to be an isomeric $Mn{=}CF_2$ complex.

6.2.6 Cyclic Voltammetry

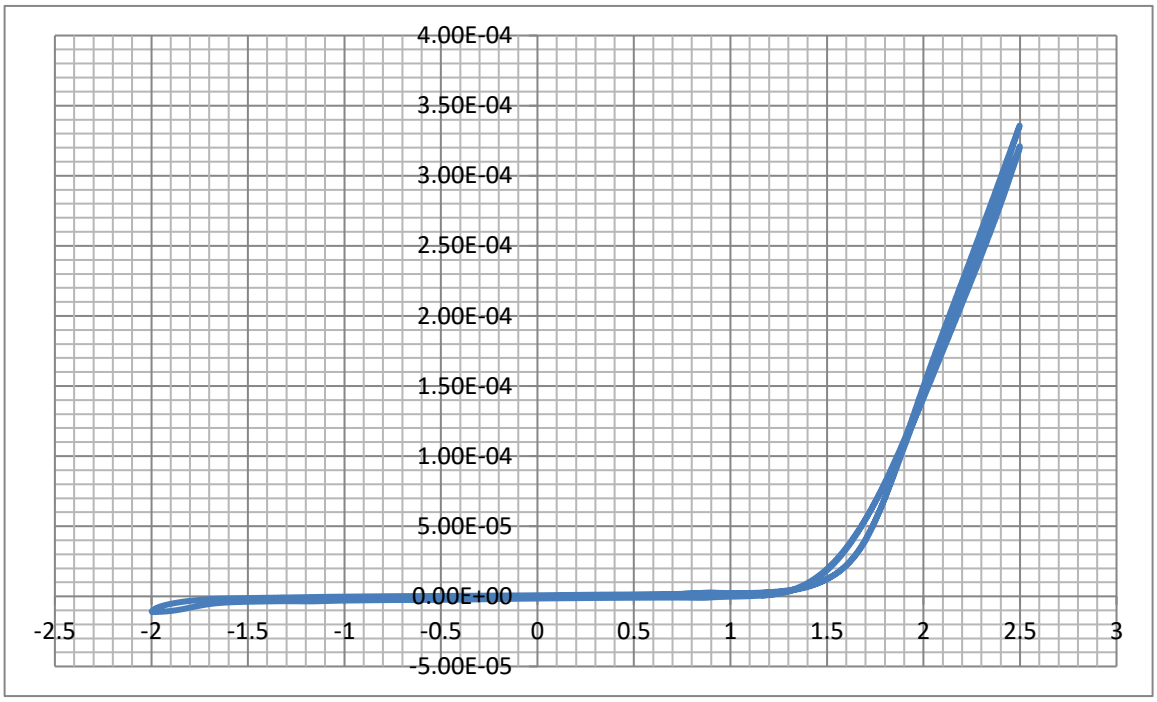

Figure 6.20: Blank Cyclic Voltammogram (0.1M THF solution of $[(Bu)_4N][BF_4]$)

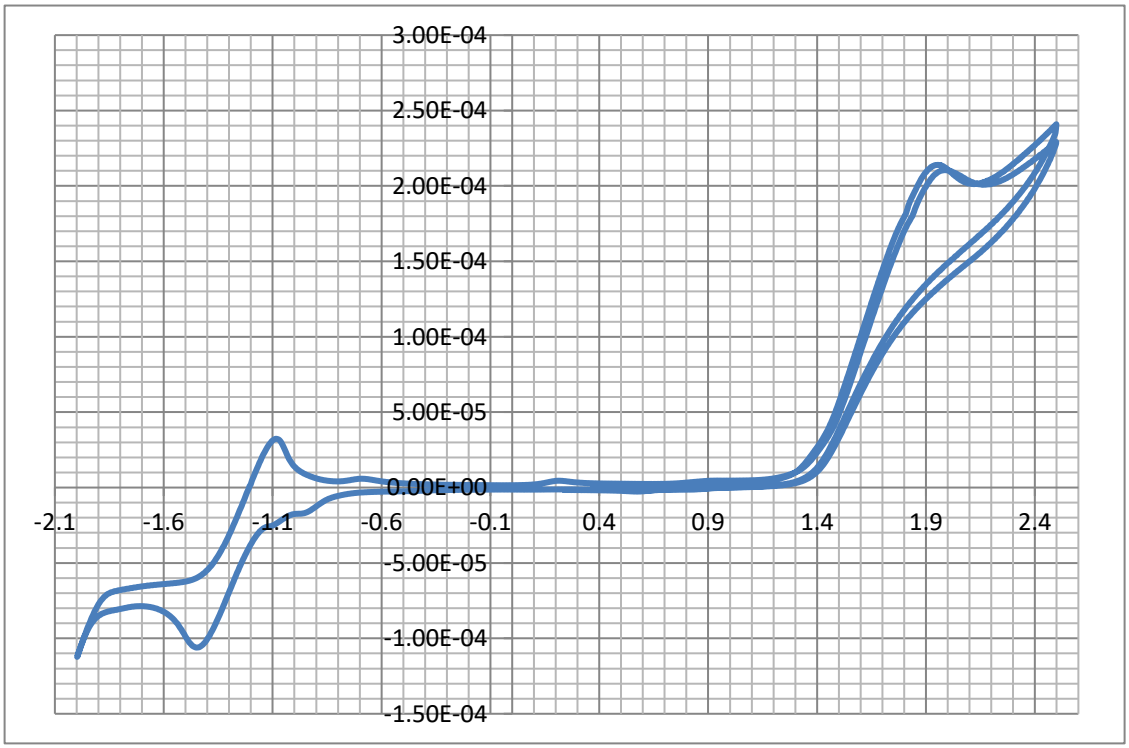

Figure 6.21: Cyclic Voltammogram of $MnCF_3(Bipy)(CO)_3$ (**3**) in THF (100mV/s sweep rate)

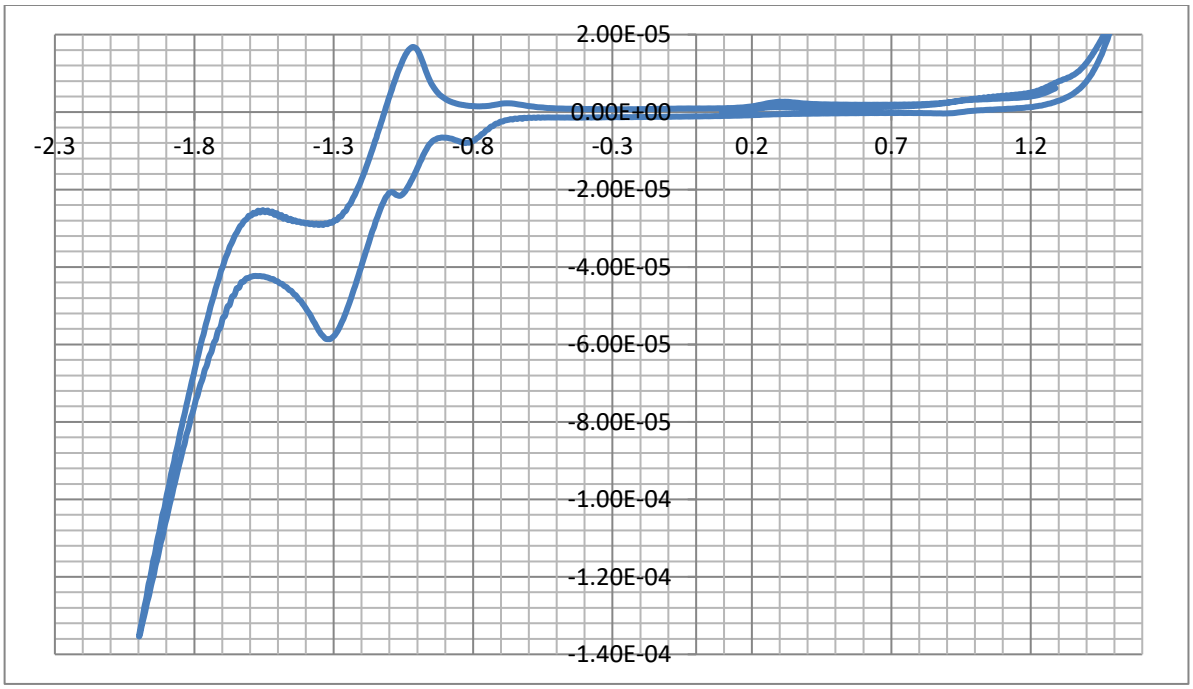

Figure 6.22: Cyclic Voltammogram of -0.5V - +1.5V region of $MnCF_3(CO)_2(Tpy)$ (**4**) in THF (100mV/s sweep rate) showing quasi-reversible reduction at -2.1 V vs. ferrocene

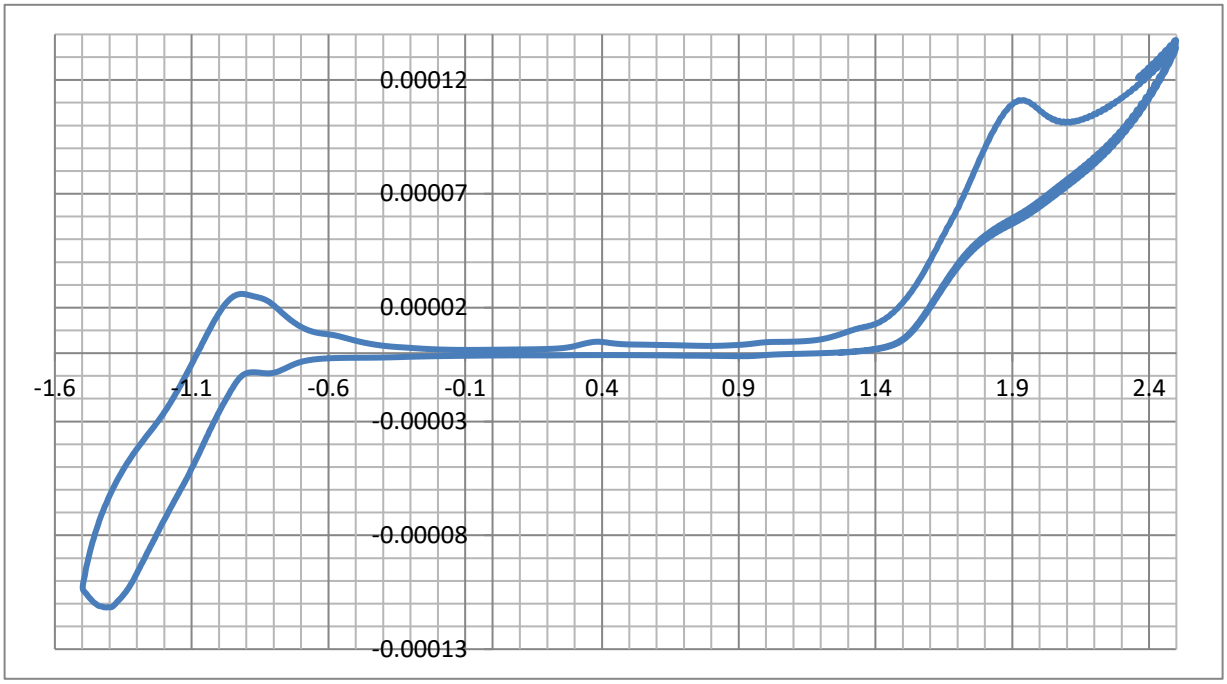

Figure 6.23: Cyclic voltammogram of -1.5 - 2.5 V region for $MnCF_3(CO)_2(Tpy)$ (**4**) in THF (100mV/s sweep rate) showing non-reversible oxidation at 0.66V vs ferrocene

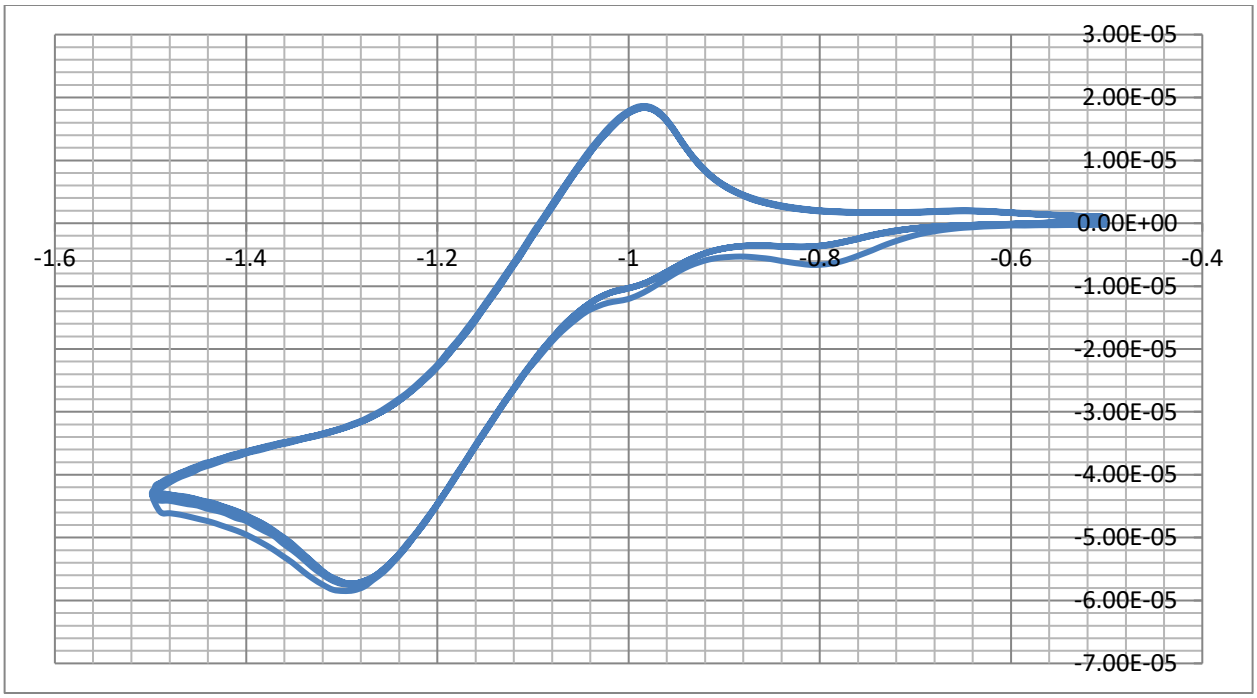

Figure 6.24: Cyclic voltammogram of -0.5V - -1.5V region for $MnCF_3(CO)_2(Tpy)$ (**4**) in THF (100 mV/s sweep rate) showing possible irreversible oxidation and quasi-reversible reduction

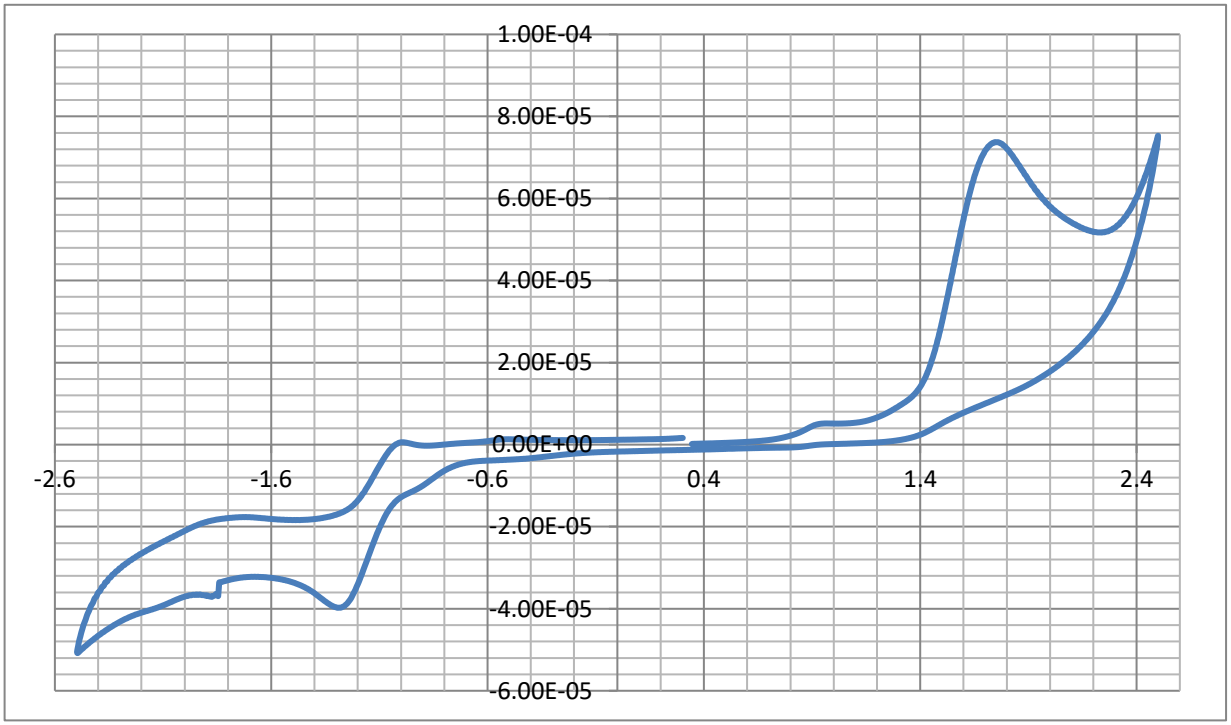

Figure 6.25: Cyclic voltammogram of $MnCF_3(CO)_2(NNS)$ (**7**) in THF (100 mV/s sweep rate) showing possible irreversible oxidation and quasi-reversible reduction

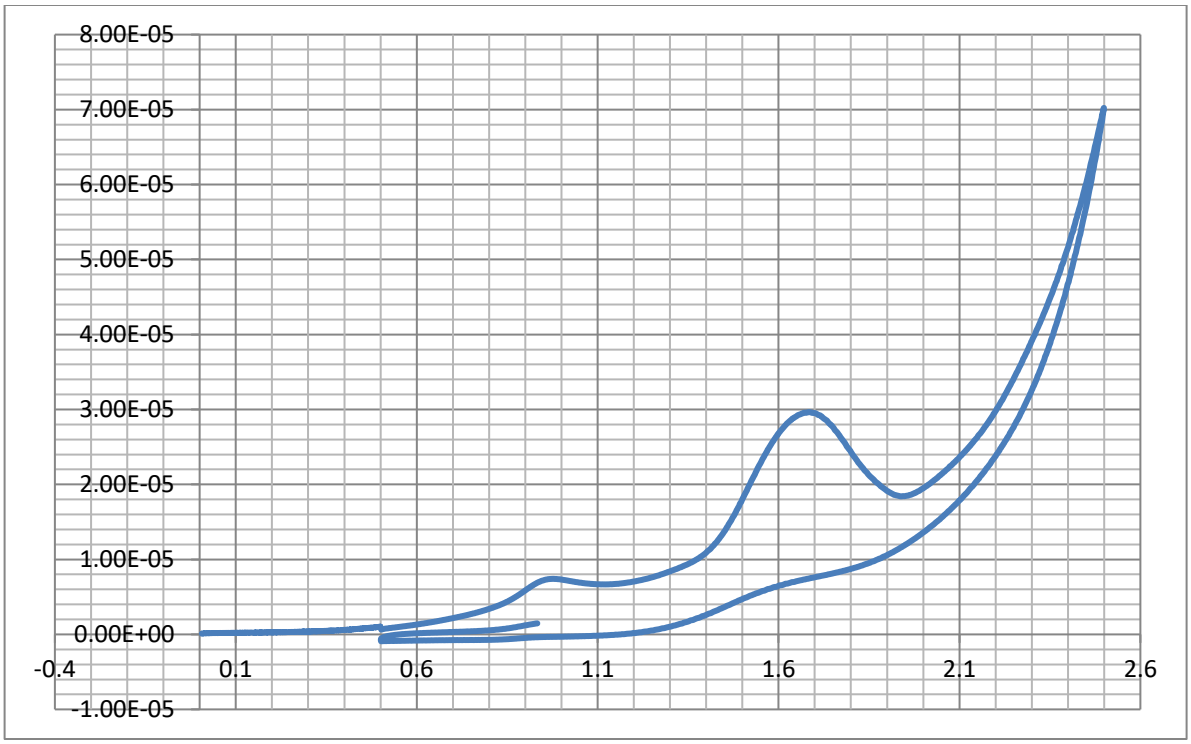

Figure 6.26: Cyclic voltammogram of $MnCF_3(CO)_2(NNS)$ (**7**) in THF (100 mV/s sweep rate) showing possible irreversible oxidation and quasi-reversible reduction

6.2.7 EI-MS Data

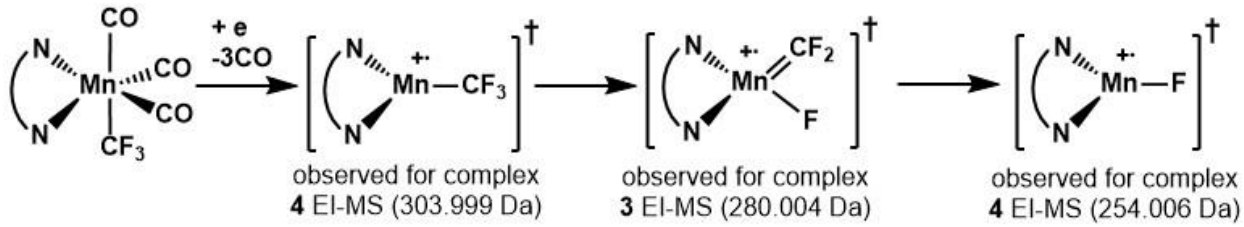

Figure 6.27: Hypothetical fragmentation of complex **3** and **4** after electron impact (EI) mass spectrometry (shown in Figures 6.28-6.32)

Formula search on scan 10 of 2d3940

Mass	Int%	Dev mmu	1 H	12 C	14 N	19 F	55 Mn
280.00375	0.20	-2.39	0	21	2	0	0
		-8.70	2	20	0	2	0
		3.87	0	19	1	2	0
		-8.50	1	15	3	3	0
		-4.77	9	18	0	0	1
		7.80	7	17	1	0	1
		-4.57	8	13	3	1	1
		8.00	6	12	4	1	1
		1.69	8	11	2	3	1

Figure 6.28: Exact mass search for $N_2(F)Mn{=}CF_2$ (N_2 = Bipy) of mass 280.00375 Da

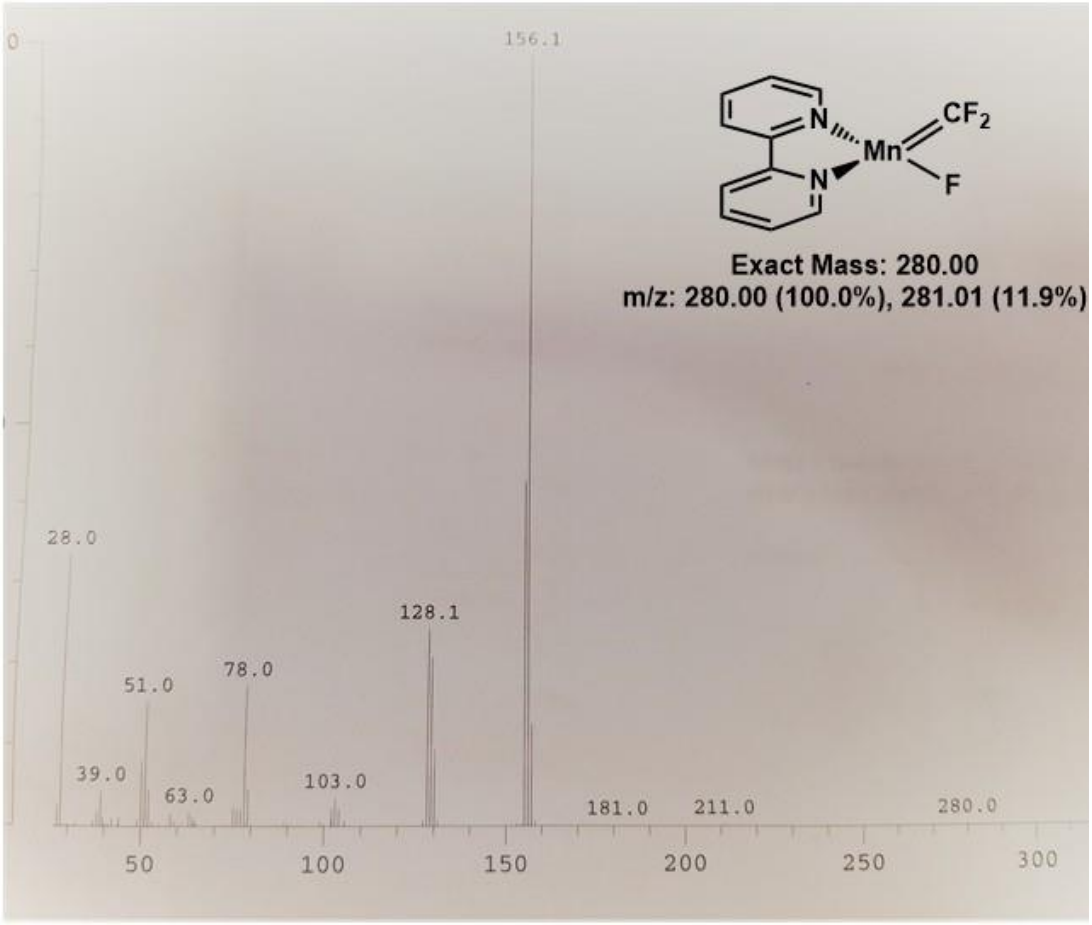

Figure 6.29: EI-MS spectrum of fragmentation of complex **3** showing $N_2(F)Mn{=}CF_2$ fragment.

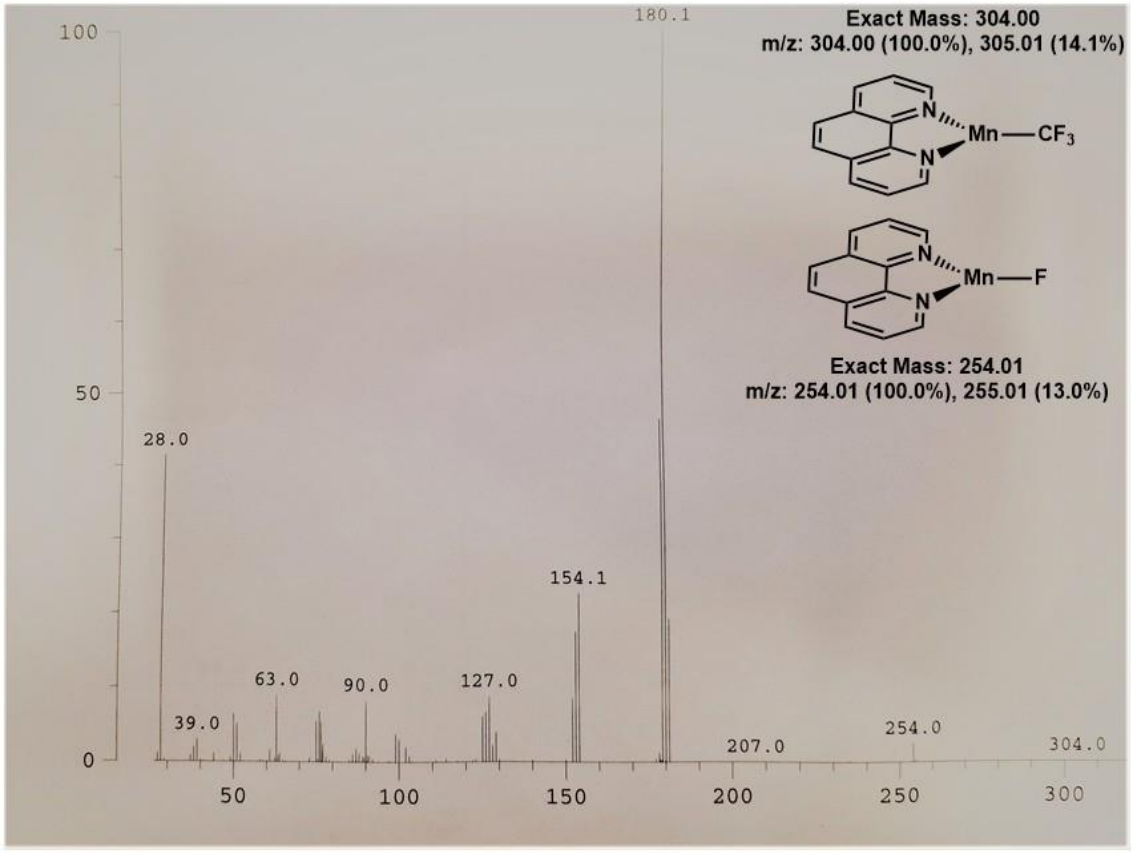

Figure 6.30: EI-MS for complex **4** showing $N_2Mn\text{-}CF_3$ and $N_2Mn\text{-}F$ fragments (304.0 and 254 Da respectively)

Formula search on scan 11 of 2d3939

Mass	Int%	Dev mmu	1 H	12 C	14 N	19 F	55 Mn
303.99905	0.09	-7.09	0	23	2	0	0
		-0.83	0	21	1	2	0
		-9.47	9	20	0	0	1
		3.10	7	19	1	0	1
		-9.27	8	15	3	1	1
		3.30	6	14	4	1	1
		9.37	7	17	0	2	1
		-3.01	8	13	2	3	1
		9.57	6	12	3	3	1

Figure 6.31: Exact mass for $N_2Mn\text{-}CF_3$ (N_2 = Phen) exact mass of 303.99905 Da

Formula search on scan 11 of 2d3939

Mass	Int%	Dev mmu	1 H	12 C	14 N	19 F	55 Mn
254.00625	2.55	-9.40	2	21	0	0	0
		3.17	0	20	1	0	0
		-9.20	1	16	3	1	0
		9.44	0	18	0	2	0
		-2.94	1	14	2	3	0
		0.99	8	12	2	1	1
		-5.31	10	11	0	3	1
		7.26	8	10	1	3	1

Figure 6.32: Exact mass of $N_2Mn\text{-}F$ (N_2 = Phen) exact mass of 254.00625 Da

References

[1] Steinborn, D. Fundamentals of Organometallic Catalysis; Wiley-VCH: Weinheim, 2012.

[2] Chiusoli, G. P.; Maitlis, P. M., Eds. Metal-Catalysis in Industrial Organic Processes, RSC Publishing: Cambridge, 2006.

[3] Taw, F. L.; Clark, A. E.; Mueller, A. H.; Janicke, M. T.; Cantat, T.; Scott, B. L.; Hay, P. J.; Hughes, R. P.; Kiplinger, J. L. Titanium(IV) Trifluoromethyl Complexes: New Perspectives on Bonding from Organometallic Fluorocarbon Chemistry. *Organometallics*. **2012**, *31*, 1484−1499.

[4] Hughes, R. P. Adv. Organo-transition Metal Compounds Containing Perfluorinated Ligands. *Organomet. Chem*. **1990**, *31*, 183−267.

[5] Brothers, P. J.; Roper, W. R. Transition-metal Dihalocarbene Complexes. *Chem. Rev*. **1988**, *88*, 1293−1326.

[6] Ojima, I. Fluorine in Medicinal Chemistry and Chemical Biology; Blackwell: Chichester, U.K., 2009.

[7] Chambers, R. D. Fluorine in Organic Chemistry; Blackwell: Oxford, 2004.

[8] Kirsch, P. Modern Fluoroorganic Chemistry: Synthesis, Reactivity, Applications; Wiley-VCH: Weinheim, 2004.

[9] Alonso, C.; de Marigorta, E. M.; Rubiales, G.; Palacios, F. Carbon Trifluoromethylation Reactions of Hydrocarbon Derivatives and Heteroarenes. *Chem. Rev*. **2015**, *115*, 1847−1935

[10] Wang, J.; Sánchez-Roselló, M.; Aceña, J. L.; del Pozo, C.; Sorochinsky, A. E.; Fustero, S.; Soloshonok, V. A.; Liu, H. Fluorine in Pharmaceutical Industry: Fluorine-Containing Drugs Introduced to the Market in the Last Decade (2001-2011). *Chem. Rev*. **2014**, *114*, 2432−2506.

[11] Zhu, W.; Wang, J.; Wang, S.; Gu, Z.; Aceña, J. L.; Izawa, K.; Liu, H.; Soloshonok, V. A. Recent Advances in Trifluoromethylation Methodology and new CF_3-containing Drugs. *J. Fluorine Chem*. **2014**, *167*, 37−54.

[12] Müller, K.; Faeh, C.; Diederich, F. *Science* **2007**, *317*, 1881−1886.

[13] Jeschke, P. The Unique Role of Fluorine in the Design of Active Ingredients for Modern Crop Protection. *ChemBioChem*. **2004**, *5*, 570−589. See also ref 3a.

[14] Im, J.; Walshe-Langford, G. E.; Moon, J-W.; Löffler, F. E. Environmental Fate of the Next Generation Refrigerant 2,3,3,3-Tetrafluoropropene (HFO-1234yf). *Environ. Sci. Technol*. **2014**, *48*, 13181−13187.

[15] Panferova, L. I.; Miloserdov, F. M.; Lishchynskyi, A.; Martinez Belmonte, M.; Benet-Buchholz, J.; Grushin, V. V. Well-Defined CuC_2F_5 Complexes and Pentafluoroethylation of Acid Chlorides. *Angew. Chem., Int. Ed*. **2015**, *54*, 5218−5222.

[16] Konovalov, A. I.; Lishchynskyi, A.; Grushin, V. V. Mechanism of Trifluoromethylation of Aryl Halides with $CuCF_3$ and the Ortho Effect. *J. Am. Chem. Soc*. **2014**, *136*, 13410−13425.

[17] Morimoto, H.; Tsubogo, T.; Litvinas, N. D.; Hartwig, J. F. A Broadly Applicable Copper Reagent for Trifluoromethylations and Perfluoroalkylations of Aryl Iodides and Bromides. *Angew. Chem., Int. Ed*. **2011**, *50*, 3793−3798.

[18] Dubinina, G. G.; Furutachi, H.; Vicic, D. A. Active Trifluoromethylating Agents from Well-Defined Copper(I)-CF_3 Complexes. *J. Am. Chem. Soc*. **2008**, *130*, 8600−8601.

[19] Wiemers, D. M.; Burton, D. J. Pregeneration, Spectroscopic Detection and Chemical Reactivity of (Trifluoromethyl)copper, an Elusive and Complex Species. *J. Am. Chem. Soc*. **1986**, *108*, 832−834.

[20] McLoughlin, V. C. R.; Thrower, J. Route to Fluoroalkyl-substituted Aromatic Compounds Involving Fluoroalkylcopper Intermediates. *Tetrahedron* . **1969**, *25*, 5921−5940.

[21] Choi, W. J.; Choi, S.; Ohkubo, K.; Fukuzumi, S.; Cho, E. J.; You, Y. Mechanisms and Applications of Cyclometalated Pt(II) Complexes in Photoredox Catalytic Trifluoromethylation. *Chem. Sci*. **2015**, *6*, 1454−1464.

[22] Nagib, D. A.; MacMillan, D. W. C. Trifluoromethylation of Arenes and Heteroarenes by Means of Photoredox Catalysis. *Nature* **2011**, *480*, 224−228.

[23] Natta, G. New Class of Polymers of α-olefin Having Exceptional Regularity of Structure. *Atti. Acc. Naz. Lincei Mem*. **1955**, *4*, 61.

[24] Breil, H.; Natta, G.; Pino, P.; Mazzanti, G.; Ziegler, K. *JP Appl.JP*, **1957**, 1957-7445.

[25] Natta, G.; Pino, P.; Corradini, P.; Danusso,F.; Mantica, E.; Mazzanti, G.; Moraglio, G. Crystalline High Polymers of α-Olefins. *J. Am. Chem. Soc*. **1955**, *77*, 1708.

[26] Boday, D. J. The State of Fluoropolymers. In Advances in Fluorine-Containing Polymers; Smith, D. W. Jr., Iacono, S. T., Boday, D. J., Kettwich, S. C., Eds.; American Chemical Society: Washington, **2012**; pp 1-5.

[27] Kim, C. U.; Lee, J. M.; Ihm, S. K. *J. Fluorine Chem.* **1999**, *96*, 11.

[28] Kim, C. U.; Lee, J. M.; Ihm, S. K. *J. Appl. Polym. Sci.* **1999**, *73*, 777.

[29] Sianesi, D.; Caporiccio, G.; Stereospecific Polymerization of Perfluoroolefins. *Makromol. Chem*. **1963**, *60*, 213.

[30] Huang, Y.; Li, J.; Zhou, J.; Zhu, Z.; Hou. G. π-Bis(Benzene)Chromium(0)-Catalyzed Oligomerization of Perfluoropropylene. *J. Organomet. Chem*. **1981**, *205*, 185-191.

[31] Clot, E.; Megret, C.; Kraft, B. M.; Eisennstein, O.; Jones, W. D.; Defluorination of Perfluoropropene Using $Cp^*_2ZrH_2$ and Cp^*_2ZrHF: A Mechanism Investigation from a Joint Experimental-Theoretical Perspective. *J. Am. Chem. Soc*. **126**, 5647-5653.

[32] . Smart, B. E. in The Chemistry of Functional Groups, Supplement D; Patai, S., Rappoport, Z., Eds.; John Wiley & Sons: New York, **1983**; Chapter 14.

[33] Wilford, J. B.; Stone. F. G. A. Chemistry of the Metal Carbonyls. XXVIII. Addition of Rhenium Pentacarhonyl Hydride to Fluoro Olefins. *Inorg. Chem*. **1965**, *4*, 93-97

[34] Fujisawa, K.; Nabika, M. Development of New Polymerization Catalysts with Manganese(II) Complexes. *Coord. Chem. Rev*. **2013**, *257*, 119-129

[35] Algarra, A. G.; Grushin, V. V.; Macgregor. S. A. Natural Bond Orbital Analysis of the Electronic Structure of [LnM(CH_3)] and [LnM(CF_3)] Complexes. *Organometallics*, **2012**, *31*, 1467-1476.

[36] McClellan, W. R. Perfluoroalkyl and Perfluoroacyl Metal Carbonyls. *J. Am. Chem. Soc*. **1961**, *83*, 1598-1600.

[37] Naumann, D.; Kaiser. M. A New Synthesis of Perfluoroorgano Manganese and Rhenium Compounds. *Z. Anorg. Allg. Chem*. **1995**, *621*, 812-816.

[38] Banerjee, S.; Karunananda, M. K.; Bagherzadeh, S.; Jayarathne, U.; Parmelee, S. R.; Waldhart, G. W.; Mankad, N. P. Synthesis and Characterization of Heterobimetallic Complexes with Direct Cu-M Bonds (M = Cr, Mn, Co, Mo, Ru, W) Supported by N-Heterocyclic Carbene Ligands: A Toolkit for Catalytic Reaction Discovery. *Inorg. Chem*. **2014**, *53*, 11307-11315.

[39] Sublimation occurred at atmospheric pressure at 100^{o}C. This caused partial decarbonylation of $Mn(CO)_5(COCF_3)$ to $Mn(CO)_5CF_3$; however, given the volatility of the complexes, the cold-finger collected a mixture containing 40-50% of $Mn(CO)_5COCF_3$.

[40] Lumsden, S. E. A.;Durgaprasad, G.; Muthiah, K. A. T.; Rose, M. J. Tuning Coordination Modes of Pyridine/thioether Schiff Base (NNS) Ligands to Mononuclear Manganese Carbonyls. *Dalton Trans*. **2014**, *43*, 10725-10738.

[41] Welch, K. D.; Dougherty, W. G.; Kassel, W. S.; Dubois, D. L.; Bullock, R. M. Synthesis, Structure and Reactions of Manganese Complexes Containing Diphosphine Ligands and Pendant Amines. *Organometallics*, **2010**, *29*, 4532-4540.

[42] Van Putten, R.; Uslamin, E. A.; Garbe, M.; Liu, C.; Gonzalez-de-Castro, A.; Lutz, M.; Junge, K.; Hensen, E. J. M.; Beller, M.; Lefort, L.; Pidko, E. A. Non-Pincer-Type Manganese Complexes as Efficient Catalysts for the Hydrogenation of Esters. *Angew. Chem. Int. Ed*. **2017**, *56*, 7531-7534.

[43] Liu, S. Tripodal Phosphine Ligands. Syntheses and Coordination Chemistry Toward Mn(I). *J. Chin. Chem. Soc*. **1992**, *39*, 611-616.

[44] Ligands attempted: PPh_3, PMe_3, DPPE, DPPF, DMPE, Tripod, Triphos, $P(O^iPr)_3$, $P(OPh)_3$

[45] Luh, T-Y. Trimethylamine N-oxide - a Versatile Reagent for Organometallic Chemistry. *Coord. Chem. Rev*. **1984**, *60*, 255-276.

[46] Morrison, J. A. Trifluoromethyl-containing Transition Metal Complexes. *Adv. Organomet. Chem*. **1993**, *35*, 211.

[47] Leyssens, T.; Peeters, D.; Orpen, A. G.; Harvey, J. N. How Important is Metal-Ligand Back-bonding toward YX3 Ligands (Y = N, P, C, Si)? An NBO Analysis. *Organometallics*, **2007**, *26*, 2637-2645.

[48] Welch, K. D.; Dougherty, W. G.; Kassel, W. S.; Dubois, D. L.; Bullock, R. M. Synthesis, Structures, and Reactions of Manganese Complexes Containing Diphosphine Ligands with Pendant Amines. *Organometallics*, **2010**, *29*, 4532-4540.

[49] Specific reduction waves occurred at -2.3 V (Complex **3**), -2.2 V (Complex **4**) and -2.4 V (Complex **7**)

[50] Electrospray ionization mass spectroscopy (ESI-MS) was initially performed; however this led to significant fragmentation of the parent ions due to a presumed oxidation to unstable Mn(II) species for all Mn–CF_3 complexes. For this reason we turned to EI-MS.

[51] EI-MS spectral data and proposed reaction pathway for gas-phase formation of $[(N\text{-}N)MnF]^+$ and $[(N\text{-}N)(F)Mn{=}CF_2]^+$ are available in the SI.

[52] Reactions involving stoichiometric quantities of complex **3-6** with aryl-iodides were done at various temperatures (25°C, 60°C, 100°C) utilizing various solvents (THF, Toluene) and ^{19}F NMR spectra showed only starting material after 1 and 24 h.

[53] Richmond, T. G.; Shriver, D. F. Electrophillic Halogen Exchange between Lewis Acids and Transition-Metal Perfluoroalkyl Complexes. Synthesis and Characterization of Transition Metal α-Haloalkyl Complexes. *Organometallics*, **1984**, *3*, 305-314.

[54] Richmond, T. G.; Crespi, A. M.; Shriver, D. F. Nucleophillic, Electrophillic, and Homolytic Reaction Chemistry of Transition Metal Carbonyl Trihalomethyl (X = F, Cl, Br) Complexes. *Organometallics*, **1984**, *3*, 314-319.

[55] Harrison, D. J.; Daniels, A. L.; Guan, J.; Gabidullin, B. M.; Hall, M. B.; Baker, R. T. Nickel Fluorocarbene Metathesis with Fluoroalkenes. *Angew. Chem. Int. Ed*. **2018**, *57*, 5772 – 5776.

[56] Harrison, D. J.; Daniels, A. L.; Korobkov, I.; Baker. R. T. d^{10} Nickel Difluorocarbenes and Their Cycloaddition Reactions with Tetrafluoroethylene. *Organometallics*. **2015**, *34*, 5683-5686.

[57] Harrison, D. J.; Lee, G. M.; Leclerc, M. C.; Korobkov, I.; Baker, R. T. Cobalt Fluorocarbenes: Cycloaddition Reactions with Tetrafluoroethylene and Reactivity of the Perfluorometallacyclic Products. *J. Am. Chem. Soc*. **2013**, *135*, 18296-18299.

[58] See Experimental section for ^{19}F NMR spectra.

[59] Brandt, S.; Helquist, P. Cyclopropanation of Olefins with a Stable, Iron-containing Methylene Transfer Agent. *J. Am. Chem. Soc*. **1979**, *101*, 6473.

[60] O'Connor, E. J.; Brandt, S.; Helquist. P. $(\eta^5\text{-}C_5H_5)(CO)_2FeCH_2S^+(CH_3)_2\ BF_4^-$: A Methylene Transfer Reagent for the Direct Cyclopropanation of Alkenes. *J. Am. Chem. Soc.* **1987**, *109*, 3739.

[61] Only preliminary reactivity studies were performed for the formation of the $(NNS)(CO)_2Mn{=}CF_2$ and $(Bpy)(CO)_3Mn{=}CF_2$ complexes. ^{19}F NMR spectra are included in the SI.

7 Summary and Outlook

"The true delight is in the finding out rather than in the knowing" ~ Isaac Asimov

7.1 Overview

There is still a great deal of research required before there is sufficient understanding of transition metal fluorocarbenes and their reactivity to craft an efficient system for catalytic fluoroalkene oligomerization or metathesis. However, the work presented within this thesis represents a significant leap forward towards this final goal. This chapter summarizes this research and provides an outlook for future projects.

7.2 Chapter 2

Base metal complexes bearing perfluoro-alkyl ligands are rare although highly sought after as key precursors for the synthesis of metal fluorocarbene complexes. In this chapter, the modified synthesis of a zinc cobaltate and subsequent reaction with trifluoroacetic anhydride (TFAA) provides us with an easily modifiable Co–CF_3 scaffold with which new metal perfluoro-alkyl complexes can be obtained. This coordinatively labile complex provided us with four unique Co–CF_3 complexes, including one bearing an NHC ligand (NHC = SIPr), all of which were completely characterized.

Additionally, abstraction of fluoride from several of these complexes using a Lewis acid afforded rare $\{[Co]=CF_2\}^+$ difluorocarbenes that were observed using ^{19}F NMR spectroscopy. Although these electrophilic carbenes are unreactive towards TFE, we showed that the electron-rich Co fluoro-alkyl $P_3(CO)Co–CF_3$ transfers fluorine irreversibly to the less electron-rich fluorocarbene, $[P_2(CO)_2Co=CF_2]^+$, showcasing the effect of ancillary ligands on both perfluoro-carbene/-alkyl moieties.

Further reactivity of these new Co-CF_3 and Co=CF_2 complexes has yet to be determined. Given the rich coordination chemistry of the $Co(CO)_4CF_3$ scaffold, a wide variety of untested ligand systems including non-innocent and hard donor ligands represents a potentially large body of work to discern the effects of these modifications.

7.3 Chapter 3

Sluggish reactivity or electrophilic behavior in reactions utilizing neutral or cationic d^8 cobalt perfluoro-carbenes pointed us towards a more electron-rich metal such as nickel(0). In addition to the preparation of the first d^{10} metal fluorocarbenes, the work presented in this chapter sought to compare and contrast the reactivity of these new [Ni]=CF_2 carbenes with the half-sandwich CpLCo=CF_2 complexes that originally showed promising results with TFE and terminal acetylenes. Synthesis of the [Ni]=CF_2 complexes was accomplished through oxidative addition of TFAA with a Ni(0) precursor and subsequent reduction/fluoride abstraction with a powerful reductant in the presence of a stabilizing ligand.

It was immediately apparent that these nickel difluorocarbenes were significantly more reactive towards metallacycle formation when compared with the cobalt difluorocarbenes insofar as kinetics was involved. Metallacycle formation with nickel was complete within hours as opposed to days (>48 h) for cobalt. This difference is attributed to the increase in electron density when moving to a neutral d^{10} system, thereby increasing the nucleophilic character of the carbene itself. Moreover, the mechanism for nickel metallacycle formation involves initial ligand (L) loss as evidenced by decreased reaction rates in the presence of excess L. This is intriguing given that DFT results suggest that pre-coordination of the olefin is not necessary for metallacycle formation that results from attack of the terminal carbene on one carbon of TFE via a singlet diradical process. Nonetheless, reactions of these d^8 metallacycles with Lewis or Brønsted acids gave cis/trans-perfluorovinyl species or nickel perfluoroalkene complexes, respectively, as seen previously with the d^6 cobalt analogues. Even the most electron-rich Ni difluorocarbene, (dppe)[$P(OMe)_3$]Co=CF_2 afforded exclusively the stable metallacyclobutane on reaction with TFE, with no indication of the retro [2+2] cycloaddition required for metathesis. These results encouraged us to pursue alternate nickel perfluoro-carbenes as viable candidates.

7.4 Chapter 4

To access a fluorocarbene with a more stabilized triplet state, we targeted a [Ni]=$CF(CF_3)$ complex, surmising that a more covalent (nucleophilic/reactive) carbene may successfully activate the retro-cycloaddition reactivity, giving us successful fluoroalkene metathesis. However, these complexes were significantly more difficult to synthesize from

pentafluoropropionic anhydride so an alternate method was adopted. This required use of the toxic $Cd(CF_2CF_3)_2$ reagent to both transfer the $^-CF_2CF_3$ group and abstract fluoride from the resultant $P_3Ni\text{-}CF_2CF_3$, giving the desired $P_3Ni{=}CF(CF_3)$ complex directly [$P = P(O^iPr)_3$].

Upon reaction of this new nickel perfluorocarbene with TFE we observed via ^{19}F NMR spectroscopy the formation of the expected metallacycle product *and* the desired metathesis products, $Ni{=}CF_2 + CF_2{=}CF(CF_3)$, This represented the first example of successful metathesis of a fluoroalkene with a metal fluorocarbene. However, when left under an atmosphere of TFE there was no interconversion between the metallacycle and the new olefin as would be expected if the reaction occurred via the well-known Chauvin mechanism. Computational details were then discerned through collaboration with Dr. Jia Guan and Prof. Michael Hall from Texas A&M University which showed that formation of the metallacycle and metathesis products occurs through separate reaction pathways. Unlike the singlet diradical mechanism, the metathesis pathway includes coordination of the fluoroalkene to the nickel through a novel 4-coordinate transition state. Moreover, while C-C bond formation occurs in the NiP_2 plane for metallacycle formation, a tetrahedral transition state for metathesis leads to C-C bond formation in a plane perpendicular to the NiP_2 plane.

Moving to more electron-rich olefins such as TrFE and VDF showed a steady increase towards the metathesis reaction pathway forming greater ratios of metathesis to metallacycle products. DFT studies of this phenomenon determined that the more electron-rich olefins decrease the activation barrier for fluoroalkene coordination. The metallacycles formed using these substrates also have unique chemistry such as regioselective formation from VDF, due presumably to stabilization of the diradical intermediate, and unprecedented instability when the metallacycle contains a CHF moiety as was the case using TrFE. In the latter case, the regioisomeric metallacyclobutanes rearranged to a nickelacyclopropane and a fluoronickel alkenyl species.

This chapter solidifies the idea that base metal fluorocarbenes are promising candidates for the fluoro-variant of the alkene metathesis reaction. Given that the major hurdle in regards to metathesis of fluorinated substrates utilizing both Grubbs and Schrock catalysts is the highly stabilized $[M]{=}CFR^F$ intermediate, our discovery offers hope towards the progression of this chemistry.

7.5 Chapter 5

It is apparent that the nickel-mediated fluoro-metathesis reaction required a wider scope of substrates to better understand this chemistry, to determine if the metallacycle pathway could be subdued through careful selection of substrates and determining if these metal fluorocarbenes could be utilized in traditional non-fluorinated metathesis. In total, seven new substrates were utilized to better understand the reactivity of the [Ni]=CF(CF_3) carbenes including Tr^FOCF_3, perfluorocyclobutene, ethylene, 4-methoxy-styrene, pentafluorostyrene, cyclopentene and methyl-5-norbornene 2-carboxylate.

The reaction with perfluorocyclobutene was expected to generate a new fluorocarbene of similar energy to Ni=CF(CF_3) allowing for its interception by additional substrate, promoting oligomerization through unprecedented fluoroalkene ring-opening metathesis. However, time-resolved ^{19}F NMR experiments showed that the new carbene was quickly consumed to produce a novel product with a spiro carbon connecting a cyclopropane ring to the nickelacyclobutane. Although it is still unclear at which stage the required fluoride migration occurs, rapid formation of this stable product has so far stifled attempts to intercept the ring-opened nickel fluorocarbene with additional perfluorocyclobutene. In contrast, reaction of [Ni]=CF(CF_3) with bulky CF2=CF(CF_3) produced the metallacycle exclusively, as the direct attack diradical pathway obviates the need for nickel to coordinate this fluoroalkene.

Based on the observed trend going from TFE to VDF, reactions with smaller, more electron-rich substrates such as ethylene were predicted to afford higher yields of metathesis products when in fact only metallacycles were observed. These results suggest that fluoroalkene metathesis may require stabilized metal carbene products to out-compete the metallacycle pathway. This was the case even when ring-strain was employed to destabilize the metallacycle product utilizing either cyclopentene or a bicyclic norbornene substrate both of which produced metallacycle products exclusively.

This chapter focused on the effect of substrates in regard to productive metathesis as well as regio- and stereoselectivity in regards to metallacycle formation. Although this chapter certainly ascertained that successful stoichiometric and catalytic fluoroalkene metathesis transformations

will require new catalyst designs, our detailed knowledge of the competing reaction pathways provides some basis for these designs.

7.6 Chapter 6

Following our successful demonstration of a fluoro-variant of alkene metathesis, we aimed to demonstrate a fluoro-variant of the Cossee-Arlman mechanism for coordination polymerization of alkenes. While several publications have demonstrated the insertion of TFE into a Mn(I)–C_{Me} bond, examples of such an insertion into an M-C^F bond have not yet been reported. It was our aim that formation of an electron-rich manganese complex in the +2 oxidation state would remove the crystal field stabilization, therefore increasing the overall lability of the Mn–C^F bond and the likelihood for insertion of fluorinated alkenes.

This research began with the synthesis of the first examples of new Mn–CF_3 complexes in 50 years. In fact, our preparation gave easy access to 4 new manganese trifluoromethyl complexes. However, oxidation of these Mn(I) complexes, even in the presence of TFE, led to cleavage of the Mn-C_{CF3} bond as determined by X-ray crystallography of the resulting Mn(II) complex.. Indeed, cyclic voltammetry (CV) experiments showed an irreversible oxidative wave confirming a subsequent chemical reaction. Intriguingly, however, a quasi-reversible reduction was also observed, suggesting formation of a Mn(0) complex which may prove useful in later studies. Moreover, reaction of the Mn-CF_3 complexes with trimethylsilyl triflate (TMS-OTf) afforded new$\{[Mn]=CF_2]\}^+$ cations. the first examples of Mn fluorocarbenes. Although reactions of this electrophilic carbene with ethylene did not produce the expected cyclopropanation product, the ^{19}F NMR carbene resonance disappeared, indicating that further investigation is called for.

This chapter explored the possibility of utilizing perfluoro-alkyl manganese complexes as possible initiators for the formation of fluoropolymers. In so doing, a new route to Mn–CF_3 complexes was discovered along with formation of the first $\{[Mn]=CF_2\}^+$ carbenes. There remains a great deal of unexplored possibilities utilizing both $Mn^{(I)}$ and $Mn^{(0)}$–CF_3 complexes as well as better understanding the fate of [Mn=CF_2] carbenes in their reactions with non-fluorinated alkenes.

7.7 Outlook

Our results from Chapter 2 were initially disappointing for the simple reason that successful [2+2] cycloadditions with fluoroalkenes were not possible for the cationic d^8 cobalt difluoro-carbenes. However, knowing now that the diradical pathway employed by both d^8 cobalt and d^{10} nickel complexes is non-productive for metathesis, it would be worth determining whether a more electron-rich, coordinatively unsaturated cobalt variant is capable of reacting with fluoroalkenes. For example, trimethylamine N-oxide and/or UV-light are both excellent methods to promote CO loss, opening up the possibility for coordinatively unsaturated [Co]=CF_2 moieties. That being said, these cationic species may still be poor choices to capture electrophilic fluoroalkenes. With this in mind, the neutral Co–CF_3 precursors or their paramagnetic d^9 Co(0) anionic analogs may still be good candidates for the elusive Cossee-Arlman fluoroalkene polymerization process. The results we obtained from chapters 3-5, on the other hand, provided us with new ideas for tailoring the fluoroalkene metathesis reaction. For example, it is becoming abundantly clear that complexes with triplet-stabilized carbenes such as [Ni]=CF(CF_3), as opposed to [Ni]=CF_2, are necessary for productive metathesis to occur. In addition, the overall geometry of the transition state is a major contributing factor towards the ratio of metathesis vs. metallacycle products formed. For example, the main difference between the transition state leading to metallacycle and metathesis products are the nickel oxidation state and the position of the ancillary ligands {perpendicular (tetrahedral) versus eclipsed (square planar)} with respect to the C-C bond-forming plane. Therefore, by utilizing a ligand system that makes a square planar geometry difficult due to steric crowding, the metallacycle pathway may be subdued. In addition, use of p-accepting ligands will tend to favor the zerovalent metathesis transition state over the Ni(I) diradical intermediate on the metallacycle pathway.

It may also be possible to create an ideal system by revisiting chapter 6 in which manganese (I) difluoro-carbenes were synthesized. Interactions of a triplet carbene with the metal are favored if appropriate singly occupied metal orbitals (SOMOs) are available. By reacting anionic ligands such as tris-pyrazolyl ligands (Tp) with the formed [L_5Mn=CF_2][OTf] complexes we could produce neutral d^6 carbenes along with K[OTf] salts. Not only would these complexes be neutral and therefore more likely to react with fluoroalkenes, if the carbonyls could be removed via photolysis the resulting tetrahedral d^6 complex would contain singly occupied dx^2-y^2 and dz^2

orbitals. Additionally, use of a bulky Tp ligand such as 2,5 dimethyl Tp (^{Me,Me}Tp = Tp*) may discourage formation of a stable metallacycle due to both steric and electronic restraints. Further research on these new carbenes may provide additional insight into the effects of metal fragment geometry and electronic structure on this process. Finally, photolysis may also be employed to generate a transient triplet state while also encouraging ligand dissociation.

The work that I have accomplished throughout this thesis has extended the fields of both base metal fluoro-alkyl complexes as well as transition metal fluorocarbenes**.** It was particularly fortunate that the first examples of d^{10} [Ni]=CF(CF_3) complexes gave rise to fluoroalkene metathesis reactions as many attempts at ligand diversification have not yet met with success. The one successful synthesis after a year of work was the formation of (Bipy)(MeCN)-Ni=CF(CF_3) via a multi-step synthesis involving oxidative addition of pentafluoropropionic anhydride to Ni(PPh_3)$_2$, subsequent addition of bipyridine to the isolated product, and KC_8 reduction in acetonitrile. Although this complex was capable of the desired metathesis transformation, it did so with a poor ratio of metathesis to metallacycle products and was impure even after attempted isolation steps and therefore not included in publications. However, 2,2'-di-substituted bipyridines may be able to 'enforce' the tetrahedral transition state needed to outcompete metallacycle formation. Moreover, use of electron-withdrawing substituents such as chloride may electronically favor the zerovalent Ni metathesis transition state over formation of the divalent metallacycle.

In summary, this research paves the way for the next group of chemists to discover effective catalysts for the formation of new fluoroalkenes, cyclic structures and polymers via metal-mediated (or –catalyzed) fluoro-variants of alkene metathesis and 1,2-alkene insertions.

"Satisfaction of one's curiosity is one of the greatest sources of happiness in life." ~ Linus Pauling